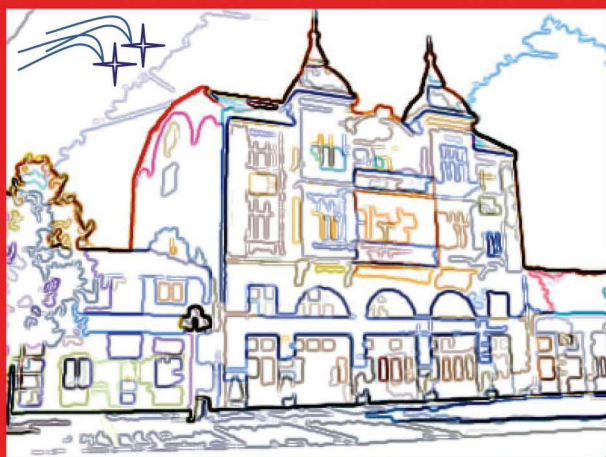


PROCEEDINGS OF THE VIII SERBIAN-BULGARIAN ASTRONOMICAL CONFERENCE

Leskovac, Serbia, May 8-12, 2012

Eds. Milan S. Dimitrijević and Milcho K. Tsvetkov



BELGRADE, 2013

**PROCEEDINGS OF THE VIII SERBIAN-BULGARIAN
ASTRONOMICAL CONFERENCE**

Leskovac, Serbia, May 8-12, 2012

Eds. Milan S. Dimitrijević and Milcho K. Tsvetkov



**БЕОГРАД
2013**

SCIENTIFIC COMMITTEE

Milan S. Dimitrijević (Co-chairman)
Milcho K. Tsvetkov (Co-chairman)
Žarko Mijajlović (Co-vice chairman)
Ognyan Kounchev (Co-vice Chairman)
Tanyu Bonev
Dimo Dimov
Dragana Ilić
Darko Jevremović
Predrag Jovanović
Andjelka Kovačević
Jelena Kovačević
Petko Nedialkov
Nadežda Pejović
Luka Č. Popović
Zoran Simić
Katya Tsvetkova
Dejan Urošević

LOCAL ORGANIZING COMMITTEE

Milan S. Dimitrijević (Co-chairman)
Žarko Mijajlović (Co-chairman)

Scientific secretary:

Andjelka Kovačević

Members:

Luka Č. Popović
Darko Jevremović
Nadežda Pejović
Jelena Kovačević
Marko Stalevski
Tanja Milovanov
Miodrag Dačić
Zoran Simić

Under the auspices of
Serbian Ministry of Education, Science and Technological Development
Bulgarian Academy of Sciences

ORGANIZERS:

Society of Astronomers of Serbia and Astronomical Observatory
Institute of Astronomy with National Astronomical Observatory, BAS

Co-organizers:

Faculty of Mathematics and Department of Astronomy, University of Belgrade
Institute of Mathematics and Informatics of the Bulgarian Academy of Sciences
Department of Astronomy, Faculty of Physics, Sofia University “St. Kliment Ohridski”

On the front cover: logo of the conference made by Zoran Simić

On the back cover: In the beginning, author Zoran Simić

Text arrangement by computer: Tatjana Milovanov

Published and copyright © by Astronomical Society “Rudjer Bošković”, Kalemegdan,
Gornji Grad 16, 11000 Belgrade, Serbia
President of the Astronomical Society “Rudjer Bošković”: Miodrag Dačić

Financially supported by the Ministry of Education, Science and Technological
Development of Serbia

ISBN 978-86-89035-02-5

Production: Siga Star, Mrakovička 48/4, Beograd, in 100 copies

CONTENTS

INVITED LECTURES

Alexandra Költzsch, Amalya Poghosyan and Valeri Hambaryan
**ON A CYCLIC ACTIVITY AND DIFFERENTIAL ROTATION OF
Par 1724 = V1321 Ori** 7

Jelena Kovačević, Luka Č. Popović, Milan S. Dimitrijević
**CORRELATIONS BETWEEN SPECTRAL PROPERTIES IN AGN
TYPE 1: INFLUENCE OF STARBURSTS** 15

Georgi T. Petrov
LINUX ASTRONOMICAL SOFTWARE 21

Georgi Petrov, Momchil Dechev, Emanouil Atanasov
**BULGARIAN GRID, BULGARIAN VIRTUAL OBSERVATORY
AND SOME ASTRONOMICAL APPLICATIONS** 57

Jan Vondrák
LONG TERM PRECESSION MODEL 91

CONTRIBUTED PAPERS

E. Atanassov, M. Dechev, G. Petrov, A. Karaivanova, T. Gurov and
M. Durchova
**HPC CLUSTER WITH GPGPU CAPABILITIES. PERFORMANCE
AND FEATURES EVALUATION** 105

Daniela Boneva, Lachezar Filipov, Deyan Gotchev
**3D NUMERICAL ANALYSIS AND STRUCTURES FORMATION
IN ACCRETING WHITE DWARFS** 113

Yavor Chapanov
**4-PARAMETER TRANSFORMATION OF DIGITIZED
ASTRONOMICAL IMAGES** 121

Luka Ćirić and Dušan Ćirić
RELATIVE EXISTENCE OF PHYSICAL OBJECTS 127

Zorica Cvetković, Goran Damljanović, Rade Pavlović MORE ACCURATE FOCAL LENGTH DETERMINATION FOR THE ROZHEN 2 m TELESCOPE	135
M. Dechev, K. Koleva, M. S. Madjarska, P. Duchlev, J.-C. Vial, E. Buchlin KINEMATICS OF A LOOP-LIKE ERUPTIVE PROMINENCE AS OBSERVED BY AIA/SDO	143
Milan S. Dimitrijević SOCIETY OF ASTRONOMERS OF SERBIA 2008-2011	153
Milan S. Dimitrijević TEN YEARS OF THE SCIENTIFIC SOCIETY “ISAAC NEWTON” AND OF “YUGOSLAVIA” BRANCH OF THE INTERNATIONAL ASTRONOMICAL INSTITUTE ISAAC NEWTON OF CHILE	173
Milan S. Dimitrijević ACTIVITIES OF PARTICIPANTS OF THE PROJECTS 146001 AND 176002 “INFLUENCE OF COLLISIONAL PROCESSES ON THE ASTROPHYSICAL PLASMA SPECTRA” – 2010-2011	189
Milan S. Dimitrijević, Magdalena Christova, Zoran Simić, Andjelka Kovačević, Sylvie Sahal-Bréchet ON THE STARK BROADENING OF B IV SPECTRAL LINES	205
Dimo Dimov and Milan S. Dimitrijević IMAGE PROCESSING SUGGESTIONS FOR ASTRONOMICAL MULTIEXPOSURE WIDE FIELD PLATES	219
Sava Donkov, Orlin Stanchev, Todor Veltchev MODELING OF MOLECULAR CLOUDS WITH FORMATION OF PRESTELLAR CORES	239
Daniela Kirilova, Mariana Panayotova INHOMOGENEOUS BARYOGENESIS MODEL AND ANTIMATTER IN THE UNIVERSE	249
Žarko Mijajlović, Aleksandar Simonović, Nadežda Pejović A METHOD FOR ENHANCED IMAGE PROCESSING AND SEARCH FOR VARIABLE STARS	257

Ivana S. Milić and Goran Damljanović OBSERVATIONS OF ERS FROM ICRF2 LIST USING ASV 60 cm AND ROZHEN 2 m TELESCOPES	263
Petko Nedialkov, Antoniya Valcheva, Evgeni Ovcharov and Yanina Metodieva WIDE-FIELD STELLAR PHOTOMETRY WITH THE 50/70 cm SCHMIDT TELESCOPE OF NAO ROZHEN	271
Grigor B. Nikolov, Mary Kontizas, Anastasios Dapergolas, Maya K. Belcheva, Valery K. Golev and Ioannis Bellas-Velidis DISTRIBUTION OF STARS IN MAGELLANIC CLOUDS' STAR CLUSTERS	279
Plamen Nikolov, Tanyu Bonev, Nikola Petrov, Pawel Rudawy, Bogdan Rompolt, Petar Duchlev FINE STRUCTURE OSCILLATIONS OF A QUIESCENT PROMINENCE	283
Aleksandra Nina PERTURBATIONS OF THE TERRESTRIAL LOW IONOSPHERE CAUSED BY SOLAR FLARES	289
Slobodan Ninković, Milan Stojanović, Zorica Cvetković THE KINEMATICS OF STARS FROM THE SOLAR NEIGHBOURHOOD CASE OF THE TWO DISC COMPONENTS	297
Georgi Petrov, Michel Dennefeld ON THE COMPOSITE NATURE OF THE GALAXY NGC 5929	303
N. Petrov, P. Duchlev, K. Koleva, M. Dechev PROMINENCE ERUPTION ON 22 AUGUST 2006 OBSERVED WITH THE H_α CORONAGRAPH IN NAO ROZHEN	321
Lyuba Slavcheva-Mihova BAR PARAMETERS IN SEYFERT AND INACTIVE GALAXIES	329
V. A. Srećković, A. A. Mihajlov, Lj. M. Ignjatović, M. S. Dimitrijević, A. Metropoulos THE MANIFESTATIONS OF THE NON-SYMMETRIC ION-ATOM ABSORPTION PROCESSES IN THE SOLAR ATMOSPHERES IN UV AND VUV REGION	333

K. A. Stoyanov, R. K. Zamanov, G. Y. Latev, S. Boeva, M. F. Bode, S. V. Tsvetkova, N. Kacharov UBVRI_{α} ’ OBSERVATIONS OF THE FLICKERING OF THE JET EJECTING SYMBIOTIC STAR MWC 560	339
Katya Tsvetkova and Milcho Tsvetkov WFPDB METADATA FORMAT PREPARATION	349
Katya Tsvetkova, Milcho Tsvetkov, Nikolay Kirov, Damyan Kalaglarsky THE LAST PLATE OBSERVATIONS WITH ROZHEN OBSERVATORY SCHMIDT TELESCOPE	359
Sonja Vidojevic, Arnaud Zaslavsky, Milan Maksimovic, Säm Krucker, Milan Drazic, Olga Atanackovic LANGMUIR WAVES, TYPE III RADIO BURSTS AND IMPULSIVE ELECTRON EVENTS	367
Krasimira D. Yankova GENERATION AND DEVELOPMENT OF THE DISK CORONA	375
AUTHORS’ INDEX	382
PHOTOS	383

INVITED LECTURES

ON A CYCLIC ACTIVITY AND DIFFERENTIAL ROTATION OF Par 1724 = V1321 Ori

ALEXANDRA KÖLTZSCH, AMALYA POGHOSYAN and VALERI HAMBARYAN

*Astrophysical Institute and University Observatory
Friedrich Schiller University of Jena, Germany
E-mail: vvh@astro.uni-jena.de*

Abstract. We applied the Gregory-Loredo method (for periodic signal detection of unknown shape in time-series with Gaussian errors) to the 200000 year old naked, weak-line, run-away T Tau type star Par 1724, located north to of the Trapezium cluster in Orion, for which measurements of the stellar magnitudes in V-band and corresponding errors spanning more than 50 years are available. Preliminary results indicating on a cyclic activity of Par 1724 with a period of ~ 18 years. It also revealed a second significant periodic signal, in the range of 5.85-5.95 days (together with 5.67 days period, known as rotational one), which might be a mimic on a differential rotation.

1. INTRODUCTION

The K0 pre-main sequence star Par 1724 in Orion is listed as star number 1724 in Parenago (1954), it is located at $\alpha = 5^{\text{h}}35^{\text{m}}4.21^{\text{s}}$ and $\delta = -5^{\circ}8'13.2''$ (J2000.0), 15' north of the Trapezium cluster in Orion. Par 1724 is one of the most active and variable young stars known. It is known to show photometric variability since 1996 (Cutispoto et al. 1996). An extensive photometric study was made by Neuhauser et al. in 1998 (Neuhauser et al. 1998). The origin of the photometric variation is a rotational modulation due to a large polar spot, detected indirectly by Doppler imaging (Fig. 1). Par 1724 rotates with a period of $P \approx 5.7\text{d}$, the amplitude of variation is about 0.2 mag in V-band. This period is seen so far in all data sets from 1968 to 1997. Beside this rotational period, the star may also show a long-term change of its optical brightness, namely getting fainter in V over 40 years, see Fig. 5 in Neuhauser et al. (1998).

2. DATA ANALYSIS AND RESULTS

For our analysis of the rotation period we used data obtained in 2007 (nine nights between March 15 and April 14) at the University Observatory in Jena. Eight nearby bright comparison stars were used to determine the photometric amplitude of Par 1724 relative to these eight stars. We then calculated the mean of relative magnitude

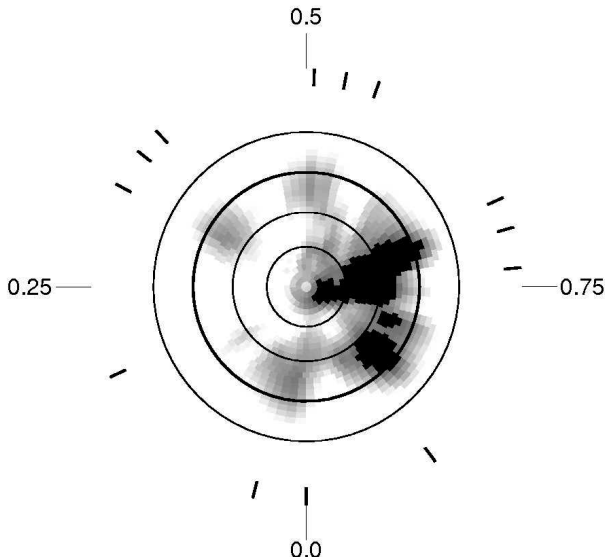


Figure 1: Doppler Image of Par 1724 obtained in 1997 showing the location of the spot. The ticks mark the rotational phase spectra were taken.

changes between Par 1724 and each comparison star between the first and any other night, see Neuhäuser *et al.* (2009) for further information.

Beside these data points obtained in Jena, we used V-band data available online¹ from the All Sky Automated Survey (ASAS), where the whole observable sky (down to 14 mag) is monitored using telescopes on Las Campanas, Chile and Haleakala, Hawaii. Almost 700 fully reduced V-band data points for Par 1724 are available.

To analyse the long-term brightness change we used all available data from the 1960ies on and in addition to this own data from La Silla, Chile (1998) and Wendelstein Observatory, Germany (2004).

2. 1. PREVIOUS STUDY

We searched for periodicity signals in all data using the standard methods stringlength (Broeg *et al.* 2005 and references therein), Lomb-Scargle (Scargle 1982, Horne 1986) and a Fourier analysis (Lenz and Breger 2005).

For both data sets (Jena and ASAS), we obtain the already known 5.7d period. Fig. 2 shows the phase-folded lightcurves for the ASAS data.

To obtain information about the long-term change we used all available data from the 1960ies to 2009, covering about 40 years of observation. Using the same tools for analysis, we found five different possible periods: $P_1 = 6.05$ yr (Power 12.98), $P_2 = 8.96$ yr (Power 34.04), $P_3 = 36.9$ yr (Power 104.33), $P_4 = 17.5$ yr with a stringlength of 42.7 and $P_5 = 27.9$ yr with high false alarm propability of 0.059. Figure 3 shows the periodograms of the stringlength algorithm (top) and Lomb-Scargle (bottom).

¹www.astrouw.edu.pl/asas

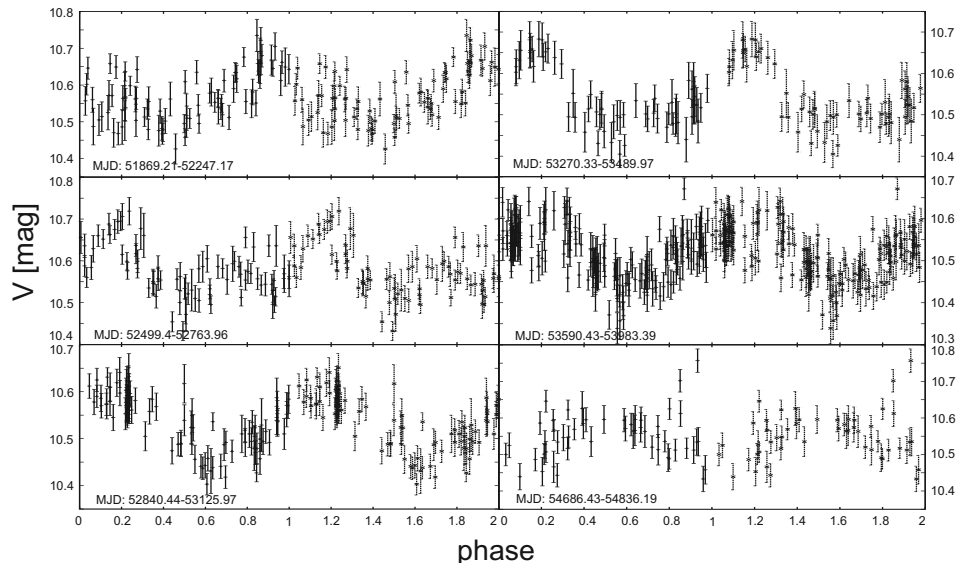


Figure 2: The phase-folded lightcurves for the ASAS data. The data are always plotted in phase with the 5.7d period.

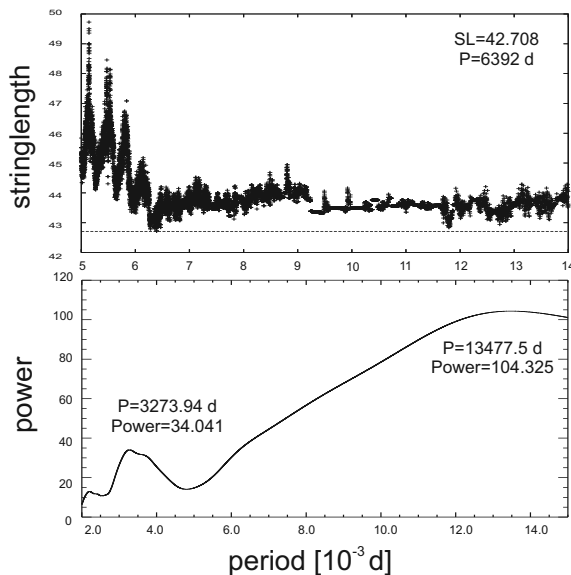


Figure 3: Periodograms of stringlength and Lomb-Scargle with the most probable periods (or cycle lengths) of 9 and 17.5 years.

The two periods that describe the long-term variation best, are $P_2 = 9$ yr and $P_4 = 17.5$ yr. This would indicate a cycle similar to the 11 year solar cycle.

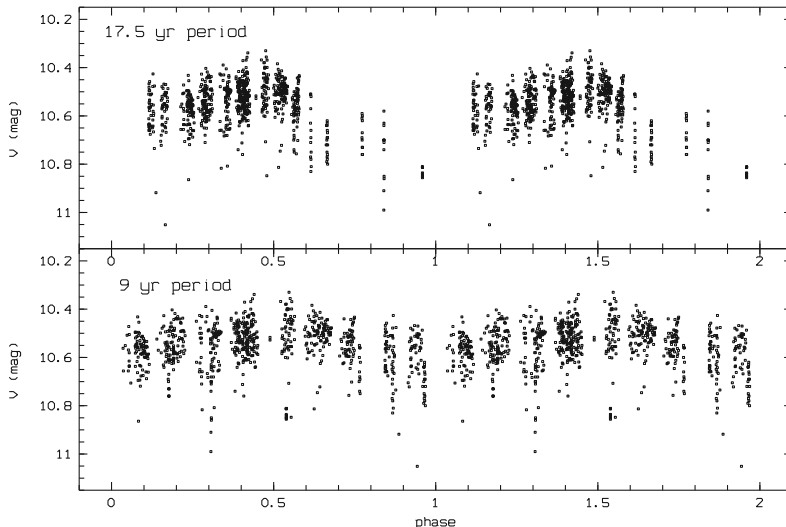


Figure 4: Absolute photometry data for Par 1724. We plot absolute magnitude in mag versus phase for the two best periods, namely 17.5 years and 9 years.

2. 2. BAYESIAN APPROACH

In order to detect cyclic activity of Par 1724 we applied a method developed by Gregory & Loredó (1992) in the case of Gaussian errors (Gregory 1999, 2005).

The method is using a Bayesian approach to the problem of detection and characterization of a periodic signal in a time series when we have no specific prior knowledge of the existence of such a signal or of its characteristics, including shape.

Originally, the method was developed to deal with photon arrival time data sets in X-ray and gamma-ray astronomy, where the appropriate sampling distribution is the Poisson distribution.

In the current approach, we are dealing with stellar magnitude measurements (or timing residuals after folding into the rotational period), i.e. analyzing a sampled time series with Gaussian noise (Gregory 1999). This analysis does not assume uniform sampling; the approach allows us to draw optimal inferences about the nature of the signal for whatever data is available.

Thus, the Par 1724 data sets, for which long term observations are available (Neuhäuser 2009), we can represent the measurements of the stellar magnitudes in V-band and corresponding errors spanning more than 50 years, by the equation

$$V_i^O = V_i^M + \epsilon_i + \epsilon_0$$

where V_i^O is the measured data at time t_i , V_i^M the periodic model or constant model prediction at time t_i , ϵ_i the component of V_i^O , which arises from measurement errors, and ϵ_0 is any additional unknown measurement errors plus any real signal in the data that cannot be explained by the model prediction V_i^M .

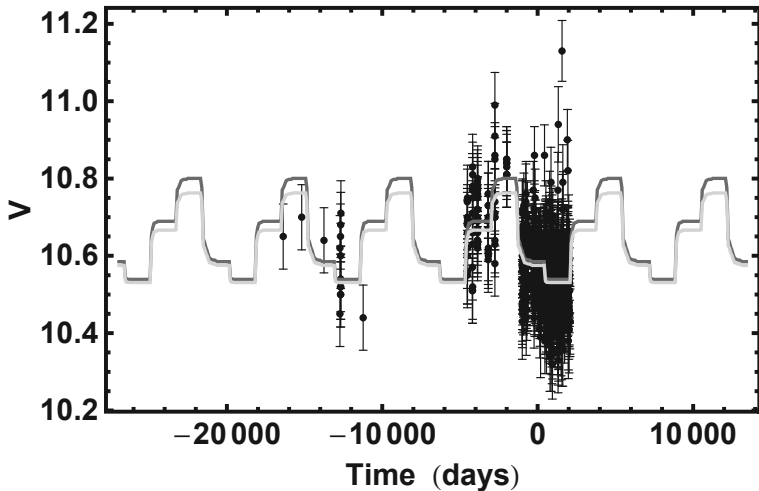


Figure 5: Long-term light curve of Par 1724 for cyclic activity period of ~ 18 years is shown. The shape of the phase folded light curve shape determined by application of the GL method, a Bayesian approach for periodic signal detection of unknown shape with Gaussian noise (for details, see text).

Under the proposition that the quantity $V^O - V^M$ obeys to the Gaussian distribution, we computed the ratio of the probabilities (odds ratio) of two models, ie. periodic and constant. Periodic model is a family of models capable of describing a background plus a periodic signal of arbitrary shape.

A priori, we assumed that constant and periodic models have equal probability. Each member of the family of periodic models is a histogram with m bins, with m ranging from 2 to some upper limit, typically 12. The unknown parameters are P (period), ϕ (phase offset of start of data and beginning of first bin), m (number of bins), and ϵ_0 (extra Gaussian noise parameter, for details, see Gregory (1999, 2005), Hambaryan (2010), Hambaryan et al. (2010), Borisova et al. (2010)).

The long-term period search was performed in the range of 2.5 to 22.0 years. As a result, we obtained a most likely periodicity of 6665 days (e.g. 2×9 years) with a 1σ credibility range of 6635 to 6676 days cycle length. This confirms the preliminary result in Neuhäuser et al. (2009), being 17.5 years, and it also supersedes it by the fact that this new value of cycle length is shown to be more significant than the other candidate cycle length (9 years, Neuhäuser et al. (2009)) and it can now be given with a significant error range (see Fig. 5).

We also performed periodicity search analysis by applying the GL method in the range of 4-6 days. It also revealed a second significant periodic signal, in the range of 5.85-5.95 days (together with 5.67 days period, known as rotational one), which might be a mimic on a differential rotation (see Fig. 6).

P = 5.90722 ; s = 0.0834335 ; m = 2 ; chain $\beta = 1.$;

Max $\log_{10} (\text{Prior} \times \text{Likelihood}^{\beta}) = 464.957$

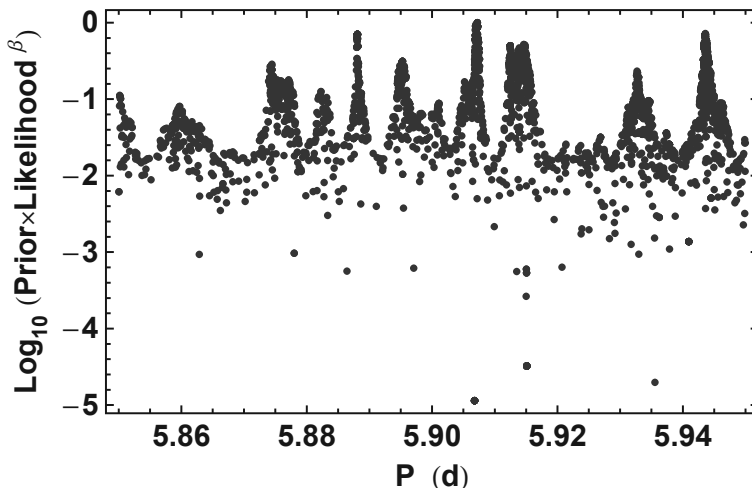


Figure 6: Markov-Chain Monte-Carlo approach for periodicity search by the GL method with Gaussian noise, in the range of 5.80-5.95 days of Par 1724. A significant peek at $P=5.90$ days together with well known 5.67 days rotational period may mimic on a differential rotation of Par 1724 (3-5% longer than rotational one).

References

- Borisova, A., Laskov, L. and Hambaryan, V.: 2010, *Bayesian probability theory in astronomy: Looking for stellar activity cycles in photometric data-series*. In *VIIIth Bulgarian-Serbian Astronomical Conference*, volume this issue.
- Broeg, C., Fernández, M. and Neuhäuser, R.: 2005, *A new algorithm for differential photometry: computing an optimum artificial comparison star*. *Astronomische Nachrichten*, **326**, 134.
- Cutispoto, G., Tagliaferri, G., Pallavicini, R. Pasquini, L. and Rodono, M.: 1996, *Photometric and spectroscopic studies of cool stars discovered in EXOSAT X-ray images. III. Photometric properties*. *Astronomy and Astrophysics Supplement*, **115**, 41.
- Gregory, P. C. and Loredo, T. J.: 1992, *A new method for the detection of a periodic signal of unknown shape and period*. *ApJ*, **398**, 146.
- Gregory, P. C.: 1999, *Bayesian Periodic Signal Detection. I. Analysis of 20 Years of Radio Flux Measurements of the X-Ray Binary LS I +61 deg303*. *ApJ*, **520**, 361.
- Gregory, P. C.: 2005, *Bayesian Logical Data Analysis for the Physical Sciences: A Comparative Approach with 'Mathematica' Support* (Cambridge University Press).
- Hambaryan, V. V.: 2010, *Bayesian probability theory in astronomy: Timing analysis of neutron stars*. In *VIIIth Bulgarian-Serbian Astronomical Conference*, volume this issue.
- Hambaryan, V., Tsvetkov, M., Tsvetkova, K. and Poghosyan, A.: 2010, *On a possible cyclic activity of Pleiades flare star HCG 377=II Tau*. In *VIIIth Bulgarian-Serbian Astronomical Conference*, volume this issue.
- Horne, J. H. and Baliunas, S. L.: 1986, *A prescription for period analysis of unevenly sampled time series*. *ApJ*, **302**, 757.
- Lenz, P. and Breger, M.: 2005, *Period04 User Guide*. *Communications in Asteroseismology*, **146**, 53.

- Neuhäuser, R., Wolk, S. J., Torres, G., Preibisch, T., Stout-Batalha, N.-M., Hatzes, A. P., Frink, S., Wichmann, R., Covino, E., Alcalá, J. M., Brandner, W., Walter, F. M., Sterzik, M. F. and Koehler, R.: 1998, *Optical and X-ray monitoring, Doppler imaging, and space motion of the young star Par 1724 in Orion*. *Astronomy and Astrophysics*, **334**, 873.
- Neuhäuser, R., Koeltzsch, A., Raetz, S., Schmidt, T. O. B., Mugrauer, M., Young, N., Bertoldi, F., Roell, T., Eisenbeiss, T., Hohle, M. M., Vaňko, M., Ginski, C., Rammo, W., Moualla, M. and Broeg, V.: 2009, *Photometric monitoring of the young star Par 1724 in Orion*. *Astronomische Nachrichten*, **330**, 493. 0905.1807.
- Parenago, P. P.: 1954, *Catalogue of stars in the area of the Orion Nebula*. *Trudy Gosudarstvennogo Astronomicheskogo Instituta*, **25**, 1.
- Scargle, J. D.: 1982, *Studies in astronomical time series analysis. II - Statistical aspects of spectral analysis of unevenly spaced data*. *ApJ*, **263**, 835.

CORRELATIONS BETWEEN SPECTRAL PROPERTIES IN AGN TYPE 1: INFLUENCE OF STARBURSTS

JELENA KOVAČEVIĆ, LUKA Č. POPOVIĆ, MILAN S. DIMITRIJEVIĆ

*Astronomical Observatory Belgrade
Volgina 7, 11060 Belgrade, Serbia
E-mail: jkovacevic@aob.bg.ac.rs*

Abstract. The possible influence of starbursts to AGN (Active Galactic Nucleus) spectra is investigated in the case of a sample of AGNs Type 1. We divided the AGN sample into two subsamples according to dominant source of ionization. It is assumed that objects with $R = \log([\text{O III}]/\text{H}\beta \text{ NLR}) < 0.5$ have a predominant starburst contribution in narrow emission lines, and objects with $R = \log([\text{O III}]/\text{H}\beta \text{ NLR}) > 0.5$ are pure AGNs. We performed correlations between different spectral properties within these two subsamples and found some significant differences: the correlations between FWHM broad $\text{H}\beta$ vs. FWHM $[\text{O III}]$, and FWHM broad $\text{H}\beta$ vs. L_{5100} , as well as EW $\text{H}\beta$ broad vs. L_{5100} , are seen only for the starburst subsample. The possible influence of starbursts on the emission of the broad lines in AGN spectra is discussed.

1. INTRODUCTION

In some cases, the kinematical or physical characteristics of AGNs may be reflected in the correlations between different AGN spectral properties. Many authors investigated these correlations, trying to find and explain their physical background (see Popović and Kovačević 2011 and references therein).

On the other hand, there are some indications that evolution of AGNs is probably related with starburst regions (see Lípári and Terlevich 2006; Mao et al. 2009; Sani et al. 2010). Namely, it is possible that AGNs in an earlier phase of their evolution are composed of starburst (star-forming) regions and the central engine, that is AGN, and, during evolution, the starburst contribution becomes weaker and/or negligible (Wang and Wei 2006, 2008; Mao et al. 2009).

In this paper we analyse how the presence/absence of the starburst contribution to the AGN spectra influences to the correlations between different spectral properties.

2. THE SAMPLE AND ANALYSIS

For this investigation we use the sample of 302 AGNs Type 1, selected with criteria described in paper Kovačević et al. (2010).

The sample has approximately an uniform redshift distribution in the range of $z=0-0.7$ and negligible host galaxy contribution.

As it is described in Kovačević *et al.* (2010), the emission lines within the 4400 – 5500 Å range are fitted with multiple Gaussians, where each Gaussian represent contribution from different emission region. For spectra with $z<0.4$, we also fitted the $H\alpha$ and forbidden [N II] lines. The Balmer lines are fitted with three components: a narrow, an intermediate and a very broad component ($H\beta$ NLR, ILR and VBLR, respectively). We assume that all narrow lines originate from the same emission region, and consequently they have the same width and shift. The $H\beta$ broad component is taken as the sum of the $H\beta$ ILR and $H\beta$ VBLR components, and FWHM (Full Width Half Maximum) of $H\beta$ line is measured only for the $H\beta$ broad line. The iron lines within 4400 – 5500 Å range are fitted with template given in Kovačević *et al.* (2010).

In order to estimate in which objects there is a significant contribution of starbursts, we plot "BPT diagram" (Baldwin, Phillips and Terlevich 1981), which use the ratio of the narrow lines for diagnostic of starburst contribution. Since we have line measurements of the $H\alpha$ and [N II] lines only for objects with $z<0.4$, the BPT diagram is performed for the 137 objects from our sample, as shown in Fig 1. As it can be seen from Fig. 1, a number of AGNs from the sample show a significant starburst contribution in narrow lines. It is interesting that these AGNs are mostly with the FWHM $H\beta$ broad $< 3000 \text{ km s}^{-1}$ (open circles), while in the AGN part of the BPT diagram, both fractions (with FWHM $H\beta$ broad $< 3000 \text{ km s}^{-1}$ and FWHM $H\beta$ broad $> 3000 \text{ km s}^{-1}$), are present. the objects with the FWHM $H\beta$ broad $> 3000 \text{ km s}^{-1}$ are denoted with full circles.

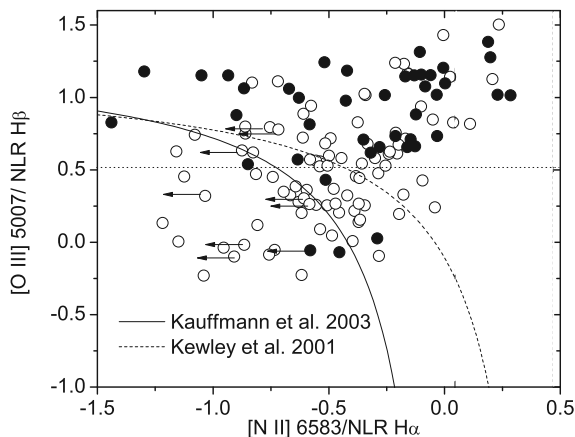


Figure 1: The BPT diagram for 137 objects from the sample. Open circles: objects with FWHM $H\beta$ broad $< 3000 \text{ km s}^{-1}$, full circles: with FWHM $H\beta$ broad $> 3000 \text{ km s}^{-1}$. Dashed line: $R=\log([\text{O III}]/H\beta \text{ NLR}) = 0.5$ (Popović and Kovačević, 2011).

The possible contribution of starbursts in AGN Type 1 spectra has been also reported (using the BPT diagnostic) in some other investigations: Popović *et al.* (2009) found that in the case of NLSy1 galaxy Mrk 493, the narrow-line ratios correspond to starbursts rather than to an AGN origin. Similar result is found in paper of Mao

et al. 2009 for the three AGN Type 1, which are mainly excited from starburst in narrow lines, since they belong to the H II part of BPT diagram.

Since we have complete measurements of line parameters only for the narrow H β and [O III] lines in the whole sample (302 AGNs), we accepted a criteria of $R = \log([\text{O III}]/\text{H}\beta \text{ NLR}) = 0.5$ (horizontal dashed line in Fig. 1) as an indicator of the predominant starburst emission contribution to the narrow emission lines. We divided our sample into two subsamples: $R < 0.5$ (91 AGNs, hereafter starburst dominant) and $R > 0.5$ (210 AGNs, hereafter AGN dominant). Then, we perform correlations between measured spectral properties for two subsamples, in order to check if there are some significant differences in correlation coefficients, which may be signature of different physical properties of emission regions.

3. RESULTS

Since our division of sample according to the dominant source of ionization (in narrow lines) into the AGN dominant and starburst dominant subsamples is very approximate (we use only the ratio of $R = \log([\text{O III}]/\text{H}\beta \text{ NLR})$, we need some additional tests, in order to check its accuracy. We perform correlation between FWHM [O III] and continuum luminosity (at 5100 Å) for which one may expect to be significant for the subsample with starburst contribution (Brungardt 1988). Indeed, as it can be seen in Fig 2., there is a significant correlation between these parameters for the starburst dominant subsample, but no correlation is seen for the AGN dominant one.

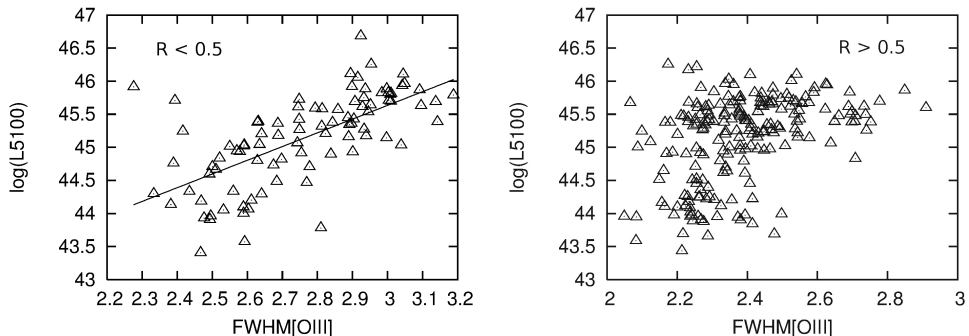


Figure 2: The correlation between FWHM [O III] and continuum luminosity (at 5100 Å) is significant for starburst dominant ($R < 0.5$) subsample, while for AGN dominant ($R > 0.5$), no correlation is seen (Popović and Kovačević, 2011).

We performed correlations between spectral properties (continuum luminosity, broad and narrow line widths, equivalent widths of lines) for two subsamples and found significant differences in some correlations. We found that the width of the broad H β is in a significant correlation with the FWHM of narrow [O III] lines and with the continuum luminosity (L_{5100}) for the starburst dominant subsample, while there are no any correlations between these parameters for the AGN dominant subsample. Correlations are shown in Fig 3 and 4. Also, we found correlation between the EW (equivalent width) of H β broad and L_{5100} for the starburst dominant subsam-

ple ($r=0.56$, $P=9E-9$), while there is no correlation for the AGN dominant subsample ($r=-0.03$, $P=0.67$). This correlation is very interesting since anticorrelations between EWs of the emission lines and continuum luminosity are commonly called the Baldwin effect (see Baldwin 1977), and their physical cause is still unclear, because they can not be explained by simple photoionization model. Additionally, in this case there is opposite trend, e.i. EW of the broad $H\beta$ increases, as continuum luminosity increases (Inverse Baldwin effect).

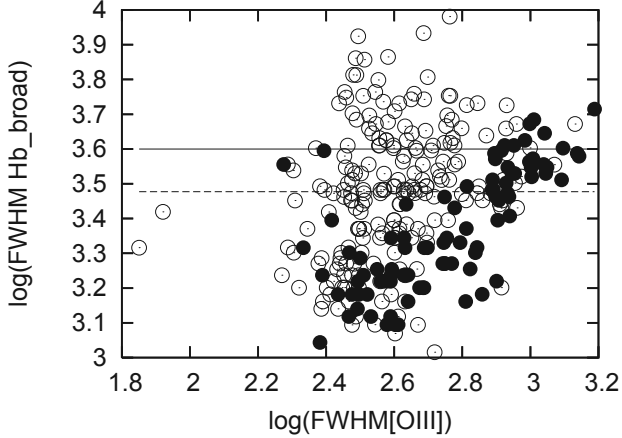


Figure 3: FWHMs of the broad $H\beta$ vs. the narrow $[O III]$ lines (which corresponds to the narrow $H\beta$). Filled circles denote the sample with $R < 0.5$, and open circles, sample with $R > 0.5$. The solid line denotes a border of $FWHM H\beta = 4000$ km/s, while the dashed line denotes $FWHM H\beta = 3000$ km/s (Popović and Kovačević, 2011).

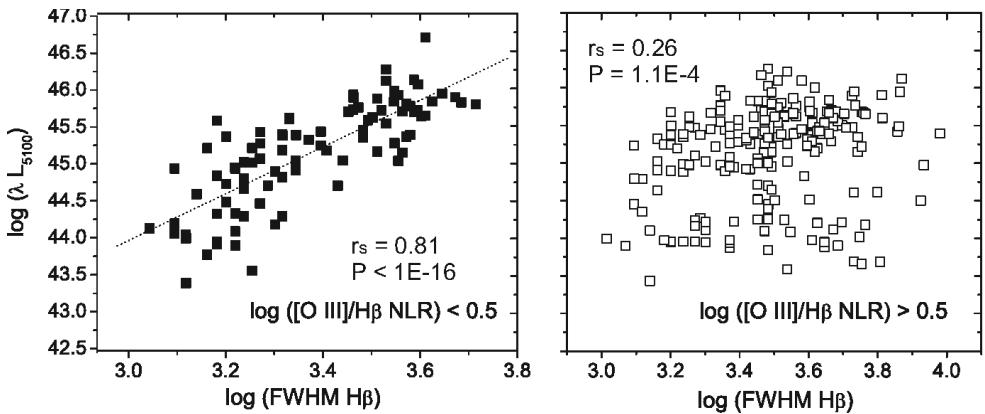


Figure 4: Correlations between continuum luminosity and $FWHM H\beta$ for starburst dominant (left) and AGN dominant subsample (right).

Since we found significant correlations of some spectral parameters and the broad component (ILR+VBLR) of $H\beta$ only for starburst dominant subsample, one may ask interesting question: is it possible that starbursts may have contribution, not only in emission of narrow lines, but also partly in the emission of the broad lines in AGN spectra? In that case, part of the flux of the broad Balmer emission lines may arise in the stellar envelopes of Wolf-Rayet and OB stars associated with multiple SN events (see Izotov et al. 2007, and references therein) and emission gas could be randomly accelerated in several bursts.

References

- Baldwin, J. A.: 1977, *Astrophysical Journal*, **214**, 679.
- Baldwin, J. A., Phillips, M. M., Terlevich, R.: 1981, *Astronomical Society of the Pacific, Publications*, **93**, 5.
- Brungardt, C. L.: 1988, *Astrophysical Journal Letters*, **327**, 51.
- Izotov, Y. I., Thuan, T. X., Guseva, N.G.: 2007, *Astrophysical Journal*, **671**, 1297.
- Kovačević, J., Popović, L. Č., Dimitrijević, M. S.: 2010, *Astrophysical Journal Supplement*, **189**, 15.
- Lípari, S. L., Terlevich, R. J.: 2006, *Monthly Notices of the Royal Astronomical Society*, **368**, 1001.
- Mao, Y-F. Wang, J., Wei, J.-Y.: 2009, *Astronomy and Astrophysics*, **9**, 529.
- Popović, L. Č., Smirnova, A., Kovačević, J., Moiseev, A., Afanasiev, V.: 2009, *Astronomical Journal*, **137**, 3548.
- Popović, L. Č., Kovačević, J.: 2011, *Astrophysical Journal*, **738**, 68.
- Sani, E., Lutz, D., Risaliti, G., Netzer, H., Gallo, L. C., Trakhtenbrot, B., Sturm, E., Boller, T.: 2010, *Monthly Notices of the Royal Astronomical Society*, **403**, 1246.
- Wang, J., Wei, J.: 2006, *Astrophysical Journal*, **648**, 158.
- Wang, J., Wei, J.: 2008, *Astrophysical Journal*, **679**, 86.

LINUX ASTRONOMICAL SOFTWARE

GEORGI T. PETROV

*Institute of astronomy and NAO, Bularian Academy of Sciences,
72 Tsarigradsko Shossee*

Abstract. The most popular astronomical software for scientists and non professional astronomers based on LINUX operational system is reviewed. The software packages are grouped in 10 directions - *Data Analysis Packages, GRID software, Modeling and Simulations, Organizers, Planetariums software, Radio & Interferometry software, Spectrum Analysis, Visualization, VO software and X ray analysis software.* Included are data reduction packages as IRAF, MIDAS and SExtractor, simulation and modeling software – e.g. GADGET, GALFIT and SYNSPEC, organisers – e.g. FITS_viewres, SKYCAL and WCS_tools, planetarium software – e.g. CELESTIA, KSTARS and XEPHEM, analysis of radio and interferometric data as AIPS, MIRIAD and SPEX_tool, spectral analysis software – e.g. SPECTRUM and SPECVIEW, visualisation software – e.g. ALADIN, DS9, QFITSview and ESO's SKYCAT and VIRGO, and analysis of X_ray data – e.g. CIAO, SAS and XSPEC. Specialised GRID and VIRTUAL OBSERVATORY software are briefly presented here. More than 100 LINUX software products are presented.

1. INTRODUCTION

The fast developing of the astronomical science, the new telescopes and equipments and tremendous quantity of astronomical data enforce the astronomers very often to know and use a lot of different, sometimes quite specialized or sophisticated astronomical software. Sometimes it is not so easy to decide which package will give you the best solution for the task you are interested in. There is a lot of free specialized astronomical software, as well as some commercial packages (e.g. IDL). Here we presented ca. 110 free astronomical software packages for LINUX – the free operational system. Distributed in 10 groups - Data Analysis Packages, GRID software, Modeling and Simulations, Organizers, Planetariums software, Radio & Interferometry software, Spectrum Analysis, Visualization, VO software and X ray analysis software, all the packages are reviewed and presented in alphabetical order in each group. Sometimes platform independent packages - Java application are presented. In some cases detailed

instruction for software installation and user guides could be found in the official WEB pages of the authors or distributors (see references here).

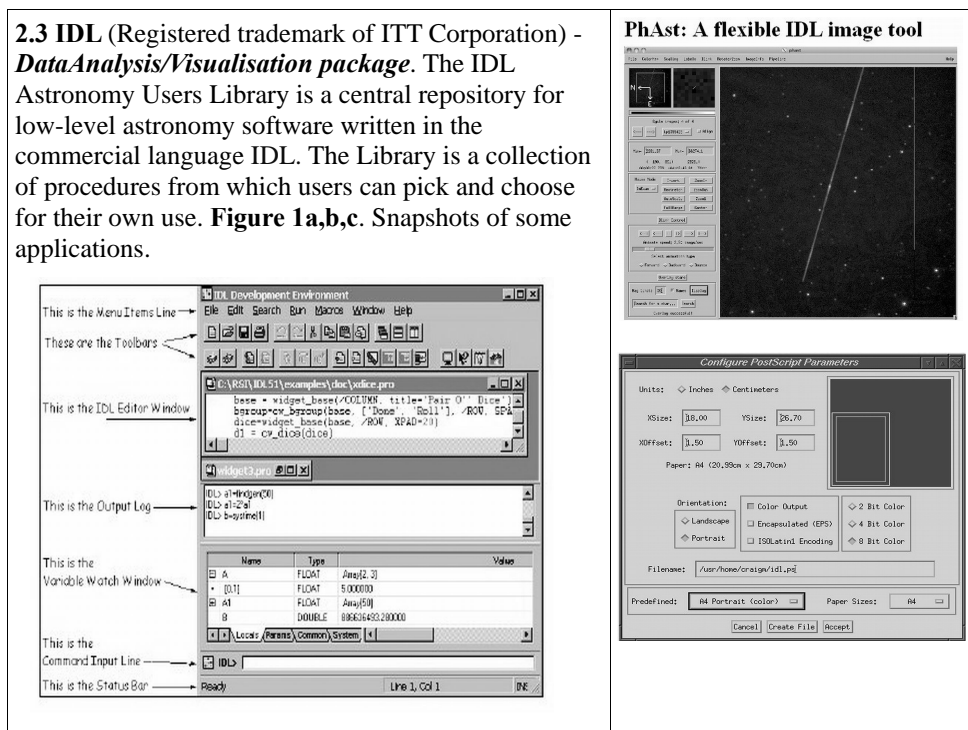
GRID and VO software are briefly mentioned here, as the full description of these special packages are presented in Petrov et al. (2012) in this volume. In the Sections 2 to 11 all the reviewed packages are presented. All the figures are snapshots from the WEB_pages or real execution of the software packages.

2. DATA ANALYSIS PACKAGE

2.1 CCDPROC (<http://www.astronomy.ohio-state.edu/~pogge/Software/>) - *performs basic reductions on raw CCD images* (overscan bias subtraction, trim, zero and/or dark subtraction, and flat fielding), creating a reduced image ready for subsequent analysis. A process control (proc) file contains the instructions for performing the reduction. **Ccdproc** is designed to be used *for fast pipeline reductions of CCD images*, but requires that the necessary zero (2D Bias) and normalized flat-field images be already prepared using standard image reduction packages like IRAF, VISTA, IDL, etc. Author R. Pogge.

2.2 FIGARO (<http://www.aao.gov.au/figaro/>) - a data reduction system that originated at Caltech at the Anglo-Australian Observatory. Although it is intended to be able to deal with any sort of data, almost all its applications to date are geared towards *processing optical and infra-red data...* (by Keith Shortridge).

2.3 IDL (Registered trademark of ITT Corporation) - *Data Analysis/Visualisation package*. The IDL Astronomy Users Library is a central repository for low-level astronomy software written in the commercial language IDL. The Library is a collection of procedures from which users can pick and choose for their own use. **Figure 1a,b,c.** Snapshots of some applications.



2.4 IRAF

(<http://iraf.noao.edu/iraf-ftp.html>) - an **Image Reduction and Analysis Facility**, a general purpose software system for the reduction and analysis of astronomical data. **Figure 2.** Snapshot of IRAF home page.



2.5 ISIS (<http://asterisk.apod.com>) - ISIS is a **complete package to process CCD images using the image Optimal subtraction method** (Alard & Lupton 1998, Alard 1999). ISIS includes a number of facilities to **compute the light curves of variables objects from the subtracted images**. **Figure 3.** Snapshot of ISIS logo.



2.6 MIDAS

(<http://www.eso.org/sci/software/esomidas/>) - the acronym for the **Munich Image Data Analysis System** which is developed and maintained by the European Southern Observatory. The official name, **ESO-MIDAS**, is a **registered trademark**. The ESO-MIDAS system provides **general tools for image processing and data reduction** with emphasis on astronomical applications including imaging and special reduction packages for ESO instrumentation at La Silla. In addition **it contains applications packages for stellar and surface photometry, image sharpening and decomposition, statistics and various others** (Grosbol & Ponz 1990).

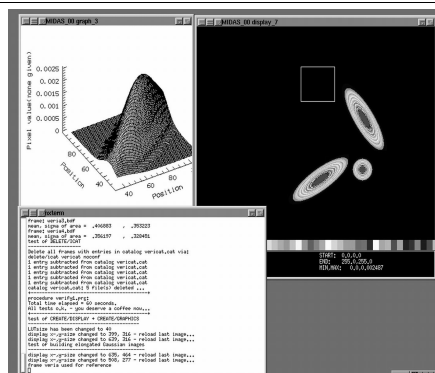
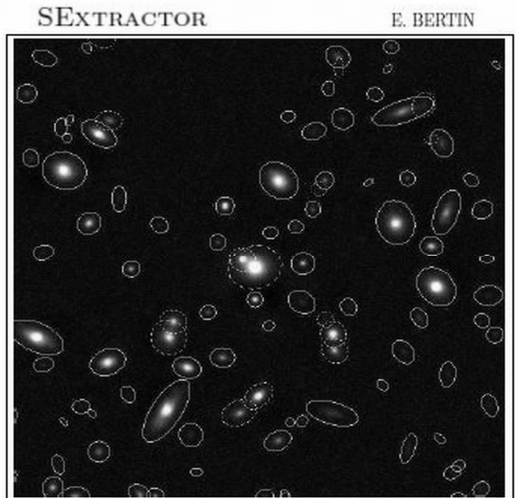


Figure 4. Snapshot of MIDAS work area.

2.7 SEXTRACTOR

(<http://www.astromatic.net/software/sextractor>) - a program that **builds a catalog of objects from an astronomical image**. Although it is particularly oriented towards reduction of large scale galaxy-survey data, it can perform reasonably well on moderately crowded star fields. A "teaching" program for object selection is **EYE** (Bertin & Arnouts 1996).
Rem.: In the site
<http://www.astromatic.net/software/>
one could find and other programs from E.Bertin...

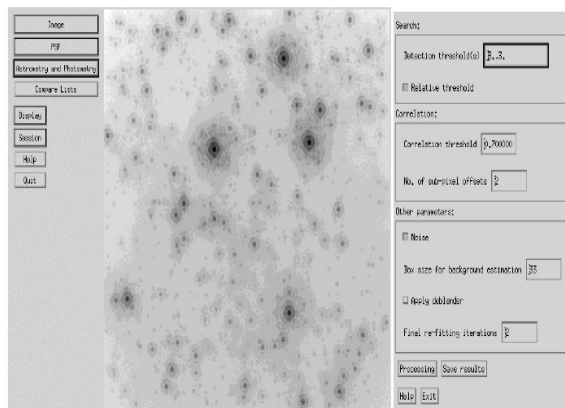
Figure 5. Snapshot of SExtractor logo.



2.8 STARFINDER.IDL

(<http://asterisk.apod.com/>) - an **code for the deep analysis of stellar fields**, designed for Adaptive Optics well-sampled images. The **Point Spread Function is extracted directly from the frame**, to take into account the actual structure of the instrumental response and the atmospheric effects. The code is written in IDL language and organized in the form of a self-contained widget-based application, provided with a series of tools for data visualization and analysis (Diolaiti et al. 2000).

Figure 6. Snapshot of STARFINDER application.



2.9 STARLINK (<http://starlink.jach.hawaii.edu/starlink>) - A full set of data reduction and analysis tools. The Starlink Project was a long running UK Project supporting astronomical data processing. It was shut down in 2005 but the software continues to be developed at the Joint Astronomy Centre and is open source (Disney et al. 1982). See a Starlink – brochure (1996) too.

2.10 STSDAS (http://www.stsci.edu/institute/software_hardware/stsdas) - The Space Telescope Science Data Analysis System (**STSDAS**) is a software package for reducing and analyzing astronomical data. It is layered on top of IRAF and provides general-purpose tools for astronomical data analysis as well as routines specifically designed for HST data. The TABLES package sits alongside STSDAS and provides tools and libraries for working with tabular data. STSDAS requires TABLES, but one may use TABLES without STSDAS.

2.11 VISTA - There are two different versions, distributed as *xvista*:

- Xvista version 7.xx (<http://ganymede.nmsu.edu/holtz/xvista/>) maintained and distributed by *Jon Holtzman* at the New Mexico State University, is an image processing program designed to be used primarily with astronomical data. It contains routines *for reading, displaying, basic image processing, and specialized tasks for the analysis of astronomical imaging and spectroscopic data*.
- *Richmond & Treffers's XVista*, (ver. 0.1.9/2010) is a suite of programs *for analyzing and displaying astronomical images* on computers running Unix-like operating systems and X Windows (Richmond et al. 1993, 1995).

3. GRID SOFTWARE

3.1 AMEEPAR (<http://www.jpl.nasa.gov/>) - parallel processing for hyperspectral imaging (Plaza et al., 2006).

3.2 CACTUS (<http://www.cactuscode.org>) - toolkit to numerically simulate extremely massive bodies, such as neutron stars and black holes.

3.3 GADGET-2 (<http://www.mpa-garching.mpg.de/gadget/>) – a freely available code for cosmological N-body/SPH simulations

3.4 COSMIC SIMULATION

(<http://www.mpa-garching.mpg.de/galform/millennium/>) - A virtual universe – GIMIC and Millennium simulations

3.5 CLUSTERFINDER

(<http://www.gac-grid.de/project-products/Applications/ClusterFinder.html>)

3.6 CRBLASTER (<http://www.noao.edu/staff/mighell/crblaster>) - a fast parallel-processing program for cosmic ray rejection (Mighell 2010)

3.7 Einstein@home (<http://boinc.berkeley.edu/wiki/Einstein@Home>)

3.8 Milkyway@home (<http://milkyway.cs.rpi.edu/milkyway/>)

3.9 Nbody6++ (<http://www.ast.cam.ac.uk/~sverre/web/pages/nbody.htm>) - direct N-body integrator used for simulations of dense star clusters, galactic nuclei, and problems of star formation (Aarseth 2001).

3.10 N_body-sh1p (http://modesta.science.uva.nl/Software/src/nbody_sh1p.tar.gz) - a parallel direct N_body code - *an educational N-body integrator* (Konecny & Fürst 2007). (see 4.9 too...).

3.11 SETI@home (<http://setiathome.berkeley.edu/>) - SETI (Search for Extraterrestrial Intelligence) - to detect intelligent life.

3.12 SKYMAKER (<http://www.astromatic.net/software/skymaker>) - a program that simulates astronomical images (Bertin 2009).

3.13 SYNTSPEC (<http://www.balticgrid.org/>) - The Synthetic spectra modeling under GRIDCOM interface (Mikolaitis & Tautvaiseine 2009).

3.14 VIRGO (<http://virgo.org.ua/>)

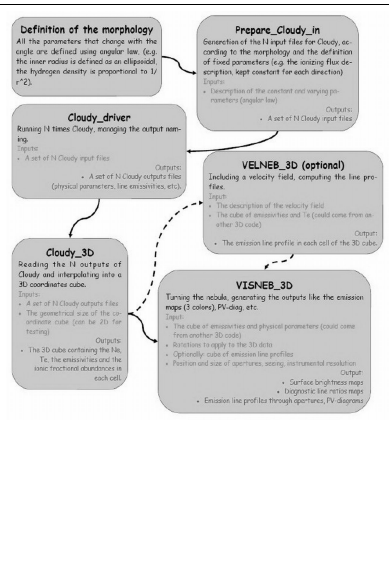
4. MODELLING & SIMULATIONS

4.1 CHANGA – (<http://www-hpcc.astro.washington.edu/tools/changa.html>) - (**Charm N-body GrAvity solver**) is a code to perform collisionless N-body simulations. It can perform cosmological simulations with periodic boundary conditions in comoving coordinates or simulations of isolated stellar systems. It also can include hydrodynamics using the Smooth Particle Hydrodynamics (SPH) technique. It uses a Barnes-Hut tree to calculate gravity, with hexadecapole expansion of nodes and Ewald summation for periodic forces. Timestepping is done with a leapfrog integrator with individual timesteps for each particle.

4.2 CHIANTI (<http://www.chiantidatabase.org/chianti.html>) - An Atomic Database for Spectroscopic Diagnostics of Astrophysical Plasmas.

4.3 CLOUDY.IDL (<http://www.nublado.org/>; <http://sites.google.com/site/cloudy3d/> - author Christophe Morisset, 2010) - designed to *simulate emission line regions ranging from the intergalactic medium to the Broad Line Regions of Quasars*. ... Dilute gas is heated and ionized by the radiation field of a central object. Under these circumstances *it is possible to predict the physical conditions* (e.g. the run of ionization, density, and temperature) *of the gas, and its resulting emission-line spectrum*, in a unique and self-consistent manner. For this the equations of statistical and thermal equilibrium, equations which balance ionization-neutralization processes, and heating-cooling processes are used.

Figure 7. Snapshot of CLOUDY flowchart.



4.4 COSMICS (<http://asterisk.apod.com/>) - a package of FORTRAN programs useful for *computing transfer functions and microwave background anisotropy for cosmological models*, and for generating Gaussian random initial conditions for nonlinear structure formation simulations of such models. Four programs are provided: (1) `linger_con` and `linger_syn` integrate the linearized equations of general relativity; (2) `matter`, and radiation in conformal Newtonian and synchronous gauge, respectively; (3) `deltat` integrates the photon transfer functions computed by the `linger` codes to produce photon anisotropy power spectra; (4) `graphic` tabulates normalized matter power spectra and produces constrained or unconstrained samples of the matter density field (Ma & Bertschinger 1995).

4.5 FASTELL (<http://asterisk.apod.com/>) - a code *to calculate quickly and accurately the lensing deflection and magnification matrix* for the softened power-law elliptical mass distribution (SPEMD) lens galaxy model. The **SPEMD consists of** a softened power-law radial distribution with elliptical isodensity contours. Because of their simplicity, axisymmetric mass distributions are often used to model gravitational lenses. Since galaxies are usually observed to have elliptical light distributions, mass distributions with elliptical density contours offer more general and realistic lens models (Barkana 1998).

4.6 GADGET (<http://www.mpa-garching.mpg.de/gadget/>) - a freely available code for *cosmological N-body/SPH simulations* on massively parallel computers with distributed memory. The code can be run on essentially all supercomputer systems presently in use, including clusters of workstations or individual PCs. ***GADGET computes gravitational forces with a hierarchical tree. It follows the evolution of a self-gravitating collisionless N-body system, and allows gas dynamics to be optionally included.*** Author - Prof. Dr. Volker Springel and later on Naoki Yoshida.

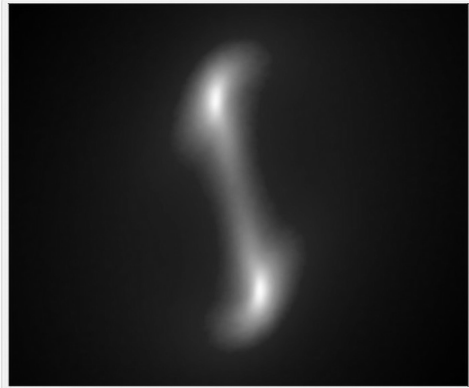


Figure 8. Snapshot from GADGET-2 working area.

4.7 GALACTICUS (<http://sites.google.com/site/galacticusmodel/downloads>) – a project, led by Andrew Benson, aims to ***build a comprehensive model of galaxy formation.*** Galacticus is ***designed to solve the physics involved in the formation of galaxies within the current standard cosmological framework.*** It is of a type of model known as "semi-analytic" in which the numerous complex non-linear physics involved are solved using a combination of analytic approximations and empirical calibrations from more detailed, numerical solutions. Models of this type aim to begin with the initial state of the Universe (specified shortly after the Big Bang) and apply physical principles to determine the properties of galaxies in the Universe at later times, including the present day. ***Typical properties computed include the mass of stars and gas in each galaxy, broad structural properties (e.g. radii, rotation speeds, geometrical shape etc.), dark matter and black hole contents, and observable quantities such as luminosities, chemical composition, etc.***

4.8 GALFIT (<http://users.obs.carnegiescience.edu/peng/work/galfit/galfit.html>) - ***A two-dimensional (2-D) fitting algorithm designed to extract structural components from galaxy images, with emphasis on closely modelling light profiles of spatially well-resolved, nearby galaxies observed with the Hubble Space Telescope.*** 2-D models such as the "Nuker" law, the Sersic (de Vaucouleurs) profile, an exponential disk, and Gaussian or Moffat functions are used. The azimuthal shapes are generalized ellipses that can fit disk and boxy

components. Many galaxies with complex isophotes, ellipticity changes, and position-angle twists can be modeled accurately in 2-D. *This is illustrated by way of seven case studies*, which include regular and barred spiral galaxies, highly disky lenticular galaxies, and elliptical galaxies displaying various levels of complexities. Author C. Y. Peng.

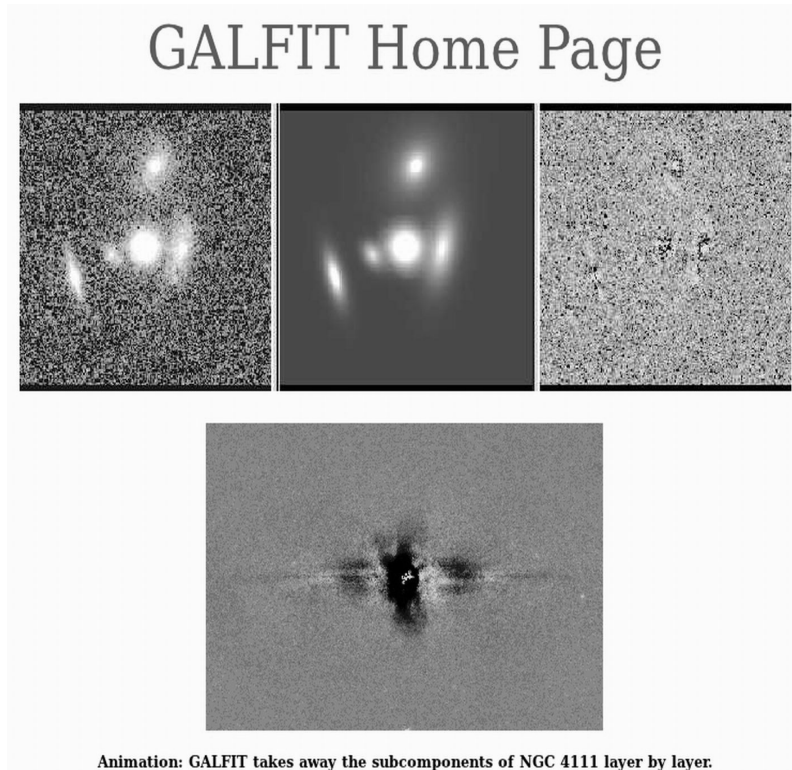
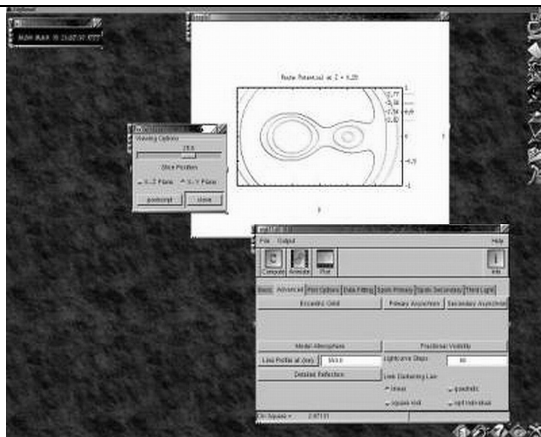


Figure 9. Snapshot from GALFIT working area.

4.9 N-BODY simulations ([http://www.scholarpedia.org/article/N-body_simulations_\(gravitational\)](http://www.scholarpedia.org/article/N-body_simulations_(gravitational))) - `nbody_sh1p` - *a parallel direct N-body code. Educational N-body integrator* with a shared but variable time step (the same for all particles but changing in time), using the Hermite integration scheme (Konecny & Fürst 2007). Typical command line (generates `n24body.out`): `*** nbody_sh1p < n24body.in > n24body.out`

4.10 NIGHTFALL

(<http://www.la-samhna.de/nightfall/nightfall-1.70.tar.gz>) - ... “astronomy application for fun, education, and science. It can produce animated views of eclipsing binary stars, calculate synthetic light curves and radial velocity curves, and eventually determine the best-fit model for a given set of observational data of an eclipsing binary star system. Nightfall comes with a user guide, and a set of observational data for several eclipsing binary star systems”. (Mahy et al. 2011). **Figure 10.** Snapshot from NIGHTFALL working area.



4.11 PANDORA (<https://www.cfa.harvard.edu/~avrett/pandora.html>) - Pandora is a *general-purpose non-LTE computer program for calculating stellar atmosphere models and detailed line and continuum spectra*. Recent applications include extensive modeling of the outer atmosphere of the Sun and other late-type stars, including effects of mass flows; the atmospheric response to external ionizing radiation; and the effects of ion diffusion (Averet & Loeser 2003).

4.12 SYNSPEC (<http://nova.astro.umd.edu/Synspec43/>) - is a *general spectrum synthesis program*. It assumes an existing model atmosphere, calculated previously with *TLUSTY* or taken from the literature, for instance from the Kurucz grid of models. The opacity sources (continua, atomic and molecular lines) are fully specified by the user. An arbitrary stellar rotation and instrumental profile can be applied to the synthetic spectrum. *Synplot* is a user-friendly IDL wrapper around Synspec. Synplot is keyword-driven and incorporates all the necessary plotting resources for spectral analysis (see 3.12 TLUSTY). Authors – Ivan Hubeny & Thiery Lanz.

4.13 TIPSYP (<ftp://ftp-hpcc.astro.washington.edu/pub/hpcc/tipsy-XX.tar.gz/>; <http://astro.washington.edu/index.html>) - the Theoretical Image Processing System. *Display and analyze the results of N-body simulations*. *TIPSYP* is a special package built to could *easily perform the following functions*: Display particle positions (as points), and velocities (as line segments) from an arbitrary

viewpoint; Zoom in to a chosen position. Due to their extremely clustered nature, structure of interest in an N-body simulation is often so small that it can not be seen when looking at the simulation as a whole; Color particles to display scalar fields. Examples of such fields are potential energy, or for SPH particles, density and temperature; Selection of a subset of the particles for display and analysis; Following selected particles from one timestep to another; Finding cumulative properties of a collection of particles. This usually involves just a sum over the particles. ***The basic data structure is an array of particle structures.*** Since TIPSY was built for use with cosmological N-body simulations, there are actually ***three separate arrays for each of the types of particle used in such simulations: collisionless particles, SPH particles, and star particles.***

4.14 TLUSTY (<http://nova.astro.umd.edu/>) - The present set of computer programs is ***a package designed to accomplish a wide range of spectroscopic diagnostics.*** In its maximum configuration, the user may start from scratch and calculate a model atmosphere of a chosen degree of complexity, and end with a synthetic spectrum in a wavelength region of interest for an arbitrary stellar rotation and an arbitrary instrumental profile. The user may also model the vertical structure of annuli of an accretion disk. Authors – Ivan Hubeny & Thierry Lanz.

5. ORGANIZERS

5.1 APT - The **Astronomer's Proposal Tool** (<http://www.stsci.edu/hst/>). Write, validate and submit proposals for the Hubble Space Telescope.

5.2 CONSKY (<http://asterisk.apod.com>) - This program addresses the question of ***what resources are needed to produce a continuous data record of the entire sky down to a given limiting visual magnitude.*** The program simulates a small camera/telescope or group of small camera/telescopes collecting light from a large portion of the sky. From a given stellar density derived from a Bahcall - Soneira Galaxy model, the program first converts star densities at visual magnitudes between 5 and 20 to number of sky pixels needed to monitor each star simultaneously. From pixels, ***the program converts input CCD parameters to needed telescope attributes, needed data storage space, and the length of time needed to accumulate data of photometric quality for stars of each limiting visual magnitude over the whole sky.*** The program steps though photometric integrations one second at a time and includes the contribution from a bright background, read noise, dark current, and atmospheric absorption (Nemiroff, Robert J.; Rafert, J. Bruce: 1999, PASP, Volume 111, Issue 761, pp. 886-897.).

5.3 FITS viewers. **Figure 11.** Snapshot of FITS viewers and converters page.



FITS Image Viewers and Format Converters

FITS Image Viewers

- [SAOImage ds9](#) - astronomical visualization application from SAO
- [fv](#) - FITS file viewer and editor (supports FITS images and FITS tables)
- [FITSview](#) - FITS image viewer from NRAO
- [SkyCat](#) - ESO tool combines image visualization and access to catalogs
- [GAIA](#) - an image display and analysis tool from the U.K. Starlink Project. It is a derivative of the ESO SkyCat tool
- [Aladin](#) - Interactive Sky Atlas
- [APLpy](#) - Astronomical Plotting Library in Python is a Python module aimed at producing publication-quality plots of astronomical imaging data in FITS format.
- [qiv](#) - A cross platform (posix and Windows) image viewer designed especially for scientific vision and computational geometry. Supports interactive brightness and contrast adjustment of 2D images and 3D cubes in various data formats, including FITS. Also supports drawing vector graphics on top of the image.
- [PhAst](#) - A flexible IDL tool to display and analyze FITS images. It can calibrate raw images, provide astrometric solutions, and do circular aperture photometry. PhAst allows the user to load, process, and blink any number of images. Requires either an IDL license, or installation of the (free) IDL Virtual Machine.
- [QFitsView](#) - An image viewer for 1-D, 2-D, and 3-D FITS images. It is written in C++ and uses the Qt widget library. Binary executables for Microsoft Windows, Linux, and Mac OSX, as well as the source code, are available.
- [Libtiffs](#) - a fully demand-driven, threaded image processing library with no image size limits and with good support for colour. Reads and writes FITS images, as well as TIFF, JPEG, PPM, PNG, and other file formats. Has interfaces to C, C++ and Python, and a command-line interface that can be called from shell scripts.

Image Format Converters - FITS to/from GIF, JPEG, etc

- [Netpbm](#) - a package of graphics programs and programming library. The [documentation](#) is on-line. In particular, see the [fitstopnm](#) and [pnmtofits](#) programs. To first order, the following command converts a jpeg image to a FITS image on most Linux systems:


```

      djpeg file.jpg | pnmtofits > file.fits
      
```

 where "djpeg" is available in the libjpeg RPM package.
- [ImageMagick](#) - read, write, and manipulate images in over 88 formats
- [pbmplus](#) - image file format conversion package
- [gimp](#) - GNU Image Manipulation Package
- [FITS2jpeg](#) - a FITS to jpeg converter provided by Bill Cotton (NRAO). It needs the CFITSIO and libjpeg libraries and produces grayscale images.
- [SAOImage ds9](#) - this FITS visualization application from SAO allows the image to be saved as a jpeg, tiff, png, or ppm file on disk (use File->Save)
- [MicroObservatory Image 2.0](#) - Image display and processing program can perform FITS to GIF conversion and create RGB color images or animated GIF files.
- [fts2gif](#) - a simple FITS to gif converter written by Michal Szymanski (Warsaw University Observatory). It requires the "raw2gif" application from the cflib-3.0 library (Linux and Solaris versions of raw2gif are included in the fts2gif tar file).

5.3.1 STIFF

(<http://www.astromatic.net/2010/02/10/stiff-2-1-release>) is a program that *converts scientific FITS images to the more popular TIFF format* for illustration purposes. Last version – 2.1 was included in ALADIN. Author E. Bertin.

Figure 12. Comparison of two types of color image creators.



The same 3 R,G and B deep-sky images processed by FITS LIBERATOR (left) and STIFF (right), using the same intensity cuts.

5.4 GASGANO (<http://www.eso.org/sci/software/gasgano/>) - a data file organizer by ESO “to manage and organize in a systematic way the astronomical data observed and produced by all VLT compliant telescopes”.

5.5 HERA (<http://heasarc.nasa.gov/hera/>) - The Hera data processing facility provides *many general utility programs for manipulating FITS format images and tables*. These general tools are organized into *several different FTOOLS packages*:

- ✧ **HEATTOOLS** - tasks for listing, editing and calculating statistics about any FITS file, image processing calculators, and general table manipulation tools (sorting, appending, selecting rows, etc.)
- ✧ **FIMAGE** - utilities for general image processing and manipulation.
- ✧ **FUTILS** - a large set of general FITS utility program mainly for manipulating FITS headers or tables; some of these are older versions of tools in the HEATTOOLS package.

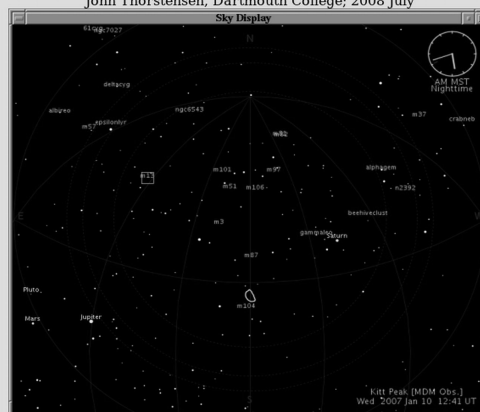
Hera also provides hundreds of more specialized programs, mainly for professional researchers, to analyze data from high-energy astrophysics missions such as ROSAT, Chandra, XMM-Newton, Swift, and Suzaku. Currently, these tools include all the hundreds of programs in the HEASARC FTOOLS and the Chandra CIAO data analysis packages, as well as several of the most frequently used programs in the XMM-Newton SAS package.

5.6 SKYCAL

(<http://www.dartmouth.edu/~physics/faculty/skycalc/JSkyCalc.jnlp>)
and

http://www.briancasey.org/artifacts/astro/skycalendar_notes.html) – *in fact a two different programs: **Skycalc** is an interactive tool which conveniently handles the time-and-the-sky calculations commonly encountered in optical astronomy. It has many features useful for planning observations at the telescope. Ver.6 and newer have a GUI interface too. The picture shows JAVA version of the SkyCalc. Skycalendar prints a table of sunrise, sunset, moonrise, moonset, and so on, organized on a nightly (double-dated) basis for any site. Author - John Thorstensen with a Web interface by Brian Casey. **Figure 13.** Snapshot of Java applet of SkyCalc.*

JSkyCalc -- A Convenient, Portable Observing Aid
 John Thorstensen, Dartmouth College, 2008 July



5.7 WCSTOOLS

(<http://tdc-www.harvard.edu/software/wcstools/wcstools.wcs.html>) - a package of programs and a library of utility subroutines for *setting and using the world coordinate systems (WCS) in the headers of the most common astronomical image formats, FITS and IRAF .imh, to relate image pixels to sky coordinates.* This software is all written in very portable C, so it should compile and run on any computer with a C compiler. The current (2011) version is 3.8.1

LINUX ASTRONOMICAL SOFTWARE

The current version is 3.8.4

	<ul style="list-style-type: none"> Handles all FITS image data types: 8-bit unsigned integer, 16- and 32-bit signed integer, 32- and 64-bit IEEE floating point, plus non-standard 16-bit unsigned integer (BITPIX=16). Accesses IRAF link (versions 1 and 2) files as well as FITS files Uses any of several reference catalog formats from CDROMs or identically-structured online files, Uses the standard SAO/NRAO world coordinate system library or Mark Calabretta's WCSLIB library, which defines the proposed FITS WCS standard. Is Y2K-compliant Implements images with more than one WCS Uses same WCS subroutines as SAOImage, SAOImage_4a9, and skymap image browsing programs. Can be installed as an IRAF package
	<ul style="list-style-type: none"> Image WCS (imwcs) (imwcs) (imwcs) (SACImage) [Getting Good Coordinates] Catalogs and Image WCS (imcat) (imcat) [Environment Variables] Image Header Utilities (delhead) (delhead) (gethead) (mhead) (mhead) (keyhead) (keyhead) Image Utilities (getfile) (getfile) (getfile) (getfile) (getfile) (getfile) Catalog Utilities (imcat) (imcat) (imcat)
	<ul style="list-style-type: none"> USNO-B1.0 Catalog HST-GSC II HST-GSC and GSC-ACT Catalogs USNO-A2.0, SA2.0, and UCAC2 Catalogs 2MASS Point-Source Catalog Copenhagen/USNO Tycho-2 Catalog Local catalogs in Starbase, ASCII, or SAO TDC binary format Environment variables for catalog paths
	<ul style="list-style-type: none"> World Coordinate System Subroutines Source Catalog Access Subroutines Image I/O and Access Subroutines Processing Subroutines
	<ul style="list-style-type: none"> Anonymous FTP from http://cfp.jp.harvard.edu/pub/irc/WCSTools/ (A legitimate domain name is needed as the password; if you have problems retrieve the package via http:) HTTP from http://tdc-www.harvard.edu/software/wcstools/wcstools-3.8.4.tar.gz You can retrieve a subset of the WCSTools subroutines which are needed for WCS conversion from http://tdc-www.harvard.edu/software/wcstools/wcstools-3.8.4.tar.gz If you are on a CP-managed system at the CJA, add <code>data/irc/wcs/bin/realnet</code> for Redhat Linux machines to your search path. Pete Ratuski has put together a Perl interface to the WCSTools libraries called Astro-WCS-lib-WCS-0.20
	<ul style="list-style-type: none"> WCS subroutines: D.Mink (1995), ADASS V (full text) Entire package: D.Mink (2001), ADASS XI, D.Mink (1996), ADASS VI (full text), D.Mink (1998), AAST/DA meeting, D.Mink (1998), ADASS VIII (full text)
	Some subroutines in the library have been adapted and amplified from software originally written by Elwood Downey of the University of Iowa Automated Telescope Facility; Bill Cotton of the U.S. NRAO; Mark Calabretta of the Australian SSB; and Pat Wallace of the UK Starlink Project. Others are translated from the Fortran code I wrote to support the <code>star</code> and <code>skymap</code> programs.
	This software was originally inspired by the impending standardization of WCS keywords in FITS as discussed at the 1994 ADASS Conference. The subroutines to translate between sky and image coordinates came first, then the utilities to use them, and then the programs to search catalogs and fit a world coordinate systems to images.

Last updated 30 December 2011 by [Jessica Mink \[email\]](#)

Figure 14. Snapshot of WCSTOOL applications.

6. PLANETARIUMS SOFTWARE

6.1 CELESTIA (<http://www.shatters.net/celestia/index.html>) is a free *real-time space simulation* that lets you visually experience our universe in three dimensions.

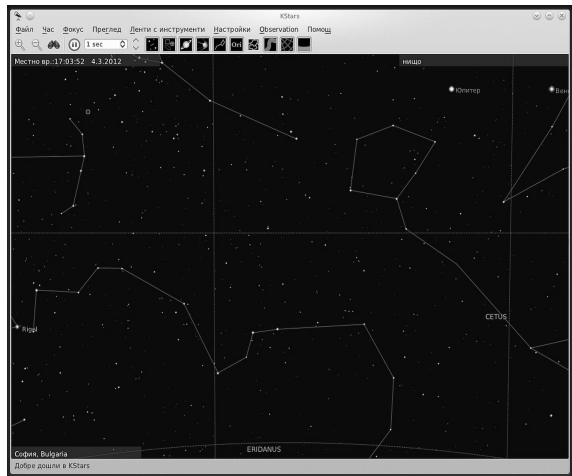


Figure 15. Snapshot of CELESTIA planetarium software.

6.2 KSTARS

(<http://edu.kde.org/applications/all/kstars/>) - *a Desktop Planetarium for KDE*. It provides an accurate graphical simulation of the night sky, from any location on Earth, at any date and time. *The display includes up to 100 million stars, 13,000 deep-sky objects, all 8 planets, the Sun and Moon, and thousands of comets and asteroids.*

Figure 16. Snapshot of KSTARS planetarium software.



6.3 OPEN UNIVERSE (<http://openuniverse.org/>)

Open Universe



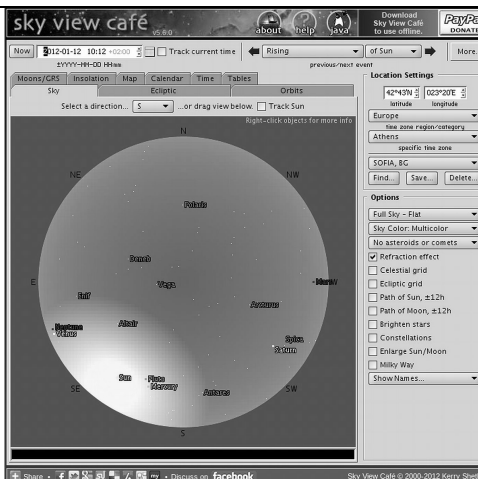
Strictly spoken it's a piece of software, simulating the Solar System's bodies in 3D on your Windows or Linux PC (will work in most *NIX's as well). In difference to quite a few other programs it does so in realtime. Meaning you can view all the planets, moons and spaceships *move* along their paths, trace them, follow them, orbit them and even control them (time and spaceship control). And you won't have to fight your way through hordes of green, slimey and one-eyed aliens for that ;-)

Figure 17. Snapshot of OPEN UNIVERSE home page.

6.4 SKYVIEW.CAFE

(<http://circumnavigational/>) - Sky View Cafe is *a Java applet that lets you see many types of astronomical information in both graphical and numerical form*. Sky View Café includes star charts, a 3-D orderly, displays of the moons of Jupiter and Saturn, an astronomical event calendar, an ephemeris generator, and many other features. Author - Kerry Shetline (2000-2010).

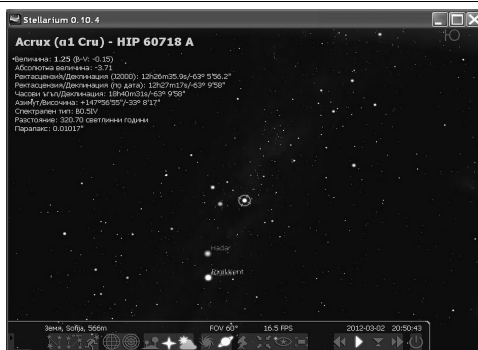
Figure 18. Snapshot of SKYVIEW.CAFE planetarium software.



6.5 STELLARIUM

(<http://www.stellarium.org/>) - a free open source planetarium for your computer. It shows a realistic sky in 3D, just like what you see with the naked eye, binoculars or a telescope. *It is being used in planetarium projectors. Stellarium includes: default catalogue of over 600,000 stars; extra catalogues with more than 210 million stars; asterisms and illustrations of the constellations; constellations for twelve different cultures; images of nebulae (full Messier catalogue); realistic Milky Way; very realistic atmosphere, sunrise and sunset; the planets and their satellites.*

Figure 19. Snapshot of STELLARIUM planetarium software.



6.6 XEPHEM

(<http://www.clearskyinstitute.com/xephem/>) - a *scientific-grade interactive astronomical ephemeris package*. XEphem: *computes* heliocentric, geocentric and topocentric information for all objects; has built-in support for all planets; the moons of Mars, Jupiter, Saturn, Uranus and Earth; downloads Digitized Sky Survey FITS files from STScI or ESO overlaid with database symbols and other graphical information; provides a handy coordinates spreadsheet for converting among equatorial, ecliptic, horizon and galactic frames; performs automatic star pattern matching to automatically solve for World Coordinate System on any image and many others. Author - Elwood Downey. Copyright'2005 by Robert Bruce Thompson and Barbara Fritchman Thompson.



Figure 20. Snapshot of XEPHEM planetarium software.

6.7 XPLNS

(<http://www.astroarts.com/products/xplns/index.html>) - reproduces real starry sky on your display of X Window System. It *calculates the position of many celestial objects (stars, galaxies, nebulae, constellations, planets, comets, etc.) very accurately*. There are *fourteen projection mode* in xplns, "Horizontal View Mode", "Equatorial Mode", "Ecliptic Mode", "Galactic Mode", "Planisphere Mode" and "Solar System Mode". Author - AJIKI Osamu.

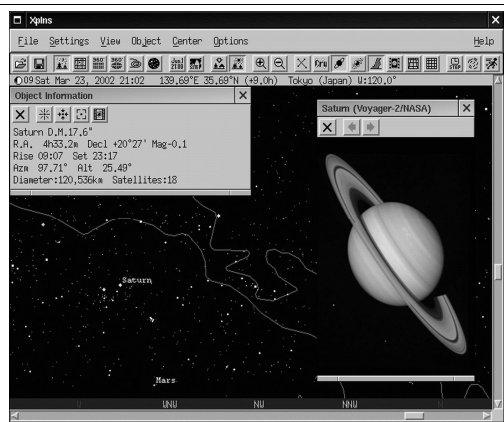
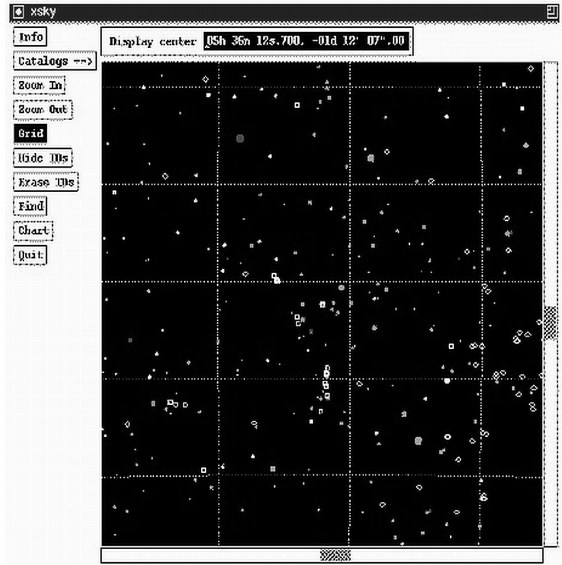


Figure 21. Snapshot of XPLNS planetarium software.

6.8 XSKY

(<ftp://arizona.edu/software/unix/xsky/>;
<http://hpux.connect.org.uk/hppd/hpux/X11/Viewers/xsky-2.01/>) - *makes the use of machine-readable astronomical object catalogues* available by the National Space Sciences Data Centre. Author - T.R.Friedrichsen, Sunquest Information Systems.

Figure 22. Snapshot of XSKY planetarium software.



6.9 XVMOONTOOL

(<http://www.paganlink.org/library/astronomy/xvmoontool.html>) - application which *displays information about the moon in real time*. Authors - John Walker and Ron Hitchens.

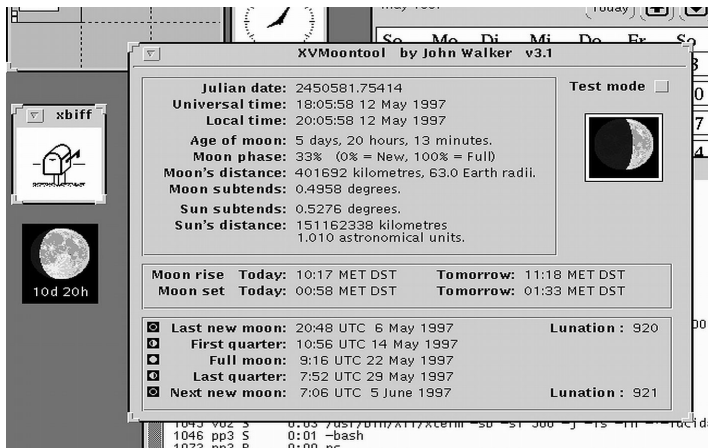
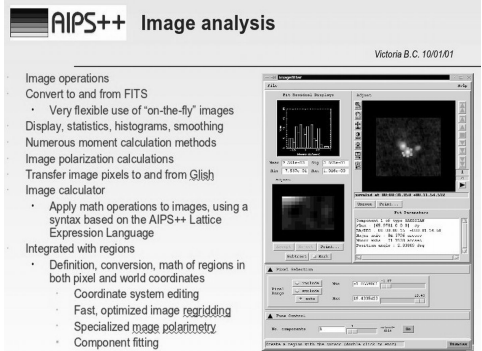


Figure 23. Snapshot of XVMOONTOOL application.

7. RADIO&INTERFEROMETRY ANALYSIS SOFTWARE

7.1 AIPS - stands for **Astronomical Image Processing System for calibration, data analysis, image display, plotting, and a variety of ancillary tasks on astronomical data.** AIPS is *not recommended for processing mm-wave observations* (30 GHz and higher) from the ATCA, e.g. One should use the MIRIAD package instead. (<http://aips2.nrao.edu>; <http://www.aips.nrao.edu/index.shtml>)

Figure 24. Snapshot of AIPS++ working area.



7.2 ASAP

(<ftp://ftp.atnf.csiro.au/pub/software/asap/current/>;

<http://svn.atnf.csiro.au/trac/asap>) - an ATNF *Spectral line Analysis package* to reduce single dish, single-pointing spectral-line observations (Marquarding M.: 2009, Astroinformatics School 2009)

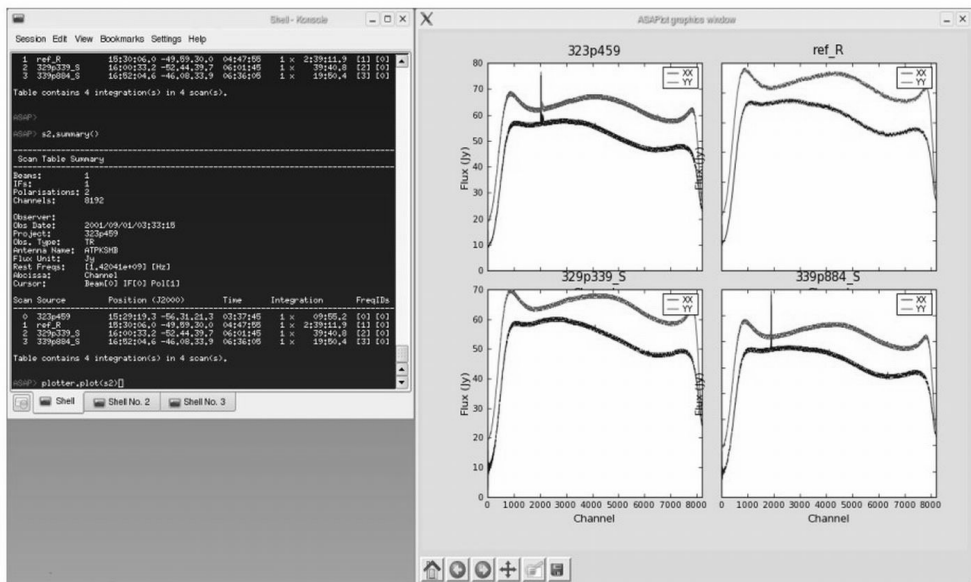


Figure 25. Snapshot of ASAP working area.

7.3 GILDAS (<http://pdb.finkproject.org/pdb/package.php/gildas>;
<http://www.iram.fr/IRAMFR/GILDAS/gildas.html>)- Grenoble Image and Line
 Data Analysis Software.

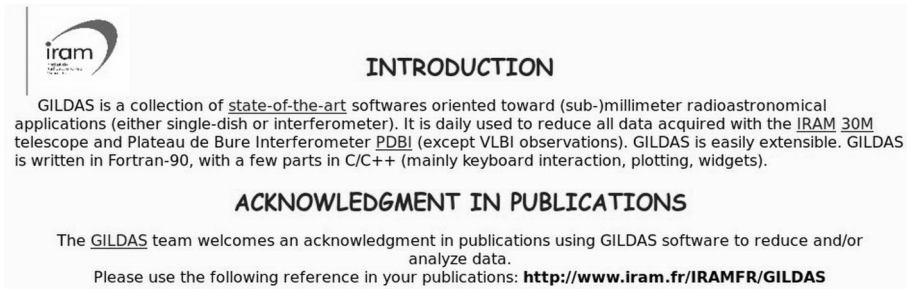


Figure 26. Snapshot of GILDAS home page.

7.4 GIPSY

(<http://www.astro.rug.nl/~gipsy/>;
<http://www.atnf.csiro.au/computing/software/gipsy/>) - a highly interactive
 software system for the *reduction and display of astronomical data*.

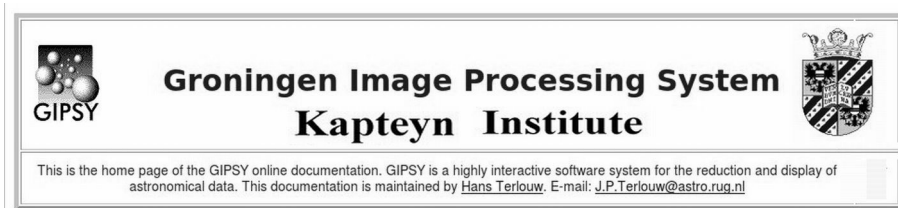


Figure 27. Snapshot of GIPSY home page.

7.5 MIRIAD (<ftp://ftp.atnf.csiro.au/pub/software/miriad/>) - radio
 interferometry reduction package e.g. of continuum and spectral line
 observations...

7.6 SPC (<http://www.atnf.csiro.au/computing/software/spc/>;
<ftp://ftp.atnf.csiro.au/pub/software/spc/>) - a *Spectral Line Reduction Package*
 used for reducing spectral line data from the Parkes and Mopra radiotelescopes.
 SPC was originally written to process data written by SPECTRA, the spectral-line
 observing program of the Parkes radiotelescope. The basic idea in using SPC is to
load in a sequence of up to 110 spectra and then use various commands to
operate on these spectra. Author - Rick Forster.

7.7 SPEXtool (<http://irtfweb.ifa.hawaii.edu/~spex/>) – an IDL-based package for
 the *reduction of spectral data obtained with SpeX IR imager and spectrograph*
 (Rayner et al. 2004, Cushing et al. 2004).

8. SPECTRUM ANALYSIS

8.1 DIPSO.STARLINK

(<http://www.starlink.rl.ac.uk/star/docs/sun50.htx/sun50.html>) - DIPSO is, historically, *a simple plotting package incorporating some basic astronomical applications*. DO read the documentation fully at some time; *DIPSO can do a lot of things, some of which you might not know that you needed* until you read about them... (by *I. D. Howarth, J. Murray, D. Mills & D. S. Berry, 5.03.2004*)

8.2 ICUR.IDL (<http://www.astro.sunysb.edu/fwalter/ICUR/icur.tar.gz>) - a generalized program which permits the user *to display and measure spectra*. Written in IDL, ICUR is a cursor-oriented spectral display and analysis program.

8.3 PINTOFALE (<http://hea-www.harvard.edu/PINTofALE/>) - originally developed to *analyze spectroscopic data from optically-thin coronal plasmas*, though much of the software is sufficiently general *to be of use in a much wider range of astrophysical data analyzes* (Kashyap & Drake 2000).

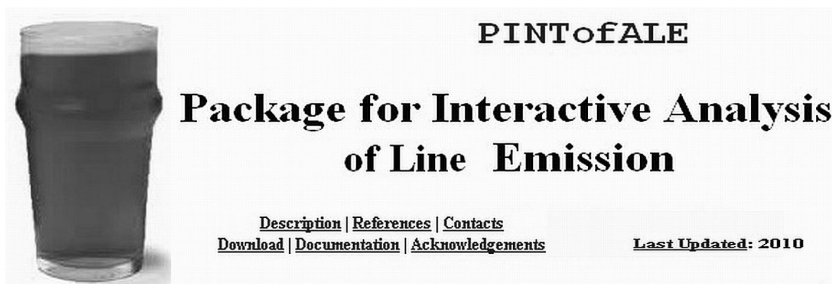


Figure 28. Snapshot of PINTofALE home page.

8.4 SHERPA (<http://cxc.harvard.edu/sherpa4.3/index.html>)



Figure 29. Snapshot of SHERPA home page.

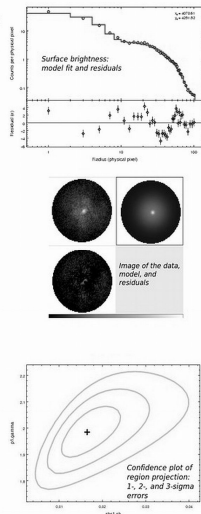
Sherpa enables the user *to construct complex models from simple definitions and fit those models to data, using a variety of statistics and optimization methods.* Sherpa lets you:

Fit 1-D data sets (simultaneously or individually), *including:* spectra, surface brightness profiles, light curves, general ASCII arrays; access the internal data arrays; build complex model expressions; import and use your own models; choose appropriate statistics for modeling Poisson or Gaussian data; import new statistics, with priors if required by analysis; visualize a parameter space with simulations or using 1-D/2-D cuts of the parameter space; calculate confidence levels on the best-fit model parameters; etc... (Freeman et al. 2001).

Figure 30. Snapshot of SHERPA modeling examples.

Sherpa lets you:

- fit 1-D data sets (simultaneously or individually), including: spectra, surface brightness profiles, light curves, general ASCII arrays;
- fit 2-D images/surfaces in the Poisson/Gaussian regime;
- access the internal data arrays;
- build complex model expressions;
- import and use your own models;
- choose appropriate statistics for modeling Poisson or Gaussian data;
- import new statistics, with priors if required by analysis;
- visualize a parameter space with simulations or using 1-D/2-D cuts of the parameter space;
- calculate confidence levels on the best-fit model parameters;
- choose a robust optimization method for the fit: Levenberg-Marquardt, Nelder-Mead Simplex or Monte Carlo/Differential Evolution;
- and use Python to create complex analysis and modeling functions, build the batch mode analysis or extend the provided functionality to meet the required needs.



8.5 SNID (<http://marwww.in2p3.fr/~blondin/software/snid/index.html>) – a software to determine the type, redshift, and age of a type Ia supernovae (Blondin & Tonry 2007).

8.6 SPECTRUM (<http://www1.appstate.edu/dept/physics/spectrum/specftp.html>) - currently, *SPECTRUM is suitable for computing stellar spectra in the spectral-type range B – mid M.* Copyrighted by Richard O. Gray, 1992-2008.

SPECTRUM *A Stellar Spectral Synthesis Program*

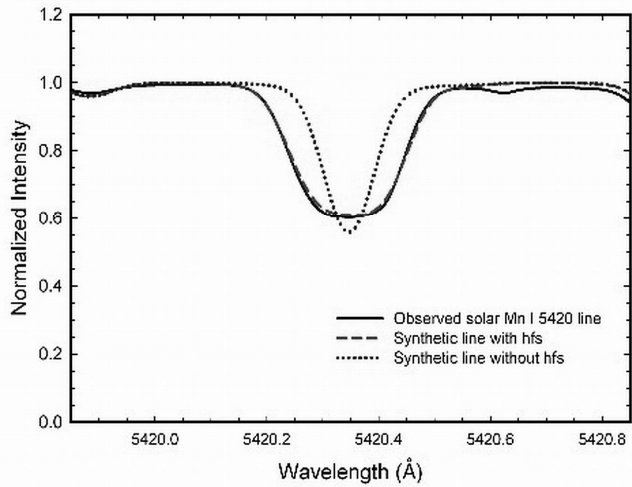


Figure 31. Snapshot of SPECTRUM application.

8.7 SPECVIEW (http://www.stsci.edu/institute/software_hardware/specview/) - a tool for 1-D spectral visualization and analysis of astronomical spectrograms.

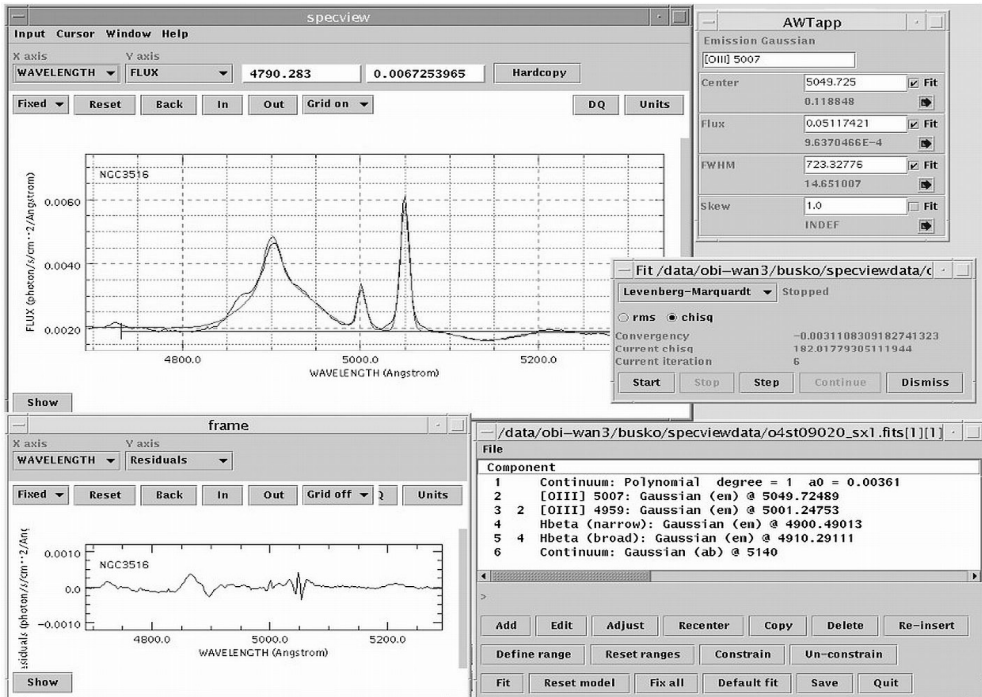


Figure 32. Snapshot of SPECVIEW working area.

8.8 SPLAT - a graphical tool *for displaying, comparing, modifying and analyzing astronomical spectra* stored in NDF, FITS and TEXT files as well as the new NDX format.

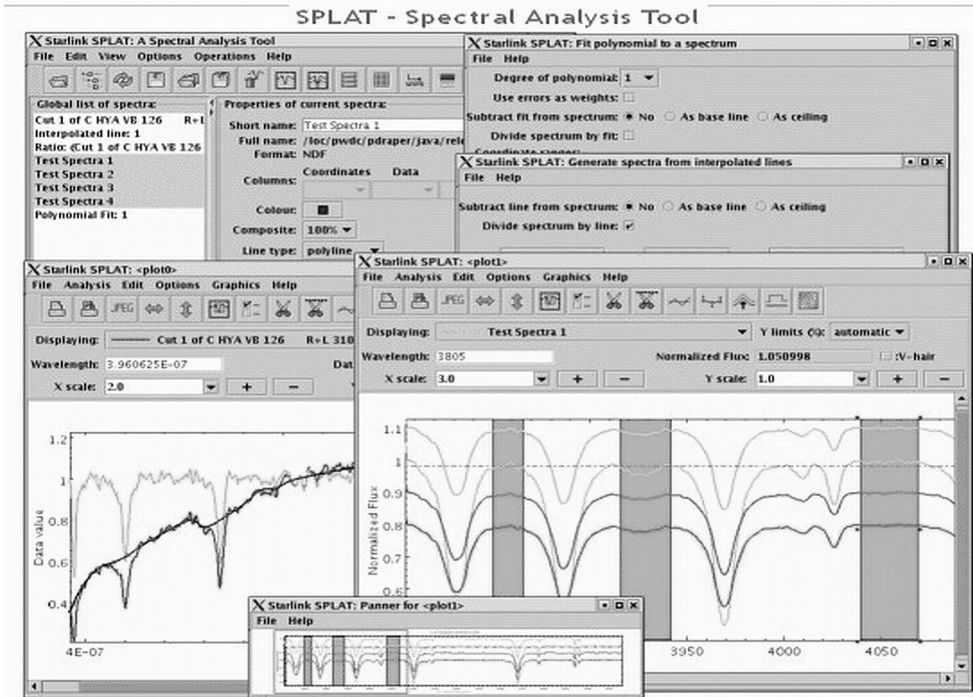


Figure 33. Snapshot of SPLAT working area.

8.9 STECKMAP (<http://astro.u-strasbg.fr/~ocvirk/indexsteckmap.html>) - a powerful toolkit for whoever wishes *to interpret the stellar absorption features of integrated light spectra of stellar populations*. It is written in *yorick* (Ocvirk et al. 2006A, 2006b).

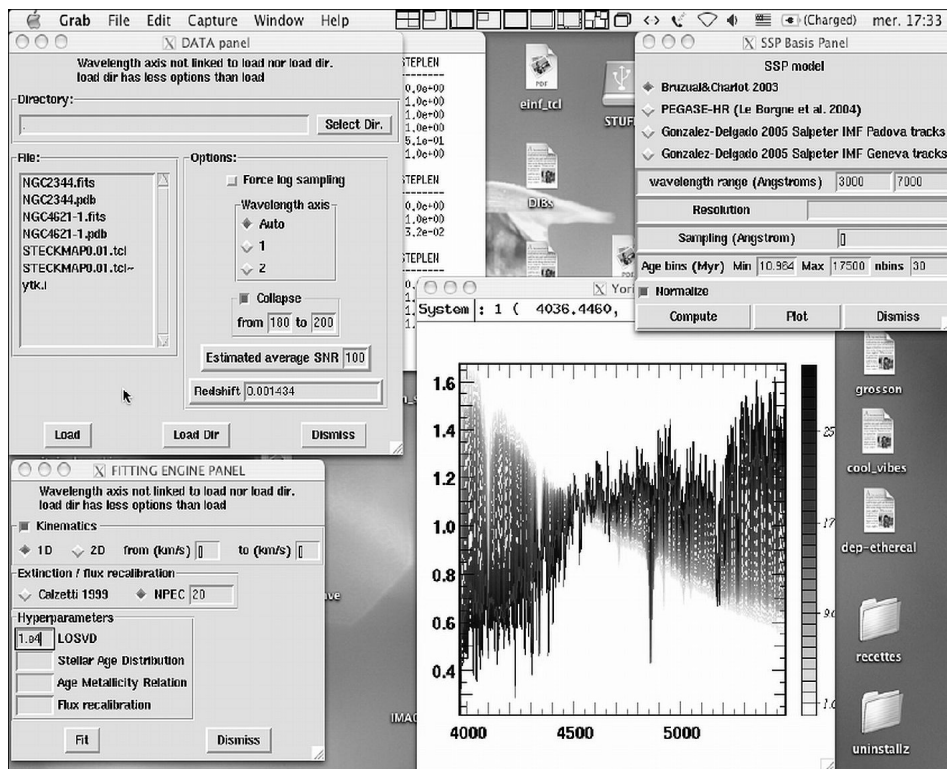


Figure 34. Snapshot of STECKMAP working area.

8.10 XSTAR (<http://heasarc.gsfc.nasa.gov/docs/software/lheasoft/xstar/xstar.html>)

- a command-driven, interactive, computer program for *calculating the physical conditions and emission spectra of photoionized gases*.

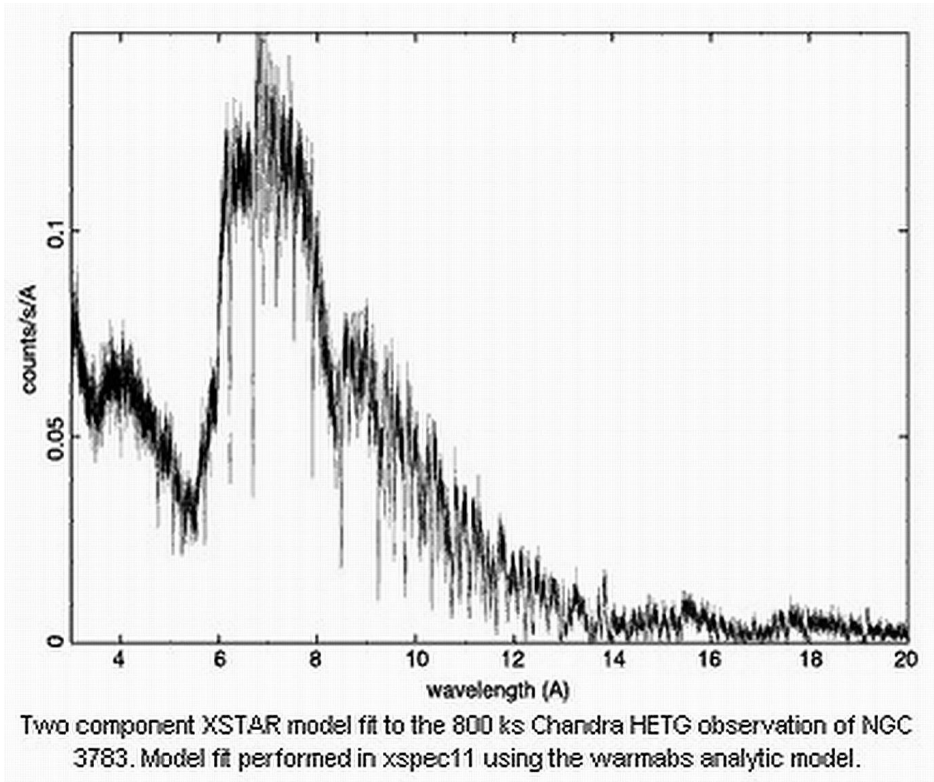
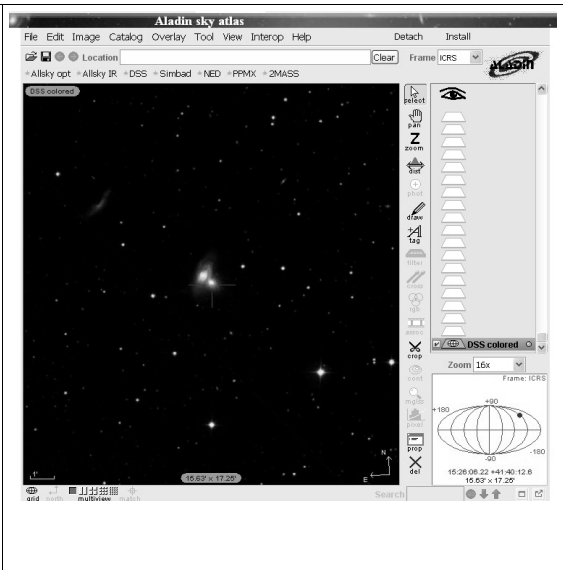


Figure 35. Snapshot of XSTAR application.

9. VISUALIZATION SOFTWARE

9.1 ALADIN (<http://aladin.u-strasbg.fr/>) - An *interactive software sky atlas* allowing the user to visualize digitized astronomical images, superimpose entries from astronomical catalogues or databases, and interactively *access related data and information from the Simbad database, the Vizier service and other archives for all known sources in the field* (Bonnarel et al. 2000).

Figure 36. Snapshot of ALADIN application.



9.2 DS9

(<http://hea-www.harvard.edu/saord/ds9/>) - **SAO Image DS9** is an astronomical imaging and data visualization application. DS9 supports FITS images and binary tables, multiple frame buffers, region manipulation, and many scale algorithms and colormaps. It provides for easy communication with external analysis tasks and is highly configurable and extensible via XPA and SAMP. DS9 is a stand-alone application. *It requires no installation or support files.* DS9 also supports FTP and HTTP access.

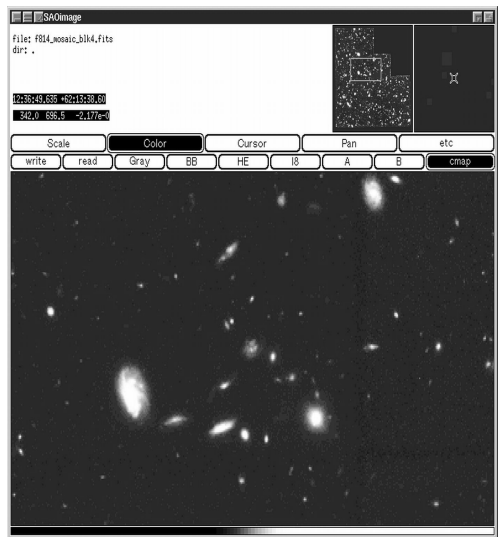
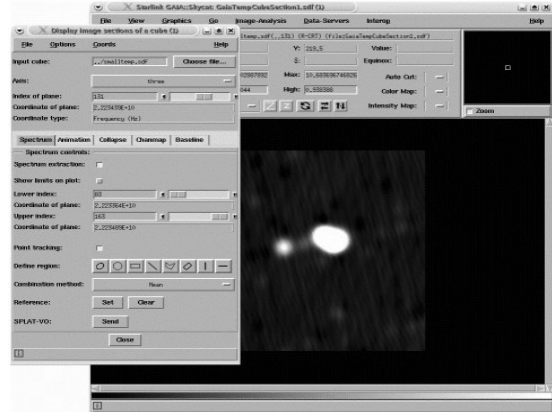


Figure 37. Snapshot of SAOimage DS9 application.

9.3 GAIA-ESO

(<http://extraterritorial/~pdraper/gaia/ontheweb/index.html>)

Figure 38. Snapshot of GAIA SkyCat application.



9.4 FUSE.IDL (<http://fuse.pha.jhu.edu/analysis/sw/>) - **IDL widget programs for displaying and manipulating FUSE data files**, written by Don Lindler. There are many features in this program for manipulating time-tag data. The following programs for the reading and display of FUSE images and spectra have been contributed at JHU: **ftv.pro**; **readit.pro**; **plorate.pro**; **showdetector.pro**; **allsegments.pro**; **hist_combine**. Authors: Alex Fullerton, Don Lindler, Ed Murphy, Bill Oegerle, Dave Sahnaw.

9.5 FV FITS VIEWER (<http://heasarc.gsfc.nasa.gov/docs/software.html>)

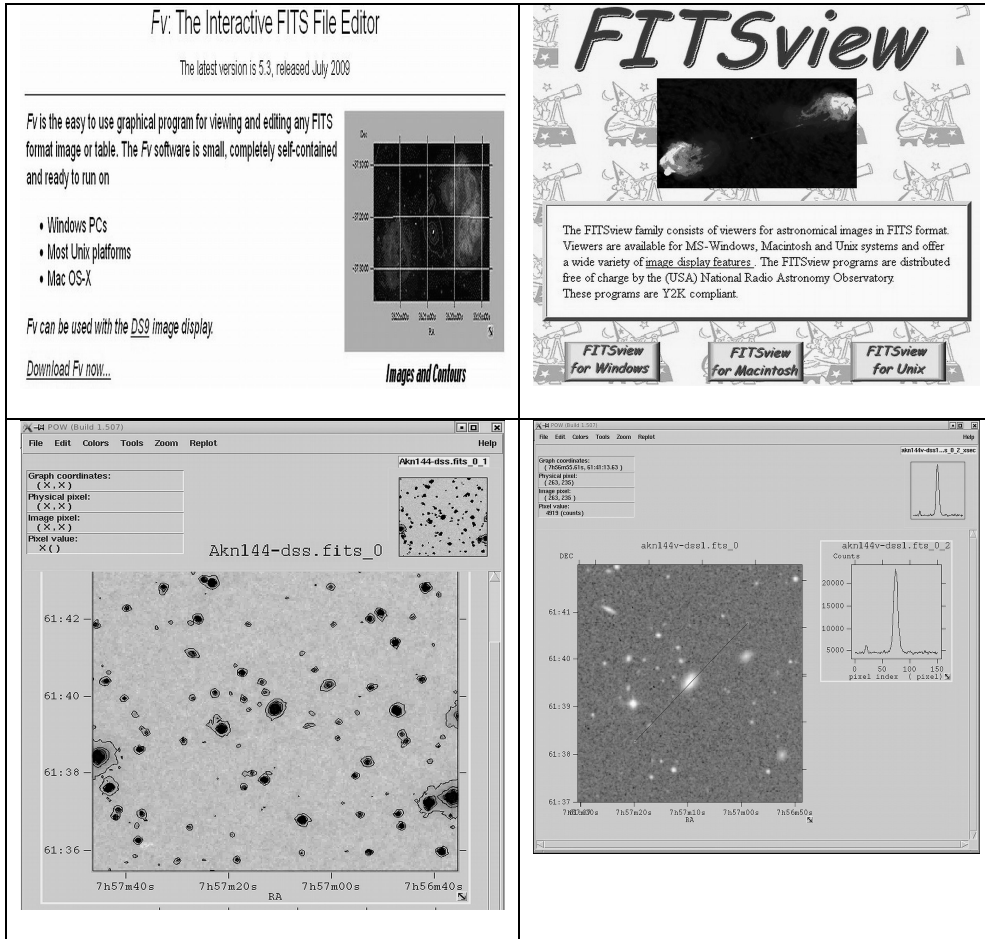


Figure 39a,b,c,d. Snapshot of fv FITS file editor application.

9.6 KARMA TOOLKIT
 (ftp://ftp.atnf.csiro.au/pub/software/karma/) - *A package for visualization multi-dimensional images, signal and image processing applications* (Gooch 1996).

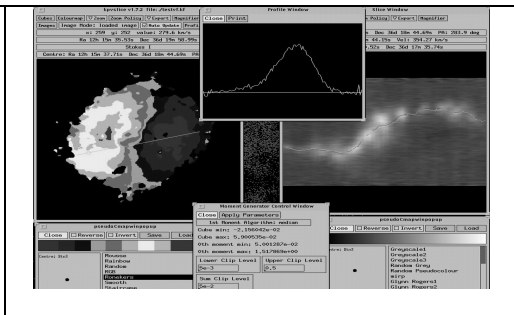


Figure 40. Snapshot of KARMA toolkit application.

9.7 PROFIT (<http://heasarc.gsfc.nasa.gov/docs/software/profit/>) - a GUI (graphical user interface) *tool for accessing high-resolution spectra*. Profit displays spectra in various formats, allowing users to identify emission lines, to convert an identified line into velocity units using a user-selected wavelength, to store (and restore) individual spectra, to fit lines to Gaussians, and other features.

9.8 QFITSVIEW (<http://www.mpe.mpg.de/~ott/dpuser/qfitsview.html>).
Copyrighted by Thomas Ott.



Figure 41. Snapshot of QFITSVIEW application.

9.9 SDSS.SKYSERVER (<http://cas.sdss.org/dr7/en/>) - the *data access site for the Sloan Digital Sky Survey*. From the site, one can view all of the SDSS data, using the same tools that professional astronomers use etc.

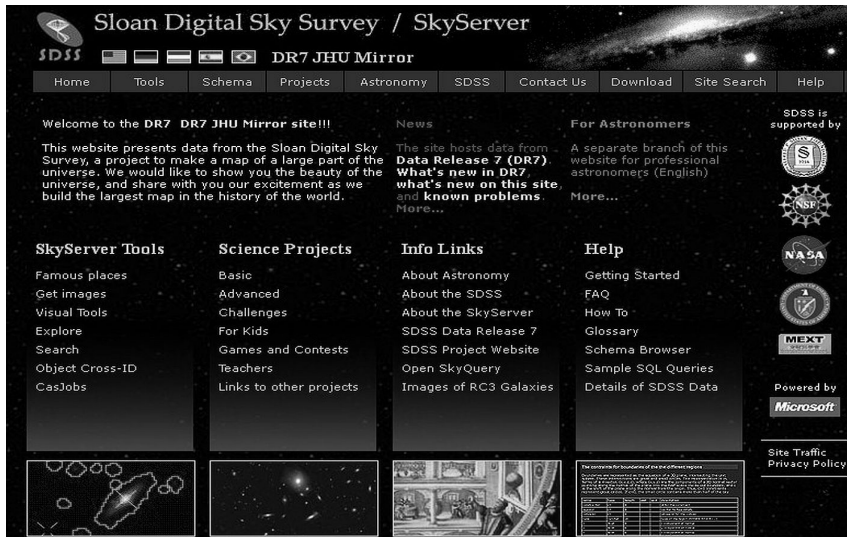


Figure 42. Snapshot of SDSS.SKYSERVER home page.

9.10 SKYCAT-ESO (<http://archive.eso.org/cms/tools-documentation/skycat>) - a tool that *combines visualization of images and access to catalogs and archive data* for astronomy. Below is Java SkyCat application

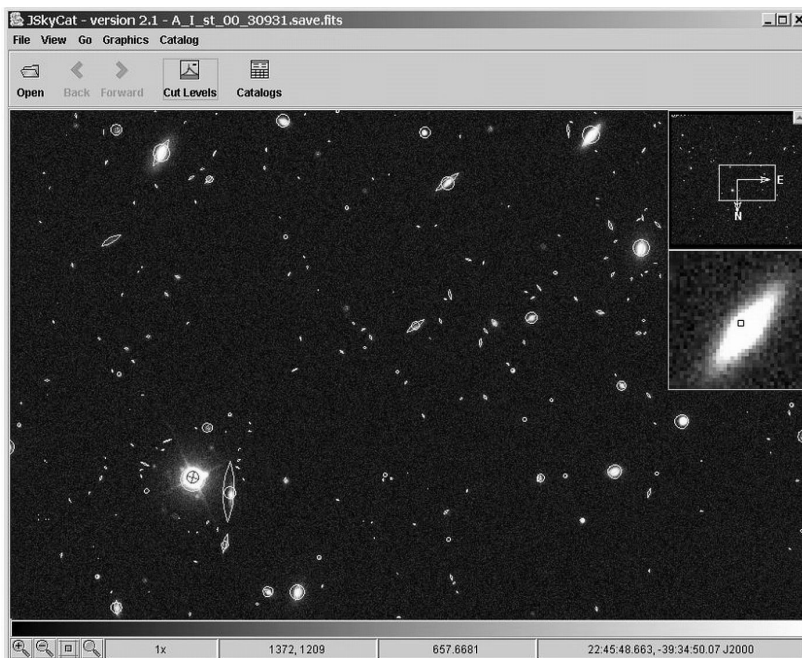


Figure 43. Snapshot of SKYCAT-ESO application.

9.10 SKYMAP (<http://tdc-www.harvard.edu/software/skymap/>) - an *astronomical mapping program* written in Fortran and C for Unix workstations by Doug Mink of the Smithsonian Astrophysical Observatory Telescope Data Center (Mink 1993).

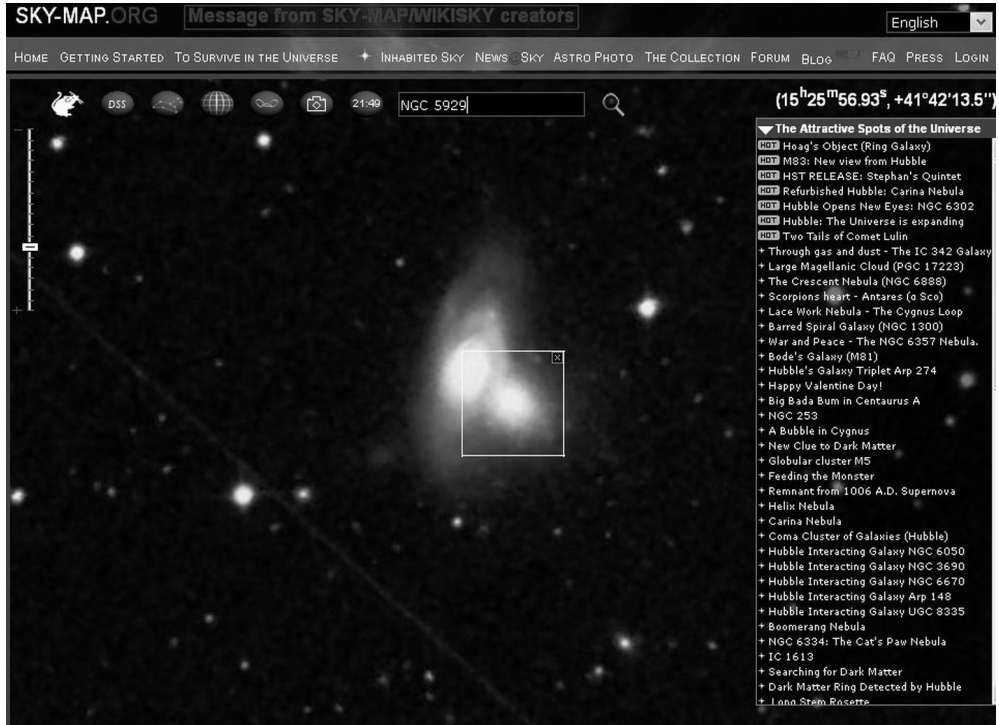


Figure 44. Snapshot of SKYMAP application.

9.12 VIRGO (<http://archive.eso.org/cms/virgo/>)



VirGO is the next generation Visual Browser for the ESO Science Archive Facility developed by the VO Systems Department. It is a plug-in for the popular open source software Stellarium with added capabilities for browsing professional astronomical data. VirGO gives astronomers the possibility to easily discover and select data from millions of observations in a new visual and intuitive way. Its main feature is to perform real-time access and graphical display of a large number of observations by showing instrumental footprints and image previews, and to allow their selection and filtering for subsequent retrieval. It reads FITS images and catalogues in VOTable format. It superimposes DSS background images and allows to view the sky in a *real life* mode as seen from the main ESO sites.

Data interfaces are based on Virtual Observatory standards enabling access to images and spectra hosted by other data centers and to exchange data with other VO applications through the PLASTIC messaging system.

These screenshots illustrate some of the main features of VirGO such as footprints, DSS background, previews or browsing through large number of data sets.

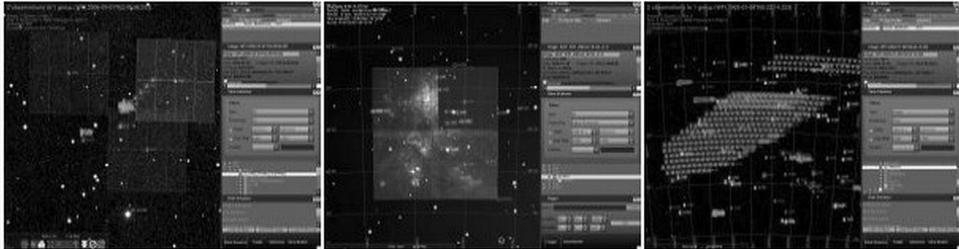


Figure 45. Snapshot of ESO VIRGO application.

9.13 VISIT (<https://wci.llnl.gov/codes/visit/home.html>) - an interactive parallel visualization and graphical analysis tool for viewing scientific data. Users can quickly generate visualizations from their data, animate them through time, manipulate them, and save the resulting images for presentations. VisIt contains a rich set of visualization features so that you can view your data in a variety of ways. It can be used to visualize scalar and vector fields defined on two- and three-dimensional (2D and 3D) structured and unstructured meshes. VisIt was designed to handle very large data set sizes in the terascale range and yet can also handle small data sets in the kilobyte range. VisIt handles 2D and 3D data equally well. VisIt also has the ability to animate data, allowing users to see the time evolution of their data. VisIt is also a powerful analysis tool. It provides support for derived fields, which allow new fields to be calculated using existing fields.

10. VO SOFTWARE - details presented during the VII_SBAC (Petrov et al. 2012)

10.1 ESO-MEX

(<http://cds.u-strasbg.fr/twiki/DCA/bin/view/EuroVODCA/DcaJune2008ESOMEx>)
- tools for publishing images and spectra

10.2 SAADA (<http://amwdb.u-strasbg.fr/saada/>) - transforms a set of heterogeneous FITS files or VOTables of various categories (images, tables, spectra...) into a database.

10.3 DAL ToolKit (<http://www.ivoa.net/cgi-bin/twiki/bin/view/IVOA/IvoaDAL>; <http://www.sciops.esa.int/SD/ESAVO/DALToolKit-v0.0.tar.gz>)

10.4 DATASCOPE (<http://heasarc.gsfc.nasa.gov/cgi-bin/vo/datascope/>) - searches everything for a given target or region of the sky.

10.5 MAKI (http://heasarc.nasa.gov/docs/astroe/prop_tools/maki.html) - investigates instrument Fields of View (FOV's), and viewing multi-mission observing windows.

10.6 PLASTIC (<http://esavo.esac.esa.int/VOSpecManual/interoperability.html>) - a protocol for communication between client-side astronomy applications.

10.7 SKYVIEW (<http://skyview.gsfc.nasa.gov/>) - generating all sky images from Radio to Gamma-Ray

10.8 SPECVIEW (http://www.stsci.edu/institute/software_hardware/specview/) - a tool for 1-D spectral visualization and analysis of astronomical spectrograms (see 8.7 too).

10.9 SPLAT (<http://star-www.dur.ac.uk/~pdraper/splat/splat.html>) - a toolbox for querying, downloading and displaying spectra from the current generation of SSAP servers.

10.10 STILTS (<http://www.starlink.ac.uk/stilts/>) - a set of command-line tools processing astronomical tables. Author - Mark Taylor.

10.11 TOPCAT (<http://www.starlink.ac.uk/topcat/>) - an interactive graphical viewer and editor for tabular data. Author - M. Taylor.

10.12 VisIVO (<http://visivo.oact.inaf.it/>) - a visualization and analysis software for astrophysical data

10.13 VOCONVERT (<http://vo.iucaa.ernet.in/~voi/VOConvert.htm>) - a tool for converting files from one format to another

10.14 VODESKTOP (<http://www.astrogrid.org/wiki/Help/IntroVODesktop>) - a core application with several interlinked tools

10.15 VOEVENT (<http://www.ivoa.net/Documents/VOEvent/>) - a standardized language used to report observations of astronomical events

10.16 VO PLOT (<http://vo.iucaa.ernet.in/~voi/voplot.htm>) - a tool for visualizing astronomical data.

10.17 VOSA (<http://svo.cab.inta-csic.es/theory/vosa/>) - a tool designed to perform the many tasks in an automatic manner (Bayo et al. 2008).

10.18 VOSPEC (<http://esavo.esa.int/vospec/>) - a multi-wavelength spectral analysis tool with access to spectra, theoretical models and atomic and molecular line databases registered in the VO.

10.19 VOSTAT (<http://astrostatistics.psu.edu/vostat/>) - statistical routines on large datasets.

11. X_RAY ANALYSIS SOFTWARE

11.1 CIAO (<http://cxc.harvard.edu/ciao/index.html>) - Chandra Interactive Analysis of Observations. The remarkable science capabilities of the Chandra X-ray Observatory demanded new, *flexible, multi-dimensional software to analyze the data* it returned. A system has been proven itself *useful for the analysis of data from other, non-X-ray missions*, because of the mission independence that is the basis of the CIAO design (Fruscione et al. 2006).

11.2 ISIS.XRAY (<http://space.mit.edu/cxc/isis/>)- a complete package to process CCD images using the *image optimal subtraction method* (Alard & Lupton 1998, Alard 1999). The ISIS package can find the best kernel solution even in case of kernel variations as a function of position in the image. (...see 1.5 too...).

11.3 PIMMS (<http://heasarc.nasa.gov/docs/software/tools/pimms.html>) - Portable, Interactive Multi-Mission Simulator software *for high-energy astrophysicists*.

11.4 SAS (http://xmm.esac.esa.int/sas/current/documentation/sas_concise.shtml) - The Science Analysis System is *a collection of tasks, scripts and libraries, specifically designed to reduce and analyze data collected by the XMM-Newton observatory*. "XMM-Newton data are available in two formats: 1) Observation Data Files (ODF), i.e. reformatted telemetry in FITS format and 2) Pipeline Processing System (PPS) products, a collection of validated, top-level scientific products".

11.5 SPEX (<http://www.sron.nl/>) - a software package *optimized for the analysis and interpretation of high-resolution cosmic X-ray spectra*. The software is especially suited for fitting spectra obtained by current X-ray observatories like XMM-Newton, Chandra, and Suzaku.

11.6 XSPEC (<http://heasarc.gsfc.nasa.gov/docs/xanadu/xspec/>) - An *X-Ray Spectral Fitting Package*. XSPEC is a command-driven, interactive, X-ray spectral-fitting program, completely detector-independent. XSPEC has been used to analyze data from HEAO-1 A2, *Einstein Observatory*, EXOSAT, Ginga, ROSAT, BBXRT, ASCA, CGRO, IUE, RXTE, Chandra, XMM-Newton, Integral/SPI, Swift and Suzaku (Arnaud 1996).

Acknowledgements

This work is partially supported by a grant of the Bulgarian National Science Foundation, Ministry of Education and Science, under number DO-02-273.

References

- Aarseth, S. J. : 2001, *New Astron.*, **6**, 277.
- Alard, C.: 1999, *A&A*, **343**, 10.
- Alard, C., Lupton, R. H.: 1998, *ApJ*, **503**, 325.
- Arnaud, K. A.: 1996, In: *Astronomical Data Analysis Software and Systems V*, Eds. George H. Jacoby and Jeannette Barnes, *ASP Conference Series*, **101**.
- Avrett, E. H., Loeser, R.: 2003, *IAU Symp.*, **210**, 21.
- Barkana, R.: 1998, *ApJ*, **502**, 531.
- Bayo, A., Rodrigo, C., Barrado y Navascués, D., Solano, E., Gutiérrez, R., Morales-Calderón, M., Allard, F.: 2008, *A&A*, **492**, 277.
- Bertin, E.: 2009, *Memorie della Societa Astronomica Italiana Supplement*, **80**, 422.
- Bertin, E., Arnouts, S.: 1996, *Astron.Astrophys., Suppl.Ser.*, **317**, 393.
- Blondin, S., Tonry, J. L.: 2007, *Ap.J*, **666**, 1024.
- Bonnarel, F., Fernique, P., Bienayme, O., Egret, D., Genova, F., Louys, M., Ochsenbein, F., Wenger, M., Bartlett, J. G.: 2000, *Astron. Astrophys., Suppl.Ser.*, **143**, 33.
- Cushing, M. C., Vacca W. D., Rayner, J. T.: 2004, *PASP*, **116**, 362.
- Diolaiti, E., Bendinelli, O., Bonaccini, D., Close, L., Currie, D., Parmeggiani, G.: 2000, *Astron.Astrophys., Suppl.Ser.*, **147**, 335.
- Freeman, P. E., Doe, S., Siemiginowska, A.: 2001, *SPIE Proceedings*, **4477**, 76.
- Fruscione et al.: 2006, *SPIE Proc.* V, Eds. D. R. Silvia, R. E. Doxsey, **6270**, 62701.
- Gooch, R.: 1996, In: *Astronomical Data Analysis Software and Systems V*, Eds. George H. Jacoby and Jeannette Barnes, *A.S.P. Conference Series*, **101**, 80.
- Grosbol, P. J., Ponz, J. D.: 1990, In: *Acquisition, Processing and Archiving of Astronomical Images*, Eds. G. Longo, G. Sedmak, OAC and FORMEZ, p. 109.
- Kashyap, V., Drake, J. J.: 2000, *BASI*, **28**, 475.
- Konecny, F., Fürst, J.: 2007, *Computers and Geosciences*, **33**, 159.
- Ma, C.-P., Bertschinger, E.: 1995, *Ap.J*, **455**, 7.
- Mahy, et al.: 2011, *Astron. Astrophys.*, **533**, 9.
- Marquarding, M.: 2009, *Astroinformatics School' 2009*.
- Mighell, K. J.: 2010, *PASP*, **122**, 1236.
- Mikolaitis, S., Tautvaiseine, G.: 2009, *EGEE'09*, 21-25 September 2009, Zurich.
- Mink, D. J. : 1993, In: *Astronomical Data Analysis Software and Systems II*, Eds. R. J. Hanisch, R. J. V. Brissenden, J. Barnes, *A.S.P. Conference Series*, **52**, 499.
- Nemiroff, R. J., Rafert, J. B.: 1999, *PASP*, **111**, 886.
- Ocvirk, P., Pichon, C., Lançon, A., Thiébaud, E.: 2006a, *MNRAS*, **365**, 46.
- Ocvirk, P., Pichon, C., Lançon, A., Thiébaud, E.: 2006b, *MNRAS*, **365**, 74.
- Plaza, A., Plaza, J., Valencia, D.: 2006, In: *International Conference on Computational Science (3), Proceedings*, p. 24.
- Petrov, G., Dechev, M., Atanasov, E.: 2012, *this volume*
- Rayner, J. T., Onaka, P. M., Cushing, M. C., Vacca, W. D.: 2004, *SPIE*, **5492**, 1498.
- Richmond, M. W. et al.: 1995, *Astronomical Journal*, **109**, 2121.
- Richmond, M. W., Treffers, R. R., Filippenko, A. V.: 1993, *PASP*, **105**, 1164.

BULGARIAN GRID, BULGARIAN VIRTUAL OBSERVATORY AND SOME ASTRONOMICAL APPLICATIONS *

GEORGI PETROV¹, MOMCHIL DECHEV¹
and EMANOUIL ATANASOV²

¹*Institute of Astronomy, Bulgarian Academy of Sciences,
72, Tsarigradsko chaossee, 1784-Sofia, Bulgaria*

²*Institute for Parallel Processing, Bulgarian Academy of Sciences,
Acad. G. Bonchev Str., Bl. 25-a, Sofia, Bulgaria*

E-mail: petrov@astro.bas.bg, mdechv@astro.bas.bg, emanouil@parallel.bas.bg

Abstract: The development of the Bulgarian GRID, new possibilities for Bulgarian Virtual Observatory and some basic astronomical GRID applications from the published papers and internet are reviewed. Amongst the basic applications are N_body simulations, looking for dark matter, dark energy and neutrino, large scale structure of the Universe, stellar and galaxy evolution, active processes on the Sun, near earth object discovery, specialised software and firmware, network telescopes architecture etc.

1. INTRODUCTION

During the 2009 – 2011 years the Bulgarian High performance computing GRID for advanced scientific applications under the NSF DO 02-115/2009 grant is establishes. The first stage of the project is over – the grid system was configured and tested and it is under regular profit. The review presented here is based on the original published papers and internet information as well. The main goal is to point the possibilities of GRID for scientific investigations for the Bulgarian astronomical community.

ACM Computing Classification System (1998): A.0, I.4.0, J.2

Key words: GRID, Virtual observatory, astronomical grid applications, grid and VO software, GRID portals, simulations, dark energy, stellar and galaxies evolution.

* Invited lecture presented on the VII Serbian-Bulgarian Astronomical Conference, Maj'2010, Chepelare.

For the beginning one always could reviewed *iSGTW* web site:

- ***International Science Grid This Week*** (www.isgtw.org)

iSGTW is an international, weekly, on-line science-computing newsletter that shows the importance of distributed computing, grid computing, cloud computing and high-performance computing. It does so by reporting about the people and projects involved in these fields, and how these types of computing technologies are being applied to make scientific advances.

2. GRID PROJECTS

The picture could be fulfilled with portals and services. In the table below the **basic Grid Projects**, including some national and older ones, are summarised.

- European Grid Initiative <u>EMI</u> - European Middleware Initiative <u>gLite</u> - European middleware distribution <u>Open Science Grid</u> - the U.S scientific Grid infrastructure <u>Virtual Data Toolkit</u> - provides middleware distribution	National Grid projects <u>Dutch Grid</u> <u>GridPP</u> <u>INFN Grid</u> <u>LCG France</u> <u>NorduGrid</u> <u>WestGrid EGI</u> <u>GÉANT</u> - European academic and research network infrastructure	Previous projects <u>EGEE</u> <u>European Data Grid</u> <u>Datatag</u> <u>Grid2003</u> <u>GriPhyN</u> <u>iVDGL</u> <u>PPDG</u>
---	---	--

- ***EGEE - Enabling Grids for E-science*** (www.eu-egee.org)

The **Enabling Grids for E-science** project is no longer active. The project **officially ended on April 30, 2010**. The distributed computing infrastructure is now supported by the **European Grid Infrastructure**. This long-term organisation coordinates National Grid Initiatives, which form the country-wide building blocks of the pan-European Grid. Here are some **Regional Web Site pages**.

<u>EGEE South East Europe</u> <u>Spain EGEE-III site</u> <u>Romanian Grid site</u>	<u>Bulgarian Grid portal</u> <u>Cyprus Grid site</u> <u>Hungarian Grid site</u>	<u>Russian website</u> <u>Portuguese website</u> <u>Slovak website</u>
--	---	--

Welcome to Bulgarian Grid Portal (www.grid.bas.bg)

Grid computing is a form of distributed computing whereby a "super and virtual computer" is composed of a cluster of networked, loosely-coupled computers, acting in concert to perform very large tasks. This technology has been applied to

computationally-intensive scientific, mathematical, and academic problems through volunteer computing, and it is used in commercial enterprises for such diverse applications as drug discovery, economic forecasting, seismic analysis, and back-office data processing in support of e-commerce and web services. What distinguishes grid computing from typical cluster computing systems is that grids tend to be more loosely coupled, heterogeneous, and geographically dispersed. Also, while a computing grid may be dedicated to a specialized application, it is often constructed with the aid of general purpose grid software libraries and middleware.

- *AstroGRID* (www2.astrogrid.org)

AstroGrid is the doorway to the Virtual Observatory (VO). It provides a suite of *desktop applications* to enable astronomers to explore and bookmark resources from around the world, find data, store and share files in VOspace, query databases, plot and manipulate tables, cross-match catalogues, and build and run scripts to automate sequences of tasks. Tools from other Euro-VO projects inter-operate with AstroGrid software, so one can also view and analyse images and spectra located in the VO.

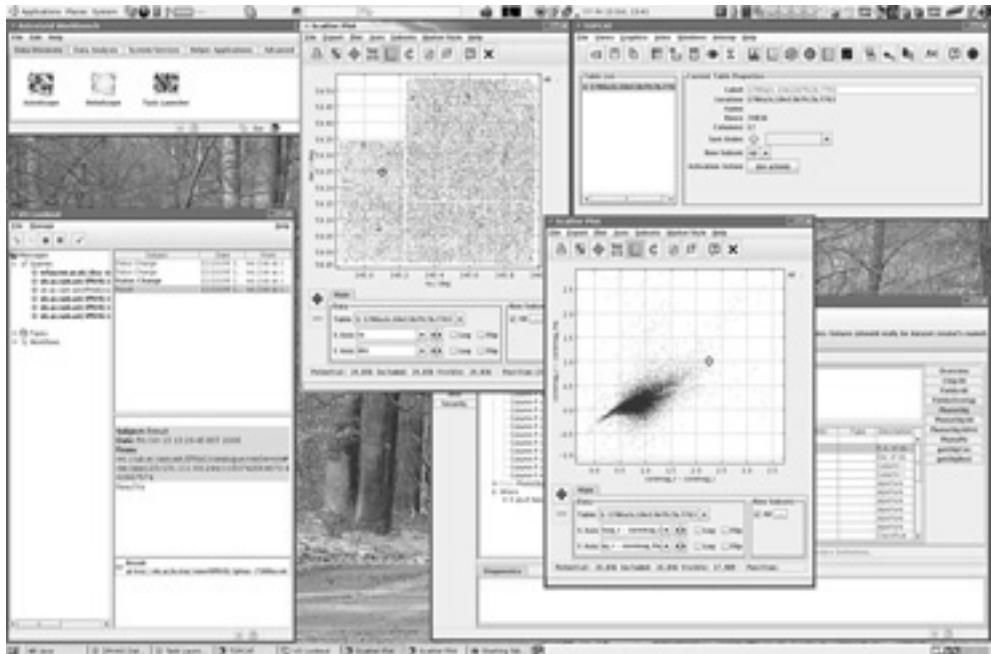


Figure 1: Screenshot from the AstroGrid WEB_page.

AstroGrid, a UK-government funded, open-source project, helps create universal access to observational astronomy data scattered around the globe. **The AstroGrid consortium**, which **consists of 11 UK university groups**, represents astronomy and computing groups with background in handling and publishing such data. The consortium worked with international partners to agree upon standards for published observational astronomy data, so that all astronomers could interact with all data sets.

The AstroGrid workbench is the main user interface for astronomers accessing the virtual observatory. The global set of standards agreed upon by the consortium and its partners allows any astronomer to query the virtual observatory to ask for information on a certain area of the sky.

Through AstroGrid, UK astronomers can also access workflows and applications for data analysis. AstroGrid has also created the “voSpace” program that allows astronomers to share their workflows. For a lot additional of possibilities see paper of Lawrence (2002).

- **AstroGRID-D** - enabling grid science in the German Astronomical community.

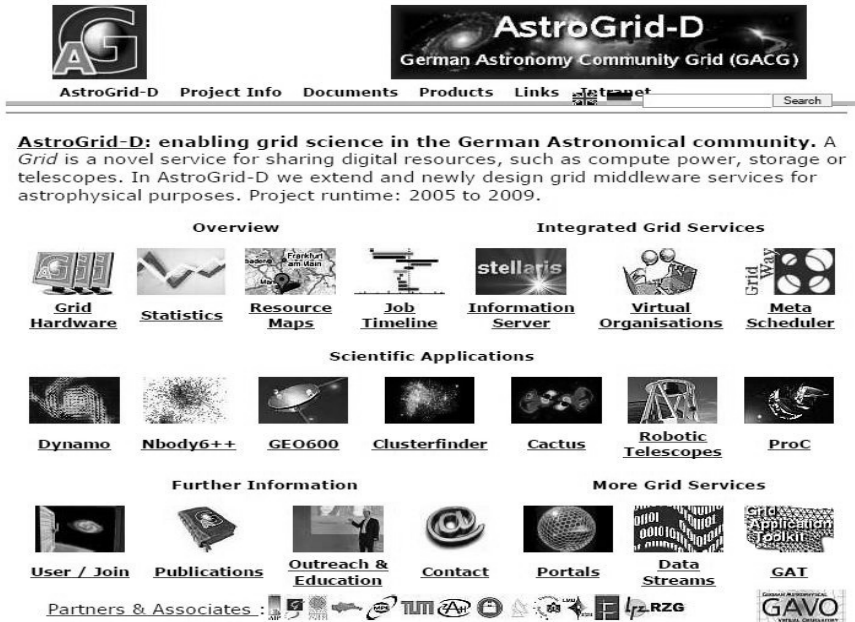


Figure 2: Screenshot from the AstroGrid-D WEB_page.

3. MIDDLEWARE and FRAMEWORKS

The structure of the instrumentation between software and hardware will be shortly reviewed in this part.

- FALKON, a Fast and Light-weight task execution framework for Clusters, Grids, and Supercomputers. Amongst the projects is *AstroPortal*. Large astronomy datasets are generally *terabytes in size* and contain *hundreds of millions of objects* separated into *millions of files*. **The key question is:** “How can the analysis of large astronomy datasets be made a reality for the astronomy community using Grid resources?” **The answer is: the “AstroPortal”**, a science gateway to grid resources that is specifically designed for the astronomy community - <http://www.cs.uchicago.edu/~iraicu/projects/Falkon/astro-portal.html>.

- **GRACIE: Grid Resource Virtualization and Customization Infrastructure** (net.pku.edu.cn). *Gracie* is a lightweight execution **framework for efficiently executing massive independent tasks in parallel on distributed computational resources**. **Three optimization strategies** have been devised to improve the performance of Grid system.

Pack up to thousands of tasks into one request.

Share the effort in resource discovery and allocation among requests by separating resource allocations from request submissions.

Pack variable numbers of tasks into different requests, where the task number is a function of the destination resource’s computability.

Gracie is a computational grid software platform developed by Peking University (Li et al. 2008).

- **NIMROD** (messagelab.monash.edu.au/NimrodPortal) - A million questions or a few good answers? The **tool set**, called *Nimrod* - <http://messagelab.monash.edu.au/Nimrod>, automates the process of finding good solutions to demanding computational experiments. Importantly, Nimrod is more than a job distribution system; it **is a high level environment for conducting search across complex spaces**.

The number of jobs, and thus the parallelism, can be varied at run time, and the Nimrod scheduler places tasks on the available resources at run time. Users can **ask complex questions such as** “Which parameter values will minimize the output of my model?” This helps shield the user from the complexity of managing lots of independent jobs. In many cases it is possible to establish a new experiment in minutes.

- **IMAGER: A Parallel Interface to Spectral Line Processing** (Roberts & Crutcher 1997).

IMAGER is an interface to parallel implementation of imaging and deconvolution tasks of the Software Development Environment (SDE) of the NRAO. The

interface is based on the MIRIAD interface of the BIMA (Berkeley-Illinois-Maryland Association) array and it allows for interactive and batch operations - with such instruments as the VLA and the BIMA telescopes one could have spectral line data sets in excess of a gigabyte... Astronomers need access to fast processing to allow the analysis of such large data sets and to use different methods of ***non-linear deconvolution***. ***Radio synthesis data reduction*** has been one of the most computer intensive operations in observational astronomy. In the common case of radio spectral line observations, large numbers of frequency channels lead to large amounts of data. The analysis of spectral line data, in which each channel is independent from every other channel, is an embarrassingly parallel problem.

- ***Parallel-Processing Astronomical Image Analysis Tools for HST and SIRTf***

NASA applied information system researches, develops and implements ***several parallel-processing astronomical image-analysis tools for stellar imaging data from the Hubble Space Telescope and the Space Infrared Telescope Facility*** – see, e.g. Mighell (2005). This project combines the enabling image-processing technology of the Principal Investigator’s ***new digital PSF-fitting MATPHOT algorithm for accurate and precise CCD stellar photometry*** with enabling technology of Beowulf clusters which offer excellent cost/performance ratios for computational power. ***Data mining tools for quick-look stellar photometry and other scientific visualization tasks*** will also be written and used in order to investigate how such tools could be used at the data servers of NASA archival imaging data like the Space Telescope Science Institute.

4. SPECIALISED SOFTWARE

Here we present some selected specialised software for astronomical grid computing.

- ***AMEEPAR - Parallel processing for hyperspectral imaging***

The wealth of spatial and spectral information provided by ***hyperspectral sensors (with hundreds or even thousands of spectral channels)*** has quickly introduced new processing challenges. In particular, ***many hyperspectral imaging applications require a response in (near) real time*** in areas such as environmental modeling and assessment, target detection for military and homeland defense/security purposes, and risk prevention and response.

At the time being only a few parallel processing algorithms exist in the open literature – Plaza (2006a, 2006b).

To address the need for integrated software/hardware solutions in hyperspectral imaging, a highly innovative processing algorithms on several types of parallel platforms, including commodity (Beowulf-type) clusters of computers, large-scale distributed systems made up of heterogeneous computing resources, and specialized hardware architectures is developed.

Several parallel algorithms to analyze the AVIRIS (Airborne Visible/Infrared Imaging Spectrometer) data were implemented. Amongst them is

- The automated morphological extraction (AMEEPAR). This is one of the few available parallel algorithms that integrate spatial and spectral information – Wozniak (2009). Using 256 processors, AMEEPAR provided a 90% accurate debris/dust map of the full AVIRIS data in 10s, while the P-ATGP algorithm was able to detect the spatial location of thermal hot spots in the WTC area in only 3s.

On the Figure 3 is *hyperspectral image* collected by the NASA Jet Propulsion Laboratory's AVIRIS (Airborne Visible/Infrared Imaging Spectrometer) system *over the World Trade Center* (WTC) area in New York City on September 16, 2001. The data comprises *614 samples, 3675 lines, and 224 spectral bands, for a total size of 964MB.*

Figure 3 shows a false-color composite of a portion of the scene, in which the spectral channels at 1682, 1107, and 655nm are displayed as red, green, and blue respectively. Here, vegetation appears green, burned areas appear dark gray, and smoke appears bright blue due to high spectral reflectance in the 655nm channel.



Figure 3: A hyperspectral image of the World Trade Center.

- *GADGET-2 – a code for cosmological simulations of structure formation.*

Gadget is a freely available *code for cosmological N-body/SPH simulations* on massively *parallel computers* with distributed memory. GADGET uses an explicit communication model that is implemented with the standardized MPI communication interface. *The code can be run on almost all supercomputer systems* presently in use, including *clusters of workstations* or *individual PCs*. All details – in <http://www.mpa-garching.mpg.de/gadget/>.

GADGET computes gravitational forces with a hierarchical tree algorithm (optionally in combination with a particle-mesh scheme for long-range gravitational forces) and represents fluids by means of smoothed particle hydrodynamics (SPH). The code can be used for studies of isolated systems, or for simulations that include the cosmological expansion of space, both with or without

periodic boundary conditions. In all these types of simulations, **GADGET** follows the evolution of a self-gravitating collisionless N-body system, and allows gas dynamics to be optionally included. Both the force computation and the time stepping of **GADGET** are fully adaptive, with a dynamic range which is, in principle, unlimited.

GADGET can therefore be used to address *a wide array of astrophysically interesting problems*, ranging from *colliding and merging galaxies*, to the *formation of large-scale structure in the Universe*. With the inclusion of additional physical processes such as radiative cooling and heating, **GADGET** can also be used to *study the dynamics of the gaseous intergalactic medium*, or to address *star formation* and its regulation by *feedback processes*.

GADGET comes with a *number of small examples* that can be run to develop a feel for working with the simulation code:

A pair of colliding disk galaxies (collisionless).

A spherical collapse of a self-gravitating sphere of gas.

Cosmological formation of a cluster of galaxies (collisionless, vacuum boundaries).

Cosmological structure formation in a periodic box with adiabatic gas physics.

- *CRBLASTER : a fast parallel-processing program for cosmic ray rejection*

Many astronomical image-analysis programs are based on algorithms that can be described as being *embarrassingly parallel*, where *the analysis of one subimage generally does not affect the analysis of another subimage*. Yet few parallel-processing astrophysical image-analysis programs exist that can easily take full advantage of today's fast multi-core servers costing a few thousands of dollars. A major reason for the shortage of state-of-the-art parallel-processing astrophysical image-analysis codes is that the writing of parallel codes has been perceived to be difficult.

CRBLASTER - a new fast *parallel-processing image-analysis program does cosmic ray rejection* using van Dokkum's L.A.Cosmic algorithm. **CRBLASTER** (Mghell 2008) is written in C using the industry standard Message Passing Interface (MPI) library. For example processing a single 800×800 HST WFPC2 image takes 1.87 seconds using 4 processes on an Apple Xserve with two dual-core 3.0-GHz Intel Xeons; the efficiency of the program running with the 4 processors is 82%.

The code can be used as a software framework for easy development of parallel-processing image-analysis programs using embarrassing parallel algorithms: the biggest required modification is the replacement of the core image processing function with an alternative image-analysis function based on a single-processor algorithm.

- *N_body-sh1p - a parallel direct N_body code* (Gualandris et al. 2007)

This is an **Educational N-body integrator** with a shared but variable time step (the same for all particles but changing in time), using the Hermite integration scheme (Hut & Makino 2003) in *The art of Computer Science*. The source code has been *adapted for a parallel ring algorithm* using the MPI library.

Typical command line (generates : n24body.out)

```
% nbody_sh1p < n24body.in > n24body.out
```

Small *timing test* (performed by A. Gualandris) for 128, 256 and 512 particles *with up to 32 processors* on the *Blue (Boewulf) linux cluster* is presented at SARA.

- *Parallel processing algorithms*

A papers and books present the parallel processing including algorithms, architectures etc. Among the basic books is one of Parhami (1999). Cosmological problems, solved with parallel processing are presented in Bode & Bertshinger (1995) and in Ferrell & Bertshinger (1995).

5. MODELLING AND SIMULATIONS

In this part selected astronomical simulations, modelling and experiments are presented.

- *SkyMaker* (www.astromatic.net/software/skymaker)

SkyMaker is a program that simulates astronomical images. It accepts object lists in ASCII generated by the Stuff program to produce realistic astronomical fields. SkyMaker is part of the EFIGI development project. The authors are Emanuel Bertin and Pascal Fouque (Bertin 2009).

Cosmic simulation - a lot of things in <http://www.igstw.org>

Cosmic structure formation theory has passed test after test, *predicting how many galaxies will form, where they will form, and what type of galaxy they will be*. But for almost 20 years, its predictions about the central mass of dwarf galaxies have been wrong.

Worldwide, there are many teams working on their own versions; each attacks the problem from a different angle.

E.g. Governato et al. (2010) say: “Potentially, *this is a very big problem for the model*. It might imply that *the dark matter particle that we think is the correct one is not the correct one*, or *maybe that gravity works differently* than we think it does. So *this is a very fundamental problem for physics*.”

A simulation running on computer resources at NASA Advanced Supercomputing Division, the Arctic Region Supercomputing Center, and TeraGrid may have resolved this conundrum. A more realistic model of how stars form and die, incorporated into the existing cosmic structure formation theory. It turns out that *when a star near the galactic center explodes, a lot of interstellar gas is blown away from the center of the galaxy.* As a result, *less stars form at the center, because there is less gas.* When stars explode they can eject gas, but it is not clear enough how much it would impact galaxy formation...

To create the simulation about *a million computer hours were used*, which means that it would have taken close to a hundred years to run the same simulation on the average desktop.

Klypin's team (Klypin et al. 1999, Klypin et al. 2007) is exploring *the large-scale effects of energy released by young stars.*

Stars are forming, and *young stars release large amounts of energy into the gas that surrounds them.* That energy finds its way to larger scales, *affecting the motion of gas in the whole galaxy* – even the way it is being accreted in the galaxy.

Over time, scientific understanding of processes such as star formation has evolved, yielding new equations. The equations can in turn be used to refine the computational model.

Bertshinger (1995) presented the COSMICS codes. Mayer et al. (2008) presented the formation of disk galaxies and on <http://hydra.susx.ac.uk> HYDRA consortium presented its N_{body} hydrodynamical simulations.

- *Flip-flopping of black hole accretion disks*

The accretion disk of a black hole forms from gas attracted by the black hole's massive gravitational pull. For the last 20 years, astrophysicists have debated *whether the whirlpool-like motion of the accretion disk will periodically reverse motion, a behavior called 'flip-flop'?* According to a new *simulation* powered by *TeraGrid*, the *whirlpools of gas flip-flop as they are sucked into black holes* (Blondin & Pope 2009).

When *flip-flopping first turned up in a 1988 numerical simulation*, some scientists argued that it explains recurrent x-ray flares observed by the European X-Ray Observatory in 1985. But in subsequent years, although *some simulations showed flip-flop, others did not*, casting doubt on the existence of the phenomenon. The earlier work was criticized for a wide variety of reasons, but the chief among them was the lack of computer power and hence accuracy of the computation.

The most basic form of the equation used in the simulation was originally formulated by Fred Hoyle and Ray Lyttleton in 1939. The simulation shows that *the accretion disk reversed direction repeatedly*, confirming that *at least in this model of black hole accretion disks, flip-flop does occur.*

- ***Millennium Simulation Project***

The Millennium Simulation Project (www.mpa-garching.mpg.de/galform/virgo/millennium) is helping ***to clarify the physical processes underlying the buildup of real galaxies and black holes***. It has ***traced the evolution of the matter distribution***. The *Millennium Run* used more than ***10 billion particles*** to trace ***the evolution of the matter distribution in a cubic region of the Universe over 2 billion light-years*** on a side. It loaded the main principal supercomputer at the Max Planck Society's Supercomputing Centre in Garching, Germany for more than a month. By applying sophisticated modelling techniques to the 25 Tbytes of stored output, *Virgo scientists* have been able to ***recreate evolutionary histories both for the 20 million or so galaxies*** which populate this enormous volume ***and for the supermassive black holes*** which occasionally power quasars at their hearts. By comparing such simulated data to large observational surveys, one can clarify ***the physical processes underlying the buildup of real galaxies and black holes***. Amongst them are:

A journey through the simulated universe.

The dark matter distribution in the universe at the present time

The galaxy distribution in the simulation

on very large scales

for a rich cluster of galaxies

Slices of the dark matter distribution

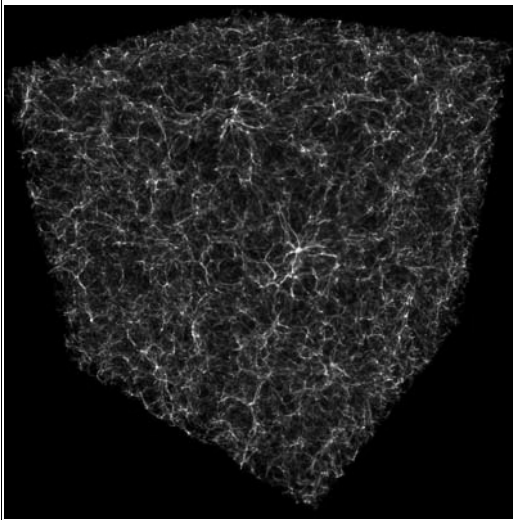
Halo and semi-analytic galaxy catalogues

How did the universe evolve into the structure we know?

The very early universe consisted of homogeneous gas with tiny perturbations. As the gas cooled over time, it collapsed under gravity into clumps and then galaxies. Bode et al. (2001) simulation is one example for large-scale simulations.

The researchers ran the largest detailed simulation of a cosmological structure to date. In the simulation, the region of study collapses from about 2 billion light years across to form a region of galaxy clusters only 25,000 light years across.

The distribution of galaxy clusters in the universe can actually help us to learn things about dark energy, how much matter there is in the universe, and how fast the universe is expanding...



The filaments indicate “*warm-hot intergalactic medium*”, or WHIM. WHIM constitutes about half of the universe's non-dark matter, yet we cannot see it very well. It emits and absorbs largely in the UV and soft X-ray portion of the electromagnetic spectrum, much of which is blocked by the earth's atmosphere.

The knot-like structures at the intersections indicate large groups and clusters of galaxies—important objects to study for understanding the fundamental properties of our universe such as the amount of matter, dark energy, and the expansion rate. The largest knot, near the center, is a galaxy cluster.

Figure 4: Example of the largest detailed simulation of a cosmological structure (see the text).

- **Dark Energy Survey** (www.darkenergysurvey.org)

To understand better dark energy and its implications on our current knowledge of matter, energy, space, and time, scientists will conduct the ***large-scale Dark Energy Survey (DES), starting in 2012*** at the Cerro Tololo Inter-American Observatory in Chile. Researchers will use the ***4-meter Blanco telescope***, equipped with the ***Dark Energy Camera***, to capture ***images of more than 300 million galaxies***. They expect to measure quantities related to pressure and energy density five times more precisely than currently possible. The startling discovery that ***the universe's expansion is accelerating*** has led scientists to postulate ***the existence of an outward-pushing dark energy***.

Astrophysicists are trying to learn more about the physics of the big bang, and the origin of the large-scale structure. Computational tools and resources are indispensable to pursuing these fundamental questions. To test and debug the image processing programs, researchers use Open Science Grid to create complex simulations of telescope signals and Teragrid to process these simulations. The scientists feed the known position, brightness, and shape of about 50 million galaxies and 5 million stars into software that renders simulated images of these objects.

- *Visualizations in planetarium show*
(www.amnh.org/rose/spaceshow/journey)

“Journey to the Stars” is a planetarium show that uses grid-generated simulations to take audiences deep under the surface of the sun. Viewers embark on a journey through the lifespan of stars and the origin of life. *Visualizations* of the universe *explain how stars first formed* and then *exploded* to produce the chemical elements that make life possible. The 25-minute journey culminates in *a flight to the center of the sun*. This was the most difficult sequence to accurately depict; the producers wanted to take viewers below the sun’s surface, through its convective layer, and down to its core to reveal the underlying mechanisms that create its powerful magnetic field.

Using *TeraGrid* supercomputers complex computer *models of the sun are build*. The *sun’s convection zone* based on a sphere of hydrogen and helium plasma is modelled. Based on that model, the *properties of hydrogen and helium*, and how they react to *the sun’s heat*, the *convective motions* is produced. The resulting *simulation allows planetarium visitors to take a peek at the sun’s convective zone*.

Sunspots are actually concentrations of strong magnetic fields that occasionally erupt above the sun’s surface. These provide *clues to the sun’s internal magnetic field*. Numerical *simulations allow us to look several thousand kilometers into the sun* and see how the surface structure we observe is related to convective motions that happen far below the visible surface. A *three-dimensional virtual domain* to replicate a region on the sun 31,000 miles in length and height and about 5,100 miles in depth. The domain was *large enough to fit an entire sunspot*, which has a typical size of 12,000 to 19,000 miles, and provided enough resolution *to view substructure on the scale of 20- to 30- miles*. The researchers then *used TACC’s Ranger supercomputer* to solve complex solar equations *for each of 268 million points spaced 20- to 30- miles* apart within the virtual domain. This involved processing approximately *a terabyte of data and took several days to run on 512 processors*.

Details could be found in

<http://physics.ucsc.edu/~joel/SimulationVisualisation.pdf> .

6. ASTROPHYSICAL APPLICATIONS AND PROJECTS

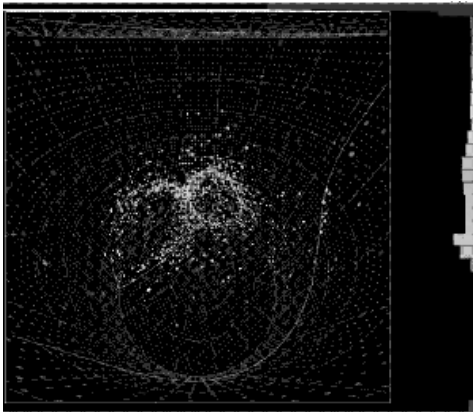
In this last part we shall make a short review of the basic astrophysical projects and applications.

- *A neutrino's journey* - the Tokai-to-Kamioka (T2K) experiment

Neutrinos are the introverts of the particle physics world. They travel through the universe largely unnoticed, except for the very rare interaction. Neutrinos are neutral – free of charge. That means that electricity and magnetism can’t draw

them out and force them to interact. We know that *there are three types of neutrinos* – *the electron neutrino* is the smallest, *the tau neutrino the largest*, with *the muon neutrino* caught in the middle. We also know that *when no one's looking, neutrinos go 'fuzzy' - an unobserved neutrino is all three types of neutrinos at the same time*. The likelihood that a scientist will see a particular type of neutrino changes periodically over time, *oscillating*. Three different constant angles determine the rate at which those probabilities oscillate. Scientists have already seen muon and tau neutrino oscillation, and measured two of the three angles. The *third angle, theta13*, is much trickier to measure, however, because it is *very small*. That is the goal of *the Tokai-to-Kamioka (T2K) experiment* in Japan.

Super-Kamiokande in essence is a giant cylindrical tank filled with 50,000 tons of pure water located 1,000 meters underground. The inside walls of the tank are covered with photomultiplier tubes, which detect any sparks of light that occur inside the tank. *When a neutrino strikes a neutron* in a water molecule's nucleus, the two particles interact via something called the Weak Force. The neutrino and neutron go in, and *out comes a proton and one of the three types of leptons (electron, muon, or tau, all of which are negatively charged)*.



The first T2K event seen in Super-Kamiokande. Each dot is a photomultiplier tube which has detected light. The two circles of hits indicate that a neutrino has probably produced a particle called a π^0 , perfectly in time with the arrival of a pulse of neutrinos from J-PARC. Another faint circle surrounds the viewpoint of this image, showing a third particle was created by the neutrino.

Figure 5: Some events in Super-Kamiokande during T2K experiment.

An electron neutrino will generate an electron, a muon neutrino a muon, and so on. The lepton is ejected, traveling at extremely high speeds. Although it does not travel as quickly as light does in a vacuum, it does travel faster than light does in water, *creating Cerenkov radiation* – the visual equivalent of a sonic boom. The *photomultiplier* tubes detect the scintillating light of the Cerenkov radiation, and in so doing, they *indirectly detect the neutrino*

Maltoni et al. (2003) presented a results of three-neutrino oscillations [20].

- *A virtual universe – GIMIC* (Frenk 2008) - www.deisa.eu/science/deci/projects2005-2006/GIMIC *and Millennium simulations*

With the aid of the grid, researchers are conducting *the largest-ever calculation to follow the formation of the dark haloes that seed galaxies*. To understand the properties of the galaxies themselves, *it is necessary to simulate how gas cools and forms stars in such haloes*.

Virgo is an international consortium of cosmologists that performs large numerical simulations of the formation of galaxies. Its *Millennium Simulation* is the largest ever calculation to follow the formation of the dark haloes that seed galaxies.

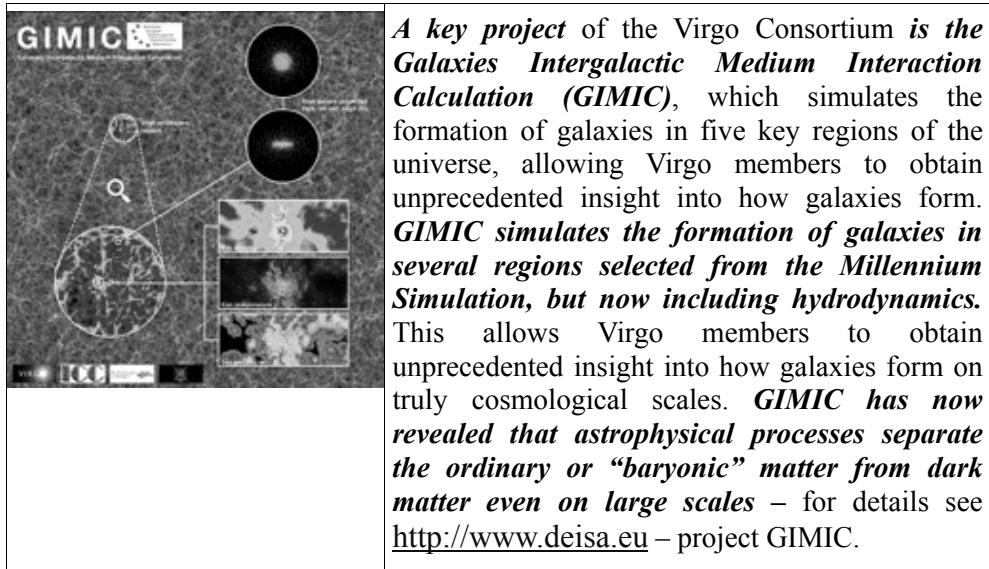


Figure 6: Titular page of the GIMIC project.

As gas collapses to make a galaxy, the *energy liberated by stars* can blow powerful winds which *heat the surrounding gas* and *pollute it with* the products of nuclear fusion in the centers of stars – *heavy elements*.

For example, the cosmological model that has been so successfully explored in the Millennium simulation assumes a particular kind of dark matter, the so-called *cold dark matter*. Since *the particles that would make up this cold dark matter have not yet been discovered* in the laboratory, we cannot be sure that our assumptions are correct.

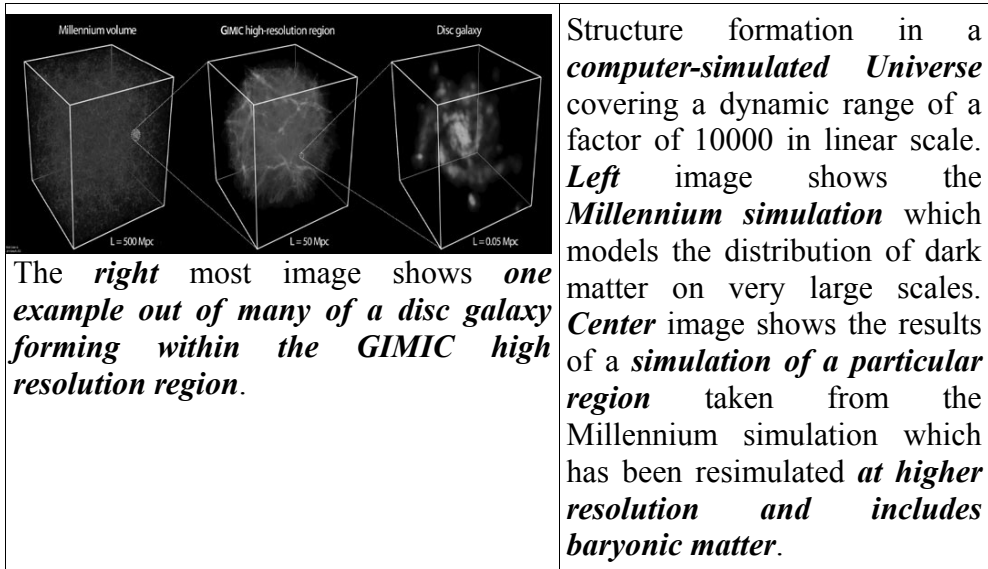


Figure 7: Examples of the computer simulated Universe.

Petaflop machines will simultaneously allow us to model the physics of galaxy formation with increasing realism and to explore alternative assumptions for the cosmological model, including the nature of the dark matter. Detail for the Millennium Simulation project could be found in www.mpa-garching.mpg.de/galform/virgo/millennium/ and in Bode et al. (2001).

- *Near Earth Objects* (neo.jpl.nasa.gov)

While scanning through images from the Sloan Digital Sky Survey, Stephen Kent noticed something unusual — a few extended streaks scattered among the millions of stars and galaxies (Kent et al. 2009). During its eight years of operation, the *SDSS obtained images* of more than a quarter of the night sky *and identified almost 400 million objects*. Although the survey was designed to detect stars and galaxies and determine their properties, it also helped identify *more than 100 NEOs*. To sift through the data for NEOs, Kent divided the SDSS data into fields, each containing about 1,000 candidate objects of all types. Using a special algorithm Kent bundled several hundred fields together and run the application on the grid.

The resulting 200 to 300 NEO candidates have been examined by eye to eliminate misclassifications and compile *the final catalog of around 100 NEOs, ranging in size from about 20 to 200 meters in diameter*.

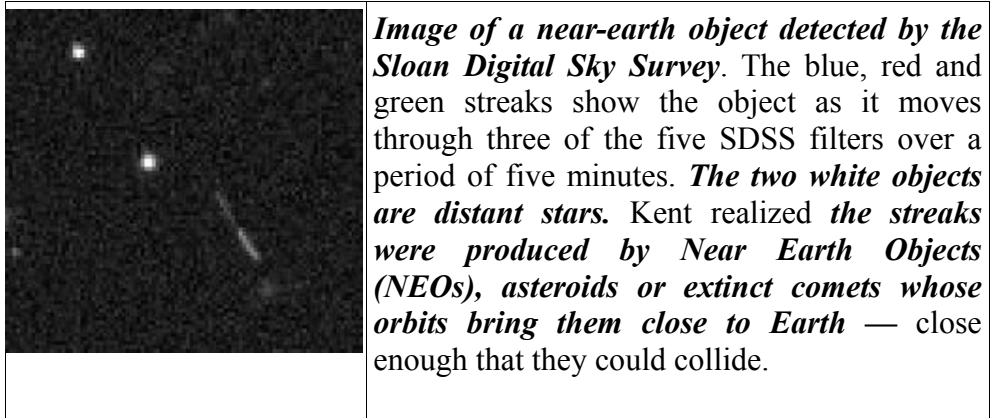


Figure 8: Detecting a Near Earth Objects.

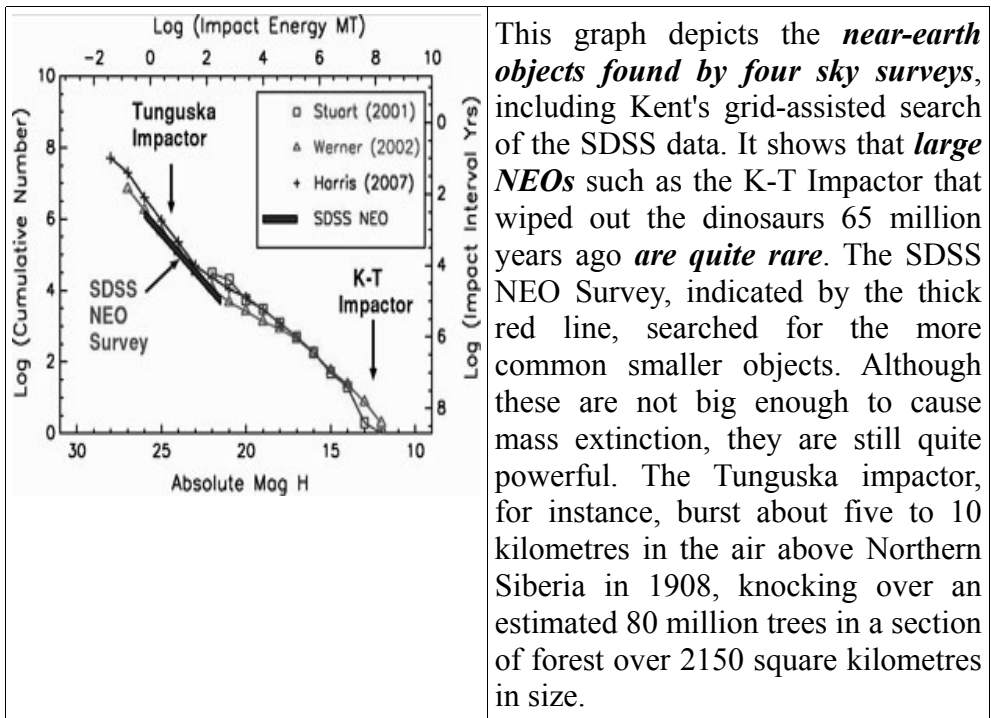


Figure 9: Near-earth objects found by four sky surveys.

Kent estimates **the total population of NEOs in the same size range to be around one million** and the estimation of **the Earth-NEO collision rate** — **about one every thousand years**.

- *Scientific Applications of AstroGRID-D* (www.gac-grid.org)



Figure 10: An extraction from the AstroGRID-D home_page.

The *Dynamo* scripts are designed to *use a large number of compute nodes and are an easy way to run many independent jobs on them*. The package was originally an application for a magnetohydrodynamic simulation, but it has been developed further so it can be used for general purposes.

Nbody6++ is a member of a family of high accuracy *direct N-body integrators used for simulations of dense star clusters, galactic nuclei, and problems of star formation*. It is a special version of Nbody-6 *optimised for massively parallel computers*. Some of the *most important applications* are *simulations of rich open and globular clusters* with a large number of binaries and *galactic nuclei with single and binary black holes*.

GEO600 Data Analysis - The **GEO600 gravitational wave detector** is contributing to the **Laser Interferometer Gravitational Wave Observatory (LIGO)**, an international effort to *directly measure the effects of gravitational waves*, as predicted in Einstein's theory of general relativity.



Clusterfinder

(www.gac-grid.org/project-products/Applications/ClusterFinder.html)

Clusterfinder is used within the AstroGrid-D project that *tests the deployment and performance of a typical data-intense astrophysical application*. The algorithm for any point in the sky depends only on the data from nearby points, so the data access and calculation can easily be parallelized, making Clusterfinder well-suited for production on the grid. The *scientific purpose* of Clusterfinder *is to reliably identify clusters of galaxies by correlating the signature in X-Ray images with that in catalogs of optical observations*.

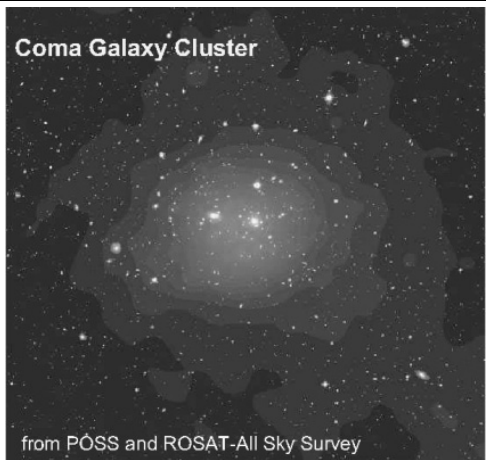


Figure 11: Coma cluster of galaxies.

Astronomy in recent years has observed a shift away from the study of individual or unusual objects to the statistics of large numbers of objects, observed at a variety of wavelengths across the electromagnetic spectrum, so that *the techniques developed for Clusterfinder are applicable to many cutting edge astronomic studies* – e.g. cosmology and galaxy clusters...

✦ **Cactus**. The **Cactus Computational Toolkit** is an open source problem solving environment designed for scientists and engineers. *Cactus is used to numerically simulate extremely massive bodies, such as neutron stars and black holes*. An accurate model of such systems requires a solution of the full set of Einstein's equations for general relativity.

✦ **Robotic Telescopes** –

(www.gac-grid.org/project-products/Software/RoboticTelescopes)

Global networks of robotic telescopes provide important advantages over single telescopes. Independent of daytime and weather, they can more efficiently perform

multiwavelength observations and continuous long-term monitoring, as well as react rapidly to transient events such as GRBs and supernovas. With the number of currently existing robotic telescopes a very powerful network could already be built - this is the idea of ***OpenTel*** - an Open Network for Robotic Telescopes. OpenTel provides the means for interconnecting single robotic telescopes to a global network for sharing observation time, observation programs and data. OpenTel is an open network. Open means open standards, open source and open for telescopes to join.

Grid technology provides an ideal framework. It provides solutions for the management of Virtual Organizations, grid resources, computational jobs and observation, data and metadata. The architecture is built on two technologies: the grid middleware of the Globus Toolkit and the Remote Telescope Markup Language (RTML) for the exchange of observation requests.

Robotic Telescopes of the Astrophysical Institute Potsdam (AIP) (www.gac-grid.de/project-products/Software/RoboticTelescopes.html)

With five robotic telescopes the AIP provides the first hardware to OpenTel. The five telescopes are RoboTel, STELLA-I and II, Wolfgang and Amadeus.

RoboTel is located at the AIP. It is a 0.8 m telescope equipped with a CCD camera for imaging and photometry. Besides its science core-program, half of the observation time is reserved for schools and universities. The remaining observation time is dedicated to testing of new instruments, software and methods for the STELLA-I and II telescopes.

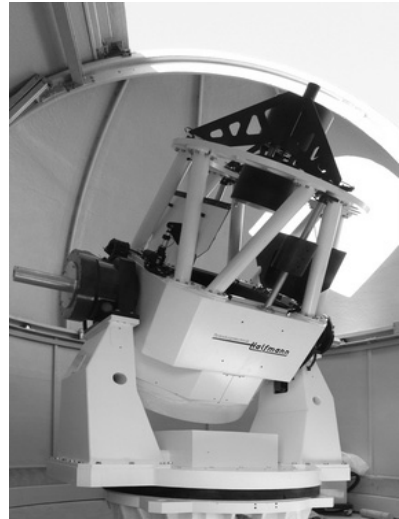


Figure 12: RoboTel - robotic telescope.

The ***STELLA robotic observatory*** is located at the Teide observatory in Tenerife, Spain. It consists of two 1.2 m telescopes, STELLA-I and STELLA-II. STELLA-I is equipped with a spectrograph and STELLA-II will be equipped with an imaging photometer. Scientific objectives are: Doppler imaging, the search for extrasolar planets, spectroscopic surveys and support observations for simultaneous observations with larger facilities.



Figure 13: The STELLA robotic observatory.

Wolfgang and Amadeus are located at the Fairborn Observatory in Arizona. They are two 0.75 m telescopes equipped with photomultipliers for photometry. The scientific objectives are the participation in multi-site observing campaigns and studies of variability timescales and life times of starspots, requiring monitoring of stars over periods of years.

Figure 14: Robotic telescopes Wolfgang and Amadeus.



ProC – The Planck Process Coordinator Workflow Engine. (www.gac-grid.de/project-products/Software/ProC_en.html)

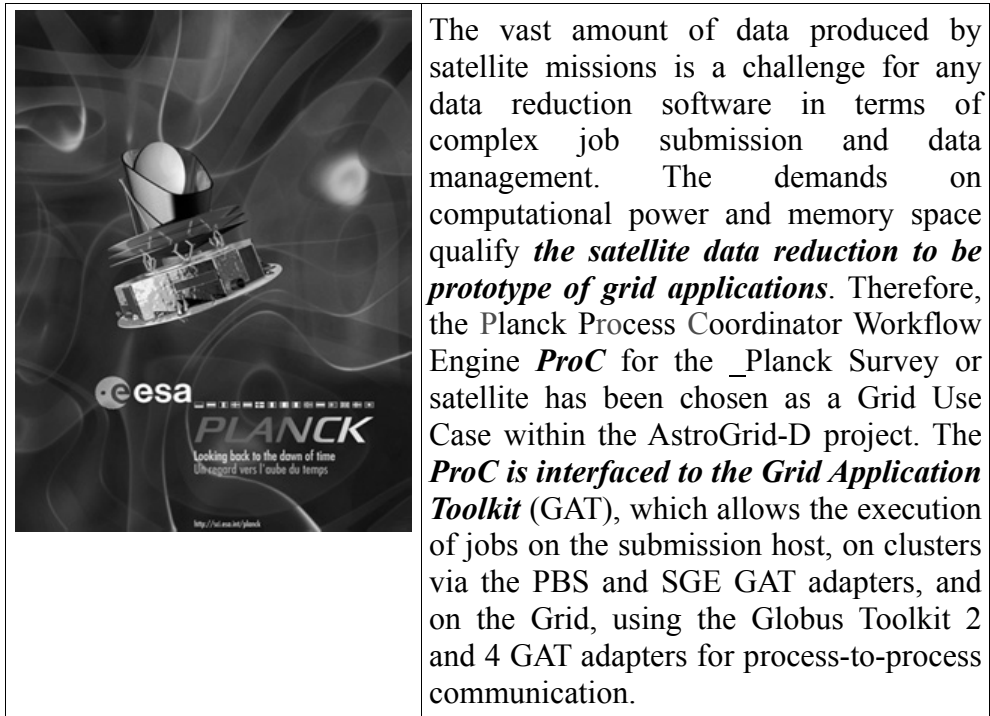


Figure 15: Titular page of the PLANK project.

Below is the block-scheme of the ProC interfaces to the Grid Application Toolkit (GAT) which via its set of adapters offers job execution on the local host, on worker nodes of a local cluster, and on remote Grid hosts. Details in <http://www.gac-grid.org/project-products/Software/ProC/proc.pdf>.

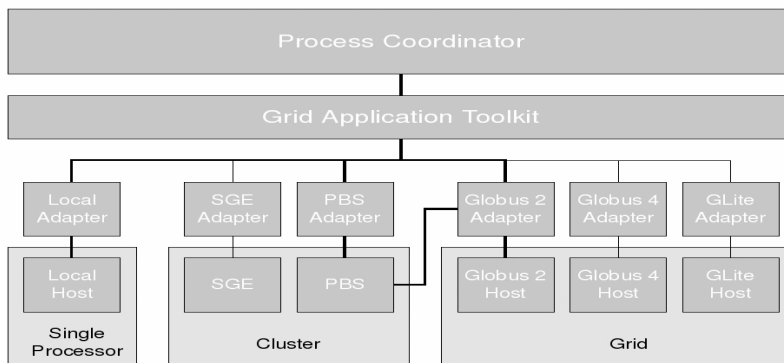


Figure 16: Block-scheme of the ProC interfaces.

- ***Black holes and their jets***

Jets of particles streaming from black holes in far-away galaxies operate differently than previously thought, according to a study published recently in Nature.

High above the flat Milky Way galaxy, ***blazars dominate the gamma-ray sky. As nearby matter falls into the black hole at the center of a blazar, “feeding” the black hole, it sprays some of this energy back out into the universe as a jet of particles.***

The recent study, which included data from more than 20 telescopes worldwide over a full year of observations, focused on one particular blazar jet, located in the constellation Virgo. Astronomers monitored it in many different wavelengths of light: gamma-ray, X-ray, optical, infrared and radio (blazars continuously flicker, and researchers expected continual changes in all types of light). As a result researchers observed a spectacular change in the jet’s optical and gamma-ray emission: a 20-day-long flare in gamma rays was accompanied by a dramatic change in the jet’s optical light.

Hayashida et al. (2010) turn suggests that the magnetic field lines must somehow help the energy travel far from the black hole before it is released in the form of gamma rays. The data suggest that ***gamma rays are produced not one or two light days from the black hole (as was expected) but closer to one light year.***

This simulation depicts ***a black hole with a dipole as a magnetic field.*** This system is sufficiently orderly to generate gamma ray bursts that travel at relativistic speeds of over 99.9% the speed of light.

The black hole pulls in nearby matter (yellow) and sprays energy back out into the universe in a jet (blue and red) that is held together by the magnetic field (green lines).

The simulation was performed on the Texas Advanced Computing Center resources via TeraGrid, consuming approximately ***400 000 service units.*** (Picture from the Internet).

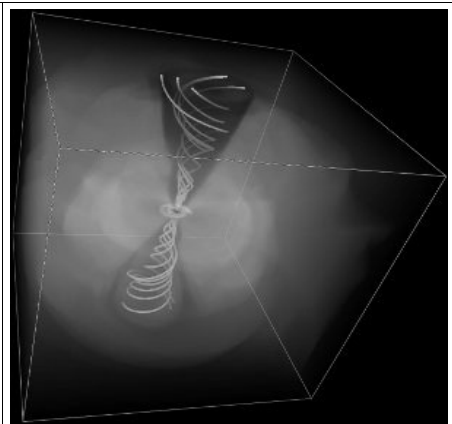


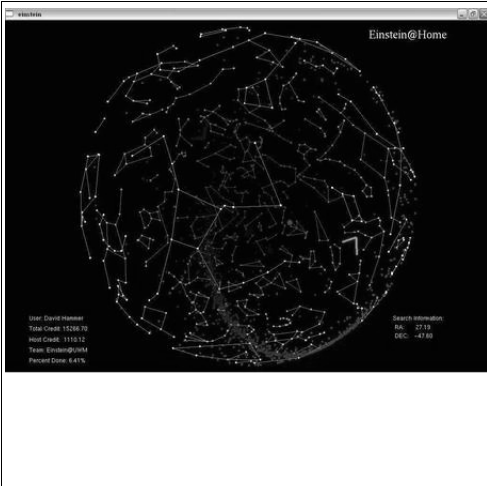
Figure 17: Simulation of the black hole and its jet in a magnetic field.

This new understanding of the inner workings and construction of a blazar jet requires a new working model of the jet’s structure, one in which the jet curves dramatically and the most energetic light originates far from the black hole.

- ***BOINC-GridRepublic Astronomy projects*** (www.grid-republic.org)

SETI@home

SETI (Search for Extraterrestrial Intelligence) is a scientific area whose goal is to ***detect intelligent life outside Earth***. One approach, known as radio SETI, uses radio telescopes to listen for narrow-bandwidth radio signals from space. Such signals are not known to occur naturally, so a detection would provide evidence of extraterrestrial technology. Radio telescope signals consist primarily of noise (from celestial sources and the receiver's electronics) and man-made signals such as TV stations, radar, and satellites. Modern radio SETI projects analyze the data digitally. More computing power enables searches to cover greater frequency ranges with more sensitivity. Radio SETI, therefore, has an insatiable appetite for computing power. See [Rosetta@home](#) and [Einstein@home](#) too.

	<h3>Einstein@Home</h3> <p>To process the vast amount of data that is being generated by GEO600 and other detectors, the Einstein@Home software framework was developed. It uses BOINC as underlying middleware to split the data analysis into small computational tasks that can be distributed to available computers on the Internet and executed on any commodity hardware.</p> <p>Figure 18: Screenshot from the Einstein@home.</p>
--	--

Einstein@Home is managing the execution of these tasks on a large set of computational resources distributed world wide. What appears to be a screen saver to the layman is in fact a supercomputer providing 70TFlops/s to the search for gravitational waves. Additional information – in [LHC@home](#) and [Milkyway@home](#) .

- ***BalticGrid-II astronomy application*** (www.balticgrid.org)

ElectroCap

This is a set of computer programs (Stellar Rates of Electron Capture) ***calculating electron capture rates with several nuclear structure models*** and modelling of core-collapse supernova requires nuclear input in terms of electron capture rates. Nuclear structure Information from the best available nuclear models is used to

calculate electron capture rates in the thermal environment of a collapsing star. Both the total and the partial electron capture rates *as well as* the *emitted neutrino spectra* are calculated for many nuclei and averaged for the stellar conditions. Both the total and the partial electron capture rates as well as the emitted neutrino spectra are loudspeaker for many nuclei and averaged for the stellar conditions. These rates and spectra are calculated for around 3000 nuclei and averaged according to the abundances at given stellar conditions.

SyntSpec - There are two demos (AVI files) in the WEB_page above. They have been presented for the first time in Catania, Italy, during the EGEE UF / OGF25, on 2-5.03.2009, at the BG-II demo stand "The Synthetic spectra modeling under GRIDCOM interface" (Mikolaitis & Tautvaišienė 2011).

- **GAJA mission** (sci.esa.int/science-e)

Gaia is an ambitious *mission to chart a three-dimensional map of our Galaxy*, the Milky Way, in the process revealing the composition, formation and evolution of the Galaxy. *Gaia will provide* unprecedented *positional and radial velocity measurements* with the accuracies needed to produce a stereoscopic and kinematic census *of about one billion stars in our Galaxy and throughout the Local Group*. This amounts to *about 1 per cent of the Galactic stellar population*. Combined with astrophysical information for each star, provided by *on-board multi-colour photometry*, these data will have the precision necessary to quantify the early formation, and subsequent dynamical, chemical and star formation evolution of the Milky Way Galaxy.


	<p>LAUNCH DATE: 2012 MISSION END: nominal mission end after 5 years (2017) LAUNCH VEHICLE: Soyuz-Fregat LAUNCH MASS: 2030 kg MISSION PHASE: Implementation ORBIT: Lissajous-type orbit around L2 OBJECTIVES: To create the largest and most precise three dimensional chart of our Galaxy by providing unprecedented positional and radial velocity measurements for about one billion stars in our Galaxy and throughout the Local Group.</p>
---	---

Figure 19: Gaja spacecraft.

Additional scientific products include detection and orbital classification of tens of thousands of extra-solar planetary systems, a comprehensive survey of objects ranging from huge numbers of *minor bodies in our Solar System*, through *galaxies in the nearby Universe*, to *some 500 000 distant quasars*. It will also provide a number of stringent new tests of general relativity and cosmology. Hobbs et al. (2008) presented astrometric solution in the light of GAJA mission.

- ***Girls Engaged in Math and Science (GEMS) program***
(gems.ncsa.illinois.edu)

The GEMS program was created in 1994 through a partnership of the Champaign Community Unit School District and NCSA to encourage local girls to consider a wide range of mathematics and science-oriented careers. Recently, ***GEMS has turned its focus to astronomy***, making use of the largest-ever digital astronomy database, the Sloan Digital Sky Survey (SDSS).

Over the course of the GEMS after-school program and summer camp, ***the girls investigate the universe***. They make ***multi-wavelength images of galaxies***, measure the ***colors of stars and quasars***, ***detect asteroids and black holes***, and even ***measure the expansion of the universe***—using the same data professional astronomers use.

The GEMS program is growing to include the use of emerging technologies and communication tools. The Girls on the Grid component of GEMS uses Access Grid technology to link girls in grades 6-12 to peers and leading women in science and mathematics world-wide.

Astronomy Programming: GEMS has recently partnered with the Department of Astronomy at the University of Illinois to offer a special Spring/Summer program, focused on introducing students to the rapidly expanding frontiers of digital astronomy. This program has been made possible through a grant from the National Aeronautics and Space Administration to Professor Robert Brunner.

- ***Distant Galaxy Search Applying Astrogrid-RU***

The first astronomical problem that has been experienced by IPI RAN together with the Special Astrophysical Observatory of RAS (SAO RAS) applying AstroGrid and Aladin is ***a distant radio galaxy search in the sky strip investigated in the “Cold” deep survey with the RATAN-600*** (large Russian radio telescope). Details are in the synthesis.ipi.ac.ru/synthesis/.

It used RC catalogue as a list of initial radio sources. One had to select optical sources with certain properties taken from DR 3 SDSS and crossmatched them with the RC catalogue. The result of the crossmatch may contain candidates for distant galaxies that should be analyzed further applying their images and Aladin capabilities. Below an example of a result image opened in Aladin is shown.

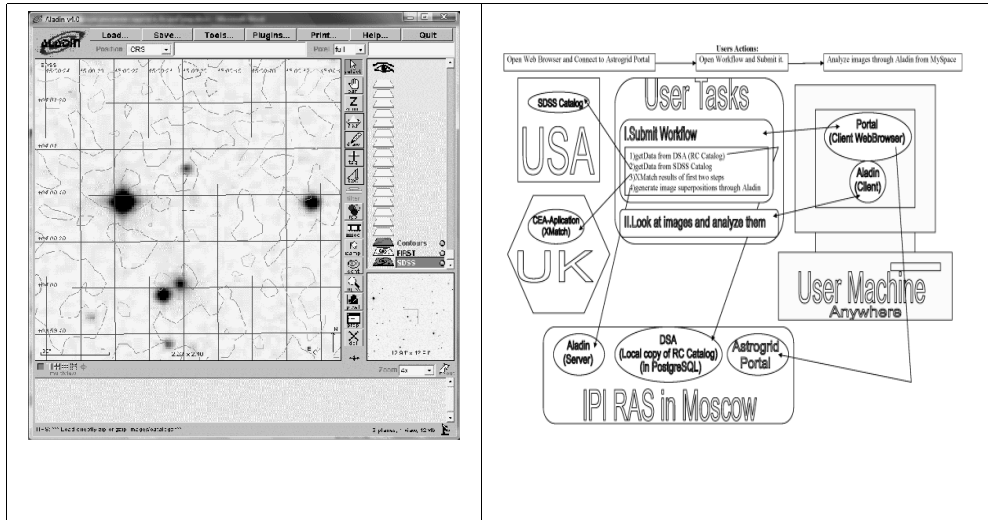


Figure 20: Screenshot from the WEB_page of Russian AstroGrid.

- **Grid in a cloud**

There are recently experiments with *running a grid inside a cloud in order to process massive datasets*, using test data drawn from something *astronomically large - data from the Gaia project* (see above). In order to execute the jobs and process the data, an in-house distributed computing framework was configured to run the *Astrometric Global Iterative Solution (AGIS)* (Hobbs et al. 2008), which runs a number of iterations over the data until it converges.

The system works as follows: Working nodes get a job description from the database, retrieve the data, process it and send the results to intermediate servers. These intermediate servers run dedicated algorithms and update the data for the following iteration. The process continues until the data converges. *The nature of the AGIS process makes it a good candidate to take advantage of cloud computing because:*

- The amount of data increases over the 5-year mission.
- Iterative processing results in 6-month Data Reduction Cycles.
- At current estimates, AGIS will run for 2 weeks every 6 months.

To process 5 years of data for 2 million stars, 24 iterations of 100 minutes each were done, which translates into 40 hours of running a grid of 20 Amazon Elastic Compute Cloud (EC2) high-CPU instances. *For the full billion-star project, 100 million primary stars will be analyzed, plus 6 years of data, which will require a total of 16,200 hours on a 20-node EC2 cluster.* The estimated cost calculated for the cloud-based solution is less than half the cost of an in-house solution, even when the additional electricity and system administration costs of the in-house

solution are not taken into account. A lot of possibilities of grid in a cloud are presented in Stanoevska-Slabova & Wozniak (2010).

- **Databases in Grid** (wwwas.oats.inaf.it/grid/)

"Databases in Grid" is a technological transfer project of INAF, co-funded by **INAF - UIT** (Ufficio di Innovazione Tecnologica) and **NICE s.r.l.**, the industrial partner for this project.

The project aims at making the Grid technology able to access Databases. A software prototype will be developed, fully compatible with standards defined in **EGEE** (Enabling Grids for E-science). The EGEE project is the UE established point of reference for what concerns the Grid technology. The so generated extended Grid, able to access Databases, is referred to with the term **G-DSE+QE**, where **G-DSE** (Grid-Data Source Engine) indicates the actual extension of the Grid middleware and **QE** (Query Element) is the new Grid element built on top of G-DSE and able to handle queries to be passed down to Databases in Grid.

- **Grid-enabled Astrophysics** – papers from workshop (Benacchio & Fabio 2006, Vuerli et al. 2008a, Vuerli et al. 2008b)

The volume collects the contributions to the **"Computational Grids for Italian Astrophysics: Status and Perspectives"** workshop, held at INAF headquarters, Rome, in **November 2005**. The workshop aimed at taking a snapshot of the status within the Italian astrophysical community of the development and usage of computational and data Grid(s) with particular reference to the status of the **Grid.it** and **DRACO** projects. The results obtained by the scientists participating in the two projects were summarised, **to evaluate the effectiveness of the porting of scientific applications on the Grid**, to recognise possible improvements, to foster cross-fertilisation with other sciences involved in Grid processing, **to bring the requirements of astronomers to the attention of middleware developers** and, maybe most important, **to disseminate results so as to allow fellow astronomers to make use of the Grid**. An attempt to define the roadmap for the future was also made, to understand which resources are needed and how to procure them. The workshop ideally closed a complete loop initiated in **July 2003**, when a first workshop called **"Grids in Astrophysics and the Virtual Observatory"** was organised. After two years of hard work and experience based on trial-and-error have shown that **Grids are actually useful and have found application in many fields of astrophysical research, ranging from theoretical simulations to data processing, from distributed databases to planning of space missions**.

- **GRID and the Virtual Observatory** – (wwwas.oats.inaf.it/grid/)

SI-GRG: GRID Research Group at INAF SI in Trieste (**SI-GRG**) **is doing research on Grid application and infrastructure development focused on Astronomical and Astrophysical problems**.

Virtual Observatories (VObs) aim at federating astronomical databases in a way that they are accessible in a uniform way irrespective of peculiarities characterizing each of them (format of data, requests syntax...). ***Virtual Observatories generally federate astronomical databases on a national basis***; they in turn join other national VObs to form wider alliances on an international basis - see Passian (2004). ***IVOA (International Virtual Observatory Alliance) is the worldwide alliance of all VObs***. The main goal of IVOA is to define a set of universally accepted standards in order to make possible a uniform vision of all federated Vobs – (Rixon 2109, Walton & Rixon 2008). ***IVOA also supplies tools and software layers to practically implement this uniformity***.

The concept of VObs therefore deals with data storage and retrieval. But astronomers need to process data once they have been retrieved and very often a considerable amount of computing power is requested to process such data. ***Because VObs offers astronomical data but not computing power a synergy between the VObs and the Grid appears as a natural choice*** (Schade 2001).

The interconnection of GRID and the VO is presented in Skoda (2009) and Taffoni et al. (2009).

DRACO Project (Datagrid for Italian Research in Astrophysics and Coordination with the Virtual Observatory) is a concept aiming at providing the scientific community with a distributed multi-functional environment allowing the use of specialized (observational, computing, storage) Grid nodes.

DRACO has been generated from a section of a project called ***"Enabling platforms for high-performance computational Grids oriented towards scalable virtual organizations"*** which has been approved and funded by the Italian Fund for Basic Research (FIRB). The ***astrophysical section of this project*** that terminated at the end of 2005 ***was composed of three demonstrators*** aiming at proving the feasibility of porting astrophysical applications within the framework of a national Grid infrastructure.

- ***HORIZON project*** (Wozniak 2009) - www.projet-horizon.fr

The HORIZON Project is built on several research teams in different institutes, namely the CEA/Sap in Saclay, the Observatories of Paris (LUTH and LERMA laboratories), Lyons and Marseilles. The scientific objective is specifically oriented towards studying galaxy formation in a cosmological framework. Its transverse and federative nature will however allow to develop in a few years high-level expertise in parallel and distributed (GRID) computing, in database management and virtual observations, in applied mathematics and computer science, and build in the same time a strong theoretical knowledge in astrophysics.

The consortium also studies the influence on the predictions of the resolution, the numerical codes, the self-consistent treatment of the baryons and of the physics included.

The main objectives are:

- the numerical study of galaxy formation in a cosmological framework using Grand Challenge applications;
- the development of advanced techniques in parallel computing and in applied mathematics to model galaxy formation and predict their observational signatures, as a function of physical parameters
- the gathering of renowned experts in computational astrophysics to share their software and expertise, and to optimize their access to national and international supercomputing facilities
- the delivery of a friendly access to state-of-the-art numerical simulations to the scientific community of both observers and theoreticians.

- ***Sifting for dark matter*** (ppd.fnal.gov/experiments/cdms/)

Think of grid computing as a sieve that physicists use to sift out those rare events that might just be signs of dark matter — the mysterious substance that appears to exert gravitational pull on visible matter, accelerating the rotation of galaxies.

FermiGrid, the campus grid of Fermilab and the interface to the Open Science Grid, ***recently helped researchers from the Cryogenic Dark Matter Search experiment to do just that: identify two possible hints of dark matter*** (Ahmed et al. 2010).

Dark matter has never been detected. And although the CDMS team cannot yet claim to have detected it, their findings have generated considerable excitement in the scientific community.

The experiment, managed by Fermilab and bringing together scientists from several universities, operates a set of detectors in the Soudan Mine in Minnesota, a half-mile underground.

Galaxies are mostly dark matter clouds: Over the evolution of the Universe, the dark matter particles formed structures, like water vapor forms clouds. These massive collections of dark matter particles became the galaxies. In fact, ***the gravitational force of dark matter helps hold galaxies together.*** The stars and interstellar dust are just icing on the cake!

WIMPs, a name for dark matter: We know that dark matter particles generate gravity, but they interact very weakly otherwise. In our conception they are ***weakly-interacting, but massive particles - WIMPs*** for short (Bykov et al. 2004).

- (c) **after observations:** the astronomer can browse the archive's holdings using customizable displays;
- (d) **prior to processing:** the astronomer can create his/her own scripts for reprocessing archival data;
- (e) **during processing:** optional viewers can be opened up to monitor, and possibly steer, the deconvolving process.

The processing is carried out using AIPS++, which employs the Glish scripting language to glue processing objects together. Its event-driven programming model (combined with the toolkit nature of AIPS++) makes it ideal for building automated processing in a distributed environment. *An important role for NCSA*, as a member of the AIPS++ development consortium, *is to enable support for parallel processing on a range of mildly to massively parallel machines*, with a particular emphasis on Linux clusters. The Intel Itanium-based supercluster that will be brought on-line at NCSA this year will handle the bulk of the imaging and deconvolution chores for the pipeline, while smaller machines will handle the serial processing.

References

- Ahmed, Z. et al.: 2010, *Science*, **327**, 1619 and <http://cdms.berkeley.edu/experiment.html> .
- Bertin, E.: 2009, *Mem.S.A.It.*, **80**, 422.
- Bertschinger, E.: 1995, *Astro-ph/9506075v1*, 20 p.
- Blondin, J., Pope, T.: 2009, *ApJ*, **700**, 95.
- Bode, P., Bertschinger, E.: 1995, *Astro-ph/9504040*, 18 p.
- Bode, P., Bahcall, N., Ford, E., Ostriker, J.: 2001, *ApJ*, **551**, 15.
- Bykov, A., Paerels, F., Petrosian, V.: 2004, *Space Sci. Rev.*, **134**, 141.
- Ferrell, R., Bertschinger, E.: 1995, *Astro-ph/9503042*, 8 p.
- Frenk, C.: 2008, *DEISA Newsletter*; **8**, 1.
- Governato, F., Brook, C., Mayer, L., Brooks, A., Rhee, G., Wadsley, J., Jonsson, P., Willman, B., Stinson, G., Quinn, T., Madau, P.: 2010, *Nature*, **463**, 203.
- Benacchio, L., Fabio Pasian F.(Eds.): 2006, *Grid-enabled Astrophysics*.
- Gualandris, A., Portegies Zwart, S., Tirado-Ramos A.: 2007, *PARCO*, **33**, 159.
- Hayashida, M. et al.: 2010, *Nature*, **463**, 919.
- Hobbs, D., Lindegren, L., Holl, B., Lammers, U., O'Mullane, W.: 2008, *IAU Symp.* No. **248**, 268.
- Hut, P., Makino M.: 2003, <http://www.artcompsci.org>.
- Kent, S., Schaffer, M., Szalay, A., Gray, J., Ivezić, Z., Quinn, T., Richmond, M., Knapp, J., Schneider, D.: 2009, *BAAS*, **41**, 707.
- Klypin, A., Gottlober, S., Kravtsov, A., Khokhlov, A.: 1999, *ApJ*, **516**, 530.
- Klypin, A., Gottlober, S., Yepes, G., Kravtsov, A.: 2007, *Wurzburg, september workshop, presentation*.
- Lawrence, A.: 2002, *Proc. SPIE*, **4846**, 6.
- Li, H., Yu, H., Li, X.: 2008, *MTAGS08*, 24.
- Maltoni, M., Schwetz, T., Tortola, M., Valle, J.: 2003, *Phys.Rev. D*, **68**, 113010.1.
- Mayer, L., Governato, F., Kaufmann, T.: 2008, *Advanced Science Letters*, **1**, 7.
- Mighell, K.: 2005, *MNRAS*, **316**, 861.

- Mighell, K.: 2008, *Proc SPIE*, **7019**, 70191F.1.
- Mikolaitis, Š., Tautvaišienė, G.: 2011, *EAS Publications Series*, **45**, 413.
- Parhami, B.: 1999, Plenum Press New York, 532 p.
- Passian, F.: 2004, *Mem.S.A.It. Suppl.*, **4**, 86.
- Plante, R., Mehringer, D., Guillaume, D., Crutcher, R.: 2001, *ASP Conf. Ser.*, **238**, 279.
- Plaza, A.: 2006a, *J. of Parallel and Distrib. Comp.*, **66**, 345.
- Plaza, A.: 2006b, *Lecture Notes in Computer Science*, **3391**, 888.
- Rixon, G.: 2009, *Mem.S.A.It.*, **80**, 584.
- Roberts, D., Crutcher, D.: 1997, *VI ASP Conference Series*, **125**, 120.
- Schade, D.: 2001, in *First Astro-Grid workshop*, January 29-30, (2001).
- Skoda, P.: 2009, *Mem.S.A.It.*, **80**, 484.
- Stanoevska-Slabova, K., Wozniak, T.: 2010, in *Grid and Cloud computing*. Eds.:
Stanoevska-Slabova K., Wozniak T., Ristol S. p. 47.
- Taffoni, G., Vuerli, C., Passian, F.: 2009, *Mem.S.A.It. Suppl.*, **13**, 147.
- Vuerli, C., Passian, F., Taffoni, G.: 2008, *ASP conf. ser.*, **394**, 281.
- Vuerli, C., Taffoni, G., Pasian, F.: 2009, *Mem.S.A.It.*, **80**, 477.
- Walton, N., Rixon, G.: 2008, *Garching workshop april'2008*.
- Wozniak, H.: 2009, *Mem.S.A.It.*, **80**, 357.

LONG TERM PRECESSION MODEL

JAN VONDRÁK

*Astronomical Institute
Academy of Sciences of the Czech Rep., Prague, Czech Republic
E-mail: vondrak@ig.cas.cz*

Abstract. Precession is the secular and long-periodic component of the motion of the Earth's spin axis in space, exhibiting a motion of about $50''$ /year around the pole of the ecliptic. All precession models, used in astronomy so far (Newcomb, IAU 1976, IAU 2006) approximate this motion by polynomial expansions of time. These models are however valid, with very high accuracy, only in the close vicinity of the reference epoch J2000.0. For epochs that are more distant (several centuries), this approximation quickly deviates from reality. As a reaction to this problem, a new model, comprising very long-period terms fitted to a numerical integration of the motion of solar system bodies, has recently been developed by the present author in cooperation with N. Capitaine (France) and P. Wallace (United Kingdom) and published in the European journal *Astronomy and Astrophysics*. A shortened description of the new model, including an evaluation of its accuracy, is presented.

1. INTRODUCTION

The transformation between the terrestrial and celestial reference frame is given by five Earth Orientation Parameters (see Fig. 1). They define the position of the spin axis in the Earth's body (polar motion), the angle of proper rotation (Universal Time) and the position of the spin axis in space (precession-nutation). The position of the axis of rotation of the Earth exhibits, under the dominant influence of the Moon and the Sun, a rather complicated motion in space. Its very long-periodic part, precession, is the slow motion of the pole of Earth's rotation P around the pole of the ecliptic C . The angle between the two poles (obliquity) is approximately constant, today roughly equal to 23.5° . Precession was known already to Hipparchos, since it causes the growth of ecliptical longitudes of the stars by about $50''$ per year; the spin axis makes one revolution in about 26 thousand years (Platonic year). This motion is in reality rather complicated: the pole of the ecliptic itself is not fixed with respect to the stars – it exhibits precession of the ecliptic (formerly called planetary precession). It is dominantly caused by the attractive forces of all bodies of the solar system on the motion of the Earth around the barycenter of the solar system. The axis of rotation of the Earth exhibits a motion around the moving pole of ecliptic under the torques exerted by the Moon, Sun, and planets on the rotating oblate Earth, precession of

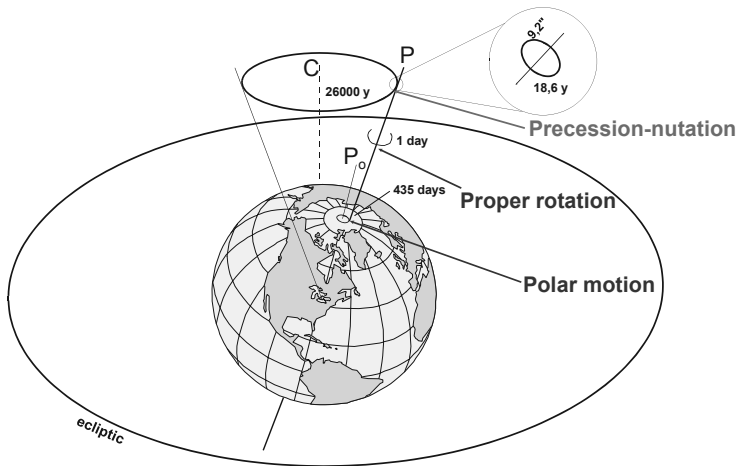


Figure 1: Earth Orientation Parameters.

the equator (formerly luni-solar precession). Neither the obliquity, nor the rate of precession are strictly constant.

All precession models used so far are expressed in terms of polynomial development of time. The most recent model IAU 2006 (Capitaine et al. 2003) is very accurate, but usable only for a limited time interval (several centuries around the epoch J2000); its errors rapidly increase with longer time spans. In reality, precession represents a very long-periodic process, whose periods reach hundreds of centuries. This can be demonstrated by comparison with the numerically integrated equations of motion of the Earth in the solar system and its rotation (Vondrák et al. 2009, 2011a). Fig. 2 (here reproduced from paper by Vondrák et al. 2009) displays the motion of the axis of rotation of the Earth during about 1.5 precession cycles, as given by long-term numerical integration (LT integration) and different analytical models – Lieske et al. (1977), Simon et al. (1994), and two models by Capitaine et al. (2003): one computed from the expansions of precession angles ζ_A , θ_A , and one from the expansions of direction cosines X_A , Y_A . The position of the axis of rotation at the basic epoch J2000.0 is the point $X = Y = 0$, pole of the ecliptic is located in the center of the figure. The models are not graphically distinguishable in the interval $\pm 50\text{cy}$ around J2000, but they start to differ significantly outside the interval $\pm 100\text{cy}$.

We assume that precession includes only periods longer than 100 centuries; shorter ones represent nutation. Our aim was to find relatively simple expressions of different precession parameters, with accuracy comparable to the IAU 2006 model near the epoch J2000.0, and lower, slowly degrading accuracy outside the interval ± 1000 years (up to several minutes of arc at the extreme epochs ± 200 thousand years). The paper describing the new model in detail has recently been published by Vondrák et al. (2011b). Below is given an abridged description of the model, followed by a new assessment of its accuracy and comparison with other models.

LONG TERM PRECESSION MODEL

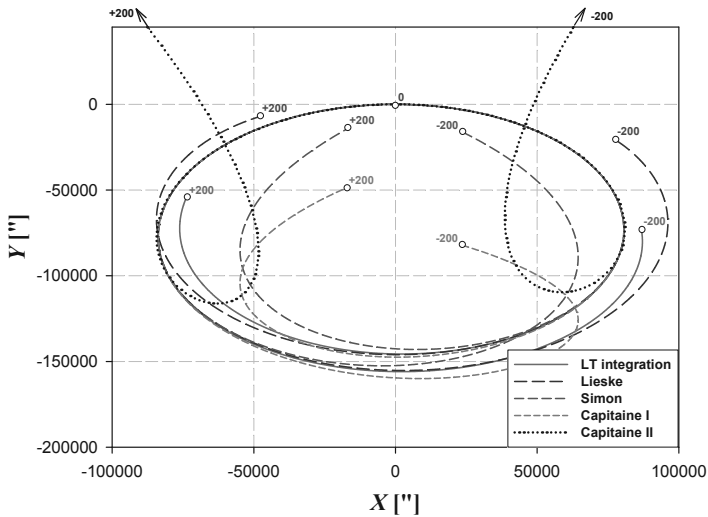


Figure 2: Different models of precession in the interval ± 200 cy around J2000.0, and comparison with numerical integration.

2. NUMERICAL INTEGRATION, LONG TERM EXPRESSIONS

We used the numerically integrated values of the following four parameters

- the precession of the ecliptic $P_A = \sin \pi_A \sin \Pi_A$, $Q_A = \sin \pi_A \cos \Pi_A$, calculated with the Mercury 6 package by Chambers (1999), considering only the eight ‘classical’ planets, and
- the general precession/obliquity p_A, ϵ_A , computed by Laskar et al. (1993),

to calculate time series for all other precession parameters in the interval ± 200 thousand years from J2000.0, with 100-year steps. The numerical integrations depend on the initial conditions that are based on observations. In the first case, these are the optical and radar observations of the planets, in the second one the observations of the Earth orientation parameters by VLBI. Namely the latter led to small corrections that we had to apply to Laskar’s values of p_A, ϵ_A (due to a slightly different value of dynamical ellipticity of the Earth, the rate of change of the dynamical form factor J_2 , planetary tilt effects and the tidal effects, neglected in Laskar’s solution).

To estimate the accuracy of the numerical integrations above, we tested them against the values obtained independently and found that the differences from other solutions at both extreme epochs do not exceed the level of 20 arcseconds. The neglected perturbations by asteroids have recently been shown by Aljabaee and Souchay (2012) to be very small - peak to peak quasi-periodic effects in Earth’s inclination are smaller than $0.05''$, the periods are typically shorter than 100 years. Thus we concluded that the accuracy of the numerical integration, including both numerical errors and imperfections of the models used, is sufficient for our purpose.

The central part of the data (± 1000 years from the epoch J2000.0) was replaced by IAU 2006 values to make the new model consistent with the recent model accepted by

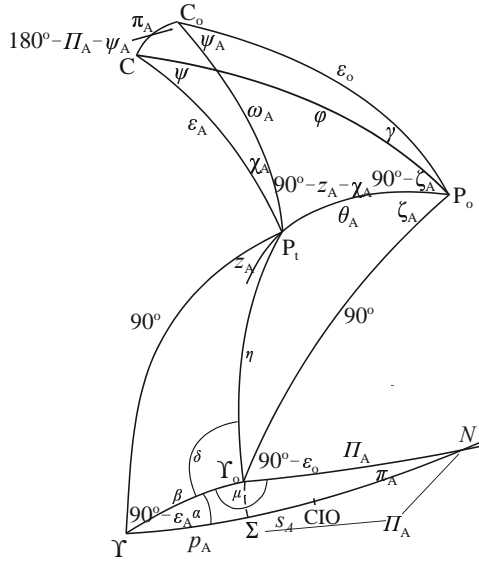


Figure 3: Precession parameters.

the IAU. From the values of the precession parameters P_A , Q_A , p_A and ϵ_A , different precession parameters were calculated in the interval ± 200 millennia from J2000.0 with 100-year steps, solving several spherical triangles depicted in Fig. 3, in which C_o and C denote the positions of the pole of ecliptic at the epochs J2000.0 and T , respectively, P_o , P_t are the poles of rotation of the Earth and Y_o , Y vernal points at the same epochs, and CIO stands for Celestial Intermediate Origin.

We proceeded from the bottom of the figure upwards and obtained first the auxiliary angles α, β, μ from the spherical triangle $Y Y_o N$, then the angles η, δ by solving the triangle $Y Y_o P_t$, and, from triangle $Y_o P_t P_o$, we got the precession angles θ_A, ζ_A . From the triangle $P_o P_t C_o$ then followed the precession parameters ω_A, ψ_A and from the triangles $P_t C C_o$, $P_o P_t C_o$ the parameters χ_A, z_A .

Instead of precession angles θ_A, z_A, ζ_A we used direction cosines $X_A = \sin \theta_A \cos \zeta_A$, $Y_A = -\sin \theta_A \sin \zeta_A$, $V_A = \sin \theta_A \sin z_A$, $W_A = \sin \theta_A \cos z_A$; the angles θ_A, ζ_A and z_A exhibit large discontinuities (of about 94° for θ_A , 180° for ζ_A and z_A) at irregular intervals: there is also a change of sign approximately each 26,000 years. This makes the long-term analytical approximation of these precession angles extremely difficult, while the direction cosines are continuous.

The time series of all parameters calculated above were then approximated by a cubic polynomial plus up to 14 long-periodic terms of the general form (T is the time in centuries from J2000.0, P_i is the period and n the number of periodic terms)

$$a + bT + cT^2 + dT^3 + \sum_{i=1}^n (C_i \cos 2\pi T/P_i + S_i \sin 2\pi T/P_i), \quad (1)$$

so that the fit is best around J2000.0. This was assured by choosing appropriate

weights (equal to 10^4 in the central part and to $1/T^2$ outside this interval). The periods were found beforehand using the Vaníček's method (Vaníček 1969), based on the least-squares method, as modified by Vondrák (1977), and verified with the ones found by Laskar et al. (1993, 2004) from much longer time series. Weighted least-squares estimation (with fixed values of the periods) was then used to determine the cosine/sine amplitudes of individual periodic terms.

We derived the long-term expressions of the following precession parameters (some of them being precession angles, some direction cosines, expressed in terms of certain precession angles):

- precession angles: $p_A, \varepsilon_A, \omega_A, \psi_A, \chi_A, \varphi, \gamma, \psi$;
- direction cosines: $P_A = \sin \pi_A \sin \Pi_A, Q_A = \sin \pi_A \cos \Pi_A, X_A = \sin \theta_A \cos \zeta_A, Y_A = \sin \theta_A \sin \zeta_A, V_A = \sin \theta_A \sin z_A, W_A = \sin \theta_A \cos z_A$.

We also derived the expression for the CIO locator (the part that is due to precession), the small angular distance between the points Σ and CIO, s_A . All these angles are depicted in Fig. 3.

3. EXAMPLES

We present here, as typical examples, the long-term expressions of direction cosines of the pole of the ecliptic C, P_A, Q_A , and of the Earth's spin axis P_t, X_A, Y_A (both expressed in arcseconds):

The long-term expressions for the precession of the ecliptic are given as

$$\begin{aligned}
 P_A &= 5851.607687 - 0.1189000T - 0.00028913T^2 + 101 \times 10^{-9}T^3 + \sum_P, \quad (2) \\
 Q_A &= -1600.886300 + 1.1689818T - 0.00000020T^2 - 437 \times 10^{-9}T^3 + \sum_Q,
 \end{aligned}$$

where the cosine/sine amplitudes of the periodic parts \sum_P, \sum_Q are given in Tab. 1. Names of some of the terms in column 1 come from Laskar et al. (1993, 2004). The comparison of the long-term model of the precession of the ecliptic, P_A (top), Q_A

Table 1: Periodic terms in P_A, Q_A

term	C/S	$P_A['']$	$Q_A['']$	$P[\text{cy}]$
σ_3	C_1	-5486.751211	-684.661560	708.15
	S_1	667.666730	-5523.863691	
$-s_1$	C_2	-17.127623	2446.283880	2309.00
	S_2	-2354.886252	-549.747450	
	C_3	-617.517403	399.671049	1620.00
$-s_6$	S_3	-428.152441	-310.998056	
	C_4	413.442940	-356.652376	492.20
	S_4	376.202861	421.535876	
	C_5	78.614193	-186.387003	1183.00
	S_5	184.778874	-36.776172	
	C_6	-180.732815	-316.800070	622.00
	S_6	335.321713	-145.278396	
	C_7	-87.676083	198.296701	882.00
	S_7	-185.138669	-34.744450	
	C_8	46.140315	101.135679	547.00
	S_8	-120.972830	22.885731	

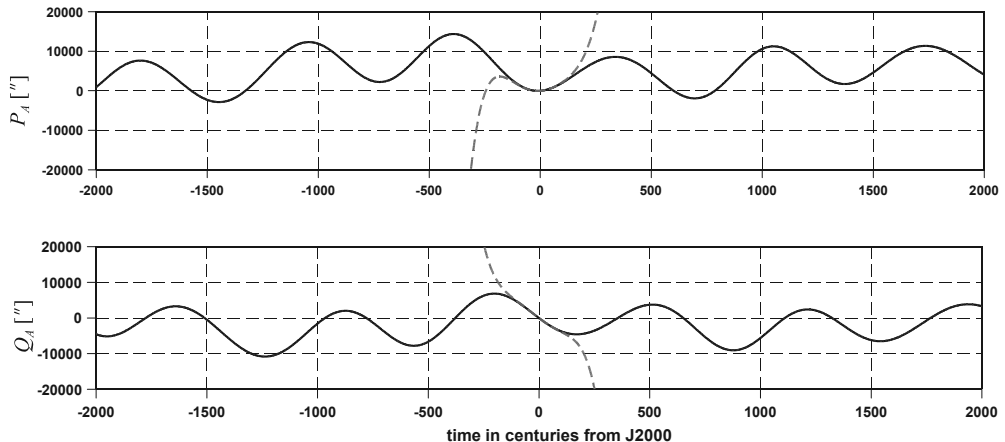


Figure 4: Long-term model of precession parameters P_A , Q_A – new model (dotted), integrated values (solid), and IAU 2006 (dashed).

(bottom) with integrated values and the IAU 2006 model is depicted in Fig. 4. The model and integrated values are so close that they are graphically indistinguishable. One can readily see that the expressions for P_A , Q_A of IAU 2006 model quickly deviate from the former ones. The pole of the ecliptic roughly describes a clockwise circular motion with the amplitude of about 1.5° and period of 71 millenia.

The expressions for the precession of the equator are

$$\begin{aligned} X_A &= 5453.282155 + 0.4252841T - 0.00037173T^2 - 152 \times 10^{-9}T^3 + \sum_X, \quad (3) \\ Y_A &= -73750.930350 - 0.7675452T - 0.00018725T^2 + 231 \times 10^{-9}T^3 + \sum_Y, \end{aligned}$$

where the cosine/sine amplitudes of the periodic parts \sum_X , \sum_Y are displayed in Tab. 2. The comparisons of the long-term models of precession angles X_A (top) and Y_A (bottom) are shown in Fig. 5. Again, the model is graphically indistinguishable from the numeral integration. The pole of rotation describes a clockwise motion around the pole of the ecliptic, once per 26 millenia, its radius quasi-periodically changes between 22.5° and 24.2° , with period of about 71 millenia. The speed of the motion (general precession) is also not constant. The behavior of other precession parameters is similar to these.

4. PARAMETRIZATION OF PRECESSION MATRIX

Different combinations of the precession angles derived above can be used to compute precession matrix \mathbf{P} , necessary to transform coordinates of celestial bodies from the fundamental epoch J2000.0 to any epoch T :

- ‘Lieske’ parametrization (Lieske et al. 1977):

$$\mathbf{P} = \mathbf{R}_3(-z_A) \cdot \mathbf{R}_2(\theta_A) \cdot \mathbf{R}_3(-\zeta_A),$$

Table 2: Periodic terms in X_A, Y_A

term	C/S	$X_A['']$	$Y_A['']$	$P[\text{cy}]$
p	C_1	-819.940624	75004.344875	256.75
	S_1	81491.287984	1558.515853	
$-\sigma_3$	C_2	-8444.676815	624.033993	708.15
	S_2	787.163481	7774.939698	
$p - g_2 + g_5$	C_3	2600.009459	1251.136893	274.20
	S_3	1251.296102	-2219.534038	
$p + g_2 - g_5$	C_4	2755.175630	-1102.212834	241.45
	S_4	-1257.950837	-2523.969396	
$-s_1$	C_5	-167.659835	-2660.664980	2309.00
	S_5	-2966.799730	247.850422	
$-s_6$	C_6	871.855056	699.291817	492.20
	S_6	639.744522	-846.485643	
$p + s_4$	C_7	44.769698	153.167220	396.10
	S_7	131.600209	-1393.124055	
$p + s_1$	C_8	-512.313065	-950.865637	288.90
	S_8	-445.040117	368.526116	
$p - s_1$	C_9	-819.415595	499.754645	231.10
	S_9	584.522874	749.045012	
$2p + s_3$	C_{10}	-538.071099	-145.188210	1610.00
	S_{10}	-89.756563	444.704518	
	C_{11}	-189.793622	558.116553	620.00
	S_{11}	524.429630	235.934465	
	C_{12}	-402.922932	-23.923029	157.87
	S_{12}	-13.549067	374.049623	
$2p + s_3$	C_{13}	179.516345	-165.405086	220.30
	S_{13}	-210.157124	-171.330180	
	C_{14}	-9.814756	9.344131	1200.00
	S_{14}	-44.919798	-22.899655	

- ‘Capitaine’ parametrization (Capitaine et al. 2003):

$$\mathbf{P} = \mathbf{R}_3(\chi_A) \cdot \mathbf{R}_1(-\omega_A) \cdot \mathbf{R}_3(-\psi_A) \cdot \mathbf{R}_1(\varepsilon_o),$$

- ‘Williams-Fukushima’ parametrization (Fukushima 2003):

$$\mathbf{P} = \mathbf{R}_1(-\varepsilon_A) \cdot \mathbf{R}_3(-\psi) \cdot \mathbf{R}_1(\varphi) \cdot \mathbf{R}_3(\gamma),$$

in which $\mathbf{R}_i(\alpha)$ denotes the rotation matrix around i -th axis by angle α . In the classical ‘Lieske’ parametrization the precession angles z_A, θ_A, ζ_A can be easily expressed in terms of direction cosines X_A, Y_A, V_A, W_A . Quite naturally, all these methods should theoretically lead to the same result.

5. ESTIMATION OF MODEL ACCURACY, COMPARISON WITH OTHER MODELS

In Vondrák et al. (2011b) the accuracy was estimated using a simple expression based on the average uncertainty of all parameters (derived from the fit to integrated values) and weights at different epochs. The uncertainty at epoch T was computed as $\sigma_o/w(T)$, where $\sigma_o = 0.365''$ was the average unit-weight uncertainty estimated from the fit of all precession parameters, and $w(T)$ the weight defined in Section 2.

Here a rigorous formula is used, based on the full variance-covariance matrix. Thus all correlations existing between estimated parameters are taken into account. For each of the parameters we first estimate the unit-weight uncertainty σ_o (from the fit

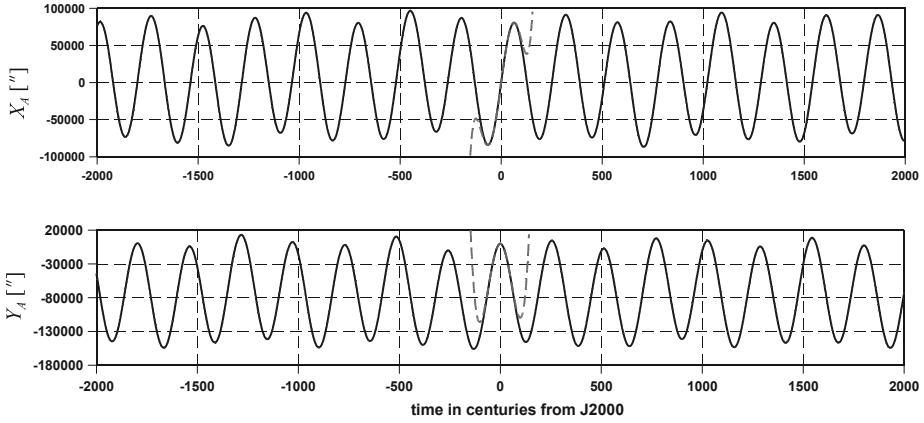


Figure 5: Long-term model of precession parameters X_A , Y_A – new model (dotted), integrated values (solid), and IAU 2006 (dashed).

to numerically integrated values) and then the uncertainty at the epoch T as

$$\sigma^2(T) = \sigma_o^2 \sum_{i=1}^{n+4} \sum_{j=1}^{n+4} f_i f_j Q_{ij}, \quad (4)$$

where $f_1 = 1$, $f_2 = T$, $f_3 = T^2$, $f_4 = T^3$, $f_5 = \cos(2\pi T/P_1)$, $f_6 = \sin(2\pi T/P_1)$..., and Q_{ij} is the element of the matrix inverse to the matrix of normal equations. The result is depicted in Fig. 6, where the accuracy of each estimated parameter is given and compared with the one from Vondrák et al. (2011b).

It is clear from the figure that our previous estimate was too conservative – the rigorous estimate yields much smaller uncertainties for all parameters, in some cases as much as two orders of magnitude lower.

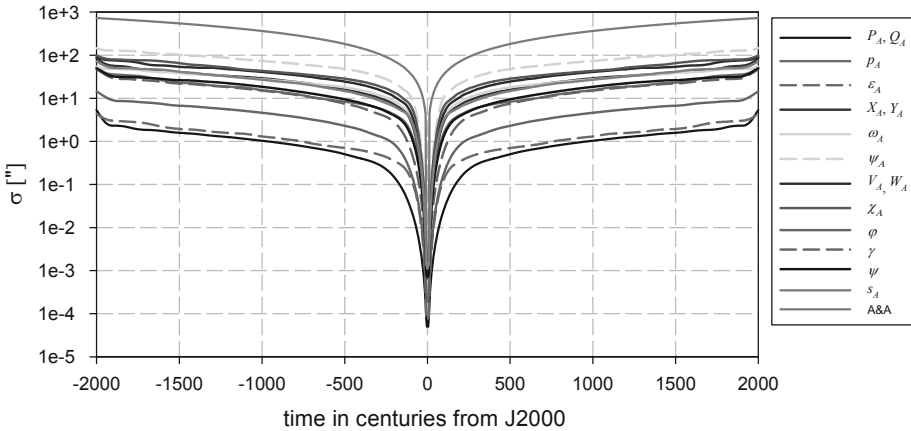


Figure 6: Estimated accuracy of all precession parameters.

LONG TERM PRECESSION MODEL

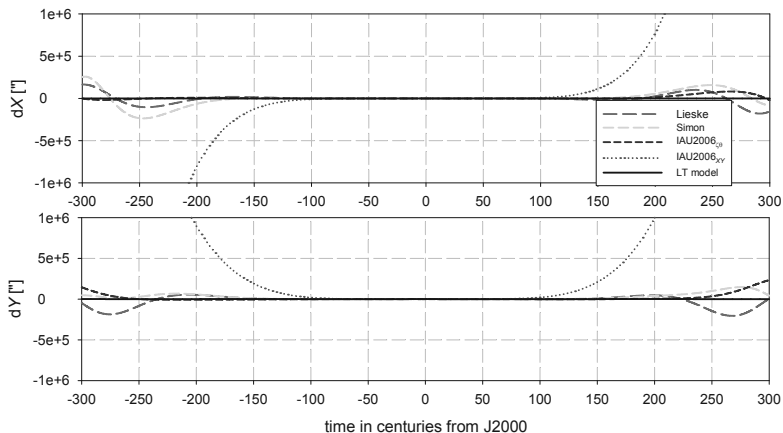


Figure 7: Comparison of different precession models with integrated values.

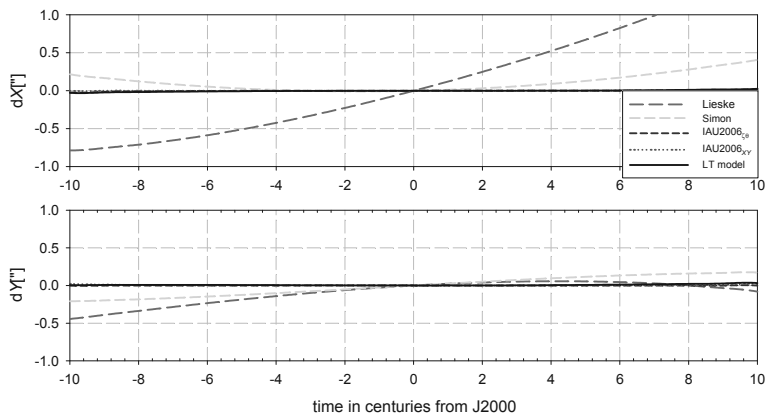


Figure 8: Comparison of precession models – closeup of the central part.

The comparison of the new long-term solution with other models of precession (X_A and Y_A parameters only) is given in Figs 7 and 8. X_A and Y_A values as computed from the values of ζ_A, θ_A by Lieske et al.(1977), Simon et al. (1994) and Capitaine et al. (2003) (denoted as Lieske, Simon, IAU2006 $_{\zeta\theta}$), computed directly from the X_A, Y_A expressions by Capitaine et al. (2003), denoted as IAU2006 $_{XY}$, and by Vondrák et al. (2011b), denoted as LT model, are compared with the numerically integrated values.

Fig. 7 depicts the comparison in the interval ± 300 centuries from J2000.0, while Fig. 8 shows close-up of the central part (± 10 centuries from J2000.0). One can see that the direct IAU 2006 expressions for direction cosines X_A, Y_A yield much worse results for more distant epochs than using the expressions of ‘traditional’ precession angles ζ_A, θ_A . The new LT model is indistinguishable from the integration at this scale, whereas all other models display deviations reaching 50 degrees for epochs more distant than 200 centuries. Fig. 8 clearly demonstrates the correction of precession

rate, and also the quadratic term in obliquity, that were recently introduced in more recent models, with respect to Lieske et al. (1977). On the other hand, all models shown are consistent with the numerically integrated precession within one arcsecond or so in the interval ± 10 centuries from J2000.0.

6. CONCLUSIONS

The presently adopted IAU 2006 model provides high accuracy over a few centuries around the epoch J2000.0. For longer periods, polynomial development of precession angles ζ_A, θ_A should be preferable to direct X_A, Y_A expressions. More than five thousand years from the fundamental epoch J2000.0 the model IAU 2006 rapidly goes away from reality. The newly proposed model of precession, developed by Vondrák et al. (2011b) and valid over ± 200 millennia, is presented. Its accuracy is comparable to IAU 2006 model in the interval of several centuries around J2000.0, and it fits the numerically integrated position of the pole for longer intervals, with gradually decreasing accuracy (several arcminutes ± 200 thousand years away from J2000.0). The estimated accuracy, as given in paper (Vondrák et al. 2011b), is too conservative. It is necessary to add that the new model is strictly valid only in the interval ± 200 millenia from J2000.0. Outside this interval, its uncertainties rapidly grow, due to strong correlations between the estimated sine/cosine amplitudes of different terms.

Acknowledgements. This work was supported by grant No. LC506 of the Ministry of Education, Youth and Sports of the Czech Republic, and also by the grant No. DO 02-275 awarded by the Bulgarian NSF.

References

- Aljabaee, S. and Souchay, J.: 2012, Specific effects of large asteroids on the orbits of terrestrial planets and the ASETEP database, *Astron. Astrophys.*, **540**, A21, doi: 10.1051/0004-6361/201118564
- Capitaine, N., Wallace, P. T. and Chapront J.: 2003, Expressions for IAU 2000 precession quantities, *Astron. Astrophys.*, **412**, 567–586.
- Chambers, J. E.: 1999, A hybrid symplectic integrator that permits close encounters between massive bodies, *MNRAS*, **304**, 793–799.
- Fukushima, T.: 2003, A new precession formula, *Astron. J.*, **126**, 494–534.
- Laskar, J., Joutel, F. and Boudin, F.: 1993, Orbital, precessional, and insolation quantities for the Earth from -20 Myr to $+10$ Myr, *Astron. Astrophys.*, **270**, 522–533.
- Laskar, J., Robutel, P., Joutel, F., Gastineau, M., Correia, A. C. M. and Levrard, B.: 2004, A long-term numerical solution for the insolation quantities of the Earth, *Astron. Astrophys.*, **428**, 261–285.
- Lieske, J. H., Lederle, T., Fricke, W. and Morando, B.: 1977, Expressions for the precession quantities based upon the IAU (1976) system of astronomical constants, *Astron. Astrophys.*, **58**, 1–16.
- Simon, J. L., Bretagnon, P., Chapront, J., Chapront-Touzé M., Francou G. and Laskar J.: 1994, Numerical expressions for precession formulae and mean elements for the Moon and the planets, *Astron. Astrophys.*, **282**, 663–683.
- Vaniček, P.: 1969, Approximate spectral analysis by least-squares fit, *Astrophys. Sp. Sci.*, **4**, 387–391.

- Vondrák, J.: 1977, The rotation of the Earth between 1955.5 and 1976.5, *Studia Geophys. Geod.*, **21**, 107–117.
- Vondrák, J., Capitaine, N. and Wallace, P. T.: 2009, Towards a long-term parametrization of precession, in *Proc. Journées 2008 Systèmes de référence spatio-temporels*, eds. M. Soffel, N. Capitaine, pp. 23–26. Lohrmann Observatorium Dresden and Observatoire de Paris.
- Vondrák, J., Capitaine, N. and Wallace, P. T.: 2011a, Some new thoughts about long-term precession formula, in *Proc. Journées 2010 Systèmes de référence spatio-temporels*, ed. N. Capitaine, pp. 24–27. Observatoire de Paris.
- Vondrák, J., Capitaine, N. and Wallace, P. T.: 2011b, New precession expressions, valid for long time intervals, *Astron. Astrophys.*, **534**, A22, doi: 10.1051/0004-6361/201117274.

CONTRIBUTED PAPERS

HPC CLUSTER WITH GPGPU CAPABILITIES. PERFORMANCE AND FEATURES EVALUATION

E. ATANASSOV¹, M. DECHEV², G. PETROV², A. KARAIVANOVA¹,
T. GUROV¹ and M. DURCHOVA¹

¹ *Institute of Information and Communication Technologies, Sofia, Bulgaria*

² *Institute of Astronomy and National Astronomical Observatory, Sofia, Bulgaria*

Abstract: The high performance computing clusters that are being deployed lately increasingly incorporate GPGPU processing cards, in order to achieve high energy and space efficiency. This leads to development of hybrid computing models that attempt to balance and optimize the performance of the CPU- and GPU-based hardware elements. After the expansion of the HPC cluster at the Institute of Information and Communication Technologies with HP SL390S G7 nodes equipped with NVIDIA M2090 cards, we performed careful evaluation and benchmarking of the new capabilities of the cluster. In this paper we present the software and hardware architecture of the cluster and the results of our benchmarking process.

1. INTRODUCTION

Last years high performance computing cluster was build at the Institute of Information and Communication Technologies, Bulgarian Academy of Sciences. It became a true center of the Bulgarian grid infrastructure and ensures a full membership into European virtual organizations. Its characteristics – infiniband connectivity (90 % efficiency) and 96TB storage volume, the High Performance Computing (HPC) Cluster at Institute of Information and Communication Technologies, Bulgarian Academy of Sciences (IICT-BAS) is more powerful than a big part of the European grid clusters. Recently it was extended with HP SL390S G7 nodes equipped with NVIDIA M2090 cards. Here we present an overview of the Bulgarian HPC infrastructure, the software and hardware architecture of the cluster and the results of our benchmarking process.

2. BULGARIAN HIGH PERFORMANCE COMPUTING INFRASTRUCTURE

The Bulgarian HPC infrastructure (Fig. 1) consists of the biggest HPC resource for research in Bulgaria – the supercomputer IBM BlueGene/P with 8192 cores, two big HPC clusters with Intel GPUs and Infiniband interconnection at IICT-BAS and Institute of Organic Chemistry with Centre of Phytochemistry approximately 1400 cores total. In addition GPU-enabled servers equipped with state of the art Nvidia GPU cards are available for applications that can take advantage of them.



Figure 1: The Bulgarian HPC infrastructure.

The main part of the HPC cluster at IICT-BAS (Fig. 2) consists of 3 chassis HP Cluster Platform Express 7000 with 36 blades BL 280c. The blades are equipped with dual Intel Xeon X5560 @ 2.8Ghz providing a total of 576 cores, 24 GB RAM per node. The cluster has 8 management servers HP DL 380 G6 with dual Intel X5560 @ 2.8 GHz and 32 GB RAM. They are connected with optical Fibre Channel connections with two SAN switches, ensuring redundant access to two Storage Area Network (SAN) storage systems - MSA2312fc and P2000 G3 FC. The total storage space is 96TB (Fig. 3). It is divided in two filesystems for users - /home and /scratch, for permanent and temporary storage, respectively. The management of these high-performance lustre filesystems is performed by 3 management nodes - one MGS/MDS and two OST nodes. The lustre filesystem is open source and popular choice for HPC computing clusters, due to its capability to perform parallel high-performance I/O.

The internal network connectivity of the cluster is provided by fully non-blocking DDR Infiniband at 20 Gbps line speed. The non-blocking feature ensures

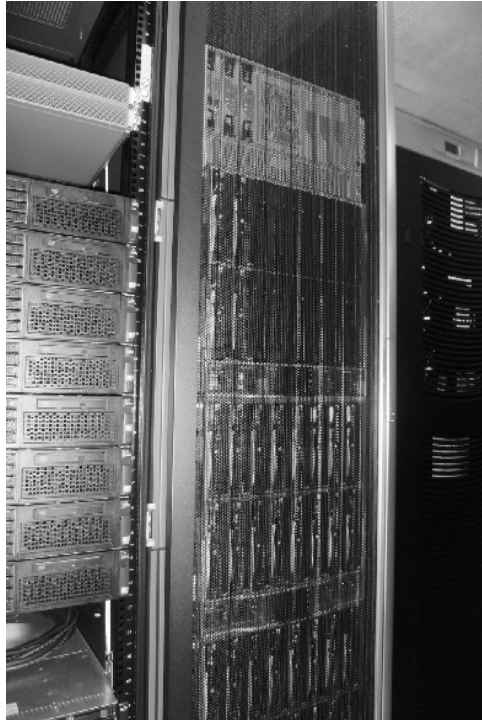


Figure 2: HPC cluster at ICT-BAS.

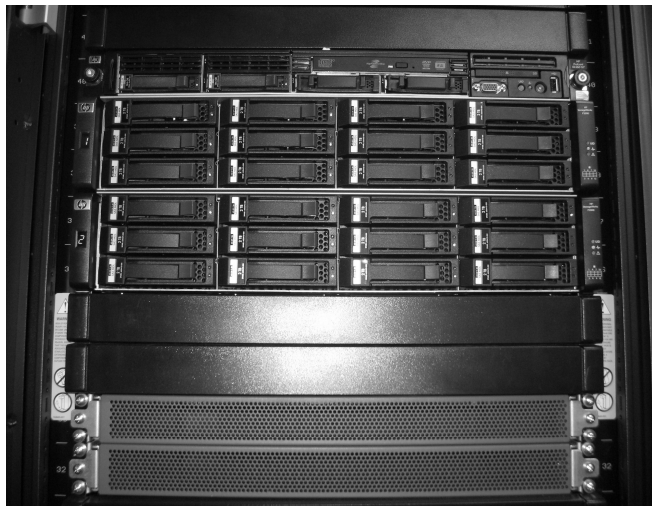


Figure 3: Cluster storage area.

that applications do not run into network bottlenecks even when the cluster is fully used. The core switch of the Infiniband interconnection is a Voltaire Grid director 2004 Infiniband switch (Fig.4). This main advantage of Infiniband versus Ethernet consists in the low-latency of point-to-point communication, where the latency is measured at 2.5 μ s between each two nodes.

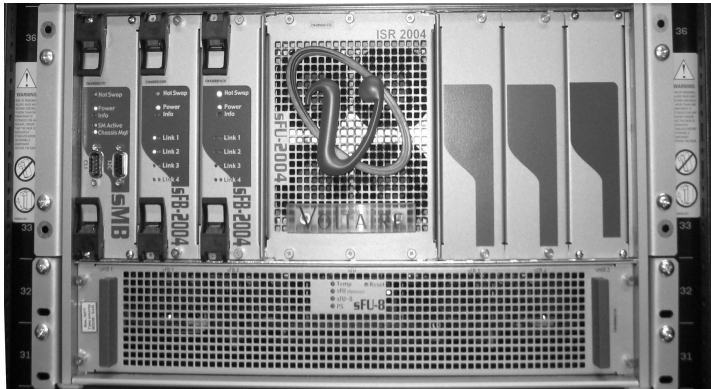


Figure 5: Voltaire Grid director 2004 Infiniband switch.

As was mentioned above, two GPU-enabled servers were added recently. They are HP ProLiant SL390s G7 servers with Intel(R) Xeon(R) CPU E5649 @ 2.53GHz and 96 GB RAM, which support maximum 8 NVIDIA Testla cards. Currently they are equipped with M2090 cards. Every such GPU card has 512 graphic cores and has peak performance of 1331 Gigaflops in single precision calculations and 665 Gigaflops in double precision.

The cluster works under operating system Scientific Linux 5. The cluster can be accessed with Grid certificates, supporting several international and national Virtual Organizations.

3. TESTS AND BENCHMARKS

During the continuous certification process of the cluster, we performed a series of benchmarks:

a) High Performance Linpack

The performance of the supercomputers usually is done in billions floating points operations (double precision). The results of the first 500 systems are regularly published at www.top500.org.

For our test we used the software High-Performance Linpack (www.netlib.org/benchmark/hpl/). All tests were done using all computing cores without hyperthreading since enabling the hyperthreading option does not improve the result. In order to provide optimal parameters for the test we used the suggestions from <http://hpl-calculator.sourceforge.net/>.

Tests showed that the ratio between reached real performance and maximal theoretical performance is 3000/3225, i. e. more than 93%. This is an exceptional result and demonstrates the excellent parallel efficiency of the cluster, mainly due to the use of non-blocking Infiniband.

b) MPI Infiniband tests

One of the most popular tests for performance of the MPI communications are *osu_latency* and *osu_bw*. They measure the latency and bandwidth between servers in the cluster. *Osu_latency* test results are presented in Table 1. They show that we can reach latency smaller than 2.5 μ s. The results from the *osu_bw* tests are shown in Table 2. One can conclude that under 131072 byte size a maximal bandwidth of 1734 MB per second is reached, which is close to the theoretical maximum.

Table 1: OSU MPI Latency Test v3.1.1

Size (bytes)	Latency (μ s)	Size (bytes)	Latency (μ s)
0	2.45	2048	8.75
1	2.54	4096	10.73
2	2.46	8192	14.74
4	2.17	16384	20.84
8	2.14	32768	33.15
16	2.18	65536	53.76
32	2.24	131072	100.04
64	2.44	262144	178.19
128	4.10	524288	333.10
256	4.45	1048576	625.75
512	5.01	2097152	1249.96
1024	6.22	4194304	2462.30

Table 2: OSU MPI Bandwidth Test v3.1.1

Size (bytes)	Bandwidth (MB/s)	Size (bytes)	Bandwidth (MB/s)
0	0	2048	936.44
1	1.13	4096	1211.40
2	2.32	8192	1528.57
4	4.68	16384	1471.90
8	8.82	32768	1572.26

16	18.51	65536	1680.17
32	36.68	131072	1727.01
64	67.71	262144	1727.80
128	124.40	524288	1731.80
256	228.00	1048576	1733.65
512	427.28	2097152	1734.14
1024	698.39	4194304	1734.69

c) Filesystem tests

One of the standard tests for filesystem is *bonnie++*. It is included into the Operating System (OS). At that test cluster reached high results. As an example the block read speed achieved was 436MB/s.

d) For the GPU cards the device query tests show the following:

Device 0: "Tesla M2090"

CUDA Driver Version / Runtime Version	4.0 / 4.0
CUDA Capability Major/Minor version number:	2.0
Total amount of global memory:	5375 MBytes
(16) Multiprocessors x (32) CUDA Cores/MP:	512 Cores
GPU Clock Speed:	1.30 GHz
Memory Clock rate:	1848.00 Mhz
Memory Bus Width:	384-bit
L2 Cache Size:	786432 bytes
Total amount of constant memory:	65536 bytes
Total amount of shared memory per block:	49152 bytes
Total number of registers available per block:	32768
Warp size:	32
Maximum number of threads per block:	1024
Texture alignment:	512 bytes

4. RESOURCE MANAGEMENT AND INFRASTRUCTURE MONITORING

The main control of the resource utilization is performed via the torque batch system and the Maui scheduler. The computational jobs can be submitted either locally or through the Grid. A special accounting system is installed to allow quick overview of the resource utilization. Currently the cluster has around 50 local users, mainly from the institutes of the Bulgarian Academy of Sciences. Most of the cluster resources are used for parallel jobs, since this is its main advantage versus regular clusters. A special accounting system is installed in order to track the utilization of the cluster as well as other HPC clusters in the region (Fig. 5).

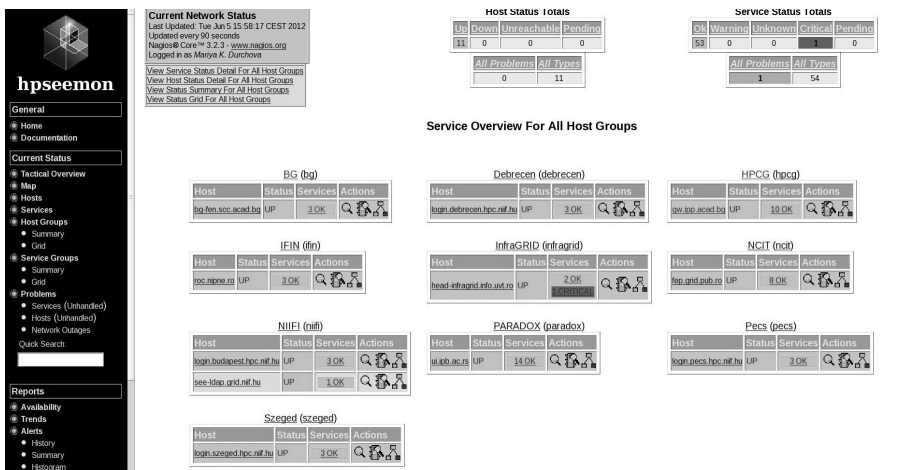


Figure 5: Web-based cluster accounting system.

The cluster health status is monitored both through a local ganglia installation and using the EGI-Inspire nagios portal and the HP-SEE project regional nagios instance. Thus the administrators of the cluster receive alarms and notifications regarding major problems at the cluster.

5. CONCLUSIONS AND FUTURE WORK

The HPC cluster at IICT-BAS provides unique HPC resources, enabling development and use of advanced CPU-based and GPU-based parallel application from various areas of science. The use of the cluster enabled scientific research that otherwise would not have been possible. The balanced state-of-the-art hardware infrastructure can be further expanded by addition of more GPU-based resources or more high-performance disk storage resources. In the future we plan to provide access also via open-source cloud middleware.

Acknowledgments

This work is supported by a grant of the Bulgarian National Science Foundation, Ministry of Education and Science, under number DVCP02/1 CoE Supper CA++ and DO-02-275.

3D NUMERICAL ANALYSIS AND STRUCTURES FORMATION IN ACCRETING WHITE DWARFS

DANIELA BONEVA¹, LACHEZAR FILIPOV², DEYAN GOTCHEV

Space Research and Technology Institute – Bulgarian Academy of Sciences

Abstract. The majority of accreting white dwarfs are dynamically bounded with a companion in a binary star configuration. We aim to examine structure's properties of the flow in accreting zone, surrounding the white dwarf star. We consider a gas-dynamical system that allows 3D modeling of physical processes in the close components. Multi-physics, multi-algorithm, adaptive numerical code is applied. The methods implied are both suitable for time-dependent, implicit computations and consist of a hydrodynamical module in their architectures. The results reveal the pattern formation character and dynamics of interaction in the binary star's flow. A density distribution model through the whole disc's structure is suggested.

1. INTRODUCTION

Binary systems in which a white dwarf accretes from a close companion star are quite common in the Galaxy. The importance of their study comes from the fact that they provide an opportunity to examine the accretion process in isolation, since other sources of luminosity, in particular the companion star, are relatively unimportant. When nuclear burning does occur on the surface of a white dwarf, it is likely that the reaction tends to produce a great brightness but short duration (Frank et al. 2002). For almost whole of its last lifetime no nuclear burning occurs, and the white dwarf may derive its entire luminosity from accretion. A critical stage in the evolution of a compact WD binary is the period just after mass transfer has been initiated (Dan et al. 2012). For the binary to survive, the mass transfer must be stable, which depends sensitively on the internal structure of the donor star, the binary mass ratio, and the angular momentum transport mechanisms (e.g. Marsh et al. 2004; Gokhale et al. 2007). In astrophysics, the problems of structures development have been investigated mainly numerically (e.g. Lithwick 2009, Godon and Livio 1999). In the papers of Shen et al. (2006) and Barranco and Marcus (2005), 2D compressible simulations and “inelastic code” in 3D simulation are applied to compute the evolution of the flow matter.

Johnson and Gammie (2006) have performed a series of runs with zero initial vorticity and perturbation wavelengths and have given a very realistic way of the initial vorticity generation.

The simulations of Meheut *et al.* (2012) show that the Rossby vortices can survive for long time scales, if they are sustained by the Rossby Wave Instability in case of permanent mechanism that forms the “overdensity” and launch the instability. They have shown that the Rossby vortices can emerge in a 3D protoplanetary disc and can survive for hundreds of years without migrating.

Although most of the problems concerning the disc’s flow morphology and dynamics are considering as solved and many papers, investigations and works have been devoting to them, there are still unanswered questions.

We aim to study the morphology of the accreting flow and to establish a part of disc’s configuration around the primary (white dwarf) star after the mass transfer through the Lagrangian point being started.

Therefore, when investigating close components, it is necessary to include physical essence of the flow dynamics response to the interaction processes.

By applying numerical calculations on the gas-dynamical flow, we suggest modeling of patterns formation and explanation of supporting physical processes in interacting flows. We present in this paper our 3D numerical calculations of the posted problem, which would be compared to the previously received 2D results. In the section II we briefly introduce the applied methods, equations and conditions of calculations. The results of current study are presented in Section 3.

2. METHODS, EQUATIONS AND CONDITIONS

2.1. Codes and methods

The complexity of the studied problem and analysis on the corresponding equations in hydrodynamical matter, require applying of numerical codes.

The Maple code is a comprehensive environment for exploring, teaching, and applying mathematics (Heal *et al.* 1998). In addition, Maple 12 is a complete mathematical problem-solving environment that supports a wide variety of mathematical operations such as numerical analysis, symbolic algebra, and graphics.

We chose to insert into the calculations methods, which are implied in the code, known as the Runge-Kutta (implicit part) method. The method treats every step in a sequence of steps in identical manner (Autar and Egwu 2008; Chang *et al.* 1991).

Finite-difference scheme. The basis for the finite-difference method of solution of differential equations is the replacing of derivatives by decrements or difference derivatives.

Alternating direction implicit method (ADI): ADI method belongs to the group of finite difference methods and follows the idea to split the finite difference

equations in two, in relation to the derivatives in coordinates taken implicitly. The system of equations then becomes symmetric and tridiagonal and is usually solved with tridiagonal matrix solver.

The advantage of implicit methods is that they are general in their application and good for partial differential equations, because of their high stability.

We test the equations with the "pdetest" tool, which checks if the solution is correct. To reduce the PDEs to a simpler problem, we applied an "ansatz" tool. Adaptive step-size control is used here (Hairer and Soderling 2005), with the purpose of achieving some predetermined correctness in the solution with minimum computational effort and resources.

Box-multiplying scheme has been suggested, which means that we could perform the calculations in limited regions of the box, defined by the boundary conditions, and then apply it to all disc's area. This could lead to some incorrect solutions, because the behavior of the flow throughout the disc's space is not uniformity. For this reason we should input in these schemes a correction for each of the considering part of the flow and include additional parameters in the calculations. Of course this takes a lot of calculation time and hard math processes. After that, it could be possible to create the model picture of the whole disc's structure. The fast and easy calculation is the advantage of the scheme.

2.2. Equations and Conditions

The gas-dynamical system of equations, which has been suggested by many authors (Frank et al. 2002; Graham 2001; Shu 1992), is applied. We consider the influence of viscous processes, gravitational forces, Coriolis force and we add the corresponding terms for viscous non-ideal fluid in the equations. Then our system of equations consists of equation of mass conservation, the Navier-Stokes equations, energy conservation, the equation of state for compressible flow.

$$\begin{aligned} \frac{\partial \rho}{\partial t} + \nabla \cdot (\rho v) &= 0 \\ \frac{\partial v}{\partial t} + v \cdot \nabla v &= -\frac{1}{\rho} \nabla P - \Omega \times (\Omega \times r) - 2\Omega \times v - \nabla \Phi + \nu \nabla^2 v \\ \frac{\partial}{\partial t} \left[\rho \left(\frac{1}{2} v^2 + \varepsilon + \Phi \right) \right] + \nabla \cdot \left[\rho v \left(\frac{1}{2} v^2 + h + \Phi \right) - 2\eta \sigma \cdot v \right] &= 0 \\ P &= c_s^2 \rho \end{aligned}$$

Where the basic notations are as follows: ρ is the mass density of the flow, v - is the velocity of the flow; P - is the pressure; ν - is the kinematic viscosity; Ω - is the angular velocity; $\Omega \times (\Omega \times r)$ - is the centrifugal acceleration of the centrifugal force; and $2\Omega \times v$ - is the Coriolis acceleration in the mean of the Coriolis force. Φ is the gravitational potential and it depends on the density

distribution inside of the each star's component (Boyarchuk et al. 2002). c_s is the sound speed.

The expression $\frac{\partial}{\partial t} \left[\rho \left(\frac{1}{2} v^2 + \varepsilon + \Phi \right) \right]$ is the total energy density, where the first term on the left denotes the kinetic energy, the second is the internal energy and the third expresses again the full potential of the gravitational fields.

Further $\left[\rho v \left(\frac{1}{2} v^2 + h + \Phi \right) \right]$ is the total energy flux, where $h = \varepsilon + P / \rho$ is the enthalpy, η is the shear (or dynamical) viscosity of the flow, and σ is the rate of shear.

The applied boundary conditions in the calculations are consistent with the studied area of the disc's flow and with a stage of mass transfer. We suggest free boundary conditions at the outer disc edge with constant density: $\rho_{out} = 10^{-6} \rho_{L_1}$, where ρ_{L_1} is the density of the inner Lagrangian point $\sim L_1$. In the inner regions, where the mass transfer and the interaction of streams take place, the values of the density could not remain constant.

We set the matter's state of the general flow to be close to the baroclinicity conditions of (Klahr & Bodenheimer 2003): $\nabla \rho(r, z, \varphi) \times \nabla p(r, z, \varphi) \neq 0$

The boundary conditions of Dirichlet- and Cauchy Type are introduced to control the area of calculations:

$$r_{v(1+n)} = K(x, y, z) - \frac{\partial K}{\partial r_v} \frac{\partial}{\partial t}; \quad r_{v0}(0) = 0 \text{ is the initial radius of the vortex;}$$

$K(x, y, z)$ - the boundary area of equations activity.

It is used the cylindrical coordinates (r, φ, z) frame for the equations and quadratic (x, y, z) set for the numerical scheme.

We use in the calculations the data for SS Cyg and U Gem that are cataclysmic variables with white dwarf star. For SS Cyg: white dwarf with a mass of $\sim 0.97 M_{\odot}$; Orbital period: 6h 38 min. **U Gem** - hot white dwarf; Mass $\sim 0.5 - 0.9 M_{\odot}$. Orbital period: 4 h 11 min.

3. RESULTS

For the purpose of this study, the functions of continuous argument are to be replaced by grid functions determined on the difference grid and, as a result, instead of the original differential equation we obtain an algebraic equation.

We divide the calculation domain into finite-difference cells, which are organized in the proposed box-sharing scheme model.

3.1. Density distribution

The calculations show that interacting flows via the inconstant tidal mass transfer rate could not remain stable, because of the disturbances in velocity and density. The variability in density and velocity may causes formation of areas with increased density. In the places where the velocity values are close to their minimum, the density starts to increase and it pulls a matter there. Thereafter, this means that the matter from a disc could be pumped out or concentrated within given places, causing the density's dilution in close areas. Based on the research of Bisikalo et al. (2001), we have explained in details in the paper of Boneva and Filipov (2012) how the dense zones in the binary mass transfer area has been formed. Here we make a confirmation of the result, as we run Pp once for in each of orbital periods (P_1, P_2, P_3). Steps in moments of rotational period:

$$\sim t_{m0} + 0.25P_p, + 0.57P_p, + 0.78P_p, + 0.92P_p$$

t_{m0} is the time step for zero initial moment; P_p is the rotational period of the binary corresponds to the values of CV. The numerical series were repeated for P_p : $P_{p1} \sim 4h, P_{p2} \sim 5h, P_{p3} \sim 6h$ and fulfilled once $5.6 P_p$.

3.2. Vortex-like formation

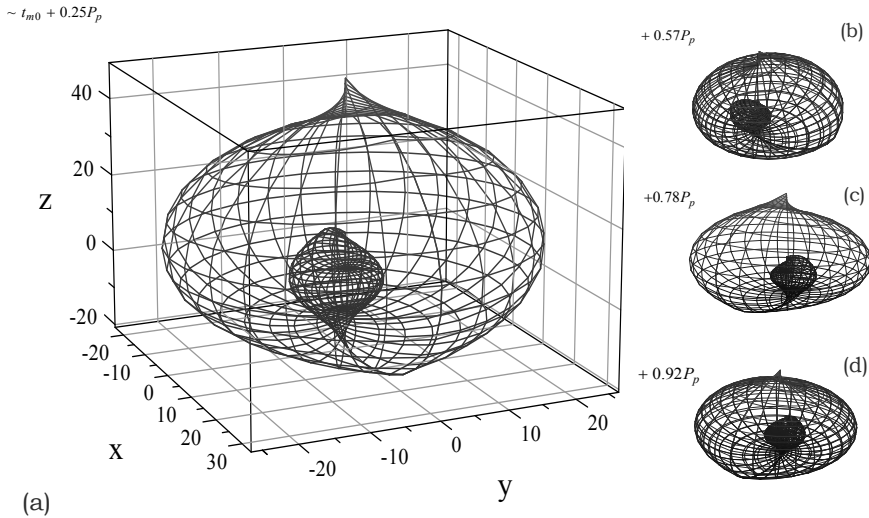


Figure 1: 3D view of the thickened zone formation, as a result of disturbances in the stability state, caused by mass transfer in a binary system. The dense pattern's (colored in light blue) behavior during the periods of time is observed in all periods at the image. The mesh grid was taken in a (x, y, z) calculation' frame of coordinates, corresponded to the density distribution in r direction over the time t[d] (Boneva and Filipov 2012).

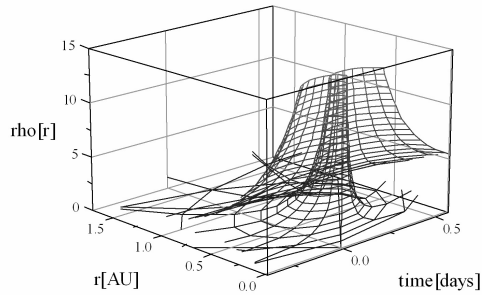


Figure 2: Flow density distribution in the area of the thickened zone formation. The image indicates matter accumulation with increased density. Here, the calculation radius r is in units $[AU].10^{(-7)}$ and the density maximum value is $\rho[rho].10^{(-3)}$ (see electronic version).

We received 3D view of the thickened zone formation, as a result of disturbances in the stability state, caused by mass transfer in a binary system. The whole system consecutive phases of rotation can be seen in four images (a),(b),(c),(d) of Fig.1. The dense pattern's behavior during the periods of time is observed in all periods at the image, colored in light blue. The mesh grid was taken to be $[50, 50, 50]$ in a (x, y, z) calculation' frame of coordinates. (Boneva and Filipov 2012).

We express the flow's density distribution in time in the area of thickened zone. Fig. 2 depicts the density variation's curves lines with the values concentration, which indicates matter accumulation with increased density. The graphical result is in conformity with the dense pattern formation in Fig. 1.

To compare with the previous results we point to the 2D simulation made by (Boneva and Filipov 2012) and Fig. 3 presents a single vortex formation, which is a part of pattern configuration frame in the covered range of about 7.687×10^{-8} AU to 6.68×10^{-7} AU ($K(x,y)$ – boundary calculation area). The picture visualizes the final stage of vortex-like development in the flow. The light blue and dark blue colors show the difference in density in the interacting flow layers. The density values are increasing from light to the dark zone.

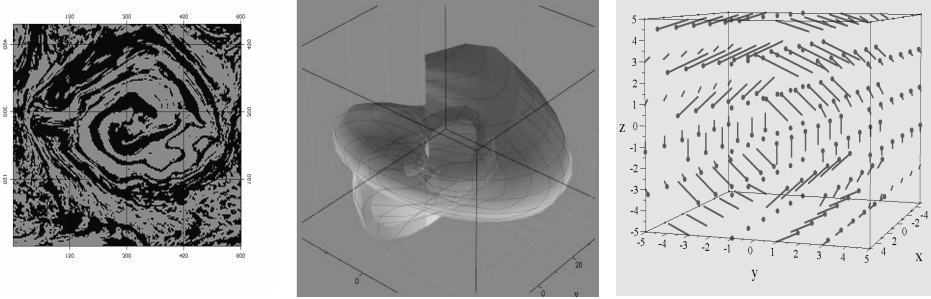


Figure 3: Single vortex-like pattern as a result of 2D calculations, with zero initial vorticity, but with initial present of turbulization value different from zero. The boundary calculation area $K(x,y)$ is covered of about $7.687 \times 10^{-8} \text{ AU} \div 6.68 \times 10^{-7} \text{ AU}$ (Fig.3a left). 3D result of a single vortex-like structure, with non-zero initial vorticity and function of turbulization is seen at Fig.3b. The boundary calculation area $K(x,y,z)$ is covered of about $7.687 \times 10^{-8} \text{ AU} \div 6.68 \times 10^{-7} \text{ AU}$. The picture shows decomposition in the vortex formation stage. The image in Fig.3c (right) depicts the vector field of vortical formation in a 3D calculation frame.

According to the conditions of the general flow and by applying the simulations we obtain the 3D view of vorticity time evolution in the accreting flow. The box boundary values in this case are: $K(x, y, z) \in [8 \cdot 10^{-9} \div 7 \cdot 10^{-10} \text{ AU}]$. The 3D “vortex”-like formation is presented as a patch graphics in the calculating mesh grid (Fig. 3b). Unlike the 2D calculations, here we perform the runs with non-zero initial vorticity and non-zero initial turbulization.

We created the vector field of initial vorticity, seen in Fig. 3c, which gives the basic shape in the calculating box area. In the result, shown in Fig. 3b, an initial deformation in the single vortex-like 3D configuration is observed.

4. CONCLUSION

We presented our study of patterns development in accreting flow around white dwarf stars. The results show that during the mass transfer and interacting processes in the binary, the flow doesn't remain laminar or homogeneous. Comparing to 2D results, 3D calculations show that the dense zone, formed by the disturbances in mass transfer through the binary, keeps its structure, place and stayed stable through the time of rotation. The different situation is observed in the initial behavior of vortex-like configuration, depicted in the box scheme of numerical calculations. We have detected the splitting of the vortex structure wholeness there. It could be seen in the figure.

The vortex, seen in 3D, started to split in small similar-like structures, which would play further role in some new formation around the accretion disc. The accumulation of much of these small dense patterns could lead to throwing of matter out of the disc's space.

Due to the 2D-3D-transition new self organization phenomena probably are observed: as a result from 3D-fluctuations of the velocity gradients the primary density nucleus breaks down into new vorticities whose trajectories draw a tor.

This is only a single result and we could not give any conclusion about the behavior of vortexes in 3D calculations and schemes. New model is needed with related correction, which will give us the construction and view of the whole disc configuration in 3D.

References

- Autar, K. K., Egwu, E. K.: 2008, Numerical methods with applications, 1st ed., self-publ., (http://numericalmethods.eng.usf.edu/topics/textbook_index.html).
- Barranco, J. A., Marcus, P. S.: 2005, *ApJ*, **623**, 1157.
- Bisikalo, D. V., Boyarchuk, A. A., Kaigorodov, P. V., and Kuznetsov, O. A.: 2003, *Astron. Rep.* **47**, 809.
- Boneva, D. V.: 2010, *BGAJ*, **13**, pp. 3-11, ISSN 1313-2709.
- Boneva, D., Filipov, L.: 2012, Density distribution configuration and development of vortical patterns in accreting close binary star system, submitted to A&A, arXive astro.
- Boyarchuk, A. A., Bisikalo, D. V., Kuznetsov, O. A., Chechetkin, V. M.: 2002, *Adv. in Astron. and Astroph.*, **Vol. 6**, London: Taylor & Francis.
- Chang, M. J., Chow, L. C., Chang, W. S.: 1991, *Numerical Heat transfer*, Part B, **19(1)**, 69-84, ISSN 1040-7790.
- Dan, M., Rosswog, S., Guillochon, J., Ramirez-Ruiz, E.: 2012, *MNRAS*, **Vol. 422**, Issue 3, pp. 2417-2428.
- Frank, J., King, A., Raine, D.: 2002, *Accretion Power in Astrophysics*, 3-rd edition, Cambridge University Press, New York.
- Godon, P., Livio, M.: 1999, *ApJ*, **523**, 350.
- Gokhale, V., Peng, X. M., Frank, J.: 2007, *ApJ*, **655**, 1010.
- Graham, J. R.: 2001, "Astronomy 202: Astrophysical Gas Dynamics", Astronomy Department, UC Berkeley.
- Heal, K. M., Hanse, M. L., Rickard, K. M.: 1998, *Maple V: Learning Guide (for Release 5)*, Springer, New York.
- Hairer, E., Soderling, G.: 2005, *SIAM J. Sci. Comput.*, **Vol. 26**, 6, pp. 1838-1851.
- Johnson, B. M., Gammie, C. F.: 2005, *ApJ*, **635**, 149-156.
- Klahr, H., Bodenheimer, P.: 2003, *ApJ*, **582**, 869-892.
- Lithwick, Y.: 2009, *ApJ*, **693**, 85.
- Marsh, T. R., Nelemans, G., Steeghs, D.: 2004, *MNRAS*, **350**, 113.
- Meheut, H., Keppens, R., Casse, F., Benz, W.: 2012, *A&A*, **542**, A9, arXiveastro:1204.4390.
- Shen, Y., Stone, J. M., Gardiner, T. A.: 2006, *ApJ*, **653**, 513.
- Shu, F. H.: 1992, *The Physics of Astrophysics, Vol II: Gas Dynamics*.

4-PARAMETER TRANSFORMATION OF DIGITIZED ASTRONOMICAL IMAGES

YAVOR CHAPANOV

*National Institute of Geophysics, Geodesy and Geography,
Bulgarian Academy of Science
Acad. G. Bonchev Str., Bl.1, Sofia 1113, Bulgaria
E-mail: astro@bas.bg*

Abstract. The accuracy of star celestial coordinates determined from astronomical images depends on various parameters. A part of these parameters are the celestial coordinates of the image center and the angle between image axes and the North direction. The 4-parameter transformation (two translations, one rotation and scale) is used to determine the orientation of the digitized astronomical images and the coordinates of their center. The transform parameters are estimated by means of coordinates of identical stars from two images. The influence of the star proper motion uncertainties on the 4-parameter transformation accuracy is investigated by models of digitized astronomical images of one and same part of the sky in different epochs and made from different instruments. The ability of application of the 4-parameter transformation of the digitized astronomical images in determination of star coordinates and proper motions is discussed.

1. INTRODUCTION

The preliminary determination of the precision of the real measurements and observations and their systematic errors and deviations are very important for the quality of scientific research, especially in the cases of observations from classical instruments whose accuracy level is relatively low in comparison with the high-technology modern equipment. When we try to use the digitized astronomical plates, we need to prove that the accuracy of the determined star coordinates from these images and the results of their processing are of the order of 1-2 tenth of arc second, which accuracy is necessary in scientific research of various geodynamic effects connected with the crust deformation, gravity and Earth rotation variations, and etc.

2. 4-PARAMETER HELMERT TRANSFORMATION

The Helmert transformation is used in geodesy. It transforms a set of points into another by rotation, scaling and translation. When both sets of points are given, then least squares can be used to solve the inverse problem of determination of the parameters, or the parameters of the so-called 7 parameter transformation can be obtained by standard methods (Awange et al., 2004). The classic Helmert transformation between two coordinate spatial systems depends on 7 parameters – 3 translations, 3 rotation and a scale parameter. The general form of 7-parameter Helmert transformation between two reference systems A and B is:

$$\begin{bmatrix} X \\ Y \\ Z \end{bmatrix}_B = \begin{bmatrix} C_X \\ C_Y \\ C_Z \end{bmatrix} + (1 + s \times 10^{-6}) \cdot \begin{bmatrix} 1 & -r_Z & r_Y \\ r_Z & 1 & -r_X \\ -r_Y & r_X & 1 \end{bmatrix} \cdot \begin{bmatrix} X \\ Y \\ Z \end{bmatrix}_A, \quad (1)$$

where X , Y and Z are rectangular coordinates, c_X , c_Y , and c_Z are translations, r_X , r_Y , and r_Z are rotations and s is the scale, so that the value of the scale factor $\mu=1+s$ to be around 1. The 4-parameter transformation is obtained from (1) where Z , c_Z , r_X and r_Y are zeroes, so the 2-dimension coordinate systems are transformed by the 4-parameter Helmert transformation in the form

$$\begin{aligned} X_B &= c_X + (1 + s \times 10^{-6}) \cdot (X_A - r_Z Y_A), \\ Y_B &= c_Y + (1 + s \times 10^{-6}) \cdot (r_Z X_A + Y_A). \end{aligned} \quad (2)$$

3. STAR IMAGES AND ERROR MODEL

The model of simulated observations is created by a set of star coordinates from sky image, containing 317 generated by the program StarGazer (author Rumen Bogdanovski, a member of Astrominformatics Project team) with 2arcmin field width (Fig.1). The star image is possible to enlarge and to rescale star coordinates so that the output field width reach 2 degrees. The resulting star coordinates form the first set of points which coordinates correspond to a given star catalog. The second set of identical points is formed from the first set with the assumption that if the simulated star image center is shifted from the true point, small rotation of the image in the focal plane exists and the image scale, which transforms photo coordinates to celestial coordinates is known approximately. The initial values of these systematic errors are chosen as follow: shift of the center coordinates $X_0=180$ arcsec, $Y_0=240$ arcsec, rotation around Z axis $r_Z= -120$ arcsec, plate scale uncertainty $s = 100$ ppm (part per million). The model of random errors of the second set of simulated star coordinates, obtained from the digitized astronomical plate is described in details in (Chapanov et al., 2011). Three different cases of the level of random errors are considered (I) – with standard 0.5 arcsec, which is the best case, (II) – with standard 1.0 arcsec, which corresponds

to the case of middle precision, (III) – with standard 5.00 arcsec, a case with poor accuracy. Two more cases are considered: (IV) – with standard 0.5 arcsec and 0.5 arcsec/a uncertainties of the star proper motions on 10-year time spans, and (V) – a case with huge scale error ($s = 10^6$ ppm).

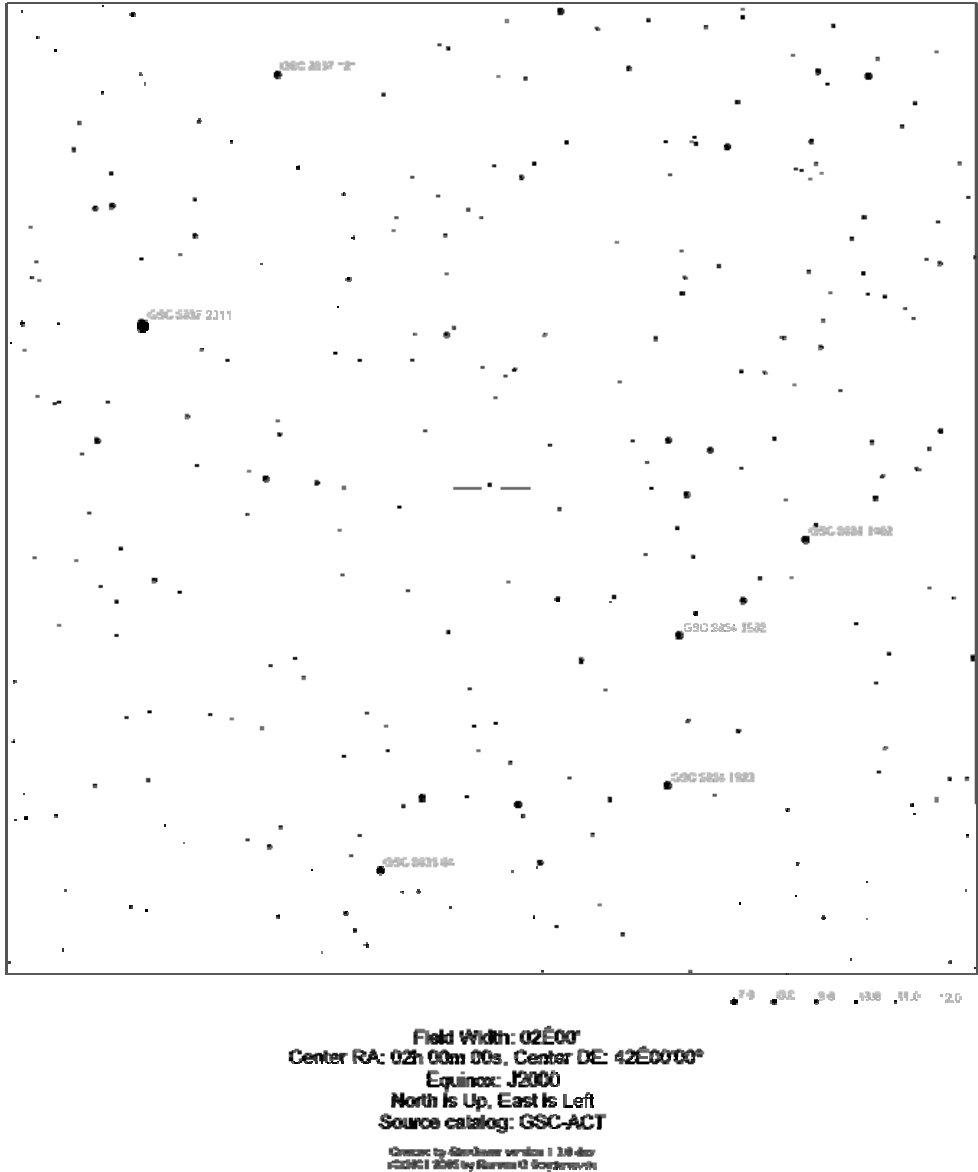


Figure 1: Map of the chosen sky field, containing 317 stars. The map is generated by the program StarGazer, version 1.3.0-dev and source star catalog GSC-ACT.

4. RESULTS

The results for 5 cases of application of 4-parameter transformation to the simulated star coordinates derivation from digitized astronomical plates are given in Tables 1-5.

4.1. Results for error model I, $\sigma=0.5$ as

Max. errors $<0''.05$

Table 1: Results for error model I, $\sigma=0.5$ as

Model		Solution	Differences	Errors [as]
Parameters	Initial values			
X [as]	180.0	180.03	-0.03	0.03
Y [as]	240.0	240.02	-0.02	0.02
Rz [as]	-120.0	-119.48	-0.52	
S [ppm]	100.0	92.96	7.04	

4.2. Results for error model II, $\sigma=1.0$ as

Table 2: Results for error model II, $\sigma=1.0$ as

Model		Solution	Differences	Errors [as]
Parameters	Initial values			
X [as]	180.0	180.03	-0.03	0.03
Y [as]	240.0	240.01	-0.01	0.01
Rz [as]	-120.0	-121.28	1.28	
S [ppm]	100.0	99.20	0.80	

4.3. Results for error model III, $\sigma=5.0$ as

Table 3: Results for error model III, $\sigma=5.0$ as

Model		Solution	Differences	Errors [as]
Parameters	Initial values			
X [as]	180.0	180.24	-0.24	0.24
Y [as]	240.0	240.15	-0.15	0.15
Rz [as]	-120.0	-121.12	1.12	
S [ppm]	100.0	87.20	12.80	

Max. errors $<0''.4$

4.4. Results for error model I with proper motion errors

Table 4: Results for error model I with proper motion errors

Model		Solution	Differences	Errors [as]
Parameters	Initial values			
X [as]	180.0	180.22	-0.22	0.22
Y [as]	240.0	240.15	-0.15	0.15
Rz [as]	-120.0	-112.78	-7.22	
S [ppm]	100.0	143.54	0.80	

Max. errors <0".5

4.5. Case of large scale

Table 5: Results for the case of large scale

Model		Solution	Differences	Errors [as]
Parameters	Initial values			
X [as]	360.0	180.22	-0.22	0.22
Y [as]	480.0	240.15	-0.15	0.15
Rz [as]	-120.0	-112.78	-7.22	
S [ppm]	1×10^6	1000085.93	-85.93	

Max. errors <0".6

5. CONCLUSIONS

It is possible to estimate the rotation and image center of digitized astronomical plates by the 4-parameter Helmert transformation if the number of identical stars is more than 100. The estimation accuracy is better than 0.4 as at the image borders and better than 0.1as in the center for plates with 100"/mm scale, scan resolution 2400dpi and total RMS errors of star positions below 5 as.

The necessary preprocessing of digitized astronomical images are image convert to small scale, determination of identical stars from the image and star catalog and correction of the atmosphere refraction and distortions due to telescope optics and projection of celestial sphere over the focal plane.

Acknowledgments

This work is supported by a grant of the Bulgarian National Science Foundation, Ministry of Education and Science, under number DO 02-275.

References

- Awange, J. L., Fukuda, Y. and E. Grafarend: 2004, Exact solution of the nonlinear 7-parameter datum transformation by Groebner basis, *Bollettino di Geodesia e Scienze Afini* **63**, 117-127 2004.
- Chapanov, J. Vondrák, C. Ron, V. Štefka: 2011, Proper motion accuracy of WFPDB stars, Proc. VII SBAC, Chepelare 01-04 June 2010, 169-176.

RELATIVE EXISTENCE OF PHYSICALE OBJECTS

LUKA ĆIRIĆ¹ and DUŠAN ĆIRIĆ²

¹*Institute of Complex Matter, EPFL, Station 3, 1015 Lausanne, Switzerland*

²*Dept. of Math., Fac. of Nat. Sci. and Math., Višegradska 33, Niš, Serbia*

E-mail: luka.ciric@epfl.ch, dusancir@yahoo.com

Abstract. In this article we investigate the structure of the time and propose a new concepts of the local times with which is possible to work in physics. Novel concept of the local times allows parameterizations of the local times not only by the full real line but as well by the certain proper subsets of the real line. It is shown that local times for each point seen as the ordered set of moments can be compared one with another by their size or inclusion and it is demonstrated that the size of each local time depends on the observer. We elaborate how the existence of the physical objects depends on the observer and how it posses strictly relative character.

1. INTRODUCTION

Two notions determine our perception of time, its order and its flow. By the order of time we understand set of ordered moments T , with precisely defined ordering properties. The impression of the existence of the time flow is coming from our belief that the motion exists.

The standard theory of relativity introduces the concepts of time locality and the speed of the time flow (Einstein, 1955). Locality means that the time is strictly assigned to each point of space. It is assumed that each local time flows steadily with the certain flow rate that depends on the observer and that local times can be compared with respect to their "speed" of flow. Therefore, one can say that the Theory of Relativity is in fact theory of relativity of the speeds of the time flows.

Time, as the ordered set of moments, we believe, has all the properties of the ordered set R of the real numbers. That is the reason why we are used to parameterize the time by the real numbers. The order properties of the real numbers were precise by theorems of Dedekind and Cantor.¹ Each local time, as it has all the order properties of real numbers is linearly ordered, unbounded and complete with respect to order set of moments in which exist the ordered dense subset, linearly ordered with respect to induced order, unbounded and countable.

¹See T. Jech, *Set theory*, Academic Press, New York, San Francisco, London 1978.

2. PARAMETRIZATION OF LOCAL TIMES

The same ordering properties as the set of all real numbers possess as well infinitely many its proper subsets. This can be seen from numerous examples.² In Čirić and Čirić (2012) we examine the possibility that local times related to each point of space can be parameterized not only by "full parametrization" R but by any proper subset of R that has all order properties as R as well. Here, each subset R^* of the set R , with induced order from R , such that there exists at least one ordering isomorphism $f : R \rightarrow R^*$ can be called parametrization of the local times.

Parametrization of the local time we relate to each point in space in the following manner. Lets suppose that $x \in X$ is any point in space X and $R^*_x \subset R$ its time parametrization. That the point $x \in X$, exists as material point, that has reality, it has to have extensionality in its space and its time. It has extensionality in space as $\{x\} \subset X$, and it has extensionality in time as $t \in R^*_x$. Point $x \in X$ does not have time extensionality in the set $R - R^*_x$, therefore it does not exist as the material point for the elements of that set. Size of the parametrization $R^*_x \subset R$ we determine by the size of the existence of the point x within the full time R . Thus, we can say that for the point $x \in X$ we have corresponding parametrization $R^*_x \subset R$ what means that the point $x \in X$ exists in the moments that are elements of the set R^*_x , and not exists in the "moments" that are elements of the set $R - R^*_x$.

The non-empty subsets of the real set that can be parameterizations of the local times are described in details in the Theorem 3., of Čirić and Čirić (2012). Namely, we saw that the following statement holds:

Theorem 1. (Characterization of the parameterizations of the local times.) Any non-empty subset R^ of the set R with respect to the order induced from R , is parametrization of local time if and only if the following conditions are fulfilled:*

1. *As the subset of the ordered set R , set R^* does not have minimal and maximal element in R .*
2. *It exists most countable family $\{X_i\}_{i \in I}$ of disjoint, finite or infinite intervals, such that:*

$$R^* = \bigcup_{i \in I} X_i,$$

where the closed intervals, if they exist can be reduced to the point.

3. *If X_i and X_j are two neighbouring intervals, such that X_i is before X_j , than either X_i is closed from the right and X_j open from the left or X_i open from the right and X_j is closed from the left side.*

²See example 1., in Čirić and Čirić (2012).

3. MORE ABOUT THE PARAMETERIZATIONS OF THE LOCAL TIMES

From the definition of the parameterizations of the local times R^* one can see that there exists ordering isomorphism $f : R \rightarrow R^*$ that represents parametrization R^* . In the general case there can be infinitely many isomorphisms that represent the same parametrization. Each representation of the parameterizations of the local times on the set R^* defines order, algebraic structure and structure of the metric space. We saw from the Theorem 4., in Ćirić and Ćirić (2012) that all the representations define the same topological and order structure on the set R^* and up to isomorphism unique algebraic structure on that set. Each representation of parameterizations of the local times is isomorphism with respect to all mentioned structures.

That every representation induces same topology on the set R^* one sees from the following statement.

Proposition 1. Let R^ be parametrization of local times and $f, g : R \rightarrow R^*$ ordering isomorphisms that represents that parametrization. If d_f and d_g are metrics on set R^* defined as:*

$$\forall y, \forall z, y, z \in R^*, d_f(y, z) = d(f^{-1}(y), f^{-1}(z)),$$

or:

$$\forall y, \forall z, y, z \in R^*, d_g(y, z) = d(g^{-1}(y), g^{-1}(z)),$$

than topologies induced on R^* are the same. Here d is the usual metrics on R .

Proof. If $y_0 \in R^*$ is arbitrary point and set

$$\begin{aligned} K_f(y_0, \epsilon) &= \{y \mid d_f(y, y_0) < \epsilon\} = \\ &= \{y \mid d(f^{-1}(y), f^{-1}(y_0)) < \epsilon\} = \{y \mid x_0 - \epsilon < f^{-1}(y) < x_0 + \epsilon\} \end{aligned}$$

open ball in metrics d_f sa $x_0 = f^{-1}(y_0)$. There exist numbers u and v such that $x_0 - \epsilon < u < x_0$ and $x_0 < v < x_0 + \epsilon$ $g((u, v)) \subset K_f(y_0, \epsilon)$. As g is homeomorphism, (u, v) open subset of R , than $g((u, v))$ is open subset as well in metric space (R^*, d_g) which than with each its point, and the point y_0 contains at least one d_g - open ball $K_g(y_0, \eta)$. Therefore, it holds:

$$y_0 \in K_g(y_0, \eta) \subset g((u, v)) \subset K_f(y_0, \epsilon).$$

Each open set in metric space (R^*, d_f) that with each point in the set contains d_f open ball, with each point contains and at least one d_g open ball, so it is open in the metric space (R^*, d_g) . Similarly can be proved that each open set in metric space (R^*, d_g) , is open in the metric space (R^*, d_f) , what makes proposition proved.

Proposition 2. If R^ is parametrization of local times and $f : R \rightarrow R^*$ arbitrary ordering isomorphism, topology induced by the metrics d_f is interval topology on R^* .*

The proof is obvious.

Proposition 3. If $f : R \rightarrow R^*$, is ordering isomorphism, and if there exists at least one $y \in R - R^*$ such that $L_y = (-\infty, y] \cap R^*$ and $D_y = [y, +\infty) \cap R^*$ are non-empty, then, (and only then) there exists the point $x_0 \in R$ in which function f seen as function $R \rightarrow R$, does not have limit.

The proof is obvious.

We saw that one can state the existence of the time flow with a certain flow rate. If the local time of the point $x \in X$ is parameterized by the set R^* its time flow is driven by the whole R but the existence and materiality of the point $x \in X$ is restricted when time flows over the set R^* . Finally, that local time flows, and that flow has certain speed now means that point $x \in X$ moves towards its future through full time R with certain speed but exist only in the moments that belong to the set $R^*_x \subset R$, and it does not exist as a material point, as reality in the "moments" that are elements of the set $R - R^*_x$.

Set R is parametrization of the local times and it can be represented not only by identical function, but as well with another isomorphism that keeps order structure $f : R \rightarrow R$. Each such isomorphism is derivable function on R and its derivative f' shows change of the speed of flow of the local time R . *The choice of the representation of the local times means choice of the configuration of the speed of the time flow.* For example, requirement that local time R flows steadily is equivalent to the requirement that speed of flow is the same in each moment or that function f that represents local time R is of the form $f(x) = \alpha x + \beta$, where $\alpha > 0$.

It can be proved that *the set $R^* \subset R$ is unbounded parametrization of the local time in R if and only if for each isomorphism that keeps order $f : R \rightarrow R$, function:*

$$f^*(x) = \begin{cases} f(x) + \mu([x, 0] \cap (R - R^*)), & x < 0 \\ f(x) - \mu([0, x] \cap (R - R^*)), & x \geq 0 \end{cases}$$

is isomorphism that keeps order of the set R^ in the set R .* As the inversion function of the function f^* is representation of the parametrization of the local time, that means that every and therefore linear function as well $f(x) = \alpha x + \beta$, where $\alpha > 0$, induces an arc by arc linear representation of the set R^* that has derivative $\frac{1}{\alpha}$ in all except the mostly countable points. Therefore, we have the following situation. We suppose that "full time" R is prominent parametrization with steady flow and the speed of flow that is taken as the unity in analyzing speeds of flows of other local times. Unbounded local time R^* we see inside "full time" R and its flow as the part of the flow of "full time" that contains it. The existence of the function f^{*-1} that represents parametrization R^* whose derivative where is defined is $\frac{1}{\alpha}$, means that time through set R flows with speed $\frac{1}{\alpha}$. Therefore, one can compare the speed of the flow of certain local time with speed of the flow of the "full time" for which we assume that has unity of speed flow.

As the speed of the flow of each unbounded in R local time R^* , with the speed of the flow of full time, we can compare speeds of unbounded local times one with another as well. *Thus, for the class of unbounded parameterizations of local times the Theory of Relativity is possible.*

We have to stress that *there are local times that could not flow steadily.*

Although parameterizations of the local times are bounded in R , and do not have linear representation, *it is possible to compare the speeds of local time flows of the same or different parameterizations of in many cases.* For example, if set R^* is bounded parametrization of local times, and $f : R^* \rightarrow R$ is isomorphism that keeps order, than the function $\alpha f : R^* \rightarrow R$ for $\alpha \neq 1$ is also isomorphism with respect to order. Let local times of the points x and y be parameterized by the set R^* which is in the point x represented by the function f^{-1} , and in the point y by the function $(\alpha f)^{-1}$, we can say that the speeds of flow of local times in the points x and y are comparable and that time in the point y flows with the factor $\frac{1}{\alpha}$ with respect to the speed of flow of the time in the point x .

4. PHYSICAL OBJECTS AND RELATIVITY OF THEIR EXISTENCE

Every set of points, as the subset of the space, has extensionality in space. That set of the points has reality, or existence, it has to have extensionality in time as well. Only the objects that have extensionality in space and time can be seen as the material objects or the objects that exist in reality. *Therefore, one can ask the following question: how to select physical objects from the material objects.*

Physics is not formal theory, and it does not have its formal language. However, we can extend the language of the standard mathematics, or the language of Theory of Sets, by proper relations relevant for physics and obtain *the language of physics* with which we can formulate *physical properties*. The objects that are considered in physics or *the physical objects are therefore, among the sets of the points, subsets of the space, determined by the totality of their physical properties.*³ We allow as well that physical objects as mathematical can be determined by its elements and by some physical property that collect elements of the physical objects in that concrete physical object.

Primer properties of all physical objects are their material existence, their reality and extensionality in space and time. The fact that the physical objects are some subsets of the space X means their extensionality in space. Let $\mathfrak{R} = \{x|\varphi(x)\}$ be any physical object whose elements x have physical property φ . Each element $x \in \mathfrak{R}$ is the point in which local time is defined with parametrization $R^*_x \subset R$. Each local time $R^*_x \subset R$ except its size in the "full time" R has its flow, and the speed of flow. Flow of the local time R^* in the point we see as the flow of "full time" R that contains it, so that the point exist while its time passes over the set R^* , and does not exist on the set $R - R^*$. That \mathfrak{R} presents physical object it has to have extensionality in time as well, and obviously it has to be the set $\bigcap_{x \in \mathfrak{R}} R^*_x \neq \emptyset$. Also, in order to define time flow of the object and its speed of flow, all the elements that make constitutes object \mathfrak{R} need to have local times that flow steadily and whose time flows are of the equal speed. This means that parametrization of local times of the points

³It is known that sets or objects that mathematics treats are determined by totality of their collectivizing properties and due to Axiom of extensionality in Set Theory by their elements as well, which are collected in some set by some of the collectivizing mathematical property.

that make physical object \mathfrak{R} need to be unbounded in R . Hence, the non-empty set $T_{\mathfrak{R}} = \bigcap_{x \in \mathfrak{R}} R^*_x$ will be *the time of physical object \mathfrak{R} , or time in which the physical object exists*.

We can therefore say (see Ćirić and Ćirić, 2012) that *each non-empty set \mathfrak{R} of the space X whose elements are collected via certain physical property is physical object, if all local times of its points flow steadily, with the same speed, and if the time in which the object \mathfrak{R} , $T_{\mathfrak{R}} = \bigcap_{x \in \mathfrak{R}} R^*_x$ exists as a non-empty set*.

We define physical object \mathfrak{R} , as non-empty subset of the space determined with corresponding physical property. Here one precise and size of the object \mathfrak{R} in the time. Namely, on the non-empty set $T_{\mathfrak{R}} \subset R$ the object exists, and on the set $R - T_{\mathfrak{R}}$, it does not exist. While it exists, the object \mathfrak{R} has reality and materiality.

Numerous, simple properties of physical object are proved in Ćirić and Ćirić (2012). Here we will analyze the existence of the physical objects.

Let $(\mathfrak{R}_1, T_{\mathfrak{R}_1})$ and $(\mathfrak{R}_2, T_{\mathfrak{R}_2})$ be two different physical objects in material space X . Lets imagine that we placed the observers A and B , in the objects \mathfrak{R}_1 and \mathfrak{R}_2 respectively.

Lets suppose that the time of the object \mathfrak{R}_1 is proper subset of the set R , so that $T_{\mathfrak{R}_1} \neq R$. In the moments $t \in T_{\mathfrak{R}_1}$ the observer A exists, and does not exist as physical object on the set $R - T_{\mathfrak{R}_1}$, as on that set at least one of its point has not reality, and has not extensionality in its local time. Taking into account that on set $R - T_{\mathfrak{R}_1}$ the observer A does not exist, there is no way for the observer A to detect the discontinuities in its time flow. Time $T_{\mathfrak{R}_1}$ in which the observer A exists, the observer A sees as one, continuous interval, subset of the "full time" R . Its proper time $T_{\mathfrak{R}_1}$, the observer A sees with all order properties of interval that is subset of the ordered set R of the real numbers.

For the observer A the time flow exists, this is the time flow of all elements of the physical object \mathfrak{R}_1 , reduced on its time $T_{\mathfrak{R}_1}$. The observer A does not exist on the set $R - T_{\mathfrak{R}_1}$, it exist while its time passes through the set $T_{\mathfrak{R}_1}$. Time flow of the $T_{\mathfrak{R}_1} \subset R^*_x$ for every $x \in \mathfrak{R}_1$ is steady and it has a speed of flow that is equal to speeds of flow of all its points.

On the set $T_{\mathfrak{R}_1}$ we have induced order, topological and algebraic structure. The observer A sees structures on $T_{\mathfrak{R}_1}$ like they are induced from R .

All what we said for the observer A we can say for the observer B .

Existence of the observer A is reducing to the existence of the observer A in its time $T_{\mathfrak{R}_1}$. The observer A exists in its local reality. Naturally one ask the question *when for the observer A exists the observer B* .

Lets suppose here that *the object \mathfrak{R}_2 is near enough to the object \mathfrak{R}_1 that the information transfer about the existence of the object \mathfrak{R}_2 to the object \mathfrak{R}_1 is almost instantaneous and that relativistic effects are negligible*.

In that case if $T_{\mathfrak{R}_1}$ and $T_{\mathfrak{R}_2}$ are times in which the objects \mathfrak{R}_1 and \mathfrak{R}_2 exist, it can be $T_{\mathfrak{R}_1} \cap T_{\mathfrak{R}_2} \neq \emptyset$ or not.

If $T_{\mathfrak{R}_1} \cap T_{\mathfrak{R}_2} = \emptyset$ in reality of the observer A the observer B can never exist.

If $T_{\mathfrak{R}_1} \cap T_{\mathfrak{R}_2} \neq \emptyset$ for the observer A the observer B exists in the time $T_{\mathfrak{R}_1} \cap T_{\mathfrak{R}_2} \subset T_{\mathfrak{R}_1}$. In the time $T_{\mathfrak{R}_1} \cap (R - T_{\mathfrak{R}_2})$, of the observer A , the observer B does not exist. The observer A can detect, that the local time $T_{\mathfrak{R}_2}$ is proper subset of the R , but it does not have to be the case if $R - T_{\mathfrak{R}_2} \subset R - T_{\mathfrak{R}_1}$. If the observer A in certain moments of its time $T_{\mathfrak{R}_1}$, sees disappearance of the object \mathfrak{R}_2 , and equally after some time interval it sees reappearance of the object \mathfrak{R}_2 on the place and characteristics as it has been never disappeared, the observer A can state that it is about the same object \mathfrak{R}_2 . *Therefore, the observer A can state that the time $T_{\mathfrak{R}_2}$ of the object \mathfrak{R}_2 has discontinuities, as it sees the discontinuities in the existence of the object \mathfrak{R}_2 .*

The following question arises, is it possible for the observer A to detect the discontinuities in its local time, and if it can how it can do it? We saw that this is impossible within its proper time. Let now the observer B with respect to the observer A moves on arbitrary trajectory with variable speed with neglecting relativistic effects again. It could happen than that in the reality of the observer A that the object \mathfrak{R}_2 abruptly change the place in space. By assuming that there is no abrupt change in space, the observer A can only conclude that there was interruption in its own existence. The reason is simple, namely in the interval of the interruption of the existence of the object \mathfrak{R}_1 , or the observer A the object \mathfrak{R}_2 existed as the physical object in its own time and it has change the place in the space meanwhile. The observer A does not see the discontinuities in its own existence and therefore for him the displacement of the object \mathfrak{R}_2 is instantaneous. Here, of course it is about the abrupt displacement or change of any physical characteristics.

References

- Ćirić, Luka, Ćirić, Dušan: 2012, New concept of time and Relativity of existence in physics, submitted to *Physical Review D*.
- Einstein, A.: 1955, *The principle of Relativity*, A Collection of Original Memoir New York Dover Publication Inc.
- Jech, T.: 1978, *Set theory*, Academic Press, New York, San Francisco, London.

MORE ACCURATE FOCAL LENGTH DETERMINATION FOR THE ROZHEN 2 m TELESCOPE

ZORICA CVETKOVIĆ, GORAN DAMLJANOVIĆ, RADE PAVLOVIĆ

Astronomical Observatory, Volgina 7, 11060 Belgrade 38, Serbia
E-mail: zorica@aob.rs, gdamljanovic@aob.rs, rpavlovic@aob.rs

Abstract. The focal length of a telescope is an important parameter in determining the relative coordinates (angular separation and position angle) of double and multiple stars, as well as in determining the precise coordinates of extragalactic radio sources visible in optical part of wavelengths. With the 2 m telescope of National Astronomical Observatory at Rozhen we have collected a large number of observations of these objects. To determine the telescope focal length more accurately for attached detector, we used angular-separation measurements from CCD images. The obtained focal length is $F = (15774 \pm 21)$ mm using the CCD camera VersArray 1300B attached to the telescope.

1. INTRODUCTION

The telescope focal length is an important parameter in determining the angular pixel size. It is used for the purpose of determining the relative coordinates (angular separation and position angle) of double and multiple stars, as well as in determining the precise optical coordinates of extragalactic radio sources (ERS).

In this paper we present the first results of determining the effective focal length of 2 meter Ritchey-Chretien-Coude telescope installed at National Astronomical Observatory at Rozhen (NAOR) for the CCD camera VersArray 1300B. We observed with system Ritchey-Chretien. Both primary and secondary mirrors are hyperbolic. The telescope focal length is 16 m with focal ratio of f/8 as given by the manufacturer. The NAOR is located in southern Bulgaria. The geographic coordinates of the station are: the longitude $24^\circ 44' 18''$, latitude $41^\circ 41' 41''$ and altitude above the sea level 1730 m. More details can be found at website¹.

2. EQUIPMENT AND METHOD

From 2004 till now a group of astronomers from the Belgrade Observatory has stayed several times at the NAOR in Bulgaria taking frames of visual double and multiple stars. Series of observations of double and multiple stars at the Bulgarian NAOR have been made with a CCD camera attached to their 2 m telescope. Only in

¹<http://www.nao-rozhen.org/>

the observations from 2004 the Photometrics CE200A CCD camera was used. The dimensions of CCD chip are 1024×1024 pixels, the pixel size is 24×24 micrometers. The angle corresponding to one pixel is 0.31 arcsec. All later observations have been performed with the CCD camera VersArray 1300B with characteristics: 1340×1300 pixels, the pixel size is 20×20 micrometers and one pixel is 0.26 arcsec.

The effective focal length F for a two-mirror system is given by Bely (2003):

$$F = \frac{f_1 f_2}{f_1 + f_2 - s},$$

where f_1 and f_2 are the focal length of the primary and the secondary mirrors respectively, and s is the distance between the two mirrors (Fig.1). As can be seen, the effective focal length depends on s . For each detector (CCD cameras) s is varied during the focus finding procedure which changed the effective focal length F too.

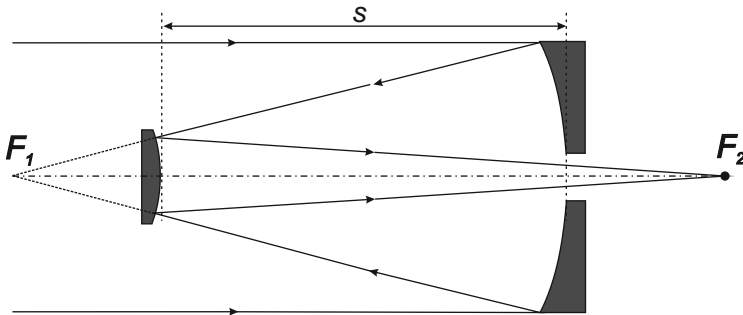


Figure 1: Scheme of a two-mirror system: F_1 is the primary mirror focus, F_2 is the effective focus and s is the distance between the two mirrors.

The effective focal length can be determined by comparing the measured separation d_m between the images of two objects on a CCD frame with the separation d_c calculated by using their coordinates taken from a catalogue.

The positions of objects in frames were measured by using the AIP4WIN software (Berry and Burnell 2002).

3. OBSERVATIONS

Our team has performed eight series of CCD observations of visual double and multiple stars at the NAO Rozhen in the period from 2004 to 2012. Also, we have performed three series of CCD observations of compact ERS that are visible at optical wavelengths in order to investigate the relation between the optical and radio reference frames.

The first series was in the middle of October 2004 (the frames were obtained by using the Photometrics CE200A CCD camera). The other seven series of CCD observations of visual double and multiple stars were: in the end of October 2005, on December 16/17 2006, on July 20/21 2009, on September 7-10 2010, from March 29 to April 01 2011, on October 27-28 2011 and on April 24-26 2012. In the last seven series the frames were obtained by using the CCD camera VersArray 1300B. A total of 891 pairs were measured. The results of observations obtained by 2011 have been

published in Pavlović et al. (2005), Cvetković et al. (2006, 2007, 2010, 2011). The results of observations performed during 2011 will be published (Cvetković et al., in preparation).

The three series of CCD observations of ERS were done: from March 29 to April 01 2011, on October 27-28 2011 and on April 24-26, 2012. About 100 ERS objects were measured.

As examples four CCD frames obtained with the CCD camera VersArray 1300B are given in Fig. 2.

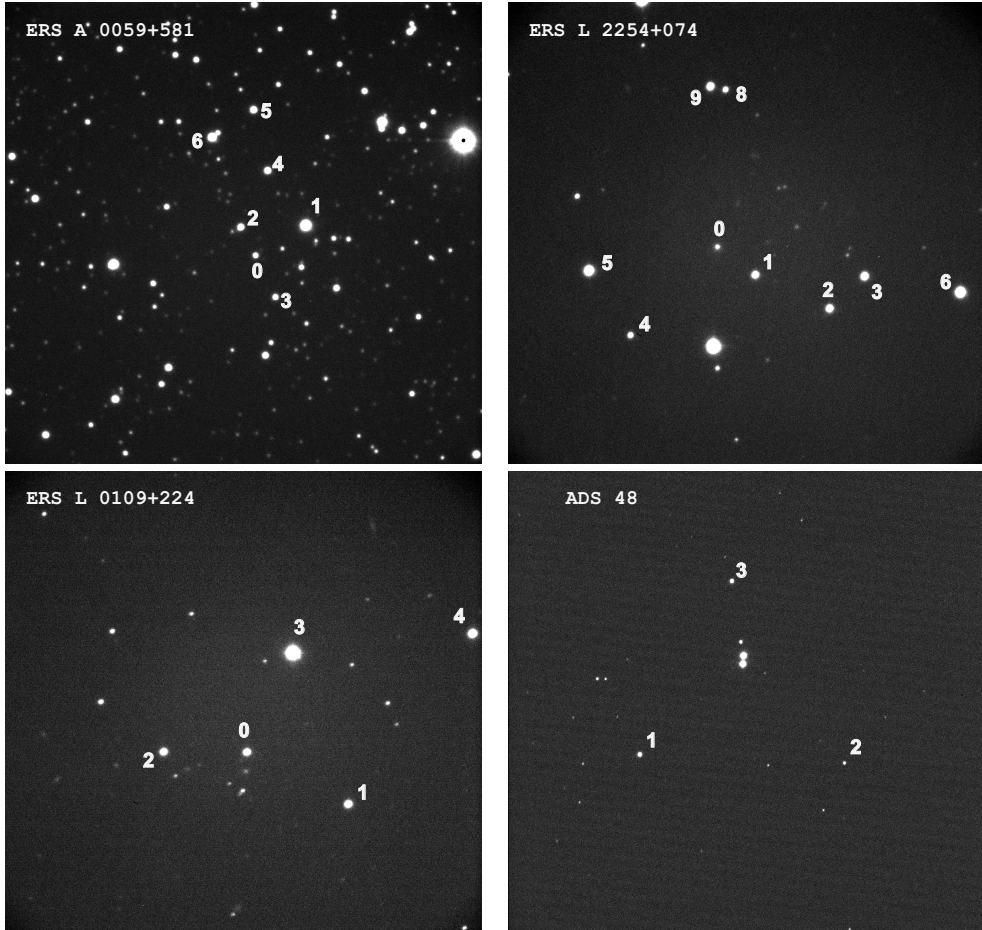


Figure 2: CCD frames obtained with camera VersArray 1300B at NAOR. The separations were measured between either two stars from field of view or a star and an extragalactic radio source and used to determine the telescope focal length.

During the summer of 2011 the first observations of celestial bodies from the new Astronomical Station on the mountain of Vidojevica (ASV) took place. This Station belongs to the Astronomical Observatory of Belgrade. From June to November 2011 we carried out several series of CCD observations of visual double or multiple stars

at Astronomical Station Vidojevica aimed at determining the relative coordinates (angular separation and position angle). For these series we used either SBIG ST-10ME or Apogee Alta U42 CCD cameras. Also, during September and October 2011, we observed about 20 compact ERS that are visible at optical wavelengths in order to investigate the relation between the optical and radio reference frames. The optical positions of ERS (α and δ) have been calculated using the positions of reference stars from some of big modern star catalogues. For these observations we used Apogee Alta U42 CCD camera only.

During the autumn of 2011 we observed the same objects at both NAOR and ASV. We noticed that the measured separations (ρ_{NAOR} , ρ_{ASV}) differ for the same pairs of stars and the differences increase with increasing angular separation. Therefore, we measured the angular separations between images of objects visible in our CCD frames. The results for measured separations and their corresponding separation differences $\Delta\rho = \rho_{NAOR} - \rho_{ASV}$ are given in Table 1 and Fig.3. It is clear that their dependence is linear and it can be given by the following equation:

$$\Delta\rho = 0.0019 + 0.0137\rho \quad .$$

The separation depends on the angle corresponding to one pixel, i.e. the focal length of the telescope. The result of determining the focal length of 60 cm telescope at the ASV are given in Cvetković *et al.* (2012), and of 2 m NAOR telescope in this paper (see Table 2). The differences are relatively small, the order of 1.4%. For pairs of stars with angular separations smaller than $10''$, the differences are approximately equal to measurement errors. Our observational program of double and multiple stars contains mainly pairs with angular separations less than $10''$ and therefore small deviations in separations resulting from inaccurate telescope focal length could not be previously noticed.

Table 1: The separations (in arcsec) measured for the same pairs of objects from CCD frames obtained at NAO Rozhen and ASV as well as the separation differences.

ρ_{NAOR}	ρ_{ASV}	$\Delta\rho$
44.61	45.23	0.62
62.90	63.76	0.86
107.41	108.86	1.45
109.72	111.26	1.54
115.45	117.03	1.58
120.59	122.21	1.63
142.43	144.39	1.97
148.39	150.47	2.08
155.05	157.17	2.13
189.11	191.69	2.58

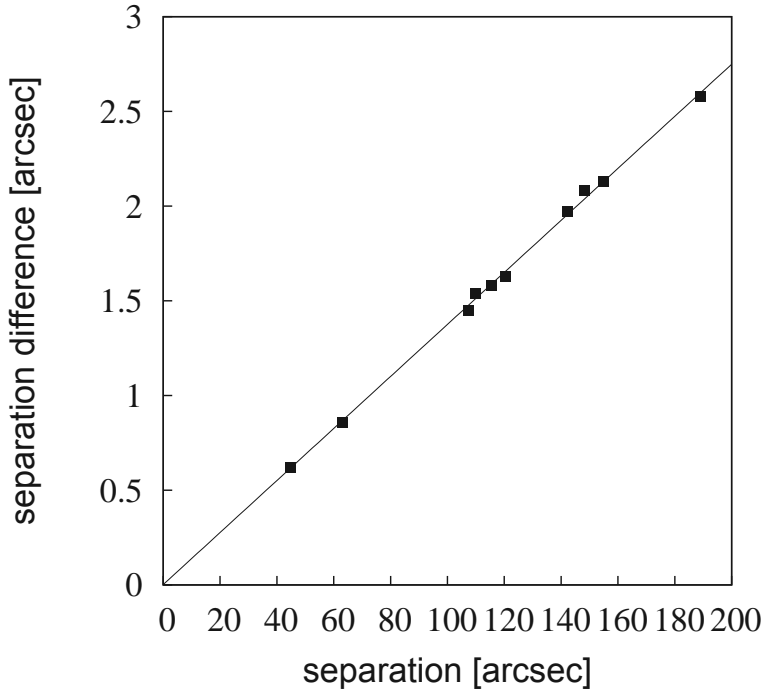


Figure 3: The separation differences versus separation measured for the same pairs of objects at NAOR and ASV.

4. CALCULATION AND RESULTS

The telescope effective focal length for detector (CCD camera VersArray 1300B) was determined by comparing the measured separations d_m of images of two stars or a star and an ERS on the CCD frames, with the separations d_c calculated from their coordinates and proper motions.

For data reduction we used the XPM catalogue² that contains the positions and proper motions of 314 million stars distributed all over the sky for the epoch J2000.0. Since the catalogue coordinates (α_0 and δ_0) are given for J2000.0, the corresponding positions for the epoch of the observations (α_i and δ_i) are calculated by taking proper motions into account. The coordinates of radio sources are taken from the ICRF2 list (Fey et al. 2009). These are remote sources with proper motions negligibly small.

The angular separation d_c between two objects (arc along a great circle of celestial sphere) is calculated from their coordinates α_i and δ_i , $i = 1, 2$ for the epoch of observations according to the formula

$$\cos d_c = \sin \delta_1 \sin \delta_2 + \cos \delta_1 \cos \delta_2 \cos(\alpha_2 - \alpha_1) .$$

The measured separation d_m is calculated from:

²<http://astrodata.univer.kharkov.ua/catalogs/XPM/>

$$d_m = \frac{3600 \times 180}{\pi} \sqrt{(x_1 - x_2)^2 + (y_1 - y_2)^2},$$

where x_i and y_i , $i = 1, 2$ are the measured coordinates from the CCD frame.

The field of view of CCD frames is small enough (its size is 5.8×5.6 arcmin) and we did not apply the corrections for apparent displacements such as the differential refraction (Aslan *et al.* 2010, Kiselev 1989). The main steps for processing the CCD images are the detection of star-like objects (ERS) and stars, and measuring the positions (x, y) .

The focal length of the telescope is obtained from:

$$F = \frac{d_m}{d_c}.$$

The calculated values of F are given in Table 2 as well as the coordinates and proper motions of the objects used in these determinations. The radio sources are faint, their apparent magnitudes exceed 14 so that the corresponding exposures lasted about one minute. The frames containing visual double stars were obtained with shorter exposures. Their apparent magnitudes are below 12 so that the exposure times were from a few tenths to a few seconds. Due to this, the frames with the radio sources contain more images of stars for which the separations were measured than the frames with double stars.

Numbers of objects identified on the CCD frames, where a radio source is assigned zero and stars numbers exceeding zero, are given in the first column in Table 2. Right ascensions and declinations (in degrees) and proper motions $\mu_\alpha \cos \delta$ and μ_δ (in mas/yr) are given in columns 2-5 and in columns 6-9 for the first and second object of a pair respectively. The focal length of the telescope is given in the tenth column. The year of observation is given in the last column. An empty row separates the measurements on different CCD frames for ERS or the measurements of different pairs for double stars.

When the CCD camera VersArray 1300B was attached to the 2 m telescope, we obtained the focal length $F = (15774 \pm 21)$ mm. It is the average of the 40 values given in Table 2.

The temperature variation of the focal length has not been studied because the need for determining the focal length of the telescope more accurately appeared only when we had the observations of the same objects at both NAOR and ASV (autumn 2011). Therefore, the temperature effects on the focal length are left for future observations.

Table 2.: Focal length of 2 m telescope at NAO Rozhen with attached CCD camera VersArray 1300B.

Table 2.: Focal length of 2 m telescope at NAO Rozhen with attached CCD camera VersArray 1300B.										
pairs	α_1 [$^{\circ}$]	δ_1 [$^{\circ}$]	$\mu_{\alpha_1} \cos \delta_1$ [mas/yr]	μ_{δ_1} [mas/yr]	α_2 [$^{\circ}$]	δ_2 [$^{\circ}$]	$\mu_{\alpha_2} \cos \delta_2$ [mas/yr]	μ_{δ_2} [mas/yr]	F [mm]	year
0- 1	18.024270	22.744107	0.00	0.00	18.002064	22.755148	-3.57	-8.12	15765	2011
0- 2	18.024270	22.744107	0.00	0.00	18.042636	22.743713	-5.48	2.30	15824	2011
0- 3	18.024270	22.744107	0.00	0.00	18.013677	22.724062	-4.44	-26.81	15755	2011
0- 4	18.024270	22.744107	0.00	0.00	17.973797	22.720838	9.26	-4.07	15781	2011
0- 1	15.690677	58.403094	0.00	0.00	15.671078	58.397176	-33.78	0.87	15761	2011
0- 2	15.690677	58.403094	0.00	0.00	15.696223	58.397288	-6.16	-13.82	15769	2011
0- 3	15.690677	58.403094	0.00	0.00	15.683303	58.411670	-4.40	-1.35	15775	2011
0- 4	15.690677	58.403094	0.00	0.00	15.685314	58.385840	1.86	-2.47	15773	2011
0- 5	15.690677	58.403094	0.00	0.00	15.690276	58.373386	0.16	-1.28	15770	2011
0- 6	15.690677	58.403094	0.00	0.00	15.706665	58.378832	30.57	13.97	15783	2011
0- 1	343.280705	19.709619	0.00	0.00	343.270844	19.688776	7.53	2.00	15812	2011
0- 2	343.280705	19.709619	0.00	0.00	343.254917	19.704537	26.80	-5.09	15775	2011
0- 3	343.280705	19.709619	0.00	0.00	343.277107	19.723909	45.25	-3.12	15722	2011
0- 4	343.280705	19.709619	0.00	0.00	343.297852	19.733495	0.06	-14.81	15758	2011
0- 5	343.280705	19.709619	0.00	0.00	343.308839	19.738109	6.73	-0.82	15764	2011
0- 6	343.280705	19.709619	0.00	0.00	343.316243	19.739516	-4.73	-3.72	15754	2011
0-10	343.280705	19.709619	0.00	0.00	343.235601	19.744564	-6.24	-12.42	15780	2011
0- 1	344.322096	7.720084	0.00	0.00	344.314393	7.725902	16.93	-12.71	15860	2011
0- 2	344.322096	7.720084	0.00	0.00	344.299252	7.733080	0.37	-0.88	15767	2011
0- 3	344.322096	7.720084	0.00	0.00	344.291939	7.726671	-3.45	0.04	15779	2011
0- 4	344.322096	7.720084	0.00	0.00	344.340401	7.737714	7.81	4.88	15734	2011
0- 5	344.322096	7.720084	0.00	0.00	344.348585	7.724290	27.90	-7.18	15753	2011
0- 6	344.322096	7.720084	0.00	0.00	344.272324	7.730363	-19.47	-13.71	15779	2011
0- 8	344.322096	7.720084	0.00	0.00	344.319724	7.688006	9.70	-8.88	15761	2011
0- 9	344.322096	7.720084	0.00	0.00	344.322800	7.687318	22.00	-23.82	15762	2011
1- 2	1.392738	45.791748	6.47	-5.84	1.420091	45.827052	13.85	-7.68	15781	2005
1- 2	1.392738	45.791748	6.47	-5.84	1.420091	45.827052	13.85	-7.68	15781	2006
1- 2	1.392738	45.791748	6.47	-5.84	1.420091	45.827052	13.85	-7.68	15773	2010
1- 2	1.392738	45.791748	6.47	-5.84	1.420091	45.827052	13.85	-7.68	15773	2011
1- 2	1.392738	45.791748	6.47	-5.84	1.420091	45.827052	13.85	-7.68	15767	2012
1- 3	1.392738	45.791748	6.47	-5.84	1.452613	45.789707	6.68	-8.17	15775	2005
1- 3	1.392738	45.791748	6.47	-5.84	1.452613	45.789707	6.68	-8.17	15780	2006
1- 3	1.392738	45.791748	6.47	-5.84	1.452613	45.789707	6.68	-8.17	15779	2010
1- 3	1.392738	45.791748	6.47	-5.84	1.452613	45.789707	6.68	-8.17	15778	2011
1- 3	1.392738	45.791748	6.47	-5.84	1.452613	45.789707	6.68	-8.17	15780	2012
2- 3	1.420091	45.827052	13.85	-7.68	1.452613	45.789707	6.68	-8.17	15773	2005
2- 3	1.420091	45.827052	13.85	-7.68	1.452613	45.789707	6.68	-8.17	15781	2006
2- 3	1.420091	45.827052	13.85	-7.68	1.452613	45.789707	6.68	-8.17	15773	2010
2- 3	1.420091	45.827052	13.85	-7.68	1.452613	45.789707	6.68	-8.17	15772	2011
2- 3	1.420091	45.827052	13.85	-7.68	1.452613	45.789707	6.68	-8.17	15767	2012

5. CONCLUSION

The focal length of the NAOR 2 m telescope is close to that declared at the factory. Its values can differ when diverse detectors are used in the observations.

In the case of frames taken with VersArray 1300B the telescope focal length obtained here differs from the manufacturer's one by less than 2%. This fact indicates a good quality of the telescope (mirror and construction).

The temperature variation of the focal length should be examined.

The focal-length values corresponding to other detectors: another CCD, adaptive optics, filters, etc, should be also determined.

Acknowledgements

The authors from the Astronomical Observatory in Belgrade gratefully acknowledge the observing grant support from the Institute of Astronomy and Rozhen National Astronomical Observatory, Bulgarian Academy of Sciences. This research has been supported by the Ministry of Education and Science of the Republic of Serbia, Project No 176011 "Dynamics and kinematics of celestial bodies and systems".

References

- Aslan, Z., Gumerov, R., Jin, W., Khamitov, I., Maigurova, N., Pinigin, G., Tang, Z. and Wang, S.: 2010, *A&A*, **510**, A10.
- Bely, P. Y. (Editor): 2003, *The Design and Construction of Large Optical Telescopes*, Springer-Verlag, New York, Inc.
- Berry, R. and Burnell, J.: 2002, *The Handbook of Astronomical Image Processing*, Includes AIP4WIN Software, Willmann-Bell, Inc., Richmond, USA.
- Cvetković, Z., Novaković, B., Strigachev, A. and Popović, G. M.: 2006, *Serb. Astron. J.*, **172**, 53.
- Cvetković, Z., Pavlović, R., Strigachev, A., Novaković, B. and Popović, G. M.: 2007, *Serb. Astron. J.*, **174**, 83.
- Cvetković, Z., Pavlović, R. and Boeva, S.: 2010, *Serb. Astron. J.*, **180**, 103.
- Cvetković, Z., Pavlović, R., Damljanović, G. and Boeva, S.: 2011, *AJ*, **142**, 73C.
- Cvetković, Z., Damljanović, G., Pavlović, R., Vince, O., Milić, I. S. and Stojanović, M.: 2012, *Serb. Astron. J.*, **184**, in press.
- Fey, A. L., Gordon, D. and Jacobs, C. S.: 2009, IERS Technical Note, No. 35.
- Kiselev, A. A.: 1989, *Theoretical foundations of photographic astrometry*, Nauka, Moskva.
- Pavlović, R., Cvetković, Z., Olević, D., Strigachev, A., Popović, G. M. and Novaković, B.: 2005, *Serb. Astron. J.*, **171**, 49.

KINEMATICS OF A LOOP-LIKE ERUPTIVE PROMINENCE AS OBSERVED BY AIA/SDO

M. DECHEV¹, K. KOLEVA¹, M. S. MADJARSKA², P. DUCHLEV¹,
J.-C. VIAL³, E. BUCHLIN³

¹*Institute of Astronomy and National Astronomical Observatory, BAS,*

²*Armagh Observatory, College Hill, Armagh, N. Ireland*

³*Univ Paris-Sud, Institut d'Astrophysique Spatiale, Orsay, France*

Abstract. We examined the kinematic and helicity pattern, as well as the morphological and geometrical evolution of an EP on 2010 March 30. We used the He II 304 Å AIA/SDO and EUVI/STEREO B observations. The unique combination of high-resolution limb observations of the EP in AIA and a central meridian position in EUVI permitted a view from significantly different perspectives and detailed analysis of the prominence eruption. The eruption process consists of prominence activation, acceleration, and a phase of constant velocity. The prominence body was composed of left-hand twisted threads around the main prominence axis. The twist during the eruption was estimated at 3 turns (6π). The prominence reformed in the same place two days after its eruption. The same sign of the prominence body twist and writhe, as well as the amount of twisting above the critical value of 2π after the activation phase indicate that the conditions for kink instability were present. The fact that the erupted filament re-formed at the same place two days after the eruption implies a confined type of eruption.

1. INTRODUCTION

Prominence eruptions are large-scale eruptive phenomena, which occur in the low solar atmosphere. Eruptive prominences (EP), in contrast to active ones, could be defined as prominences in which all or some of the prominence material appears to escape the solar gravitational field (Gilbert et al., 2000). Gilbert et al. (2007) summarize three types of prominence eruptions: a full eruption, when all of the material is expelled; a partial, when only a part of the mass erupts; or a failed eruption, if the material resettles or falls back to the surface. The observations show that prominence/filament activations include a wide range of eruptive-like dynamic activity, from the full eruption (Plunkett et al., 2000) through partial eruption (Zhou et al. 2006; Liu et al., 2008) to failed eruption. Several studies

(Sterling & Moore, 2004 a, b) have unveiled a common pattern of prominence (filament) eruptions: an initial slow-rise phase (with very small acceleration), during which the filament gradually ascends, followed by a sharp change to a fast-rise phase of fast acceleration. The eruption onset has been defined as the transition between these two phases. There are three scenarios for a prominence rising after its fast rise phase: 1) an EP can continue to raise with acceleration, 2) an EP fast rise can be followed by a constant velocity phase, or 3) a constant velocity phase of a EP can be followed by a deceleration phase (Vrsnak, 1998).

The slow rise motion of an EP is accompanied by a gradual morphological evolution from an initially intricate structure into an apparently toroidal shape, exposing sometimes a twisted pattern, that is most often prominent in the legs of the prominence (Vrsnak et al., 1991). EPs very often develop a clearly helical axis shape in the course of the eruption, which is the characteristic signature of a MHD kink instability (KI) of a twisted magnetic flux rope (MFR) (Rust & LaBonte, 2005). A MFR becomes kink-unstable if the twist, a measure of the number of windings of the field lines about the rope axis, exceeds a critical value of 2π (Hood and Priest, 1981). The axis of an MFR then undergoes writhing (kinking) motions and part of the twist of the field is transformed into helical writhe of the axis, since the magnetic helicity is essentially conserved (Rust & LaBonte, 2005). The conservation of helicity in ideal MHD (Berger, 1984) requires the resulting writhe to be of the same sign as the transformed twist (Green et al., 2007). The kink instability has long been investigated as a possible triggering mechanism for solar eruptive phenomena, especially in flux rope models (Liu and Alexander, 2009).

2. OBSERVATIONAL MATERIAL

The prominence eruption was observed at the North-East solar limb between 17:30 UT and 19:30 UT on 2010 March 30. The EP was located at mean heliographic co-ordinates N22.63°; E78.80° and centered mean position angle 66°.

The analyzed images were taken with 1 min cadence in the He II 304 Å pass-band of AIA/SDO (Lemen et al., 2011). The AIA instrument consists of seven Extreme Ultra-Violet (EUV) and three Ultra-Violet (UV) channels which provide an unprecedented view of the solar corona with an average cadence of about 12s. The AIA image field-of-view reaches 1.3 solar radii with a spatial resolution of about 1.5 arcsec.

First, we selected a partial field-of-view (FOV) from the AIA He II 304 Å images. We used level 1 reduced data, i.e. the dark current removed and flat-field correction applied. We extracted 700 x 1000 pixels² cut-outs from the full FOV images. The images were further stabilized for the satellite movements by applying intensity cross-correlation analysis. For the purpose of our analysis we defined the visible limb from the He II 304 Å images.

We also analyzed observations from the Extreme Ultraviolet Imager (EUVI) aboard STEREO Behind (B) spacecraft. EUVI has a field-of-view of 1.7 R_{\odot} and

observes in four spectral channels that cover the 0.1 to 20 MK temperature range (Wuelser et al., 2004). The EUVI detector has pixel size of 1.6 arcsec.

In the present study we used EUVI images in the He II 304 Å channel with an average cadence of 10 minutes.

3. MORPHOLOGY AND HELICITY EVOLUTION

The prominence eruption evolved as a height expanding twisted loop with both legs anchored in the chromosphere of a plage area.

The prominence can be observed in H-alpha before the activation at 17:19 UT (Fig.1) as a few bright clouds above the limb with no distinguishable fine structure.

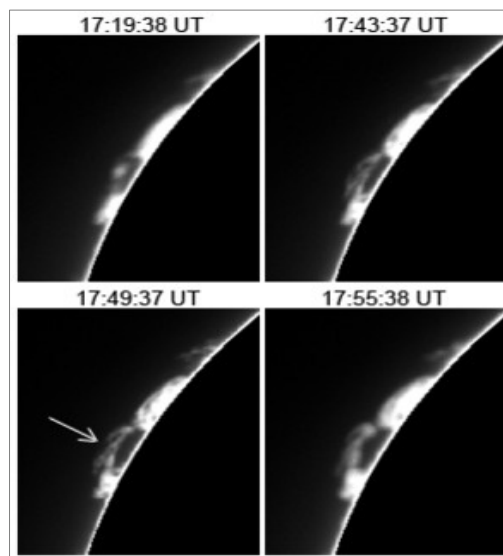


Figure 1: Mauna Loa H-alpha images before and during the start of the prominence activation. The arrow points at the region revealing twisted structure.

The first signature of a twisted prominence fine structure appears at 17:49 UT in the AIA He II 304 Å image (Fig.2). From part of the prominence where the fine structure is visible, we could estimate a 2π twist, i. e. one turn of the prominence rope around its main axis. This time coincides with the beginning of the prominence slow rise during the activation phase. The total twist was estimated to be of about 6π (3 turns) of the eruptive prominence body.

After 18:25 UT the eruption can also be followed on the EUVI/STEREO image differences shown in Fig. 3. Here, thanks to the different view point we could see

that the filament upper body underwent a left-hand writhe, which increase with time, reaching $\pi/2$ at 19:26 UT.

The helical twist of the prominence and its evolution in time can be clearly seen in AIA He II 304 Å images after 18:20 UT. During the prominence rise the twist transfers from the lower (legs) to the upper prominence body causing the prominence to evolve from a loop-shaped into a ribbon-like structure. From the EUVI B difference images (Fig. 3), we established the footpoint location in order to determine the type of twist and writhe, and their evolution in time. Based on the magnetic field polarity configuration obtained from the magnetograms, the H-alpha images and the prominence drawings (Fig. 7), we could determine in which magnetic polarity the southern and the northern legs of the prominence were located. We determined that the prominence underwent a left-hand writhe as a result of counter-clockwise rotation with respect to the two polarity fluxes.

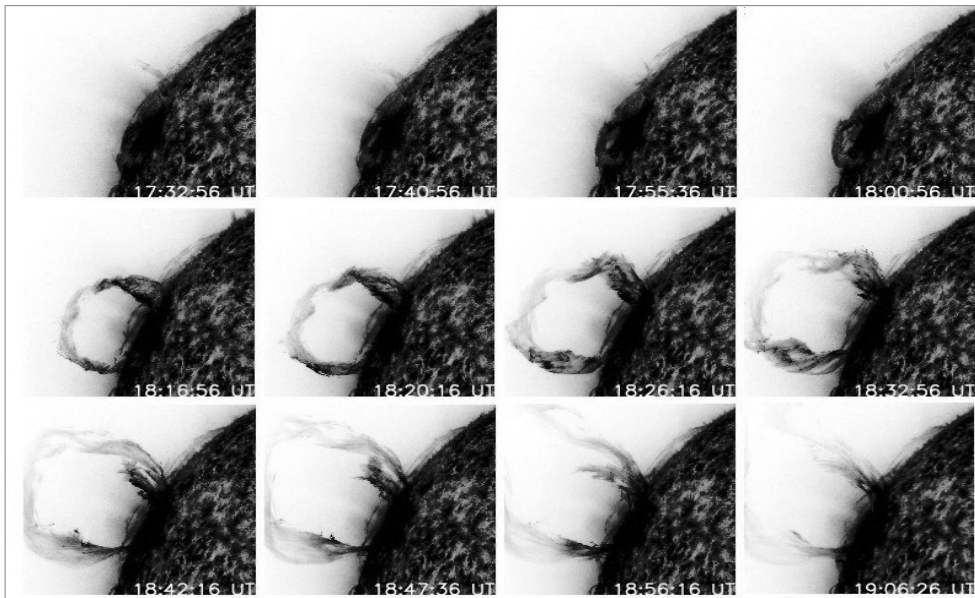


Figure 2: He II 304 Å images (in reversed colour table) showing the morphology and, in particular, the helicity evolution of the erupting prominence.

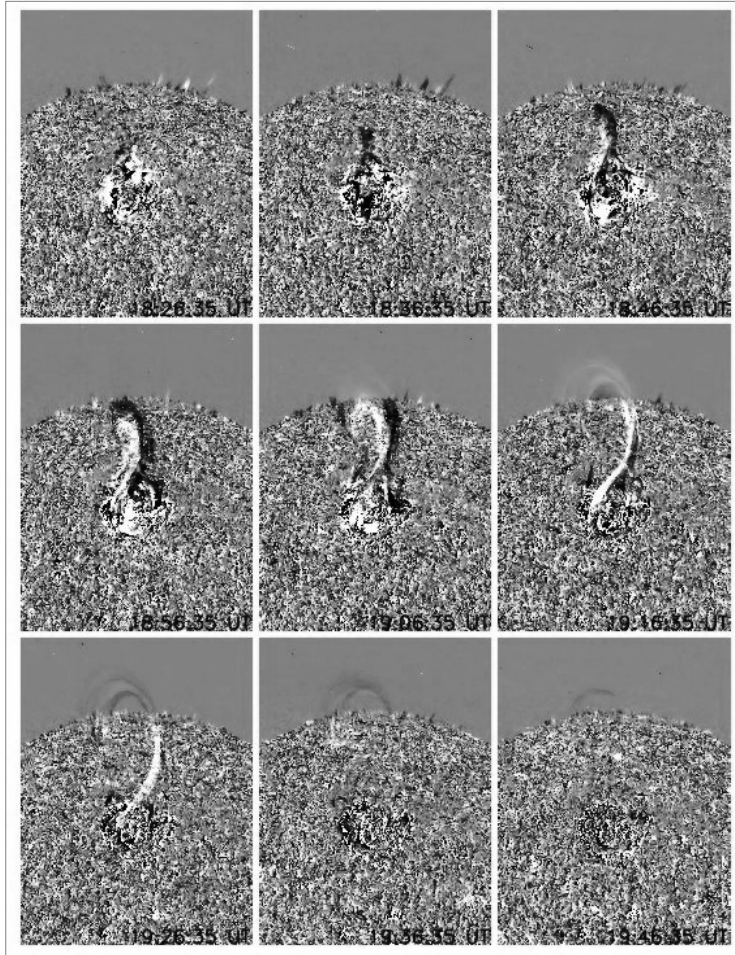


Figure 3: Running difference images from EUVI B in the He II 304 Å channel.

4. KINEMATICS

The prominence height was determined as the height of the main axis of the prominence above the visible limb as observed in the He II 304 Å channel of the AIA/SDO images (Fig. 4). The time evolution of the height reveals three distinctive phases of the prominence eruption: prominence activation, an eruption with acceleration, and an eruption with a constant velocity. The height-time diagram of the prominence eruption is presented in Fig. 5. From the first and second derivatives of the polynomial fit of the height-time curve, we defined the speed and the acceleration of the prominence eruption. The prominence activation is defined as the time period of a slow rise of the loop system with a velocity of 10 km/s. The activation is already in progress at the beginning of the AIA observations around 17:33 UT. Until 18:00 UT the height of the prominence

changed from 18 Mm to 34 Mm. The eruption onset was registered at 18:00 UT and it was determined from the AIA images as a sudden increase of the prominence height. It lasted until around 18:12 UT (Fig. 5). During this phase the prominence height changed from 34 Mm to 121 Mm and the speed of the prominence rise increased from 15 km s^{-1} to a maximum of 166 km s^{-1} with an acceleration from 46 to 430 ms^{-2} . The constant velocity phase was measured until 18:44UT. After this time the top of the looped prominence is outside the AIA field-of-view.

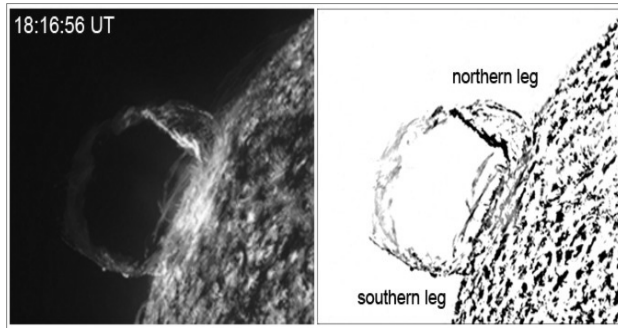


Figure 4: The eruptive prominence on 2010 March 30 observed in the 304 \AA AIA/SDO channel at 18:17 UT (left) and its corresponding edge-enhanced image (right).

We used also, as an additional geometrical parameter, the diameter at the summit \mathbf{D} of the main prominence MFR. Its dependence as a function of time is given in Fig.6. The time profile of \mathbf{D} clearly shows two phases in its behavior: slow decrease during a 51-minute time interval and strong increase during an 8-minute time interval. The comparison of the time profiles of \mathbf{D} and the EP height in Fig.6 shows that the decrease of \mathbf{D} covers the activation, acceleration, and half of the constant velocity phase of the EP.

The kinematics of the different phases of the eruptive process is summarized in Table 1.

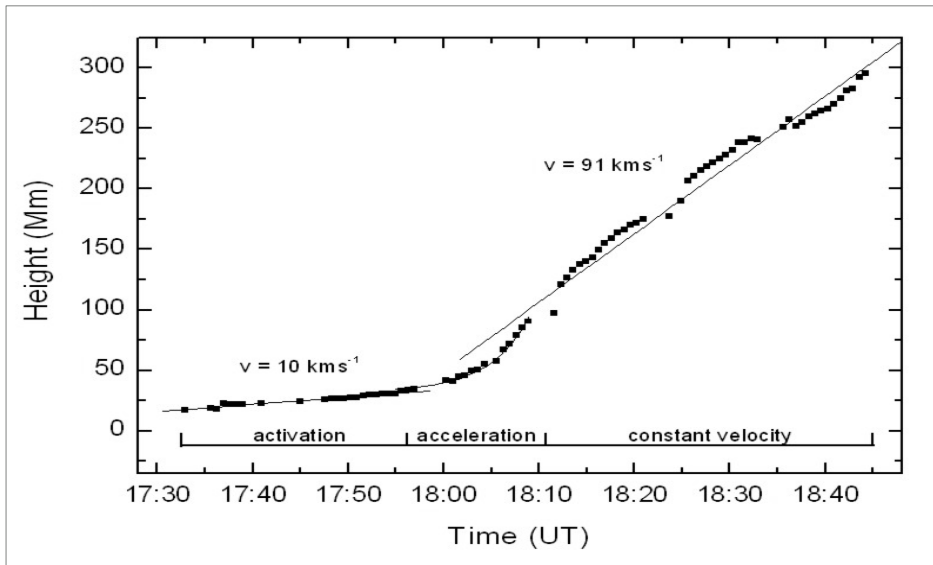


Figure 5: Height-time profile of the prominence eruption for the three phases of the EP evolution: the activation, the acceleration, and the constant velocity.

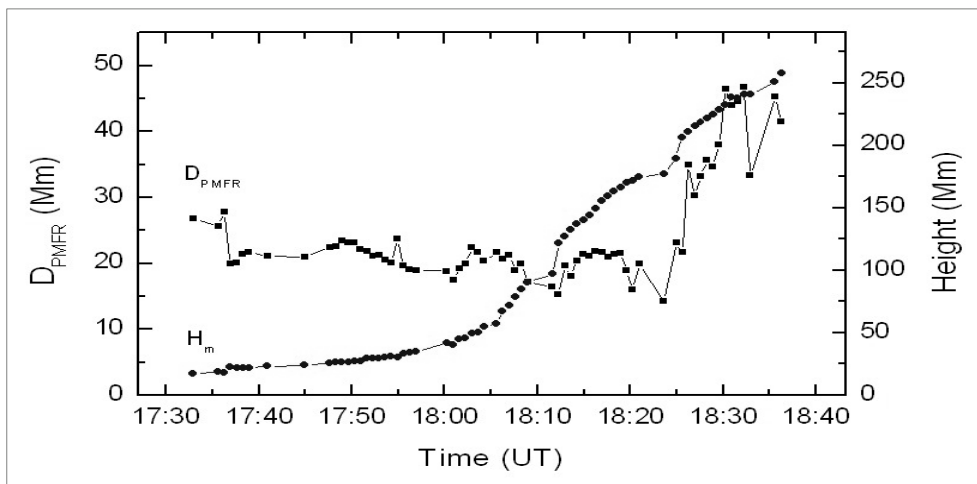


Figure 6: Time profile of the diameter D of the main prominence magnetic flux rope (PMFR) at the EP summit. The time profile of the height of the axis of main PMFR is shown, too.

Table.1: Kinematics of the eruptive prominence derived from the AIA images.

Phase	Time (UT)	Height (Mm)	Velocity (km s^{-1})	Acceleration (m s^{-2})
Activation	17:33 - 18:00	18 - 34	10	0
Acceleration	18:00 - 18:12	34 - 121	15 - 166	46 - 430
Constant velocity	18:12 - 18:44	121 - 295	91	0

5. REFORMATION

The prominence reformed in the same place two days after its eruption. In Fig. 7 the re-formation of the filament is presented from March 31 to April 2. On March 31, one day after its eruption, the filament can be traced above and below the plage area on the Coimbra Solar Observatory H-alpha (Fig.7a). The magnetic field of the plage area associated with the reforming filament can be seen in Fig.7b. Figs.7 c, d, e and f show H-alpha images and drawings of the area from the Pulkovo Observatory, confirming the reformation of the filament. However, we can notice that the H-alpha filament is rather faint. We searched for its reformation in the EUV lines of EUVI B, but even in He II it was not possible to detect it. One can conclude that even if the eruption failed, the material was not totally recovered at the low temperature typical of a filament.

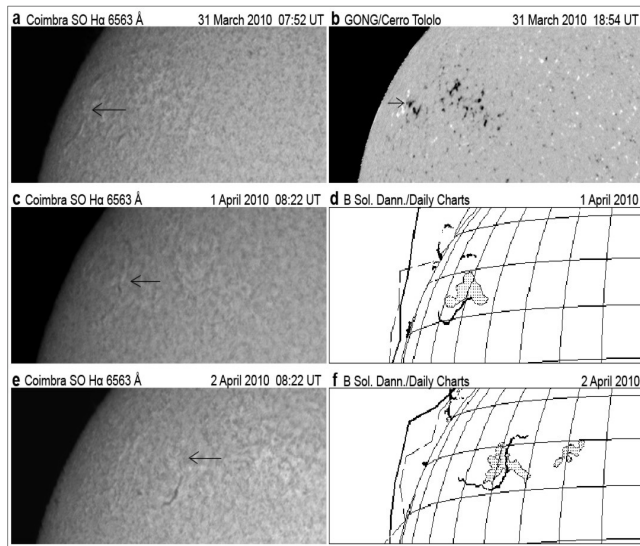


Figure 7: The prominence reformation as seen on the disk as a filament traced in Coimbra Solar Observatory H-alpha images (**a**, **c**, **e**), a GONG magnetogram (**b**), and daily drawings of the Sun from the electronic Bulletin "Solnechnye Dannye" of Pulkovo Observatory (**d** and **f**).

6. RESULTS

We examined the kinematic and helicity pattern together with the morphological and geometrical evolution of an EP, based on He II 304Å AIA/SDO and EUVI/STEREO B observations. The unique combination of high-resolution limb observations of the EP in AIA and a central meridian position in EUVI B permitted a detailed analysis of the prominence eruption on 2010 March 30. The obtained results can be summarized as follow:

- The EP appeared as a helically twisted MFR with fixed foot-points. The prominence's body was composed of left-hand twisted threads around the main prominence axis. The twist during the eruption was estimated to be 6π (3 turns).
- The EP twist progressively converted into a left-hand writhe that is clearly traced in the EUVI/STEREO B images.
- The prominence contracted to its primary location after reaching a maximum height of 526 Mm. The prominence/filament partially reformed, suggesting that either part of the material has drained into the photosphere or that not all of the prominence material returned to its primary temperature.

Acknowledgments

One of the authors (M. D.) is supported by a grant of the Bulgarian National Science Foundation, Ministry of Education and Science, under number DO-02-275.

References

- Berger, M. A.: 1984, *Geophysical and Astrophysical Fluid Dynamics*, **30**, 79.
 Gilbert, H. R., Alexander, D., Liu, R.: 2007, *Sol. Phys.*, **245**, 287.
 Gilbert, H. R., Holzer, T. E., Burkepile, J. T., Hundhausen, A. J.: 2000, *ApJ*, **537**, 503.
 Green, L. M., Kliem, B., Torok, T., van Driel-Gesztelyi, L., Attrill, G. D. R.: 2007, *Sol. Phys.*, **246**, 365.
 Hood, A. W., Priest, E. R.: 1981, *Geophysical and Astrophysical, Fluid Dynamics*, **17**, 297.
 Lemen, J. R., Title, A. M., Akin, D. J., et al.: 2011, *Sol. Phys.*, 172.
 Liu, R., Alexander, D.: 2009, *ApJ*, **697**, 999.
 Liu, R., Gilbert, H. R., Alexander, D., Su, Y.: 2008, *ApJ*, **680**, 1508.
 Plunkett, S. P., Vourlidas, A., Simberova, S., et al.: 2000, *Sol. Phys.*, **194**, 371.
 Rust, D. M., LaBonte, B. J.: 2005, *ApJ*, **622**, L69.
 Sterling, A. C., Moore, R. L.: 2004a, *ApJ*, **602**, 1024.
 Sterling, A. C., Moore, R. L.: 2004b, *ApJ*, **613**, 1221.
 Vršnak, B.: 1998, In: IAU Colloq. 167: *New Perspectives on Solar Prominences*, Eds.. D. F. Webb, B. Schmieder, D. M. Rust, *Astronomical Society of the Pacific Conference Series*, **150**, 302.
 Vršnak, B., Ruždjak, V., Rompolt, B.: 1991, *Sol. Phys.*, **136**, 151.

- Wuelser, J., Lemen, J. R., Tarbell, T. D., et al.: 2004, In: *Society of Photo-Optical Instrumentation Engineers (SPIE) Conference Series*, Eds.S. Fineschi, M. A. Gummin, **5171**, 111.
- Zhou, G. P., Wang, J. X., Zhang, J., et al.: 2006, *ApJ*, **651**, 1238.

SOCIETY OF ASTRONOMERS OF SERBIA 2008-2011

MILAN S. DIMITRIJEVIĆ

Astronomical Observatory, Volgina 7, 11060 Belgrade, Serbia
E-mail: mdimitrijevic@aob.bg.ac.rs

Abstract: The review of activities of the Society of Astronomers of Serbia within the period 2008-2011 is presented.

1. INTRODUCTION

Society of astronomers of Serbia (SAS) is founded on 25. 02. 1981, and author of this contribution was elected for president on Assembly held in October 2008. Activities of the Society from October 2008 up to the end of 2011 are:

- International Year of Astronomy 2009;
- Olympiads in astronomy;
- Mobile planetarium and project "Popularization of astronomy in educational and cultural institutions and schools";
- Scientific meetings organized by DAS;
- Publishing activity of SAS;
- Foreign scientists – guests of Society of Astronomers of Serbia;
- Links with the European Astronomical Society;
- Links with the International Astronomical Union;

2. INTERNATIONAL YEAR OF ASTRONOMY 2009

On the proposition of UNESCO, in December 2007, the United Nations General Assembly adopted a resolution, that 2009 was declared the International Year of Astronomy, in order to mark the anniversary of the start of the telescopic era, the 400th anniversary of the first astronomical observation through a telescope made by Galileo Galilei.

IYA 2009 was a global celebration of astronomy and its contributions to society and culture, with the following objectives:

- Popularization of astronomy and related sciences;

Strengthening of the astronomical communities and of the international cooperation;

Astronomical education (formal and informal);

Promotion of the importance and attraction of the scientific work;

Strengthening of amateur community and improvement of the cooperation of amateurs and professionals;

Preservation and protection of world cultural and natural heritage of dark skies and historical astronomical sites.

Preparations for the marking of IYA in Serbia began in 2007, and since September 2008 until the end of IYA, national coordinator and president of the National Organizing Committee for the marking of IYA in Serbia was Nikola Božić. Beside him, from October 2008 (after the Assembly of the Society of Astronomers of Serbia), other members of the National Organizing Committee (NOC of IYA) are Ištvan Vince, Predrag Jovanović, Nadežda Pejović, Slobodan Ninković, Milan Dimitrijević, Dejan Urošević, Zoran Knežević, Nataša Stanić and Aleksandar Bogojević. Ministry of Science and Technological Development approved to SAS 600 000 RSD for projects for marking IYA 2009 in Serbia. With these funds disposed NOC of IYA and Nikola Božić reported to Directional Board of SAS on NOC of IYA activities. In celebration of IYA in Serbia, besides SAS, and all other astronomical institutions and society of amateur astronomers took part.

Coordinators of global projects were:

100 Hours of Astronomy - Janko Mravik;

Galileoscops - Goran Pavičić;

Cosmic Diary - Milan Ćirković;

Gates of the Universe - Aleksandar Zorkić;

She is an astronomer - Tijana Prodanović;

Conscience on dark sky - Nikola Božić;

Astronomical Heritage - Zorica Cvetković;

Galilean Ambassadors - Slobodan Ninković;

Conscience on the Universe - Nataša Stanić;

The universe as seen by eyes of Earth - Dragana Ilić;

Global development of astronomy - Olga Atanacković.

The most important activities realized during International Year of Astronomy, ordered chronologically, are:

Student's seminar "Architecture in Space", Research Station Petnica, January;

Series of lectures "The universe yours to discover" Kolarac Foundation, January / February:

Milutin Milanković - Canon of insolation, Zoran Knežević;

Great astronomical discoveries from Galileo until now, Nikola Božić;

- Galileo Galilei - the beginning of modern astronomy*, Milan Ćirković;
Radio Astronomy, Dr Jelena Milogradov-Turin;
 Ceremony of the proclamation of IYA in Serbia, Faculty of Science, February;
 Publishing of a brochure dedicated to IYA, March;
 Public telescopic observations in, at least, around fifteen cities throughout the year;
 The popular lectures, in at least two dozen cities throughout the year;
 Workshops for preschoolers, 7 Children's Theatre Festival "Zvezdarište", Municipality of Zvezdara, April;
 Program for preschool and primary school children, Children's Fair, Belgrade Fair, April;
 Participation at the manifestation "Night of Museums", Faculty of Science, AS "R. Bošković", Belgrade, May;
 Organization of participation in the international competition "Be astronomer of the Integral", May-June;
 Participation in the realization of the international photo competition "Earth and Sky", Summer; Media activity in *Politika, Novosti, Blic, 24 sata, Borba*, B92, RTS, Radio Beograd, Radio 021, *Prosvetni pregled, Vreme, Mikro, Playboy, Planeta, Astronomija, Glas javnosti, National Geography*, RTV, Pink, E-newspapers...;
 The third workshop of students of astronomy, Faculty of Science, June;
 Seventh Serbian Conference on spectral line shapes in astrophysics, Zrenjanin 15-19. June;
 Lecture for prisoners in the Prison for Juveniles in Valjevo, June;
 International Astronomical camp "Letenka" Fruška Gora, with more than 220 astronomers from around the region. The central activity of IYA in Serbia, July;
 International cooperation with countries of the region, but also with distant Ethiopia, the whole year;
 Public discussion of the phenomenon of concealment during the total solar eclipse, ten years later, in August;
 The projection of the popular science television series of Milan S. Dimitrijević, the Cinematheque, Autumn (organized by Andjelka Kovačević);
 Projections of science fiction films in the Cinematheque, Autumn (organized Andelka Kovačević);
 Exhibition dedicated to the cooperation between Serbia and France in the field of astronomy, the French Cultural Center, September;
 Astronomy and the arts, debates, exhibition of paintings and installations, Belgrade City Library, Youth Center, September;
 Series of lectures "In honor to Milanković", AS "R. Bošković", in September:
 Milan S. Dimitrijević: *Milanković and astronomy*;
 Jelena Milogradov-Turin: *How we repaid to Milutin Milanković*;
 Goran Pavičić: *On the Life and Work of Milutin Milanković*;
 Nataša Stanić: *Milanković as a popularizer of science: "Through Space and Centuries"*.

VI SREAC conference of professional astronomers with the participation of amateur astronomers, under the auspices of UNESCO, the Ministry of Science and Astronomical Observatory of Belgrade, September;

The cycle of lectures on "Women in Astronomy" in Kolarac Foundation, October:

Dragana Ilić: *The Astronomical Instruments – The Sky seen by the eyes of women*;

Olga Atanacković: *Women at Harvard - through Light to the Stars*;

Andjelka Kovačević: *The Stars of Miss Leavitt*;

Tijana Prodanović: *The missing Space - The story of Vera Rubin*;

Exhibition of astronomical photographs, within the frame of the project "From the Earth to the Universe," Education Fair and Book Fair, Belgrade Fair, October;

Art competition for children on topics in astronomy, during whole year;

Conference of Secondary school pupils - participants in programs of Research station "Petnica", "A Step into Science," November;

Astronomical exhibition and an exhibition of astronomical photos on the III Festival of Science, December;

The competition for primary school children for essays in connection with astronomy. The ceremony of handling the prizes on Belgrade Astronomical Observatory in cooperation with "Mladinska knjiga", December;

Encouragement of cooperation among amateur societies and professionals with them, during the whole year;

Seminars for teachers of physics, about astronomy, AD "R. Bošković ", autumn;

Encouragement and training for the establishment of school sections in Serbia, RS "Petnica", during the whole year;

To obtain a donation of 100 galileoscopes for schools in Serbia, December;

The start of the formation of the Museum of Astronomy at Belgrade Astronomical Observatory. the whole year, Vojislav Protić Benišek;

Purchase of a mobile planetarium, with the financial support of UNESCO, in December. The idea and project Nataša Stanić, about the practical realization the most is done by Goran Pavičić.

3. OLYMPIADS IN ASTRONOMY

Competitors from Serbia in this period took part in the following international Olympiads covering astronomy and astrophysics:

XIII International Astronomical Olympiad (International Astronomy Olympiad), Trieste, 13-21 October 2008, eight competitors, three over the quota (the success of the previous year), two seniors, three juniors, team leaders were Ratomirka Miller and Slobodan Ninković; silver medals obtained Nataša Dragović and Filip Živanović, bronze Milena Milošević, Aleksandar Miladinović and Dušan Joksimović.

III International Olympiad on Astronomy and Astrophysics (International Olympiad on Astronomy and Astrophysics) Teheran, 17-26 October 2009, four competitors, team leaders were Slobodan Ninković and Ivan Milić, silver medalists Aleksandar Vasiljković, Nataša Dragović and Filip Živanović, Milena Milošević commended, and Filip Živanović as the best observer received a special award and gift (lap-top) from the organizers.

XIV International Astronomical Olympiad, Hangzhou, 8-16 November 2009, the four contestants, two seniors and two juniors, team leaders were Ratomirka Miller and Slobodan Ninković, bronze medalist Ognjen Marković.

IV International Olympiad on Astronomy and Astrophysics, Beijing, 12-21 September 2010, five competitors, team leaders were Sonja Vidojević and Slobodan Ninković, Aleksandar Vasiljković won the gold medal, Ognjen Marković and Filip Živanović silver, and bronze Stefan Andjelković. Milena Milošević was commended.

XV International Astronomical Olympiad, Sudak in the Crimea, 16-24 of October 2010, five competitors, two seniors and three juniors, team leaders were Slobodan Ninković and Ivan Milić; Ivan Tanasijević won gold, silver Luka Bojović, and bronze Stefan Badža and Djordje Žikelić.

V International Olympiad in astronomy and astrophysics, Katowice, from 25 August to 4 September 2011, five competitors, team leaders Slobodan Ninković and Aleksandar Vasiljković; Stefan Andjelković and Ognjen Marković won the silver medal, bronze Filip Živanović, and Stefan Badža was commended.

XVI International Astronomical Olympiad, Alma-Ata, 22-30 September 2011, the five contestants, two over quota, two senior and one junior, team leaders Nikola Božić and Ivan Milić. The success was the following: Aleksandar Miladinović, Dušan Šobot and Ivan Tanasijević won the bronze medals.

In the period 2008-2011, Society of Astronomers of Serbia took part in eight Olympiads in astronomy, in which participants from Serbia won two gold medals, ten silver and eleven bronze medals, three participants were commended and one received a special award.

Team leaders were: Slobodan Ninković seven times, Ivan Milić three, Ratomirka Miller two and by once Sonja Vidojević, Aleksandar Vasiljković and Nikola Božić.

4. PROJECT "POPULARIZATION OF ASTRONOMY IN EDUCATIONAL AND CULTURAL INSTITUTIONS AND SCHOOLS"

For popularization of astronomy using a mobile planetarium, SAS was applied at the Ministry of Science and Technological Development with the project "Popularization of astronomy in educational and cultural institutions and schools", and for 2010 as well as for 2011 received 300 000 RSD for each year. Program activities are primarily designed to popularize astronomy in the towns in the interior of Serbia and the Republic Srpska. To this end, the lecturers with the mobile planetarium, obtained in 2009 thanks to the donation of UNESCO, visited

particular towns, organizing a day of astronomy, in order to acquaint students, educators and concerned citizens with the phenomena and objects in the night sky and the results and achievements in this science.

Activities achieved during the realization of project in 2010 year are shown here in tables.

<i>Date</i>	<i>Lecture and Place</i>	<i>Attendies</i>	<i>Lecturer</i>
08/04/10	Electromagnetic spectrum and objects which we observe – Kragujevac	50	Luka Č. Popović
08/04/10	The secret of big silence of cosmic civilisations – Kragujevac	50	Milan S. Dimitrijević
08/04/10	Planetarium projection (mobile planetarium) – Kragujevac	120	Goran Pavičić
15/04/11	The secret of big silence of cosmic civilisations - Dobož	50	Milan S. Dimitrijević
15/04/10	Planetarium projection (mobile planetarium) – Dobož	180	Goran Pavičić
16/04/10	Planetarium projection (mobile planetarium) – Banja Luka	240	Goran Pavičić
16/04/10	The secret of big silence of cosmic civilisations - Banja Luka	50	Milan S. Dimitrijević
17/04/10	Planetarium projection (mobile planetarium) – Banja Luka	120	Goran Pavičić
28/04/10	Electromagnetic spectrum and objects which we observe – Vršac	60	Luka Č. Popović
28/04/10	The secret of big silence of cosmic civilisations – Vršac	60	Milan S. Dimitrijević
28/04/10	Planetarium projection (mobile planetarium) – Vršac	180	Goran Pavičić
15/05/2010	Planetarium projection (mobile planetarium)- Avio Museum – Belgrade	690	N. Trajković, A. Zlatanović, N. Radovanović, S. Maćušev
22/05/2010	Planetarium projection (mobile planetarium) – Novi Sad	690	A. Brajović, K. Savić, K. Kaćanski, Goran Pavičić
23/05/2010	Planetarium projection (mobile planetarium) – Novi Sad	690	A. Brajović, K. Savić, K. Kaćanski, Goran Pavičić

26/05/2010	Planetarium projection (mobile planetarium) – Kikinda	180	Goran Pavičić
26/05/2010	Electromagnetic spectrum and objects which we observe – Kikinda	60	Luka Č. Popović
26/05/2010	Astronomy of XXI century – Kikinda	60	Milan S. Dimitrijević
26/05/10	Milutin Milanković - Novi Bečej	60	Petar Vuča
17/09/10	Planetarium projection (mobile planetarium)- Secondary school, Zrenjanin	150	Goran Pavičić
18/09/10	Planetarium projection (mobile planetarium)- Primary school „2 October”, Zrenjanin	150	Goran Pavičić
24/09/10	Planetarium projection (mobile planetarium) – Night of researchers, Novi Sad	600	Kristina Kačanski, Goran Pavičić
27/09/10	Planetarium projection (mobile planetarium), Secondary school „Svetozar Marković“, Niš	300	Goran Pavičić
27/09/10	The secret of big silence of cosmic civilisations – where are they?, Faculty of Sciences, Niš	40	Milan S. Dimitrijević
28/09/10	Mobile planetarium – Secondary school, Prokuplje	210	Goran Pavičić
28/09/10	The secret of big silence of cosmic civilisations – where are they?, Secondary school, Prokuplje	40	Milan S. Dimitrijević
09/10/10	The secret of big silence of cosmic civilisations - „Days of Eureka” – Kruševac	60	Milan S. Dimitrijević
09/10/10	„Miraculous astrophysical objects” - „Days of Eureka” – Kruševac	60	Luka Č. Popović
09/10/10	Mobile planetarium - „Days of Eureka” – Kruševac	180	Goran Pavičić
26/10/10	Mobile planetarium - „Fair ZVONCE” - Belgrade	120	A. Brajović, N. Popović, Goran Pavičić
27/10/10	Mobile planetarium - „Fair ZVONCE” - Belgrade	120	A. Brajović, N. Popović, Goran Pavičić

28/10/10	Mobile planetarium - „Fair ZVONCE” - Belgrade	120	A. Brajović, N. Popović, Goran Pavičić
29/10/10	Mobile planetarium - „Fair ZVONCE” - Belgrade	120	A. Brajović, N. Popović, Goran Pavičić
30/10/10	Mobile planetarium - „Fair ZVONCE” - Belgrade	120	A. Brajović, N. Popović, Goran Pavičić
10/11/10	Mobile planetarium – Novi Bečej	120	Goran Pavičić
11/11/10	The secret of big silence of cosmic civilisations – Novi Bečej	60	Milan S. Dimitrijević
11/11/10	Milutin Milanković - Novi Bečej	60	Petar Vuca
12/11/10	Mobile planetarium – Novo Miloševo	120	Goran Pavičić
12/11/10	Mobile planetarium – Novi Kneževac	120	Goran Pavičić
13/11/10	The secret of big silence of cosmic civilisations - Novi Kneževac	60	Milan S. Dimitrijević
13/11/10	Milutin Milanković - Novi Kneževac	60	Petar Vuca
03/12/10	Mobile planetarium, Festival of Science - Belgrade	810	A. Brajović, N. Grubač, F. Čolaković, Goran Pavičić
04/12/10	Mobile planetarium, Festival of Science - Belgrade	810	A. Brajović, N. Grubač, F. Čolaković, Goran Pavičić
05/12/10	Mobile planetarium, Festival of Science - Belgrade	810	A. Brajović, N. Grubač, F. Čolaković, Goran Pavičić
27/12/10	Mobile planetarium, Secondary school - Smederevo	120	Goran Pavičić

To the above listed activities 9250 listeners were present in 2010. On total of 19 lectures were 960 listeners, and 276 planetarium projections with lectures, were attended by 8290 listeners (since in a planetarium projection the number of

listeners is limited to 30, the total number of listeners during the day is shown in the table).

Such "Days of Astronomy" were organized during 2010 in Kragujevac, Doboj, Banja Luka, Vršac, Belgrade, Novi Sad, Kikinda, Zrenjanin, Niš, Prokuplje, Kruševac, Novi Bečej, Novo Miloševo and Novi Kneževac.

Under the program, to schools in Kragujevac, Doboj, Banja Luka, Vršac, Kikinda, Niš, Prokuplje, Kruševac, Novi Bečej, Novo Miloševo and Novi Kneževac, Galileoscops, purchased during IYA with the assistance of the Ministry, were donated.

In the realization of the project were involved Goran Pavičić, Milan S. Dimitrijević, Luka Č. Popović, Darko Jevremović, Petar Vuca, Nenad Trajković, Ana Zlatanović, Nataša Radovanović, Slavica Maćušev, Ana Brajović, Kristina Savić, Kristina Kaćanski, Natalija Popović, Nevena Grubač, and Filip Čolaković.

In 2011, "Days of Astronomy" are organized in Niš, Pančevo, Smederevska Palanka, Leskovac, Rusko Selo, Banatsko Karadjordjevo, Novi Sad, Gradiška, Banja Luka, Modriča, Trebinje, Sutjeska, Subotica, Sečanj, Kruševac, Vršac, Belgrade and Kučevo.

- др Лука Ч. Поповић
 - др Милан С. Димитријевић
 „ТАЈНА ВЕЛИКОГ БУТАЊА
 ВАНЗЕМАЉСКИХ ЦИВИЛИЗАЦИЈА“
 (16.04. од 16 часова у Дому омладине)

БАЊА ЛУКА
ДОМ ОМЛАДИНЕ
16. и 17.04.2010.
од 9 часова

ДОБОЈ
ГИМНАЗИЈА
15.04.2010.
од 10 часова

УЛАЗ БЕСПЛАТАН

Figure 1: Poster for the lectures in Doboj and Banja Luka.



Figure 2: Dobrivoje Grčak, director of the Secondary school in Kruševac and Milan S. Dimitrijević with Acknowledgement. In front of him, books that he donated to the Secondary school, Kruševac 9. 10. 2010.

Activities on the Project realized during 2011 are presented in the table below.

<i>Date</i>	<i>Lecture and Place</i>	<i>Attendies</i>	<i>Lecturer</i>
25/02/11	Mobile planetarium – Niš	240	Goran Pavičić
26/02/11	Mobile planetarium – Niš	300	Goran Pavičić
26/02/11	Astronomy of XXI century – Niš	60	Milan S. Dimitrijević
16/03/11	Mobile planetarium – Pančevo	180	Goran Pavičić
16/03/11	Astronomy of XXI century – Pančevo	43	Milan S. Dimitrijević
24/03/11	Mobile planetarium – Smederevska Palanka	180	Goran Pavičić
24/03/11	Astronomy of XXI century – Smederevska Palanka	35	Milan S. Dimitrijević
16/04/11	Mobile planetarium – Leskovac	150	Goran Pavičić
16/04/11	Astronomy of XXI century - Leskovac	60	Milan S. Dimitrijević

SOCIETY OF ASTRONOMERS OF SERBIA 2008-2011

17/04/11	Mobile planetarium - Leskovac	150	Goran Pavičić
05/05/11	Mobile planetarium – Rusko Selo	60	Goran Pavičić
05/05/11	Astronomy of XXI century – Rusko Selo	60	Milan S. Dimitrijević
05/05/11	Milutin Milanković – Rusko Selo	60	Petar Vuca
06/05/11	Mobile planetarium – Banatsko Karadjordjevo	120	Goran Pavičić
06/05/11	Astronomy of XXI century – Banatsko Karadjordjevo	120	Milan S. Dimitrijević
06/05/11	Milutin Milanković – Banatsko Karadjordjevo	120	Petar Vuca
07/05/11	Mobile planetarium – Novi Sad	240	Goran Pavičić, K. Savić, N. Grubač, R. Džudžar
08/05/11	Mobile planetarium – Novi Sad	240	Goran Pavičić, K. Savić, N. Grubač, R. Džudžar
23/08/11	Mobile planetarium – Kragujevac	120	Goran Pavičić
19/09/11	Mobile planetarium – Gradiška	240	Goran Pavičić
19/09/11	The secret of big silence of cosmic civilisations – where are they? – Gradiška	75	Milan S. Dimitrijević
20/09/11	Mobile planetarium – Banja Luka	180	Goran Pavičić
20/09/11	The secret of big silence of cosmic civilisations – where are they? – Banja Luka	50	Milan S. Dimitrijević
21/09/11	Mobile planetarium – Modriča	180	Goran Pavičić
23/09/11	Mobile planetarium – Subotica	180	Ana Brajović, Nevena Grubač
29/09/11	Astronomy of XXI century – Sečanj	60	Milan S. Dimitrijević
29/09/11	Milutin Milanković – Sečanj	60	Petar Vuca
30/09/11	Astronomy of XXI century – Sutjeska	60	Milan S. Dimitrijević
30/09/11	Milutin Milanković – Sutjeska	60	Petar Vuca

06/10/11	Mobile planetarium – Trebinje	300	Goran Pavičić
06/10/11	Astronomy of XXI century – Trebinje	50	Milan S. Dimitrijević
07/10/11	Mobile planetarium – Trebinje	300	Goran Pavičić
15/10/11	Astronomy of XXI century – Kruševac	80	Milan S. Dimitrijević
15/10/11	Dark matter and Dark energy – Kruševac	80	Slobodan Ninković
15/10/11	A journey across the Space – Kruševac	80	Luka Č. Popović
15/10/11	Mobile planetarium – Kruševac	240	Ana Brajović, Nevena Grubač
28/10/11	Astronomical theory of climatic changes – Vršac	20	Milan S. Dimitrijević
23-30/10/11	Mobile planetarium – Fair of education „ZVONCE”, Belgrade	1700	N. Radovanović, Lj. Isaković, Goran Pavičić
08/11/2011	Mobile planetarium – Kučevo	150	Nevena Grubač, Goran Pavičić
2-4/12/11	Mobile planetarium – Festival of Science, Belgrade	2000	N. Grubač, N. Radovanović, Goran Pavičić

To the above listed activities 8638 listeners were present in 2011. On total of 19 lectures were 1233 listeners, and 249 planetarium projections with lectures, were attended by 7405 listeners.

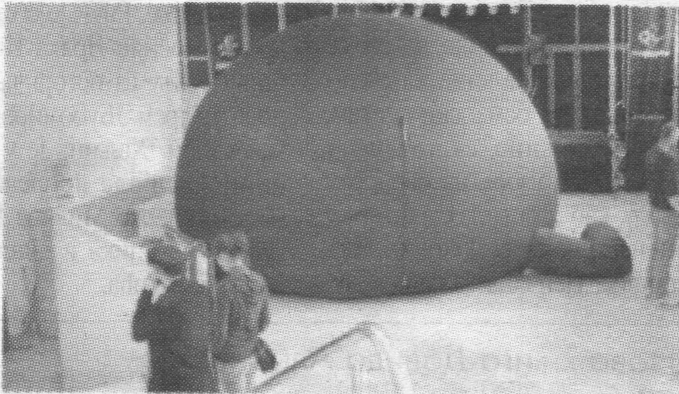
In the realization of the project were involved Goran Pavičić, Milan S. Dimitrijević, Luka Č. Popović, Darko Jevremović, Petar Vuca, Slobodan Ninković, Nataša Radovanović, Ana Brajović, Kristina Savić, Nevena Grubač, Robert Džudžar and Ljubisa Isaković.

ГЛАС СРПСКЕ сриједа, 21. септембар 2011. 23

ПОМУ

Ово је "Гласу Српске коње - казала је Мирко
изјавила директор овог вићева. А. П.

Одушевљење планетаријумом



Вићена симулација ноћног неба

ФОТО: С. ЈОКИЋ

Универзитетско астрономско друштво Бањалука већ другу годину заредом уз помоћ београдског астрономског друштва "Руђер Бошковић" довело је мобилни планетаријум помоћу кога су бројни Бањалучани имали прилику да на едукативан начин виде симулацију ноћног неба.

Рекао је ово после јучерашњег предавања члан бањалучког астрономског друштва Немања Ракић.

- Реализацију овог пројекта подржали су Министарство науке и технологије РС те бројни искусни предавачи из ове области који су корисним информацијама овај необични догађај учинили још интересантнијим. Оно на што смо посебно поносни је предавање професора Милана С. Димитријевића који важи за велико име у астрономији - додао је Ракић. С. Ј.

Figure 3: Article in „Glas Srpske“.



Figure 4: Mobile planetarium. Trebinje 6. 10. 2011.



Figure 5: Trebinje 6. 10. 2011. Lecture of Milan S. Dimitrijević.

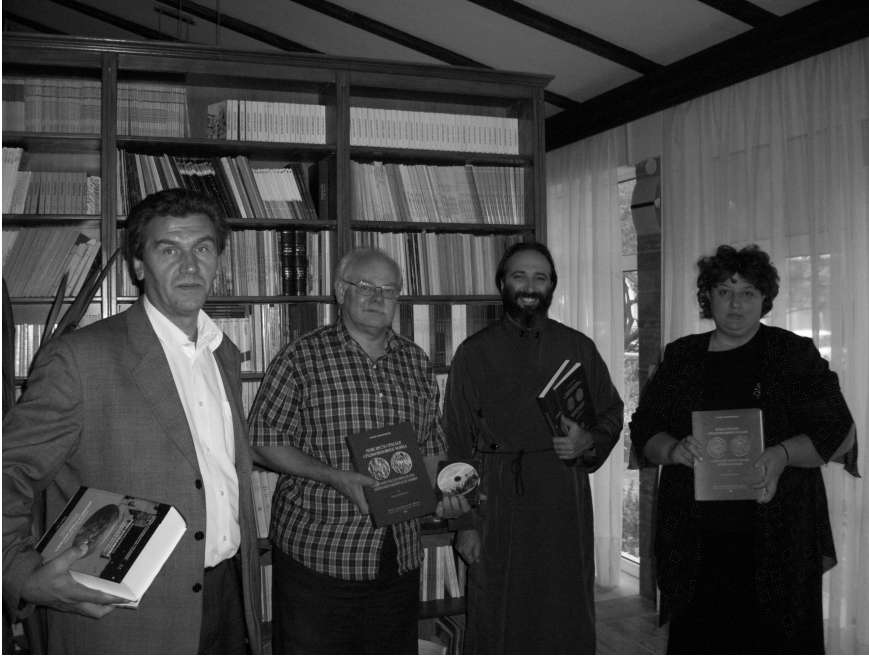


Figure 6: Trebinje. Luka Č. Popović and Milan S. Dimitrijević in Church Library with the donated books.

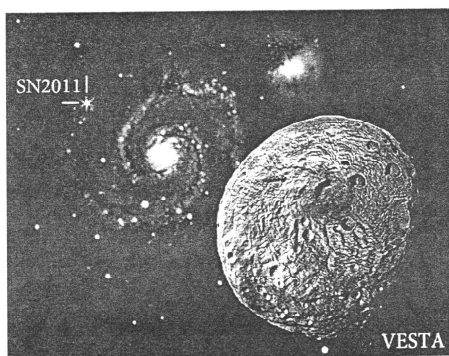


Figure 7: Kruševac „Day of Eureka“ 15th of October 2011.
First row: Milan S. Dimitrijević, Luka Č. Popović, Dobrivoje Grčak,
Slobodan Ninković, Danica Milićević.

Природњачко друштво
ГЕА

11. ВРШАЧКИ АСТРОНОМСКИ СУСРЕТ

Преглед актуелних открића у астрономији



Вршац
28 и 29. октобар 2011. год.
Сала Дома омладине Вршац

11. ВРШАЧКИ АСТРОНОМСКИ СУСРЕТ

Сала Дома омладине Вршац

ПРОГРАМ:

ПЕТАК 28. октобар

- 16.00 - Свечано отварање
- 16.10 - Милутин Миланковић - Астрономска теорија климатских промена
предавач: Др Милан Димитријевић
- 17.10 - Супернове - експлозије звезда
Супернова 2011
предавач: Александар Оташевић
- 18.10 - Најновија открића екстрасоларних планета орбиталним телескопима Кеплер и Корот
предавач: Срђан Ђукић
- 19.10 - 50 година од првог лета човека у космос - Гагаринов поухват
предавач: Драган Лазаревић

СУБОТА 29. октобар

- 17.00 - Шта нам откривају радиотелескопи
предавач: Дарко Донеvски
- 18.00 - Космичке кише
предавач: Јован Алексић
- 18.30 - Актуелности у истраживању Сунчевог система међупланетарним сондама
предавач: Срђан Пењивраг
- 19.30 - Први кораци човечанства у космосу
предавач: Драган Лазаревић

Покровитељи:
Центар за промоцију науке
Скупштина општине Вршац
Дом омладине Вршац

Могуће су мање измене у програму предавања

Figure 8: Astronomical Meetings of Vršac.

5. SCIENTIFIC CONFERENCES ORGANIZED BY SAS

Within the considered period, SAS has expanded its activities and on scientific meetings and for the first time organized two scientific conferences.

First is 1st Workshop "Spectroscopy as a tool to investigate Active Galactic Nuclei and gravitational lenses," Hotel "Kantri club", Babe, Kosmaj, Serbia, 7-11.07. 2010. The meeting was conceived as a workshop, so in the morning were lectures (during the Meeting in total eight lectures), and in the afternoon, participants worked in groups on specific topics or mini projects.

The main conclusions of the meeting are that such work, where three to six researchers are grouped around a well defined topics, enable a quality work. Two papers were finished on the workshop and sent in the days that followed to the leading journals, and seven future papers were considered in different forms.

Second was I Workshop on Astrophysical Spectroscopy, Vila "Alexander", Orašac, 26-30. August 2011, organized by the same principle as the previous one.

In addition, SAS was co-organizer of international conferences VII Serbian Conference on Spectral Line Shapes in Astrophysics, Zrenjanin, 15-19. June 2009 and VIII Serbian Conference on Spectral Line Shapes in Astrophysics, Divčibare, 6-10. Jun 2011, as well as of the National Conference with international participation "Development of astronomy among Serbs V", Belgrade, 18-22 April 2008.

6. PUBLISHING ACTIVITY

Within the considered period, SAS for the first time started and with the publishing activity. Published were a brochure on the International Year of Astronomy, Proceedings of the Sixth Serbian-Bulgarian Astronomical Conference (with the Astronomical Society "Rudjer Bošković"), Book of Abstracts of the Seventh Serbian Conference on Spectral Line Shapes in Astrophysics and four electronic optical DVD discs (two were published together with the Astronomical observatory and one with the Astronomical Society "Rudjer Bošković").

Published bibliographic units are:

1. INTERNATIONAL YEAR OF ASTRONOMY (IN SERBIAN)
2. PROCEEDINGS OF THE 6TH SERBIAN-BULGARIAN ASTRONOMICAL CONFERENCE, Belgrade 7-11 May 2008, eds. M. S. Dimitrijević, M. Tsvetkov, L. Č. Popović, V. Golev, Publ. Astron. Soc. »Rudjer Bošković«, No. 9.
3. VII SERBIAN CONFERENCE ON SPECTRAL LINE SHAPES IN ASTROPHYSICS (VII SCSLSA), Zrenjanin 15-19 June 2009, Book of abstracts, eds. L. Č. Popović, M. S. Dimitrijević, D. Jevremović, D. Ilić, Serbian Astronomical Society and Astronomical Observatory, Belgrade 2009.
4. ABSTRACTS, PROGRAM AND PHOTOS [Electronic Source], 7th Serbian Conference on Spectral Line Shapes in Astrophysics, June 15-19, 2009, Zrenjanin, Serbia; eds. Luka Č. Popović, M. S. Dimitrijević, D. Jevremović, D. Ilić, Organized by Serbian Astronomical Society and Astronomical Observatory, Belgrade. DVD prepared by Milan S. Dimitrijević, Miodrag Dačić and Tatjana Milovanov - Belgrade: Serbian Astronomical Society: Astronomical Observatory, 2009 (Beograd: Astronomical Observatory). - 1. Electronic optical disk (DVD).
5. PROCEEDINGS, PHOTOS AND VIDEOS [Electronic Source], The 5th Bulgarian-Serbian Conference on Astronomy and Space Science, May 9-12, 2006, Sofia, Bulgaria, edited by M. K. Tsvetkov, L. Filipov, M. S. Dimitrijević, L. Č. Popović, organized by the Space Research Institute of the Bulgarian Academy of Sciences. DVD prepared by Milan S. Dimitrijević and Tatjana Milovanov - Belgrade: Serbian Astronomical Society: Astronomical Observatory, 2009 (Belgrade: Astronomical Observatory). - 1. Electronic optical disk (DVD).
6. DEVELOPMENT OF ASTRONOMY AMONG SERBS V, Belgrade 18-22. April 2008. [Electronic source], editor Milan S. Dimitrijević, organizer

Astronomical Society "Rudjer Bošković", disk prepared by Milan S. Dimitrijević and Tatjana Milovanov, - Belgrade: Astronomical Society "Rudjer Bošković", Society of Astronomers of Serbia 2009 (Belgrade: Astronomical Society "Rudjer Bošković") - 1 electronic optical disc (DVD).

7. ABSTRACTS, PRESENTATIONS AND PHOTOS [Electronic Source], 1st Workshop "Spectroscopy as a Tool to Investigate Active Galactic Nuclei and Gravitational Lenses", Kosmaj, Babe, July 7-11, 2010; eds. Milan S. Dimitrijević, Luka Č. Popović and Miodrag Dačić, Organized by Serbian Astronomical Society and Astronomical Observatory, Belgrade. DVD prepared by Milan S. Dimitrijević, Miodrag Dačić and Tatjana Milovanov - Belgrade: Astronomical Observatory: Serbian Astronomical Society, 2009 (Beograd: Astronomical Observatory). - 1. Electronic optical disk (DVD).

7. FOREIGN SCIENTISTS – GUESTS OF SOCIETY OF ASTRONOMERS OF SERBIA

For the first time in its history the Society had within the considered period twelve stays of foreign guests, which opened up the possibility for another type of activities and applications to competitions at the Ministry of Education and Science. Guests Scientists from abroad who stayed in Serbia as guests of SAS were:

Magdalena Christova, Bulgaria,
Giovanni La Mura, Italy,
Martin Gaskel, USA,
Piero Rafanelli, Italy,
Ala Shapovalova, Russia,
Aleksandr F. Zakharov, Russia,
Jonathan Francisco Leon Tavares, Finland,
Eduardo Guerras Valera, Spain,
Nebil Ben Nesib, Tunisia.

They were the guests of the Conference *1st Workshop on "Spectroscopy as a tool to investigate Active Galactic Nuclei and gravitational lenses"*, Hotel Kantri club, Babe, Kosmaj, Serbia, 7-11.07.2010. At the meeting *I Workshop on astrophysical spectroscopy*, Orašac, 26-30.08.2011, SAS guests were:

Magdalena Christova, Bulgaria,
Giovanni La Mura, Italy,
Jacopo Fritz, Belgium.

8. OTHER ACTIVITIES

8.1. Links with the European Astronomical Society

Directional Board of SAS regularly collected and paid annual dues for the European Astronomical Society, for those members who wanted to.

Milan S. Dimitrijević and Andjelka Kovačević participated in all meetings of the bodies of the European Astronomical Society and its assembly on JENAM 2009 "European Week of Astronomy and Space Science" in Hatfield, near London, 20-23 April 2009, as representatives of the Society of Astronomers of Serbia, and Dimitrijević and as a Councilor of the European Astronomical Society.

On JENAM 2011 in St. Petersburg, the official representative of the SAS in the EAS was Vojislava Protić Benišek.

8.2. Links with the International Astronomical Union

Links with the International Astronomical Union (IAU) were held from one side through the National Committee for Astronomy, whose president within the period considered was Ištvan Vince, and from the other side the SAS paid the membership fee of Republic of Serbia to IAU.

9. CONCLUSION

We can conclude that in the period since 2008 up to 2011. Society of Astronomers of Serbia successfully participated in activities related to International Year of Astronomy, organized preparation and participation of our competitors at eight international Olympiads in astronomy, where they won two gold medals, ten silver and eight bronze. The Society has purchased portable planetarium and the Ministry accepted its project "Popularization of astronomy in educational and cultural institutions and schools". During its realization a series of popular lectures and planetarium projections were organized in different places in Serbia and Republic Srpska. Only in 2010, to the activities covered by this project, within which was organized "Astronomy Day" in different places, attended 9250 listeners. On that occasion, to schools have been donated Galileoscopes, purchased in 2009th. The Society expanded its activities and to the organization of scientific conferences, publishing and inviting scientists from abroad, and also maintained and developed links with the European Astronomical Society and the International Astronomical Union.

References

Božić, Nikola: 2010, *International Year of Astronomy 2009 in Serbia*, Proceedings of the conference "Development of astronomy among Serbs VI", Belgrade, 18-22 April 2008, editor M. S. Dimitrijevic, *Publ. Astr. Soc. "Rudjer Bošković"*, **10**, 367.

TEN YEARS OF THE SCIENTIFIC SOCIETY "ISAAC NEWTON" AND OF "YUGOSLAVIA" BRANCH OF THE INTERNATIONAL ASTRONOMICAL INSTITUTE ISAAC NEWTON OF CHILE

MILAN S. DIMITRIJEVIĆ

Astronomical Observatory, Volgina 7, 11060 Belgrade 74, Serbia
E-mail: mdimitrijevic@aob.bg.ac.rs

Abstract. On the occasion of ten years from the foundation, activities of Scientific Society "Isaac Newton" and of "Yugoslavia Branch" of the Isaac Newton Institute of Chile in Eastern Europe and Eurasia are reviewed.

Ten years ago, on 11th April 2002, the director of the Astronomical Observatory and the Director and Founder of the International Astronomical Institute "Isaac Newton" from Chile, Gonzalo Alcaino, signed an agreement on establishment of a Branch of this Institute in Yugoslavia (Fig. 1). The circumstances leading up to it are presented in detail in the journal "Vasiona" (Universe - Dimitrijevic, 2002). The initial years of the Branch (2002-2004), are described in the article Dimitrijević et al. (2005).

Associates of the Branch "Yugoslavia", which founded it, were: Edi Bon, Srdjan Z. Bukvić, Zorica Cvetković, Miodrag Dačić, Milan S. Dimitrijević (Branch Director), Stevan. Djeniže, Gojko R. Djurašević, Sanja R. Erkapić, Ljubinko M. Ignjatović, Predrag Jovanović, Aleksandar Dj. Kubičela, Anatolij A. Mihajlov, Vladimir Milosavljević, Nenad Milovanović, Slobodan Ninković, Dragomir Olević, Luka Č. Popović, Srdjan S. Samurović, Zoran Simić, Aleksandar Srećković, Nataša M. Stanic and Dragana Tankosic. They were later joined by: Dejan Urošević (second session of the Assembly – 30th January 2003), Dragan Ilić, Andjelka Kovačević, Jelena Kovačević, Nataša Gavrilović (fourth session of the Assembly on March 5th, 2007), Darko Jevremović (sixth session of the Assembly on 16th July 2008). In 2009, Marko Stalevski was admitted and on 17th November, on the eighth session of the Assembly, Sonja Vidojević, so that, at 1 February 2012, Branch has 29 members.

The first, constitutive meeting was held at the Astronomical Observatory on 8th May 2002. On it is confirmed and adopted the earlier signed agreement, establishing the Branch, and Jovan Grujić photographed participants, according to the wish



ASTRONOMICAL OBSERVATORY
Volgina 7, 11160 Belgrade, Yugoslavia
Tel.: +381-11-419-357 Fax: +381-11-419-553

AGREEMENT

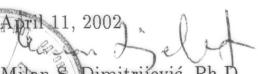
AMONG THE
BELGRADE ASTRONOMICAL OBSERVATORY IN YUGOSLAVIA
AND
THE ISAAC NEWTON INSTITUTE OF CHILE

Wishing to contribute to further development of scientific research in observational and theoretical astrophysics, and using the possibilities of international cooperation enhanced by the globalized use of internet, we have decided to open a Branch of the Isaac Newton Institute at the Belgrade Astronomical Observatory in Yugoslavia.

At the Observatory in Belgrade, a group of astronomers from the local staff, have been unified as to create the Isaac Newton Institute Branch in Yugoslavia. The scientists involved will remain in the staff of their observatory and simultaneously become members of the Isaac Newton Institute. Scientists from other astronomical centers in Yugoslavia are as well entitled to join our Branch.

As the results of the research with the Isaac Newton Institute Branch in Yugoslavia, are considered only results submitted to the three most prestigious journals in astronomy, namely, the Astrophysical Journal and the Astronomical Journal in the United States, and Astronomy and Astrophysics, in Europe. The two institutions involved will be explicitly mentioned as the affiliations of the corresponding authors.

The present document officially establishes the creation of the Isaac Newton Institute of Chile Branch in Yugoslavia at the Belgrade Astronomical Observatory.

April 11, 2002

Milan S. Dimitrijević, Ph.D.
Director
Belgrade Astronomical Observatory



Gonzalo Alcaino
President
Isaac Newton Institute

Figure 1: The agreement between Belgrade Astronomical Observatory and Isaac Newton Institute of Chile on establishment of the Branch of this Institute in Yugoslavia.



Figure 2: Members of the Branch of the Institute Isaac Newton of Chile in Yugoslavia. Seated: Dragomir Olević, Dragan Tankosić, Slobodan Ninković, Stevan Djeniže, Milan S. Dimitrijević, Luka Č. Popović, Gojko Djurašević, Aleksandar Kubičela, Srdjan Bukvić. Standing: Zoran Simić, Predrag Jovanović, Miodrag Dačić, Vladimir Milosavljević, Aleksandar Srećković, Zorica Cvetković, Anatolij A. Mihajlov, Ljubinko Ignjatović, Sanja Erkapić.

of Gonzalo Alcaino, who wanted to publish a picture of the members of the Branch in the publication of the Institute (***, no year, a copy in the library of Matica Srpska within the legacy of M. S. Dimitrijevic). Two images were selected and one published in the said publication and the other is here as Fig. 2. The second meeting was convened for the 25th July (see Fig. 3). Item 3 in the invitation, organizational issues, has been turned into the founding assembly of the as-

sociation of citizens: the Scientific Society "Isaac Newton." The meeting adopted the statute, and for the President of the Managing Board and for director of the Branch was elected Milan. Dimitrijević, for his deputy Stevan Djeniže, for the secretary Miodrag Dačić. In the Managing Board has been elected also Luka Č. Popović and Anatolij A. Mihajlov, and in the Supervisory Board Gojko Djurašević, Aleksandar Srećković and Zorica Cvetković.

In the Register of associations, social organizations and political organizations, led by the Federal Ministry of Justice, the Society was included on the 4th September 2002. It is interesting that the Society has received a copy of the decision that differ from original (Fig. 7), to which we draw attention to future researchers. In the decision, signed by the Minister Savo Marković, is written that the Society "was included in the registry list no. 1645 under the number 4352, and on the copy, signed for the Minister by (illegible) is: "in the registry list no. 1642 under the number 4344".



У четвртак 25. јула 2002. у
библиотеци АОБ
у 14 часова
одржаће се други сасланак
ЈУГОСЛОВЕНСКОГ
ОГРАНКА ИНСТИТУТА
ИСАК ЊУТН

Дневни ред

1. Предавање
Лука Ч. Поповић
ОБЛАСТ БАЛМЕРОВЕ ЕМИСИЈЕ У NGC 3516:
КИНЕМАТИЧКА И ФИЗИЧКА СВОЈСТВА
2. Стеван Ђениже
ЕКСПЕРИМЕНТАЛНЕ ШТАРКОВЕ ШИРИНЕ 1
ПОМАЦИ У СПЕКТРУ ТРОСТРУКО ЈОНИЗОВАНОГ
СУМПОРА
3. Организациона питања

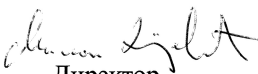

Директор
Југословенског огранка
Милан С. Димитријевић

Figure 3: Call for the second meeting of the Yugoslav Branch of the Institute Isaac Newton.



У понедељак 9. септембра
2002. у библиотеци АОЅ
у 11 часова
одржаће се трећи састанак
ЈУГОСЛОВЕНСКОГ
ОГРАНКА ИНСТИТУТА
ИСАК ЊУТН

Дневни ред

1. Предавање

Profesor Gonzálo Alcaino Barros
THE ISAAC NEWTON INSTITUTE OF CHILE IN
EASTERN EUROPE AND EURASIA

Директор Југословенског огранка


Милан С. Димитријевић

Figure 4: Invitation to the lecture of Gonzalo Alcaino.

It should be noted that the Society, on the third General Assembly, held on 30th April 2003, proposed Dimitrijević for a corresponding member of SASA, and also on the seventh General Assembly, held on 10th May 2009. Luka Č. Popović proposed (acts no. 5 and 6/08 of 07.16.2008), that the Society initiates the process for awarding the title of scientist emeritus for M. S. Dimitrijević and A. A. Mihajlov. Both proposals were adopted at the 6 General Assembly, held on 16th July 2008.

The National Council for Science, elected M. S. Dimitrijević for scientist emeritus. According to the new law on associations, the Company has registered on 5th August 2011, in the Agency for Business Registers (Fig. 8).

By 1st January 2012, Branch Associates have published 76 papers in Astronomy and Astrophysics, Astrophysical Journal (including Letters and Supplement Series), Astronomical Journal and the Monthly Notices of the Royal Astronomical Society, and their list is presented here.




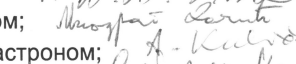





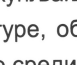

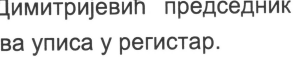
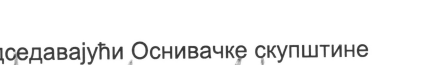

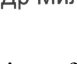
At the beginning, Alcaino published annual report of the Isaac Newton Institute of Chile (***, 2003, 2004, Alcaino, 2003, 2004, 2005), where was also the report on the scientific work of the Branch.

ОДЛУКА О ОСНИВАЊУ

На основу члана 10. став 2. Закона о удруживању грађана у удружења, друштвене и политичке организације које се оснивају на територији СРЈ, као и члана 13. Статута, на оснивачкој скупштини одржаној 25. јула 2002. године донета је одлука о оснивању Удружења грађана "ЈУГОСЛОВЕНСКИ ОГГРАНАК МЕЂУНАРОДНОГ АСТРОНОМСКОГ ИНСТИТУТА – ИСАК ЊУТН".

Седиште удружења је у Београду.

Оснивачи Удружења су:

1. Др. Милан С. Димитријевић; астроном 
2. Др. Срђан С. Буквић, физичар; 
3. Проф. Др. Стеван Ђениже, физичар; 
4. Др Лука Ч. Поповић, астроном; 
5. Др Анатолиј А. Михајлов, физичар; 
6. Др Миодраг Д. Дачић, астроном; 
7. Др Александар Ђ. Кубичела, астроном; 
8. Др Слободан Нинковић, астроном; 
9. Др Александар Срећковић, физичар; 
10. Мр. Еди Бон, астроном; 
11. Мр. Предраг Јовановић, астроном; 
12. Мр Ненад Миловановић, астроном; 
13. Мр Драгомир Олевић, астроном; 
14. Мр Наташа Станић, астроном; 
15. Зоран Симић, астроном. 

Основни задатак Удружења је окупљање заинтересованих грађана и правних лица у циљу развоја Науке, културе, образовања, информатике и грађанског друштва, као и очувања природне средине.

Овлашћује се Др. Милан С. Димитријевић председник Управног одбора Удружења, за извршавање послова уписа у регистар.

Председавајући Оснивачке скупштине

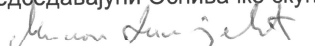

Др Милан С. Димитријевић

Figure 5: The decision on foundation of the Scientific society „Isaac Newton“.



Figure 6: Visit of Alcaino to the Astronomical Observatory on 9th September 2002: Aleksandar Kubičela, Milan S. Dimitrijević, Zorica Cvetković, Gonzalo Alcaino.

Following ten years of work, we can conclude that the great merit of Gonzalo Alcaino is that he assembled the most creative scientists in Serbia working in astronomy, supported and helped their work and stimulated them to publish in most prestigious international journals. If one looks at the list of publications, given below, one can see that the Branch "Yugoslavia" of the Isaac Newton Institute of Chile, created and supported by Gonzalo Alcaino, is scientifically the most productive astronomical institution in Serbia which gave a significant contribution to this Science, and has the richest list of scientific results in Astronomy in Serbia.



Савезна Република Југославија
САВЕЗНО МИНИСТАРСТВО ПРАВДЕ
Број 31-12132/2002-07

04.09.2002. године
Београд

На основу члана 13. Закона о удруживању грађана у удружења, друштвених организација и политичке организације који се оснивају за територију Србије (Службени лист СФРЈ, бр. 42/80) и члана 192. став 1. Закона о општем управном поступку (Службени лист СФРЈ, бр. 33/87; и Решењем по пријави удружења "ИСАК ЊУТН" из Београда за упис у Регистар удружења, друштвених организација и политичких организација, Савезно министарство правде доноси

РЕШЕЊЕ

1. Научно друштво "ИСАК ЊУТН" уписује се у Регистар удружења, друштвених организација и политичких организација, који се води код Савезног министарства правде, као удружење грађана, на регистарском листу број 1645 подредним бројем 4352.
2. Седиште Научног друштва "ИСАК ЊУТН" налази се у Београду, улица Волгина број 7.
3. Научно друштво "ИСАК ЊУТН" заснуло и представља др Милан С. Димитријевић, председник Управног одбора.

Образложење

Научно друштво "ИСАК ЊУТН" из Београда поднело је пријаву за упис у Регистар удружења, друштвених организација и политичких организација, који се води код Савезног министарства правде.
Решавајући по поднетој пријави утврђено је да су испуњени сви услови предвиђени Законом, па је одлучено као у диспозитиву Решења.
Правна поука: Сво решење је коначно у управном поступку и против њега се може покренути управни спор тужбом Савезном суду у року од 30 дана од дане пријема Решења.

Достављено:
- организацији
- у досије
- архиви



Савезна Република Југославија
САВЕЗНО МИНИСТАРСТВО ПРАВДЕ
Број 31-12132/2002-07

34.09.2002. године
Београд

На основу члана 13. Закона о удруживању грађана у удружења, друштвених организација и политичке организације који се оснивају за територију Србије (Службени лист СФРЈ, бр. 42/80) и члана 192. став 1. Закона о општем управном поступку (Службени лист СФРЈ, бр. 33/87; и Решењем по пријави удружења "ИСАК ЊУТН" из Београда за упис у Регистар удружења, друштвених организација и политичких организација, Савезно министарство правде доноси

РЕШЕЊЕ

1. Научно друштво "ИСАК ЊУТН" уписује се у Регистар удружења, друштвених организација и политичких организација, који се води код Савезног министарства правде, као удружење грађана, на регистарском листу број 1642 под редним бројем 4344.
2. Седиште Научног друштва "ИСАК ЊУТН" налази се у Београду, улица Волгина број 7.
3. Научно друштво "ИСАК ЊУТН" заснуло и представља др Милан С. Димитријевић, председник Управног одбора.

Образложење

Научно друштво "ИСАК ЊУТН" из Београда поднело је пријаву за упис у Регистар удружења, друштвених организација и политичких организација, који се води код Савезног министарства правде.
Решавајући по поднетој пријави утврђено је да су испуњени сви услови предвиђени Законом, па је одлучено као у диспозитиву Решења.
Правна поука: Сво решење је коначно у управном поступку и против њега се може покренути управни спор тужбом Савезном суду у року од 30 дана од дане пријема Решења.

Достављено:
- организацији
- у досије
- архиви



Figure 7: Original and copy of the decision of registration with different numbers in the registry and different signatures.



Регистар удружења



5000049075415

Број БУ 13544/2011

Дана 05.08.2011. године
Београд

Агенција за привредне регистре, Регистратор који води Регистар удружења, на основу чланова 26. и 32. Закона о удружењима („Службени гласник РС“ бр. 51/09), поступајући по пријави за упис усклађивања у Регистар удружења друштвених организација, удружења грађана и њихових савеза уписаних у Регистар друштвених организација и удружења грађана и Регистар удружења, друштвених организација и политичких организација, који је поднет од стране "НАУЧНО ДРУШТВО - ИСАК ЊУТН", преко:

Име и презиме: Милан Димитријевић

доноси:

РЕШЕЊЕ

УПИСУЈЕ СЕ у Регистар удружења усклађивање удружења, са следећим подацима:

Облик организовања: Удружење

Назив: "НАУЧНО ДРУШТВО - ИСАК ЊУТН"

Назив у преводу на страни језик:

- Пун назив (енглески језик): „SCIENTIFIC SOCIETY ISAAC NEWTON“

Седиште и адреса: Волгина 7, Београд-Звездара, Србија

Матични број удружења: 28056494

ПИБ: 107192151

Датум оснивања: 25.07.2002

Датум доношења Статута: 05.11.2010

Делатност удружења: 9412 - Делатности струковних удружења

Подаци о заступнику:

Име и презиме: Милан Димитријевић

ЈМБГ: 2408947710415

Адреса: Булевар Краља Александра 126, Београд-Звездара, Србија

Страна 1 од 2



Предвиђено време на које се удружење оснива: Неограничено

Област остваривања циљева:

Рад на популаризацији и унапређењу астрономских наука.

Образложење

Подносилац пријаве број БУ 13544/2011, поднео је дана 20.07.2011. године, усаглашену пријаву за упис усклађивања:

"НАУЧНО ДРУШТВО - ИСАК ЊУТН"

у Регистар удружења, и документацију заведену у потврди о примљеној пријави број БУ 13544/2011.

Како су испуњени услови прописани одредбом члана 79. Закона о удружењима („Сл.гласник РС“ бр.51/09.) и члана 30. Правилника о садржини, начину уписа и вођења Регистра удружења („Сл.гласник РС“ број 80/09), Регистратор је одлучио као у диспозитиву.

Упис усклађивања у Регистар удружења, врши се без накнаде.

Поука о правном средству:

Против овог решења може се изјавити жалба министру надлежном за људска и мањинска права, послове државне управе и локалне самоуправе, у року од 15 дана од дана пријема решења. Жалба се предаје преко Агенције за привредне регистре, уз доказ о уплати таксе од 500,00 динара, прописану тарифним бројем 7., Закона о републичким административним таксама на рачун број:840-742221843-57, примацац Буџет Републике Србије.



Figure 8: The decision on the registration of Scientific Society "Isaac Newton" in the Register of Associations.

PUBLISHED SCIENTIFIC WORKS OF ASSOCIATES OF THE SCIENTIFIC SOCIETY „ISAAC NEWTON“

1. Djeniže S., Srecković A., Jelisavčić M., Bukvić S.: 2002, „Experimental Stark widths and shifts in the triply ionized Sulphur spectrum", *Astronomy and Astrophysics*, **389**, 1086-1089.
2. Popović L. Č., Mediavilla E. G., Kubičela, A., Jovanović, P.: 2002, "Balmer lines emission region in NGC 3516: Kinematical and physical properties" *Astronomy and Astrophysics*, **390**, 473-480.
3. Milosavljević V., Djeniže S.: 2002, "Ion contribution to the astrophysical important 447.15, 587.6 and 667.82 nm He I spectral lines broadening", *Astronomy and Astrophysics*, **393**, 721-726.
4. Djeniže, S., Dimitrijević, M. S., Srećković, A., Bukvić, S.: 2002, "Stark shifts and transition probabilities in Si III and Si IV spectra", *Astronomy and Astrophysics*, **396**, 331-336.

5. Milosavljević, V., Djeniže, S.: 2003, "Ion contribution to the prominent NeI, ArI and KrI spectral lines broadening", *Astronomy and Astrophysics*, 398, 1179-1184.
6. Popović L. Č., Mediavilla E. G., Jovanović P., Munoz J. A.: 2003, "The influence of microlensing on the shape of the AGN Fe K alpha line", *Astronomy and Astrophysics*, 398, 975-982.
7. Tankosić, D. Popović, L. Č., Dimitrijević, M. S.: 2003, "The electron-impact broadening parameters for Co III spectral lines", *Astronomy and Astrophysics*, 399, 795-797.
8. Dimitrijević, M. S., Dacić, M., Cvetković, Z., Sahal-Bréchet, S.: 2003, "Stark broadening of spectral lines of multicharged ions of astrophysical interest. XXIII. Be III", *Astronomy and Astrophysics*, 400, 791-793.
9. Srecković, A., Dimitrijević, M. S., Djeniže, S., Bukvić, S.: 2003, "Stark broadening parameters in the S III spectrum", *Astronomy and Astrophysics*, 400, 1155-1159.
10. Djurašević, G., Rovithis-Livaniou, H., Rovithis, P., Georgiades, N., Erkapić, S., Pavlović, R.: 2003, "Gravity-darkening coefficients in semi-detached binary systems from their photometric observations: Part I", *Astronomy and Astrophysics*, 402, 667-682
11. Mihajlov A. A., Jevremović D., Hauschildt P., Dimitrijević M. S. Ignjatović Lj. M., Alard, F.: 2003, "The influence of chemi-ionization and chemi-recombination processes on the Rydberg states populations of the hydrogen atoms in low-temperature layers of M type red dwarf atmospheres", *Astronomy and Astrophysics*, 403, 787-791.
12. Dimitrijević, M. S., Ryabchikova, T., Popović, L. C., Shulyak, D., Tsymbal, V.: 2003, "On the influence of Stark broadening on Si I lines in stellar atmospheres", *ASTRONOMY AND ASTROPHYSICS 2003*, Djeniže 404, 1099-1106.
13. Mihajlov A. A., Ignjatović Lj. M., Dimitrijević M. S., Djuric, Z.: 2003, "Symmetrical chemi-ionization and chemi-recombination processes in low-temperature layers of helium rich DB white dwarf atmospheres", *ApJs* 2003, Djeniže 147, 369-377.
14. Milosavljević V., Djeniže S.: 2003, "Astrophysical plasma diagnostics through analysis Ar I line shape characteristics", *ASTRONOMY AND ASTROPHYSICS 2003*, Djeniže 405, 397-403.
15. Popović, L. Č.: 2003, "Balmer Lines as Diagnostics of Physical Conditions in AGN Broad Emission Line Region", *ApJ* 2003, Djeniže 599, 140-146.
16. Zboril, M., Djurašević, G.: 2003, "SV Cam spot activity in February 2001 - March 2002", *ASTRONOMY AND ASTROPHYSICS 2003*, Djeniže 406, 193-201.
17. Djeniže, S., Bukvić, S., Srecković, A., Kalezić, S.: 2003, "Experimental transition probabilities and Stark shifts in O III and OIV spectra", *ASTRONOMY AND ASTROPHYSICS 2003*, Djeniže 406, 759-764.

18. Cakirh, O., Ibanoglu, C., Djurasević, G., Erkapic, S., Evren, S., Tas, G.: 2003, "Long-term photometric behaviour of the RS CVn binary RT Lacertae", *ASTRONOMY AND ASTROPHYSICS* 2003, Djeniže 405, 733-745.
19. Dimitrijević, M. S., Jovanović, P., Simić, Z.: 2003, "Stark broadening of neutral germanium spectral lines", *Astronomy and Astrophysics*, **410**, 735-739.
20. Djeniže, S., Bukvić, S., Srećković, A.: 2003, "On the Bowen fluorescence mechanism in the helium-oxygen plasmas", *Astronomy and Astrophysics*, **411**, 637-640.
21. Popović, L. Č., Mediavilla, E. G., Bon, E., Stanić, N., Kubičela, A.: 2003, "The Line Emission Region in III Zw 2: Kinematics and variability", *Astrophysical Journal*, **599**, 185-192..
22. Olević, D., Cvetković, Z.: 2004, "Orbits for 10 interferometric binary systems calculated by using the improved Koval'Skij's method", *Astronomy and Astrophysics*, **415**, 259-264.
23. Milovanović, N., Dimitrijević M. S., Popović, L. Č., Simić Z.: 2004, "Importance of Collisions with Charged Particles for Stellar UV Line Shapes: Cd III" *Astronomy and Astrophysics*, **417**, 375-380.
24. Djurašević, G., Albayrak, B., Tanriverdi, T., Erkapic, S.: 2004, "A Photometric Study of NN Virginis", *Astronomy and Astrophysics*, **415**, 283-287.
25. Mihajlov, A. A., Ermolaev, A. M., Ignjatović, Lj. M.: 2004, "H + H(1s) collisions at intermediate impact velocities as a new source of UV and VUV radiation", *Astronomy and Astrophysics*, **419**, 1-5.
26. Srećković, A., Bukvić, S., Djeniže, S., Dimitrijević, M. S.: 2004, "Stark broadening parameters in singly and doubly ionized fluorine spectra", *Astronomy and Astrophysics*, **420**, 769-774.
27. Zakharov, A. F., Popović, L. Č., Jovanović, P.: 2004, "On the contribution of microlensing to X-ray variability of high-redshifted QSOs", *Astronomy and Astrophysics*, **420**, 881-888.
28. Albayrak, B., Djurašević, G., Erkapic, S., Tanriverdi, T.: 2004, "Modeling the changing spot features of SW Lacertae: A three year study", *Astronomy and Astrophysics*, **420**, 1039-1045.
29. Ben Nessib, N., Dimitrijević, M. S., Sahal-Bréchet, S.: 2004, "Stark broadening of the four times ionized silicon spectral lines", *Astronomy and Astrophysics*, **423**, 397-400.
30. Dimitrijević, M. S., Dačić, M., Cvetković, Z., Simić, Z.: 2004, "Stark broadening of Ga I spectral lines", *Astronomy and Astrophysics*, **425**, 1147-1152.
31. Popović, L. Č., Mediavilla, E., Bon, E., Ilić, D.: 2004, "Contribution of the Disk Emission to the Broad Emission Lines in AGNs: Two-component model", *Astronomy and Astrophysics*, **423**, 909-918.
32. Djeniže, S., Bukvić, S., Srećković, A., Platiša, M.: 2004, "Mg II spectral line broadening in helium, oxygen and argon-helium plasmas", *Astronomy and Astrophysics*, **424**, 561-564.

33. Mahmoudi, W. F., Ben Nessib, N., Dimitrijević, M. S.: 2004, "Modified semiempirical electron width calculations of singly-ionized oxygen spectral lines", *Astronomy and Astrophysics*, **423**, 397-400.
34. Urošević, D., Pannuti, T. G., Duric, N., Theodorou, A.: 2005, "The Sigma-D Relation for Supernova Remnants in Nearby Galaxies", *Astronomy and Astrophysics*, **435**, 437-447.
35. Dimitrijević, M. S., Ryabchikova, T., Popović, L. Č., Shulyak, D., Khan, S.: 2005, "On the influence of Stark broadening on Cr I lines in stellar atmospheres", *Astronomy and Astrophysics*, **435**, 1191-1198.
36. Mihajlov, A. A., Ignjatović, Lj. M., Dimitrijević, M. S.: 2005, "Processes of (n-n')-mixing in collisions of Rydberg H*(n) atoms with H(1s) in the Solar atmosphere", *Astronomy and Astrophysics*, **437**, 1023-1028.
37. Simić, Z., Dimitrijević, M. S., Milovanović, N., Sahal-Bréchet, S.: 2005, "Stark broadening of Cd I spectral lines", *Astronomy and Astrophysics*, **441**, 391-393.
38. Djurašević, G., Rovithis-Livaniou, H., Rovithis, P., Georgiades, N., Erkapić, S., Pavlović, R.: 2006, "Gravity-Darkening exponents in Semi-Detached Binary Systems from their photometric observations: Part II", *Astronomy and Astrophysics*, **495**, 291-303.
39. Popović, L. Č., Jovanović, P., Mediavilla, E., Zakharov, A. F., Abajas, C., Muñoz, J. A., Chartas, G.: 2006, "A study of the correlation between the amplification of the Fe K alpha line and the X-ray continuum of quasars due to microlensing", *Astrophysical Journal*, **637**, 620-630.
40. Urošević, D., Pannuti, T. G., Leahy, D. : 2007, "An analysis of the broadband (22-3900 MHz) radio spectrum of HB3 (G132.7+1.3): The detection of thermal radio emission from an evolved supernova remnant?", *Astrophysical Journal Letters*, **655**, L41.
41. Hamdi, R., Ben Nessib, N., Dimitrijević, M. S., Sahal-Bréchet, S.: 2007, "Stark broadening of the four times ionized neon lines", *Astrophysical Journal Supplement Series*, **170**, 243-250.
42. Dimitrijević, M. S., Ryabchikova, T., Simić, Z., Popović, L. Č., Dačić, M.: 2007, "The influence of Stark broadening on Cr II spectral line shapes in stellar atmospheres", *Astronomy and Astrophysics*, **469**, 681-686.
43. Mihajlov, A. A., Ignjatović, Lj. M., Sakan, N. M., Dimitrijević, M. S.: 2007, "The influence of H₂⁺ - photo-dissociation and (H + H⁺) - radiative collisions on the solar atmosphere opacity in UV and VUV regions", *Astronomy and Astrophysics*, **469**, 749-754.
44. Mihajlov, A. A., Jevremović, D., Hauschildt, P., Dimitrijević, M. S., Ignjatović, Lj. M., Allard, F.: 2007, "Influence of chemi-ionization and chemi-recombination processes on Hydrogen line shapes in M dwarfs", *Astronomy and Astrophysics*, **471**, 671-673.
45. La Mura, G., Popović, L. Č., Ciroi, S., Rafanelli, P., Ilić, D.: 2007, "Detailed Analysis of Balmer Line in a SDSS Sample of 90 Broad Line AGN", *Astrophysical Journal*, **671**, 104-117.

46. Djurašević, G., Vince, I., Atanacković, O.: 2008, "Accretion disk in massive binary RY Scuti", *Astronomical Journal*, **136**, 767-772.
47. La Mura, G., Di Mille, F., Ciroi, S., Popović, L. Č., Rafanelli, P.: 2009, "Balmer Emission Line Profiles and the Complex Properties of Broad Line Regions in Active Galactic Nuclei", *Astrophysical Journal*, **693**, 1437-1448.
48. Popović, L. Č., Smirnova, A. A., Kovačević, J., Moiseev, A. V., Afanasiev, V. L.: 2009, "Three-dimensional Spectroscopic Study of the Line-Emitting Regions of Mrk 493", *Astronomical Journal*, **137**, 3548-3557.
49. Urošević, D., Vukotić, B., Arbutina, B., Ilić, D., Filipović, M., Bojičić, I., Šegan, S., Vidojević, S.: 2009, "The Sigma-D relation for planetary nebulae", *Astronomy and Astrophysics*, **495**, 537-546.
50. Ignjatović, Lj. M., Mihajlov, A. A., Sakan, N. M., Dimitrijević, M. S., Metropoulos, A.: 2009, "The total and relative contribution of the relevant absorption processes to the opacity of DB white dwarf atmospheres in UV and VUV regions", *Monthly Notices of the Royal Astronomical Society*, **396**, 2201-2210.
51. Djurašević, G., Vince, I., Khruzina, T. S., Rovithis-Livaniou, E.: 2009, "Accretion disk in the massive V448 Cygni system", *Monthly Notices of the Royal Astronomical Society*, **396**, 1553-1558.
52. Vukotić, B., Urošević, D., Filipović, M. D., Payne, J. L.: 2009, "The Sigma - D Analysis of Recently Detected Radio Planetary Nebulae in the Magellanic Clouds", *Astronomy and Astrophysics*, **503**, 855-858.
53. Bon, E., Popović, L. Č., Gavrilović, N., La Mura, G., Mediavilla, E.: 2009, "Contribution of a Disk Component to Single Peaked Broad Lines of Active Galactic Nuclei", *Monthly Notices of the Royal Astronomical Society*, **400**, 924-936.
54. Shapovalova, A. I., Popović, L. Č., Burenkov, A. N., Chavushyan, V. H., Ilić, D., Kovačević, A., Bochkarev, N. G., Leon-Tavares, J.: 2010, "Long-term variability of the optical spectra of NGC 4151: II. Evolution of the broad H α and H β emission-line profiles", *Astronomy and Astrophysics*, **509**, A106.
55. Cubarsi, R., Alcobe, S., Vidojević, S., Ninković, S.: 2010, "Disk and halo kinematic populations from HIPPARCOS and Geneva-Copenhagen surveys of the solar neighbourhood", *Astronomy and Astrophysics*, **510**, A102.
56. Shapovalova, A. I., Popović, L. Č., Burenkov, A. N., Chavushyan, A. N., Ilić, D., Kollatschny, W., Kovačević, A., Bochkarev, N. G., Carrasco, L., Leon-Tavares, J., Mercado, A., Valdes, J. R., Vlasuyk, V. V., de la Fuente, E.: 2010, "Spectral optical monitoring of 3C390.3 in 1995-2007: I. Light curves and flux variation of the continuum and broad lines", *Astronomy and Astrophysics*, **517**, A42.
57. Srećković, V. A., Ignjatović, Lj. M., Mihajlov, A. A., Dimitrijević, M. S.: 2010, "The electrical conductivity of plasmas of DB white dwarf atmospheres", *Monthly Notices of the Royal Astronomical Society*, **406**, 590-596.
58. Kovačević, J., Popović, L. Č., Dimitrijević, M. S.: 2010, "Analysis of the optical Fe II lines in a sample of AGN spectra", *Astrophysical Journal Supplement Series*, **189**, 15-36.

59. Jovanović, P., Popović, L. Č., Stalevski, M., Shapovalova, A.I.: 2010, "Variability of the H β line profiles as an indicator of orbiting bright spots in accretion disks of quasars: a case study of 3C 390.3", *Astrophysical Journal*, **718**, 168-176.
60. Urošević, D., Vukotić, B., Arbutina, B., Sarevska, B.: 2010, "The orthogonal fitting procedure for determination of the empirical Sigma - D relations for supernova remnants: Application to starburst galaxy M82", *Astrophysical Journal*, **719**, 950-957.
61. Djurašević, G., Latković, O., Vince, I., Cseki, A.: 2010, "Accretion disk in the eclipsing binary AU Mon", *Monthly Notices of the Royal Astronomical Society*, **409**, 329-336.
62. Djurašević, G., Yilmaz, M., Basturk, O., Kilicoglu, T., Latković, O., Caliskan, S.: 2010, "Physical parameters of close binaries QX And, RW Com, MR Del and BD +07o 3142", *Astronomy and Astrophysics*, **525**, A66.
63. Popović, L. Č., Moiseev, A. V., Mediavilla, E., Jovanović, P., Ilić, D., Kovačević, J., Muñoz, J.: 2010, "RXJ 0921+4529: a binary quasar or gravitational lens?", *Astrophysical Journal Letters*, **721**, L139-L142.
64. Mihajlov, A. A., Ignjatović, Lj. M., Srećković, V. A., Dimitrijević, M. S.: 2011, "Chemi-ionization in Solar Photosphere: Influence on the Hydrogen Atom excited States Populations", *Astrophysical Journal Supplement Series*, **193**, 2.
65. Popović, L. Č., Shapovalova, A. I., Ilić, D., Kovačević, A., Kollatschny, W., Burenkov, A. N., Chavushyan, V. H., Bochkarev, N. G., Leon-Tavares, J.: 2011, "Spectral optical monitoring of 3C 390.3 in 1995-2007: II. Variability of the spectral line parameters", *Astronomy and Astrophysics*, **528**, A130.
66. Popović, L. Č., Kovačević, J.: 2011, "Different spectral properties of a sample of the broad line AGNs: Baldwin effect and EV 1", *Astrophysical Journal*, **738**, 68.
67. Donnarumma, I., De Rosa, A., Vittorini, V., Miller, H. R., Popović, L. Č., Simić, S., Tavani, M., Eggen, J., Maune, J., Kuulkers, E., Striani, E., Vercellone, S., Pucella, G., Verrecchia, F., Pittori, C., Giommi, P., Pacciani, L., Barbiellini, G., Bulgarelli, A., Cattaneo, P., Chen, A. W., Costa, E., Del Monte, E., Evangelista, Y., Feroci, M., Fuschino, F., Gianotti, F., Giuliani, A., Giusti, M., Lazzarotto, F., Longo, F., Lucarelli, F., Pellizzoni, A., Piano, G., Soffitta, P., Trifoglio, M., Trois, A.: 2011, "The remarkable gamma-ray activity in the gravitationally lensed blazar PKS 1830-211", *Astrophysical Journal Letters*, **736**, 30.
68. Elabidi, H., Sahal-Bréchet, S., Dimitrijević, M. S., Ben Nessib, N.: 2011, "Quantum Stark broadening data for C IV, N V, O VI, F VII and Ne VIII resonant transitions", *Monthly Notices of the Royal Astronomical Society*, **417**, 2624-2630.
69. Baes, M., Verstappen, J., De Looze, I., Fritz, J., Saftly, W., Vidal Perez, E., Stalevski, M., Valcke, S.: 2011, "Efficient 3D NLTE dust radiative transfer with SKIRT", *Astrophysical Journal Supplement Series*, **196**, 22.
70. Stalevski, M., Fritz, J., Baes, M., Nakos, T., Popović, L. Č.: 2012, "Three-dimensional radiative transfer modeling of AGN dusty tori as clumpy two-phase medium", *Monthly Notices of the Royal Astronomical Society*, **420**, 2756 (accepted 2011).
71. Popović, L. Č., Jovanović, P., Stalevski, M., Antoniu, S., Andrei, A. H., Kovačević, J., Baes, M.: 2012, "Photo-centric variability of quasars caused by var-

- iations in their inner structure: Consequences on GAIA measurements", *Astronomy and Astrophysics*, **538**, A107 (accepted, 2011).
72. Kovačević, A.: 2012, "Determination of Ceres mass based on most gravitationally efficient close encounters", *Monthly Notices of the Royal Astronomical Society*, **419**, 2725-2736 (accepted 2011).
73. Djurašević, G., Vince, I., Antokhin, I. I., Shatsky, N. I., Cseki, A., Zakirov, M., Eshankulova, M.: 2012, "A study of the active binary system V455 Cygni", *Monthly Notices of the Royal Astronomical Society*, **420**, 3081 (accepted 2011).
74. Mennickent, R.E., Djurašević, G., Kolaczowski, Z., Michalska, G.: 2012, "The Double Periodic Variable V 393 Scorpii: evolution stage and possible massive disk", *Monthly Notices of the Royal Astronomical Society*, **421**, 862 (accepted 2011).
75. Bozzetto, L.M., Filipović, M. D., Crawford, E.J., Haberl, F., Sasaki, M., Urošević, D., Pietsch, W., Payne, J. L., De Horta, A. Y., Stupar, M., Tothill, N., Dickel, J., Chu, Y.-H., Gruendl, R.: 2012, "Multi-frequency study of the Large Magellanic Cloud Supernova Remnant J0529-6653 near Pulsar B0529-66", *Monthly Notices of the Royal Astronomical Society*, **420**, 2588-2595 (accepted 2011).
76. Arbutina, B., Urošević, D., Andjelić, M., Pavlović, M., Vukotić, B.: 2012, "Modified equipartition calculation for supernova remnants", *Astrophysical Journal*, **746**, 79 (accepted 2011).

Acknowledgements

This work is a part of the Project III44002, of the Ministry for Education, Science and Technological development of Republic of Serbia

References

- ***: *Isaac Newton Institute of Chile in Eastern Europe and Eurasia*.
- ***: 2003, *Isaac Newton Institute of Chile in Eastern Europe and Eurasia*, in INI - Isaac Newton Institute of Chile in Eastern Europe and Eurasia, Santiago, Chile, 1-714.
- ***: 2004, *Isaac Newton Institute of Chile in Eastern Europe and Eurasia*, in INI - Isaac Newton Institute of Chile in Eastern Europe and Eurasia, Santiago, Chile, 1-511.
- Alcaino, G.: 2003, *Isaac Newton Institute of Chile in Eastern Europe and Eurasia*, *Bulletin of the American Astronomical Society*, **35**, 109.
- Alcaino, G.: 2004, *Isaac Newton Institute of Chile in Eastern Europe and Eurasia*, *Bulletin of the American Astronomical Society*, **36**, 59.
- Alcaino, G.: 2005, *Isaac Newton Institute of Chile in Eastern Europe and Eurasia*, *Bulletin of the American Astronomical Society*, **37**, 78.
- Димитријевић, М. С.: 2002, *Васиона*, бр. 5, 141.
- Димитријевић, М. С., Поповић, Л. Ч., Симић, З., Јовановић, П., Миловановић, Н., Бон, Е.: 2005, „Огранак „Југославија“ Међународног астрономског „Исак Њутн“, Зборник радова конференције „Развој астрономије код Срба III“, Београд 25-28. Април 2004, уредник М. С. Димитријевић, Публ. Астрон. Друштва „Пуђер Бошковић“, **6**, 255.

ACTIVITIES OF PARTICIPANTS OF THE PROJECTS 146001 AND 176002 "INFLUENCE OF COLLISIONAL PROCESSES ON THE ASTROPHYSICAL PLASMA SPECTRA" – 2010-2011

MILAN S. DIMITRIJEVIĆ

Astronomical Observatory, Volgina 7, 11060 Belgrade, Serbia
E-mail: mdimitrijevic@aob.bg.ac.rs

Abstract. The brief review is given, of activities of participants of the projects 146001 (in the 2010 year) and 176002 (in the 2011 year) "Influence of collisional processes on the astrophysical plasma spectra", within the period from 1st January 2010 up to 31st December 2011. Besides the bibliography of scientific results, other activities of the project participants, such as activities in popularization of science and in literature, editing, organization of scientific conferences, etc. are presented.

The period described here was specific, since in 2010 one project cyclus was completed (project 146001) and started a new one in which the project 176002 was submitted with the same name: "Influence of collision processes on astrophysical plasma spectra", but with a much broader content. In addition, the group of Anatolij Mihajlov was included and their experimental investigations of the influence of solar activity on the characteristics of the earth-ionosphere waveguide. Sonja Vidojević with a new topic of research of solar wind was also included as well as foreign associates.

The new Project is the continuation of long standing research of the influence of atomic collisional processes on the spectra of astrophysical and laboratory plasmas, and contains also two Project tasks where the investigations in two new research fields will start. The topics proposed to the Ministry of Education and Science are:

1. Determination of parameters of Stark broadening and investigations of its influence on spectral lines of white dwarfs and of chemically peculiar A and B type stars. This research field is particularly actualized with the development of satellite born astronomy, which provides the good quality spectra with unreachably before resolution, so that spectral lines of trace elements are becoming more and more astrophysically significant. Particularly is interesting recently discovered

new type of white dwarfs with carbon atmospheres,¹ which spectra contain numerous C II lines broadened by impacts with charged particles. Data on their Stark broadening available in literature are scarce and insufficient, and in order to understand the origin and evolution of this new type of stars the inclusion of accurate spectral line broadening is crucial for this type of white dwarf atmosphere modelisation.

The influence of Stark broadening on other types of white dwarf spectra, as well as on that of A and B type stars, will be investigated as well. For determination of Stark broadening parameters, semiclassical perturbation and modified semiempirical method will be used, and the results will be compared with observed stellar spectra and synthetic ones, modeled with SYNTH2 and PHOENIX code. These results enter within the frame of FP7 project VAMDC 239108 (<http://www.vamdc.org/>), in STARK-B database (<http://stark-b.obspm.fr/>), and Serbian Virtual Observatory (<http://servo.aob.rs/~darko/>).

Except for Astrophysics, obtained results will be of importance and for research of laboratory plasma, plasma technologies, lightning, lasers, laser produced plasmas and inertial fusion.

2. The influence of solar activity on the characteristics of waveguide Earth-ionosphere (Space weather), as well as the influence of electrical discharges in the Earth's atmosphere will be studied experimentally, by permanent measuring of the amplitude and phase of VLF radio-waves which propagate through the waveguide Earth-ionosphere. Measuring of the amplitude and phase of narrowband transmitters within the range 10-30 kHz, by using AbsPAL (*Absolute Phase and Amplitude Logger*) and AWESOME (*Atmospheric Weather Electromagnetic System for Observation Modeling and Education*) systems. On the base of obtained data will be analyzed daily changes in the ionosphere which are caused by reinforced radiation from the Sun during flares and the electron density profiles during the flares as well as in the period when regular conditions in the D layer of ionosphere are established. Also, it will be studied the perturbation of the electron density in the D layer of ionosphere during night conditions which are caused by falling down high energy electrons from the radiative bands (*Lightning-induced electron precipitation, LEP event*). We plan the continuation of the work within European action COST ES0803 «Developing space weather products and services in Europe», as well as of the bilateral collaboration with the University of Nova Gorica (Slovenia).

3. We will study the influence of inelastic atom-Rydberg atom and radiative ion-atom collision processes on the kinetics of weakly ionized plasma of Sun, white dwarfs and Earth's ionosphere. As the result, the needed rate coefficients of chemi-ionization/recombination and excitation/deexcitation processes in atom-Rydberg atom collisions, as well as the coefficients of the absorption caused by ion-atom collisions in UV and VUV spectral regions will be determined. On the base of these data the influence of atom-atom and ion-atom collision processes to

¹ Dufour, P., Liebert, J., Fontaine, G., Behara, N. : 2007, White dwarf stars with carbon atmospheres, *Nature*, **450**, 522.

the kinetic transport properties of weakly ionized solar, stellar and ionospheric plasmas will be studied.

4. Within the Project frame is the Project task "Solar wind", led by Sonja Vidojević. By analysis of observations with different devices on the satellites "Wind" and "STEREO", in collaboration with Paris Observatory (Milan Maksimović) will be investigated the interaction of beams with highly energetic electrons, formed in various violent events on the the Sun, with interplanetary plasma (Solar wind), through which they propagate on lines of force of the solar magnetic field. One will work and on the investigation of relationship between Langmuir oscillations/waves, and the type III solar radio bursts. As the result, one expect to determine reliably a large number of parameters of Langmuir oscillations/waves and to prove the cause and effect relationship with the type III solar radio bursts.

5. The second Project's task is "Investigation of exoplanet's reflectance spectra" in order to search biomarkers in them. This is the beginning of such investigations here, and in collaboration with Siegfried Franck from Potsdam our younger researcher will be trained to synthesize, with the JPL (Jena, Potsdam, Lund) code, the reflectance spectrum of a planet and to investigate observability of the influence of biosphere on it. The spectrum of host-star, which should be subtracted, will be modeled with the PHOENIX code or obtained by observations. Unfortunately, this activity stopped, since Professor Siegfried Franck passed away.

Besides the scientific investigations, what is the principal objective of the Project, it will be (as in the previous Project's cycle) a basis for wide international collaboration in this research field, as it is the work on FP7 project VAMDC 239108 (Virtual Center for Atomic and Molecular Data <http://www.vamdc.org/>), which has participants from 9 countries (and the Project's leader, and the author of this text, is a member of the Project Board and leader of the Serbian node - AOB node), and on COST action ES0803 «Developing space weather products and services in Europe» (<http://www.costes0803.noa.gr/>). Because of needed equipment for the Project (observations from satellites „Wind» and "STEREO", observations of stellar spectra) will be continued and enlarged the collaboration with Paris Observatory and Russia. On the other hand, in order to obtain results of high quality, in the work on Project will participate our coauthors and colleagues from France, Russia, Greece, Spain, Germany, Tunisia, Bulgaria, Belgium (Jovo Vranješ) and Slovenia (Vida Žigman). The Project will be and a basis for scientific training and education of the young, so that we expect that at least three PhD Theses will be defended until the end of this Project, and that some tasks on the Project become themes for Diploma theses of Master studies.

Within the 2010-2011 period, participants of the Project published 7 papers in leading international journals, namely (the number of papewrs is in the brackets): Astronomy and Astrophysics (1), Astrophysical Journal (1), Astrophysical Journal Supplement Series (2), Monthly Notices of the Royal Astronomical Society (2), Journal of Physics A: Mathematical and Theoretical Physics (1).

In international journals European Physical Journal: Applied Physics (1), Journal of Quantitative Spectroscopy and Radiative Transfer (1) Physica Scripta (1) Baltic Astronomy (14) and Acta Astronomica (1), 18 papers are published. Moreover, three papers, not connected with project, are published in the journal from SSC list, and in international journals not in SCI list, and books of international publishers 20 papers are published.

The other results are: Invited lectures on international conferences published in journals and books of international publishers (8), national monographies (2), scientific papers in national journals and books (13), scientific papers in proceedings of international conferences (3), contributions on national conferences (12), abstracts of invited lectures on international conferences (12), abstracts of contributions to international conferences (27), abstracts of invited lectures on national conferences (1), book reviews in national journals (1) and 13 entries for Serbian Encyclopedia. In the considered period Dragana Tankosić defended her PhD Thesis.

In total, associates of the Project published 141 bibliographic item, from which 95 are connected with Project and 46 not.

Associates of the Project have organized also four conferences and one summer school, giving and in this way a contribution to the development of scientific collaboration. These meetings are:

1. „DEVELOPMENT OF ASTRONOMY AMONG SERBS VI“, Belgrade, 22 – 26 April 2010, M. S. Dimitrijević Chair of Scientific Committee, M. Dačić member; M. Dačić Chair of Local Organizing Committee, M. S. Dimitrijević member.
2. THE THIRD INTERNATIONAL SCHOOL IN ASTRONOMY: ASTROINFORMATICS – VIRTUAL OBSERVATORY, Belgrade, 29 Jun – 1 July 2010, M. S. Dimitrijević and A. Kovačević Co-Chairs of Scientific Committee, D. Jevremović Co-Vice chair, Z. Simić member, A. Kovačević Chair of Local Organizing Committee, J. Kovačević, M. Dačić, Z. Simić members.
3. I WORKSHOP: SPECTROSCOPY AS A TOOL TO INVESTIGATE ACTIVE GALACTIC NUCLEI AND GRAVITATIONAL LENSES, Бабе (Космај), 7-11. јули 2010, M. S. Dimitrijević, D. Jevremović, A. Kovačević members of Scientific Committee, J. Kovačević Chair of Local Organizing Committee, A. Kovačević member.
4. 8th SERBIAN CONFERENCE ON SPECTRAL LINE SHAPES IN ASTROPHYSICS, Divčibare, 6-10 Jun 2011, D. Jevremović Co-Chair of Scientific Committee, M. S. Dimitrijević, A. A. Mihajlov members, D. Jevremović Co-Chair of Local Organizing Committee, A. Kovačević Secretary, M. S. Dimitrijević, J. Kovačević, M. Dačić, Z. Simić members
5. I WORKSHOP ON ASTROPHYSICAL SPECTROSCOPY, Orašac, 26-30. August 2011. M. S. Dimitrijević co-Chair of the Scientific and Local Organizing Committees, D. Jevremović, Z. Simić, A. Kovačević members,

A. Kovačević Co-Chair of Local Organizing Committee, M. Dačić, J. Kovačević, Z. Simić members.

In addition, associates of the Project contributed and to the organization of the following conferences:

1. 7th BULGARIAN-SERBIAN ASTRONOMICAL CONFERENCE, ASTROINFORMATICS, Chepelare, 1 – 4. June, 2010, M. S. Dimitrijević, D. Jevremović, Z. Simić members of Scientific Committee.
2. IX CONFERENCE NEW TECHNOLOGIES AND STANDARDS: NATIONAL HERITAGE DIGITIZATION, Belgrade, 16-17. June 2010, M. S. Dimitrijević member of the Organizing Committee.
3. 20th International Conference on Spectral Line Shapes, 6-11 June 2010, St. Johns, Newfoundland, Canada, Milan S. Dimitrijević member of Scientific Committee.
4. 12th International Conference on Computer Systems and Technologies, CompSysTech'11, Wien, 16-17 June 2011, International Programme Committee, M. S. Dimitrijević, member.
5. 10th CONFERENCE NEW TECHNOLOGIES AND STANDARDS: NATIONAL HERITAGE DIGITIZATION, Belgrade, 22-23 September 2011, M. S. Dimitrijević member of the Organizing Committee.

During 2010, on the project 146001 seven associates participated, six from Astronomical Observatory and Andjelka Kovačević from Mathematical Faculty (MF). The Project Leader was Zoran Simić and the list of associates is:

1. **Miodrag Dačić**, (born 1946) with 10 rm (research months)
2. **Milan S. Dimitrijević**, (born 1947) with 12 rm
3. **Darko Jevremović**, (born 1968) with 9 rm
4. **Andjelka Kovačević**, (born 1972, MF) with 8 rm
5. **Nenad Milovanović**, (born 1972) with 12 rm
6. **Zoran Simić**, (born 1967) with 12 rm
7. **Dragana Tankosić**, (born 1968) with 4 rm

During 2011, twenty six researches have been engaged on the new project 176002, sixteen from Serbia and ten from abroad. Among researches from Serbia, seven was from Astronomical Observatory (AO), four from Institute of Physics (IF), three from Mathematical Faculty (MF), one from Mathematical Institute (MI) and one from Institute for chemical power sources (IHIS). The Project leader was M. S. Dimitrijević and the list of participants is:

1. **Sonja Vidojević**, (born 1960, IHIS) with 12 rm (research months)
2. **Miodrag Dačić**, (born 1946, AO) with 0 rm
3. **Milan S. Dimitrijević**, (born 1947, AO) with 9 rm

4. **Sanja Životić**, (born 1984, MF) with 2 rm
5. **Ljubinko Ignjatović**, (born 1959, IF) with 12 rm
6. **Darko Jevremović**, (born 1968, AO) with 3 rm
7. **Andjelka Kovačević**, (born 1972, MF) with 7 rm
8. **Jelena Kovačević**, (born 1981, AO) with 1 rm
9. **Dušan Marčeta**, (born 1980, MF) with 4 rm
10. **Nenad Milovanović**, (born 1972, AO) with 2 rm
11. **Anatolij Mihajlov**, (born 1941, IF) with 0 rm
12. **Aleksandra Nina**, (born 1977, IF) with 5 rm
13. **Zoran Simić**, (born 1967, AO) with 10 rm
14. **Vladimir Srečković**, (born 1972, IF) with 5 rm
15. **Dragana Tankosić**, (born 1968, AO) with 6 rm
16. **Brankica Šurlan**, (born 1974, MI) with 6 rm

Foreign participants of the Project were **Jovo Vranješ** (Belgium), **Milan Maksimović** (France), **Tatjana Ryabchikova** (Russia), **Magdalena Christova** (Bulgaria), **Emanouel Danezis** (Greece), **Antonios Antoniou** (Greece), **Sylvie Sahal-Bréchet** (France), **Nebil Ben Nessib** (Tunisia), **Maria Dolores Calzada** (Spain) and **Siegfrid Franck** (Germany).

In 2010, seven participants of the project 146001 realized 67 months of research, ie. 5.6 years. Average age of researchers was 1963.9 or about 46 years. In 2011 the situation is different because we have ten foreigners and two retired with zero months. If we consider only funded researchers, fourteen associates participated with a total of 84 months of research or 7 years. Average age was 1970.6 or about 40.4 years.

An important result of the project is the PhD thesis defended by Dragana Tankosić in 2010. The information concerning the achieved scientific results and extensive international cooperation, provides the bibliography of published works, listed in the Appendix. The new project, which was accepted by the Ministry of Education and Science in the new cycle, which began in 2011, greatly exceeded the old, completed in 2010, both in scope and in number of research assistants, as well as with opportunities for further education of the young. Also, a fruitful and successful international cooperation with a number of colleagues from other countries has been developed and the obtained results are, and will be included in European projects such as FP7 (Virtual Atomic and Molecular Data Center) and COST action.

BIBLIOGRAPHY OF SCIENTIFIC WORKS OF PARTICIPANTS OF THE PROJECTS 146001 AND 176002 WITHIN THE PERIOD 2010-2011

PhD THESES

1. Dragana Tankosić: EXPERIMENTAL INVESTIGATIONS OF THE OPTICAL AND PHYSICAL PROPERTIES OF INTERSTELLAR AND LUNAR DUST, PhD Thesis defended 16.09.2010, on the University of State Alabama, Huntsville, USA.

SCIENTIFIC PAPERS IN LEADING INTERNATIONAL JOURNALS

1. J. Kovačević, L. Č. Popović, M. S. Dimitrijević: 2010, ANALYSIS OF OPTICAL Fe II EMISSION IN A SAMPLE OF ACTIVE GALACTIC NUCLEUS SPECTRA, *Astrophysical Journal Supplement Series*, **189**, 15-36.
2. V. A. Srećković, Lj. M. Ignjatović, A. A. Mihajlov, M. S. Dimitrijević: 2010, "ELECTRICAL CONDUCTIVITY OF PLASMAS OF DB WHITE DWARF ATMOSPHERES" *Monthly Notices of the Royal Astronomical Society*, **406**, 590-596.
3. A. A. Mihajlov, Lj. M. Ignjatović, V. A. Srećković, M. S. Dimitrijević: 2011, CHEMI-IONIZATION IN SOLAR PHOTOSPHERE: INFLUENCE ON THE HYDROGEN ATOM EXCITED STATES POPULATION, *Astrophysical Journal Supplement Series*, **193**, 2(1-7).
4. H. Elabidi, S. Sahal-Bréchet, M. S. Dimitrijević, N. Ben Nessib: QUANTUM STARK BROADENING DATA FOR THE C IV, N V, O VI, F VII AND NE VIII RESONANCE DOUBLETS, *Monthly Notices of the Royal Astronomical Society* **417** (2011), 2624-2630.
5. L. Č. Popović, A. I. Shapovalova, D. Ilić, A. Kovačević, W. Kollatschny, A. N. Burenkov, V. H. Chavushyan, N. G. Bochkarev, J. León-Tavares: SPECTRAL OPTICAL MONITORING OF 3C 390.3 IN 1995-2007. II. VARIABILITY OF THE SPECTRAL LINE PARAMETERS, *Astronomy and Astrophysics*, **528** (2011), A130.
6. A. A. Mihajlov, N. M. Sakan, V. A. Srećković, Y. Vitel: MODELING OF CONTINUOUS ABSORPTION OF ELECTROMAGNETIC RADIATION IN DENSE PARTIALLY IONIZED PLASMAS, *Journal of Physics A: Mathematical and Theoretical Physics*, **44** (2011), 095502.
7. L. Č. Popović, J. Kovačević: OPTICAL EMISSION-LINE PROPERTIES OF A SAMPLE OF THE BROAD-LINE ACTIVE GALACTIC NUCLEI: THE BALDWIN EFFECT AND EIGENVECTOR 1, *Astrophysical Journal*, **738** (2011), 68.

**SCIENTIFIC PAPERS IN INTERNATIONAL JOURNALS FROM SCI AND
SSCI LISTS**

1. R. Qindeel, M. S. Dimitrijević, N. M. Shaikh, N. Bidin, Y. M. Daud: SPECTROSCOPIC ESTIMATION OF ELECTRON TEMPERATURE AND DENSITY OF ZINC PLASMA OPEN AIR INDUCED BY Nd:YAG LASER, *European Physical Journal: Applied Physics*, **50** (2010), 30701.
2. M. L. Dubernet, V. Boudon, J. L. Culhane, M. S. Dimitrijevic, A. Z. Fazliev, C. Joblin, F. Kupka, G. Leto, P. Le Sidaner, P. A. Loboda, H. E. Mason, N. J. Mason, C. Mendoza, G. Mulas, T. J. Millar, L. A. Nuñez, V. I. Perevalov, N. Piskunov, Y. Ralchenko, G. Rixon, L. S. Rothman, E. Roueff, T. A. Ryabchikova, A. Ryabtsev, S. Sahal-Bréchet, B. Schmitt, S. Schlemmer, J. Tennyson, V. G. Tyuterev, N. A. Walton, V. Wakelam, C. J. Zeippen: VIRTUAL ATOMIC AND MOLECULAR DATA CENTRE, *Journal of Quantitative Spectroscopy and Radiative Transfer*, **111** (2010), 2151-2159.
3. E. Theodossiou, V. Manimanis, M. S. Dimitrijević: THE INCONVENIENT RELATION BETWEEN RELIGION AND SCIENCE: THE PREVALENCE OF THE HELIOCENTRIC THEORY, *European Journal for Science and Theology* **6** (3) (2010), 47-56.
4. B. Zmerli, N. Ben Nessib, M. S. Dimitrijević, S. Sahal-Bréchet: 2010, STARK BROADENING CALCULATIONS OF NEUTRAL COPPER SPECTRAL LINES AND TEMPERATURE DEPENDENCE, *Physica Scripta* **82**, 055301 (9pp).
5. E. Theodossiou, V. Manimanis, M. S. Dimitrijević: THE CONTRIBUTION OF BIZANTINE PRIESTS IN ASTRONOMY AND COSMOLOGY. I. THE CHURCH FATHERS: THREE BISHOPS ST. BASIL THE GREAT, ST. GREGORY OF NAZIANZUS AND ST. JOHN CHRYSOSTOM, *European Journal for Science and Theology* **7** (2) (2011), 33-47.
6. E. Theodossiou, V. Manimanis, M. S. Dimitrijević: THE CONTRIBUTION OF BIZANTINE PRIESTS IN ASTRONOMY AND COSMOLOGY. II. GREAT CHURCH SCHOLARS IN THE EARLY BYZANTINE EMPIRE, *European Journal for Science and Theology* **7** (4) (2011), 25-45.
7. S. Sahal-Bréchet, M. S. Dimitrijević, N. Ben Nessib: COMPARISONS AND COMMENTS ON ELECTRON AND ION IMPACT PROFILES OF SPECTRAL LINES, *Baltic Astronomy* **20**, (2011) 523-530.
8. P. Dufour, N. Ben Nessib, S. Sahal-Bréchet, M. S. Dimitrijević: STARK BROADENING OF CARBON AND OXYGEN LINES IN HOT DQ WHITE DWARF STARS: RECENT RESULTS AND APPLICATIONS, *Baltic Astronomy* **20**, (2011) 511-515.
9. F. Kupka and the VAMDC (participant M. S. Dimitrijević) collaboration (P.[rincipal] I.[nvestigator] M.-L. Dubernet): VAMDC AS A RESOURCE FOR ATOMIC AND MOLECULAR DATA AND THE NEW RELEASE OF VALD, *Baltic Astronomy* **20**, (2011) 503-510.

10. M. S. Dimitrijević, A. Kovačević, Z. Simić, S. Sahal-Bréchet: STARK BROADENING AND WHITE DWARFS, *Baltic Astronomy* **20**, (2011) 495 -502.
11. R. Hamdi, N. Ben Nessib, M. S. Dimitrijević, S. Sahal-Bréchet: AB INITIO DETERMINATION OF ATOMIC STRUCTURE AND STARK BROADENING PARAMETERS: Pb IV AND RECENT RESULTS, *Baltic Astronomy* **20**, (2011) 552-557.
12. A. A. Mihajov, Lj. M. Ignjatović, V. A. Srećković, M. S. Dimitrijević: THE INFLUENCE OF CHEMI-IONIZATION AND RECOMBINATION PROCESSES ON SPECTRAL LINE SHAPES IN STELLAR ATMOSPHERES, *Baltic Astronomy* **20**, (2011) 566-571.
13. E. Lyrtzi, E. Danezis, L. Č. Popović, A. Antoniou, M. S. Dimitrijević, D. Stathopoulos: THE COMPLEX BROAD ABSORPTION LINE PROFILES IN A SAMPLE OF QSO SPECTRA, *Baltic Astronomy* **20**, (2011) 448-452.
14. Z. Simić, M. S. Dimitrijević, A. Kovačević, S. Sahal-Bréchet: STARK BROADENING OF In III LINES IN ASTROPHYSICAL AND LABORATORY PLASMA, *Baltic Astronomy* **20**, (2011) 613-617.
15. M. S. Dimitrijević, A. Kovačević, Z. Simić, S. Sahal-Bréchet: STARK BROADENING OF SEVERAL Ne II, Ne III AND O III SPECTRAL LINES FOR THE STARK-B DATABASES, *Baltic Astronomy* **20**, (2011) 580-586.
16. M. S. Dimitrijević, A. Kovačević, Z. Simić, S. Sahal-Bréchet: STARK BROADENING OF SEVERAL Ar I SPECTRAL LINES IN THE VISIBLE SPECTRUM, *Baltic Astronomy* **20**, (2011) 576-579.
17. A. Antoniou, E. Danezis, E. Lyrtzi, D. Stathopoulos, M. S. Dimitrijević: A STATISTICAL STUDY OF THE Si IV RESONANCE LINE PARAMETERS IN 19 Be STARS, *Baltic Astronomy* **20**, (2011) 548-551.
18. A. I. Shapovalova, L. Č. Popović, D. Ilić, A. Kovačević, J. Kovačević, A. N. Burenkov, V. H. Chavushyan: SPECTRAL MONITORING OF AGN: PRELIMINARY RESULTS FOR ARK 564 AND ARP 102B, *Baltic Astronomy* **20**, (2011) 476-480.
19. S. Šegan, S. Milisavljević, D. Marčeta: A COMBINED METHOD TO COMPUTE THE PROXIMITIES OF ASTEROIDS, *Acta Astronomica*, **61** (2011) 275-283.
20. A. Nina, V. Čadež, V. Srećković, D. Šulić: THE INFLUENCE OF SOLAR SPECTRAL LINES ON ELECTRON CONCENTRATION IN TERRESTRIAL IONOSPHERE, *Baltic Astronomy*, **20** (2011), 609–612.
21. A. Mihajlov, N. Sakan, V. Srećković, Y. Vitel: MODELING OF THE CONTINUOUS ABSORPTION OF ELECTROMAGNETIC RADIATION IN DENSE HYDROGEN PLASMA, *Baltic Astronomy*, **20** (2011), 604-609.

**INVITED LECTURES ON INTERNATIONAL CONFERENCES
PUBLISHED IN BOOKS AND JOURNALS OF INTERNATIONAL
PUBLISHERS**

1. E. Lyratzi, E. Danezis, E., L. Č. Popović, A. Antoniou, M. S. Dimitrijević, D. Stathopoulos: STUDYING THE COMPLEX BAL PROFILES IN THE BALQSOS SPECTRA, *Journal of Physics: Conference Series* **257**, (2010) 012035 (1-8).
2. M. S. Dimitrijević, S. Sahal-Bréchet, A. Kovačević, D. Jevremović, L. Č. Popović: EUROPEAN VIRTUAL ATOMIC DATA CENTRE - VAMDC, *Journal of Physics: Conference Series* **257**, (2010) 012032 (1-8).
3. K. Tsvetkova, M. Tsvetkov, M. S. Dimitrijević, V. Protić-Benišek, V. Benišek, D. Jevremović: WIDE-FIELD PLATE ARCHIVES IN ROZHEN AND BELGRADE OBSERVATORIES, *Memorie della Societa Astronomica Italiana Supplementi* **15**, (2010) 192-203.
4. M. Christova, M. S. Dimitrijević: STARK BROADENING OF SPECTRAL LINES OF INERT GASES, *Memorie della Societa Astronomica Italiana Supplementi* **15**, (2010) 126-137.
5. M. S. Dimitrijević: ASTRONOMICAL SPECTRA AND COLLISIONS WITH CHARGED PARTICLES, *Memorie della Societa Astronomica Italiana Supplementi* **15**, (2010) 32-43.
6. E. Danezis, E. Lyratzi, A. Antoniou, L. Č. Popović, M. S. Dimitrijević: STUDYING THE COMPLEX SPECTRAL LINE PROFILES IN THE SPECTRA OF HOT EMISSION STARS AND QUASARS, *Memorie della Societa Astronomica Italiana Supplementi* **15**, (2010) 13-31.
7. M. S. Dimitrijević, S. Sahal-Bréchet, A. Kovačević, D. Jevremović, L. Č. Popović: 2011, NEW CHALLENGES OF ASTROINFORMATICS – STARK-B DATABASE AND SERBIAN VIRTUAL OBSERVATORY ' – SerVO, AND RELATIONS TO VIRTUAL ATOMIC AND MOLECULAR DATA CENTER – VAMDC, INFLUENCE OF COLLISIONS WITH CHARGED PARTICLES ON ASTRONOMICAL SPECTRA, in *Computer Systems and Technologies, Proceedings of the 12th International Conference CompSysTech'11*, eds. B. Rachev, A. SmrikarovAngelopoulos, ACM (Association for Computing Machinery) ICPS (International Conference Proceedings Series), ACM Press, New York **578**, 23-31.
8. Rixon, G., Dubernet, M. L., Piskunov, N., Walton, N., Mason, N., Le Sidaner, P., Schlemmer, S., Tennyson, J., Akram, A., Benson, K., Bureau, J., Doronin, M., Endres, C., Heiter, U., Hill, C., Kupka, F., Nenadović, L., Marquart, T., Mulas, G., Ralchenko, Y., Shih, A., Smith, K., Schmitt, B., Witherick, D., Boudon, V., Culhane, J. L., Dimitrijević, M. S., Fazliev, A. Z., Joblin, C., Leto, G., Loboda, P. A., Mason, H. E., Mendoza, C., Millar, T. J., Nunez, L. A., Perevalov, V. I.,

Rothman, L. S., Roueff, E., Ryabchikova, T. A., Ryabtsev, A., Sahal-Bréchet, S., Tyuterev, V. G., Wakelam, V., Zeippen, C. J.: 2011, VAMDC - THE VIRTUAL ATOMIC AND MOLECULAR DATA CENTRE - A NEW WAY TO DISSEMINATE ATOMIC AND MOLECULAR DATA - VAMDC LEVEL 1 RELEASE, 7th International Conference on Atomic and Molecular Data and their Applications - ICAMDATA - 2010, Vilnius, Lithuania 21-24 September 2010, eds. A. Bernotas, R. Karazija, Z. Rudzikas, American Institute of Physics Conference Proceedings **1344**, 107-115.

PAPERS IN INTERNATIONAL JOURNALS WHICH ARE NOT ON SCI LIST AND IN BOOKS OF INTERNATIONAL PUBLISHERS

1. A. Antoniou, E. Danezis, E. Lyratzi, L. Č. Popović, M. S. Dimitrijević, D. Stathopoulos: 2010, A NEW APPROACH OF THE GR MODEL, in "Advances in Hellenic Astronomy during the IYA09", K. Tsinganos, D. Hatzidimitriou, and T. Matsakos, eds., Astronomical Society of the Pacific (ASP) Conference Series, **424**, 187-188.
2. E. Danezis, E. Lyratzi, L. Č. Popović, M. S. Dimitrijević, A. Antoniou: 2010, INVESTIGATING DACS/SACS PHENOMENA IN HOT EMISSION STARS AND QUASARS, in "Advances in Hellenic Astronomy during the IYA09", K. Tsinganos, D. Hatzidimitriou, and T. Matsakos, eds., Astronomical Society of the Pacific (ASP) Conference Series, **424**, 305-307.
3. E. Lyratzi, E. Danezis, L. Č. Popović, M. S. Dimitrijević, A. Antoniou: 2010, WAYS OF CREATION OF DACS AND SACS IN THE SPECTRA OF PG 0946+301 AND PG 1254+047, in "Advances in Hellenic Astronomy during the IYA09", K. Tsinganos, D. Hatzidimitriou, and T. Matsakos, eds., Astronomical Society of the Pacific (ASP) Conference Series, **424**, 308-310.
4. N. Larbi-Terzi, S. Sahal-Bréchet, N. Ben Nessib, M. S. Dimitrijević: 2010, VAMDC FP7 PROJECT AND STARK-B DATABASE: C II STARK BROADENING PARAMETERS FOR WHITE DWARF ATMOSPHERES RESEARCH, in 17th European White Dwarf Workshop, eds. M. K. Werner, T. Rauch, American Institute of Physics Conference Proceedings **1273**, 428-431.
5. V. A. Srećković, Lj. M. Ignjatović, A. A. Mihajlov, M. S. Dimitrijević: 2010, ELECTRICAL CONDUCTIVITY OF PLASMA IN DB WHITE DWARF ATMOSPHERES, in 17th European White Dwarf Workshop, eds. M. K. Werner, T. Rauch, American Institute of Physics Conference Proceedings **1273**, 428-431.
6. M. Christova, M. S. Dimitrijević, A. Kovačević: SIMILARITIES IN CALCULATED STARK BROADENING PARAMETERS OF ARGON SPECTRAL LINES, Journal of Physics: Conference Series **207**, (2010) 012024 (1-6).

7. M. Christova, M. S. Dimitrijević, Z. Simić, S. Sahal-Bréchet: STARK BROADENING PARAMETERS OF Ne I 837.8 nm SPECTRAL LINE, *Journal of Physics: Conference Series* **207**, (2010) 012025 (1-4).
8. J. Kovačević, L. Č. Popović, M. S. Dimitrijević: THE OPTICAL Fe II EMISSION LINES IN ACTIVE GALACTIC NUCLEI, *Memorie della Societa Astronomica Italiana Supplementi* **15**, (2010) 176-181.
9. E. Lyratzi, E. Danezis, L. Č. Popović, M. S. Dimitrijević, A. Antoniou, D. Stathopoulos: KINEMATIC PROPERTIES OF THE BROAD ABSORPTION LINE REGIONS IN THE SPECTRA OF QUASARS, *Memorie della Societa Astronomica Italiana Supplementi* **15**, (2010) 161-165.
10. J. Muñoz, C. Yubero, M. S. Dimitrijević, M. D. Calzada: VAN DER WAALS BROADENING IN ATMOSPHERIC PRESSURE SURFACE WAVE DISCHARGES SUSTAINED IN RARE GASES, *Memorie della Societa Astronomica Italiana Supplementi* **15**, (2010) 157-160.
11. B. Zmerli, N. Ben Nessib, M. S. Dimitrijević, S. Sahal-Bréchet: ON THE STARK BROADENING OF Cu I SPECTRAL LINES, *Memorie della Societa Astronomica Italiana Supplementi* **15**, (2010) 152-156.
12. R. Hamdi, N. Ben Nessib, M. S. Dimitrijević, S. Sahal-Bréchet: AB INITIO CALCULATIONS OF Ca V STARK BROADENING PARAMETERS, *Memorie della Societa Astronomica Italiana Supplementi* **15**, (2010) 148-151.
13. Z. Simić, M. S. Dimitrijević, A. Kovačević: ON THE STARK BROADENING IN HOT STARS, *Memorie della Societa Astronomica Italiana Supplementi* **15**, (2010) 143-147.
14. A. Antoniou, E. Danezis, E. Lyratzi, L. Č. Popović, M. S. Dimitrijević, E. Theodossiou: STUDYING THE LOCATION OF SACS AND DACS REGIONS IN THE ENVIRONMENT OF HOT EMISSION STARS, *Memorie della Societa Astronomica Italiana Supplementi* **15**, (2010) 138-142.
15. N. A. Walton, M. L. Dubernet, N. J. Mason, N. Piskunov, G. T. Rixon and VAMDC Consortium: 2011, VAMDC: The Virtual Atomic and Molecular Data Center, in “ ASTRONOMICAL DATA ANALYSIS SOFTWARE AND SYSTEMS XX”, I. N. Evans, A. Accomazzi, D. J. Mink, A. H. Rots, eds., *Astronomical Society of the Pacific (ASP) Conference Series*, **442**, 89-92.
16. M. S. Dimitrijević: 2011, PROBLEMS OF CALENDAR REFORM AND EASTER DATE DETERMINATION AND A PROPOSITION TO THE SERBIAN ORTHODOX CHURCH, MADE BY DJORDJE STANOJEVIĆ, *Transdisciplinary Studies* **1** (2011), 147-156.
17. E. Th. Theodossiou, V. N. Manimanis, P. Z. Mantarakis M. S. Dimitrijević: 2011, ASTRONOMY AND CONSTELLATIONS IN ILIAD AND ODYSSEY, *Journal of Astronomical History and Heritage* **14(1)** (2011), 22-30.

18. E. Theodossiou, P. Mantarakis, M. S. Dimitrijević, V. N. Manimanis, E. Danezis: FROM THE INFINITY (APEIRON) OF ANAXIMANDER IN ANCIENT GREECE TO THE THEORY OF INFINITE UNIVERSES IN MODERN COSMOLOGY, *Astronomical and Astrophysical Transactions* **27** (2010/2011), 172-176.
19. E. Th. Theodossiou, V. N. Manimanis, M. S. Dimitrijević, P. Z. Mantarakis: 2011, SIRIUS IN ANCIENT GREEK AND ROMAN LITERATURE: FROM THE ORPHIC ARGONAUTICS TO THE ASTRONOMICAL TABLES OF GEORGIOS CHRYSOCOCCA, *Journal of Astronomical History and Heritage* **14(3)** (2011), 180-189.
20. B. Šurlan, J. Kubát: LINE PROFILES OF OB STAR WINDS USING A MONTE CARLO METHOD, *Proceedings of the International Astronomical Union, IAU Symposium*, **272** (2011) 214-215.

NATIONAL MONOGRAPHS

1. Мр Јелена Ковачевић, АКТИВНА ГАЛАКТИЧКА ЈЕЗГРА И ЊИХОВИ ЕМИСИОНИ РЕГИОНИ, *Academia*, **235**, Задужбина Андрејевић, Београд, 2010.
2. Др Зоран Симић, ШТАРКОВО ШИРЕЊЕ СПЕКТРАЛНИХ ЛИНИЈА У ХЕМИЈСКИ НЕОБИЧНИМ ЗВЕЗДАМА, *Dissertatio*, **245**, Задужбина Андрејевић, Београд, 2010.

SCIENTIFIC WORKS IN NATIONAL JOURNALS AND BOOKS

1. E. Danezis, E. Theodossiou, M. S. Dimitrijević, A. Dacanalis, Ch. Katsavrias: THE COSMOLOGY OF DEMOCRITUS, *Bulgarian Astronomical Journal* **13** (2010), 140-152.
2. J. Kovačević: SPECTRAL PROPERTIES OF AGN WITH VERY WEAK [O III] LINES, *Serbian Astronomical Journal*, **182** (2011), 17-24.
3. E. Theodossiou, A. Dacanalis, M. S. Dimitrijević, P. Mantarakis: GAIA, HELIOS, SELENE AND OURANOS: THE THREE PRINCIPAL CELESTIAL BODIES AND THE SKY IN THE ANCIENT GREEK COSMOGONY, *Bulgarian Astronomical Journal*, **16** (2011), No. 2, 1-19.
4. E. Theodossiou, V. N. Manimanis, M. S. Dimitrijević: SIX CALENDAR SYSTEMS IN THE EUROPEAN HISTORY FROM 18TH TO 20TH CENTURY, *Bulgarian Astronomical Journal*, **16** (2011), No. 6, 1-20.
5. Емануил Данезис, Ефстратиос Т. Теодосију, Милан С. Димитријевић, Арис Даканалис: 2010, КОЗМОЛОГИЈЕ АЛКМАНА, ЛЕУКИПА И ДЕМОКРИТА И НЕКЕ СЛИЧНОСТИ СА МОДЕРНИМ НАУЧНИМ КОНЦЕПТИМА, *Античка култура, европско и српско наслеђе, Друштво за античке студије Србије, Институт за теолошка истраживања, Београд*, 162-173.

6. M. S. Dimitrijević, ELECTRONIC EDITIONS FROM ASTRONOMICAL INSTITUTIONS OF BELGRADE, Pregled NCD, 17, 2011, 17-24.
7. E. Danezis, E. Th. Theodossiou, M. S. Dimitrijević, A. Dacanal: 2010, COSMOLOGIES OF ALCMAN, LEUCIPPUS AND DEMOCRITUS AND SOME SIMILARITIES WITH MODERN SCIENTIFIC CONCEPTS, Зборник Матице српске за класичне студије, бр. 12, Нови Сад 2010, 281-297.
8. E. Theodossiou, V. Manimanis, M. S. Димитријевић: 2011, НЕПОДЕСАН ОДНОС ИЗМЕЂУ РЕЛИГИЈЕ И НАУКЕ: ПРЕВЛАДАВАЊЕ ХЕЛИОЦЕНТРИЧНЕ ТЕОРИЈЕ, Антика и савремени свет: Религија и култура, Друштво за античке студије Србије, Институт за теолошка истраживања, Београд, 374-386.
9. E. Theodossiou, V. Manimanis, M. S. Димитријевић: 2011, КОЗМОЛОГИЈА ГНОСТИКА, Антика и савремени свет: Религија и култура, Друштво за античке студије Србије, Институт за теолошка истраживања, Београд, 366-373.
10. E. Theodossiou, V. Manimanis, M. S. Dimitrijević: 2011, THE COSMOLOGICAL THEORIES OF PRE-SOCRATIC GREEK PHILOSOPHERS AND THEIR PHILOSOPHICAL VIEWS FOR THE ENVIRONMENT, Facta Universitatis, Series: Philosophy, Sociology, Psychology and History, **10**, 89-99
11. E. Theodossiou, V. Manimanis, M. S. Dimitrijević, M. Katsiotis: THE PYRAMIDS OF GREECE – ANCIENT MERIDIAN OBSERVATORIES?, Bulgarian Astronomical Journal, 16, 2011, 130-143.
12. Евстратије Теодосију, Василије Н. Маниманис, Милан С. Димитријевић: 2010-2011, „ТЕОРИЈА СВЕГА“ БЕНЦАМИНА ЛЕЗБИОСА, Phlogiston, 18, 2010-2011, 7-16.
13. Efstratios Theodossiou, Vassilios N. Manimanis, Milan S. Dimitrijević: 2010-2011, THE THEORY OF PANTANEKINETON OF BENJAMIN LESBIOS, Phlogiston, 18, 2010-2011, 17-32.

CONTRIBUTED PAPERS IN PROCEEDINGS OF INTERNATIONAL CONFERENCES

1. V. Srećković, Lj. M. Ignjatović, A. A. Mihajlov, M. S. Dimitrijević: 2010, ELECTRICAL CONDUCTIVITY OF PLASMAS IN DB WHITE DWARF ATMOSPHERES, Publ. Astron. Obs. Belgrade **89**, 383.
2. N. Larbi-Terzi, S. Sahal-Bréchet, N. Ben Nessib, M. S. Dimitrijević: 2010, C II STARK BROADENING PARAMETERS FOR WHITE DWARF ATMOSPHERES RESEARCH, Publ. Astron. Obs. Belgrade **89**, 375.
3. M. S. Dimitrijević, VAMDC Consortium (Dubernet, P. I. M- L.) A. Kovačević, D. Jevremović, L. Č. Popović, S. Sahal-Bréchet: EUROPEAN VIRTUAL ATOMIC DATA CENTRE - VAMDC, XIXth Symposium of Physics of Switching Arc, Invited Lectures and

Contributed Papers, Nove Mesto na Morave, 5-9 September 2011, Brno University of Technology, Faculty of Electrical Engineering and Communication, 201,1 153-156.

CONTRIBUTED PAPERS IN PROCEEDINGS OF NATIONAL CONFERENCES

1. Евстратије Теодосију, Василије Н. Маниманис, Милан С. Димитријевић: 2011, ДОПРИНОС ВИЗАНТИЈЕ ПРИРОДНИМ НАУКАМА; ВИЗАНТИЈСКИ АСТРОНОМИ И НАУЧНИЦИ, Зборник радова конференције "Развој астрономије код Срба VI", Београд, 22-26. април 2010, уредник М. С. Димитријевић, Публ. Астр. друш. "Руђер Бошковић" св. 10, 693-706.
2. Евстратије Теодосију, Василије Н. Маниманис, Милан С. Димитријевић: 2011, ШЕСТ КАЛЕНДАРСКИХ СИСТЕМА У ЕВРОПСКОЈ ИСТОРИЈИ ОД 18. ДО 20. ВЕКА, Зборник радова конференције "Развој астрономије код Срба VI", Београд, 22-26. април 2010, уредник М. С. Димитријевић, Публ. Астр. друш. "Руђер Бошковић" св. 10, 745-769.
3. Милан С. Димитријевић: 2011, ФИЛАТЕЛИЈА И АСТРОНОМИЈА, Зборник радова конференције "Развој астрономије код Срба VI", Београд, 22-26. април 2010, уредник М. С. Димитријевић, Публ. Астр. друш. "Руђер Бошковић" св. 10, 845-865.
4. Еди Бон, Милан С. Димитријевић, Игор Стојић, Весна Мијатовић: 2011, МОТИВИ АСТРОНОМСКИХ ПОЈАВА У ХРИШЋАНСКОЈ УМЕТНОСТИ, Зборник радова конференције "Развој астрономије код Срба VI", Београд, 22-26. април 2010, уредник М. С. Димитријевић, Публ. Астр. друш. "Руђер Бошковић" св. 10, 931-939.
5. Милан С. Димитријевић: 2011, НЕБЕСКИ ЗНАЦИ И КОСМИЧКА ТРАГАЊА У ПОЕЗИЈИ ДРАГАНА ДРАГОЈЛОВИЋА, Зборник радова конференције "Развој астрономије код Срба VI", Београд, 22-26. април 2010, уредник М. С. Димитријевић, Публ. Астр. друш. "Руђер Бошковић" св. 10, 1061-1068.
6. Милан С. Димитријевић: 2011, ЛИРСКО-ПОЕТСКО И ДОКУМЕНТАРИСТИЧКО ВИЂЕЊЕ АСТРОНОМИЈЕ У „БЛАГОДАРНИКУ“ МИЛАНА С. КОСОВИЋА, Зборник радова конференције "Развој астрономије код Срба VI", Београд, 22-26. април 2010, уредник М. С. Димитријевић, Публ. Астр. друш. "Руђер Бошковић" св. 10, 1069-1082.
7. Милан С. Димитријевић: 2011, „С ГЕОМ НА РЕДУТУ“ ПОД ЗВЕЗДАМА, Зборник радова конференције "Развој астрономије код Срба VI", Београд, 22-26. април 2010, уредник М. С. Димитријевић, Публ. Астр. друш. "Руђер Бошковић" св. 10, 1093-1124.

8. Милан С. Димитријевић: 2011, КОСМИЧКЕ ИНСПИРАЦИЈЕ СТРАТОСА ТЕОДОСИЈУА, Зборник радова конференције “Развој астрономије код Срба VI”, Београд, 22-26. април 2010, уредник М. С. Димитријевић, Публ. Астр. друш. “Руђер Бошковић” св. 10, 1125-1132.
9. Милан С. Димитријевић: 2011, ПЕСНИЧКИ ДЕКОНСТРУИСАНА ЛИРСКО-СОНЕТНА КОСМОГОНИЈА У ИЗВРНОМ ОГЛЕДАЛУ; Поетски дар Петковићевом уздарју, Зборник радова конференције “Развој астрономије код Срба VI”, Београд, 22-26. април 2010, уредник М. С. Димитријевић, Публ. Астр. друш. “Руђер Бошковић” св. 10, 1185-1189.
10. Анђелка Ковачевић, Милан С. Димитријевић, Лука Ч. Поповић: 2011, ДРУГА ЛЕТЊА ШКОЛА ИЗ АСТРОНОМИЈЕ, Зборник радова конференције “Развој астрономије код Срба VI”, Београд, 22-26. април 2010, уредник М. С. Димитријевић, Публ. Астр. друш. “Руђер Бошковић” св. 10, 1257-1284.
11. Анђелка Ковачевић, Милан С. Димитријевић, Лука Ч. Поповић: 2011, VII СРПСКА КОНФЕРЕНЦИЈА О ОБЛИЦИМА СПЕКТРАЛНИХ ЛИНИЈА У АСТРОФИЗИЦИ, Зборник радова конференције “Развој астрономије код Срба VI”, Београд, 22-26. април 2010, уредник М. С. Димитријевић, Публ. Астр. друш. “Руђер Бошковић” св. 10, 1285-1308.
12. Милан С. Димитријевић: 2011, АКТИВНОСТИ САРАДНИКА ПРОЈЕКТА 146001 „УТИЦАЈ СУДАРНИХ ПРОЦЕСА НА СПЕКТРЕ АСТРОФИЗИЧКЕ ПЛАЗМЕ“ – 2008-2009, Зборник радова конференције “Развој астрономије код Срба VI”, Београд, 22-26. април 2010, уредник М. С. Димитријевић, Публ. Астр. друш. “Руђер Бошковић” св. 10, 289-341.

ON THE STARK BROADENING OF B IV SPECTRAL LINES

MILAN S. DIMITRIJEVIĆ^{1,2}, MAGDALENA CHRISTOVA³, ZORAN SIMIĆ¹,
ANDJELKA KOVAČEVIĆ⁴, SYLVIE SAHAL-BRÉCHOT²

¹*Astronomical Observatory, Volgina 7, 11060 Belgrade 38, Serbia*

²*Observatoire de Paris, 92195 Meudon Cedex, France*

³*Department of Applied Physics, Technical University-Sofia, 1000 Sofia, Bulgaria*

⁴*Department of Astronomy, Faculty of Mathematics, Studentski Trg 16,
11000 Belgrade, Serbia.*

E-mail: mdimitrijevic@aob.rs, mchristo@tu-sofia.bg, zsimic@aob.rs,
andjelka@matf.bg.ac.rs, sylvie.sahal-brechot@obspm.fr

Abstract. The preliminary results for Stark broadening parameters of B IV lines from 8 spectral series have been calculated using Sahal-Bréchet theory based on the semi-classical perturbation formalism.

1. INTRODUCTION

A major interest consists in the understanding of the evolution of the Universe, of the birth, growing, evolution and death of stars, which eject their material into the interstellar medium at the end of their life. The light trace elements lithium, beryllium, and boron (LiBeB) are at the centre of astrophysical puzzles involving sites as diverse as the primordial fireball, interstellar (IS) or even intergalactic space, and stellar surfaces and interiors (Venn et al., 2002). The origins of the light element trio are connected, by varying degrees, to the big bang nucleosynthesis, cosmic-ray spallation, and stellar evolution. Abundance determinations of Li, Be, and B in a variety of stars provide data on the above astrophysical processes that can both produce and destroy these rare elements. The light elements are sensitive probes of stellar models due to the fact that the stable isotopes of all three consist of nuclei with small binding energies that are destroyed easily by (p, α) reactions at modest temperatures (Cunha and Smith, 1999). The origin and evolution of boron are of special interest because it is hardly produced by the standard big bang nucleosynthesis (BBN), and cannot be produced by nuclear fusion in stellar interiors (Tan, Shi and Zhao, 2010). The light isotopes ^{10}B and ^{11}B are believed to be primarily formed via spallation of carbon and oxygen nuclei (Proffitt et al.,

1999). Traditional models for this process (Meneguzzi, Audouze and Reeves, 1971), where cosmic ray protons and alpha-particles collide with pre-existing CNO nuclei in the interstellar medium, predicted that beryllium and boron would scale quadratically with the overall metal abundance and that the ratio $^{11}\text{B}/^{10}\text{B} \approx 2.5$. However, boron and beryllium abundances actually scale linearly with the total metal abundance, and it has long been known that the meteoritic ratio of $^{11}\text{B}/^{10}\text{B} \approx 4$ (Proffitt *et al.*, 1999, Meneguzzi, Audouze and Reeves, 1971, Duncan, Lambert and Lemke, 1992, Duncan *et al.*, 1997, Shima, 1963). These papers are concerned primarily with boron's role in testing models of stellar interiors and evolution. This role arises because boron nuclei are destroyed by warm protons, and thus even quite shallow mixing of the atmosphere with the interior reduces the surface abundance by bringing boron-depleted material to the surface. Lithium and beryllium are similarly affected. Thus, a determination that the surface abundance of a light element is less than the star's initial abundance is an observational constraint for testing models of stellar interiors (Venn *et al.*, 2002).

Boron alone is observable in hot stars. A principal goal of most of studies of hot stars was to establish the present-day boron abundance in order to improve the understanding of the Galactic chemical evolution of boron (Venn *et al.*, 2002). In Tan, Shi and Zhao (2010) has been reported that, the abundances of the nine stars which are not depleted in Be or B show that, no matter what the strength of collisions with neutral hydrogen may be, both Be and B increase with O quasilinearly in the logarithmic plane, which confirms the conclusions that Be and B are mainly produced by the primary process in the early Galaxy. Boron in hot stars, like lithium in cool stars, is shown to be a tracer of some of the various processes affecting a star's surface composition that are not included in the standard models of stellar evolution. If the initial boron abundances of local hot stars are similar from star to star and association to association, then the large spread in boron abundances shows that boron abundances are a clue to unravelling the nonstandard processes that affect young hot stars.

The cosmic abundances of ^{11}B is of major importance for the model of Galactic chemical evolution (GCE) (Ritchey *et al.*, 2011), where the authors conclude that a major portion of the cosmic abundances of ^{11}B can be attributed to neutrino nucleosynthesis. Thus, it is necessary to accurately describe the stellar evolution, and the formation of elements, which are closely connected. To make progress in these developments chemical abundances are crucial parameters to be determined. This needs an accurate interpretation of the detailed line spectra of the stellar objects.

2. STARK BROADENING OF BORON LINES

Pressure broadening of spectral lines arises when an atom, ion, or molecule which emits or absorbs light in a gas or plasma, is perturbed by its interactions with the other particles of the medium. Interpretation of this phenomenon is currently used for modelling of the medium and for spectroscopic diagnostics, since the broadening of the lines depends on the temperature and density of the

medium. The physical conditions in the Universe are very various, and collisional broadening with charged particles (Stark broadening) appears to be important in many domains. For example, at temperatures around 10^4 K and densities 10^{13} - 10^{15} cm^{-3} , Stark broadening is efficient for modelling and analysing spectra of moderately hot (A), hot (B) and very hot (O) types of stars Sahal-Bréchet, 2010). In white dwarfs, especially, Stark broadening is the dominant collisional line broadening process. The theory of Stark broadening is well applied, especially for accurate spectroscopic diagnostics and modelling. This requires the knowledge of numerous profiles, especially for trace elements, as boron in this case, which are used as useful probes for modern spectroscopic diagnostics. Interpretation of the spectra of white dwarfs, which are very faint, allows understanding the evolution of these very old stars, which are close to death.

The primary results for Stark broadening parameters of BIV lines from 8 spectral series have been calculated using Sahal-Bréchet theory based on the semi-classical perturbation formalism. (Sahal-Bréchet, 1969ab). Within the Sahal-Bréchet theory the full width at half intensity maximum (W) and the shift (d) of an isolated line originating from the transition between the initial level i and the final level f is expressed as:

$$W = n_e \int_0^{\infty} v f(v) dv \left[\sum_{i' \neq i} \sigma_{ii'}(v) + \sum_{f' \neq f} \sigma_{ff'}(v) + \sigma_{el} \right] \quad (1)$$

$$d = \int_0^{\infty} v f(v) dv \int_{R_3}^{R_d} 2\pi \rho d \rho \sin 2\varphi_p \quad (2)$$

where i' and f' are perturbing levels, n_e and v are the electron density and the velocity of perturbers respectively, and $f(v)$ is the Maxwellian distribution of electron velocities.

The inelastic cross sections $\sigma_{ii'}(v)$ (respectively $\sigma_{ff'}(v)$) can be expressed by an integration of the transition probability $P_{ii'}$ over the impact parameter ρ :

$$\sum_{i' \neq i} \sigma_{ii'}(v) = \frac{1}{2} \pi R_1^2 + \int_{R_1}^{R_d} 2\pi \rho d \rho \sum_{i' \neq i} P_{ii'}(\rho, v) \quad (3)$$

The elastic collision contribution to the width is given by:

$$\sigma_{el} = 2\pi R_2^2 + \int_{R_2}^{R_d} 8\pi \rho d \rho \sin^2 \delta \quad (4)$$

$$\delta = (\varphi_p^2 + \varphi_q^2)^{1/2} \quad (5)$$

The phase shifts φ_p and φ_q are due to the polarization and quadrupole potential respectively. The cut-offs parameters R_1 , R_2 , R_3 , the Debye cut-off R_d and the symmetrization procedure are described in Sahal-Bréchet (1969ab). The collisions of emitters with electrons, protons and ionized helium have been examined, and the contribution of different perturbers in the total Stark broadening parameters have been discussed.

3. RESULTS AND DISCUSSION

Stark broadening width and shift for spectral lines of 8 series are presented in Table 1. The temperature dependence of Stark width and shift for the $1s^2 1S - 1s2p \ ^1P^\circ$ transition at electron density $1.10^{18} \text{ cm}^{-3}$ have been presented in Table 1., Fig. 1 and Fig. 2, respectively. The both parameters dramatically change at lower temperature values up to 10 000 K then they vary slowly, the width decreases while the shift increases. The electron contribution in total width decreases from almost 100% to 60%, the proton one increases to 13 %, and the ionized helium one increases too, up to 26 % within the temperature interval of interest. We observe the same tendency for the Stark shift. The contribution of electron perturbers decrease from 97 % to 11 %, the role of collisions with protons increase from 1 % to 27 %, and the ionized helium perturbers broad the line from 2 % to 72 % in all temperature interval. The values of Stark shift due to collisions with different perturbers are negative in the considered case. The principal quantum dependence of the electron impact width within the series is illustrated in Fig. 3. The examined conditions of interest are 100 000 K and $1.10^{14} \text{ cm}^{-3}$ electron density. The calculated data are fitted with polynomial function of 4-th order; the fit-curve is added in the figure. The polynomial function permits the interpolation and extrapolation to obtain electron impact width for other lines within the series where there is a lack of the data to perform the calculations. The analytical function is given below:

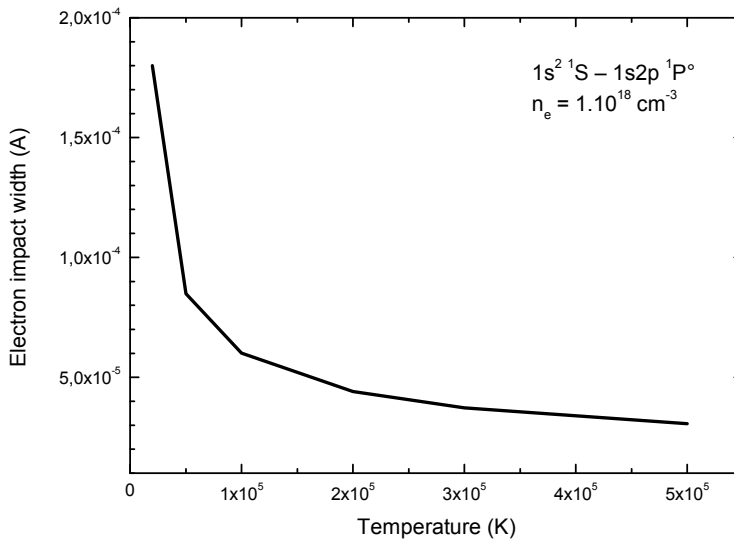


Figure 1: Temperature dependence of the electron impact width for $1s^2 1S - 1s2p \ ^1P^\circ$ transition at electron density $1.10^{18} \text{ cm}^{-3}$.

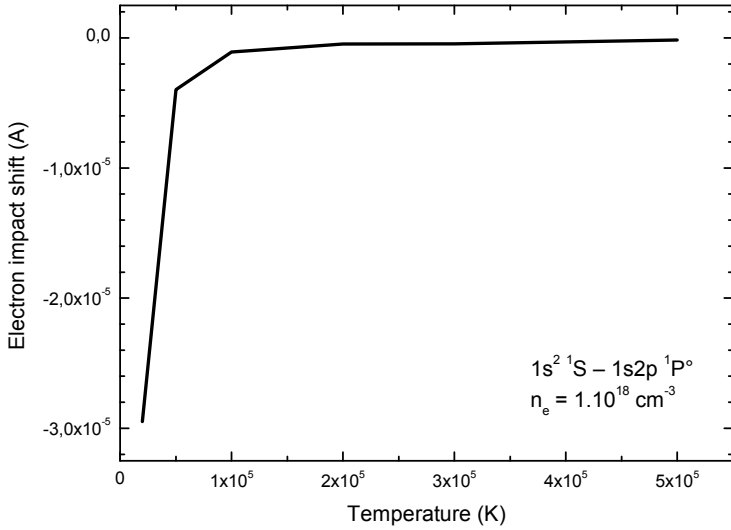


Figure 2: Temperature dependence of the electron impact shift for $1s^2 1S - 1s2p 1P^\circ$ transition at electron density $1.10^{18} \text{ cm}^{-3}$.

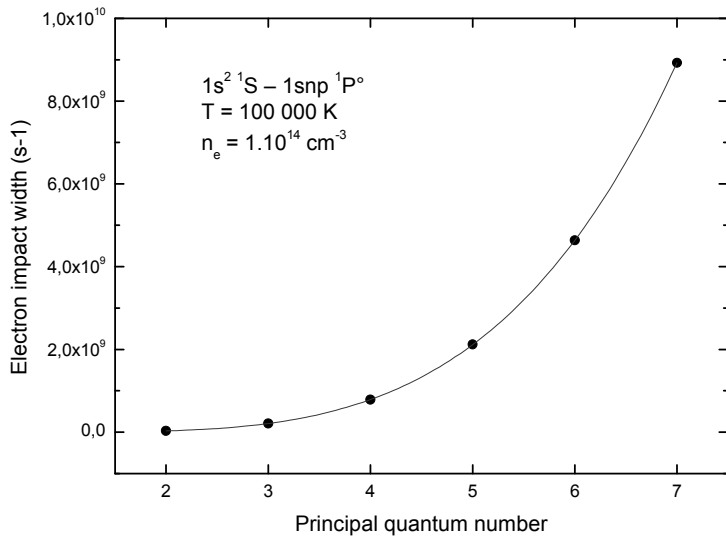


Figure 3: Principal quantum number dependence of the electron impact width for transitions within $1s^2 1S - 1snp 1P^\circ$ series at electron density $1.10^{14} \text{ cm}^{-3}$ and 100 000 K

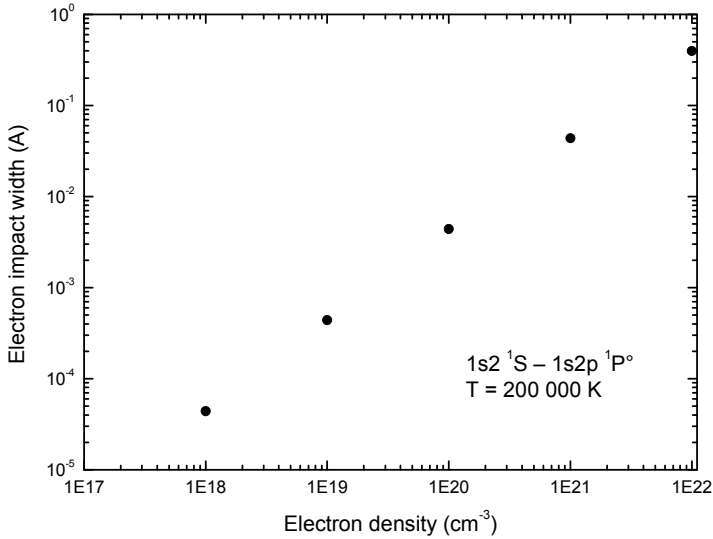


Figure 4: Electron density dependence of the electron impact width of $1s^2\ ^1S - 1s2p\ ^1P^\circ$ transition at 200 000 K.

$$W(n) = a_4 n^4 + a_3 n^3 + a_2 n^2 + a_1 n + a_0 \quad (6)$$

Where $W(n)$ is the full width at half-maximum in rad.s, $a_0 = 3.36 \times 10^7$, $a_1 = -2.00 \times 10^7$, $a_2 = 2.96 \times 10^6$, $a_3 = -5.77 \times 10^6$, $a_4 = 4.53 \times 10^6$. The fit curve is added in the figure.

The electron density dependence of the electron impact width for $1s^2\ ^1S - 1s2p\ ^1P^\circ$ transition at 200 000 K have been obtained (see Fig.4). For the electron density values above $1.1 \times 10^{21}\ \text{cm}^{-3}$ the small deviation from linear function has been observed.

The second studied spectral series in this paper is $1s2s\ ^1S - 1snp\ ^1P^\circ$. We have obtained the similar temperature dependence (see Fig.1) of the electron impact width for the lowest transition within the spectral series, $1s2s\ ^1S - 1s2p\ ^1P^\circ$. The variation of Stark width within the studied temperature range has been shown in Fig. 5.

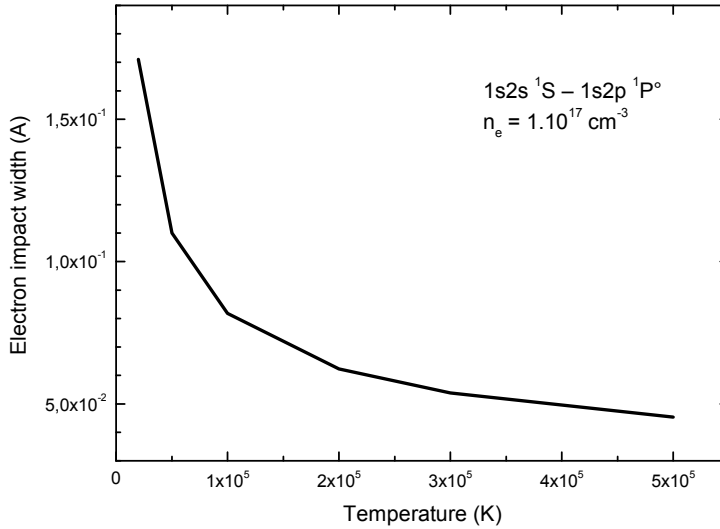


Figure 5: Temperature dependence of the electron impact width for $1s2s^1S - 1s2p^1P^\circ$ transition at electron density $1.10^{17} \text{ cm}^{-3}$.

The electron contribution in total width decreases from 99 % to 57 %, the proton one increases up to 12 %, and the ionized helium one increases to 30 % in the whole temperature interval. All shift values are negative. The impact electron Stark shift decreases from 61 % to 16 %, the role of collisions with protons increases from 13 % to 22 %, and the ionized helium shift varies from 26 % to 61 %.

4. CONCLUSION

The results for Stark broadening parameters of boron lines could be applicable for the adequate interpretation of the observed spectra to determine reliable chemical boron abundance which is of major importance for the model of Galactic chemical evolution, interstellar and intergalactic space, and stellar interiors and surfaces as white dwarfs.

Table 1: Stark broadening parameters for B IV lines for a perturber density 10^{14} cm⁻³ and temperatures from 20 000 to 500 000 K. The width (FWHM) W and shift d values from different perturbers are given in (Å). The ratio of the included parameter C versus the corresponding Stark width estimates the maximal perturber density for which the line may be treated as isolated. W_e - electron-impact width, d_e - electron-impact shift, W_p - proton-impact width, d_p - proton-impact shift, W_{He^+} - singly charged helium-impact width, d_{He^+} - singly charged helium-impact shift.

Transition	T(K)	W_e (Å)	d_e (Å)	W_p (Å)	d_p (Å)	W_{He^+} (Å)	d_{He^+} (Å)
B IV 1s2-2	20000	0.180E-07	-0.130E-08	0.687E-10	-0.478E-10	0.524E-10	-0.956E-10
60.3 Å	50000	0.860E-08	-0.118E-09	0.211E-09	-0.113E-09	0.204E-09	-0.236E-09
C = 0.81E+14	100000	0.601E-08	-0.697E-10	0.365E-09	-0.191E-09	0.470E-09	-0.429E-09
	200000	0.441E-08	-0.434E-10	0.524E-09	-0.269E-09	0.823E-09	-0.663E-09
	300000	0.372E-08	-0.447E-10	0.582E-09	-0.317E-09	0.106E-08	-0.805E-09
	500000	0.306E-08	-0.162E-10	0.658E-09	-0.361E-09	0.131E-08	-0.971E-09
B IV 1s2-3p	20000	0.584E-07	-0.434E-08	0.282E-08	-0.387E-08	0.496E-08	-0.956E-08
52.7 Å	50000	0.403E-07	-0.349E-08	0.537E-08	-0.551E-08	0.118E-07	-0.148E-07
C = 0.39E+13	100000	0.314E-07	-0.316E-08	0.701E-08	-0.665E-08	0.174E-07	-0.179E-07
	200000	0.249E-07	-0.268E-08	0.867E-08	-0.783E-08	0.223E-07	-0.212E-07
	300000	0.218E-07	-0.234E-08	0.976E-08	-0.847E-08	0.250E-07	-0.235E-07
	500000	0.186E-07	-0.196E-08	0.110E-07	-0.947E-08	0.290E-07	-0.260E-07
B IV 1s2-4p	20000	0.182E-06	-0.182E-07	0.195E-07	-0.205E-07	0.432E-07	-0.550E-07
50.4 Å	50000	0.133E-06	-0.166E-07	0.272E-07	-0.261E-07	0.691E-07	-0.704E-07
C = 0.14E+13	100000	0.106E-06	-0.144E-07	0.344E-07	-0.302E-07	0.879E-07	-0.832E-07
	200000	0.854E-07	-0.115E-07	0.408E-07	-0.354E-07	0.108E-06	-0.974E-07
	300000	0.753E-07	-0.101E-07	0.455E-07	-0.377E-07	0.120E-06	-0.106E-06
	500000	0.642E-07	-0.816E-08	0.518E-07	-0.403E-07	0.130E-06	-0.114E-06
B IV 1s2-5p	20000	0.453E-06	-0.582E-07	0.660E-07	-0.651E-07	0.167E-06	-0.175E-06
49.5 Å	50000	0.340E-06	-0.504E-07	0.898E-07	-0.804E-07	0.232E-06	-0.220E-06
C = 0.69E+12	100000	0.275E-06	-0.414E-07	0.101E-06	-0.918E-07	0.277E-06	-0.254E-06
	200000	0.222E-06	-0.330E-07	0.124E-06	-0.101E-06	0.327E-06	-0.283E-06
	300000	0.196E-06	-0.279E-07	0.131E-06	-0.117E-06	0.362E-06	-0.305E-06
	500000	0.166E-06	-0.222E-07	0.146E-06	-0.117E-06	0.407E-06	-0.340E-06
B IV 1s2-6p	20000	0.915E-06	-0.143E-06	0.170E-06	-0.159E-06	0.434E-06	-0.430E-06
48.9 Å	50000	0.714E-06	-0.118E-06	0.215E-06	-0.190E-06	0.583E-06	-0.529E-06
C = 0.40E+12	100000	0.589E-06	-0.948E-07	0.249E-06	-0.216E-06	0.668E-06	-0.592E-06
	200000	0.479E-06	-0.736E-07	0.299E-06	-0.245E-06	0.804E-06	-0.700E-06
	300000	0.422E-06	-0.617E-07	0.304E-06	-0.252E-06	0.870E-06	-0.739E-06
	500000	0.359E-06	-0.481E-07	0.342E-06	-0.278E-06	0.960E-06	-0.846E-06
B IV 1s2-7p	20000	0.169E-05	-0.306E-06	0.365E-06	-0.339E-06	0.976E-06	-0.940E-06
48.6 Å	50000	0.135E-05	-0.238E-06	0.464E-06	-0.398E-06	0.123E-05	-0.113E-05
C = 0.24E+12	100000	0.112E-05	-0.190E-06	0.535E-06	-0.443E-06	0.147E-05	-0.129E-05
	200000	0.917E-06	-0.143E-06	0.578E-06	-0.521E-06	0.175E-05	-0.143E-05
	300000	0.810E-06	-0.119E-06	0.664E-06	-0.527E-06	0.169E-05	-0.156E-05
	500000	0.688E-06	-0.892E-07	0.776E-06	-0.549E-06	0.182E-05	-0.164E-05

ON THE STARK BROADENING OF B IV SPECTRAL LINES

Table 1. Continued

Transition	T(K)	$W_c(\text{\AA})$	$d_c(\text{\AA})$	$W_p(\text{\AA})$	$d_p(\text{\AA})$	$W_{He^+}(\text{\AA})$	$d_{He^+}(\text{\AA})$
B IV 2s-2p	20000	0.168E-03	-0.669E-05	0.702E-06	-0.215E-05	0.642E-06	-0.444E-05
4492.1 A	50000	0.110E-03	-0.577E-05	0.274E-05	-0.417E-05	0.401E-05	-0.959E-05
C= 0.45E+18	100000	0.818E-04	-0.702E-05	0.481E-05	-0.578E-05	0.942E-05	-0.142E-04
	200000	0.623E-04	-0.687E-05	0.712E-05	-0.712E-05	0.168E-04	-0.191E-04
	300000	0.538E-04	-0.673E-05	0.820E-05	-0.787E-05	0.203E-04	-0.213E-04
	500000	0.454E-04	-0.644E-05	0.964E-05	-0.891E-05	0.245E-04	-0.243E-04
B IV 2s-3p	20000	0.336E-05	-0.207E-06	0.150E-06	-0.206E-06	0.266E-06	-0.509E-06
380.9 A	50000	0.233E-05	-0.200E-06	0.286E-06	-0.293E-06	0.627E-06	-0.785E-06
C= 0.20E+15	100000	0.181E-05	-0.189E-06	0.371E-06	-0.353E-06	0.924E-06	-0.947E-06
	200000	0.143E-05	-0.164E-06	0.461E-06	-0.419E-06	0.118E-05	-0.113E-05
	300000	0.126E-05	-0.146E-06	0.518E-06	-0.451E-06	0.134E-05	-0.126E-05
	500000	0.107E-05	-0.125E-06	0.596E-06	-0.506E-06	0.155E-05	-0.139E-05
B IV 2s-4p	20000	0.612E-05	-0.583E-06	0.636E-06	-0.669E-06	0.141E-05	-0.180E-05
288.1 A	50000	0.445E-05	-0.552E-06	0.888E-06	-0.852E-06	0.226E-05	-0.230E-05
C= 0.47E+14	100000	0.355E-05	-0.484E-06	0.112E-05	-0.986E-06	0.287E-05	-0.272E-05
	200000	0.286E-05	-0.390E-06	0.133E-05	-0.116E-05	0.353E-05	-0.318E-05
	300000	0.252E-05	-0.344E-06	0.149E-05	-0.123E-05	0.393E-05	-0.346E-05
	500000	0.215E-05	-0.279E-06	0.170E-05	-0.132E-05	0.426E-05	-0.372E-05
B IV 2s-5p	20000	0.125E-04	-0.158E-05	0.181E-05	-0.178E-05	0.459E-05	-0.479E-05
258.9 A	50000	0.942E-05	-0.139E-05	0.246E-05	-0.220E-05	0.637E-05	-0.604E-05
C= 0.19E+14	100000	0.762E-05	-0.115E-05	0.278E-05	-0.252E-05	0.759E-05	-0.696E-05
	200000	0.615E-05	-0.915E-06	0.339E-05	-0.278E-05	0.895E-05	-0.776E-05
	300000	0.541E-05	-0.775E-06	0.358E-05	-0.322E-05	0.993E-05	-0.835E-05
	500000	0.461E-05	-0.620E-06	0.400E-05	-0.322E-05	0.111E-04	-0.931E-05
B IV 2s-6p	20000	0.231E-04	-0.359E-05	0.428E-05	-0.399E-05	0.109E-04	-0.108E-04
245.3 A	50000	0.180E-04	-0.297E-05	0.540E-05	-0.476E-05	0.147E-04	-0.133E-04
C= 0.99E+13	100000	0.149E-04	-0.239E-05	0.625E-05	-0.542E-05	0.168E-04	-0.149E-04
	200000	0.121E-04	-0.186E-05	0.750E-05	-0.616E-05	0.202E-04	-0.176E-04
	300000	0.107E-04	-0.156E-05	0.764E-05	-0.633E-05	0.219E-04	-0.186E-04
	500000	0.906E-05	-0.122E-05	0.861E-05	-0.698E-05	0.241E-04	-0.213E-04
B IV 2s-7p	20000	0.404E-04	-0.730E-05	0.874E-05	-0.810E-05	0.233E-04	-0.225E-04
237.8 A	50000	0.323E-04	-0.570E-05	0.111E-04	-0.950E-05	0.295E-04	-0.270E-04
C= 0.58E+13	100000	0.269E-04	-0.456E-05	0.128E-04	-0.106E-04	0.351E-04	-0.308E-04
	200000	0.220E-04	-0.342E-05	0.138E-04	-0.125E-04	0.418E-04	-0.341E-04
	300000	0.194E-04	-0.285E-05	0.159E-04	-0.126E-04	0.404E-04	-0.373E-04
	500000	0.165E-04	-0.214E-05	0.185E-04	-0.131E-04	0.435E-04	-0.393E-04
B IV 3s-3p	20000	0.853E-02	-0.604E-03	0.321E-03	-0.455E-03	0.635E-03	-0.113E-02
15513.5 A	50000	0.591E-02	-0.658E-03	0.600E-03	-0.627E-03	0.142E-02	-0.169E-02
C= 0.33E+18	100000	0.462E-02	-0.614E-03	0.776E-03	-0.746E-03	0.197E-02	-0.202E-02
	200000	0.367E-02	-0.553E-03	0.970E-03	-0.877E-03	0.248E-02	-0.241E-02
	300000	0.324E-02	-0.515E-03	0.111E-02	-0.939E-03	0.284E-02	-0.263E-02
	500000	0.277E-02	-0.444E-03	0.120E-02	-0.103E-02	0.327E-02	-0.295E-02

Table 1. Continued

Transition	T(K)	$W_e(\text{Å})$	$d_e(\text{Å})$	$W_p(\text{Å})$	$d_p(\text{Å})$	$W_{\text{He}^+}(\text{Å})$	$d_{\text{He}^+}(\text{Å})$
B IV 3s-4p	20000	0.104E-03	-0.983E-05	0.950E-05	-0.100E-04	0.213E-04	-0.270E-04
1098.9 Å	50000	0.749E-04	-0.967E-05	0.133E-04	-0.128E-04	0.338E-04	-0.345E-04
C= 0.68E+15	100000	0.597E-04	-0.854E-05	0.165E-04	-0.147E-04	0.427E-04	-0.409E-04
	200000	0.481E-04	-0.709E-05	0.203E-04	-0.172E-04	0.537E-04	-0.470E-04
	300000	0.424E-04	-0.637E-05	0.223E-04	-0.180E-04	0.597E-04	-0.511E-04
	500000	0.363E-04	-0.525E-05	0.250E-04	-0.194E-04	0.644E-04	-0.560E-04
B IV 3s-5p	20000	0.117E-03	-0.146E-04	0.160E-04	-0.158E-04	0.406E-04	-0.423E-04
767.8 Å	50000	0.877E-04	-0.130E-04	0.218E-04	-0.195E-04	0.560E-04	-0.534E-04
C= 0.17E+15	100000	0.709E-04	-0.108E-04	0.247E-04	-0.224E-04	0.671E-04	-0.617E-04
	200000	0.572E-04	-0.874E-05	0.300E-04	-0.247E-04	0.786E-04	-0.690E-04
	300000	0.504E-04	-0.749E-05	0.321E-04	-0.283E-04	0.879E-04	-0.732E-04
	500000	0.429E-04	-0.603E-05	0.354E-04	-0.285E-04	0.991E-04	-0.825E-04
B IV 3s-6p	20000	0.172E-03	-0.264E-04	0.310E-04	-0.289E-04	0.789E-04	-0.784E-04
659.7 Å	50000	0.134E-03	-0.221E-04	0.391E-04	-0.345E-04	0.106E-03	-0.962E-04
C= 0.72E+14	100000	0.110E-03	-0.178E-04	0.453E-04	-0.393E-04	0.121E-03	-0.108E-03
	200000	0.897E-04	-0.140E-04	0.542E-04	-0.447E-04	0.146E-03	-0.127E-03
	300000	0.791E-04	-0.118E-04	0.550E-04	-0.458E-04	0.158E-03	-0.135E-03
	500000	0.673E-04	-0.923E-05	0.620E-04	-0.503E-04	0.176E-03	-0.154E-03
B IV 3s-7p	20000	0.268E-03	-0.481E-04	0.571E-04	-0.530E-04	0.153E-03	-0.147E-03
608.0 Å	50000	0.214E-03	-0.378E-04	0.725E-04	-0.622E-04	0.193E-03	-0.177E-03
C= 0.38E+14	100000	0.178E-03	-0.303E-04	0.836E-04	-0.693E-04	0.230E-03	-0.201E-03
	200000	0.146E-03	-0.228E-04	0.904E-04	-0.814E-04	0.274E-03	-0.223E-03
	300000	0.129E-03	-0.191E-04	0.104E-03	-0.824E-04	0.265E-03	-0.244E-03
	500000	0.109E-03	-0.144E-04	0.121E-03	-0.858E-04	0.284E-03	-0.257E-03
B IV 4s-4p	20000	0.165	-0.186E-01	0.130E-01	-0.138E-01	0.308E-01	-0.372E-01
37147.1 Å	50000	0.121	-0.178E-01	0.180E-01	-0.175E-01	0.467E-01	-0.472E-01
C= 0.77E+18	100000	0.969E-01	-0.160E-01	0.228E-01	-0.201E-01	0.594E-01	-0.560E-01
	200000	0.784E-01	-0.138E-01	0.263E-01	-0.228E-01	0.710E-01	-0.650E-01
	300000	0.693E-01	-0.122E-01	0.289E-01	-0.249E-01	0.768E-01	-0.682E-01
	500000	0.591E-01	-0.101E-01	0.299E-01	-0.268E-01	0.892E-01	-0.751E-01
B IV 4s-5p	20000	0.132E-02	-0.172E-03	0.161E-03	-0.158E-03	0.405E-03	-0.423E-03
2385.2 Å	50000	0.990E-03	-0.154E-03	0.216E-03	-0.193E-03	0.556E-03	-0.532E-03
C= 0.16E+16	100000	0.801E-03	-0.130E-03	0.260E-03	-0.226E-03	0.691E-03	-0.621E-03
	200000	0.649E-03	-0.108E-03	0.284E-03	-0.243E-03	0.796E-03	-0.693E-03
	300000	0.572E-03	-0.925E-04	0.331E-03	-0.283E-03	0.824E-03	-0.730E-03
	500000	0.487E-03	-0.750E-04	0.339E-03	-0.286E-03	0.102E-02	-0.831E-03
B IV 4s-6p	20000	0.107E-02	-0.166E-03	0.178E-03	-0.167E-03	0.458E-03	-0.455E-03
1580.5 Å	50000	0.830E-03	-0.139E-03	0.227E-03	-0.200E-03	0.614E-03	-0.557E-03
C= 0.41E+15	100000	0.684E-03	-0.114E-03	0.261E-03	-0.229E-03	0.702E-03	-0.633E-03
	200000	0.557E-03	-0.904E-04	0.317E-03	-0.263E-03	0.851E-03	-0.734E-03
	300000	0.492E-03	-0.765E-04	0.312E-03	-0.269E-03	0.942E-03	-0.783E-03
	500000	0.418E-03	-0.603E-04	0.357E-03	-0.292E-03	0.102E-02	-0.888E-03

ON THE STARK BROADENING OF B IV SPECTRAL LINES

Table 1. Continued

Transition	T(K)	$W_e(\text{\AA})$	$d_e(\text{\AA})$	$W_p(\text{\AA})$	$d_p(\text{\AA})$	$W_{He^+}(\text{\AA})$	$d_{He^+}(\text{\AA})$
B IV 4s-7p	20000	0.130E-02	-0.235E-03	0.266E-03	-0.248E-03	0.714E-03	-0.688E-03
1313.1 A	50000	0.104E-02	-0.185E-03	0.339E-03	-0.290E-03	0.906E-03	-0.825E-03
C= 0.18E+15	100000	0.866E-03	-0.149E-03	0.390E-03	-0.324E-03	0.108E-02	-0.941E-03
	200000	0.708E-03	-0.113E-03	0.423E-03	-0.382E-03	0.128E-02	-0.104E-02
	300000	0.625E-03	-0.951E-04	0.480E-03	-0.388E-03	0.123E-02	-0.114E-02
	500000	0.532E-03	-0.721E-04	0.565E-03	-0.405E-03	0.132E-02	-0.121E-02
B IV 5s-5p	20000	1.58	-0.251	0.175	-0.172	0.445	-0.462
72971.4 A	50000	1.22	-0.216	0.233	-0.211	0.605	-0.580
C= 0.15E+19	100000	0.998	-0.187	0.273	-0.236	0.711	-0.660
	200000	0.815	-0.151	0.323	-0.279	0.862	-0.772
	300000	0.720	-0.129	0.356	-0.293	0.953	-0.832
	500000	0.613	-0.107	0.379	-0.334	1.05	-0.875
B IV 5s-6p	20000	0.951E-02	-0.163E-02	0.143E-02	-0.137E-02	0.371E-02	-0.368E-02
4401.9 A	50000	0.748E-02	-0.135E-02	0.181E-02	-0.164E-02	0.489E-02	-0.451E-02
C= 0.32E+16	100000	0.620E-02	-0.112E-02	0.211E-02	-0.186E-02	0.562E-02	-0.513E-02
	200000	0.507E-02	-0.884E-03	0.254E-02	-0.208E-02	0.696E-02	-0.592E-02
	300000	0.448E-02	-0.750E-03	0.251E-02	-0.226E-02	0.754E-02	-0.627E-02
	500000	0.382E-02	-0.600E-03	0.277E-02	-0.242E-02	0.830E-02	-0.700E-02
B IV 5s-7p	20000	0.645E-02	-0.126E-02	0.124E-02	-0.116E-02	0.334E-02	-0.319E-02
2809.1 A	50000	0.518E-02	-0.956E-03	0.155E-02	-0.136E-02	0.425E-02	-0.384E-02
C= 0.80E+15	100000	0.433E-02	-0.779E-03	0.181E-02	-0.151E-02	0.503E-02	-0.432E-02
	200000	0.355E-02	-0.594E-03	0.193E-02	-0.178E-02	0.589E-02	-0.475E-02
	300000	0.314E-02	-0.498E-03	0.220E-02	-0.182E-02	0.567E-02	-0.536E-02
	500000	0.267E-02	-0.384E-03	0.259E-02	-0.186E-02	0.589E-02	-0.562E-02
B IV 6s-6p	20000	9.71	-2.14	1.35	-1.28	3.51	-3.47
126390. A	50000	7.79	-1.63	1.72	-1.54	4.67	-4.21
C= 0.26E+19	100000	6.54	-1.34	2.06	-1.76	5.68	-4.91
	200000	5.39	-1.02	2.31	-1.95	6.50	-5.36
	300000	4.77	-0.869	2.55	-2.22	6.89	-5.79
	500000	4.06	-0.702	2.59	-2.49	7.71	-6.54
B IV 6s-7p	20000	0.499E-01	-0.111E-01	0.911E-02	-0.823E-02	0.236E-01	-0.225E-01
7314.1 A	50000	0.405E-01	-0.830E-02	0.112E-01	-0.965E-02	0.298E-01	-0.269E-01
C= 0.55E+16	100000	0.341E-01	-0.669E-02	0.123E-01	-0.106E-01	0.347E-01	-0.307E-01
	200000	0.281E-01	-0.500E-02	0.143E-01	-0.132E-01	0.402E-01	-0.341E-01
	300000	0.248E-01	-0.422E-02	0.157E-01	-0.128E-01	0.423E-01	-0.390E-01
	500000	0.211E-01	-0.330E-02	0.181E-01	-0.135E-01	0.405E-01	-0.428E-01
B IV 7s-7p	20000	45.7	-11.6	7.56	-6.94	20.0	-19.0
201126. A	50000	37.6	-8.59	9.29	-8.41	25.0	-22.8
C= 0.41E+19	100000	32.0	-6.80	9.92	-9.69	30.1	-25.6
	200000	26.5	-5.09	12.7	-10.9	34.0	-29.0
	300000	23.5	-4.30	12.6	-11.1	37.5	-32.8
	500000	20.0	-3.35	13.4	-11.7	41.3	-36.9

Table 1. Continued

Transition	T(K)	$W_e(\text{Å})$	$d_e(\text{Å})$	$W_p(\text{Å})$	$d_p(\text{Å})$	$W_{\text{He}^+}(\text{Å})$	$d_{\text{He}^+}(\text{Å})$
B IV 2p-3s	20000	0.366E-05	0.219E-06	0.703E-07	0.139E-06	0.343E-06	0.533E-06
427.7 Å	50000	0.233E-05	0.272E-06	0.167E-06	0.211E-06	0.343E-06	0.533E-06
C= 0.12E+16	100000	0.179E-05	0.256E-06	0.239E-06	0.254E-06	0.602E-06	0.676E-06
	200000	0.141E-05	0.239E-06	0.309E-06	0.303E-06	0.795E-06	0.813E-06
	300000	0.124E-05	0.233E-06	0.345E-06	0.327E-06	0.923E-06	0.905E-06
	500000	0.105E-05	0.201E-06	0.398E-06	0.360E-06	0.108E-05	0.101E-05
B IV 2p-4s	20000	0.521E-05	0.680E-06	0.275E-06	0.370E-06	0.565E-06	0.918E-06
310.5 Å	50000	0.374E-05	0.611E-06	0.457E-06	0.475E-06	0.114E-05	0.128E-05
C= 0.26E+15	100000	0.297E-05	0.573E-06	0.583E-06	0.564E-06	0.152E-05	0.153E-05
	200000	0.239E-05	0.523E-06	0.700E-06	0.652E-06	0.188E-05	0.180E-05
	300000	0.211E-05	0.465E-06	0.761E-06	0.712E-06	0.210E-05	0.196E-05
	500000	0.180E-05	0.390E-06	0.870E-06	0.765E-06	0.237E-05	0.211E-05
B IV 2p-5s	20000	0.912E-05	0.176E-05	0.835E-06	0.905E-06	0.206E-05	0.243E-05
275.7 Å	50000	0.717E-05	0.152E-05	0.116E-05	0.114E-05	0.301E-05	0.308E-05
C= 0.10E+15	100000	0.594E-05	0.136E-05	0.143E-05	0.130E-05	0.390E-05	0.364E-05
	200000	0.488E-05	0.113E-05	0.174E-05	0.151E-05	0.454E-05	0.410E-05
	300000	0.432E-05	0.979E-06	0.188E-05	0.162E-05	0.519E-05	0.451E-05
	500000	0.367E-05	0.827E-06	0.214E-05	0.178E-05	0.533E-05	0.495E-05
B IV 2p-6s	20000	0.164E-04	0.409E-05	0.194E-05	0.199E-05	0.502E-05	0.534E-05
260.0 Å	50000	0.134E-04	0.335E-05	0.257E-05	0.243E-05	0.687E-05	0.678E-05
C= 0.53E+14	100000	0.114E-04	0.287E-05	0.320E-05	0.276E-05	0.844E-05	0.764E-05
	200000	0.948E-05	0.224E-05	0.346E-05	0.319E-05	0.957E-05	0.867E-05
	300000	0.839E-05	0.194E-05	0.409E-05	0.342E-05	0.103E-04	0.949E-05
	500000	0.713E-05	0.161E-05	0.397E-05	0.375E-05	0.122E-04	0.103E-04
B IV 2p-7s	20000	0.281E-04	0.823E-05	0.400E-05	0.399E-05	0.105E-04	0.108E-04
251.4 Å	50000	0.237E-04	0.664E-05	0.540E-05	0.473E-05	0.143E-04	0.134E-04
C= 0.31E+14	100000	0.205E-04	0.531E-05	0.615E-05	0.535E-05	0.168E-04	0.148E-04
	200000	0.171E-04	0.408E-05	0.725E-05	0.612E-05	0.188E-04	0.174E-04
	300000	0.152E-04	0.356E-05	0.762E-05	0.627E-05	0.216E-04	0.183E-04
	500000	0.129E-04	0.285E-05	0.814E-05	0.693E-05	0.209E-04	0.208E-04
B IV 3p-4s	20000	0.117E-03	0.130E-04	0.645E-05	0.776E-05	0.134E-04	0.198E-04
1221.5 Å	50000	0.846E-04	0.126E-04	0.961E-05	0.982E-05	0.248E-04	0.265E-04
C= 0.21E+16	100000	0.675E-04	0.117E-04	0.122E-04	0.116E-04	0.320E-04	0.317E-04
	200000	0.545E-04	0.104E-04	0.150E-04	0.134E-04	0.388E-04	0.366E-04
	300000	0.482E-04	0.916E-05	0.156E-04	0.144E-04	0.448E-04	0.402E-04
	500000	0.411E-04	0.769E-05	0.186E-04	0.155E-04	0.495E-04	0.428E-04
B IV 3p-5s	20000	0.965E-04	0.176E-04	0.793E-05	0.850E-05	0.197E-04	0.228E-04
816.9 Å	50000	0.747E-04	0.150E-04	0.109E-04	0.108E-04	0.285E-04	0.291E-04
C= 0.91E+15	100000	0.616E-04	0.133E-04	0.133E-04	0.123E-04	0.355E-04	0.338E-04
	200000	0.506E-04	0.109E-04	0.161E-04	0.137E-04	0.424E-04	0.390E-04
	300000	0.448E-04	0.947E-05	0.175E-04	0.149E-04	0.474E-04	0.410E-04
	500000	0.381E-04	0.800E-05	0.198E-04	0.165E-04	0.508E-04	0.471E-04

Table 1. Continued

Transition	T(K)	$W_e(\text{\AA})$	$d_e(\text{\AA})$	$W_p(\text{\AA})$	$d_p(\text{\AA})$	$W_{He^+}(\text{\AA})$	$d_{He^+}(\text{\AA})$
B IV 3p-6s	20000	0.127E-03	0.312E-04	0.141E-04	0.144E-04	0.363E-04	0.386E-04
692.8 A	50000	0.103E-03	0.248E-04	0.186E-04	0.177E-04	0.504E-04	0.490E-04
C= 0.38E+15	100000	0.877E-04	0.215E-04	0.228E-04	0.200E-04	0.607E-04	0.556E-04
	200000	0.728E-04	0.168E-04	0.251E-04	0.231E-04	0.690E-04	0.631E-04
	300000	0.645E-04	0.143E-04	0.292E-04	0.245E-04	0.744E-04	0.692E-04
	500000	0.548E-04	0.120E-04	0.287E-04	0.270E-04	0.896E-04	0.734E-04
B IV 3p-7s	20000	0.188E-03	0.546E-04	0.258E-04	0.257E-04	0.677E-04	0.692E-04
634.8 A	50000	0.158E-03	0.437E-04	0.345E-04	0.302E-04	0.922E-04	0.853E-04
C= 0.20E+15	100000	0.136E-03	0.348E-04	0.393E-04	0.342E-04	0.107E-03	0.949E-04
	200000	0.114E-03	0.268E-04	0.465E-04	0.392E-04	0.120E-03	0.112E-03
	300000	0.101E-03	0.233E-04	0.482E-04	0.400E-04	0.138E-03	0.117E-03
	500000	0.858E-04	0.186E-04	0.519E-04	0.446E-04	0.137E-03	0.135E-03
B IV 4p-5s	20000	0.129E-02	0.209E-03	0.110E-03	0.114E-03	0.275E-03	0.305E-03
2641.1 A	50000	0.992E-03	0.183E-03	0.151E-03	0.144E-03	0.390E-03	0.389E-03
C= 0.39E+16	100000	0.816E-03	0.165E-03	0.177E-03	0.167E-03	0.495E-03	0.450E-03
	200000	0.669E-03	0.136E-03	0.217E-03	0.188E-03	0.581E-03	0.529E-03
	300000	0.592E-03	0.118E-03	0.239E-03	0.204E-03	0.644E-03	0.564E-03
	500000	0.505E-03	0.986E-04	0.262E-03	0.215E-03	0.729E-03	0.600E-03
B IV 4p-6s	20000	0.852E-03	0.201E-03	0.910E-04	0.911E-04	0.233E-03	0.246E-03
1672.5 A	50000	0.685E-03	0.159E-03	0.122E-03	0.112E-03	0.319E-03	0.309E-03
C= 0.16E+16	100000	0.579E-03	0.137E-03	0.142E-03	0.126E-03	0.371E-03	0.354E-03
	200000	0.480E-03	0.106E-03	0.167E-03	0.147E-03	0.461E-03	0.409E-03
	300000	0.426E-03	0.913E-04	0.185E-03	0.155E-03	0.494E-03	0.441E-03
	500000	0.362E-03	0.759E-04	0.199E-03	0.178E-03	0.536E-03	0.464E-03
B IV 4p-7s	20000	0.947E-03	0.270E-03	0.127E-03	0.122E-03	0.330E-03	0.331E-03
1370.5 A	50000	0.789E-03	0.214E-03	0.161E-03	0.146E-03	0.440E-03	0.407E-03
C= 0.93E+15	100000	0.680E-03	0.170E-03	0.186E-03	0.166E-03	0.513E-03	0.456E-03
	200000	0.568E-03	0.131E-03	0.220E-03	0.189E-03	0.601E-03	0.538E-03
	300000	0.504E-03	0.113E-03	0.225E-03	0.195E-03	0.659E-03	0.566E-03
	500000	0.428E-03	0.908E-04	0.246E-03	0.212E-03	0.685E-03	0.650E-03

Acknowledgments

This paper is a part of the project 176002 "Influence of collisional processes on astrophysical plasma spectra" supported by Ministry of Education and Science of Republic Serbia. The partial financial support from Technical University – Sofia is also acknowledged.

References

- Cunha, K., Smith, V. V.: 1999, *ApJ*, **512**, 1006.
Duncan, D. K., Lambert, D. L., Lemke, M.: 1992, *ApJ*, **401**, 584.
Duncan, D. K., Primas, F., Rebull, L. M., Bosegaard, A. M., Deliyannis, C. P., Hobbs, L. M., King, J. R.,
Ritchey, A. M., Federman, S. R., Sheffer, Y., Lambert, D. L.: 2011, *ApJ*, **728**, 70.
Ryan, S. G.: 1997, *ApJ*, **488**, 338.
Sahal-Bréchet, S.: 1969a, *Astron. Astrophys.*, **1**, 91.
Sahal-Bréchet, S.: 1969b, *Astron. Astrophys.*, **2**, 322.
Sahal-Bréchet, S.: 2010, *J. of Phys.: Conf. Ser.*, **257**, 012028.
Shima, M.: 1963, *Geochim. Cosmochim. Acta*, **27**, 991.
Venn, K. A., Brooks, A. M., Lambert, D. L., Lemke, M., Langer, N., Lennon, D. J.,
Keenan, F. P.: 2002, *ApJ*, **565**, 571.

IMAGE PROCESSING SUGGESTIONS FOR ASTRONOMICAL MULTIEXPOSURE WIDE FIELD PLATES¹

DIMO DIMOV¹ and MILAN S. DIMITRIJEVIĆ²

¹*Inst. of Information and Communication Technologies, BAS, Sofia*

²*Astronomical Observatory, Belgrade*

E-mails: dtdim@iinf.bas.bg, mdimitrijevic@aob.bg.ac.rs

Abstract: In the article is proposed how to assess the quality of archival plates with chains. Certainly, CCD astronomy replacing classical photo astronomy recently makes senseless use of multiexposure wide-field plates (MEWFP) approaches. On the other hand, the world heritage of archive MEWFP, with 4-6 expositions estimated at over 10,000, encourages the development of specific methods for computer processing of MEWFP. Thus, our method is useful to evaluate the structural quality of archival MEWFP (whether it is exacerbated by overlapping of star copies on the plates).

1. INTRODUCTION

The method for locating non-stationary (variable and/or quickly moving) stellar objects by capturing images of star chains is known in astronomy as multiexposure method. The method consists of repeated photo exposures (on the same photo plate) of the observed celestial quadrant. Photo exposures, usually 4 to 6 in number, are equal over time (e.g. $\sim 5 \div 10$ min each) and relative (mechanical) movements of the photo plate toward the instrument (telescope) are uniform from exposure to exposure in selected fixed direction. The exception is the first shift, which is ~ 2 times larger than the other to indicate the beginning of the chains (Aniol et al., 1990, Winterberg et al., 1995).

The idea for this report comes from the difficulty of comprehensive computer processing of plates with star chains (Dimov et al., 2012). The configuration of the chains in a plate is usually static, i.e. direction of the chains and the distances

¹ This work was supported by the Institute of Information & Communication Technologies (IICT) at Bulgarian Academy of Sciences (BAS) through the Grant # DO-02-275/2008 of the National Science Fund at Bulgarian Ministry of Education & Science.

between their components (copies of the star over time) were selected from astronomers mainly on the principle of operational ease of use with the given telescope. Thus, in the inherited, during the years, archive plates we meet too many instances of (partially or completely) overlapping star chains, which hinders comprehensive identification of all chains in the plate for the accurate localization of flare star phenomena looked for.

In comparison to the original MEWFP method, the proposed method seems a little late in time, in view of the incoming CCD technology to replace the classical photography in astronomy. There are no technological limits to playing MEWFP method in CCD technology². But this is proved unnecessary because the sequence of CCD images can directly (and more efficiently) be processed by the so-called image differencing approaches³ (Sonka, Hlavac and Boyle, 1998).

On the other hand, the world heritage of archival astronomical plates with 4-6 expositions could be estimated at least over 10 000, according to the data in (Tsvetkova, 2012), which stimulates the development of specific methods for computer processing (Aniol et al., 1990, Winterberg et al., 1995, Dimov et al., 2012). Method proposed here can be used to assess the quality of existing archival images with MEWFP chains, in particular – to their structural quality determined by proximity to the optimum structure of the chains (as direction and distance between components). Evaluation is obtained a posteriori, i.e. concerns quality of an (already) conducted MEWFP experiment with star chains. It may serve to substantial improvements in computer processing of MEWFP images, e.g. Dimov et al. (2012), for an (external, independent) evaluation of the error in variable chains demand, i.e. variations caused by variable stars rather than random overlap in MEWFP experiment.

2. PROPOSED METHOD DESCRIPTION

2.1. Preliminary observations

We assume that the input image is pre-processed to an adequately binarized image, i.e. stars are presented by "white" spots against the "black" sky. This type of astro images are considered as "positives", unlike the original negative images obtained by scanning astronomical plates.

For the purposes of this experiment we will use a preview to astronomical image of the Pleiades region, see Fig. 1a, and its corresponding positive – in Fig. 1b.

² http://en.wikipedia.org/wiki/Charge-coupled_device

³ http://en.wikipedia.org/wiki/Blink_comparator

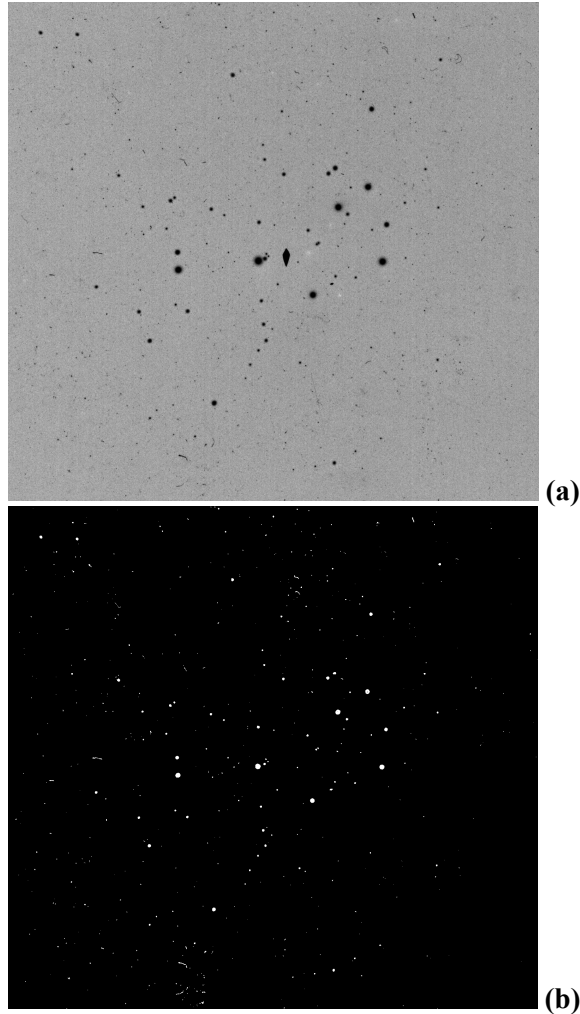


Figure 1: Image cluster "Pleiades": a) an original preview-negative 1682x1580 pix; a (diamond like) artifact is observed in the image center caused by photo plate storage in the time; b) the working positive (after binarization of the original), where the artifact is cleaned interactively.

We will mainly consider the case of linear chains (Aniol et al., 1990, Winterberg et al., 1995, Dimov et al., 2012), see also Fig. 2. Without loss of generality (and for definiteness of illustrations), we will consider the most common case:

$$d_{1,2} = 2d, \quad d_{2,3} = d_{3,4} = d_{4,5} = d_{5,6} = d, \quad d > 0, \quad (1)$$

where $d_{i,i+1}, i=1, \dots, (n-1)$ are the distances between the consecutive chain components and the length n (in number of components) is $n = 6$. Cases of "non-

linear" chains described in Dimov et al. (2012), see Fig. 2b, will be considered in discussions later on.

We substantially use analogies with the concepts, *cumulative image* and *reduced cumulative image*, introduced in [3] for the identification of chains in astro images. Here we interpret these concepts for generating images with chains from a single image of a given sky quadrant.

2.2. Idea of the method

Step S1: Let us choose an arbitrary star in the input working image. Since there black areas indicate the absence of significant stars, we can give the following trivial interpretation – black areas mark the possible vectors of displacement of the plate (to receive any chain with $n = 2$, but only for the selected star), so the shift up of this star (in the new exposure of the plate) does not cover any other star.

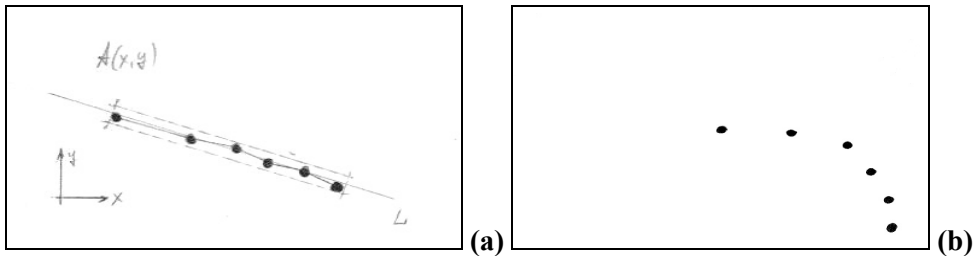


Figure 2: Chain schemes with $n = 6$ components (i.e., n exposures of the plate): a) a linear scheme of chain with illustration of the chain average direction L ; b) a non-linear scheme, for details, see [3].

For definiteness, and without loss of generality, we consider that the Cartesian coordinates' origin of the image is moved to the center of the chosen star, i.e. that the star coordinates are $(0,0)$.

Step S2: Let us choose another star with coordinates (x_2, y_2) of its center, get a copy of the input image and impose it upon the previous one, but translated so that the selected second star to coincide with the first one (from step S1). Thus, each pixel (x, y) of the input image is shift τ_2 translated to position (\tilde{x}, \tilde{y}) , and the second star is also provided with coordinates $(0,0)$ after translation:

$$\begin{aligned} (\tilde{x}, \tilde{y}) &= (x, y) - \tau_2, \\ \tau_2 &= (x_2, y_2) - (x_{\text{size}}/2, y_{\text{size}}/2), \quad 0 \leq x < x_{\text{size}}, \quad 0 \leq y < y_{\text{size}} \end{aligned} \quad (2)$$

where x_{size} and y_{size} define the size of the input working image in pixels.

Now, if we add disjunctively the both images, primary and shifted ones then the resultant black areas will mark the possible positions of the second component

of any chain of length $n = 2$ (but only for the first star and for the second star), do not cover any other star.

Step S3: Repeat the previous step S2 for all other stars in the image. Then, the black areas in resultant (disjunctive) image will mark the option for vector displacements of the plate (i.e., the formation of all chains with length $n = 2$ components), so that no chain can fall on another chain, and more precisely, any particular chain component does not cover any components of other chains.

For formal completeness, we determine starting with a blank (i.e. entirely black) image whose coordinate system is at its center, i.e. that at the current step S3 we brought all the stars found in the input image in the blank image center, like the first star (at S1) and the second one (at S2). The resultant image will be called *disjunctive accumulated image* (DAI).

DAI has the same properties as the accumulated image that had been already described, although for other purposes in Dimov et al. (2012). By analogy with Dimov et al. (2012), we also restrict a substantial square of size a , $a = \min\{x_{\text{size}}, y_{\text{size}}\} / 2$, in the central part of DAI, and we call it "*reduced DAI*" (RDI). Obviously, the area outside RDI contains incomplete information about chains overlap, because the area of the original input image, which is also used in the assessment, is uncertain therein and is formally declared by us to empty (all black). An example of DAI is illustrated in Fig. 3, and the respective and only significant RDI – in Fig. 4b. Note that zooming of images in detached figures varies for better illustration, where matching size can be traced by means of squared hints in the figures, see Fig. 3 and Fig. 4.

2.3. Formal description of the method

Step S4: Let us scale the received RDI by a factor $3/2$ and limit the result to the initial RDI size towards the coordinate origin. For the resultant, scaled and centered image to mark it as SDI(3), we can write formally:

$$\text{SDI}(3) \Leftarrow \text{RDI} : \left\{ I(\tilde{x}, \tilde{y}) = I(x, y), (\tilde{x}, \tilde{y}) = \frac{3}{2}(x, y), (\tilde{x}, \tilde{y}) \in \text{SDI}(3), (x, y) \in \text{RDI} \right\}, \quad (3)$$

where $I(\tilde{x}, \tilde{y})$ and $I(x, y)$ are the intensity values of the pixels in the SDI(3) and RDI. Let us summarize (disjunctively, pixel by pixel) the two images and indicate the result as RDI(3):

$$\text{RDI}(3) = \text{SCDI}(3) \cup \text{RDI}. \quad (4)$$

It can be shown that the black areas in the resultant image RDI(3) represent a mask for possible displacement of the plate, i.e. for optimal selection of a structure of no overlapping chains with length $n = 3$ components. Indeed, if we choose a point (pixel) in the black area of RDI(3), then it is guaranteed with a corresponding (affine, projective) point in the black area of RDI.

Repeat the previous step iteratively, i.e. scaling (3) and disjunction (4) until the desired length n of chains, for example, until $n = 6$.

If we formally write for the first step S1:

$$\text{RDI}(2) = \text{RDI}, \quad (5)$$

then we can summarize the description (3) and (4) by the following recursive formulae:

$$\text{RDI}(i) = \text{SDI}(i) \cup \text{RDI}(i-1), \quad i = 3, \dots, n; \quad (5a)$$

where

$$\text{SDI}(i) \leftarrow \text{RDI}(i-1) : \left\{ I(\tilde{x}, \tilde{y}) = I(x, y), (\tilde{x}, \tilde{y}) = \frac{i}{i-1}(x, y), (\tilde{x}, \tilde{y}) \in \text{SDI}(i), (x, y) \in \text{RDI}(i-1) \right\} \quad (5b)$$

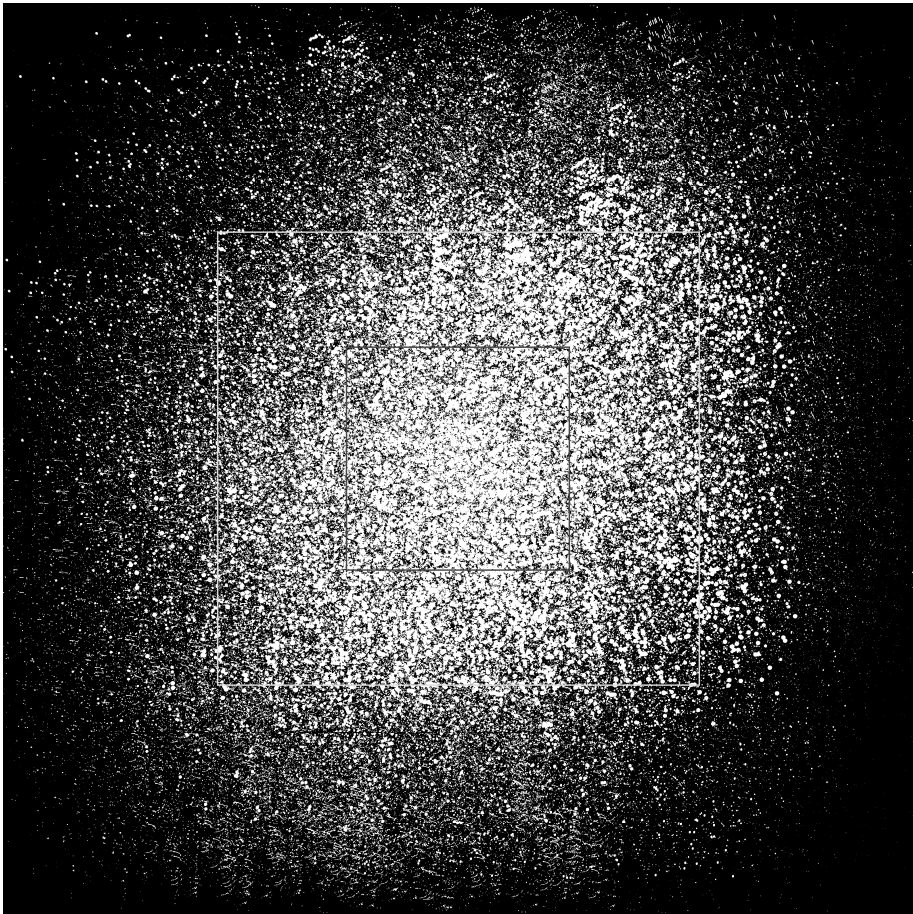


Figure 3: Full accumulated disjunctive image DAI, derived from the binarized input image (Fig. 1b). The position and size of both, the input image and the reduced disjunctive image RDI, are pointed by extra square hints.

The final image $RDI(n)$ of the sequence $RDI(i)$, $i = 2, \dots, n$, shows the optimal choice of the last, n -th component of the chains of the desired length of n components. Indeed, if we choose a point in the black area of $RDI(6)$, it follows that it is guaranteed with a series of corresponding (affine) points from black areas of each one of the images $RDI(5)$, $RDI(4)$, $RDI(3)$ and $RDI(2)$, and that these points can be used to structure the chains of type (1), which first component is the beginning $(0,0)$, i.e. the common center of these RDI images.

Now, we can specify the intuitively used concept of "*optimal choice of linear chains structure*" by the following:

Statement: Each chain structure choice by the above method is optimal in the sense that the centers of all the components of the chains generated for the stars found in the input image will fall only in the free (black) areas and not on other components and/or stars. Something else, if the mask $RDI(i)$ be empty for some i , $2 \leq i \leq n$, then the task of optimal chains with the number of components $\geq i$, has no solution.

Proof: ♦ Since working images here are black and white only, we can consider white areas (i.e., star spots) as sets of logical (Boolean) units, and black areas as sets logical (Boolean) zeros. Thus, for a set A of image pixels, we will denote by \overline{A} , $A \subset \overline{A}$, the subset of black pixels only.

Let us choose a point C_n (a vector $\overrightarrow{C_n}$) from the black field of $RDI(n)$, i.e., $C_n \in \overline{RDI(n)} \neq \emptyset$.

Then from definition (5a,b) applied to $RDI(n)$:
 $RDI(n) = \left(\frac{n}{n-1} * RDI(n-1) \right) \cup RDI(n-1)$, and from de Morgan's laws for the

Boolean intensities of each pixel, it follows that $C_n \in \left(\frac{n}{n-1} * \overline{RDI(n-1)} \right) \cap$

$C_n \in \overline{RDI(n-1)}$, where the two-place operation $a * A$ denotes scaling a given point (vector) set A by a coefficient a towards the initial point (vector) C_0 , $\left| \overrightarrow{C_0} \right| \equiv 0$. Consequently: $\exists! C_{n-1}$, $C_{n-1} \in \overline{RDI(n-1)}$, where

$\overrightarrow{C_{n-1}} = \left(\frac{n-1}{n} \right) \overrightarrow{C_n}$, for the chosen $C_n \in \overline{RDI(n)}$.

In this way, recursively it follows that for each point $C_i \in \overline{RDI(i)}$, $i = n, \dots, 3$, it exists an unique point $C_{i-1} \in \overline{RDI(i-1)}$ such that $\overrightarrow{C_{i-1}} = \frac{i-1}{i} \overrightarrow{C_i}$. Hence, the vectors $\overrightarrow{C_i}$, $i = 2, \dots, n$, are collinear, and the points C_i , $i = 1, \dots, n$ are situated on an unique line.

Finally, for the $\overline{C_2}$ component of the chains, we have $C_2 \in \overline{\text{RDI}(2)}$, wherefrom according to (5) it follows that $|\overline{C_1}| \equiv 0$, which ends the proof. ♦

Fig. 4(b÷f) show the masks $\text{RDI}(i)$ for optimal selection of the plate displacement, for each length i of the chains, respectively $i = 2,3,4,5,6$. Fig. 4a refers to the formal chain of length $i=1$ component, i.e. it coincides with the input binarized image (cf. Fig. 1b).

2.4. Enhanced interpretation of the method

In such a way, each pixel in the black area of $\text{RDI}(6)$, if non-empty, is a solution to our task.

- In case one gives some requirements for physical dimensions of the chains, as in celestial degrees (or minutes, or seconds) or in pixels, then we can sort pixels of free (black) areas according to their distances to the RDI center and look for an optimum on this sorting.

- Since stars on astro images are not ideal (mathematical) points but real spots (of significant intensity measurement), see Fig. 1(a,b), it is actually a good idea in the free (black) areas to look not as for isolated pixels but for circular areas with a diameter of more than average amount over all stellar spots in the image. For example, in the present working image of the Pleiades (Fig. 2b) the average diameter of the star spots is ~ 3.9 pixels, while the maximum diameter is ~ 17.3 pixels.

- So far, we discussed the simplest (and most used) chain structure – linear structure, in which the distances between the components of the chains are given by (1) (see also Aniol et al., 1990, Winterberg et al., 1995).

Obviously, for generality of results, we may consider arbitrary structure of chains such as Fig. 2b, i.e. when, instead of (1), we ask an arbitrary chain structure through respective vector displacements of components towards the starting component (the original star) (Dimov et al., 2012):

$$\overline{C}_i = (x_i, y_i) - (x_1, y_1), \quad i = 1, \dots, n, \quad (6)$$

where (x_i, y_i) are the vectors (i.e. centers) of components of a given chain towards the beginning (first component) $\overline{C}_1 = (0,0)$ of the chain. Furthermore to this general case, it is sufficient to add rotation of $\text{SDI}(i)$ at angle φ_i at step S4, after scaling (5b), as follows:

$$\text{rSDI}(i) \Leftarrow \text{SDI}(i) : \left\{ I(\tilde{x}, \tilde{y}) = I(x, y), (\tilde{x}, \tilde{y}) = (x, y) \left\| \begin{array}{cc} \cos \varphi_i & -\sin \varphi_i \\ \sin \varphi_i & \cos \varphi_i \end{array} \right\|, (\tilde{x}, \tilde{y}) \in \text{rSDI}(i), (x, y) \in \text{SDI}(i) \right\}$$

$$\text{SDI}(i) := \text{rSDI}(i) , \quad (6a)$$

where $\varphi_i = \angle(C_{i-1}, C_i)$, $i = 3, \dots, n$, see also Fig. 2b, where $n=6$.

By the way, the linear case (1) can be represented by (6) and (6a), like:

$$d_{1,2} = \left| \overrightarrow{C_1} - \overrightarrow{C_2} \right| = 2d , \quad d_{i,i+1} = \left| \overrightarrow{C_i} - \overrightarrow{C_{i+1}} \right| = d , \quad i = 2, \dots, (n-1), \quad (7)$$

and $\varphi_i \equiv 0$, $i = 3, \dots, n$, $n=6$.

2.5. The Algorithm Proposed

Input data:

- Astro image (a negative, an original or preview) N , $0 \leq N(x, y) < L_{\max}$, $(x, y) \in [x_{\text{size}} \times y_{\text{size}}]$, where $[x_{\text{size}} \times y_{\text{size}}]$ is the domain of N , x_{size} and y_{size} are in pixels, and $L_{\max} - 1$ is the possible maximum of image intensity values (L_{\max} is natural number usually written in the image file format).
- Number n of the components of wanted chains, usually $3 \leq n \leq 6$.

NB.: For overall processing speed use as simple preview as possible, while the stars of interest (or of given magnitude) are still visible on the preview. Over this limit, the preview precision used does not affect essentially the method performance.

Expected result:

- ◆ Slope α (in radians) of the chain direction towards the abscissa in the image N , and
- ◆ Basic distance d for the components, according to (1) or (7).

We describe the algorithm in two main steps: pre (A1) and core (A2):

A1) Preprocessing: Evaluation of the centroids (mass centers of the star spots) in the image. For this purpose:

- ♣ Invert the input image (see Fig. 1) from negative N to positive P by the formulae:

$$\forall (x, y) ((x, y) \in [x_{\text{size}} \times y_{\text{size}}]): P(x, y) = L_{\max} - N(x, y) - 1, \quad (8)$$

where $[x_{\text{size}} \times y_{\text{size}}]$ is the domain either for N or for P .

- ♣ Binarize the received positive P to get input working image B (see Fig. 1b), by the formulae:

$$\forall (x, y)(0 \leq x < x_{\text{size}}, 0 \leq y < y_{\text{size}}) : B(x, y) = \begin{cases} L_{\text{max}} - 1, & \text{if } P(x, y) < t(x, y) \\ 0, & \text{if } P(x, y) \geq t(x, y) \end{cases}, \quad (9)$$

where $t(x, y)(0 \leq x < x_{\text{size}}, 0 \leq y < y_{\text{size}})$ is binarizing (threshold) surface in the general case of locally adaptive binarization, see for example (Dimov and Dimov, 2010). In relatively "clean" images: $t(x, y) = t_0 = \text{cte}$, t_0 a threshold for global binarization, $0 \leq t_0 < L_{\text{max}}$.

♠ Find the center of mass (centroide) of each star spot. In our case, for simplicity of demonstrations, we work directly with binarized image B . For larger precision, binarized image B can be used as a mask for positive input P in assessing the centroides.

NB.: Finding centroides can be also conducted through sophisticated computer software for registration of astronomical images, e.g., the program SExtractor (Bertin and Arnouts, 1996), and then computer to generate the working image B using stars data (declination, right ascension and magnitude) registered in the corresponding to B area of used sky catalog. This approach, however, is very resource intensive and unnecessarily precise for the intended purpose here.

A2) Basic processing: As described in paragraph 2.2 and 2.3:

♥ Generate initial RDI, pursuant to paragraph 2.2 (see also Fig. 4b). Announce $\text{RDI}(2) = \text{RDI}$.

♥ Generate cyclically all $\text{RDI}(i)$, $i = 3, \dots, n$, according to (5a) and (5b) in paragraph 2.3.

♥ Look for position of the optimal chain in the black areas of the $\text{RDI}(n)$, i.e. in $\overline{\text{RDI}(n)}$.

Here, various heuristics are possible, such as:

- Find the solution $(x_{\text{opti}}, y_{\text{opti}})$, $(x_{\text{opti}}, y_{\text{opti}}) \in \overline{\text{RDI}(n)}$, as the minimum D_{min} of distances $D = \sqrt{x^2 + y^2}$ from all points $(x, y) \in \overline{\text{RDI}(n)}$ to the image center, either

- The same, but with the following premise: look for $(x_{\text{opti}}, y_{\text{opti}})$, not as an isolated pixel, but as the center of isolated circle of diameter ϕ , $\phi > 0$. An upper limit for ϕ can be determined at step A1, for example, as the average (or maximal) diameter of star spots in the working image B ;

- Other heuristics.

♥ Calculate the expected result:

$$\alpha = \text{tg}(y_{\text{opti}} / x_{\text{opti}}), \quad d = \sqrt{x_{\text{opti}}^2 + y_{\text{opti}}^2} / n \quad (10)$$

End of algorithm.

NB.: The existence of a solution for working binarized image B , i.e. $\exists(x, y) \in \text{RDI}(n) (I(x, y) = 0)$ or what is the same: $|\overline{\text{RDI}(n)}| > 0$, obviously leads to the existence of a solution for the original image N too.

3. EXPERIMENTS AND DISCUSSION

3.1. Experiments

A standard Windows-7/Vista/XP application is performed to test the proposed method for the estimation how good was the choice of the plate movements. The application is C/C++ written in a Borland C Builder 5.0 environment. The experimental computer is an IBM compatible PC: Intel Core 2 Quad CPU 2.8 GHz, MM 4,0 GB. The input images should be preliminary converted to Windows BMP/JPG format (1 bpp).

A preview image of the Pleiades region has been used for experiments, whose dimensions are $(x_{\text{size}}, y_{\text{size}}) = (1682, 1580)$, see also Fig. 1. The length n of the chains is chosen: $n = 6$.

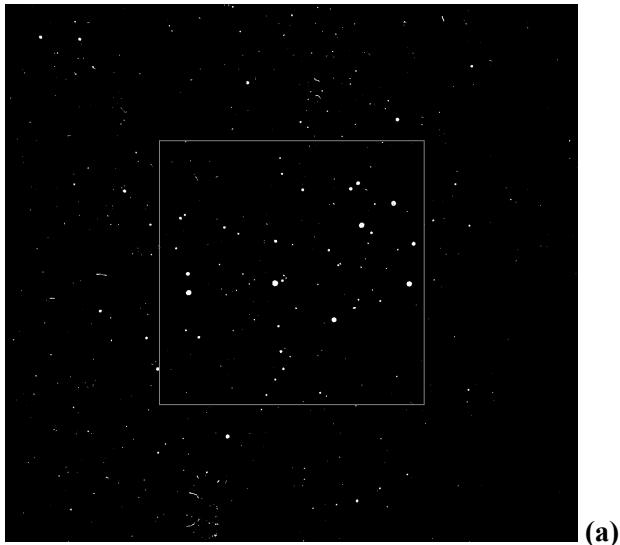
The result of the proposed algorithm performance on the image (cf. Fig. 4f) is as follows: $(x_{\text{opti}}, y_{\text{opti}}) = (331, 372)$, where the $\text{RDI}(6)$ domain is a square of size 780.

Consequently $(\tilde{x}_{\text{opti}}, \tilde{y}_{\text{opti}}) = (-59, -18)$, according to (2), wherefrom to (10), we have:

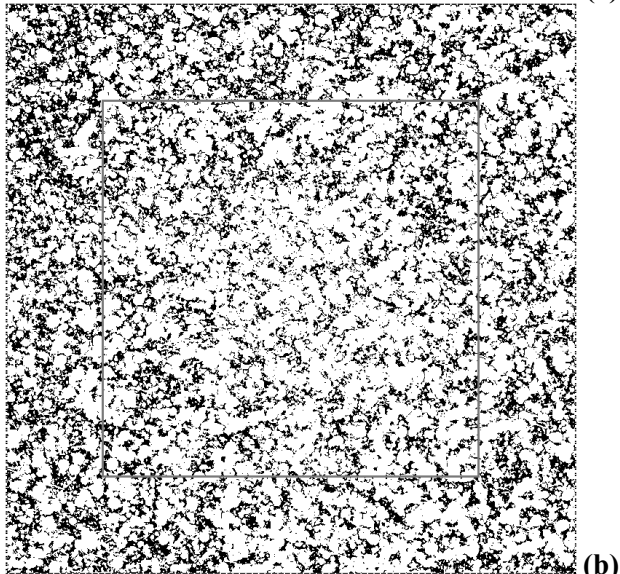
$$D_{\min} = 61.2, d = 10.2, \alpha = -163.0^\circ, \quad (11)$$

hence for the optimal structure of the chains (in central coordinates, and restrictively to pixel precision) we obtain:

$$(0, 0), (-20, -6), (-29, -9), (-39, -12), (-49, -15), (-59, -18).$$

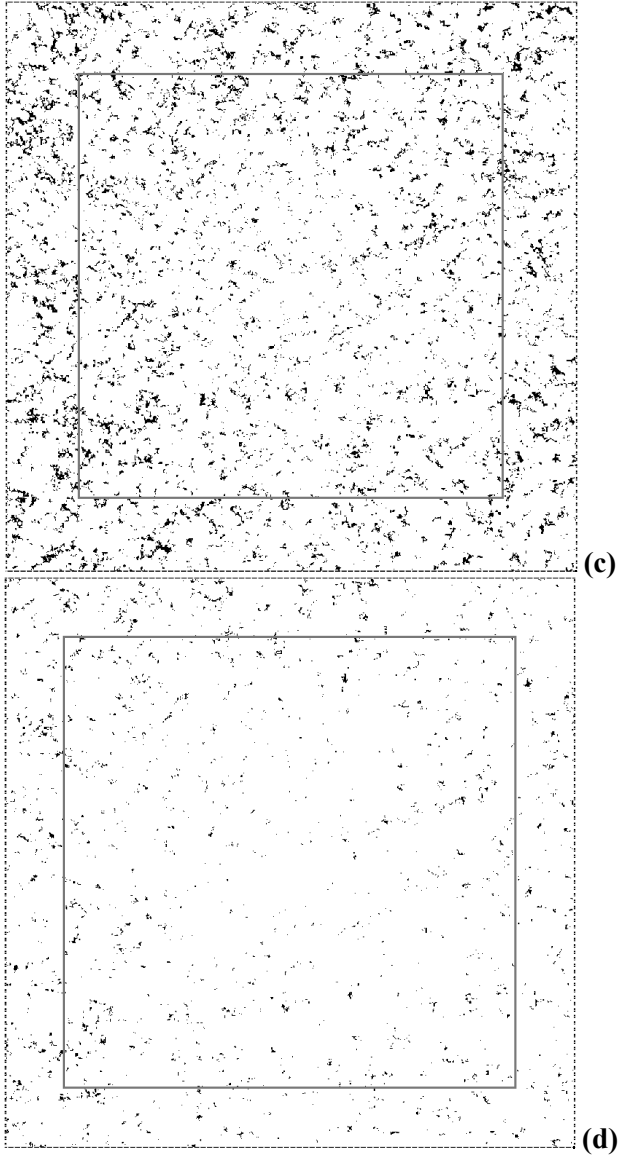


(a)



(b)

IMAGE PROCESSING SUGGESTIONS FOR ASTRONOMICAL MULTIEXPOSURE
WIDE FIELD PLATES



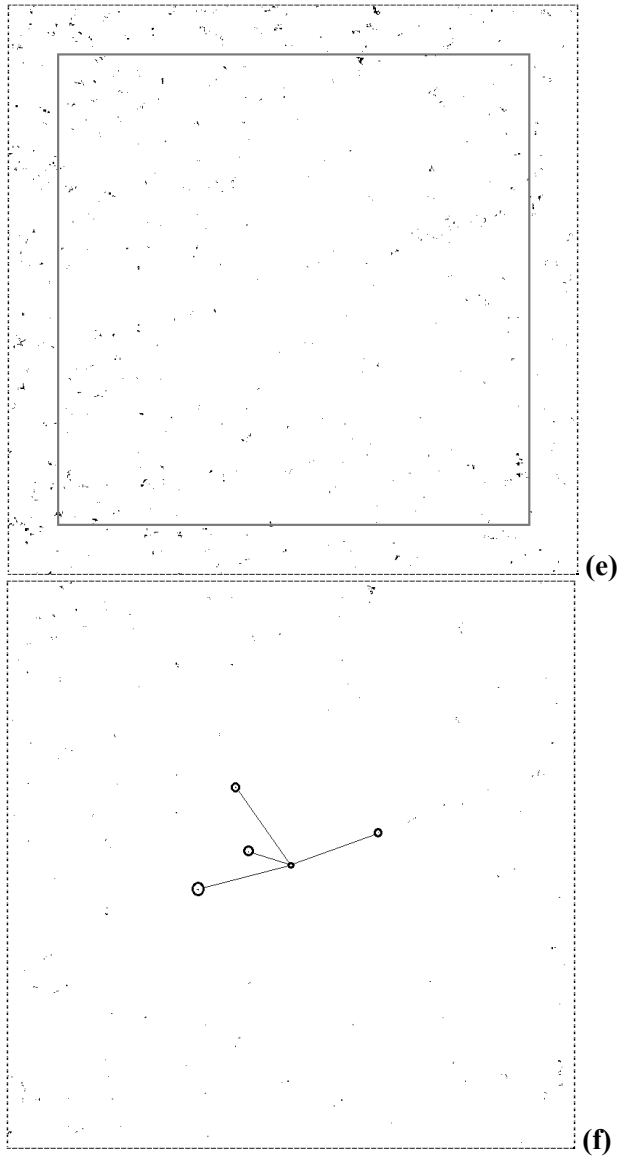


Figure 4: A sequence of reduced accumulated images RDI (n): a) $n = 1$ (formally), b) $n = 2$ (RDI), c) $n=3$, d) $n=4$, e) $n=5$, and f) $n=6$. Black areas of each RDI mark the current (n -th) component for selecting non-overlapping chains. Also, the position and size of next RDI is graphically illustrated by respective artifact-rectangle herein.

The sequence of reduced accumulated images, $RDI(i)$, $i = 1, \dots, 6$, associated with the proposed method and algorithm, is illustrated in Fig. 4(a+f). Black areas in $RDI(i)$, i.e. relevant $\overline{RDI(i)}$, mark the position of i -th component for selecting

of non-overlapping chains. An artificial square hint on each RDI(i) marks the position and size of the next RDI($i+1$), $i=1,\dots,5$, for better understanding of illustrations. For similar reasons, the sequence beginning is prefaced by the work image B (see also Fig. 1b), which plays a formal role as RDI(1). On RDI(6), i.e. last RDI, the first few (closest to the center) opportunities for chains' choice are illustrated, including the above announced optimal solution. The corresponding precise values of these solutions are given in Table 1.

Table 1: Choice of (linear) chains parameters for the image of Fig. 1a.

No.	$(x_{\text{opti}}, y_{\text{opti}})$	$(\tilde{x}_{\text{opti}}, \tilde{y}_{\text{opti}})$	D_{min}	d [pix]	α [degrees]	\emptyset [pix]	Overlaps %
1	(331, 372)	(-59, -18)	61.7	10.3	-163.0	1.5	4.9
2	(510, 345)	(120, -45)	128.2	21.4	-20.6	1.0	-
3	(313, 282)	(-77, -108)	132.6	22.1	-125.5	2.5	-
4	(261, 423)	(-129, 33)	133.2	22.2	165.7	2.5	-
*	(413, 388)	(23, -2)	24.0	4.0	-3.2	-	29.0

Each row of Table 1 corresponds to possible choice of the (linear) chains parameters for the image B , i.e., for the input image N too. The table rows are sorted in ascending order of D_{min} . Thus, row 1 represents the optimal choice for chains parameters, and the corresponding image of chains artificially generated for this choice is illustrated in Fig. 5a. The last column of the Table assesses the overlap area among the chains as a percentage of the maximum possible area A_{ovr} of overlap, $A_{\text{ovr}} = (n-1)S$, $n = 6$, and S the total area of stellar spots localized in the input image.

It is clear from Table 1 that if seeking a minimum length of the chains, and the diameter of the circle of guaranteed non-overlapping is, for example, $\phi = 2$, then instead of the obvious choice (row 1), we should prefer row 3 of the Table.

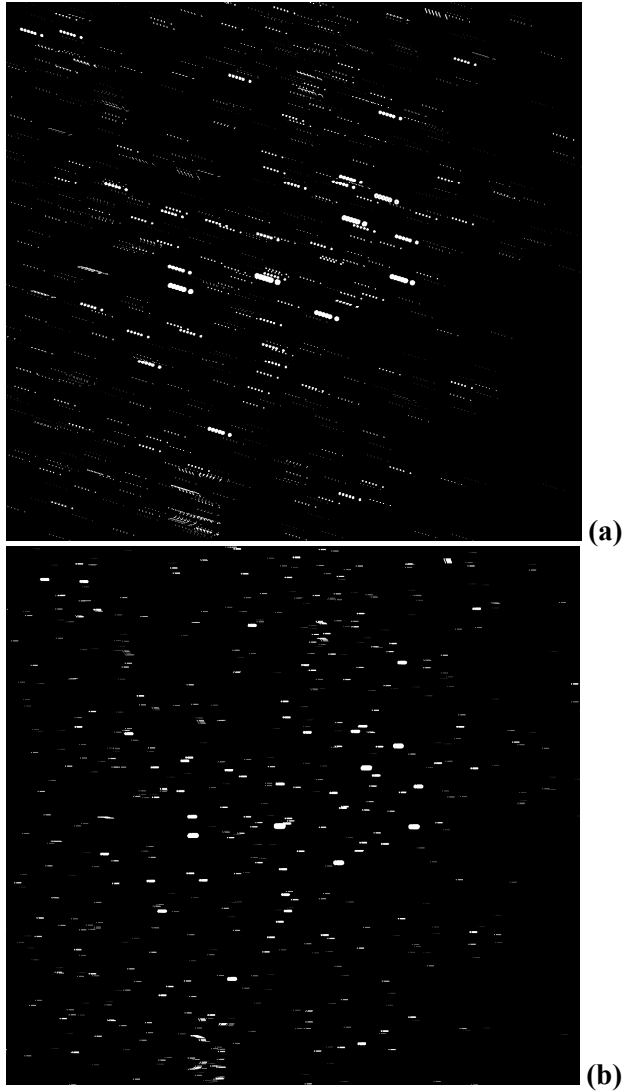


Figure 5: Astro image with chains (of 6 components' length): a) the optimal astro image (with a slope of chains $\alpha = 163.0^\circ$, $d = 61$ [pix]), generated from the working image of Fig. 1b; and b) generated (from Fig. 1b) a virtual copy of the original image ROZ050_000046 with chains' parameters: $\alpha = -3.2^\circ$, $d = 24$.

The last row marked with (*) in Table 1 refers to an image (see Fig. 5b) generated toward the choice that was (ever) made for an archival "Pleiades' chains" image, reviewed in (Dimov et al., 2012). The quantitative evaluation (29%) of overlap here is about 5 times larger than the estimated overlap for the optimal choice (row 1 of Table 1), which can be traced also by visual comparison of Fig. 5(a,b).

3.2. Discussion

The experiment illustrated in Fig. 5, shows the optimal choice of chains ($\alpha = 163.0^\circ$, $d=61$ [pix]) following the method proposed here (Fig. 5a), compared to a random choice (Fig. 5b), which parameters $\alpha = -3.2^\circ$ and $d=24$, are evaluated for the original "Pleiades chains" image, namely ROZ050_000046.bmp (Dimov et al., 2012). Both images (Fig. 5a and Fig. 5b) were obtained through the binarized input image B (Fig. 1b) by generating the appropriate software chains to simulate as close as possible experimental conditions in the two cases under comparison.

In fact, the differences in the both experiments are essential – the first one is incomplete (no actual image of chains were produced, we have only the input image of Fig. 1), while the second is represented only by an image with chains, and no initial image (like in Fig. 1). We should consider differences in experiment dates, hence varying degrees of aging of the plates, as well as differences in the type of plates, duration of exposure, type of telescopes used, etc.

Further, and beyond the illustrated comparison, we can see that the chains' overlap in the original image "Pleiades' chains" of Dimov et al. (2012), even above the optimum here defined is not as big as this occurs in its recovery (Fig. 5b) from the input image (Fig. 1). Taking note that the average diameter of the star spots in the input image is about two times larger than the one in the original image with chains from Dimov et al. (2012), explains this discrepancy.

The complexity of the proposed algorithm can be considered linear over the volume of the input image. The measured duration of the experiment is ~ 1.04 [sec], for the test image volume $V = 2.6\text{MB}$, in a BMP format. So, at the main step A1 of the algorithm proposed, we evaluate an experimental time constant τ , $\tau \sim 0.4$ [sec/MB], which can be applied to estimate the processing time t for an arbitrary input image, $t \approx V\tau$ [sec].

Interest is the ability to manage the situation of "no solution" at some step i of the proposed algorithm, i.e. when reaching $|\overline{\text{RDI}(i)}| = 0$, $i \leq n$. This will summarize two approaches: 1) by manipulating the size of the stellar spots in primary image $B \equiv \text{RDI}(1)$, and 2) by redefining the proposed method – from black-and-white (B/W) images to gray (halftone) ones.

1) If reducing the star spots' diameters ϕ in the image $B \equiv \text{RDI}(1)$ (see Fig. 4a), for example, by a specific operation such as "morphologic erosion" (Sonka, Hlavac and Boyle, 1998) but remaining unchanged the smallest spots, such as $\phi \leq 2$, then the resultant $\text{RDI}(6)$ (see Fig. 4f) will obviously contain larger black areas, i.e. more opportunities for optimal selection of chains. Conversely, if an operation like "morphologic dilation" (Sonka, Hlavac and Boyle, 1998), increases the diameter of the spots, even these few options for optimal choice (see also Table 1) will disappear from $\text{RDI}(6)$, i.e. problem will become unsolvable at $n = 6$. We already commented this effect in Fig. 5(a,b), where the differences in the

diameters of stellar spots are due to differences (most likely in duration of exposure at) in both experiment compared.

2) The proposed method was justified here for B/W images. Thus, if at the current step i of the algorithm, the black areas of $RDI(i)$, $i \leq n$, we can choose a circle ϕ , $\phi > \phi_{\max}$, where ϕ_{\max} is the diameter of the largest star spot in the initial image B , then the method ensures complete lack of overlap between the chains. This is a very strong condition. To avoid early reaching of "no decision" the key condition is weakened to $\phi > \phi_{\text{avg}}$, where ϕ_{avg} is the average diameter of the star spots in B . We still weaken to $\phi > 0$, which allows for larger values of n , at the expense of minor overlaps on the periphery of the chains. This brings the idea of an extension defined on the halftone images instead of B/W ones. To do this:

- Define a new initial image B_E , $B_E = B \cap P$, P the original input image, and B is its binarization used as mask to pass only essential (above the binarization threshold) intensities of star spots in P ;

- Instead of disjunction in (4) and (5a) use an "extended disjunction", i.e. like the conventional summation but restricted above by the intensity L_{\max} , $L_{\max} = 256$ for P and B_E images, $B_E \equiv RDI_E(1)$, as well as for the subsequent $RDI_E(i)$ and $SDI_E(i)$, $i = 2, \dots, n$;

- Look for the optimal solution $(x_{\text{opti}}, y_{\text{opti}})$ like a point (pixel) in $RDI_E(n)$, where the intensity of $RDI_E(n)$ reaches (a local) minimum.

Fig. 6(a,b) illustrates the comparison of final results obtained by the basic B/W method and by its halftone extension both applied to the same example, cf. Fig. 4f.

IMAGE PROCESSING SUGGESTIONS FOR ASTRONOMICAL MULTIEXPOSURE
WIDE FIELD PLATES

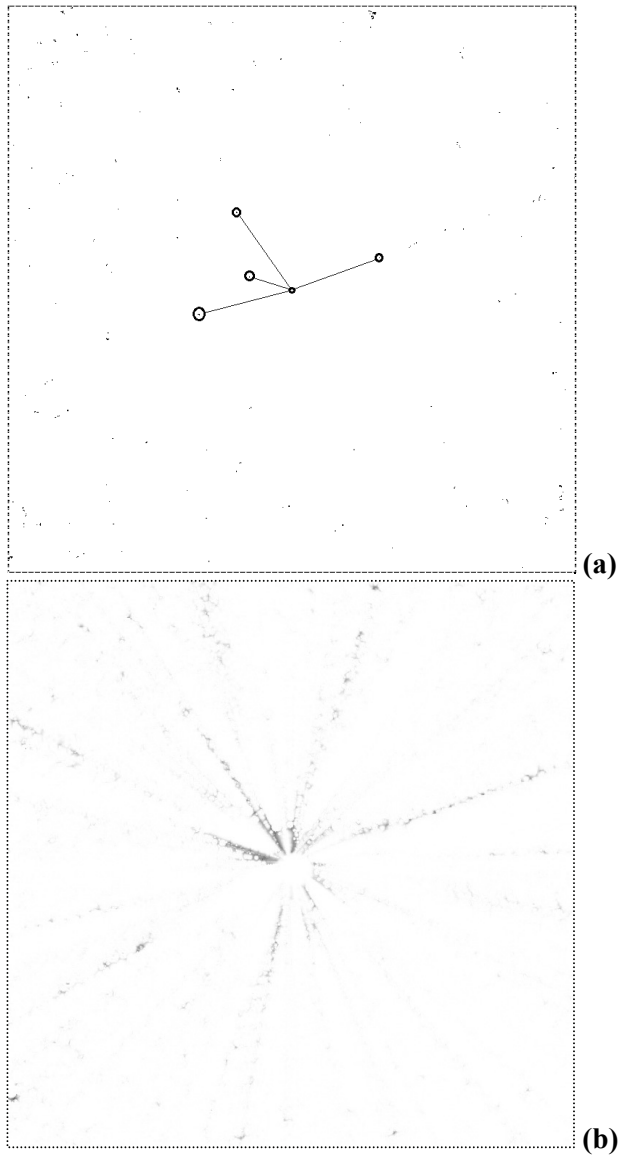


Figure 6: Comparison between of the proposed B/W method and its halftone extension: a) resultant B/W $RDI(6)$ copied from Fig. 4f; and b) corresponding halftone result $RDI_E(6)$. Obviously, the ability to define an optimal choice for the halftone expansion is significantly more flexible.

4. CONCLUSION

The method presented here, algorithm and program are developed for evaluation of optimal design parameters (slope and reference distances) of the chains in the astronomical MEWFP method.

The proposed method is described for linear chains structure and is generalized for synthesis of arbitrary (non-linear) chains structure. Various modifications of the basic B/W method are discussed including its halftone expansion, leading to an optimal compromise in no-decision cases by the basic method.

The primary purpose of this development is for a posteriori evaluation of the structural quality of (images of) astronomical archives of MEWFP type. Evaluating whether (and how much) the quality is exacerbated by overlapping stellar copies, allows improvements in demand for really variable stellar objects in archival (available, known) MEWFP. And this is considered important because of the large number of known and/or available MEWFP in astronomical observatories archives around the world.

References

- Aniol, R., Duerbeck, H. W., Seitter, W. C., Tsvetkov, M. K.: 1990, "An automatic search for flare stars in southern stellar aggregates of different ages", In *Flare Stars in Star Clusters, Associations and Solar Vicinity*, eds. L.V. Mirzoyan, B.R. Pettersen and M.K. Tsvetkov, IAU Symp. 137, Kluwer Acad. Publish., Dordrecht-Boston-London, 85-94.
- Bertin, E., Arnouts, S.: 1996, "SExtractor: Software for source extraction", *Astron. Astrophys. Suppl. Series*, **117**, 393-404.
- Dimov, D., Dimov, A.: 2010, "Data Driven Approach to Binarization of Astronomical Images", In: *Proceedings of CompSysTech'10*, June 17-18, 2010, Sofia, Bulgaria, Mini-Symposium on Astroinformatics, ACM International Conf. Proceeding Series, **471**, ACM PRESS, New York, 478-484.
- Dimov, D., Tsvetkova, K., Tsvetkov, M., Kolev, A., Kounchev, O.: 2012, "Hough Transform Approach to Flare Stars Identification in Multi-Exposure Plates Images", *Serdica J. Computing*, **6**, 121-148.
- Sonka M., Hlavac, V., Boyle, R.: 1998, *Image Processing, Analysis, and Machine Vision*, 2-d edition, Brooks/Cole Publishing Co., CA.
- Tsvetkova, K. P.: 2012, "Astroinformatics for the flare stars in stellar clusters and associations", *Proceedings of the VII Bulgarian-Serbian Astronomical Conference (VII BSAC)*, Chepelare, Bulgaria, June 1-4, 2010, Eds. M. K. Tsvetkov, M. S. Dimitrijević, K. Tsvetkova, O. Kounchev, Ž. Mijajlović, Publ. Astron. Soc. "Rudjer Bošković", **11**, 127-139.
- Winterberg, J., Nolte, M., Seitter, W. C., Duerbeck, H. W., Tsvetkov, M. K., Tsvetkova, K. P.: 1995, "Flares and Flashes", *Proc. IAU Coll. 151*, eds. J. Greiner, H.W. Duerbeck and R.E. Gershberg, Springer Verlag, Berlin, 119.

MODELING OF MOLECULAR CLOUDS WITH FORMATION OF PRESTELLAR CORES

SAVA DONKOV¹, ORLIN STANCHEV², TODOR VELTCHEV²

¹*Department of Applied Physics, Technical University*

E-mail: savadd@tu-sofia.bg

²*Department of Astronomy, Faculty of Physics, University of Sofia*

E-mail: o.stanchev@phys.uni-sofia.bg, eirene@phys.uni-sofia.bg

Abstract. We develop a statistical approach for description of dense structures (cores) in molecular clouds that might be progenitors of stars. Our basic assumptions are a core mass-density relationship and a power-law density distribution of these objects as testified by numerical simulations and observations. The core mass function (CMF) was derived and its slope in the high-mass regime was obtained analytically. Comparisons with observational CMFs in several Galactic clouds are briefly presented.

1. INTRODUCTION

Molecular clouds (MCs) are the typical regions of star formation in galaxies. Recent high-resolution observational studies in the Milky Way reveal that MCs exhibit an extremely complex, clumpy and often filamentary structure (e.g. André et al. 2010, Menseh'chikov et al. 2010), with column and spatial densities varying by many orders of magnitude. The detected large non-thermal linewidths which scale with the size of the cloud or of its larger substructures (e.g. Larson 1981, Solomon et al. 1987, Bolatto et al. 2008) have been interpreted as indicators of the presence of supersonic turbulence. Numerous works in the last two decades have demonstrated that this supersonic turbulence is among the primary physical agents regulating the birth of stars. It creates a complex network of interacting shocks, where dense cores form at the stagnation points of convergent flows. Thus, although at large scales turbulence can support MCs against contraction, at small scales it can provoke local collapse of the emerging prestellar cores. Hence, the timescale and efficiency of a protostar formation depend strongly on the wavelength and strength of turbulent driving source (Klessen, Heitsch & Mac Low 2000, Krumholz & McKee 2005).

An important structural parameter in analytical and semi-analytical models of star formation in MCs (e.g. Padoan & Nordlund 2002, Hennebelle & Chabrier 2009, Veltchev, Klessen & Clark 2011) is the probability density function (ρ -PDF), which gives the probability to measure a given density ρ in a cloud volume dV . As demonstrated from many numerical simulations, its shape is approximately lognormal in

isothermal, turbulent media that are not significantly affected by the self-gravity (e.g. Vázquez-Semadeni 1994, Padoan, Nordlund & Jones 1997, Ostriker, Gammie & Stone 1999, Federrath, Klessen & Schmidt 2008). Its lognormality should correspond to the same feature of the observed probability distributions of the *column density* N (N -PDFs) in MCs, due to the correlation between the local values of ρ along a single line of sight (Vázquez-Semadeni & García, 2001).

On the other hand, it has been argued that the PDF displays scale-dependent features and/or its shape evolves significantly in time (Federrath, Klessen & Schmidt 2008, Pineda *et al.* 2010). The lognormality is typical in the low-density, predominantly turbulent regime, whereas at higher column densities a power-law tail is emerging. Such high-density power-law (PL) tail is a characteristic feature of N -PDFs in evolved MCs where star formation processes already occur or just start (Kainulainen *et al.* 2009, Froebrich & Rowles 2010). That is confirmed as well from analysis of numerical simulations of clouds dominated by gravity (Ballesteros-Paredes *et al.* 2011). A consistent theory of cloud structure must take into account the characteristics sketched above. Probing the N - and ρ -PDFs can be used to set up constraints to analytical star formation theories.

In this work a statistical approach is suggested to derive the mass function of high-density (prestellar) cores that are possible progenitors of stars. Our starting point is a description of the PL tail of the ρ -PDF that is representative for the MC regions populated by these objects.

2. STATISTICAL DESCRIPTION OF DENSE CORES

2. 1. DESCRIPTION OF THE HIGH-DENSITY POWER-LAW TAIL OF THE PDF

Kritsuk, Norman & Wagner (2011) showed that the ρ -PDF evolves from purely log-normal shape to a combination of a lognormal ‘hat’ and a PL tail. Schematic representation of this distribution is given in Fig. 1. We use a standard designation of the logarithmic normalized density: $s \equiv \lg(\rho/\rho_0)$, where ρ_0 is a normalization unit. Parameters of the PL tail are the lower ($s_{\text{low}} \equiv \lg(\rho_1/\rho_0)$) and the upper limit ($s_{\text{up}} \equiv \lg(\rho_2/\rho_0)$) of the high-density range and its slope q . Thus, the PL tail is described by:

$$dP_s = A_s 10^{qs} ds = A_s \left(\frac{\rho}{\rho_0}\right)^q d\lg\left(\frac{\rho}{\rho_0}\right), \quad (1)$$

where the coefficient $A_s = (q \ln 10)/(10^{qs_{\text{up}}} - 10^{qs_{\text{low}}})$ is obtained from the requirement $\int_{s_{\text{low}}}^{s_{\text{up}}} dP_s = 1$.

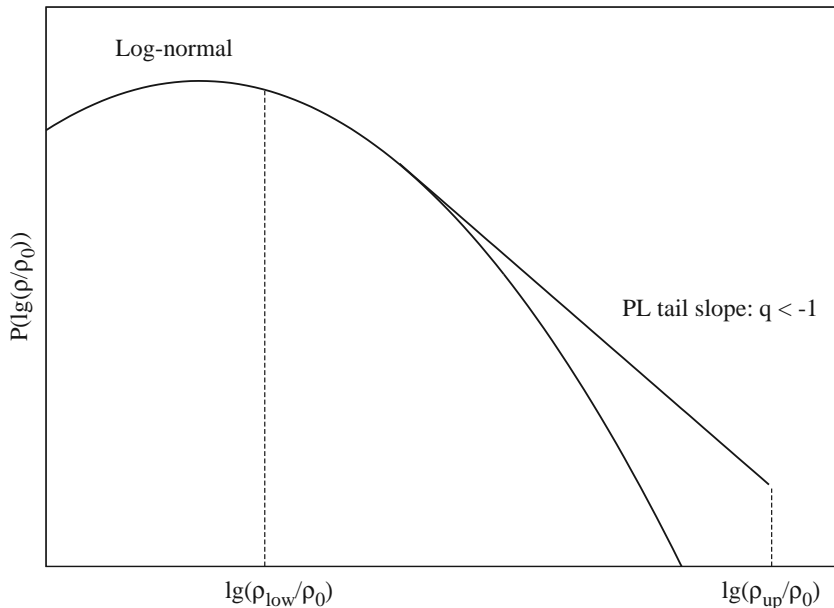


Figure 1: Schematic representation of the ρ -PDF as a combination of a lognormal function with a power-law tail in the high-density part.

2. 2. CORE MASS-DENSITY RELATIONSHIP

In observational studies, the internal structure of MCs is usually described by a sample of discrete condensations, delineated through different procedures and labelled ‘clumps’ or ‘cores’. In our approach, the set of individual clumps in a considered volume is represented by an ensemble of statistical, not individual objects as the physical characteristics of both groups obey the same statistical relations (e.g. size-mass relation, density distribution). Then the ρ -PDF corresponds to the density distribution of statistical clumps. Those with densities in the range of the PL tail are dense cores and hereafter we label them just “cores” for simplicity.

Our basic physical assumption is the existence of a core mass-density relationship:

$$\lg\left(\frac{\rho}{\rho_0}\right) = x \lg\left(\frac{m}{m_0}\right) \quad (2)$$

where m_0 is an arbitrary unit of normalization and the power-law index x is *negative* and assumed to be fixed within the whole PL tail (Lombardi, Alves & Lada, 201). Further we adopt the natural presupposition about a statistical relation between core masses m , densities ρ and sizes l ,

$$\frac{m}{m_0} = \frac{\rho}{\rho_0} \cdot \left(\frac{l}{l_0}\right)^3, \quad (3)$$

and obtain by use of Eq. 2 core size-density and size-mass (with size normalization unit l_0) as well:

$$\lg\left(\frac{\rho}{\rho_0}\right) = \frac{3x}{1-x} \lg\left(\frac{l}{l_0}\right), \quad (4)$$

$$\lg\left(\frac{m}{m_0}\right) = \frac{3}{1-x} \lg\left(\frac{l}{l_0}\right). \quad (5)$$

Taking into account the one-to-one correspondence between the core quantities ρ , m and l , one derives from Eqs. 1, 2 and 4 the probability distributions of core masses and sizes:

$$dP(m) = A_m \left(\frac{m}{m_0}\right)^{qx} d\lg\left(\frac{m}{m_0}\right), \quad (6)$$

$$dP(l) = A_l \left(\frac{l}{l_0}\right)^{q\frac{3x}{1-x}} d\lg\left(\frac{l}{l_0}\right), \quad (7)$$

where A_m and A_l are calculated from the normalization of probability measures. Note as well the obvious relation: $dP_s = dP(m) = dP(l)$. It defines the distributions of core masses and sizes in the PL tail which we label hereafter m -PDF and l -PDF, respectively.

It seems natural to choose the mean density of the cloud $\langle\rho\rangle$ and a fixed fraction κ of its size L as normalization units (Veltchev, Klessen & Clark, 2011):

$$\rho_0 \equiv \langle\rho\rangle, \quad l_0 \equiv \kappa L \quad (8)$$

2. 3. AVERAGED CORE QUANTITIES

The average core density could be calculated in two alternative ways:

Arithmetic average:

$$\left(\frac{\rho}{\rho_0}\right)_{\text{ar}} \equiv A_s \int_{\rho_1}^{\rho_2} \left(\frac{\rho}{\rho_0}\right) \cdot \left(\frac{\rho}{\rho_0}\right)^q d\lg\left(\frac{\rho}{\rho_0}\right) = \left(\frac{q}{q+1}\right) \left(\frac{\rho_1}{\rho_0}\right) \left[\frac{(\rho_2/\rho_1)^{q+1} - 1}{(\rho_2/\rho_1)^q - 1}\right], \quad (9)$$

Logarithmic average: it is a generalization of the geometric average in case of continuous density distribution and is defined as:

$$\begin{aligned} \left(\frac{\rho}{\rho_0}\right)_{\text{lg}} &\equiv 10^{\overline{\lg(\rho/\rho_0)}}, \quad \text{where} \quad \overline{\lg\left(\frac{\rho}{\rho_0}\right)} = A_s \int_{\rho_1}^{\rho_2} \lg\left(\frac{\rho}{\rho_0}\right) \cdot \left(\frac{\rho}{\rho_0}\right)^q d\lg\left(\frac{\rho}{\rho_0}\right) \implies \\ \left(\frac{\rho}{\rho_0}\right)_{\text{lg}} &= \exp\left(-\frac{1}{q}\right) \cdot \left(\frac{\rho_2}{\rho_0}\right)^{\frac{(\rho_2/\rho_0)^q}{(\rho_2/\rho_0)^q - (\rho_1/\rho_0)^q}} \left(\frac{\rho_1}{\rho_0}\right)^{-\frac{(\rho_1/\rho_0)^q}{(\rho_2/\rho_0)^q - (\rho_1/\rho_0)^q}}. \end{aligned} \quad (10)$$

Analogically, one can define and calculate arithmetic and logarithmic average of core mass and size by use of Eqs. 6 and 7. It is important to note that the approach of logarithmic averaging leads to a physically natural relationship:

$$\left(\frac{m}{m_0}\right)_{\text{lg}} = \left(\frac{\rho}{\rho_0}\right)_{\text{lg}} \cdot \left(\frac{l}{l_0}\right)_{\text{lg}}^3. \quad (11)$$

The transformation from dimensionless to physical quantities is independent on the averaging approach: $\bar{\rho} = \rho_0 \overline{(\rho/\rho_0)}$, $\bar{m} = m_0 \overline{(m/m_0)}$, $\bar{l} = l_0 \overline{(l/l_0)}$. Recalling Eq. 3, one obtains:

$$\frac{m}{\rho \bar{l}^3} = \frac{m_0}{\rho_0 l_0^3} = \frac{\bar{m}}{\bar{\rho} \bar{l}^3}. \quad (12)$$

We point out that the second sign of equality in this equation holds only in case of logarithmic averaging (cf. Eq. 11).

2. 4. RELATION BETWEEN THE NORMALIZATION UNITS AND THE FORMULA FOR TOTAL NUMBER OF CORES

The core mass is a fundamental non-observable quantity and it is crucial to avoid arbitrariness of choice of its normalization unit. Therefore we derive a relation between ρ_0 , l_0 and m_0 using the requirements for volume and mass conservation considering the whole PL tail. Its total volume V_{tot} is calculated as follows:

$$V_{\text{tot}} = \sum_{l-PDF} l^3 N_l = l_0^3 N_{\text{tot}} \sum_{l-PDF} \left(\frac{l}{l_0}\right)^3 \frac{N_l}{N_{\text{tot}}} = l_0^3 N_{\text{tot}} \int_{l_1}^{l_2} \left(\frac{l}{l_0}\right)^3 dP(l),$$

where N_l is the number of cores with size l and N_{tot} is a measure of the total number of cores. The limits l_1 and l_2 correspond to the density limits ρ_1 and ρ_2 according to Eq. 4 and one obtains after integration:

$$V_{\text{tot}} = l_0^3 N_{\text{tot}} \cdot \frac{\frac{qx}{1-x}}{\frac{qx}{1-x} + 1} \left[\frac{(\rho_2/\rho_0)^{q+\frac{1-x}{x}} - (\rho_1/\rho_0)^{q+\frac{1-x}{x}}}{(\rho_2/\rho_0)^q - (\rho_1/\rho_0)^q} \right] \equiv l_0^3 N_{\text{tot}} \cdot Q(q, x). \quad (13)$$

Analogically, the total mass of the cores is calculated through:

$$M_{\text{tot}} = \sum_{m-PDF} m N_m = \dots = m_0 N_{\text{tot}} \cdot \frac{qx}{qx + 1} \left[\frac{(\rho_2/\rho_0)^{q+\frac{1}{x}} - (\rho_1/\rho_0)^{q+\frac{1}{x}}}{(\rho_2/\rho_0)^q - (\rho_1/\rho_0)^q} \right]. \quad (14)$$

In view of $M_{\text{tot}} = \bar{\rho} \cdot V_{\text{tot}} = \rho_0 \cdot \overline{(\rho/\rho_0)} \cdot V_{\text{tot}}$, we get the relation between the normalization units:

$$\frac{m_0}{\rho_0 l_0^3} = \frac{\rho_0 \overline{(\rho/\rho_0)}}{\rho_1 \overline{(\rho_1/\rho_0)}} \frac{qx + 1}{(q-1)x + 1} \cdot \left[\frac{(\rho_2/\rho_1)^{q+\frac{1-x}{x}} - 1}{(\rho_2/\rho_1)^{q+\frac{1}{x}} - 1} \right] \quad (15)$$

Referring to Eq. 13 and the relation: $r \rho_0 V = r M = M_{\text{tot}} = \rho_0 \cdot \overline{(\rho/\rho_0)} \cdot V_{\text{tot}}$, where M and V are the mass and volume of the whole cloud, we obtain the formula for total core number as follows:

$$N_{\text{tot}} = \frac{r}{\kappa^3} \left[\overline{\left(\frac{\rho}{\rho_0}\right)} Q(q, x) \right]^{-1}, \quad (16)$$

where the filling factor r accounts for the mass fraction of cores within the whole cloud and the density average could be arithmetic as well logarithmic.

3. DERIVATION OF THE CORE MASS FUNCTION

3. 1. TOTAL NUMBER OF CORES AND SCALES DEFINED BY CHOSEN DENSITY THRESHOLD

We consider an MC as a hierarchical set of spatial scales. They are defined as effective sizes of subregions (or a set of subregions) in the cloud delineated through chosen density thresholds. Thus, a fixed density ρ' corresponds to a scale which contains the mass of the whole PL-tail substructure with densities in the range $\rho' \leq \rho \leq \rho_2$. Since the mass-density power-law index x is negative, the larger the density of a core the lower its mass. To derive the cumulative CMF correctly, one must take into account the contribution of each spatial scale in the hierarchical structure defined by threshold ρ' . The latter is a product of the total number of scales $N_{scales}(\rho')$ contained in the volume over the threshold ρ' and the total number of cores $N_{tot}(\rho')$ at each scale. Repeating the procedure in the previous sections for a subsection of the PL tail $[\rho', \rho_2]$, one obtains $N_{tot}(\rho')$ according to Eq. 16 while r , $\overline{(\rho/\rho_0)}$ and $Q(q, x)$ are functions of the given ρ' (instead of ρ_1):

$$N_{tot}(\rho') = \frac{r(\rho')}{\kappa^3} \left[\overline{\left(\frac{\rho}{\rho_0}\right)}(\rho') \cdot Q(q, x, \rho') \right]^{-1}. \quad (17)$$

Letting $\rho' \ll \rho_2$, it follows in both approaches of averaging that $\overline{(\rho/\rho_0)}(\rho') \propto (\rho'/\rho_0)$ (Eqs. 9 and 10) and $Q(q, x, \rho') \propto (\rho'/\rho_0)^{(1-x)/x}$ (Eq. 13; in this context it is important to mention that simulations predict $q \leq -1.5$). In this case $N_{tot}(\rho') \propto (r(\rho')/\kappa^3) \cdot (\rho'/\rho_0)^{-1/x}$.

The total number of scales $N_{scales}(\rho')$ is easily calculated from the filling factor r and the requirement of mass conservation at each density threshold ρ' . The total mass of cores over the given threshold ρ' in MC with mass M and volume V is $\rho_0 \cdot \overline{(\rho/\rho_0)}(\rho') \cdot V_{tot}(\rho') = M_{tot}(\rho') = r(\rho')M = r(\rho')\rho_0V$ whence

$$V_{tot}(\rho') = r(\rho') \cdot \left[\overline{\left(\frac{\rho}{\rho_0}\right)}(\rho') \right]^{-1} V$$

Obviously $r\rho_0V = M_{tot} = N_{scales}(\rho') \cdot M_{tot}(\rho') = N_{scales}(\rho') \cdot \rho_0 \cdot \overline{(\rho/\rho_0)}(\rho') \cdot V_{tot}(\rho')$ and after simple transformations one gets finally:

$$N_{scales}(\rho') = \frac{rV}{\overline{\left(\frac{\rho}{\rho_0}\right)}(\rho') \cdot V_{tot}(\rho')} = \dots = \frac{r}{r(\rho')} \quad (18)$$

3. 2. THE CUMULATIVE CMF

The cumulative CMF $\mathcal{N}(m')$ is derived by counting all cores with masses in the range $m' \geq m \geq m_2$, corresponding to densities $\rho' \leq \rho \leq \rho_2$. In our case, one has to multiply the total numbers of cores and scales over threshold $\rho' = \rho_0(m'/m_0)^x$ (Eqs. 17 and 18):

$$\mathcal{N}(m') = \frac{r}{\kappa^3} \left[\overline{\left(\frac{\rho}{\rho_0} \right)}(\rho') \cdot Q(q, x, \rho') \right]^{-1} \propto \frac{r}{\kappa^3} \left(\frac{\rho'}{\rho_0} \right)^{-\frac{1}{x}} = \frac{r}{\kappa^3} \left(\frac{m'}{m_0} \right)^{-1} \quad (19)$$

$(\rho' \ll \rho_2)$

Note that the slope Γ of a power-law differential CMF is exactly the same of its corresponding cumulative function. In other words, we derived a differential CMF with slope -1 , typical for fractal structures (Elmegreen 1997).

In view of the high densities in the PL tail, we may assume that most (if not all) cores are gravitationally unstable and contract in timescales given by the free-fall time $\tau_{\text{ff}} \propto \rho^{-1/2}$. Then a time-weighted CMF would be more representative for results one can expect from observations. Such time weighting can be done introducing a weighting factor of each scale proportional to $\tau_{\text{ff}}^{-1} \propto \overline{(\rho'/\rho_0)}^{1/2} \propto (m'/m_0)^{x/2}$. Then the time-weighted cumulative CMF will have a slope modified by addend $x/2$:

$$\mathcal{N}_\tau(m') \propto \frac{r}{\kappa^3} \left(\frac{\rho'}{\rho_0} \right)^{-\frac{1}{x} + \frac{1}{2}} = \frac{r}{\kappa^3} \left(\frac{m'}{m_0} \right)^{-1 + \frac{x}{2}} \quad (20)$$

$(\rho' \ll \rho_2)$

4. DISCUSSION

Most recent studies dedicated to the CMF show that its high-mass slope is close or identical to that of the initial stellar mass function $\Gamma = -1.35$ (Salpeter 1955). In Table 1 we illustrate the predictive capability of our model in comparison with CMFs, derived in some observational works and from simulations. The derived slopes and their variations could be explained by variations of the core mass-density power-law index in the range $0 \gtrsim x \gtrsim -0.7$ (with a single exception with an extreme value) which is consistent with the typical values of this quantity for the inner parts of several MCs as derived by Donkov, Veltchev & Klessen (2011) and testified by comparison with the observational study of Lombardi, Alves & Lada (2010).

These preliminary results are stimulating to develop further our model, including results from recent numerical simulations and/or analytical estimates of the time evolution of the ρ -PDF (Girichidis et al. 2012).

Table 1: Slopes of CMFs derived from various authors in comparison with our model predictions.

Galactic MC	Ref.	Note	Slope of the CMF	x
Pipe	1		-1.35	-0.7
Orion	2		-1.35	-0.7
Orion A	3		-1.3 ± 0.3	-0.6 ± -0.6
Perseus	4	(a) lognormal	$-1. \pm 0.1$	~ 0
		(b) time-weighted	-2.15 ± 0.08	~ -2.3
Ophiuchus	5	time-weighted	-1.35	-0.7
Perseus, Serpens, Ophiuchus	6		-1.3 ± 0.4	-0.6 ± 0.8
Simulations (PP, PPV)	7		$-1.15 \leq \Gamma \leq -1.35$	$-0.3 \geq x \geq -0.7$

[1] Alves, Lombardi & Lada 2007, [2] Nutter & Ward-Thompson 2007, [3] Ikeda & Kitamura 2009, [4] Curtis & Richer 2010, [5] André et al. 2007, [6] Enoch et al. 2008, [7] Smith, Clark & Bonnell 2008

Acknowledgement: T.V. acknowledges partial support by the *Deutsche Forschungsgemeinschaft* (DFG) under grant KL 1358/15-1.

References

- Alves, J., Lombardi, M., & Lada, C.: 2007, The mass function of dense molecular cores and the origin of the IMF, *A&A*, **462**, L17.
- André, P., Belloche, A., Motte, F., & Peretto, N.: 2007, The initial conditions of star formation in the Ophiuchus main cloud: Kinematics of the protocluster condensations *A&A*, **472**, 519.
- André, Ph., Men'shchikov, A., Bontemps, S., et al.: 2010, From filamentary clouds to prestellar cores to the stellar IMF: Initial highlights from the HERSCHEL Gould Belt Survey, *A&A*, **518**, L102.
- Ballesteros-Paredes, J., Vázquez-Semadeni, E., Gazol, A., Hartmann, L., Heitsch, F., Colín, P.: 2011, Gravity or turbulence? - II. Evolving column density probability distribution functions in molecular clouds, *MNRAS*, **416**, 1436.
- Bolatto, A. D., Leroy, A. K., Rosolowsky, E., Walter, F., & Blitz, L.: 2008, The Resolved Properties of Extragalactic Giant Molecular Clouds, *ApJ*, **688**, 9.
- Curtis, E., & Richer, J.: 2010, The properties of SCUBA cores in the Perseus molecular cloud: the bias of clump-finding algorithms, *MNRAS*, **402**, 603.
- Donkov, S., Veltchev, T., & Klessen, R. S.: 2011, Mass-density relationship in molecular cloud clumps, *MNRAS*, **418**, 916.
- Elmegreen, B. G.: 1997, The Initial Stellar Mass Function from Random Sampling in a Turbulent Fractal Cloud *ApJ*, **486**, 944.
- Enoch, M., Evans, N., Sargent, A., Glenn, J., Rosolowsky, E., Myers, P.: 2008, The Mass Distribution and Lifetime of Prestellar Cores in Perseus, Serpens, and Ophiuchus, *ApJ*, **684**, 1240.
- Federrath, C., Klessen, R. S., & Schmidt, W.: 2008, The Density Probability Distribution in Compressible Isothermal Turbulence: Solenoidal versus Compressive Forcing, *ApJ*, **688**, L79.

- Froebrich, D., & Rowles, J.: 2010, The structure of molecular clouds - II. Column density and mass distributions, *MNRAS*, **406**, 1350.
- Girichidis, P., Konstandin, L., Klessen, R. S., & Whitworth, A.: 2012 (in preparation)
- Goodman, A. A., Pineda, J. E., & Schnee, S. L.: 2009, The "True" Column Density Distribution in Star-Forming Molecular Clouds, *ApJ*, **692**, 91.
- Hennebelle, P., & Chabrier, G.: 2009, Analytical Theory for the Initial Mass Function. II. Properties of the Flow, *ApJ*, **702**, 1428.
- Ikeda, N., & Kitamura, Y.: 2009, A $C^{18}O$ Study of the Origin of the Power-Law Nature in the Initial Mass Function, *ApJ*, **705**, L95
- Kainulainen, J., Beuther, H., Henning, T., Plume, R.: 2009, Probing the evolution of molecular cloud structure. From quiescence to birth, *A&A*, **508**, L35.
- Klessen, R. S., Heitsch, F., & Mac Low, M.: 2000, Gravitational Collapse in Turbulent Molecular Clouds. I. Gasdynamical Turbulence, *ApJ*, **535**, 887.
- Kritsuk, A., Norman, M., & Wagner, R.: 2011, On the Density Distribution in Star-forming Interstellar Clouds, *ApJ*, **727**, 20.
- Krumholz, M., & McKee, C. F.: 2005, A General Theory of Turbulence-regulated Star Formation, from Spirals to Ultraluminous Infrared Galaxies, *ApJ*, **630**, 250.
- Larson, R.: 1981, Turbulence and star formation in molecular clouds, *MNRAS*, **194**, 809.
- Lombardi, M., Alves, J., & Lada, C.: 2010, Larson's third law and the universality of molecular cloud structure, *A&A*, **519**, 7.
- Men'shchikov, A., André, Ph., Didelon, P., et al.: 2010, Filamentary structures and compact objects in the Aquila and Polaris clouds observed by HERSCHEL, *A&A*, **518**, L103
- Nutter, D., Ward-Thompson, D.: 2007, A SCUBA survey of Orion - the low-mass end of the core mass function, *MNRAS*, **374**, 1413.
- Ostriker, E., Gammie, C., & Stone, J.: 1999, Kinetic and Structural Evolution of Self-gravitating, Magnetized Clouds: 2.5-dimensional Simulations of Decaying Turbulence, *ApJ*, **513**, 259.
- Padoan, P., Nordlund, Å., & Jones, B.: 1997, The universality of the stellar initial mass function, *MNRAS*, **288**, 145.
- Padoan, P., & Nordlund, Å.: 2002, The Stellar Initial Mass Function from Turbulent Fragmentation, *ApJ*, **576**, 870.
- Pineda, J., Goldsmith, P., Chapman, N., et al.: 2010, The Relation Between Gas and Dust in the Taurus Molecular Cloud, *ApJ*, **721**, 686.
- Salpeter, E.: 1955, The Luminosity Function and Stellar Evolution, *ApJ*, **121**, 161.
- Smith, R., Clark, P., & Bonnell, I.: 2008, The structure of molecular clouds and the universality of the clump mass function, *MNRAS*, **391**, 1091.
- Solomon, P. M., Rivolo, A. R., Barrett, J., & Yahil, A.: 1987, Mass, luminosity, and line width relations of Galactic molecular clouds, *ApJ*, **319**, 730.
- Vázquez-Semadeni, E.: 1994, Hierarchical Structure in Nearly Pressureless Flows as a Consequence of Self-similar Statistics, *ApJ*, **423**, 681.
- Vázquez-Semadeni, E., & García, N.: 2001, The Probability Distribution Function of Column Density in Molecular Clouds, *ApJ*, **557**, 727.
- Veltchev, T., Klessen, R., & Clark, P.: 2011, Stellar and substellar initial mass function: a model that implements gravoturbulent fragmentation and accretion, *MNRAS*, **411**, 301.

INHOMOGENEOUS BARYOGENESIS MODEL AND ANTIMATTER IN THE UNIVERSE

DANIELA KIRILOVA, MARIANA PANAYOTOVA

*Institute of Astronomy and National Astronomical Observatory,
Bulgarian Academy of Sciences*

E-mail: dani@astro.bas.bg, mariana@astro.bas.bg

Abstract. Cosmic ray and gamma-ray data at present do not rule out antimatter domains in the Universe, separated at distances bigger than 20 Mpc from us. Hence, it is interesting to explore the possible generation of vast antimatter structures during the early Universe evolution. We discuss an inhomogeneous baryogenesis model, based on a SUSY baryogenesis scenario. We have accounted for the particle creation processes that play an essential role for the correct determination of the final value of the baryon asymmetry, generated in these baryogenesis scenarios. We have explored the dependence of the produced baryon asymmetry on the parameters of the model. It is shown that for a natural range of the parameters' values this model is able to explain the value of the locally observed matter-antimatter asymmetry and also to predict antimatter domains, separated from the matter ones by baryonically empty voids.

1. INTRODUCTION: THE MATTER-ANTIMATTER ASYMMETRY OF THE UNIVERSE

One of the amazing and still unresolved mysteries of our Universe is the strong predominance of matter over antimatter in our surroundings. The baryon asymmetry (BA) in our neighborhood (within radius of 20 Mpc) is indicated by cosmic and gamma rays observations. It is usually defined by β :

$$\beta = \frac{n_B - n_{\bar{B}}}{n_\gamma} \quad (1)$$

and locally is measured to be $\beta \sim \frac{n_B}{n_\gamma} = \eta$, i.e. considerable quantity of antimatter is not observed in our vicinity.

The baryon density η is measured in several different ways, namely: The consistency between theoretically obtained and observationally measured abundances of light elements produced in BBN at $z \sim 10^9$ (Nakamura (PDG) 2010) requires

$$5.1 \times 10^{-10} \leq \eta_{BBN} \leq 6.5 \times 10^{-10} \quad \text{at } 95\% \text{ CL}; \quad (2)$$

Information for η from measurements of Deuterium towards low metallicity quasars combined with BBN data points to (Pettini 2008)

$$\eta_D = 6 \pm 0.3 \times 10^{-10} \quad \text{at } 95\% \text{ CL}; \quad (3)$$

A precise determination of η , provided by measurements of the CMB anisotropy ($z \sim 1000$) by WMAP7 (Larson, et. al. 2011):

$$\eta_{WMAP} = 6.16 \pm 0.16 \times 10^{-10} \quad \text{at } 68\% \text{ CL}. \quad (4)$$

Today we do not yet know the exact baryogenesis mechanism, i.e. different baryogenesis possibilities are studied. We discuss an inhomogeneous baryogenesis model, which has been shown in previous publications to predict a successful coexistence of matter and antimatter domains. Here we explore the possibility for a natural range of model's parameters to explain the value of the locally observed matter-antimatter asymmetry.

2. THE BARYOGENESIS MODEL

We study a scalar condensate baryogenesis model, based on the scalar baryogenesis scenario (SCB) (Dolgov, Kirilova 1991). The model has the following important ingredients:

* *Baryon charge violation at micro distances at the inflationary stage:* The baryon excess is generated at the inflationary stage and contained in a condensate of a complex scalar field φ (squark), which naturally appears in supersymmetric theories. The condensate $\langle \varphi \rangle \neq 0$ is formed during the inflationary period as a result of the rise of quantum fluctuations of φ (Vilenkin, Ford 1982, Linde 1982, Bunch, Davies 1978, Starobinsky 1982). Thus, during inflation a condensate of a baryon charge (stored in $\langle \varphi \rangle$) is developed with a baryon charge density $\sim H_I^3$, where H_I is the Hubble parameter at the inflationary stage.

While B is not conserved at large field amplitude due to the presence of the B nonconserving (BV) self-interaction terms in its potential, at low φ B-violation becomes negligible. At the B conserving stage during the decay of φ , $\varphi \rightarrow q\bar{q}l\gamma$, the baryon charge contained in the field is transferred to quarks and antiquarks. This charge, eventually diluted by some entropy generating processes, gives the observed locally BA.

* *Decrease of field's amplitude due to particle creation:* After inflation φ starts to oscillate around its equilibrium point with a decreasing amplitude due to the Universe expansion and to the particle production by the oscillating scalar field (Dolgov, Kirilova 1990).

* *Unharmonic potential of the field carrying the baryon charge:* The unharmonicity of the potential provides that different amplitudes corresponding to different space points result into different periods. Hence, the initially smooth space dependence transfers into quasiperiodic one (Dolgov, Kirilova 1991).

* *Inflationary expansion of the initially microscopic baryon distribution.* Due to inflationary growth of scales the initially microscopic domains of given baryon sign evolve into astronomically important regions of matter or antimatter.

3. THE EVOLUTION OF THE BARYON CHARGE AFTER INFLATION

In the expanding Universe φ satisfies the equation

$$\ddot{\varphi} - a^{-2}\partial_i^2\varphi + 3H\dot{\varphi} + \frac{1}{4}\Gamma\dot{\varphi} + U'_\varphi = 0, \quad (5)$$

where $a(t)$ is the scale factor and $H = \dot{a}/a$.

In this concrete model the potential was chosen of the form:

$$U(\varphi) = m^2\varphi^2 + \frac{\lambda_1}{2}|\varphi|^4 + \frac{\lambda_2}{4}(\varphi^4 + \varphi^{*4}) + \frac{\lambda_3}{4}|\varphi|^2(\varphi^2 + \varphi^{*2}) \quad (6)$$

The mass is assumed small in comparison with the Hubble constant during inflation $m \ll H_I$. In supersymmetric theories the constants λ_i are of the order of the gauge coupling constant α . We have studied the natural range of m : $10^2 \div 10^4$ GeV. The initial values for the field variables were taken to be $\varphi_o^{max} \sim H_I\lambda^{-1/4}$ and $\dot{\varphi}_o = (H_I)^2$.

We have assumed a predominance of the inflanton density: $\rho_\psi \gg \rho_\varphi$, i.e. the Hubble parameter was $H = 2/(3t)$.

Fast oscillations of φ after inflation result in particle creation due to the coupling of the scalar field to fermions $g\varphi\bar{f}_1f_2$, where $g^2/4\pi = \alpha_{SUSY}$. The term $\Gamma\dot{\varphi}$ in the equations of motion explicitly accounts for the damping of φ as a result of particle creation processes (Chizhov, Kirilova 1996). The amplitude of φ is damped as $\varphi \rightarrow \varphi \exp(-\Gamma t/4)$ and the baryon charge, contained in the φ , is exponentially reduced during BV stage, i.e. while φ is large.

It is known that if the production rate is a decreasing function of time the damping process may be slow enough for the baryon charge contained in φ to survive until the B -conservation epoch t_b (Dolgov, Kirilova 1991). Then the baryon charge of φ due to its decays is transferred to quarks and antiquarks and thus the observed excess of matter is produced.

4. RESULTS OF THE NUMERICAL ANALYSIS

For different sets of studied parameter values of the model λ_i , α , m and H_I , we have provided a numerical analysis of the scalar field φ evolution and the evolution of the baryon excess $B(t)$ for the period after the inflationary stage until the BC epoch when φ decays, in the energy range $10^{12} \div 100$ GeV. We have used Runge-Kutta 4th order method with step 10^{-6} to solve the system of ordinary differential equations representing the equation of motion for the real and the imaginary part of $\varphi(t)$. The ranges of model's parameters studied are: $\lambda = 10^{-2} \div 5 \times 10^{-2}$, $\alpha = 10^{-3} \div 5 \times 10^{-2}$, $H = 10^7 \div 10^{12}$ GeV, $m = 100 \div 1000$ GeV.

In our analysis the particle creation processes were accounted in two different ways - semi-analytically, using $\Gamma = \alpha\Omega$, where $\Omega \sim \lambda^{1/2}\varphi$ and $\alpha = g^2/4\pi$ and numerically, calculating Ω at each step as $\Omega = 2\pi/T$, where T is the period of the field oscillations. As it was found in previous publications (Dolgov, Kirilova 1991, Kirilova, Panayotova 2006), the account of particle creation processes strongly reduces the baryon charge contained in the condensate. The precise numerical account of the particle creation in

this analysis points to stronger and earlier reduction of the generated baryon excess (see Fig. 1) in comparison with the case of analytical account. We have found that the values of the final B , obtained with numerical and semi-analytical account of particle creation, may differ by up to two orders of magnitude.

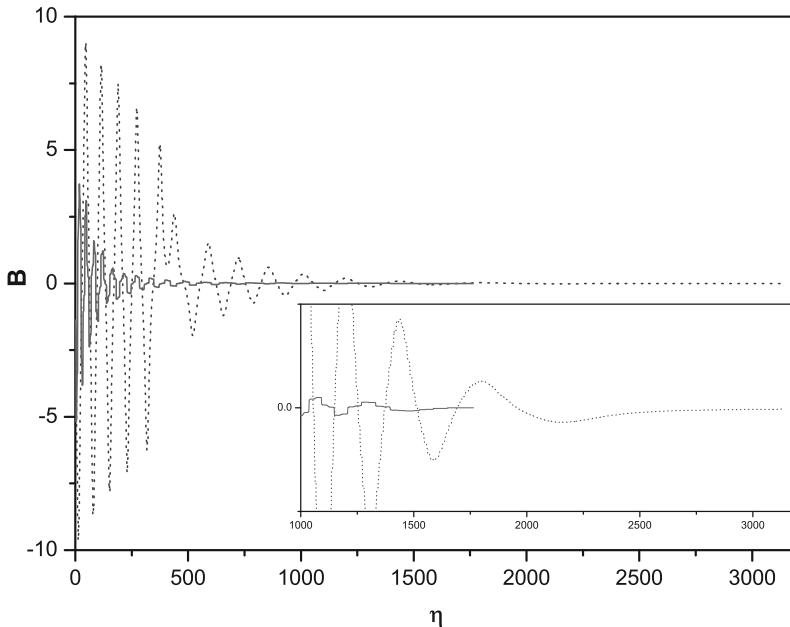


Figure 1: The evolution of the baryon charge $B(\eta)$ for $\lambda_1 = 5 \times 10^{-2}$, $\lambda_2 = \lambda_3 = 10^{-3}$, $\alpha = 10^{-2}$, $H = 10^{10} GeV$, $m = 350 GeV$, $\varphi_o = H_I \lambda^{-1/4}$ and $\dot{\varphi}_o = H_I^2$. The case of particle creation processes accounted for analytically is presented by the dotted curve and the case of numerical account for the particle creation is given by the solid curve.

We have studied the dependence of the generated baryon excess on different parameters of the model. Due to the oscillatory character of B , the generated BA is very sensitive both to small shifts of the model's parameters and to numerical methods used. This observation is in accordance with the results of other surveys of similar models (Kirilova, Valchanov 2005). Nevertheless, it is possible to determine the main trend of the behavior of the final BA on the parameters values.

The next figure (Fig. 2) presents the dependence of the baryon charge, at the BC conserving epoch, on the mass of the condensate. The numerical study confirms the expected dependence, namely, the produced baryon charge decreases with m increase. This can be easily understood having in mind that the longer φ decays till BC epoch the smaller the charge, that remains stored in it. The time of its decay is proportional to $\sim m^{-1}$.

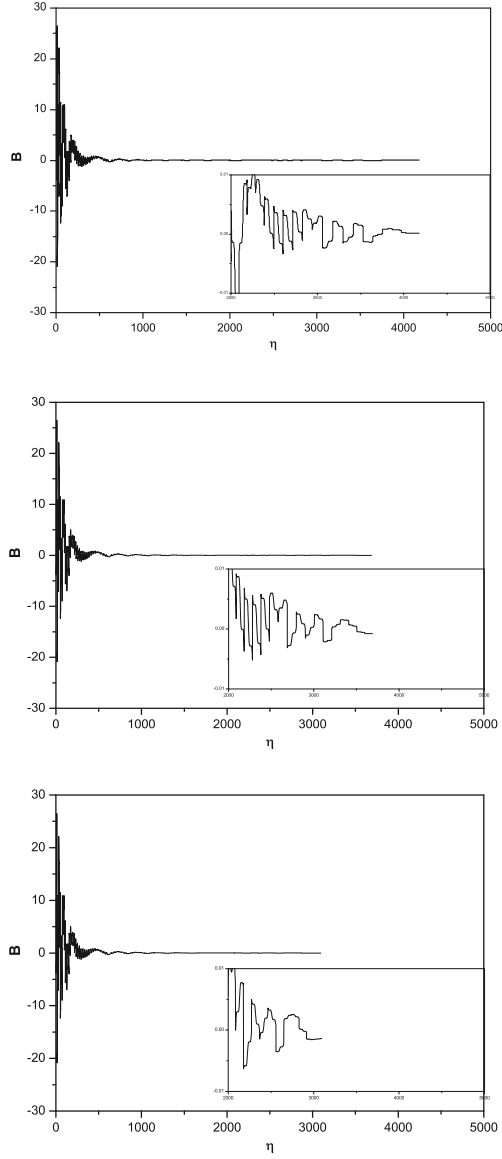


Figure 2: The evolution of the baryon charge $B(\eta)$ for $\lambda_1 = 10^{-2}$, $\lambda_2 = \lambda_3 = 10^{-3}$, $\alpha = 10^{-2}$, $H = 10^{11} \text{ GeV}$, $\varphi_o = H_I \lambda^{-1/4}$ and $\dot{\varphi}_o = H_I^2$. The upper curve is for $m = 350 \text{ GeV}$, the middle is for $m = 500 \text{ GeV}$ and the lower - for $m = 800 \text{ GeV}$. The particle creation processes are accounted for numerically.

The last figure (Fig. 3) presents the dependence of the generated baryon charge on the value of H_I . The numerical study shows that the produced baryon charge decreases when increasing H_I . Qualitatively, this dependence is an expected result because the initial value of φ is proportional to H_I and on the other hand particle creation is proportional to φ , $\Gamma \sim \Omega \sim \varphi$.

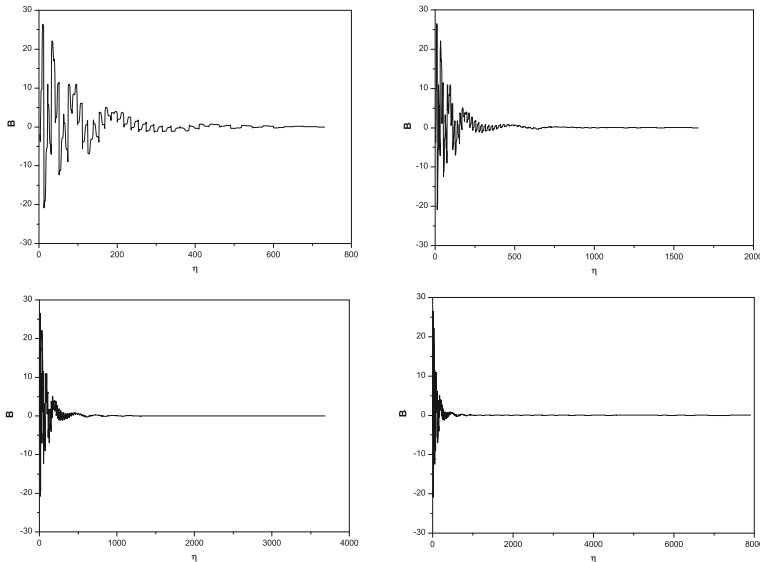


Figure 3: The evolution of the baryon charge $B(\eta)$ for $\lambda_1 = 10^{-2}$, $\lambda_2 = \lambda_3 = 10^{-3}$, $\alpha = 10^{-2}$, $m = 500\text{GeV}$, $\varphi_o = H_I \lambda^{-1/4}$ and $\dot{\varphi}_o = H_I^2$. The upper left curve corresponds to $H = 10^9\text{GeV}$, the upper right curve to $H = 10^{10}\text{GeV}$, the lower left curve to $H = 10^{11}\text{GeV}$ and the lower right curve to $H = 10^{12}\text{GeV}$. The particle creation processes are accounted for numerically.

This baryogenesis model is interesting also because it naturally predicts safely separated domains of matter and antimatter, discussed shortly in the next section.

5. THE PREDICTED ANTIMATTER DOMAINS

The preliminary results of our analysis of the evolution of the spacial distribution of the field shows that the initial natural monotonic distribution of the field due to the unharmonicity of its potential transfers into quasiperiodic distribution. Thus, an initially baryon excess region results into regions with baryon excess and such of baryon underdensities. This result is in accordance with similar previous surveys (Kirilova, Chizhov 1996, 2000). For a natural range of the model's parameters this model is able to predict astronomically interesting vast antimatter domains, separated from the matter ones by baryonically empty voids, as discussed in (Kirilova, Panayotova, Valchanov 2002, Kirilova 2003).

6. CONCLUSIONS

Within a scalar condensate baryogenesis model we have investigated the dependence of the baryon charge evolution and its final value on the model's parameters. Provided that correct account for particle creation processes is made, this model is able to provide the generation of the observed baryon asymmetry for a natural initial conditions. Besides, the model is capable to provide a natural separation between matter and antimatter regions, eventually present in the Universe.

The results of this analysis may be useful for construction of realistic baryogenesis models. Moreover, from the observed value of the baryon asymmetry it is possible to put cosmological constraints on the SUSY parameters within a concrete inflationary scenario, or/ and point to the preferable inflationary model.

1Acknowledgements. The authors thank the organizers for the financial support of their participation into the Conference and for the good organization and the pleasant atmosphere of the meeting.

References

- Affleck, I., Dine, M.: 1985, *Nucl. Phys.*, **B249**, 361.
 Bunch, T., Davies, P.: 1978, *Proc. Roy. Soc.*, **A360**, 117.
 Dolgov , A., Kirilova , D.: 1991, *J. Moscow Phys. Soc.*, **1**, 217.
 Dolgov , A., Kirilova , D.: 1990, *Sov.J.Nucl.Phys.*, **51**, 172.
 Kirilova, D., Chizhov, M.: 1996, *AATr*, **10**, 69.
 Kirilova, D., Chizhov, M.: 2000, *MNRAS*, **314**, 256.
 Kirilova, D., Panayotova, M., Valchanov, T.: 2002, *Proc. XIVth Rencontres de Blois "Matter-Antimatter Asymmetry"*, 439.
 Kirilova, D.: 2003, *Nucl. Phys. Proc. Suppl.*, **v.122**, 404.
 Kirilova, D., Panayotova, M.: 2007, *Bulg. J. Phys.*, **34**, 330.
 Larson, D.: 2011, *ApJS*, **192**, 16.
 Kirilova, D., Valchanov, T.: 2005, *Publications of the Astronomical Society "Rudjer Boskovic"*, **5**, 209.
 Linde, A.: 1982, *Phys. Lett.* , **B116**, 335.
 Nakamura, K., et. al. (Particle Data Group): 2010, *J. Phys.*, **G37**, 075021 and 2011 partial update for the 2012 edition.
 Pettini , M., et al.: 2008, *MNRAS*, **391** , 1499.
 Starobinsky, A.: 1982, *Phys. Lett.*, **B117**, 175.
 Vilenkin, A., Ford, L.: 1982, *Phys. Rev.*, **D26**, 1231.

A METHOD FOR ENHANCED IMAGE PROCESSING AND SEARCH FOR VARIABLE STARS

ŽARKO MIJAJLOVIĆ, ALEKSANDAR SIMONOVIĆ, NADEŽDA PEJOVIĆ

Faculty of Mathematics, University of Belgrade, Serbia

E-mail: zarkom@matf.bg.ac.rs, simonovicaleksandar79@yahoo.com,
nada@matf.bg.ac.rs

Abstract. The purpose of this report is to explain an enhancement in the standard procedure of processing signals extracted from astronomical images. We tested the method in confirmations of the transits of exoplanets *Tres 2b* and *Tres 3b*. We also found suspects of the variability of two stars: 3UC 317-048727 and TYC 3549-2704-1.

1. INTRODUCTION

There are well known problems related to imaging used in astrophotography. For example, images taken with ground based telescopes are subject to the blurring effect of atmospheric turbulence. Another one is coming from the errors arising from the use of equipment such as:

- dark and readout signals generated by CCD cameras,
- vignetting and
- uneven field illumination created by dust or smudges in the optical system.

On the other hand, many astronomical imaging programs require higher resolution than is possible without some correction of the images. All these problems are multiplied if modest equipment is used. Of course, there are many methods used in post processing. It should be noted that these procedures are in fact mathematical algorithms applied on digitized, numerical data representing extracted signals. There are also preprocessing procedures applied on the series of astronomical photographs such as photo stacking, and they are mostly based on physical enhancement of the signal such as the strength of the signal by accumulating it from a group of photos. As far as we know this procedure is used mainly for production of final images, therefore not for a dynamic analysis of a time process related to the series of photos.

Our method is the mixture of these two approaches. For a given set of photos representing a time process such as the variability of a star, we build a list of groups of images. Groups are built in a certain pattern in order to preserve the physical characteristics of the time process, its strength, shape and periodicity. We implemented special software for building the list of groups of photos concordant to the prescribed pattern. Then each group is preprocessed by stacking photos in this group.

In this way we averaged the signal strength, significantly reduced the noise coming from atmosphere turbulence, and eliminated errors generated by the used equipment.

At this stage we used the software DeepSkyStacker for processing the groups of images. So obtained, the new series of frames is then the subject to the analysis of the original time process, such as the star variability. At this stage we used software MaximDL and Peranso. A much better resolution of data and the curve representing the variability of the star is achieved compared to the data and the graph obtained by direct numerical analysis without the described preprocessing. In this way we confirmed transits of two exoplanets Tres 2b and Tres 3b. We also found suspects of the variability of two stars; they are 3UC 317-048727 and TYC 3549-2704-1.

2. LUCKY IMAGING

For better understanding of our procedure, we give a brief explanation of the method known as *lucky imaging*. Lucky imaging is a remarkably effective technique for delivering near-diffraction-limited imaging on ground-based telescopes. The basic principle is that the atmospheric turbulence that normally limits the resolution of ground-based observations is a statistical process. If images are taken fast enough (at least less than 0.1 sec) to freeze the motion caused by the turbulence we find that a significant number of frames are very sharp indeed where the statistical fluctuations are minimal. Imaging through atmospheric turbulence is a random process, and there is a small probability that any one image will be perfect, i.e. limited only by diffraction. In 1966 R. Hufnagel (1966, 1989) gave an estimate of this probability based upon the statistical properties of the speckles formed within a point image. He predicted that, for large diameter systems, the probability of a good exposure would vary as e^{-D^2} , D is the telescope aperture. So, telescopes with smaller D have greater probability to obtain good image. This result was confirmed by D. Fried in 1978. In 1981 D. Bensimon et al measured the probability of lucky imaging and verified this probability.

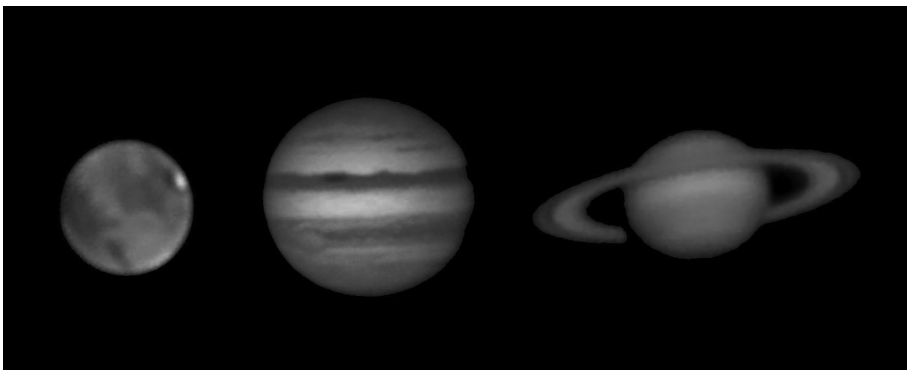


Figure 1: Images of planets obtained by lucky imaging.

By combining (stacking) these sharp images we can produce a much better one than is normally possible from the ground. We have routinely taken images of 1 arcsec resolution on the 12 cm refractor. Better results can be obtained with the assistance of adaptive optics system. These principles have been used quite extensively by the amateur astronomy community who has been able to take very high quality images of bright objects such as Jupiter and the other planets. Recently this method became of interest in professional astronomy too, see for example doctoral dissertations of N. M. Law (2007) and A. Pál (2009), and the paper by Zhang et al (2011).

In Figure 1 images of Mars, Jupiter and Jupiter are presented that we made by the lucky imaging method. These photos were obtained in April 2012. Each photo is produced from the choice of about 800 best frames selected from 1000 raw frames. One can see that the theoretical resolution limit of 1 arcsec for our instrument (see below) is achieved.

3. ALGORITHM

Suppose that there are n astro-images S_1, S_2, \dots, S_n . The idea is to divide these exposures into k equal groups G_1, G_2, \dots, G_k , each group G_i having m consecutive images. Further, if G_i and G_{i+1} are successive groups, then the first exposure S_p in G_i has the lower index than the first exposure S_q in G_{i+1} , i.e. $p < q$. Finally, the groups G_i and G_{i+1} may overlap, and in fact in most cases we make the sequence of overlapping groups. The number Δ of images contained in the intersections of G_i and G_{i+1} is called the offset. We suppose that any two consecutive groups have the same offset.

After such a grouping of images of the sequence S_1, S_2, \dots, S_n , we apply the standard preprocessing procedure (adding dark, bias and flat frames) on each group G_i and then stack all frames in G_i . In that way we produce the new sequence P_1, P_2, \dots, P_k of images. So obtained images P_i are called block frames. In this way we eliminated to the highest extent all imperfections of the equipment (dead pixels of the camera, electronic obstructions and vignetting), but also, due to the stacking, the blurring effect of atmospheric turbulence is lowered. Finally, the signal that we measured (such as the variability of the stellar magnitude) is multiplied i.e. it is strengthened.

In this way even with a modest astronomical cameras (and not so expensive), including commercial DSLR cameras, attractive results can be achieved, comparable to those obtained by professional (and expensive) astronomical cameras. Of course, some stages in the described procedure can be omitted if the professional cameras are used, e.g. the application of dark frames. However, the stacking would enhance to the great extent even the measurements done with professional astronomical cameras.

It should be mentioned that the offset Δ plays here the important role. For greater Δ blocks G_i are more overlapping, so the length k of the new sequence P_i is more close to the length of the basic sequence of raw images. The drawback of large Δ is that then more computation is needed.

Once we have the new and "clean" sequence of frames P_1, P_2, \dots, P_k , now containing the strengthened signal, one can proceed the intended analysis of the physical process (such as the variation of the stellar magnitude) represented by this signal.

To summarize, here are some basic properties of the sequence of groups G_i :

- Each individual group G_i contains the same number of images, say m .
- Each S_i (except several those at the beginning and the end of the sequence S_i) is covered by the same number of groups.
- Each group G_i has the constant increment Δ in the series S_1, S_2, \dots, S_n .
- For the fictive exposure time of the image P_i it is taken the arithmetic mean of the exposure times of images in the group G_i .

As already said, the series of block frames P_1, P_2, \dots, P_k represents, for example, the change in time of the brightness of a star and it is the subject of the appropriate analysis (statistical or astrophysical). The first author wrote a FORTRAN program FL77 for dividing the series S_1, S_2, \dots, S_n into groups G_1, G_2, \dots, G_k . The working pipeline of our procedure is summarized in Figure 2. (adaptation from Zhang et al, 2011).

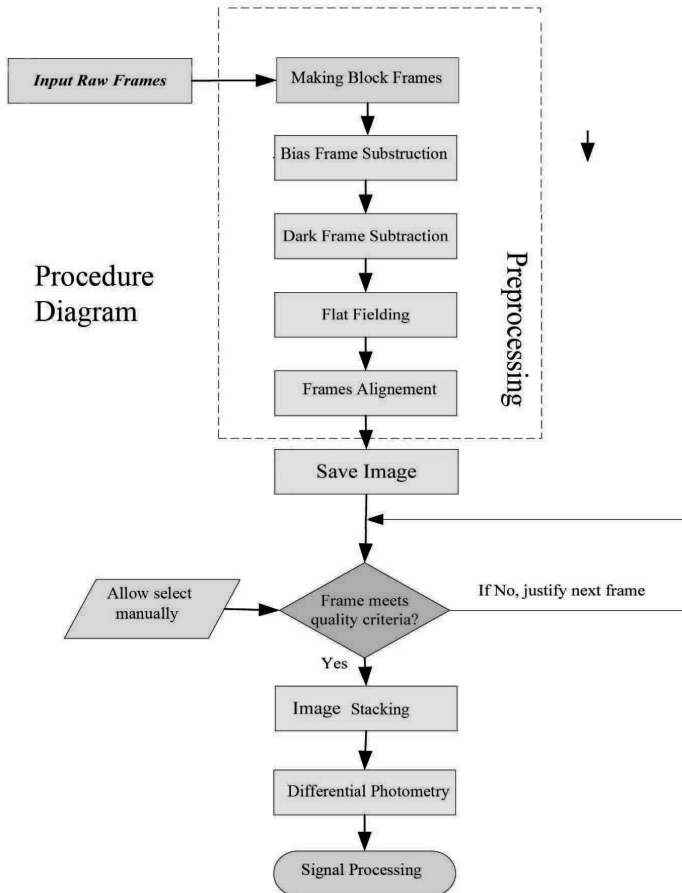


Figure 2: Flowchart of the procedure.

Blue rectangle in diagram denoted by "Making Block Frames" represents our procedure in the production process of stacked images. As seen, this is the first stage and a part of preprocessing procedure, before the images are available for further analysis.

Here is the good choice of constants for given n , the length of the series S_i : the number of groups $k = \sqrt{n}$, the offset $\Delta = k/2$, or $\Delta = n^{1/3}$. One can show that in the limit case, i.e. when n tends to infinity, the signal represented by P_1, P_2, \dots, P_k coincides with the signal obtained by ideal measurement. Particularly interesting applications is the use of lucky imaging in the analysis of processes that change in time, such as photometry, study of variable stars and search for exoplanets. New and cheap video cameras that are very sensitive to low light (such as Astrovid) based on L3CCD technology would play the crucial role in such projects.

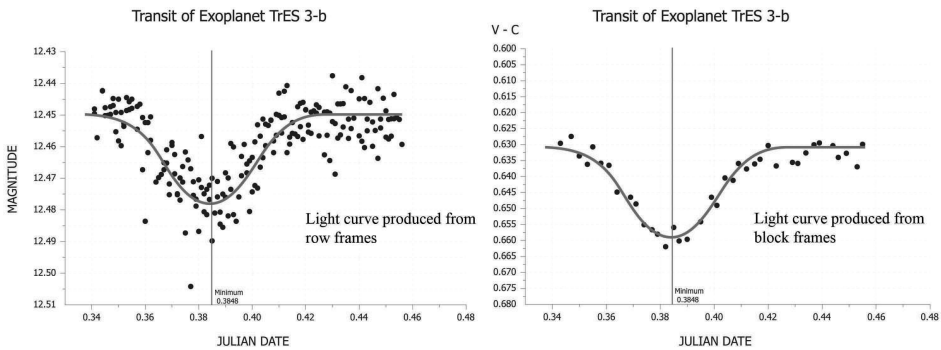


Figure 3: Transit of exoplanet Tres 3b.

As an example, we applied our method to find the light curve of the transit of the exoplanet Tres 3b in Hercules. We used a popular method for the study of variable stars, particularly short-term variables, the technique known as "differential photometry". Instead of measuring the magnitude of a variable star on an absolute scale, measurements are made over time relative to one or more non-variable stars in the field of an image and these differences are then plotted to show relative or differential change in magnitude. In Figure 3, each dot represents the magnitude of the parent star over which the exoplanet crosses. These magnitudes were measured from the corresponding frames by use of differential photometry. The light curve of the transit process is made by best fits method. The left hand graph (light curve) is produced from raw images (230 of them), while the right hand graph is made from block frames. Each block frame was obtained by stacking six consecutive raw frames. We have chosen the offset $\Delta = 0$. As seen, data are very well smoothed. While on the left diagram the measure points are widely scattered, on the right diagram they are very close to the light curve.

4. EQUIPMENT

In testing our procedure we used the following equipment:

- 1 Equinox 120ED APO 120mm $f/7.5$ fluorite apochromatic refractor.
- 2 Computerized Sky-Watcher NEQ6 PRO SynScan (EQ6 PRO): Equatorial mount with computerized GOTO system.
- 3 Computerized auto-guiding system with the supplementary guiding telescope of the aperture 90mm. Includes Opticstar PL-130M COOLAIR air-cooled, 1.3 mega-pixel monochrome video camera that connects to the computer's USB 2.0 port and can stream and store full resolution video at 12 frames per second (20fps at 640x480).
- 4 Canon EOS 50D photo camera.

References

- Hufnagel, R. E.: 1966, *Restoration of Atmospherically Degraded Images*, National Academy of Sciences - National Research Council, Washington D.C. **3**, App. 2, 11.
- Hufnagel, R. E.: 1989, *The Probability of Lucky Exposure*, The Perkin-Elmer Corporation, Technical Memorandum.
- Fried, D. L.: 1978, Probability of getting a lucky short-exposure image through turbulence, *J. Opt. Soc. Am.*, **68**, 1851.
- Bensimon, D., Englander, A., Karoubi, R., Weiss, M.: 1981, Measurement of the probability of getting a lucky short exposure image through turbulence, *J. Opt. Soc. Am.*, **71**, No.9, 1138.
- Law, N. M.: 2007, *Lucky Imaging: Diffraction – Limited Astronomy; From the Ground in the Visible*, PhD Dissertation, Inst. Astron. & Selwyn College, Cambridge Univ.
- Pál, A.: 2009, *Tools for discovering and characterizing extrasolar planets*, PhD Dissertation, Loránd Eötvös University, Faculty of Sciences PhD School of Physics.
- Zhang, S., Zhao, J., Wang, J.: 2011, *An Efficient Lucky Imaging System for Astronomical Image Restoration*, 2011 AMOS Conference technical papers, 8p. (www.amostech.com/TechnicalPapers/2011.cfm)

OBSERVATIONS OF ERS FROM ICRF2 LIST USING ASV 60 cm AND ROZHEN 2 m TELESCOPES

IVANA S. MILIĆ and GORAN DAMLJANOVIĆ

Astronomical Observatory, Volgina 7, 11060 Belgrade, Serbia
E-mail: ivana@aob.rs, gdamljanovic@aob.rs

Abstract. During 2011 we observed the extragalactic radio sources (ERS, which are visible in the optical domain) from ICRF2 list using the ASV $D = 60$ cm (Serbia) and Rozhen $D = 2$ m (Bulgaria) telescopes with CCD camera. It is of importance to compare the ERS optical and radio positions (VLBI ones) and to search for a relation between optical and radio reference frames. A few ERS were observed with both telescopes, and it is useful to check the possibilities of ASV 60 cm instrument via the Rozhen 2 m results. At the ASV 60 cm we used the CCD camera Apogee U42 (2048x2048 pixels, the pixel size is $13.5 \times 13.5 \mu\text{m}$, and at the Rozhen 2 m it is the CCD VersArray 1300B (1340x1300 pixels, the pixel size is $20 \times 20 \mu\text{m}$). The observations, reduction and preliminary results of common ERS are presented here.

1. INTRODUCTION

The reference systems are based on the resolutions of international scientific unions. So, the celestial system is based on IAU (International Astronomical Union) Resolution A4 (1991). It was officially initiated and named International Celestial Reference System (ICRS) by IAU Resolution B2 (1997). The fundamental celestial reference frame (International Celestial Reference Frame – ICRF) was adopted by the IAU (1997). There were the original list of radio objects and two extensions (ICRF-ext1 and ICRF-ext2). Now, they are referred to as ICRF1: all in all 717 sources, 212 defining ones, 109 new ones, 294 candidate ones, and 102 additional sources. At the IAU XXVII GA (2009), the second realization of the ICRF (the ICRF2) was adopted with the list of precise positions for 3414 compact radio astronomical sources. The investigation of a relation between optical and radio reference frames is of importance. For that subject, we need to make the observations of some ICRF2 ERS which are visible in the optical domain, and to compare their optical and radio positions (VLBI ones). The optical positions (α and δ) could be calculated using reference stars from some of nowadays big star catalogues. To do that comparison we can use our CCD observations of ERS made at the RCC telescope¹ of Rozhen National Astronomical Observatory (Bulgarian Academy of Sciences) and at the Astronomical Station

¹Based on observations with the 2 m RCC telescope of the Rozhen National Astronomical Observatory operated by the Institute of Astronomy, Bulgarian Academy of Sciences.



Figure 1: Telescope Cassegrain 60 cm, ASV.

Vidojevica – ASV of the Astronomical Observatory in Belgrade (Serbia). Here, we presented the possibilities of ASV telescope comparing our ASV 60 cm and Rozhen 2 m results for 6 ERS objects observed with both instruments.

2. DATA

The Hipparcos reference frame was realizing the ICRS in optical wavelengths, and the accuracy is significantly better than in the case of FK5. So, the HCRF, Hipparcos Celestial Reference Frame, is the optical one. It was linked to the ICRF1 (radio one) with an accuracy of ± 0.6 mas in position (for the epoch 1991.25) and ± 0.25 mas per year in rotation (Kovalevsky et al. 1997). That accuracy degrades over time because of the error in proper motions of stars. And, it is necessary to verify and refine the relation between the HCRF and ICRF2 by using different telescopes and methods. We can investigate the relation between optical and radio reference frames via ERS visible in the optical domain. To do that we made the observations of ERS using the Rozhen 2 m ($D = 2$ m, $F = 15.77$ m) and ASV 60 cm ($D = 60$ cm, $F = 6$ m) telescopes. The CCD fields around ERS were observed using CCD camera VersArray 1300B (1340x1300 pixels, the pixel size is $20 \times 20 \mu\text{m}$, the scale is 0.26 arcsec/pix, the field of view – FOV is about 5.5×5.5 arcmin) with 2 m Rozhen telescope, and using CCD Apogee U42 (2048x2048 pixels, the pixel size is $13.5 \times 13.5 \mu\text{m}$, 0.46 arcsec/pixel, the FOV is about 15.8×15.8 arcmin) with 60 cm ASV one (Fig. 1).

Table 1: Observed ERS using ASV 60 cm and Rozhen 2 m telescopes.

ERS	RA (VLBI)		DEC (VLBI)		Mag	Exp		Exp	
						V	R	V	R
	(h,m,s)		($^{\circ}$,', $''$)			Rozh	Rozh	ASV	ASV
					(s)	(s)	(s)	(s)	
L0109+224	01 12 05.8247	22 44 38.786	16.4	10	15,10	60	60		
A0059+581	01 02 45.7624	58 24 11.137	16.1	15	10	60	60		
Q2250+190	22 53 07.3692	19 42 34.629	16.7	20	20	60	60		
G0007+106	00 10 31.0059	10 58 29.504	14.2	5	5	60	60		
L2254+074	22 57 17.3031	07 43 12.302	17.0	20	20	60	60		
G0309+411	30 13 01.9621	41 20 01.183	16.5	15	15	60	60		

The ERS (extragalactic radio sources) are compact extragalactic objects, mostly quasars (quasi stellar objects, QSO), BL Lacertae (BL Lac) sources and a few active galactic nuclei (AGNs). The ERS are far away and their proper motions should be negligibly small. The current VLBI positions are known to better than 1 mas. The total number of objects is 3414 in ICRF2: 295 'defining', and additional 3119 ones. Alignment of ICRF2 with the ICRS was made using common ICRF2/ICRF-Ext. 2 138 stable ERS. From 1 January 2010, the realization of the ICRS is the ICRF2, and the two largest weaknesses of ICRF1 were eliminated: more uniform sky distribution of ERS and the position stability of the 295 ICRF2 defining sources.

The densification catalogues derived from the HCRF because the HCRF was primary realization of the ICRS at optical wavelengths. Some of these catalogues are: Tycho-2, UCAC3, 2MASS (near-IR), PPMXL, XPM, etc. We used here XPM catalogue (Fedorov et al., 2010). And we assume that the centers of emission of radio/optical sources coincide between each other in line with the accuracy level of the optical observations.

We need to observe the common radio/optical objects to align radio frame (ICRF2) and optical one (HCRF) with high accuracy. To do that, we calculated the accurate optical positions of ERS. So, the ground based astrometric observations of ERS are very important. During autumn 2011, we made the observations with the Rozhen 2 m and ASV 60 cm telescopes. Some of ERS were observed at both sites. And it is a good opportunity to check the ASV results via the Rozhen ones.

A total of 6 optical counterparts of ERS were observed on both sites (see Table 1): L 0109+224, A 0059+581, Q 2250+190, G 0007+106, L 2254+ 074 and G 0309+411. We made 6 frames per ERS (3 at R filter and 3 at V one). The magnitudes ranged from 14.2 to 17.0 (ICRF, V domain). All exposures were guided. The exposure time ranged from 5^s to 20^s for the Rozhen 2 m telescope and 60^s for ASV 60 cm (see Table 1). The main columns of Table 1 are: the source name and type of ERS is in the first column (Q – quasar L – BL Lac, A – active galactic nuclei or quasar, G – galaxy), the next two columns are α and δ (from ICRF2 list) of ERS, then the magnitude which is obtained for V domain, and our exposure time is presented for V and R domains (last four columns).



Figure 2: The ERS G 0007+106 with magnitude of 14.2 observed with ASV 60 cm.

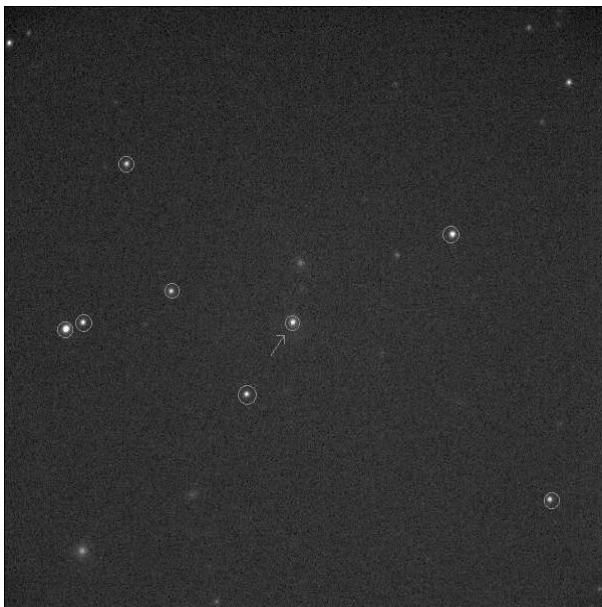


Figure 3: The ERS G 0007+106 with magnitude of 14.2 observed with Rozhen 2 m.

3. CALCULATION AND RESULTS

The detection of star-like objects (ERS) and reference stars is the first step for processing the CCD images. The next step is measuring the positions of centers (x , y) of ERS and stars. And the reduction, to get tangential and equatorial coordinates. The linear model was used, it is a standard astrometric "plate" reduction with the available reference stars,

$$\xi = ax + by + c$$

$$\eta = dx + ey + f$$

to transform the measured CCD coordinates (x , y) to tangential ones (ξ , η). The unweighted Least – Squares Method (LSM) was applied to calculate the unknown values of parameters a , b and c to get α . And d , e , and f ones to get δ . The FOV of CCD frames was small and we did not apply the corrections for apparent displacements, as differential refraction (Aslan et al. 2010, Kiselev 1989). So, we need at least 3 reference stars, but sometime in small FOV there are not enough reference stars with precise coordinates and proper motions to calculate the values of α and δ of ERS. On the other side, we need the good precision of astrometric data of reference stars (from some catalogue) to determine precise link between the radio and optical frames.

The bias and flat-field frames were not applied to our raw frames. The dark correction is not significant at Rozhen site because the CCD chip was cooled to -110° C (good for ERS fainter objects). The AIP4WIN image processing package (Berry and Burnell 2002) was applied for CCD observations. All frames were reduced individually. The XPM catalogue which was used for reduction contains the positions and proper motions for 314 million stars distributed all over the sky for the epoch 2000.0. To calculate the stellar apparent positions, some programmes from SOFA package were used. So, the positions of ERS were calibrated with respect to the XPM catalogue by using CCD observations. In this way, we determined the optical coordinates of mentioned 6 ERS objects. The ERS radio ones are from the ICRF2 list (Fey et al. 2009). Some of XPM stars did not taken into account because of their very low signal to noise ratio.

In Fig. 2, as an example of ASV observation, the CCD frame of ERS G 0007+106 is presented, and in the Fig. 3 it is the same ERS but observed with 2 m Rozhen telescope. All 7 stars are marked with circles. The ERS is near the central part of the images and marked with the direction arrow and a circle.

We compared the optical positions of ERS with the radio ones to determine the values $(O-R)_\alpha$ and $(O-R)_\delta$ (see Table 2). There are the unweighted mean offsets of $(O-R)_\alpha$ (the second column for the Rozhen side and the sixth one for the ASV side) and $(O-R)_\delta$ (the third column for the Rozhen side and the seventh one for the ASV side) values with their standard errors.

From both telescopes, these offsets in α are close to each other for bright ERS G 0007+106 with magnitude 14.2 (also, in δ); see Table 2. The errors of ASV offsets are small and close to suitable Rozhen ones. The similar situation is for the ERS L 0109+224 with magnitude of 16.4. The errors of ASV offsets of other ERS objects are

Table 2: Differences between optical (our results) and radio (VLBI) positions of ERS observed with ASV 60 cm and Rozhen 2 m telescopes.

ERS	Rozh				ASV			
	$(O-R)_\alpha$	$(O-R)_\delta$	σ_α	σ_δ	$(O-R)_\alpha$	$(O-R)_\delta$	σ_α	σ_δ
	(//)	(//)	(//)	(//)	(//)	(//)	(//)	(//)
L0109+224	-0.111	0.001	0.015	0.019	-0.049	-0.036	0.138	0.158
A0059+581	0.138	-0.028	0.050	0.098	0.026	0.317	0.226	0.495
Q2250+190	0.131	0.159	0.166	0.040	-0.181	0.224	0.400	0.120
G0007+106	-0.151	0.089	0.042	0.055	-0.115	0.053	0.038	0.076
L2254+074	0.074	0.007	0.095	0.040	0.145	0.180	0.381	0.556
G0309+411	-0.347	-0.250	0.133	0.271	0.064	-0.353	0.315	0.263

remarkably bigger than the corresponding Rozhen ones. Also, some of ASV offsets are different from the corresponding Rozhen ones.

4. CONCLUSIONS

In the paper by Damljanić and Milić (2012) we presented our first results of ERS observations using 2 m Rozhen telescope, and concluded that this kind of observations and investigations is possible with that instrument.

From just 6 ERS objects observed at both sites (with Rozhen 2 m and ASV 60 cm telescopes), we can conclude that the optical observations of ERS are possible by using 60 cm ASV telescope and a good CCD camera, but at present it is better to observe ERS with magnitudes less than about 16.5. The corresponding offsets (in α and in δ), as the results of 2 m Rozhen and 60 cm ASV observations, are very similar for bright ERS objects (for example G 0007+106 and L 0109+224). Moreover, from ASV observations and in the case of G 0007+106 (with magnitude 14.2) the errors of offsets are small and close to the corresponding Rozhen ones. Some problems during the calculation of ERS optical positions can be caused by: faintness of the optical counterparts to ERS, atmospheric influences and technical problems. We could improve the ASV results by using: star guider (to use the exposures longer than 1.5 minutes), dark, bias and flat during reduction of data, and stacking of data. Anyway, it is better to use the Rozhen 2 m telescope for observations of faint ERS objects; it means with magnitude exceeding 17.

Acknowledgements

The authors from the Astronomical Observatory in Belgrade gratefully acknowledge the observing grant support from the Institute of Astronomy and Rozhen National Astronomical Observatory, Bulgarian Academy of Sciences. This research has been supported by the Ministry of Education and Science of the Republic of Serbia (Project No. 176011 "Dynamics and kinematics of celestial bodies and systems").

References

- Aslan, Z., Gumerov, R., Jin, W., Khamitov, I., Maigurova, N., Pinigin, G., Tang, Z., Wang, S.: 2010, *A&A*, **510**, A10.
- Berry, R., Burnell, J.: 2002, *The Handbook of Astronomical Image Processing, Includes AIP4WIN Software*, Willmann-Bell, Inc., Richmond, USA.
- Damljanović, G., Milić, I. S.: 2012, in the Proc. of the Journées 2011, in press.
- Fedorov, P. N., Akhmetov, V. S., Bobylev, V. V., Bajkova, A. T.: 2010, *MNRAS*, **406**, 1734-1744.
- Fey, A. L., Gordon, D., Jacobs, C. S.: 2009, IERS Technical Note, No. 35.
- Kiselev, A. A.: 1989, *Theoretical foundations of photographic astrometry*, Nauka, Moskva.
- Kovalevsky, J., Lindegren, L., Perryman, M. A. C., Hemenway, P. D., Johnston, K. J., Kislyuk, V. S., Lestrade, J.-F., Morrison, L. V., Platais, I., Röser, S., Schilbach, E., Ticholke, H.-J., de Vegt, C., Vondrák, J., Arias, F., Gontier, A.-M., Arenou, F., Brosche, P., Florkowski, D. R., Garrington, S. T., Preston, R. A., Ron, C., Rybka, S. P., Scholz, R.-D., Zacharias, N.: 1997, "The Hipparcos Catalogue as a realization of the extragalactic reference system", *A&A*, **323(2)**, 620-633.

WIDE-FIELD STELLAR PHOTOMETRY WITH THE 50/70 cm SCHMIDT TELESCOPE OF NAO ROZHEN

PETKO NEDIALKOV, ANTONIYA VALCHEVA, EVGENI OVCHAROV and
YANINA METODIEVA

*Department of Astronomy
University of Sofia, Bulgaria
E-mail: japet@phys.uni-sofia.bg*

Abstract. We used observations of Stetson standard photometric field L104 obtained in V-band with the 50/70-cm Schmidt telescope at NAO Rozhen on March 17-18, 2012, in order to check the FWHM, the ellipticity and the position angle of the stellar profile as a function of its position over the studied area of view for different altitude of the telescope pointing. A misalignment between the center of used CCD camera and the optical axis of the telescope is clearly demonstrated via image profile degradation over large area of the detector. Systematic changes of the image profile FWHM and its orientation, probably due to the tension of the telescope tubus before and after the culmination are also seen. Estimated color terms are ~ 0.15 mag while the residual radial dependence is smaller than 0.04 mag within the region of unbiased profiles.

1. INTRODUCTION

Schmidt telescope at NAO Rozhen has 70 cm spherical mirror and 50 cm corrector plate. The focal length is 172 cm. Since 2009 the telescope is equipped with FLI PL 16803 CCD camera with 4096 x 4096 pixels with $9 \times 9 \mu\text{m}$ size and image scale of 1.08 arcsec/px. This gives field of view 73.6×73.6 arcmin². The reader is redirected to the manuscript from Markishki (2009) for more detailed information about the telescope design.

Wide field imaging with such a telescope imposes tight requirements to the optics in order to perform accurate photometry. Varying scale factor, misalignment between the detector and the optical axis, tubus tension when telescope is pointing towards different altitudes above the horizon may lead to a significant focus gradient. Thus, the derived stellar magnitudes are subject to spatially dependent systematic errors - a problem already established for images taken with the 2-m telescope of NAO Rozhen (Markov, 2005ab).

In this paper we combine both qualitative and quantitative approach in order to study stellar profile degradation over the detector area.

2. OBSERVATIONS AND DATA REDUCTION

Standard Stetson field L104 with RA(J2000)=12:42:19.4 and DEC(J2000)=-00:34:36 is very suitable target for our study because its size of 88.7 x 58.0 arcmin² is comparable to Schmidt field of view and contains 728 stars with known magnitudes in V-band. Observations were carried out on March 17-18 2012 with the 50/70-cm Schmidt telescope at NAO Rozhen.

We took images three times per night: before, during culmination and after that in order to study the effect of telescope position on stellar profiles and photometry. In every run, we took short and long exposure only in V-band. Observing log is presented in Table 1.

Table 1: Observing log

Date	Hour	Exposure	Altitude	< FWHM >
yyyy-mm-dd	UT	sec	deg	arcsec
2012-03-17	20:48:06	30	37	2.5
2012-03-17	20:58:14	300	37	2.5
2012-03-17	23:21:35	30	47	2.1
2012-03-17	23:22:58	300	47	2.1
2012-03-18	01:41:51	300	37	2.5
2012-03-18	01:48:03	30	37	2.5
2012-03-18	20:03:42	30	30	2.7
2012-03-18	20:14:07	300	30	2.7
2012-03-18	23:21:50	30	47	2.1
2012-03-18	23:36:53	300	47	2.1
2012-03-19	02:18:32	300	30	2.5
2012-03-19	02:25:02	30	30	2.5

The initial reduction was made with standard IRAF routines and includes dark current and flatfield corrections. DAOFIND task found all stellar-like objects in the observed fields and PSFMEASURE was used to determine individual FWHM, ellipticity and orientation of the stellar profile as a function of its position over the detector. In total, we measured 1727, 1996, and 1698 stars on the 300 sec exposures, taken in the three positions of the telescope. We choose to work with images, take on March 18 2012, because the pointings of the telescope are most distant. Aperture photometry was performed for all objects in the three positions of the telescope using PHOT/APPHOT routine. After that, a cross-identification with Stetson standard stars was made and standard V-magnitude was attributed to ~ 450 stars on each image.

3. RESULTS AND DISCUSSION

We started with the spatial variations of image profile width. In Figure 1 (left panels) we plotted FWHM vs. radial distance for all detected stellar-like objects (≈ 2000 in total). Irrespectively to the altitude, the samples can be divided into two subsamples: one - with a normal, and the another - with deviating, bigger FWHM.

We will refer them as sample with normal and biased FWHM. Another striking difference emerges - the mean values of the normal FWHM at culmination are rather smaller (~ 2.1 arcsec) than before (~ 2.7 arcsec) and after (~ 2.5 arcsec) the culmination. In order to distinguish between the samples with normal and biased FWHM we tentatively put a single value discriminator, equal to 3.0, 2.5 and 2.7 arcsec for the telescope pointing before, at, and after the culmination and plotted the sample with biased FWHM on the same figure (right panels). As one can see immediately, the sample with the biased FWHM has an inhomogeneous spatial distribution over the detector, covering $\approx 30\%$ of total area.

Contrary to that, the sample with normal FWHM, not shown there for clarity, populate the shifted void on each image. The offset is ~ 4 arcmin in R.A. and ~ 15 arcmin in DEC. This spatial distribution is stable in time and we attribute this to a misalignment of the detector center from the optical axis of the telescope. Defocusing of the telescope at lower altitudes can be due to the changes of the seeing quality during the night, which does not seem to be the case, and both to the tension of the telescope tubus and the higher refraction closer to the horizon. It will be checked in a forthcoming paper.

Later on, we continue with a study of the sample of cross-identified standard stars with unbiased FWHM and restricted it to stars with standard V magnitudes between 12 and 17.5 magnitudes in order to avoid significant aperture corrections for the brighter stars and to account only for the most accurate standards on the other side.

In Figure 2, the objects position angle is shown at right as a function of image polar angle, and at left - as a function of image profile ellipticity. Here we took the position angles and ellipticities derived within $2 \times FWHM$ in order to be more sensitive to the periphery of the image profile. Neither the position angles, nor ellipticities, which are mostly within 20%, are radially dependent. As expected, the position angle and the ellipticity of the stellar profile are only weakly, if at all, correlated. However, there is an obvious symmetrical change of the position angle of the stellar profile from positive ($\approx 10^\circ$ on average) to negative ($\approx -10^\circ$ on average) values when altitude varies, being $\approx 0^\circ$ during the culmination. It could be explained with a symmetrical tension of the telescope tubus before and after the culmination.

At last, as shown in Figure 3, we performed a comparison between our V-band photometry, after accounting for the color term, and that of Stetson (2012). It was found that zero-point of the photometry varies with altitude, being largest at the culmination due to the lowest atmospheric extinction. Unlike it, the color term coefficient is rather constant (~ -0.1) resulting in a correction of 0.15 mag for the reddest stars. The left panels in the figure demonstrate the lack of color dependence, after accounting for the color term, while the right panels hint a small residual radial trend, less than 0.04 mag, within distances of 1500 px from the center. The possible simultaneous correction of the instrumental magnitudes for the color and the radial terms will be considered in a forthcoming paper.

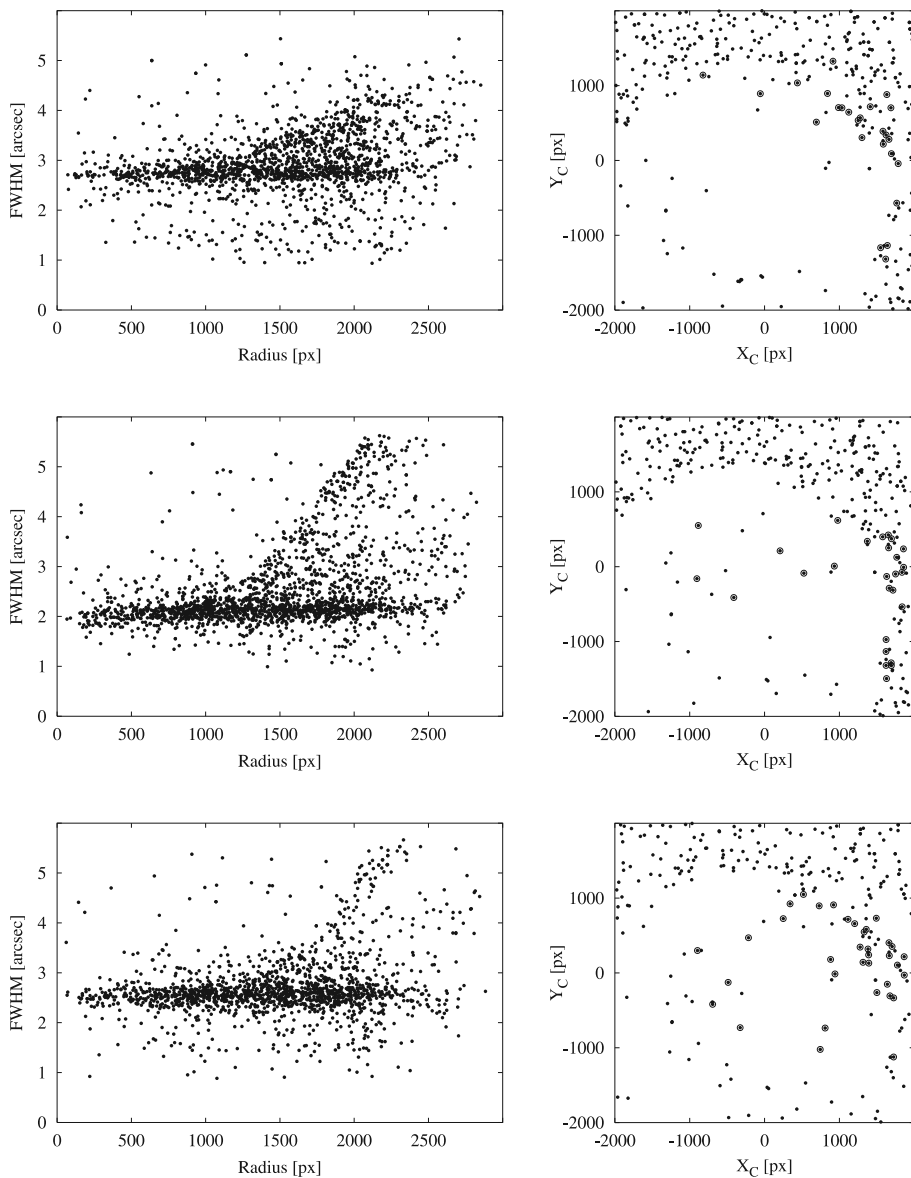


Figure 1: Variations of the FWHM of all detected stellar-like objects as a function of the radial distance (left panels) and the location of the outliers (with FWHM above the main cloud on the left panels) on image plane (right panels) relative to the center for different telescope altitudes 30° before (upper panels), 47° at (middle panels) and 30° after (lower panels) the culmination. Note, the smallest FWHM at the culmination. Only a few cross-identified standard stars, depicted with extra open circles, are outliers. The bulk of rest ~ 400 standard stars with unbiased FWHM populate the shifted void on each image due to an offset of the detector center from the optical axis of the telescope.

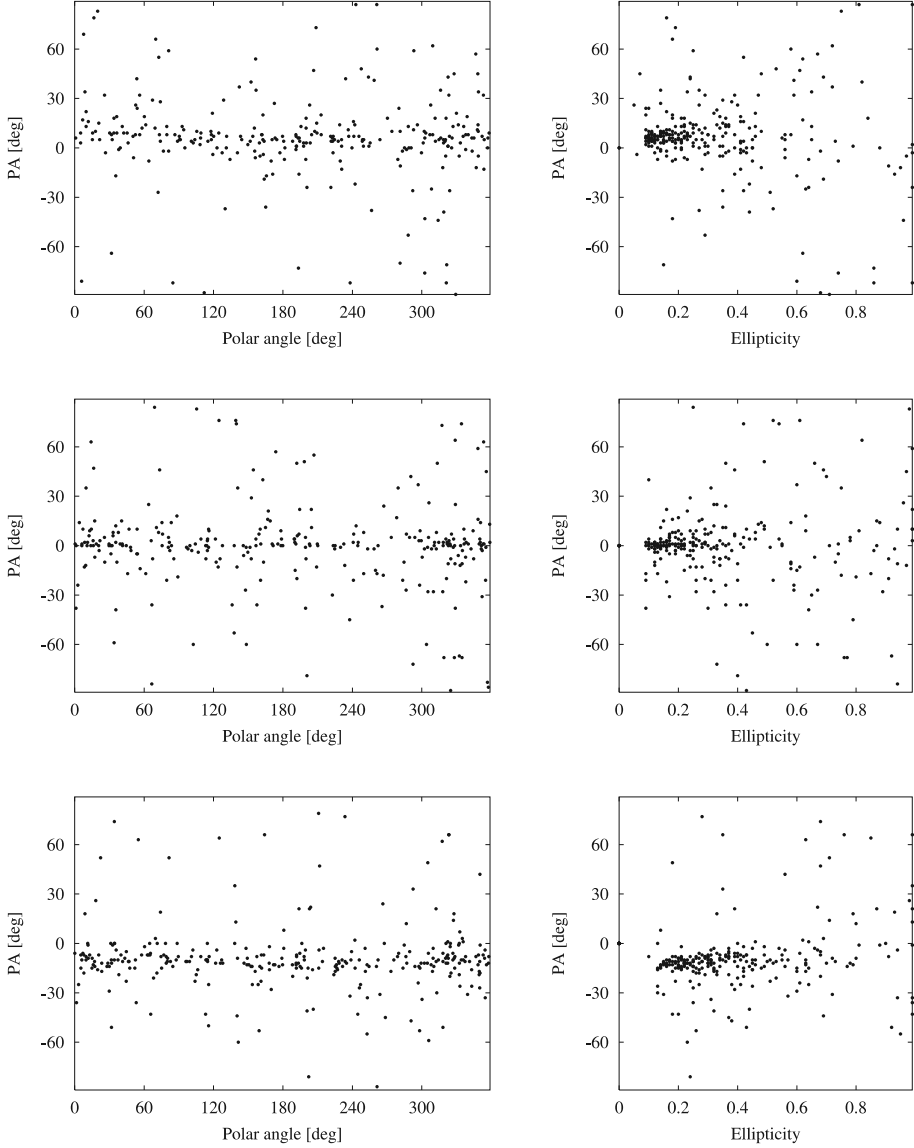


Figure 2: Position angle of the cross-identified standard stars with unbiased FWHM as a function of the object polar angle (left panels) and the stellar profile ellipticity (right panels) for different telescope altitudes: 30° before (upper panes), 47° at (middle panels) and 30° after (lower panels) the culmination. Note the reorientation of the stellar profile from positive ($\sim 10^\circ$ on average) to negative ($\sim -10^\circ$ on average) position angle values when altitude varies. As expected, the position angle and the ellipticity of the stellar profiles are not correlated. In these plots we have restricted the sample to stars with standard V magnitudes between 12 and 17.5.

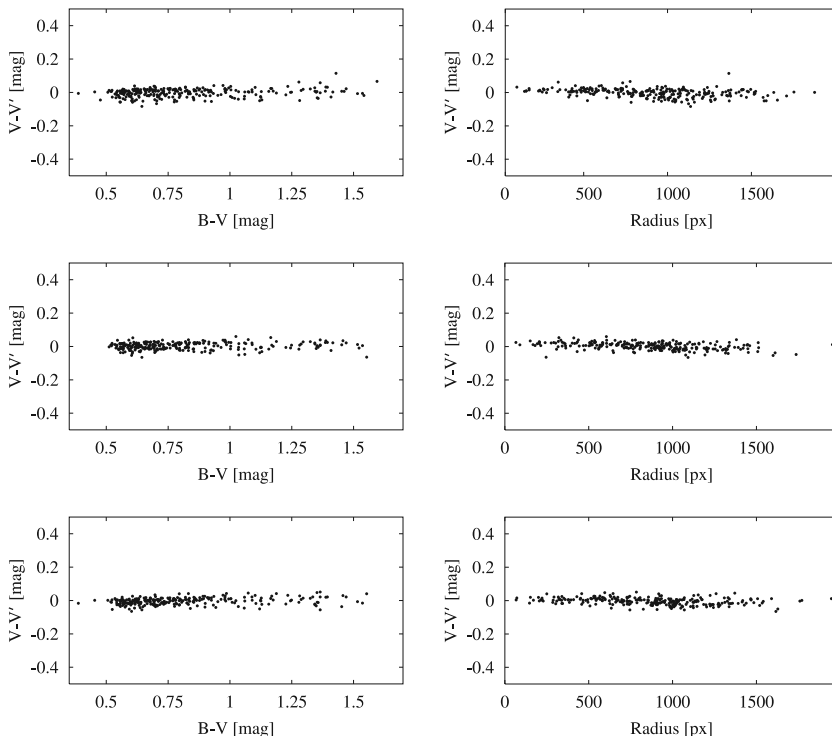


Figure 3: Comparison between our photometry V' , after accounting for the color term, and that of Stetson et al. (2012) for the cross-identified standard stars with unbiased FWHM and standard V magnitudes between 12 and 17.5. The left panels demonstrate the lack of color dependence while right panels hint a residual radial trend less than 0.04 mag within distances of 1500 px from the center. Upper panels correspond to the telescope altitude of 30° before the culmination, middle panels – to 47° at culmination, and the lower ones – to 30° after the culmination.

4. CONCLUSIONS

In brief, we may conclude that:

There is yet a lot of mechanical work to be done in order to improve the focusing over the detector. First of all is to remove the offset between the center of CCD camera and the optical axis of the telescope and later - to check once again the perpendicularity between the optical axes and the detector.

Image profile quality (FWHM and PA) is a subject to systematic changes strongly dependent on the telescope pointing being smallest at culmination and increasing at lower altitudes. We attribute this effect to the tension of the telescope tube before and after the culmination.

Nevertheless, the residual radial dependence in magnitudes within the region of unbiased profiles is smaller than 0.04 mag.

Acknowledgements

This work was partially supported by following grants: SU-068/12, DO02-340/08 and DO02-362/08.

References

- Markishki, P.: 2009, Tests of the optics of the 50/70 cm Schmidt telescope in the National Astronomical Observatory *unpublished*.
- Markov, H. S.: 2005a, Spatially Dependent Errors in Stellar Photometry. I. Qualitative Approach *Bulg. J. Phys.*, **32**, 51.
- Markov, H. S.: 2005b, Spatially Dependent Errors in Stellar Photometry. II. Quantitative Approach *Bulg. J. Phys.*, **32**, 59.
- Stetson, P. B.: 2012, Photometric Standard Fields <http://www3.cadc-ccda.hia-ihp.nrc-cnrc.gc.ca/community/STETSON/standards/>.

DISTRIBUTION OF STARS IN MAGELLANIC CLOUDS' STAR CLUSTERS

GRIGOR B. NIKOLOV¹, MARY KONTIZAS², ANASTASIOS DAPERGOLAS³,
 MAYA K. BELCHEVA¹, VALERI K. GOLEV⁴ and IOANNIS BELLAS-VELIDIS³

¹*Institute of Astronomy with National Astronomical Observatory,
 Bulgarian Academy of Sciences, Bulgaria*

²*Dpt. of Astrophysics, Astronomy and Mechanics, National and Kapodistrian
 University of Athens, Greece*

³*IAA, National Observatory of Athens, Greece*

⁴*Department of Astronomy, Sofia University "St Kliment Ohridski", Bulgaria*

Abstract. In this contribution we present our investigation of a sample of Large Magellanic Cloud star clusters. This galaxy is the closest neighbour of the Milky Way. The LMC cluster system comprises a large number of young and intermediate age clusters. In our sample we selected clusters with similar ages of 10 Gyr. We construct the radial profiles of the clusters, derive structural parameters and study the distribution of the stars within the clusters.

1. THE STUDIED CLUSTERS

All three studied clusters are old, metal-poor and populous. Clusters NGC 2005 and NGC 2019 are located in the inner parts of LMC, thus the field contribution from the host galaxy is significant. NGC 1754 is located in the outskirts of LMC and is less affected by field stars contamination than the other two. The three studied clusters are possible post-core-collapsed listed by Mackey & Gilmore (2003) from surface brightness profiles. Literature values are listed in Table 1. The V magnitudes and $B - V$ colours are from Bica et al. (1996, 1999). Age is from Frogel et al. (1990). Metallicity $[Fe/H]$ is from Olsen et al. (1998). Half-light r_h and tidal radius r_t of the King-model cluster fit is from the catalogue of McLaughlin & van der Marel (2005).

Table 1: Literature data for the studied clusters.

Cluster Name	V	B-V	Age	[Fe/H]	r_h	r_t
NGC 1754	11.57	0.75	10 Gyr	-1.42	11.2	142.9
NGC 2005	11.57	0.73	10 Gyr	-1.35	8.65	98.8
NGC 2019	10.86	0.76	10 Gyr	-1.23	9.72	121.6

2. PHOTOMETRY

In this study we use archival data from the WFPC2 on-board the Hubble Space Telescope (available on <http://archive.stsci.edu/hst/>). The images were obtained for HST proposal ID 5916.

Table 2: List of observations used.

Cluster Name	Filter	Exptime	Filter	Exptime
NGC 1754	F555W	3x500, 2x20	F814W	2x600, 2x20
NGC 2005	F555W	3x500, 2x20	F814W	3x600, 3x20
NGC 2019	F555W	3x500, 2x20	F814W	3x600, 3x20

We obtained calibrated files from the archive which were processed prior downloading by the standard STScI pipeline and calibrated using the latest WFPC2 calibrations (bad-pixel, bias and flat field correction). The photometry was performed simultaneously on the calibrated images with HSTphot (Dolphin 2000). During photometry extensive completeness tests were performed. Representative photometric uncertainties are indicated on the CMDs of Fig. 1.

3. CMD

The three LMC star clusters are well evolved. Stars brighter than $V = 23$ are evolved beyond the Main Sequence. At the distance of the LMC ($M - m = 18.5$) this corresponds to $M_V = 4.5$, or roughly stars more massive than $0.8M_\odot$ have left the Main Sequence. The photometry of all three clusters reaches very faint stars down to 26th magnitude in V . Stars fainter than $V = 24$ are most affected by incompleteness and this is why we do not consider them in the analysis. The CMDs are shown on Fig. 1 on the left side for each cluster.

4. STRUCTURAL PARAMETERS

We construct the Radial Density Profiles (RDPs) by counting stars in concentric rings around the cluster centre. This number is corrected for the incompleteness of the stars and divided by the area of the ring. The resulting density profiles with radius r are fitted with a King profile (King 1962)

$$f(r) = f_{0K} \left(\frac{1}{\sqrt{1 + (r/r_c)^2}} - \frac{1}{\sqrt{1 + (r_t/r_c)^2}} \right)^2 + f_b, \quad (1)$$

where f_{0K} is the central density, r_c and r_t are the core and tidal radius, respectively, and f_b is the background. We construct the RDPs for several ranges of magnitude, fit those profiles and derive the core radii of every subsample of the cluster. Thus we can study the variation of the core radius with magnitude. This is a method commonly used to search for mass-segregation in star clusters (Brandl et al. 1996, de Grijs et al. 2002).

DISTRIBUTION OF STARS IN MAGELLANIC CLOUDS' STAR CLUSTERS

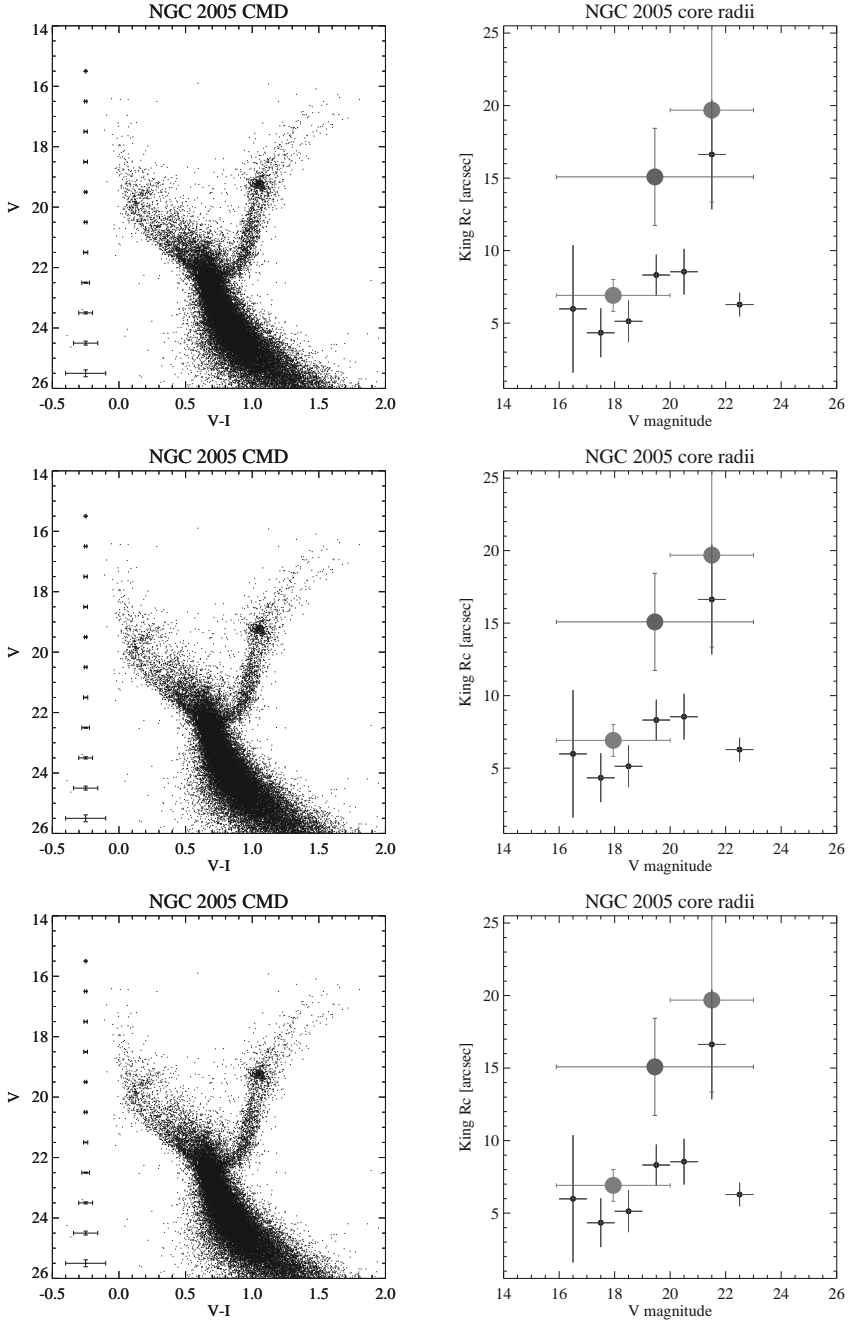


Figure 1: (left) CMDs of the studied clusters; (right) stellar segregation diagnostics diagrams, core radius from model fitting is on y-axis, magnitude of the stars is on the x-axis.

Table 3: Structural parameters derived from King-like model fitting, f_{0K} is the central density, r_c is the core radius and r_t is the tidal radius.

Cluster Name	$f_{0K} \times 10^3$ (arcmin ⁻²)	r_c (arcsec)	r_t (arcsec)
NGC 1754	42.9 ± 5.9	11.7 ± 2.1	98.5 ± 39.8
NGC 2005	29.7 ± 5.2	15.1 ± 3.3	56.0 ± 7.9
NGC 2019	47.9 ± 2.9	11.0 ± 0.9	62.9 ± 5.6

5. STELLAR SEGREGATION

When we consider stars in groups, the faint stars (shown with red circle) have core radii approx twice as large as the bright stars (shown with blue circle). The green circle marks the core radius derived for the cluster considering all magnitudes of stars. If we look at the variation of the core radius with magnitude in NGC 1754 (Fig. 1 top-right) the stellar distribution varies with magnitude – brighter stars are more centrally distributed, an indication of stellar segregation, possibly of dynamical origin.

The variation of the core radius with magnitude in NGC 2005 shows a trend – increasing with increasing magnitude, and the groups of bright and faint stars support it (see Fig. 1 centre-right). The first and last data points are outliers, but this is not unexpected. The profile for the brightest stars with $16 < V < 17$ suffers from low-number statistics and the uncertainties of the derived parameters are larger (indicated with the error bars in the right figures on Fig. 1). The faintest stars with $22 < V < 23$, on the other hand are more affected by crowding and incompleteness, which distort the profile making it steeper with small core radius.

The profiles of NGC 2019 are very smooth but they are similar for all magnitudes (Fig. 1 bottom-right). This is the reason there is no significant variation of the derived core radius with magnitude.

Acknowledgements

G. Nikolov and V. Golev acknowledge the financial support from Bulgarian Science Fund DO 02-85/2008 and DO 02-362/2008. G. Nikolov and M. Belcheva would like to thank the organizers of the VII Serbian-Bulgarian Conference for financial support.

References

- Bica, E., Claria, J. J., Dottori, H., Santos, Jr., J. F. C., and Piatti, A. E.: 1996, *ApJS*, **102**, 57.
- Bica, E. L. D., Schmitt, H. R., Dutra, C. M., and Oliveira, H. L.: 1999, *AJ*, **117**, 238.
- Brandl, B., Sams, B. J., Bertoldi, F., et al.: 1996, *ApJ*, **466**, 254.
- de Grijs, R., Gilmore, G. F., Johnson, R. A., Mackey, A. D.: 2002, *MNRAS*, **331**, 245.
- Dolphin, A. E.: 2000, *PASP*, **112**, 1383.
- Frogel, J. A., Mould, J., and Blanco, V. M.: 1990, *ApJ*, **352**, 96.
- King, I.: 1962, *AJ*, **67**, 471.
- Lyubenova, M., Kuntschner, H., Rejkuba, M., Silva, D. R., Kissler-Patig, M., Tacconi-Garman, L. E., Larsen, S. S.: 2010, *A&A*, **510A**, 19.
- Mackey, A. D., Gilmore, G. F.: 2003, *MNRAS*, **338**, 85.
- McLaughlin, D. E. and van der Marel, R. P.: 2005, *ApJS*, **161**, 304.
- Olsen, K. A. G., Hodge, P. W., Mateo, M., et al.: 1998, *MNRAS*, **300**, 665.

FINE STRUCTURE OSCILLATIONS OF A QUIESCENT PROMINENCE

PLAMEN NIKOLOV¹, TANYU BONEV¹, NIKOLA PETROV¹,
PAWEL RUDAWY², BOGDAN ROMPOLT², PETAR DUCHLEV¹

¹*Institute of Astronomy, Bulgarian Academy of Sciences*

²*Astronomical Institute of Wroclaw University*

E-mail: pnikolov@astro.bas.bg, tbonev@astro.bas.bg, nikipetrov@yahoo.com,
rudawy@astro.uni.wroc.pl, rompolt@astro.uni.wroc.pl, duchlev@astro.bas.bg

Abstract. High resolution H-alpha spectrum observations of a quiescent prominence (QP) obtained at Pic du Midi Observatory are digitized and studied. The long time series (~ 2.5 hours) of spectrograms reveal similar periods of oscillations from different parts of the prominence body. The computed line-of-sight velocities of the fine structure exhibit no changes of the amplitudes with time. The analyzed fine structures represent kink-mode oscillations of average periods.

1. INTRODUCTION

The average duration of a stable magnetic configuration that supports quiescent prominences (QPs) is about 3 hours. Observations of such prominences on the solar limb are a good base for exploring the periodic changes in their fine structure. Disturbances of the prominence plasma magnetic fields may readily produce quasi-oscillatory motions of local parts or even of the whole prominence (Wiehr, 2004).

When such prominences are observed on the solar disk as filaments the Doppler shift measurements indicate both upward and downward line of sight directed plasma motions. Internal motions in QPs have been long time under study but there is still little knowledge about their origin, behavior, and range of velocities (Petrov, 2007). Pettit (1932) has found, from time sequences of filtergrams, plasma velocities of 5 to 10 km/s. The H-alpha high-resolution observations of Yi (1992) have given velocities of about ± 1 km/s.

There is a big amount of observations implying oscillations in QPs, and cyclic velocity and intensity changes are a commonplace there. The oscillations have a large range of periods, of the order from 3÷5 min up to one hour. High-resolution observations of quiescent filaments (QFs) show oscillations that are strongly tied to their fine threads (Yi, Engvold, and Keil, 1991). High resolution H-alpha spectral observations often present non attenuation periodicity changes of line of sight (l.o.s.) velocities with period 50-60 min (Petrov, 1997; Dermenjiev, 2001). For observations longer

than 2.5 hours some investigations show similar periods with attenuation amplitudes (Wiehr, 2004; Terradas, 2002).

2. DATA SET AND DATA REDUCTION

We examine the structure and the l.o.s velocity variations of a QP on the base of high resolution H-alpha spectra and filtergrams obtained by one of the authors (BR) on October 16, 1977 at Pic du Midi Observatory. The prominence was located at the northeastern (N52-E55) limb, according to Meudon synoptic map for Carrington rotation - 1660 (Fig. 1). The filament lasted for two solar rotations and during the observations it was on its first rotation.

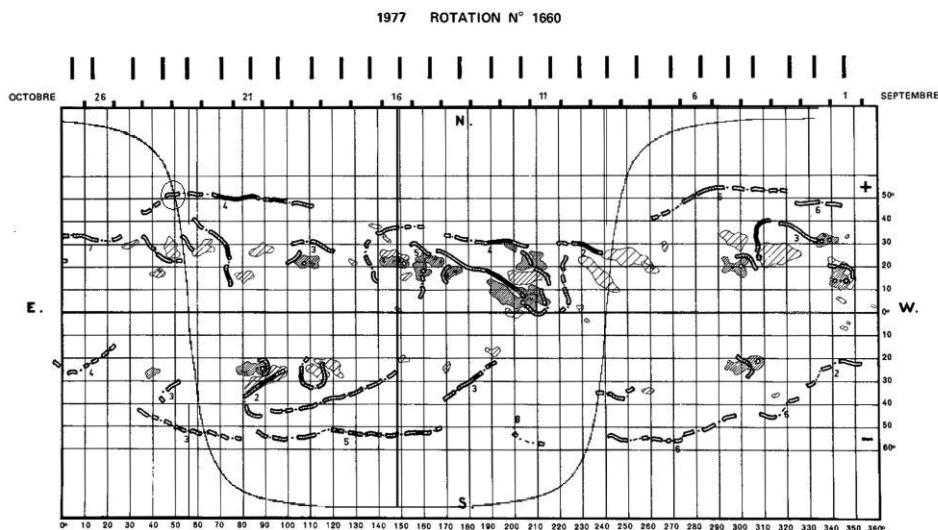


Figure 1: Part of synoptic map and the QP position on the solar limb (MSP, 1977).

The series of high-resolution H-alpha spectra have been recorded on photographic plate using the 11-m solar horizontal telescope equipped with a 9-m spectrograph (Mouradian and Leroy, 1977). A spectrohelioscan, developed at the Astronomical Institute of the Wroclaw University, was used for precise positioning of the slit. A slit-jaw unit coupled with an H-alpha camera has provided H-alpha filtergrams together with the actual slit position against the prominence body. The spectra from the QP have been taken with an exposure time of 5 s and 0.75 mm slit width.

The H-alpha filtergrams, presented on Figure 2, show that the QP consists of several arches. Our data include time series of 37 H-alpha spectra at 42 consecutive slit positions on the body of the prominence. For the purpose of this study we took data for two slit positions, 06 and 25, marked on Figure 2. The spectra obtained at position 25 were divided into two subregions, denoted 25a and 25b, respectively. The locations of these positions are chosen according to the quality of the observational

data and include all spectra obtained during the observation run. The spectra have been obtained in a time interval of about ~ 150 min (from 08:36:50 UT to 11:00:29 UT) with a nearly equal time step of 3.5 min between the consecutive scans.

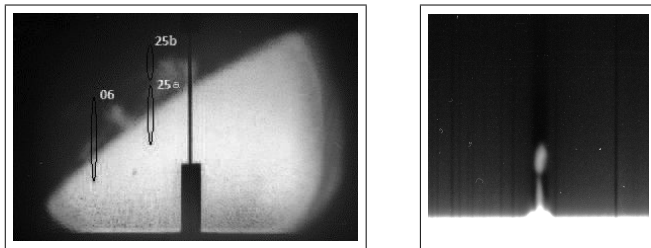


Figure 2: H-alpha filtergrams (left) together with the actual slit position against the prominence body and the respective H-alpha spectrogram, slit position 25 (right) with telluric lines of absorption.

The selected spectra and filtergrams have been digitized with an aperture of 0.016 mm which corresponds to ~ 117 km at the QP body. The first step of the data reduction is the proper orientation of the spectral images, i.e. the alignment of the transition line between background and photosphere exactly along the columns of the image. In the second step we derive the dispersion of the spectrograms by use of telluric lines well expressed in the background next to the H_{α} absorption. The value derived for the inverse linear dispersion is equal to $0.012514 \text{ \AA}/\text{px}$. We selected the minimum of the telluric H_{α} absorption to be the zero point for the wavelength measurements. Profiles of the QP's emission were taken along to the dispersion at different heights, starting 3000 km above the photosphere. The maximum of intensity of each profile was considered as representative for the l.o.s velocity of the QP at the corresponding height. The maxima were derived by fitting the profiles with parabolic function

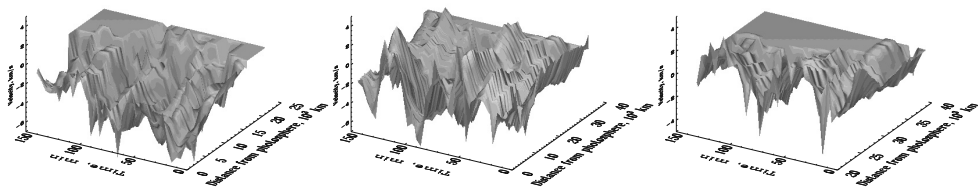


Figure 3: Distribution of l.o.s velocities in space and time for the three slit positions. Left, middle, right: slit position 06, 25a, 25b, respectively. The x-axis represents the distance along the slit in 10^3 km and the y-axis shows the time in minutes.

In a third step we corrected for solar rotation (Snodgrass, 1989) under accounting for the QP position on the solar limb. And finally, in a fourth step, all profiles obtained at a given slit position at different times were combined in 3-D maps. These maps, shown in Figure 3, represent the l.o.s. velocity dependence on time at different heights above the photosphere.

3. RESULTS AND DISCUSSIONS

The velocity fluctuations shown in Figure 3 are distributed, with some exceptions, in the range $[-5\div 5]$ km/s. The fluctuations exhibit quasi-periodic structure in time but only small variations in space, along the slit. The observed globally coherent structure is a characteristic feature of the kink mode (Van Doorselaere, 2008).

The variations of l.o.s velocities were measured from the photosphere to distance of up to 50 000 km over a time interval of about 2.5 hours. In order to derive periods of the oscillations we selected those regions along the slit which are characterized with the highest signal-to-noise ratio, extracted the profiles around these positions, calculated average profiles by integration along the space direction, and approximated the averaged profiles with the following function:

$$v = v_{mean} + v_o \sin(\omega t + \phi) + a \times t,$$

where t is the time, v_{mean} is a constant velocity along the l.o.s., v_o is the amplitude of the periodic variations, ω is the cyclic frequency, and ϕ is the initial phase. The term $a \times t$ has been added finally to account for possible constant increase/decrease of the radial velocity.

Figure 4 shows the averaged profiles extracted at the three regions and the best approximations with the function given above. At slit position 06 the velocity variations are characterized by periodic changes superimposed on a gradual constant increase of the mean radial velocity from approximately -6 km/s at the beginning of the series to about -3 km/s, 2.5 hours later. The profiles at positions 25a and 25b are well described by the periodic term only, slightly blue shifted to a constant mean values of -2 km/s, and -1 km/s, respectively.

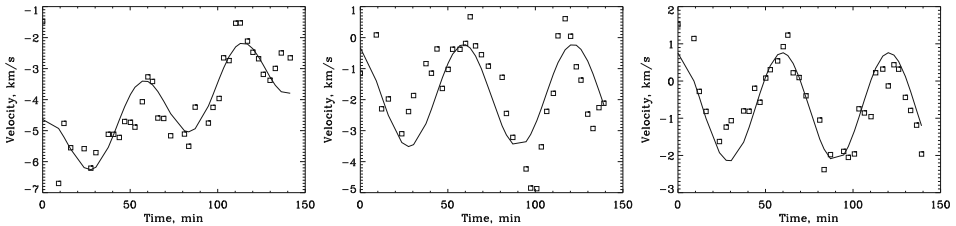


Figure 4: Squares: Measured line of sight velocities of the QP fibril for profiles extracted at slit positions 06 (left), 25a (middle), and 25b (right). Full lines: Fits to the data.

The cyclic frequency derived from the fit of the data obtained at slit position 06 is $\omega = 2\pi/T = 1.74 \times 10^{-3} \text{ s}^{-1}$, which corresponds to a period $T=60$ min. For slit positions 25a and 25b the frequency derived from the fits is $\omega = 2\pi/T = 1.69 \times 10^{-3} \text{ s}^{-1}$ corresponding to a period of 62 min. Assuming that one period is equivalent to the time interval which is needed for the plasma flow to move along the full length of the arch, we can calculate that length if we know the velocity of the flow. Typical flow velocities are given by Tandberg-Hanssen (1995) and amount to 55 km/s. With the derived periods this yields an arch length of about 200 000 km.

The Doppler shift measured with respect to the averaged H-alpha profile of the chromosphere, indicates cyclic displacement or vibration of the arches, which are typical for kink modes with average periods. The morphological structure of kink modes is presented on Figure 5.

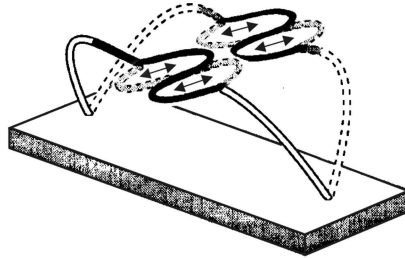


Figure 5: The diagram shows the pattern of kink mode fine structure oscillations of a quiescent prominence.

4. CONCLUSIONS

Three time series of l.o.s velocities of QP were analysed. The variations of l.o.s velocities were measured from the photosphere to distance of up to 50 000 km over a time interval of about 2.5 hours. The changes in velocities are in the range $[-5 \div 5]$ km/s. From the time sequencies obtained at two different slit positions we found oscillations with periods of about 60 and 62 min. The derived periods in combination with typical flow velocities yield a prominence arch length of about 200 000 km. The results obtained for the observed QP are typical for kink mode oscillations (Wiehr, 2004).

Acknowledgments

This study was financially supported by the National Scientific Foundation under Grants DO-02-273, DO 02-362, DO 01-34, and DO 02-85. B.R. would like to thank to Prof. J. Roesch for kind invitation to Pic du Midi Observatory, to Dr. Z. Mouradian for permission to use the solar horizontal telescope and to Dr. J.-L. Leroy for the help and stimulating discussions.

References

- Dermendjiev, V., Petrov, N., Detchev, M., Rempel, B., Rudawy, P.: 2001, On a mechanism of intensification of field-aligned currents at the solar chromosphere-quiet prominence boundaries, *Solar Phys.*, **202**, p. 99.
- Mouradian, Z., and Leroy, J. L.: 1977, Temperature and microturbulence in the outer regions of prominences, *Solar Phys.*, **51**, 103.
- Petrov, N., Dermendjiev, V., Rempel, B.: 1997, Internal Motions and Oscillatory Phenomena in a QP, *JOSO Annual Report*, p. 145.
- Petrov, N., Duchlev, P., Rempel, B., Rudawy, P.: 2007, Fine structure and Alfvén string-mode oscillations of a quiescent prominence, *Bulgarian Astronomical Journal*, **9**, p. 93.
- Pettit, E.: 1932, Characteristic Features of Solar Prominences, *ApJ.*, **76**, p. 9.

- Snodgrass, Hershel, B. and Ulrich Roger, K.: 1989, Rotation of Doppler features in the solar photosphere, *ApJ.*, **351**, p. 309.
- Tandberg-Hanssen, E.: 1995, The nature of solar prominences, *Astrophysics and space science library*, v. **199**, p. 275
- Terradas, J., Molowny-Horas, R., Wiehr, E., Balthasar, H., Oliver, R., Ballester, J. L.: 2002, Two-dimensional distribution of oscillations in a quiescent solar prominence, *A&A*, **393**, p. 637.
- Van Doorselaere, T., Nakariakov, V. M., and Verwichte, E.: 2008, Detection of waves in the Solar corona: Kink or Alfvén?, *The Astrophysical Journal*, **676**, p. L73.
- Wiehr, E.: 2004, Proc. of SOHO 13 "Waves, Oscillations and Small-Scale Transient Events in the Solar Atmosphere: A Joint View from SOHO and TRACE", Palma de Mallorca, Balearic Islands (Spain), 29 Sep-3 Oct 2003 (ESA SP-547, January 2004).
- Wiehr, E.: 2004, Observational aspects of Doppler oscillations in solar prominences, *ESA*, **SP-547**, p. 185W
- Yi, Z.: 1992, Doctoral Thesis, University of Oslo.
- Yi, Z., Engvold, O., and Keil, S. L.: 1991, Structure and oscillations in quiescent filaments from observations in He I 10830 Å, *Solar Phys.*, **132**, p. 63.

PERTURBATIONS OF THE TERRESTRIAL LOW IONOSPHERE CAUSED BY SOLAR FLARES

ALEKSANDRA NINA

Institute of Physics, University of Belgrade, Serbia

Abstract. This paper considers the most important way of investigation of terrestrial low ionosphere by VLF waves as "ionospheric probes" and explains the significance of such studies. Also, the characteristics of the Belgrade VLF station located in Institute of Physics in Belgrade are described. Finally, the attention is focused to analyses of low ionosphere response to solar X-flares.

1. INTRODUCTION

The earth's gaseous atmosphere is under permanent influence of ionizing radiation of different origins. The resulting concentration of charged particles has local maxima in the region called ionosphere at altitudes somewhere between 60 km and 1000 km. The highest periodic daily changes of electron concentration at a specific location are related to the diurnal day-night and night-day transitions, which suggests the solar radiation being the dominant source of ionization.

The electron concentration in the low ionosphere is more than one order of magnitude higher during the day than at night. Because of this difference, the ionosphere in studies is generally divided into the daytime and nighttime ionosphere. At daytime, the influence of solar background radiation is rather strong so that only sufficiently large variations in the charged particle concentration can be detected. Contrary, during the night time, much smaller changes in electric concentration are measurable.

Solar radiation is the most important origin of ionization processes in the ionosphere. Variations of its affect on the earth's atmosphere can be regular and transient. Regular changes are diurnal, seasonal and solar cycle related (Bremer and Singer 1977). Transient variations are caused by solar flares (McRae and Thomson 2004, Nina et al. 2012a) and solar coronal mass ejections (Balan et al. 2008).

The ionizing radiation in the ionosphere can originate in the outer space but it may also have a terrestrial source. The γ -ray bursts from magnetars is one of the influences on the terrestrial ionosphere that comes from very distant origins (Fishman and Inan 1988). Also, some processes occurring in the earth atmosphere, like lightnings (Cummer 1997), and in the lithosphere, like earthquakes (Hayakawa et al. 2010), can cause ionization of the low ionosphere.

Processes in the terrestrial ionosphere are rather complex which makes their exact scientific studies practically impossible. Consequently, relevant models like the Sodankyla Ion Chemistry (SIC) model (Turunen et al. 1992) and the International Reference Ionosphere (IRI) model (Rawer et al. 1978) become necessary in studies of these phenomena.

The experimental data included in the theoretical models can be obtained by different techniques related to ground-based facilities, sounding rockets, and satellites.

In this paper the attention will primarily be focused on experimental and theoretical research of the daytime low ionosphere electron concentration changes induced by solar X-flares.

2. LOW IONOSPHERE INVESTIGATIONS

The methods used in investigations of the ionospheric layer are numerous and they depend on the altitude of the considered medium. The investigations of low ionosphere find applications in pure science as well as in information technologies. In science, they are of importance in ionospheric diagnostics, studies of physical and chemical processes, and for detections of different pure natural and man-induced events. On the other hand, knowing the structure and dynamics of the ionosphere is very important in telecommunications like radio communications, planning networks of new mobile communications satellites, applications of global navigation satellite systems of high precision, etc.

The main way to analyze the low ionosphere (altitudes between 60 and 90 km) is based on properties of propagating VLF waves. Namely, during propagation from a transmitter to a receiver, the signals are reflected from the low ionosphere. The wave reflection height depends on the electron concentration and its induced changes result into some characteristic time variations of the signal amplitude and phase. For this reason, the recorded signal properties can be used to analyze the ionospheric electron concentration in situ as we are going to show below.

The advantage of this method is a continuous emission of signals by transmitters. Also, the VLF signal transmitters and receivers (incorporated in several networks such as AWESOME, AbsPAL, SAVNET and AARDDVARK) are located worldwide which allows for analyses covering large areas.

In theoretical analyses, a few numerical programs, such as LWPC (Long-Wave Propagation Capability) (Ferguson 1998) and ModeFinder (Morfitt and Shellman 1976), are used for simulations of VLF signal propagations. Calculations in these programs are based on approximations of electromagnetic waves propagating inside a spherical waveguide bounded by the earth's surface and the ionospheric layer where the VLF wave reflection occurs.

3. BELGRADE VLF STATION

There are two different VLF receivers located in the Institute of Physics in Belgrade which are incorporated into AbsPal and AWESOME international receiver networks (Fig. 1).

The AbsPal receiver, with an electrical antenna, operates as of 2004 and it can simultaneously record 6 signals from different transmitters.



Figure 1: VLF receiver systems at Belgrade station: AbsPAL (left) and AWESOME (right) antennas.

The AWESOME receiver has two loop magnetic antennas and it can simultaneously record maximum 15 signals from different transmitters. It works as of 2008.

4. RESULTS AND DISCUSSIONS

During the daytime, the most important affects on the terrestrial ionosphere have solar flares (Nina et al. 2012a, 2012b). The electron concentration variations are dependent on radiation spectra and the local atmospheric characteristics in the considered periods. Such changes induce variations in signal amplitude and phase which makes the analysis of recorded VLF signal applicable in investigations of solar flares influences on low ionosphere.

In this paper, we choose the event that occurred on March 24, 2011 between 12:01 UT and 12:11 UT as a typical example of an ionospheric response to a solar X-flare. The radiative flux intensity variation, as recorded by GOES-15 satellite, is shown in Fig. 2, the top panel, while the signal amplitude and phase variations relative to values in the case of the unperturbed ionosphere and registered by the Belgrade AWESOME receiver are presented in the bottom and the middle panels, respectively. The considered signal is the one being transmitted by the DHO transmitter in Germany at 23.4 kHz.

In the theoretical analysis, we use the Wait's model for the ionosphere which is characterized by two independent parameters the sharpness β and the reflection height H' . The VLF signal propagation is simulated by the LWPC numerical program with input parameters β and H' while the output data we used in our calculations are the signal amplitude and its phase.

In the case of unperturbed ionosphere, the program gives 0.3 km^{-1} and 74 km for β and H' , respectively. When the ionosphere is perturbed, these two parameters are chosen as a pair combination that gives the best matching of the amplitude and phase values obtained by LWPC with those recorded directly by the receiver. The time distributions of these parameters are presented in Fig. 3. In the considered case, we can see that H' has a minimum and β a maximum in the time of maximal ionospheric perturbation.

Knowing the time dependence of these values, the electron concentration $N(t, h)$ at altitude h and time t can be calculated from the Wait's theory by:

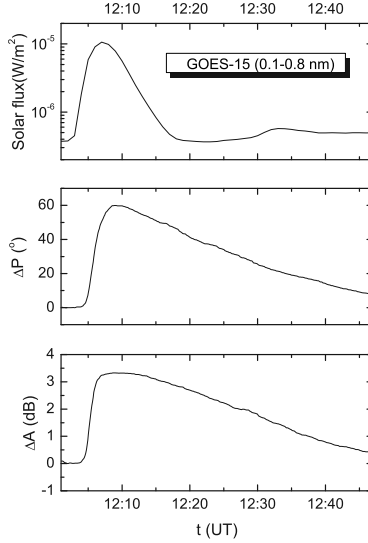


Figure 2: Solar flux registered by GOES-15 satellite and phase and amplitude changes of signal emitted from DHO transmitter (Germany) and recorded by the AWESOME receiver in Belgrade (Serbia) at the time of the observed flare. Zero values correspond to the amplitude and phase recorded when the ionosphere is unperturbed.

$$N(t, h) = 1.43 \times 10^{13} e^{-\beta(t)H'(t)} e^{(\beta(t)-0.15)h}. \quad (1)$$

The time distributions of the electron concentration at 70, 75 and 80 km are shown in Fig. 4. Very interesting is the fact that the start of rise and the maximum of the electron concentration $N(t, h)$ both occur with a time delay after the satellite recorded the related changes in the radiation flux as can be seen from a comparison of the top panel of Fig. 2 and Fig. 4.

The electron concentration dynamics in the low ionosphere can be analyzed by:

$$\frac{dN(t, h)}{dt} = G(t, h) - L(t, h). \quad (2)$$

This equation is very complicated in its general form because of the complexity of terms $G(t, h)$ and $L(t, h)$ that describe the electron gain and electron loss processes respectively.

The dominant electron gain process in the D-region at the daytime is the photoionization but below $h = 70-75$ km also the contribution of cosmic radiation has to be taken into account. Moreover, a few processes, such as electron-ion, ion-ion and three-body recombination influence the electron loss mechanism. A quantitative analysis of these processes requires knowledge of the temperature and concentration of neutral and charged particles as functions of altitude, longitude, latitude, and time. However, these data are practically not available in real time and only results of approximate calculations are obtainable for specific models.

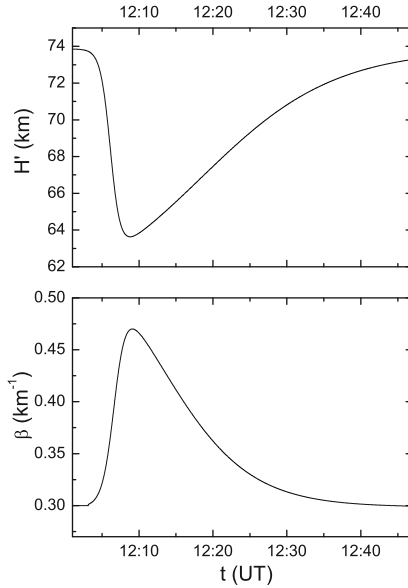


Figure 3: The reflection height H' and sharpness β obtained by comparative LWPC simulation and by the recorded signal characteristic values.

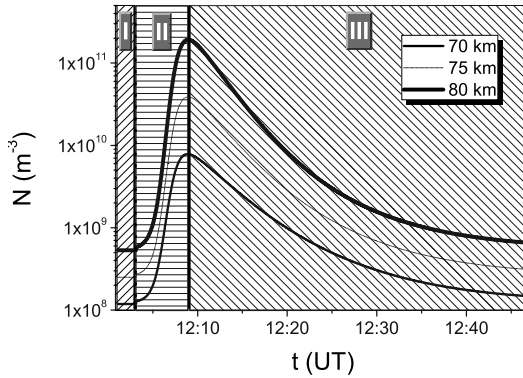


Figure 4: The time distribution of electron concentration during a quasi equilibrium (I), photo-ionization (II) and recombination regime (III) at altitudes 70, 75 and 80 km.

Fig. 5. shows the time distributions of the total electron concentrations rate.

Fig. 4 and Fig. 5 indicate that the ionospheric response can be divided into three regimes:

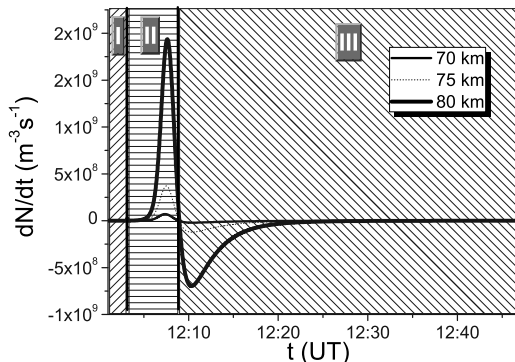


Figure 5: The temporal dependence of the electron concentration time derivative during the quasi equilibrium (I), photo-ionization (II), and recombination regime (III) at altitudes $h=70, 75$ and 80 km.

Regime 1 - the quasi equilibrium regime - where the flux increase does not cause electron concentration changes as the electron generation is instantaneously balanced by the electron recombination.

Regime 2 - the photo-ionization regime - where the photo-ionization dominates recombination resulting in electron concentration increase.

Regime 3 - the recombination regime - where the recombination dominates photo-ionization resulting in electron concentration decrease.

5. CONCLUSIONS

In this paper, we pointed out the significance of studies of low ionosphere by VLF waves and their applications in science and information technologies. Also, the Belgrade VLF station located in the Institute of Physics in Zemun is presented.

The main focus was on explanation of experimental and theoretical analyses of the low ionospheric response to a particular solar X-flare event by studying the recorded VLF signal characteristics. We showed an analogy of the time distributions of the radiation flux registered by GOES-15 satellite and those of the amplitude and phase time variations of the signal emitted by the DHO transmitter (Germany) and recorded by the Belgrade AWESOME receiver. The comparison of the electron concentration time distributions with that of the radiation flux reveals the evidence that ionospheric response to the solar X-flares has three regimes: the quasi equilibrium, photo-ionization and recombination.

Acknowledgement

The present work was supported by the Ministry of Education and Science of the Republic of Serbia as a part of the projects no. III 44002 and 176002. Author is grateful for very useful discussions with prof. dr Vladimir Čadež.

References

- Balan, N., Alleyne, H., Walker, S., Reme, H., McCrea, I., and Aylward, A.: 2008, Magnetosphere ionosphere coupling during the CME events of 07 12 November 2004, *Journal of Atmospheric and Solar-Terrestrial Physics*, **70**, 2101.
- Bremer, J. and Singer, W.: 1977, Diurnal, seasonal and solar-cycle variations of electron densities in the ionospheric D- and E-regions, *Journal of Atmospheric and Terrestrial Physics*, **39**, 25.
- Cummer, S. A.: 1997, Lightning and ionospheric remote sensing using VLF/ELF radio atmospherics, Ph. D. Dissertation, Department Electrical Engineering of Stanford University, Stanford, USA.
- Ferguson, J. A.: 1998, Computer Programs for Assessment of Long-Wavelength Radio Communications, Version 2.0, Space and Naval Warfare Systems Center, San Diego, CA.
- Fishman, G. J. and Inan, U. S.: 1988, Observation of an ionospheric disturbance caused by a gamma-ray burst, *Nature*, **331**, 418.
- Hayakawa, M., Horie, T., Muto, F., Kasahara, Y., Ohta, K., Liu, J. and Hobara, Y.: 2010, Subionospheric VLF/LF Probing of Ionospheric Perturbations Associated with Earthquakes: A Possibility of Earthquake Prediction, *SICE Journal of Control, Measurement, and System Integration*, **3**, 1, 010.
- McRae, W. M. and Thomson, N. R.: 2004, Solar flare induced ionospheric D-region enhancements from VLF phase and amplitude observations, *Journal of Atmospheric and Solar-Terrestrial Physics*, **66**, 77.
- Morfitt, D. G. and Shellman, C. H.: 1976, MODESRCH, an improved computer program for obtaining ELF/VLF mode constants, Interim report 77T, NTIS, ADA 032473, Naval Electronics Laboratory Center, USA.
- Nina, A., Čadež, V., Srećković, V., and Šulić, D.: 2012a, Altitude distribution of electron concentration in ionospheric D-region in presence of time-varying solar radiation flux, *Nuclear Instruments and Methods in Physics Research B*, **279**, 110.
- Nina, A., Čadež, V., Šulić, D., Srećković, V. and Žigman, V.: 2012b, Effective electron recombination coefficient in ionospheric D-region during the relaxation regime after solar flare from February 18, 2011, *Nuclear Instruments and Methods in Physics Research B*, **279**, 106.
- Rawer, K., Bilitza, D. and Ramakrishnan, S.: 1978, Goals and Status of the International Reference Ionosphere, *Rev. Geophys.*, **16**, 177.
- Turunen, E., Matveinen, H. and Ranta, H.: 1992, Sodankyla Ion Chemistry (SIC) Model, Sodankyla Geophysical Observatory, Rept. 49, Sodankyla, Finland.

ON THE KINEMATICS OF STARS FROM THE SOLAR NEIGHBOURHOOD CASE OF THE TWO DISC COMPONENTS

SLOBODAN NINKOVIĆ, MILAN STOJANOVIĆ, ZORICA CVETKOVIĆ

Astronomical Observatory, Volgina 7, 11060 Belgrade 38, Serbia
E-mail: sninkovic@aob.rs, mstojanovic@aob.rs, zorica@aob.rs

Abstract. The kinematics of stars from the Solar neighbourhood which belong to either of the two discs – thin or thick – is modelled following particular Gaussian distributions of their random velocities. As the mean motion in both cases rotation (circular motion of the centroid) is admitted. Assuming a given value for the galactocentric speed of Local Standard of Rest (LSR) it is possible to model the same samples in their motion with respect to LSR. Here for each sample (each of the discs) one has five parameters: three velocity dispersions, rotation speed and LSR speed. Varying these parameters we find the fractions of stars, members of either disc, which occupy a given volume in the velocity subspace centred on the LSR. In the case of the thin disc we find that almost all stars are within a sphere centred on LSR with radius equal to 120 km s^{-1} and this result is practically independent of the value assumed for the galactocentric speed of LSR. In the case of the thick disc almost all stars are within a sphere centred on LSR with radius equal to 250 km s^{-1} , but this result appears to be slightly dependent of the value assumed for the galactocentric speed of LSR.

1. INTRODUCTION

In the case of stars from the Solar neighbourhood very often the mere knowledge of the speed of a star can be indicative for the purpose of the kinematical membership of this star. Recently we studied the case of stars supposed to belong to the Galactic halo (Ninković et al. 2012 Paper I). That time we indicated the limits in the velocity subspace which contain given fractions of halo stars. However, any study of the halo is incomplete if the Galactic disc is not taken into account. Therefore, here we apply the same procedure for stars of the Galactic disc.

2. APPROACH

We assume that in general the Galactic disc, at least, at the galactocentric position of the Sun, can be split in two components known as thin disc and thick disc. The speed of a star taken here into account is that with respect to the local standard of rest (LSR).

As described in Paper I, for a given component (sample) we have five parameters: velocity dispersions along the standard axes (x-axis, velocity component U towards Galactic centre; y-axis, velocity component V in sense of Galactic rotation and z-axis, velocity component W towards north Galactic pole), centroid velocity (rotation speed) and galactocentric speed of LSR. Here we have two artificial star samples representing the two disc components. Every sample star is assigned component values U , V , W of its random velocity. Its speed with respect to LSR is calculated by using the following formula:

$$v = \sqrt{U^2 + (u + V - v_0)^2 + W^2} . \quad (1)$$

Here v is the speed of the star with respect to LSR, u is the rotation speed and v_0 is the galactocentric speed of LSR. The value of v is further used in determining to which part of the velocity subspace the star belongs. Such values are referred to as interval limits in Table 1. In this table under each interval the corresponding fraction of stars is given.

For the thin disc we assume only one set of velocity dispersions: 34, 22, 17 (along the three axes, respectively, in km s^{-1} , Fig. 1) following the result of Vidojević & Ninković (2009). The rotation speed is assumed to be always by 10 km s^{-1} slower than the galactocentric speed of LSR. In the case of the thick disc taking into account the existing evidence (e.g. Alcobé and Cubarsí 2005) we assume for the velocity dispersions values approximately twice as those for the thin disc; the rotation speed is assumed to be always by 60 km s^{-1} slower than the galactocentric speed of LSR (Fig. 2).

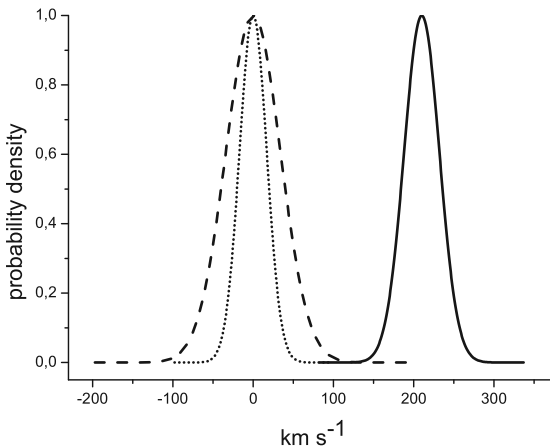


Figure 1: Gaussian velocity distribution for thin-disc stars: dashed curve x axis (centred on 0 km s^{-1} , dispersion 34 km s^{-1}); solid curve y axis (centred on 210 km s^{-1} , dispersion 22 km s^{-1}); dotted curve z axis (centred on 0 km s^{-1} , dispersion 17 km s^{-1}).

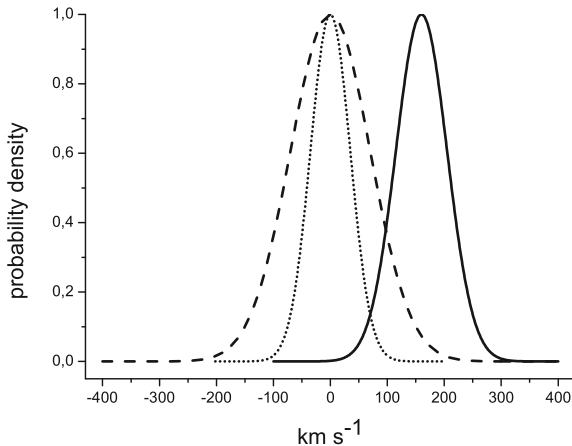


Figure 2: Gaussian velocity distribution for thick-disc stars: dashed curve x axis (centred on 0 km s^{-1} , dispersion 70 km s^{-1}); solid curve y axis (centred on 160 km s^{-1} , dispersion 45 km s^{-1}); dotted curve z axis (centred on 0 km s^{-1} , dispersion 35 km s^{-1}).

3. RESULTS

The speed of LSR is varied between 190 and 250 km s^{-1} (step equal to 30 km s^{-1}). For each particular value we calculate for every sample star its speed with respect to LSR v (formula 1) and determine the fractions of sample stars within an inner sphere centred on LSR, beyond an outer concentric sphere and between the two spheres. The radius of the inner sphere is varied to include three different values: 80 , 100 and 120 km s^{-1} , that of the outer sphere is always the same: 250 km s^{-1} . What we obtain is that for the thin disc practically all stars are within 120 km s^{-1} from LSR and this is practically independent of the assumed value for the galactocentric speed of LSR. In the case of the 80 km s^{-1} sphere the obtained fractions indicate a dependence on the assumed speed of LSR, if 190 km s^{-1} is used, the fraction is substantially lower than in the cases of the other two values for which the corresponding fractions are rather similar. The randomiser has a very weak influence.

In the case of the thick disc the situation is similar, but this time the results corresponding to the LSR speed of 250 km s^{-1} show a somewhat more significant deviation yielding lower fractions. Clearly, as in the case of the thin disc, there is a speed value (with respect to LSR) beyond which the fraction of stars is practically zero. This time it is 250 km s^{-1} . Within the speed value playing the analogous role in the case of the thin disc (120 km s^{-1}) a dependence of the fraction of thick-disc stars on the value assumed for the galactocentric speed of LSR is manifested. In particular, if 250 km s^{-1} is assumed, we have 60% , but as this value decreases, the fraction within 120 km s^{-1} increases, to attain about 75% .

In a more complete way the results are given in Table 1. The columns contain: first – the disc component; second – the galactocentric speed of LSR; the other ones – speed limits and corresponding fractions of stars.

Table 1. The fractions of stars for both discs depending on LSR speed.

Comp.	LSR speed [km s ⁻¹]	Speed km s ⁻¹	Frac. %	Speed km s ⁻¹	Frac. %	Speed km s ⁻¹	Frac. %
THIN DISC	220	[0,80]	76.6	(80,250)	23.4	[250,∞)	0
		[0,100]	92.2	(100,250)	7.8	[250,∞)	0
		[0,120]	98.8	(120,250)	1.2	[250,∞)	0
	190	[0,80]	61.6	(80,250)	38.4	[250,∞)	0
		[0,100]	81.6	(100,250)	18.4	[250,∞)	0
		[0,120]	96.0	(120,250)	4.0	[250,∞)	0
THICK DISC	220	[0,80]	37.2	(80,250)	62.8	[250,∞)	0
		[0,100]	55.2	(100,250)	44.8	[250,∞)	0
		[0,120]	73.6	(120,250)	26.4	[250,∞)	0
	250	[0,80]	24.4	(80,250)	75.4	[250,∞)	0.2
		[0,100]	41.2	(100,250)	58.8	[250,∞)	0
		[0,120]	59.2	(120,250)	40.6	[250,∞)	0.2

4. CONCLUSIONS

In studying the distribution of stars from the Solar neighbourhood we find some limiting values of speed with respect to LSR. In particular, we find that within a sphere centred on LSR with radius equal to 120 km s⁻¹ practically all stars of the thin disc are contained and also about two thirds of stars belonging to the thick disc. The fraction of thick-disc stars shows a dependence on the value assumed for the LSR speed with respect to the Galactic centre. This can be expected with regard that the velocity dispersion for the thick disc exceeds that for the thin disc. So the fraction of two thirds corresponds to the value of 220 km s⁻¹ for LSR around the centre of the Milky Way. Taking into account the results of Paper I, that beyond the sphere of 250 km s⁻¹ centred on LSR we have approximately half halo stars from the Solar neighbourhood, we can say that these very-high velocity are dominated by the halo, unlike those within 120 km s⁻¹ where the percentage of halo stars is very low (usually under 10%).

Acknowledgements

The authors acknowledge that this research has been supported by the Ministry of Education and Science of the Republic of Serbia: Project No 176011 "Kinematics and Dynamics of Celestial Bodies and Systems".

References

- Alcobé, S. and Cubarsí, R.: 2005, *Astronomy and Astrophysics*, **442**, 929.
Ninković, S., Cvetković, Z. and Stojanović, M.: 2012, Proceed. XVI National Conference of Astronomers of Serbia, *Publ. Astron. Obs. Belgrade*, in press.
Vidojević, S. and Ninković, S.: 2009, *Astronomische Nachrichten*, **330**, 46.

ON THE COMPOSITE NATURE OF THE GALAXY NGC 5929

GEORGI PETROV¹, MICHEL DENNEFELD²

¹*Institute of astronomy and National astronomical observatory, Sofia, Bulgaria*

²*Institut d'Astrophysique de Paris, University of Paris, France*

Abstract. The galaxy NGC 5929 is a member of the double system NGC 5929/5930. The two objects are at a distance of 0'.5 from each other. They figure under No. 90 in the Arp Catalogue of Peculiar Galaxies, and Zwicky mentioned them as compact objects (I Zw 112). Karachentsev included them under No. 466 in his catalogue of isolated double galaxies. Huchra et al. (1982) classified it as SyG type2. CCD spectra of the nucleus of the galaxy NGC 5929 for two different emission line regions obtained January 2012 with 1.93-m OHP telescope (M.D.) and covered spectral interval from $\lambda 3650$ to $\lambda 7300$ Å are analyzed. Dual emission line regions, reported from other authors too, are revised. A lot of emission lines as H α , H β , H γ , $\lambda 6300$, $\lambda 6363$ [OI], $\lambda 3727$ [OII], $\lambda 4959$, $\lambda 5007$ [OIII], $\lambda 6717$, $\lambda 6731$ [S II], $\lambda 6548$, $\lambda 6584$ [N H], $\lambda 6312$ [SIII], etc. and several absorption lines have been identified. The $\lambda 5199$ [N I] line is faintly visible, as well as the Fraunhofer absorption feature *b*, representing the neutral magnesium line $\lambda 5175$ Mg I. The components found in the line profiles of the NGC 5929 nucleus by other authors too can be interpreted as evidence for radial motion of gaseous masses at speeds of 200-300 km/sec. The physical parameters of the nucleus are estimated. The relative abundance of several ions is evaluated. For the emission-line spectrum to result from shock heating of the gas is inconsistent with the observational evidence. The discovery of kinematic shock signatures associated with a localized radio jet interaction in the merging Seyfert galaxy NGC 5929 and their interpretation the relative prominence of shocks to the high density of gas in nuclear environment as other models are briefly discussed.

1. INTRODUCTION

The galaxy NGC 5929 is a member of the double system NGC 5929/5930. The two objects are at a distance of 0'.5 from each other. They figure under No. 90 in the Arp Catalogue of Peculiar Galaxies (see Fig. 1a below), and Zwicky mentioned them as compact objects (I Zw 112). Karachentsev included them under No. 466 in his catalogue of isolated double galaxies. Huchra et al. (1982) classified them as SyG type2. NGC 5929 is nearby Seyfert galaxy. Because of its interesting optical and radio structure, it is investigated very intensively – more

then 300 references in SIMBAD and more than 270 in NED databases. During the last years the IR and X_{ray} investigations of NGC 5929 become leading.

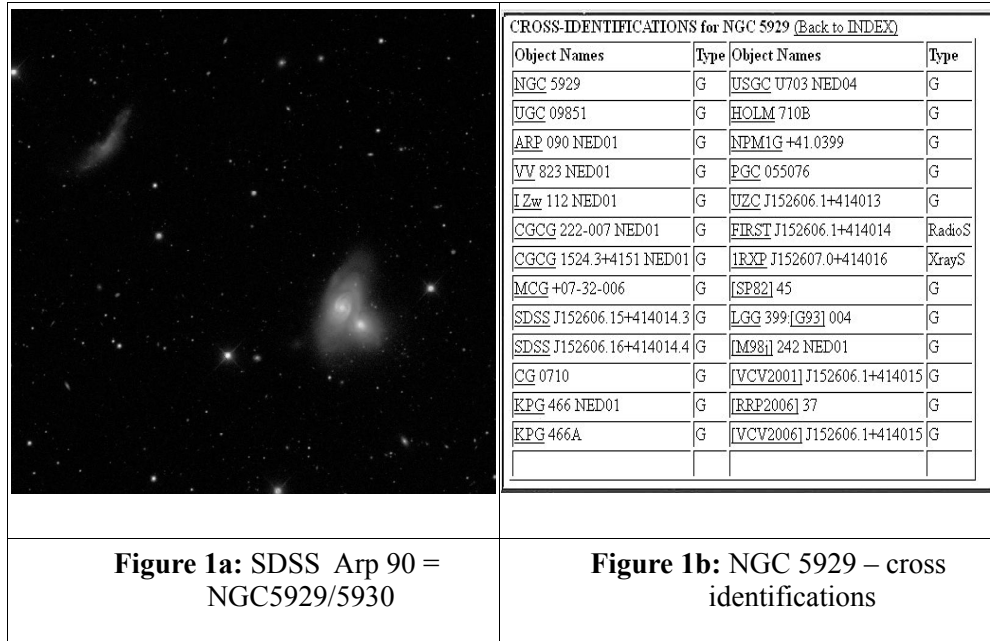
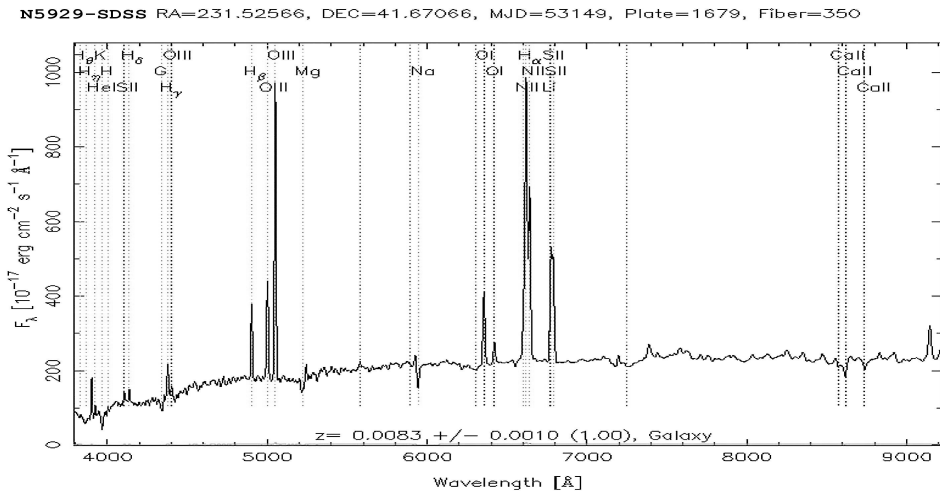


Figure 1b from NED shows all the cross-identifications of NGC 5929. In Fig.2 below the integrated spectrum of NGC 5929 from SDSS is shown. A lot of absorption features and emission lines are identified.



2. HISTORICAL OVERVIEW

Below we will try to have a look mainly of optical investigations of NGC 5929. First time double pick emission was shown in G. Petrov's PhD thesis (Fig. 12) using spectrograms obtained with the 125-cm reflector of the Crimean station, Sternberg Astronomical Institute. In Fig.3 below the registrogram of the H_α regions of the spectrum of NGC 5929 is shown. Double_picked emission in the lines of [OI], [NII] and [SII] is clearly visible.

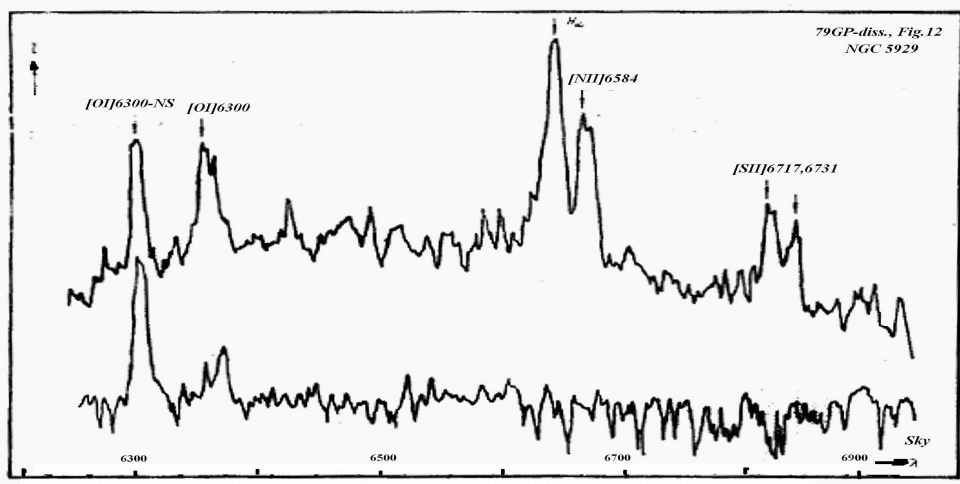


Figure 3: Registrograms of the spectra of NGC 5929 from the 6_m telescope.

The first spectrophotometric investigations of the integrated spectrum of the galaxy are presented in Petrov (1979a). Here NGC 5929 was classified as “emission-line galaxy”, not as a SyG one and double pick emission is not commented. Spectra of the nucleus of the galaxy NGC 5929 obtained with the 1.25-m and 6-m telescopes show emission lines with separate components in the wings. In the blue and red wings of each line one can see components shifted 5-6 Å away from the center, nucleus appears to be devoid of structure. A spectrum of the other member of the pair, NGC 5930, obtained at the same resolution in wavelength, does not show components in the wings of the lines. We have found that the components in the line profiles of the NGC 5929 nucleus can be interpreted as evidence for radial motion of gaseous masses at speeds of 200-300 km/sec (Golev et al. 1980). We make an evaluation the Ly_c-radiation of ca. 1000 young hot stars O5 V class in the nucleus of the galaxy is the most probable source of gas ionization.

Huchra et al. (1982) classified NGC 5929 as SyG type 2. Kennikutt & Keel (1984) investigated the effect of close galaxy-galaxy interactions on the level of nuclear activity in spiral galaxies. They demonstrated that “...galaxies with nearby

companions possess significantly higher nuclear emission-line luminosities and equivalent widths, and their nuclei exhibit a significantly higher level of ionization on average. A much higher fraction of galaxies with Seyfert or Seyfert-type nuclei is found in the sample of multiple systems... The radio and optical results make a strong case for the presence of environmentally influenced nuclear activity in a significant fraction of spiral galaxies... In any case, it is clear that conditions in the nuclei are not isolated from the outer disks". A low-dispersion spectrum taken through a 4.7-arcsec circular aperture shows a red continuum with absorption lines characteristic of an old population.

Keel (1985) investigates the "dual emission-line regions in the Seyfert galaxy NGC 5929". He shows that the type 2 Seyfert nucleus of NGC5929 contains two emission regions situated symmetrically about the center of the galaxy with the ionization levels normally associated with Seyfert nuclei. Whittle et al. (1986) provided a detailed investigations of extended forbidden O III emission associated with nuclear radio lobes of the galaxy. As they mentioned, "...NGC 5929 is a nearby Seyfert 2 galaxy with particularly simple double-lobed radio structure. The [OIII] emission-line distribution closely matches that of the radio emission, showing two distinct components of different velocity straddling the optical nucleus. The Narrow Line Region (NLR) of Seyfert galaxies appears to be closely related to the nuclear non-thermal radio emission...The absence of a young stellar population is evident from the 5150 Å continuum image, which shows no enhancement in the vicinity of the radio lobes".

It is very likely Wakamatsu & Nishida (1988) to be the first authors showing the dual emission-line clouds take the place in two members of the interacting pair Arp 90. "On optical spectra, dual-peak emission-line clouds have been discovered in both nuclei of an interacting pair Arp 90 (NGC 5929 + NGC 5930). The clouds in each galaxy are quite similar in their spatial, kinematical, and radio properties, but quite different in the excitation levels of the ionized gas, i.e., classified as H II region type for NGC 5930 or Seyfert 2 type for NGC 5929. NGC 5930 was detected as an IRAS source with the luminosity $L_{\text{IR}} = 2.0 \times 10^{10} L_{\text{sun}}$, while NGC 5929 was not...". The authors have detected 2.6 mm CO (J = 1-0) line emission from the nuclear region of NGC 5930 but not from NGC 5929.

Taylor et al. (1989) explained the narrow emission lines of NGC 5929 with a plasmon driven bowshock model, in which the linear motion of radio-emitting bubbles of plasma ejected from the nucleus drives bowshocks into the ambient nuclear medium. The cooled shocked gas, photo-ionized by the UV nuclear continuum, produces the optical NLR emission. The two nuclear components at both radio and optical wavelengths of NGC 5929 galaxy they model as two plasmon driven bowshocks on either side of the nucleus.

In their "High-Resolution Observations Of The Multicomponent Nucleus of NGC 5929" Wilson & Keel (1989) shows "...the central region of the Type 2 Seyfert galaxy NGC 5929 is known to contain double radio-continuum and optical emission-line clouds separated by $\sim 1''$ ". When the radio continuum and [O III] 5007 image of Whittle et al. (1986) are compared at the same spatial resolution, there is

no evidence that the separations or position angles of the radio and emission-line clouds differ. The double H α clouds appear to differ in position angle by $\sim 20^\circ$ from the radio lobes.”

Afanas'ev & Sil'chenko (1991) show the two gas clouds being the main forbidden line emitters in the center of NGC 5929 are found to possess the relative line-of-sight velocities -50 km/s (the eastern cloud) and $+270$ km/s (the western cloud). They suppose “the emission brightness centers which coincide with the radio lobes are probably the shock wave regions forming on the border between the clouds and the galactic disk”.

HST images of NGC 5929 and 5930 show the nuclei of both galaxies contain emission line gas. Previous ground-based observations of the Seyfert galaxy NGC 5929 include [O III] and H α + [N II] images, showing that its nucleus contains an elongated region of high-excitation emission line gas. In these HST images, this gas is clearly separated into two distinct regions separated by about $1''$ (Bower et al. 1993). Bower et al. (1994) show the correspondence between the emission line gas and the radio morphology suggests that the structure of the NLR in NGC 5929 is governed by matter ejected from the AGN. The high-excitation gas in the narrow line region (NLR) of NGC 5929 is resolved into individual clouds in the central $1.5''$. Although the [O III] emission is clearly not spherically symmetric with respect to the nucleus and no direct evidence for the reddening and/or obscuration effects characteristic of a dusty torus, which, in the context of "unified models", is expected to obscure the active galactic nucleus (AGN) in type 2 Seyfert galaxies.

Su et al. (1996) confirm the triple radio structure reported in earlier studies. The weak central source of the triplet is almost certainly associated with the active nucleus. The radio structure of NGC 5929 to recent HST images was compared and the possible models to relate the radio and optical structures (bowshock model - Taylor et al. 1989), plasmon model (Pedlar et al. 1985) have been discussed.

Ferruit et al. (1997) report observations of the galaxy NGC 5929 with the integral field spectrograph Tiger covering the [NII], H α and [SII] emission associated with the two radio-lobes. The two optical line emission components have been kinematically separated using Gaussian fitting of the spectra... All models predict edge-brightened bow shock or cylindrical shell structures for the ionized gas, which seems to conflict with the HST imaging. They noted the high spatial resolution spectrography is needed to obtain the velocity structure of both the NE and SW components and to understand the relationship between the relativistic and thermal gases.

H II region population in a sample of nearby galaxies with nuclear activity have been studied by Gonzalez Delgado et al. (1997). They showed the emission-line morphology in the two disks of the interacting pair NGC 5929/C 5930 formed by a Sy2 nucleus, NGC 5929, and a starburst nucleus in a Sb galaxy, NGC 5930 are very different. NGC 5929 only shows some weak H II regions, however, the disk of NGC 5930 shows bright H II regions, mainly along the spiral arms.

Kotilainen (1998) detects extended blue continuum components in the circumnuclear region of several galaxies. These components form a double structure across the NGC 5929 nucleus. "...The nucleus of NGC 5929 is situated between two blue maxima at opposite sides of the nucleus... they possibly represent extranuclear scattering mirrors of anisotropically escaping nuclear light".

Ferruit et al. (1999) carry out spectroscopy of spatially resolved narrow line regions in NGC 5929 with HST Faint Object Spectrograph. It displays an "extended emission-line region with two main components, one blueshifted and one redshifted, located northeast and southwest of the nucleus, respectively. Radio observations show a triple radio source with two lobes straddling an unresolved nuclear component. Comparison between the radio maps and the emission-line observations reveals a close morphological and kinematical association between the ionized gas and the radio-emitting material. The observed line ratios are compared with the predictions of the two component (matter- and ionization-bounded, MB-IB), central source photoionization models of Binette et al. (1996) and of the fast, photoionizing ("autoionizing") shock models of Dopita & Sutherland (1995). In NGC 5929, the MB-IB models have problems reproducing the strengths of the neon lines, while shock/precursor models with a velocity ca. 300 km/s provide a good match to the data".

Rhee & Larkin (2000) show significant obscuration to the narrow-line region of the galaxy.

Gonzalez Delgado et al. (2001) search for the direct spectroscopic signature of massive stars and thereby probe the role of circumnuclear starbursts in the Seyfert phenomenon. They consider the possibility that there may be two distinct subclasses of Seyfert 2 nuclei - "starbursts" and "hidden broadline regions". NGC 5929 belongs to the group of objects with a continuum dominated by an old stellar population (the stellar lines are similar to those of an old population. Later-on Rainmann et al. (2003) showed the NGC 5929 galaxy is in a group dominated by 10-Gyr metal-rich stellar population (with solar or above metallicity).

Rosario et al. (2010) carried out a direct detection of shocked gas studying the radio jet interaction in NGC 5929. They report the discovery of kinematic shock signatures associated with a localized radio jet interaction and find that low ionization gas at the interaction site is significantly more disturbed than high ionization gas, which we attribute to a local enhancement of shock ionization due to the influence of the jet. The characteristic width of the broad low-ionization emission is consistent with shock velocities predicted from the ionization conditions of the gas.

3. OBSERVATION AND REDUCTION

Spectra of the two emission-line regions of the galaxy NGC 5929 have been taken by M. Dennefeld with the Carelec spectrograph attached to the 1.93 m OHP telescope during the night of 19/20/01/2012. The slit width

was 2 arcsec. The spectra were reduced and calibrated by standard OHP MIDAS procedure. Table 1 summarizes the data for the telescope, spectrograph, CCD receiver, exposure time, etc. Observed line fluxes are calibrated in 10^{-14} ergs s^{-1} cm^{-2} . Fig. 4 shows the two spectra – of NE and SW lobes of NGC 5929, using SPECVIEW possibilities to add some typical emission nebulae lines.

Table 1: Observational data for our spectrophotometric study of NGC 5929	
Date of observation:	19.01.2012 r.
Telescope and spectrograph:	1.93_m OHP telescope, CARELEC spectrograph
Spectroscopic data:	136 A/mm, $\lambda\lambda$ 3600 – 7200 A,
	slit: width = 0.302 mm – corresponding to 2 arcsec on the sky
	length = 50 mm - corresponding to 5.5 arcmin on the sky
Observer:	M. Dennefeld
Time exposure:	1800 sec
Dev_type:	CCD EEV 42-20
Objects:	NGC 5929A = NE_lobe, NGC 5929B = SW lobe of NGC 5929
Observed line flux:	in 10^{-14} ergs s^{-1} cm^{-2}

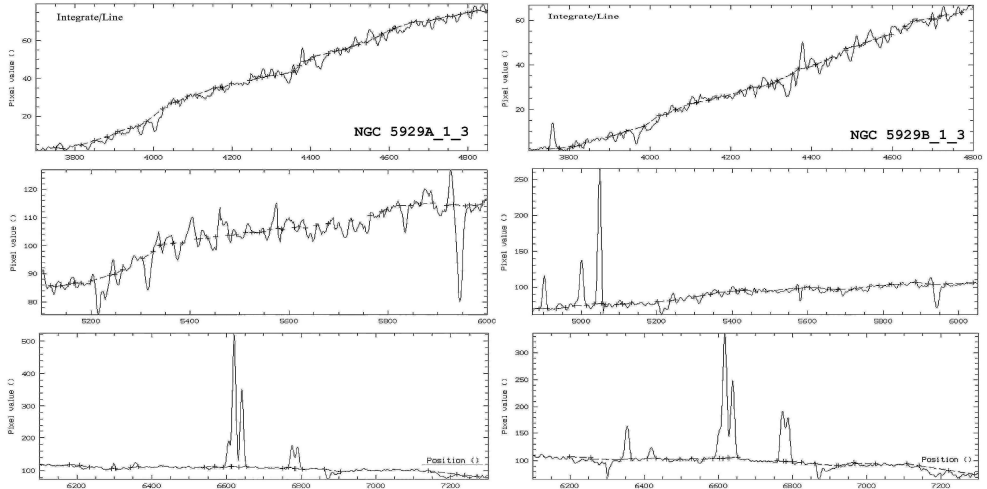


Figure 5: Results from MIDAS “INTEGRATE/LINE” procedure for NGC 5929A and B.

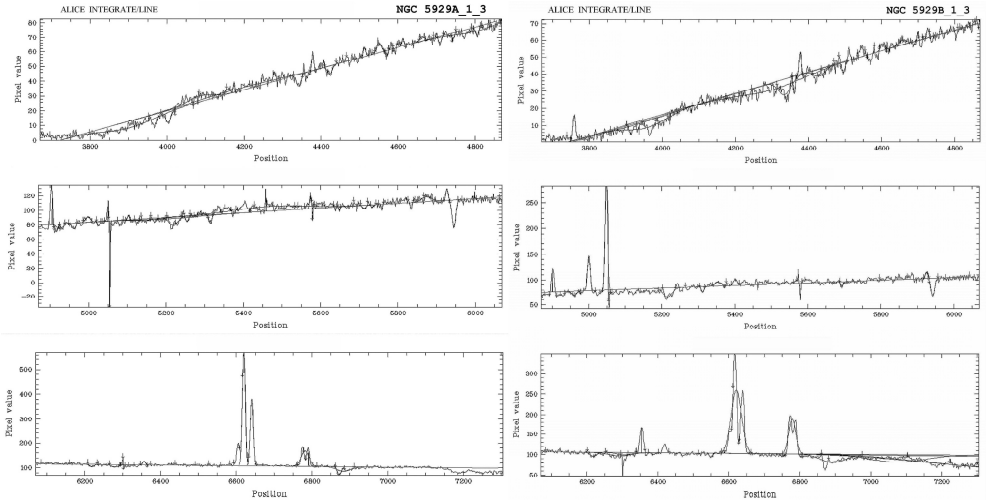


Figure 6: Results from MIDAS “ALICE - INTEGRATE/LINE” procedure for NGC 5929A and B.

Fig. 6 demonstrates ALICE INTEGRATE/LINE procedure. The same spectra subdivided in 3 parts covering ca. 1000 Å each were used. The continuum showed by continuous line was determined by ca. 20 points over the spectra fitted by different order polynoms.

Table 2 summarize the results of emission and absorption lines identifications, equivalent widths and fluxes for NE (NGC 5929A) and SW (NGC5929B) lobes of the galaxy. Absorption features bandpasses are mainly acc. to Trager et al. (1998).

Objects			NGC 5929A		NGC5929B	
X0	Ident	Bandpass	Flux	EQWT	Flux	EQWT
3727.42	[OII]		21.05	-6.26	106.33	-38.02
3840.00	H9_blend	3822-3858	-25.09	3.35		
3868.76	[NeIII]				18.47	-2.43
3889.00	HeI&H8				-25.70	2.94
3930.00	K_CaII	3908-3952	-65.78	4.15	-67.71	6.50
3970.00	H_CaII	3952-3988	-160.59	7.78	-55.17	3.91
4068.60	[SII]				28.52	-1.25
4225.44	Ca4227	4222-4234			-25.89	0.86
4301.00	G_band	4284-4318	-72.48	1.70	-177.25	5.15
4340.48	H_gamma		61.05	-1.29	109.85	-2.86
4368.74	[OIII]+?	Blend?			37.76	-0.96
4386.06	Fe4383	4369-4420	-147.29	2.81	-48.37	1.18
4471.60	HeI		26.24	-0.45	23.78	-0.49
4536.88	Fe4531	4514-4559	-42.52	0.68	-49.10	1.29
4541.60	HeII		7.19	-0.12		
4552.00	Fe4531	4514-4559	-38.54	0.60		
4656.25	C2-4668	4634-4720	-40.84	1.24		
4668.62	C2-4668	4634-4720			-43.48	0.70
4685.70	HeII		22.69	-0.32	25.24	-0.41
4698.23	C2-4668	4634-4720	-32.30	0.45		
4861.34	H_beta		403.47	-5.28	456.73	-6.50
4871.98	Hbeta	4847-4876	-27.66	0.36		
4893.40	[FeVII]				65.58	-0.92
4924.00	FeII				-37.29	0.51
4931.00	[OIII]		34.45	-0.43	12.64	-0.17
4958.90	[OIII]				753.70	-10.09
4972.10	[FeVI]		14.47	-0.18		

5006.80	[OIII]				1820.00	-23.50
5015.55	Fe5015	4977-5054	-245.40	2.96		
5027.85	Fe5015	4977-5054			-28.75	0.76
5102.90	MgI	5069-5134			-57.63	1.07
5107.89	MgI	5069-5134	-7.30	0.36		
5158.98	[FeVII]		15.80	-0.18		
5168.29	Mg2	5154-5196	-198.57	2.25	-306.15	3.85
5191.82	[ArIII]		78.06	-0.96		
5199.00	[NI]		30.17	-0.34	78.06	-0.96
5270.20	Fe5270	5245-5285	-144.90	1.50	-126.41	1.42
5328.43	Fe5335	5312-5352	-48.00	0.48	-93.23	1.00
5398.30	Fe5406	5387-5415	-86.55	0.83		
5423.90	[FeVI]		29.26	-0.28		
5517.66	[CIII]		68.35	-0.65	27.19	-0.28
5630.82	[FeVI]		19.44	-0.18		
5699.24	Fe5709	5696-5720	-102.62	0.94	-112.99	1.13
5784.96	Fe5782	5776-5796	-102.07	0.89	-45.76	0.44
5790.70	Hg		-87.50	0.77	-46.96	0.45
5875.65	HeI		114.32	-1.01	65.61	-0.63
5897.23	NaD	5876-5909	-411.68	3.80	-471.42	4.54
5971.30	TiO1	5936-5994	-22.87	0.20	-107.41	1.02
6228.50	TiO2	6189-6272	-124.97	1.14	-591.21	5.79
6300.00	[OI]		145.08	-1.32	783.29	-7.62
6363.80	[OI]+?				239.90	-2.31
6374.00	[FeX]				227.61	-2.18
6548.88	[NII]		766.65	-7.00	754.41	-7.20
6562.81	H_alpha		4387.74	-38.96	3308.84	-31.70
6583.83	[NII]		2494.67	-22.30	1928.58	-18.24
6716.42	[SII]		807.25	-7.42	1286.89	-13.01
6730.78	[SII]		730.68	-6.91	1290.31	-13.10

In Fig.7 we present an extraction of the NGC 5929B spectrum round H_alpha (ca. 900 Å) and H_beta (ca. 400 Å) lines and ALICE INTEGRATE/LINE analyze - strong narrow absorption feature near the

[OIII] 5007 strong emission can be seen. Continuum is shown with almost straight line. The procedure „propose“ gauss-fitting of the emission features, but obviously the resolution in H_alpha region is not enough, so the result of such „decompositions“ is far from satisfactory. In Tab.3 we summarize the more accurate line identification, fluxes and equivalent widths of the line in above mentioned regions of the spectrum.

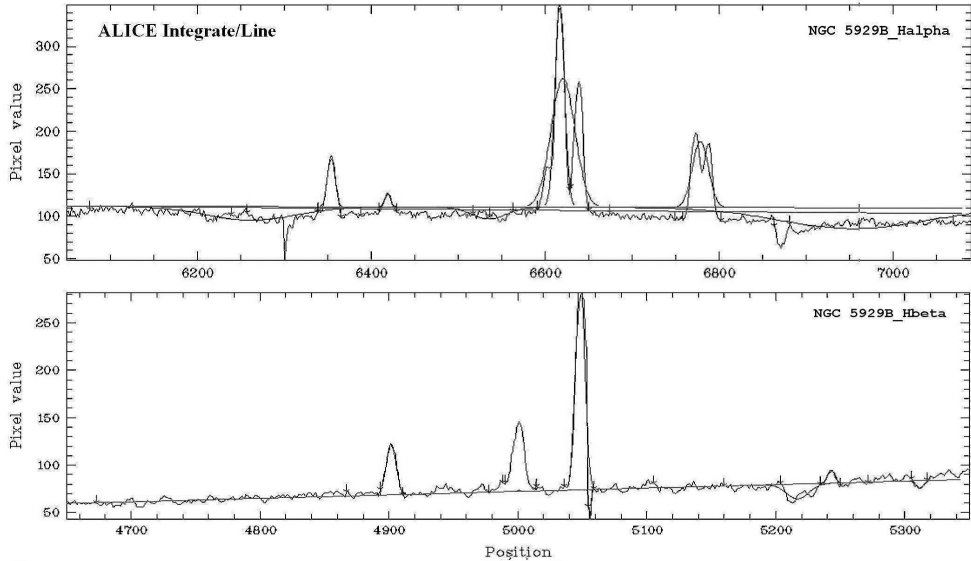


Figure 7: Results from MIDAS “ALICE - INTEGRATE/LINE” procedure for NGC 5929 B - H $_{\alpha}$ and H $_{\beta}$.

Table 3: n5929B h $_{\beta}$ h $_{\alpha}$		Rem.: EQWT > 0 means “absorption”			
X start	X end	Flux	EQWT	X0	Ident
4953.74	4970.56	-39.76	0.50	4920.510	Fe I
4983.88	5010.51	134.27	-1.63	4958.930	[O III]
5039.95	5051.16	73.19	-0.87	5006.860	[O III]
5051.16	5068.68	-273.54	3.27	5015.000	
5239.00	5248.11	36.12	-0.40	5197.940	[N I]
5239.00	5248.11	36.12	-0.40	5200.410	[N I]
5302.08	5326.61	-156.76	1.62	5269.550	Fe I
6590.32	6612.28	942.80	-8.49	6548.060	[N II]
6606.59	6630.99	4741.59	-42.39	6562.808	H_alpha
6630.99	6654.58	2580.90	-23.23	6583.370	[N II]
6763.60	6784.75	771.67	-6.99	6716.420	[S II]
6781.49	6800.20	731.93	-6.87	6730.780	[S II]

4. SPECTROPHOTOMETRIC STUDY

Table 4 presents all the spectrophotometric results for the two emission regions. Identifications, equivalent widths, fluxes and flux ratios are summarized. The highest ionization stage line in NGC 5929A is $\lambda 5159$ [FeVII] and in NGC 5929B – $\lambda 6374$ [FeX]. Forbidden lines of N⁰ doublet [NI] $\lambda 5199$, C^{II+} - [CIII] $\lambda 5517$, HeI $\lambda 4472$, 5876 and HeII $\lambda 4686$, 5411 present in both spectra. Unexpected is a present of serial of [FeVI] lines in NGC 5929A and a present of less prominent [OIII] line $\lambda 4931$ when the “traditional” $\lambda 4959$, 5007 are missing (see below). Low ionization forbidden lines of [OI] $\lambda 6300$, [OII] $\lambda 3727$, [NII] $\lambda 6548$, 6584 and [SII] $\lambda 6717$, 6731 present in both spectra too. H α /H β flux ratio – 10.845 for NGC 5929A and 7.245 for NGC 5929B confirms significant obscuration to the narrow-line region of the galaxy, mentioned by Rhee & Larkin (2000).

Oobject			NGC 5929A			NGC 5929B		
Seq	X0	Ident	Flux	EQWT	F/F_H β	Flux	EQWT	F/F_H β
1	3727.42	[OII]	21.05	-6.26	0.052	106.33	-38.02	0.233
2	3868.76	[NeIII]				18.47	-2.43	0.040
3	4068.60	[SII]				28.52	-1.25	0.062
4	4340.48	H_gamma	61.05	-1.29	0.15	109.85	-2.86	0.240
5	4368.74	[OIII]+?				37.76	-0.96	0.083
6	4471.60	HeI	26.24	-0.45	0.065	23.78	-0.49	0.052
7	4541.60	HeII	7.19	-0.12	0.018			
8	4685.70	HeII	22.69	-0.32	0.056	25.24	-0.41	0.055
9	4861.34	H_beta	403.47	-5.28	1.00	456.73	-6.50	1.00
10	4893.40	[FeVII]				65.58	-0.92	0.144
11	4931.00	[OIII]	34.45	-0.43	0.085	12.64	-0.17	0.028
12	4958.90	[OIII]				753.70	-10.09	1.650
13	4972.10	[FeVI]	14.47	-0.18	0.036			
14	5006.80	[OIII]				1820.00	-23.50	3.985
15	5158.98	[FeVII]	15.80	-0.18	0.039			
16	5199.00	[NI]	35.28	-0.39	0.087	78.06	-0.96	0.171
17	5410.80	HeII	56.16	-0.54	0.139	27.19	-0.28	0.060

18	5423.90	[FeVI]	29.26	-0.28	0.072			
19	5517.66	[ClIII]	68.35	-0.65	0.169	65.61	-0.63	0.144
20	5630.82	[FeVI]	19.44	-0.18	0.048	783.29	-7.62	1.715
21	5875.65	HeI	114.32	-1.01	0.283	239.90	-2.31	0.525
22	6300.00	[OI]	145.08	-1.32	0.360	227.61	-2.18	0.498
23	6363.80	[OI]+?				1134.14	-10.96	2.483
24	6374.00	[FeX]				227.61	-2.18	0.498
25	6548.88	[NII]	1099.54	-9.83	2.725	754.41	-7.20	1.652
26	6562.81	H_alpha	4387.74	-38.96	10.875	3308.84	-31.70	7.245
27	6583.83	[NII]	2494.67	-22.30	6.183	1928.58	-18.24	4.222
28	6716.42	[SII]	807.25	-7.42	2.001	1286.89	-13.01	2.818
29	6730.78	[SII]	730.68	-6.91	1.811	1290.31	-13.10	2.825

In Table 5 we summarize some important flux ratios to check the validity of some models above mentioned by Ferruit et al. (1999), using Binette et al. 1996 (B96) and Binette et al. 1997 (B97) models.

In our opinion our observational data do not fit well with any of these models. Remember Ferruit et al (1999) observed with HST/FOR SW lobe only – i.e. “our” NGC 5929B and the two spectrophotometric serials are quite different – e.g. $H\alpha/H\beta = 4.7$ and 7.2 respectively. As their result differs from others observations too one possible explanation could be changes in the physical conditions and ionization status of the emitting gas. Electron temperature defined by [OIII] ratios is ca. 14000 K and the electron densities in the [SII] – [OII] zone are ca. $4 - 5 \cdot 10^2 \text{ cm}^{-3}$. Our previous spectrophotometric study based on the integrated spectra of NGC 5929 are presented in Petrov (1979b). In the same time [OIII] $\lambda 4931$ line tell us for electron densities of 40 cm^{-3} as the critical electron density for this line to be observable is 40 cm^{-3} (Gurzadyan 1997). These evaluations confirm models with quite complex cloud structure with different temperatures, densities and ionization stages.

	NGC 5929A	NGC 5929B	models	
Rad. Velocities [km/sec]	2595	2526	$V_s = 300$ km/s (B96)	L_model (B97)
Ratio				
[OIII] 5007 / Hbeta		3.956	5.9 – 6.5	0.32 – 0.58
[OII] 3727 / Hbeta	0.017	0.232	1.7 – 5.2	< 0.62
[OI] 6300 / Halpha	0.033	0.254	0.32 – 0.47	< 0.39
[OII] 3727 / [OIII] 5007		0.058	0.3 – 0.8	0.57 – 0.28
[OI] 6300 / [OIII] 5007		0.300	0.15 – 0.23	0.35 – 0.17
[OIII] 5007 / [OIII] 4363		48.20	103 - 108	3.8 – 0.78
[NII] 6583 / Halpha	0.568	0.590	0.23 – 0.65	< 101
[SII] 6724 / Halpha	0.350	0.785	0.41 – 0.56	2.3 – 0.30
[He II 4686 / Hbeta	0.056	0.055	0.23 – 0.28	< 0.57
[NeIII] 3869 / Hbeta		0.040	0.50 – 0.72	1.0 – 8.7
[SII] 6717 / [SII] 6731	1.105	1.129		
[OIII] 4959+5007 / [OIII] 4363		68.16		
Ne for Te = 10 000 K	470	450		

	NGC 5929A	NGC 5929B
Log N+ (λ 6584/Hbeta)	7.99	7.83
Log S+ (λ (6717+6731)/Hbeta)	7.22	7.39
Log O++ (λ 5007/Hbeta)	-	8.10
Log O+ (λ 3727/Hbeta)	5.96	7.00
Log O ^o (λ 6300/Hbeta)	7.70	7.84
Log He+ (λ 5876/Hbeta)	11.32	11.59
Log He++ (λ 4685/Hbeta)	9.75	9.74

Based on the spectrophotometric data some evaluations of ionic abundances have been made using the methods of Pagel et al. (1979), Peimbert (1968, 1995), Oey & Shields (2000) etc. No total elemental abundances have been determined because of the lack of near IR spectra or low spectral resolution. In Tabl.6 abundances of some ions are presented assuming electron temperature $T_e = 10000$ K. As usual hydrogen abundance was set to $\text{Log}H = 12.00$. These results are close to our previous determination of the ionic abundance from the integrated spectrum of NGC 5929. In Table 7 we summarize average ionic N^+ and S^+ abundances for different kind of emission type objects – from PIN and HII regions to SyG. Pay attention – these are ionic abundances and not a chemical composition – i.e here we include ionization stage of the emitting regions.

	PIN		HII regions		Mrk Gal		Akn Gal		SyG type 2		SyG type1		Norm.Gal	
	LgN+	LgS+	LgN+	LgS+	LgN+	LgS+	LgN+	LgS+	LgN+	LgS+	LgN+	LgS+	LgN+	LgS+
$\langle X \rangle$	6.58	5.37	6.91	6.11	7.34	6.68	7.43	6.82	7.54	6.70	6.27	5.51	7.71	6.76
σ	0.84	0.63	0.41	0.32	0.22	0.30	0.20	0.36	0.26	0.29	0.44	0.44	0.34	0.26
n	37	28	36	37	28	23	18	14	28	28	25	23	20	17

Detailed results from the spectrophotometric investigation and chemical abundance of the two lobes of the galaxy together with some modeling of the cloud structure will be an object of another paper.

5. CONCLUSION

Based on the low resolution spectra from the 1.93 m OHP France telescope and CARELEC spectrograph we provided a preliminary study of the two emission lobes of the Seyfert galaxy NGC 5929. A lot of absorption features and emission lines have been identified in the two lobes. Evidences for low density clouds with $N_e \sim 40 \text{ cm}^{-3}$ in the two lobes are presented, based on the presence of [OIII] $\lambda 4931$ line.

NGC 5929A (i.e. NE-lobe) is an old star dominated region with a lot of absorption features. No signs of young stellar population have been found in accordance with the previous investigations. [OII]-[NII]-[SII] zone is characterized with $N_e \sim 470 \text{ cm}^{-3}$. No independent determination of the electron temperature was possible. Ionic abundances is quite higher in comparison with different type of emission line objects. The highest ionization lines are [FeVII] $\lambda 5159 \text{ \AA}$. It is remarkable to mention absence of [OIII] $\lambda \lambda 4363, 4959$ and 5007 \AA . Redshift determined from the emission line spectrum is $z = 0.00865$.

NGC 5929B (i.e. SW-lobe) is a typical Sy2G spectrum with a lot of strong emission lines. Redshift determined from the emission line spectrum is $z = 0.00842$. The highest ionization lines are [FeX] $\lambda 6374 \text{ \AA}$. Electron temperature in the [OIII] zone is ca. 14000K and the electron density in [OII]-[NII]-[SII] zone is characterized with $N_e \sim 450 \text{ cm}^{-3}$. Ionic abundances is quite higher in comparison with different type of emission line objects. N+ ionic abundances ($\lg N^+ = 7.83$) is lower than in NGC 5929A ($\lg N^+ = 7.99$) but all other ionic abundances are higher – e.g. $\lg O^+ = 5.96$ and 7.00 respectively. Remember practically no O++ in NCG 5929A.

References

- Afanas'ev, V. L., Sil'chenko, O. K.: 1991, *BSAO*, **33**, 103.
- Binette, L., Wilson, A. S., Raga, A., Storchi-Bergmann, T.: 1997, *A&A*, **327**, 909.
- Binette, L., Wilson, A. S., Storchi-Bergmann, T.: 1996, *A&A*, **312**, 365.
- Bower, G. A., Wilson, A. S., Mulchaey, J. S., Miley, G. K., Heckman, T. M., Krolik, J. H.: 1993, *BASS*, **182**, 406.
- Bower, G. A., Wilson, A. S., Mulchaey, J. S., Miley, G. K., Heckman, T. M., Krolik, J. H.: 1994, *AJ*, **107**, 1686.
- Dopita, M. A., Sutherland, R. S.: 1995, *ApJ*, **455**, 468.
- Ferruit, P., Pecontal, E., Wilson, A. S., Binette, L.: 1997, *A&A*, **328**, 493.
- Ferruit, P., Wilson, A. S., Whittle, M., Simpson, C., Mulchaey, J. S., Ferland, G. F.: 1999, *ApJ*, **523**, 147.
- Golev, V. K., Yankulova, I. M., Petrov, G. T.: 1980, *Sov. Astr. Lett.*, **6**, 290.
- Gonzalez Delgado, R. M., Heckman, T., Leitherer, C.: 2001, *ApJ*, **546**, 845.
- Gonzalez Delgado, R. M., Perez, E., Tadhunter, C., Vilchez, J. M., Rodriguez-Espinosa, J. M.: 1997, *ApJ Suppl. Ser.*, **108**, 155.
- Grosbol, P. J., Ponz, J. D.: 1990, In: *Acquisition, Processing and Archiving of Astronomical Images*, Eds. G. Longo, G. Sedmak, OAC and FORMEZ. p. 109.
- Gurzadyan, G. A.: 1997, *The physics and dynamics of planetary nebulae*, Springer-Verlag Berlin Heidelberg.
- Huchra, J. P., Wyatt, W. F., Davis, M.: 1982, *ApJ*, **86**, 1628.
- Keel, W. C.: 1985, *Nature*, **318**, 43.
- Kennicutt, R. C., Jr., Keel, W. C.: 1984, *ApJ*, **279**, L5.
- Kotilainen, J. K.: 1998, *A&A Suppl. Ser.*, **132**, 197.
- Oey, M. S., Shields, J. C.: 2000, *ApJ*, **539**, 687.
- Pagel, B. E. J., Edmunds, M. G., Blackwell, D.E., Chun, M. S., Smith, G.: 1979, *MNRAS*, **189**, 95.
- Pedlar, A., Dyson, J. E., Unger, S. W.: 1985, *MNRAS*, **214**, 463.
- Peimbert, M.: 1968, *ApJ*, **154**, 33.
- Peimbert, M.: 1995, In: *The Analysis of Emission Lines*, Ed. R. E. Williams, Cambridge University Press.
- Petrov, G.: 1979a, *Sov. Astr. Lett.*, **5**, 141.
- Petrov, G.: 1979b, *Astrofizika*, **17**, 43.
- Raimann, D., Storchi-Bergmann, T., Gonzalez Delgado, R. M., Fernandes, R. C., Heckman, T., Leitherer, C., Schmitt, H.: 2003, *MNRAS*, **339**, 772.
- Rhee, J. H., Larkin, J. E.: 2000, *ApJ*, **538**, 98.
- Rosario, D. J., Whittle, M., Nelson, C. H., Wilson, A. S.: 2010, *ApJ*, **711**, L94.

- Su, B., M., Muxlow, T. W. B., Pedlar, A., Holloway, A. J., Steffen, W., Kukula, M. J., Mutel, R. L.: 1996, *MNRAS*, **279**, 1111.
- Taylor, D., Dyson, J. E., Axon, D. J., Pedlar, A.: 1989, *MNRAS*, **240**, 487.
- Trager, S. C., Worthey, G., Faber, S. M., Burstein, D., Gonzalez, J. J.: 1998, *ApJ Suppl.Ser.*, **116**, 1.
- Wakamatsu, K.-I., Mitsugu T. Nishida, M. T.: 1988, *ApJ*, **325**, 596.
- Whittle, M., Haniff, C. A., Ward, M. J., Meurs, E. J. A., Pedlar, A., Unger, S. W., Axon, D. J., Harrison, B. A.: 1986, *MNRAS*, **222**, 189.
- Wilson, A. S., Keel, W. C.: 1989, *AJ*, **98**, 1581.

PROMINENCE ERUPTION ON 22 AUGUST 2006 OBSERVED WITH THE H α CORONAGRAPH IN NAO ROZHEN

N. PETROV, P. DUCHLEV, K. KOLEVA, M. DECHEV

Institute of Astronomy, Bulgarian Academy of Sciences

Abstract. An eruptive prominence (EP) on 22 August 2006 was observed with the H α coronagraph in the National Astronomical Observatory (NAO) – Rozhen, Bulgaria. The kinematic pattern of the EP was studied and the basic parameters of its eruption were determined. The associations of the EP with the filament on the solar disc and solar radio events are presented.

1. BACKGROUND

The EP occurred at the southwestern solar limb (S16° W) between 04:28 UT and 11:00 UT. The eruptive event presents seven successive eruptions during that time interval (Table 1). Each eruption, after first one, reaches smaller maximum height than previous one. The eruptions run at an angle of 45° about the limb and show two distinctive phases: rising phase and post-eruptive phase, when the prominence plasma flow back to the chromosphere by the same trajectory (Fig.1).

The eruptions are associated with a filament located at the western end of an active region NOAA 10904 at approximately the same place. The EP is associated with some activity events in solar radio emissions at 164 MHz (Nancay Radioheliograph) and 17 GHz (Nobeyama Radioheliograph).

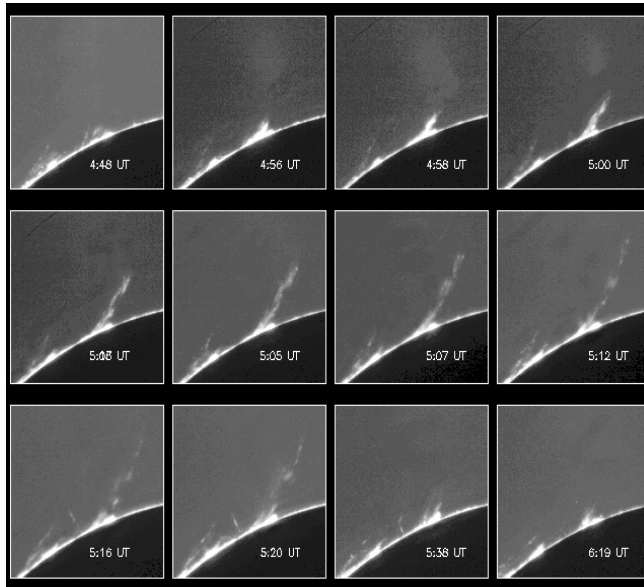


Figure 1: A sample of the EP observed on 22 August 2006 between 04:29 and 08:43 UT.

Table 1: Time of the onset and H_{\max} of the seven successive eruptions of the eruptive event.

UT	Time (min)	Eruption Number	Remark
04:47:55	19,1	1	start
05:13:21	44,6		H_{\max}
06:22:09	113,4	2	start
06:53:08	144,4		H_{\max}
07:21:15	172,5	3	start
07:32:56	184,2		H_{\max}
07:49:34	200,8	4	start
08:03:44	215,0		H_{\max}
08:06:03	217,3	5	start
08:19:51	231,1		H_{\max}
08:24:20	235,6	6	start
08:31:26	242,7		H_{\max}
08:33:07	244,3	7	start
08:35:15	246,5		H_{\max}

2. OBSERVATIONS

The EP was observed in NAO Rozhen by 15-cm coronagraph with H α filter (1.8 Å bandpass). The coronagraph (Fig. 2) has 225 cm focal length of the main objective and an effective focal length of its optical system of 450 cm. The resolution of H α filtergrams is of about 2". The images were registered with digital camera Canon EOS 350D (8 Mpxs). The first eruption was registered with an average cadence 1.3 minutes. The registered images, at maximal camera resolution, have size of 3456x2304 pxs and one pixel corresponds to size of 6.4 x 6.4 μm.

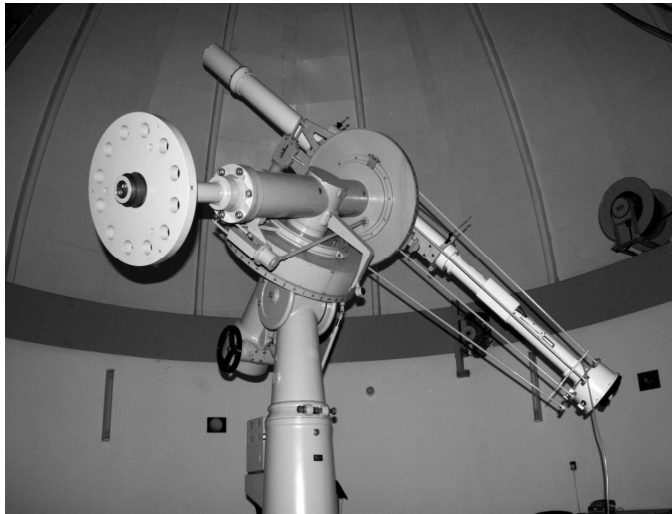


Figure 2: The 15-cm H α coronagraph mounted in the solar tower at NAO Rozhen, Bulgaria.

3. RESULTS

This work presents the kinematic pattern of the first of the seven eruptions of the event on 22 August 2006. The first eruption presents two main phases: eruption and post-eruption ones. During the eruption phase, the EP rises with almost constant velocity of 153 km/s and it reaches a maximum height of 270 000 km at 05:13 UT (Fig.3a). During the post-eruptive phase, the EP shows return motion by the same trajectory with an increasing velocity that reached a value of about 300 km/s near the solar limb (Fig. 3b). The kinematics of the eruptive process is summarized in Table 2.

The EP shows a specific behavior during its eruptive activity. The presence of several successive eruptions during its observations suggests recurrent eruptive activity like those of the surges. However, in contrast to the surges where the time

between successive eruptions is approximately one hour, this time for the EP progressive increases from 94.3 min between the first two eruptions to 8.7 min between last two eruptions (see Table 1). On the other hand, the prominence plasma visible in H α line clearly outlines a helical twisted structure of the prominence body that is typical for the eruptive prominences, while the surges occur in approximately radial magnetic field (Roy 1973a, b).

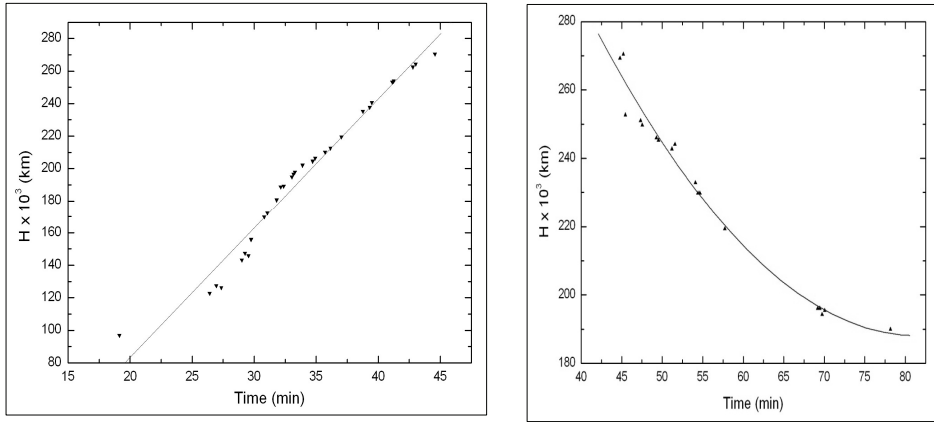


Figure 3: (*left*) Height-Time diagram of the EP eruptive phase. (*right*) Height-time diagram of the EP post-eruptive phase. The time is given in minutes after 04:28 UT.

Table 2: Basic kinematics parameters of the first eruption of the EP

Parameter	Eruptive phase		Post-eruptive phase	
	Onset	End	Onset	End
UT	04:47:55	05:13:21	05:13:34	05:46:48
Velocity km/s	153		230	302
Acceleration m/s ²	0		32	32

The EP on 22 August 2006 is associated with a part of a filament located at the western end of an active region NOAA 10904 (Fig. 4). The EP appeared along the polarity inversion line (PIL) of NOAA AR 10904 (S12°W91°) during its last stage when AR’s magnetic configuration is α/β according to the Hale classification (Hale and Nicholson, 1938). Eight soft X-ray flares of class C appeared in the AR on 20 and 21 Aug 2006. The filament erupted part was situated along the PIL

in the AR 10904 (Figs. 5 and 6). The filament has almost ring shape that encircles the positive magnetic polarity in the east of the PIL. Therefore, the filament has a “normal” magnetic configuration.

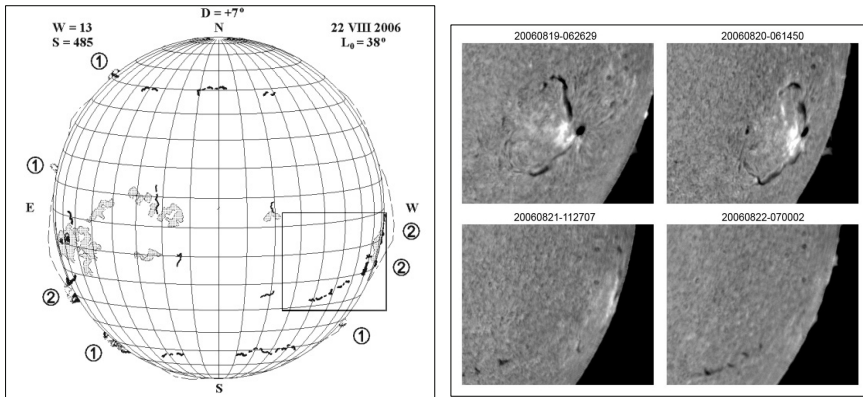


Figure 4: (left) Daily chart of the Sun from the Bulletin “Solnechnye Dannye” of Pulkovo Observatory. (right) Kanzelhöhe Solar Observatory H α filtergrams of the NOAA AR 10904 between 19 and 22 Aug 2006.

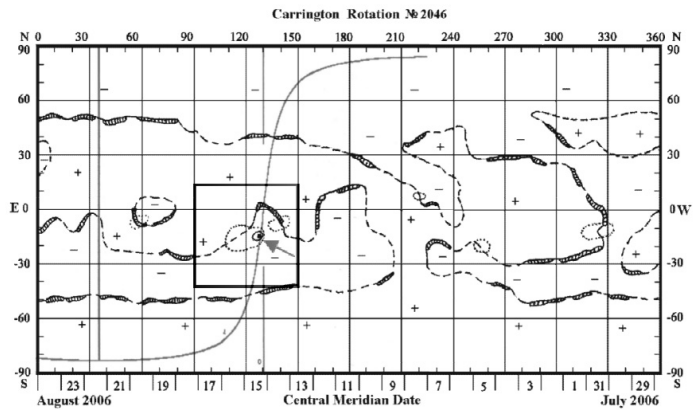


Figure 5: Pulkovo H α synoptic chart of the filament channels with the overlaid solar limb for the date 22 August 2006. The red arrow indicates the EP position (see electronic version).

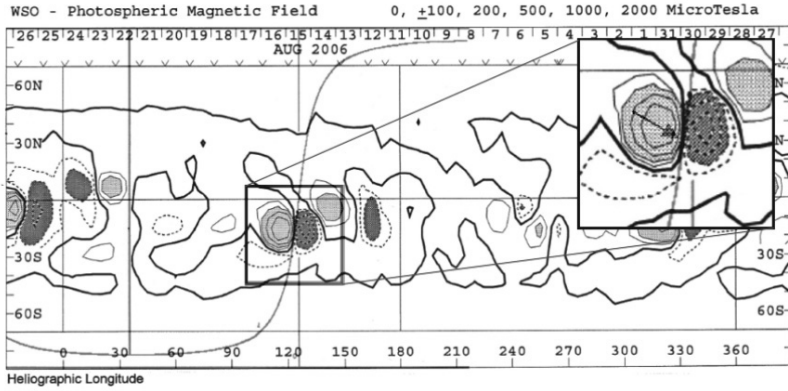


Figure 6: WSO synoptic chart of the photospheric magnetic field with the overlaid solar limb for 22 August 2006. The red arrow in the enlarged selected field indicates the EP position (see electronic version).

The EP is associated with the solar radio emissions at 164 MHz and 17 GHz. The Nancay radio images at 164 MHz (Fig. 7) indicate expanding loops (EL) inside a CME-like large magnetic system, which are observed because they are illuminated by the gyro-synchrotron emission of MeV accelerated electrons. The source and direction of movement of EL are the same as those of the EP on 22 August 2006. The Nobeyama radio images at 17 GHz show the radio analog of the EP on 22 August 2006 at the time when the first eruption in H α reaches a maximum height (Fig. 8, left). The right images on Fig. 8 show the EP radio analog at the time when the second eruption in H α reaches a maximum height.

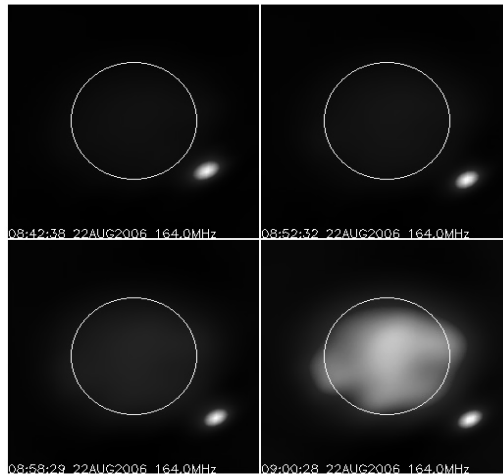


Figure 7: Nancay radio images of the Sun at 164 MHz on 22 August 2006.

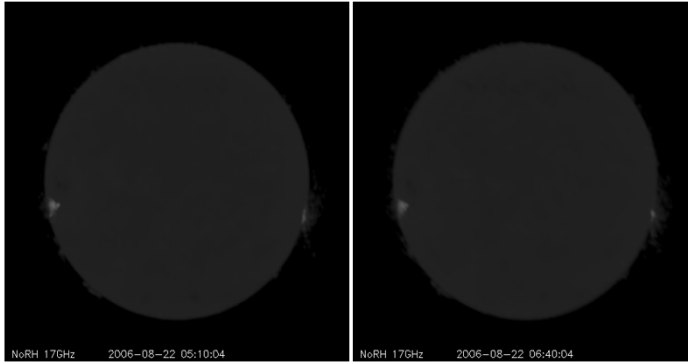


Figure 8: Nobeyama radio images of the EP on 22 August 2006 at 17 GHz.

4. CONCLUSIONS

The EP on 22 August 2006 is interesting case that presents series of seven successive eruptions during the observation time. The first eruption of the EP shows two distinctive phases: eruptive phase with constant velocity 153 km/s and post-eruptive one, during which the EP shows return motion by the same trajectory with increasing velocity reaching 300 km/s near the limb. The EP presents an erupted part of an active region filament with a “normal” magnetic configuration. There is no association of the EP with coronal mass ejection (CME) but the EP is associated with radio structures at 164 MHz, which suggest expanding loops inside a CME-like large magnetic system. In the forthcoming study, the kinematic patterns of the next six eruptions will be studied and compared with those of the first eruption of the prominence.

Acknowledgments

This work is partially due to the National Scientific Foundation under Grants DO-02-273, DO 01-34, and DO 02-85.

References

- Hale, G. E. Nicholson, S. B.: 1938, “Magnetic Observations of Sunspot 1917-1924”, *Publ. Carnegie Inst.*, **498**,
Roy, J. R.: 1973a, *Solar Phys.* **28**, 95.
Roy, J. R.: 1973b, *Solar Phys.* **32**, 139.

BAR PARAMETERS OF SEYFERT AND INACTIVE GALAXIES

LYUBA SLAVCHEVA-MIHOVA

Institute of Astronomy and NAO, Bulgarian Academy of Sciences
E-mail: lslav@astro.bas.bg

Abstract. We present a comparative analysis of the distribution and correlations of the bar parameters ellipticity, length, and relative length for a sample of Seyfert galaxies and a control sample of inactive galaxies. We extend the relation between the bar length, corresponding to the ellipticity maximum and to a 15% decrease in ellipticity maximum, with seven more galaxies. There is no significant difference in the distribution of both absolute and relative bar length for the two samples; the bar ellipticity appears lower for the Seyfert galaxies. We found no strong correlation for the (relative) bar length vs. bar ellipticity and for the bar length vs. galaxy radius with similar behaviour for the two samples.

1. INTRODUCTION

Galaxy total energy would be minimal in the presence of outflowing angular momentum (Lynden-Bell & Kalnajs 1972). Angular momentum exchange is the motor of secular evolution of galaxies. The main internal angular momentum transfer mechanism is due to the torques exerted by the bar on the gas. Depending on the relative angular frequency of the bar and disk, resonances can occur. The torques change sign at each resonance and drive the accumulation of gas in the form of rings (Combes 2001).

The basic bar parameters are length and strength. Bar length is proportional to the part of the host galaxy that can be affected dynamically by the bar (Erwin 2005). There are various bar length estimation methods: visual inspection, analysis of the surface brightness profile over the bar major axis, ellipse fitting, Fourier analysis (Erwin 2005; Michel-Dansac and Wozniak 2006). The semi-major axis corresponding to the ellipticity maximum is considered the most objective and reproducible bar length estimate. However, it is not related to any of the bar dynamical characteristics (Michel-Dansac and Wozniak 2006). Bar strength is the maximal tangential force in terms of the mean radial force (Combes and Sanders 1981). It was shown that deprojected bar ellipticity is a first order approximation of bar strength (Athanasoula 1992; Block et al. 2004).

2. DATA ANALYSIS AND RESULTS

We use a sample of 35 Seyfert galaxies and a control sample of inactive galaxies. The sample selection and data reduction are described in Slavcheva-Mihova and Mihov (2011a). In Slavcheva-Mihova and Mihov (2011b) we estimated the bar length, ℓ , and ellipticity, ϵ . Inspired by the finding of Martinez-Valpuesta et al. (2006) that the bar length corresponding to 15% decrease of ellipticity from its maximal value is related to the size of the maximal stable x_1 orbit, as bar length we adopted the minimum of the semi-major axes corresponding to 15% ellipticity decrease at both sides of the profile. The so estimated bar length was found to correlate tightly with the bar semi-major axis corresponding to the ellipticity maximum, ℓ_{\max} , with a median ratio of 1.216 ± 0.019 based on 14 Seyfert galaxies (Slavcheva-Mihova and Mihov 2011b). Now we extend this ratio with seven inactive galaxies. The median value of ℓ/ℓ_{\max} is 1.218 ± 0.023 based on the inactive galaxies and 1.218 ± 0.014 for the combined set of 21 Seyfert and inactive galaxies.

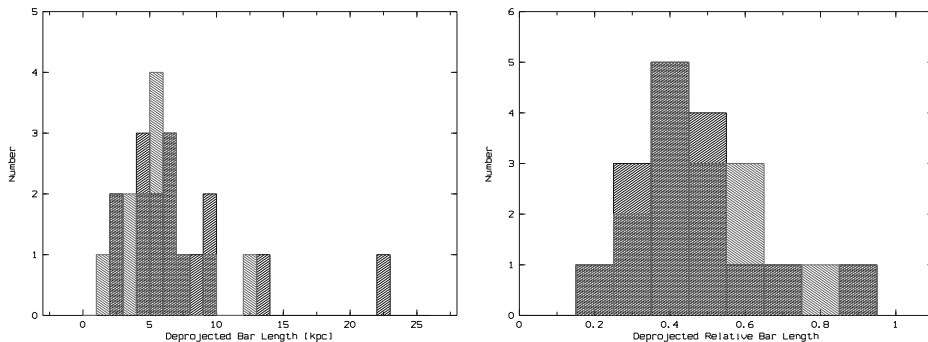


Figure 1: Distribution of the deprojected bar length (left panel) and deprojected relative bar length (right panel) for the Seyfert (left hashed, red) and inactive (right hashed, black) galaxies (see electronic version).

Both bar length and ellipticity were deprojected. The relative bar length is in terms of the galaxy radius corresponding to the 25 B mag arcsec $^{-2}$ isophote, corrected for Galactic extinction as reported in HyperLeda¹ (Paturel et al. 2003). We further applied K- and E- corrections, as well as a correction for cosmological dimming. The deprojection and corrections are described in Slavcheva-Mihova and Mihov (2011b).

We compared the distribution of bar parameters for the two samples (Figs. 1-2). The median value of the bar length, relative bar length, and bar ellipticity is $5.44 \pm 0.63/6.12 \pm 1.27$, $0.45 \pm 0.05/0.43 \pm 0.04$, and $0.39 \pm 0.04/0.49 \pm 0.04$ for the Seyfert/inactive galaxies. The difference in the distribution of both bar length and relative bar length is insignificant for the two samples at the 95% confidence level. At this confidence level the Seyfert bars have lower bar ellipticity than the inactive ones, i.e. the Seyfert bars appear weaker as discussed in Slavcheva-Mihova and Mihov (2011a).

¹<http://leda.univ-lyon1.fr>

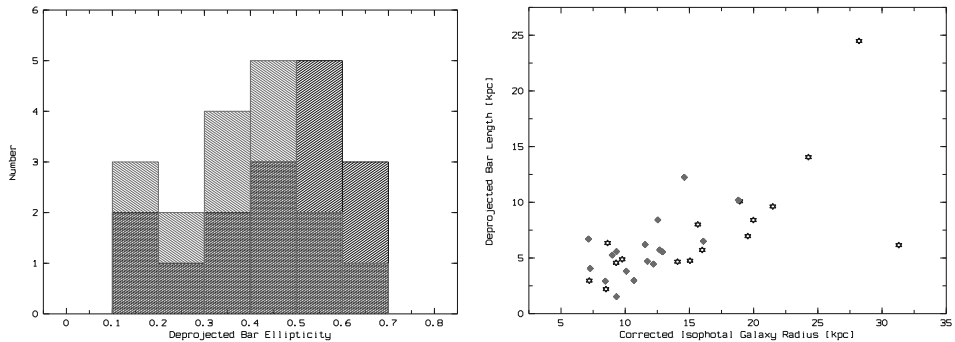


Figure 2: The same as in Fig.1 but for the deprojected bar ellipticity (left panel) and deprojected bar length vs. corrected isophotal galaxy radius for the Seyfert (red diamonds) and inactive (black stars) galaxies (right panel) (see electronic version).

Furthermore, we studied the correlations among the bar parameters and between them and the galaxy parameters. We found a weak correlation between the deprojected bar length and corrected isophotal galaxy radius with a Pearson correlation coefficient $r = 0.63$ for the Seyfert and $r = 0.65$ for the inactive galaxies (Fig. 2). The deprojected bar length/relative bar length shows no clear correlation with the deprojected bar ellipticity (with $r = 0.44/r = 0.51$ for the Seyfert and $r = 0.36/r = 0.30$ for the inactive galaxies; Fig. 3).

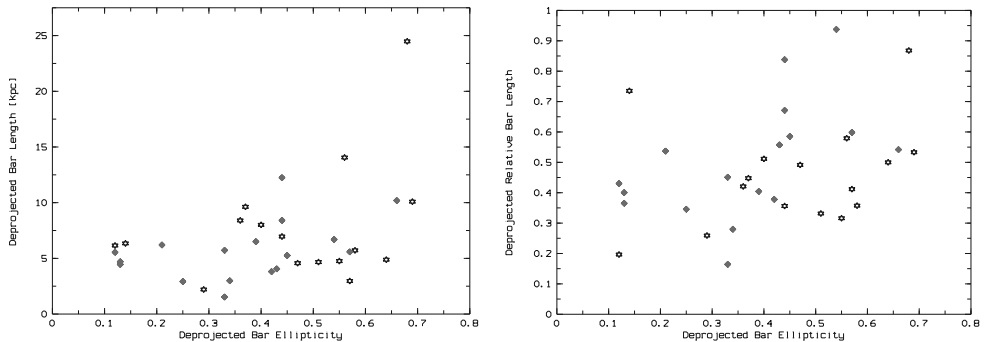


Figure 3: Deprojected bar length vs. deprojected bar ellipticity (left panel) and deprojected relative bar length vs. deprojected bar ellipticity (right panel); the symbols are as in Fig. 2.

References

- Athanassoula, E.: 1992, Morphology of bar orbits, *MNRAS*, **259**, 328.
 Block, D. L., Buta, R., Knapen, J. H., Elmegreen, D. M., Elmegreen, B. G., and Puerari, I.: 2004, Gravitational Bar and Spiral Arm Torques from K_S -band Observations and Implications for the Pattern Speeds, *AJ*, **128**, 183
 Combes, F.: 2001, Fueling the AGN, in Advanced Lectures on the Starburst-AGN held June 26-30, 2000, ed. I. Aretxaga, D. Kunth, and R. Mujica, 223

- Combes, F. and Sanders, R. H.: 1981, Formation and properties of persisting stellar bars, *A&A*, **96**, 164.
- Erwin, P.: 2005, How Large Are the Bars in Barred Galaxies?, *MNRAS*, **364**, 283.
- Lynden-Bell, D. and Kalnajs, A. J.: 1972, On the generating mechanism of spiral structure, *MNRAS*, **157**, 1.
- Martinez-Valpuesta, I., Shlosman, I., and Heller, C.: 2006, Evolution of Stellar Bars in Live Axisymmetric Halos: Recurrent Buckling and Secular Growth, *ApJ*, **637**, 214.
- Michel-Dansac, L. and Wozniak, H.: 2006, The length of stellar bars in SB galaxies and N-body simulations, *A&A*, **452**, 97.
- Paturel, G., Petit, C., Prugniel, P., et al.: 2003, HYPERLEDA. I. Identification and designation of galaxies, *A&A*, **412**, 45.
- Slavcheva-Mihova, L. and Mihov, B.: 2011a, Optical multiband surface photometry of a sample of Seyfert galaxies. I. Large-scale morphology and local environment analysis of matched Seyfert and inactive galaxy samples, *A&A*, **526**, A43.
- Slavcheva-Mihova, L. and Mihov, B.: 2011b, Optical multiband surface photometry of a sample of Seyfert galaxies: III. Global, isophotal, and bar parameters, *AN*, **332**, 191.

THE MANIFESTATIONS OF THE NON-SYMMETRIC ION-ATOM ABSORPTION PROCESSES IN THE SOLAR ATMOSPHERES IN UV AND VUV REGION

V. A. SREĆKOVIĆ¹, A. A. MIHAJLOV¹, LJ. M. IGNJATOVIĆ¹,
M. S. DIMITRIJEVIĆ², A. METROPOULOS³

¹*University of Belgrade, Institute of physics, P.O. Box 57, 11001, Belgrade, Serbia*

²*Astronomical Observatory, Volgina 7, 11060 Belgrade 74 Serbia*

³*Theoretical and Physical Chemistry Institute, National Hellenic Research
Foundation, Athens, Greece*

Abstract. In this work we draw attention to the radiative processes in strongly non-symmetric ion-atom collisions as factors of influence on the opacity of the solar atmosphere in UV and VUV region. For several ion-atom systems, $\text{He} + \text{H}^+$ and $\text{H} + \text{A}^+$, where A is the atom of one of the metal (Mg, Si, Al etc), some characteristics have been determined, such as molecular potential curves and dipole matrix elements. Here the non-symmetric radiative processes are considered under the conditions characterizing the non-LTE standard model of the solar atmosphere. In this work the calculations of the corresponding spectral absorption coefficients have been performed. It is shown that the examined processes generate rather wide and firm molecular absorption stripes in the UV and VUV regions, whose intensity is comparable and sometimes even larger than the intensity of known one's generated in the $\text{H} + \text{H}^+$ radiative collision processes. Due to all these reasons the processes have to be consistently included in standard models of the solar atmosphere.

1. INTRODUCTION

The important influence of some ion-atom radiative collision processes on the optical characteristics of the stellar atmospheres was already established. Here we have in mind the symmetric radiative processes of the photo absorption/emission and radiative charge exchange which can be presented by

$$\varepsilon_{\lambda} + A_2^+ \leftrightarrow A + A^+ \quad (1)$$

$$\varepsilon_{\lambda} + A^+ + A \leftrightarrow A + A^+ \quad (2)$$

where $A = \text{H}(1s)$ or $\text{He}(1s^2)$, A^+ and A_2^+ are the corresponding positive, single charged atomic and molecular ions in the ground electronic states, and ε_{λ} is the photon energy. Previously, it was shown in Mihajlov *et al.* (1993, 2007) that these processes can influence to the opacity of Solar atmospheres. Nevertheless, the mentioned papers have leaved opened the questions of the significance of the non-symmetric radiative processes.

The main objective of this paper is to draw attention to the possible significance of the non-symmetric radiative processes as factors which influence to the opacity of stellar atmosphere in UV and VUV region. Here we will consider the processes of absorption charge exchange and photo-dissociation of the type

$$\varepsilon_{\lambda} + AB^+ \leftrightarrow A^+ + B \quad (3)$$

$$\varepsilon_{\lambda} + A + B^+ \leftrightarrow A^+ + B \quad (4)$$

$$\varepsilon_{\lambda} + A + B^+ \leftrightarrow (AB^+)^* \quad (5)$$

where B is the ground state atom with the ionization potential I_B which is less than the ionization potential I_A of the atom A , and AB^+ - the corresponding molecular ion in one of the electronic states which are asymptotically correlated with the state of the system $A + B^+$. One can see that the processes of charge exchange and photo-dissociation i.e. (3) and (4) represent the analogues of the processes (1) and (2), while the process (5) has not it's symmetric analog.

In this paper the strongly non-symmetric radiative processes are investigated under the conditions characterizing the model of the solar atmosphere presented in Vernazza *et al.* (1981). All needed data for the calculations of the spectral absorption coefficients are provided in tabular form only in chosen models. In accordance with this model is possible that atom $A = \text{He}(1s^2)$ and $B = \text{H}(1s)$, and $A = \text{H}(1s)$ and $B = \text{Mg}, \text{Si}$ and Al .

We should point out that for the molecular ions HeH^+ and $(\text{HeH}^+)^*$ the corresponding potential curves and the dipole matrix elements, as the functions of the internuclear distances, are taken from Green *et al.* (1974a,b), while for all other considered molecular ions the mentioned quantities are calculated within this manuscript and in Srećković *et al.* (2011).

The spectral absorption coefficients calculated here, as the function of the local temperature T , wavelength λ , and the particle densities are determined in the region $40 \text{ nm} \leq \lambda \leq 230 \text{ nm}$.

2. RESULTS AND DISCUSSION

The strongly non-symmetric processes (3)-(5) are schematically shown in Fig. 1, where: bf-, ff-, and fb denote the bound-free, free-free and free-bound radiative transitions; $\Delta I = I_A - I_B$; $E = E_{\text{imp}}$ and E'_{imp} are the impact energies of the corresponding ion-atom systems; $U_{\text{in}}(R)$ and $U_{\text{fin}}(R)$ - are the adiabatic potential curves of the initial and final molecular electronic states; v, J , and v', J' - the quantum numbers of the corresponding bound ro-vibration and free states.

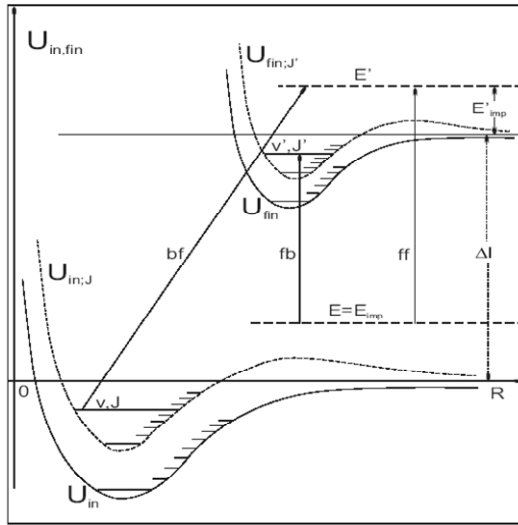


Figure 1: Schematic presentation of the non-symmetric processes (3)-(5) caused by the bf-, ff-, and fb- radiative transitions.

The contribution of the considered non-symmetric ion-atom absorption processes (3) - (5) to the opacity of the solar atmosphere is described here by the spectral absorption coefficient $\kappa_{\text{ia,nsim}}(\lambda; T)$. The behavior of $\kappa_{\text{ia,nsim}}(\lambda; T)$ for several values of λ is illustrated by Fig.2, where h is the distance of considered layer from the referent one ($h=0$) in accordance with Vernazza et al. (1981).

The behavior of the quantity $G = \kappa_{\text{ia,nsim}}(\lambda; T) / \kappa_{\text{ia,tot}}(\lambda; T)$, where $\kappa_{\text{ia,tot}}(\lambda; T)$ characterize the total contribution of all ion-atom absorption processes, i.e. (1) - (5), is shown in Fig.3. Then, in Fig.4 is presented the behavior of the quantities $F_{\text{sim}} = \kappa_{\text{ia,sim}}(\lambda; T) / \kappa_{\text{ea}}(\lambda; T)$ and $F_{\text{tot}} = \kappa_{\text{ia,tot}}(\lambda; T) / \kappa_{\text{ea}}(\lambda; T)$, dash and full lines respectively. Here $\kappa_{\text{ia,sim}}(\lambda; T)$ characterizes the contribution of the symmetric ion-atom absorption processes (1) and (2), and $\kappa_{\text{ea}}(\lambda; T)$ - the contribution of the concurrent electron-atom processes i.e. H^- continuum, which were treated until recently as the absolutely dominant.

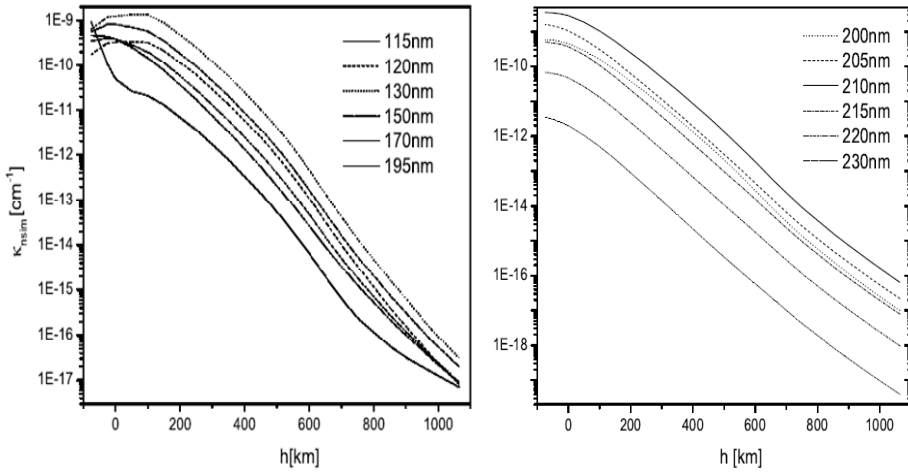


Figure 2: Spectral absorption coefficients $\kappa_{ia,nsim}(\lambda; T)$ as the function of h for the Solar atmosphere for $115 \text{ nm} \leq \lambda \leq 230 \text{ nm}$.

On the basis of the above mentioned it follows that the non-symmetric absorption processes (3)-(5) should be *ab initio* included in the relevant models.

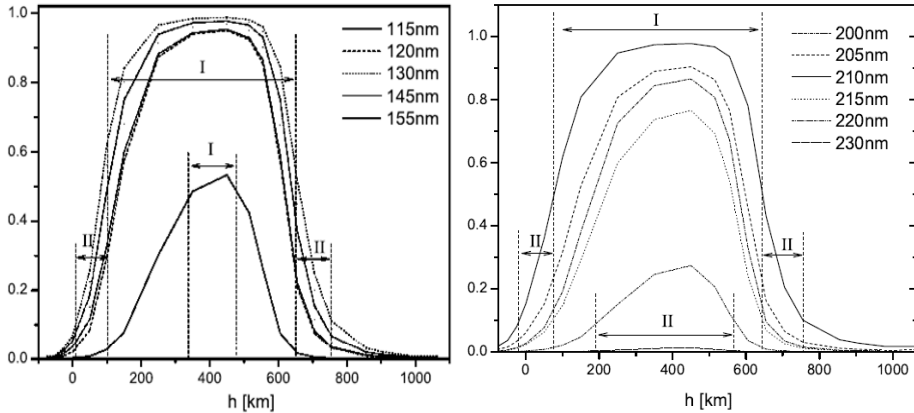


Figure 3: The behavior of the quantity $G = \kappa_{ia,nsim}(\lambda; T) / \kappa_{ia,tot}(\lambda; T)$ as the function of h for the Solar atmosphere for $115 \text{ nm} \leq \lambda \leq 230 \text{ nm}$.

Even only the results presented in figures 3 and 4 show that the neglecting of the contribution of the non-symmetric processes (3) - (5) to the opacity of the solar atmosphere, in respect to the contribution of symmetric processes (1) and (2) would caused noticeable errors.

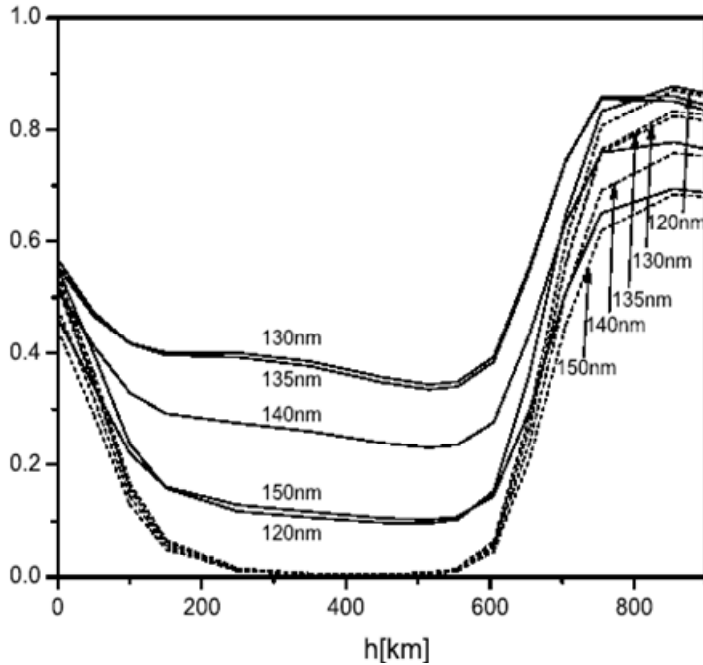


Figure 4: The behavior of the quantities F_{sim} (dash lines) and F_{tot} (full lines) as the function of h for the Solar atmosphere for $115 \text{ nm} \leq \lambda \leq 230 \text{ nm}$.

Acknowledgments

This work was supported by the Ministry of Education and Science of the Republic of Serbia as a part of the projects 176002, III4402.

References

- Green, T., Browne, J., Michels, H., Madsen, M.: 1974a, *J. Chem. Phys.*, **61**, 5198.
 Green, T. A., Michels, H. H., Browne, J. C., Madsen, M. M.: 1974b, *J. Chem. Phys.*, **61**, 5186.
 Mihajlov, A., Dimitrijević, M. S., Ignjatović, Lj.: 1993, *A&A*, **276**, 187.
 Mihajlov, A., Ignjatović, Lj., Sakan, N., Dimitrijević, M. S.: 2007, *A&A*, **437**, 1023.
 Srećković, V. et al.: 2011, JENAM Saint-Petersburg, Russia, *Contrib. Papers* p. 84.
 Vernazza, J., Avrett, E., Loser, R.: 1981, *ApJS*, **45**, 635.

*UBVR*I*u*' OBSERVATIONS OF THE FLICKERING OF THE JET EJECTING SYMBIOTIC STAR MWC 560

K. A. STOYANOV¹, R. K. ZAMANOV¹, G. Y. LATEV¹, S. BOEVA¹
M. F. BODE², S. V. TSVETKOVA¹, N. KACHAROV¹

¹*Institute of Astronomy and National Astronomical Observatory Rozhen,
Bulgarian Academy of Sciences, 72 Tsarigradsko Shousse Blvd., 1784 Sofia, Bulgaria*

E-mail: kstoyanov@astro.bas.bg, rkz@astro.bas.bg, glatev@astro.bas.bg,
sboeva@astro.bas.bg

²*Astrophysics Research Institute, Liverpool John Moores University,
Twelve Quays House, Birkenhead, CH41 1LD, UK*

Abstract. We report observations of the flickering variability of the symbiotic star MWC 560 on the basis of simultaneous observations in *UBVRI* bands. We find that MWC 560 has a flickering source with $(U - B)_0 = -0.93 \pm 0.05$, $(B - V)_0 = 0.01 \pm 0.06$, $(V - R)_0 = 0.43 \pm 0.08$, a source temperature $T_{\text{fl}} = 11780 \pm 300$ K and luminosity $L_{\text{fl}} \approx 20 L_{\odot}$ on 2009 November 14 (using a distance of $d = 2.5$ kpc and $E_{B-V} = 0.15$). On 2010 January 11, we find $(U - B)_0 = -0.61 \pm 0.05$, $(B - V)_0 = -0.01 \pm 0.05$, $(V - R)_0 = 0.46 \pm 0.02$, $T_{\text{fl}} \approx 9100 \pm 300$ K, $L_{\text{fl}} \approx 38 L_{\odot}$.

1. INTRODUCTION

Discovered by Merrill & Burwell (1943) as an object with bright hydrogen lines, MWC 560 (V694 Mon) is a symbiotic binary system, which consists of a red giant and a white dwarf. Gromadzki et al. (2007), using optical and near-IR light curves, refined it as $P_{\text{orb}} = 1931 \pm 162$ day. The white dwarf mass is ~ 0.9 (Zamanov, Gomboc & Latev, 2011). and the orbit is highly eccentric, with $e \sim 0.7$ (Zamanov et al. 2010).

The most spectacular features of this object are the collimated ejections of matter with velocities of up to ~ 6000 km s⁻¹ (Tomov et al. 1992; Stute & Sahai 2009) and the resemblance of its emission line spectrum to that of the low-redshift quasars (Zamanov & Marziani 2002).

The flickering (stochastic light variations on timescales of a few minutes with amplitude of a few $\times 0.1$ magnitudes) is a variability observed in the three main types of binaries that contain white dwarfs accreting material from a companion mass-donor star: cataclysmic variables (CVs), supersoft X-ray binaries, and symbiotic stars (Sokoloski 2003). The systematic searches for flickering variability in symbiotic stars and related objects (Dobrzycka et al. 1996; Sokoloski, Bildsten & Ho 2001; Gromadzki et al. 2006) have shown that among ~ 200 symbiotic stars known, to-

date flickering has only been detected in 9 objects. The flickering of MWC 560 was detected by Tomov et al. (1990) and Michalitsianos et al. (1993).

To improve our understanding of this object, our aims are: (1) to perform *UBVRIu'* observations of the flickering, and (2) to throw light on the origin of the flickering.

2. OBSERVATIONS

On 2004 December, as exploratory observations that led to the full programme, we obtained two runs with the RATCam CCD camera (2048x2048 pixel, field of view 4.6 arcmin) on the 2-m Liverpool Telescope (Steele et al. 2004) in the Sloan *u'* band. The amplitude of the flickering in *u'* was 0.34 and 0.49 mag for the first and second runs respectively (see Table 1).

On the night of 2009 November 14, we observed MWC 560 simultaneously with four telescopes equipped with CCD cameras. The 2m RCC telescope of the National Astronomical Observatory Rozhen observed in the *U* band, equipped with a CCD VersArray 1300 B (1340x1300 px, field of view 6'x6'). The 50/70 cm Schmidt telescope observed in the *B* band (CCD FLI PL 16803, 4096x4096 px, used 1024x1024 px, 19' x 19'). The 60 cm Rozhen telescope observed in the *R* band (FLI PL 9000 CCD with 3056 x 3056 pixels and 18'x18'); the 60 cm telescope of the Belogradchick Astronomical Observatory in the *V* band (FLI PL 9000 CCD, 3056 x 3056 px, 18'x18').

On the night of 2010 January 11, we observed MWC 560 simultaneously with three telescopes of NAO Rozhen. The 2m RCC telescope of the National Astronomical Observatory Rozhen equipped with a dual channel focal reducer observed in *U* and *V* bands. In the *U* band a Photometrics CCD (1024x1024 px, field of view 7.6'x7.6') has been used, and in the *V* band a VersArray CCD (512x512 px, 7.6'x7.6'). The 50/70 cm Schmidt telescope observed in the *B* band. The 60 cm Rozhen telescope observed in the *R* and *I* bands.

On the night of 2010 March 15, we observed MWC 560 with the 60 cm Rozhen telescope repeating *V* and *I* bands.

All the CCD images have been bias subtracted, flat fielded, and standard aperture photometry has been performed. The data reduction and aperture photometry are done with IRAF and have been checked with alternative software packages. The comparison stars of Henden and Munari (2006) have been used.

The results of our observations are summarized in Table 1 and plotted in Fig. 1. For each run we measure the minimum, maximum, and average brightness in the corresponding band, plus the standard deviation of the run.

3. FLICKERING LIGHT SOURCE

As can be seen in Fig. 1 and Table 1, during our observations MWC 560 exhibited variability on a time scale of 1-30 minutes with amplitude 0.1 – 0.3 mag in *V*. The amplitude increases to shorter wavelengths and decreases to longer. In the *I* band this variability is almost undetectable.

The distance to MWC 560 is estimated $d = 2.5 \pm 0.3$ kpc (Meier et al. 1996). Schmid et al. (2001) give $d = 2.5 \pm 0.7$ kpc and $E_{B-V} = 0.15 \pm 0.05$ mag. We assume $d = 2.5$ kpc, $E_{B-V} = 0.15$ mag, and an extinction law as given in Zombeck (1990). This gives the interstellar absorption to MWC 560: $A_U = 0.754$ mag, $A_B =$

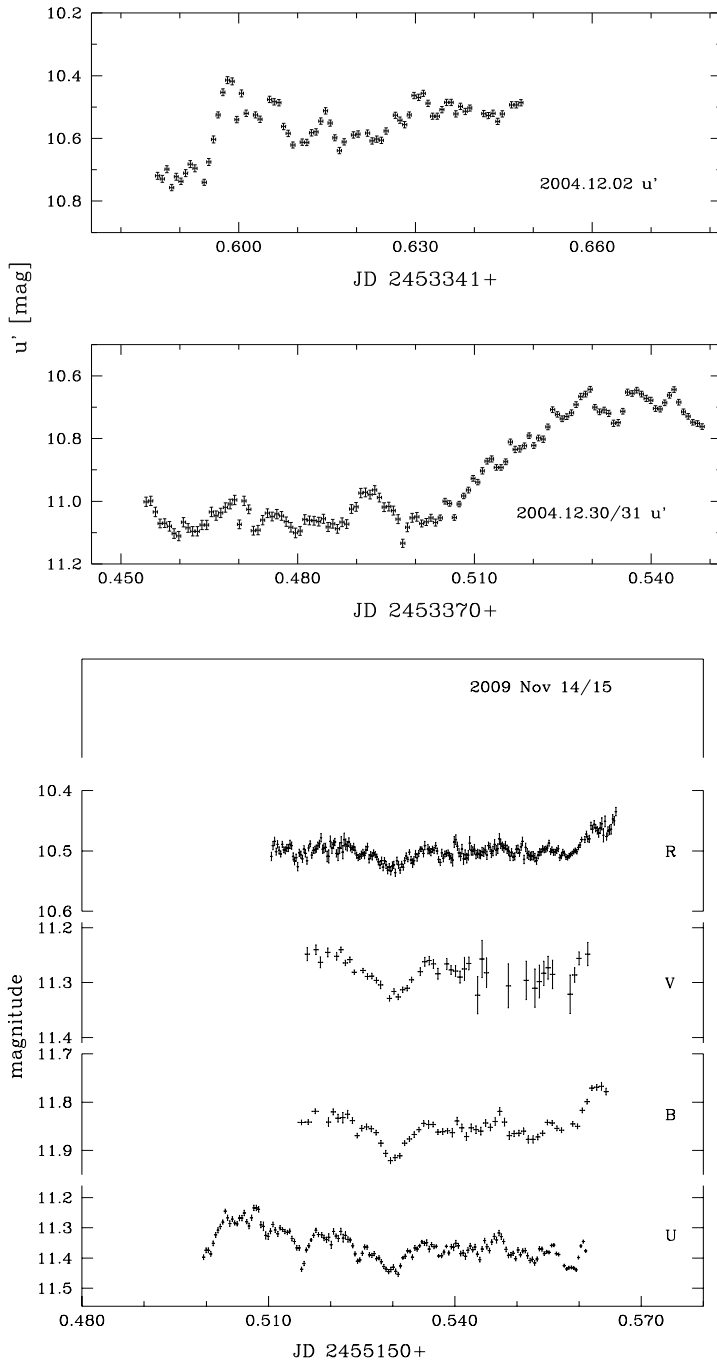


Figure 1: Variability of MWC 560: in the SDSS u' band on 2004 December 02; in the SDSS u' band on 2004 December 30/31; in the $UBVR$ bands on 2009 November 14/15;

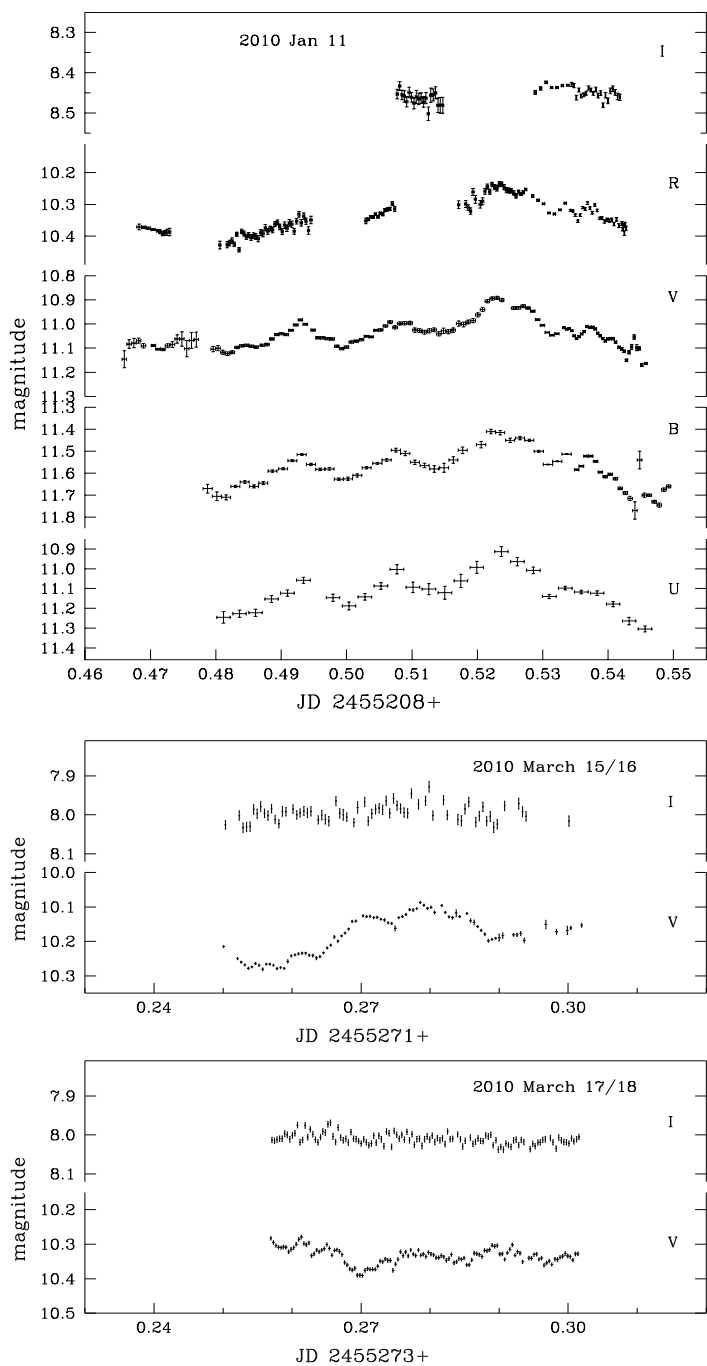


Figure 2: Variability of MWC 560: in the *UBVRI* bands on 2010 January 11/12; in the *VI* bands on 2010 March 15/16; in the *VI* bands on 2010 March 17/18.

Table 1: CCD observations of MWC 560. In the table are given as follows: the telescope, band, UT-start and UT-end of the run, exposure time and number of CCD images obtained.

date telescope	band	UT start-end	Exp-time [sec]	N _{pts}
<hr/>				
2004 Dec 02		JD 2453341		
2.0m LT	SDSS <i>u'</i>	02:04 - 03:33	60	69
2004 Dec 30/31		JD 2453370		
2.0m LT	SDSS <i>u'</i>	22:54 - 01:10	60	120
<hr/>				
2009 Nov 14/15		JD 2455150		
2m RCC	<i>U</i>	23:59 - 01:28	30	159
50/70 cm Schmidt	<i>B</i>	00:21 - 01:33	60	60
60 cm Belogr	<i>V</i>	00:23 - 01:28	60	45
^a part	<i>V</i>	00:23 - 00:59	60	29
60 cm Rozhen	<i>R</i>	00:14 - 01:35	20	221
<hr/>				
2010 Jan 11/12		JD 2455208		
2m RCC	<i>U</i>	23:31 - 01:07	180	26
50/70 cm Schmidt	<i>B</i>	23:28 - 01:11	120,60	58
2m RCC	<i>V</i>	23:11 - 01:06	60,30	117
60 cm Rozhen	<i>R</i>	22:34 - 01:02	10,30	120
60 cm Rozhen	<i>I</i>	00:11 - 01:00	30,10	48
<hr/>				
2010 March 15		JD 2455271		
60 cm Rozhen	<i>V</i>	18:00 - 19:16	30	82
60 cm Rozhen	<i>I</i>	18:00 - 19:17	3	67
<hr/>				
2010 March 17		JD 2455273		
60 cm Rozhen	<i>V</i>	18:10 - 19:14	15	120
60 cm Rozhen	<i>I</i>	18:10 - 19:14	5	117
<hr/>				

^a only the first (better) part of the *V* band observations with the 60 cm Belogr. telescope

Table 2: CCD observations of MWC 560. In the table are given as follows: the telescope, band, average magnitude in the corresponding band, minimum – maximum magnitudes in each band, standard deviation of the mean, the range of observational error.

date telescope	band	average [mag]	min-max [mag]-[mag]	stdev [mag]	err [mag]
<hr/>					
2004 Dec 02		JD 2453341			
2.0m LT	SDSS <i>u'</i>	10.562	10.414 - 10.757	0.084	0.010-0.011
2004 Dec 30/31		JD 2453370			
2.0m LT	SDSS <i>u'</i>	10.924	10.643 - 11.134	0.159	0.009-0.015
<hr/>					
2009 Nov 14/15		JD 2455150			
2m RCC	<i>U</i>	11.358	11.234 - 11.454	0.048	0.005-0.014
50/70 cm Schmidt	<i>B</i>	11.850	11.767 - 11.921	0.031	0.005-0.011
60 cm Belogr	<i>V</i>	11.281	11.240 - 11.329	0.024	0.004-0.040
^a part	<i>V</i>	11.279	11.240 - 11.329	0.025	0.004-0.012
60 cm Rozhen	<i>R</i>	10.499	10.435 - 10.536	0.016	0.004-0.011
<hr/>					
2010 Jan 11/12		JD 2455208			
2m RCC	<i>U</i>	11.118	10.913 - 11.304	0.094	0.009-0.033
50/70 cm Schmidt	<i>B</i>	11.586	11.410 - 11.770	0.085	0.002-0.040
2m RCC	<i>V</i>	11.045	10.892 - 11.169	0.056	0.002-0.035
60 cm Rozhen	<i>R</i>	10.338	10.236 - 10.443	0.051	0.002-0.012
60 cm Rozhen	<i>I</i>	8.454	8.424 - 8.502	0.016	0.002-0.020
<hr/>					
2010 March 15		JD 2455271			
60 cm Rozhen	<i>V</i>	10.183	10.087 - 10.281	0.058	0.003-0.012
60 cm Rozhen	<i>I</i>	7.995	7.928 - 8.033	0.021	0.011-0.015
<hr/>					
2010 March 17		JD 2455273			
60 cm Rozhen	<i>V</i>	10.334	10.279 - 10.391	0.023	0.005-0.006
60 cm Rozhen	<i>I</i>	8.011	7.969 - 8.038	0.013	0.007-0.007

^a only the first (better) part of the *V* band observations with the 60 cm Belogr. telescope

Table 3: Magnitudes and colours of the flickering light source of MWC 560 (only the colours are corrected for interstellar extinction).

	14.11.2009	11.01.2010	29.12.2010
<i>U</i>	14.04 ± 0.05	13.12 ± 0.04	12.08 ± 0.07
<i>B</i>	14.85 ± 0.06	13.60 ± 0.02	13.11 ± 0.07
<i>V</i>	14.69 ± 0.06	13.46 ± 0.02	12.75 ± 0.06
<i>R</i>	14.19 ± 0.07	12.93 ± 0.02	12.94 ± 0.09
$(U - B)_0$	-0.93 ± 0.05	-0.61 ± 0.05	-1.16 ± 0.08
$(B - V)_0$	0.01 ± 0.06	-0.01 ± 0.02	0.21 ± 0.09
$(V - R)_0$	0.43 ± 0.08	0.46 ± 0.02	-0.26 ± 0.10
$L_{\text{fl}} [L_{\odot}]$	20 ± 2	38 ± 3	88 ± 8
$T_{\text{fl}} [\text{K}]$	11800 ± 300	9100 ± 300	13550 ± 500
$R_{\text{fl}} [R_{\odot}]$	1.1 ± 0.1	2.7 ± 0.2	1.68 ± 0.16

0.628 mag, $A_V = 0.477$ mag, $A_R = 0.400$ mag, $A_I = 0.304$ mag. If we use the extinction law as given in Cardelli et al. (1989) than we have $A_U = 0.729$ mag, $A_B = 0.616$ mag, $A_V = 0.464$ mag, $A_R = 0.392$ mag, $A_I = 0.285$ mag, and the results will be practically the same.

3. 1. COLOURS OF THE FLICKERING SOURCE

Bruch (1992) proposed that the light curve of CVs can be separated into two parts – constant light and variable (flickering) source. We assume that all the variability in each night is due to flickering. In these suppositions the flickering light source is considered 100% modulated. Following these assumptions, we calculate the flux of the flickering light source as $F_{\text{fl}} = F_{\text{av}} - F_{\text{min}}$, where F_{av} is the average flux during the run and F_{min} is the minimum flux during the run (corrected for the typical error of the observations). F_{fl} has been calculated for each band, using the values given in Table 1 and Bessel (1979) calibration for the fluxes of a zero magnitude star.

The calculated magnitudes and colours of the flickering light source are given in Table 3. Adopting these results, we find that the flickering light source contributes about 3% of the light in the *R* band, 4% in *V*, 6% in *B*, and 8% in *U* (Nov 2009); 9% of the light in the *R* band, 11% in *V*, 16% in *B*, and 16% in *U* (Jan 2010).

Zamanov et al. (2011) reported simultaneous observations in 5 bands of MWC 560 on 2010 December 29/30 during the recent active phase. For completeness all the results are given in Table 3.

3. 2. TEMPERATURE AND SIZE OF THE FLICKERING SOURCE

The derived $(U - B)_0$ colour corresponds to a B1-B5V star ($T_{\text{eff}} \approx 24000 - 16000$ K) and a black body with $T \approx 8000 - 12000$ K. The $(B - V)_0$ colour corresponds to an

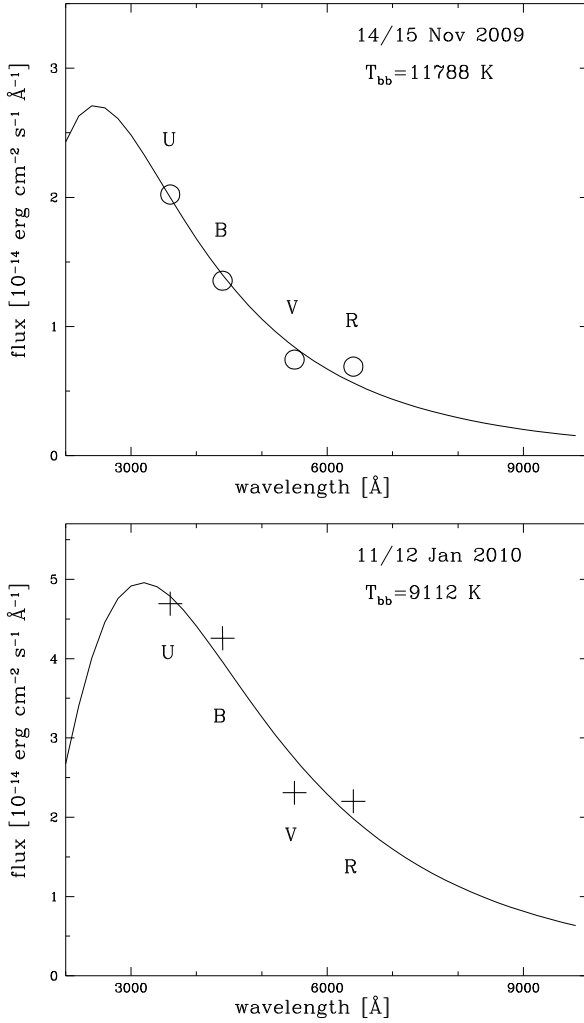


Figure 3: Dereddened fluxes of the flickering light source of MWC 560. The solid line represents a black body fit.

(upper panel): 2009 Nov 14/15 (circles). The fit is $T_{bb} = 11788 \text{ K}$, radius $R = 1.07 R_{\odot}$, located at distance $d = 2.5 \text{ kpc}$.

(down panel): 2010 Jan 11/12 (pluses), $T_{bb} = 9112 \text{ K}$, radius $R = 2.74 R_{\odot}$.

B8-A8V ($T_{\text{eff}} \approx 8000 - 13000 \text{ K}$) star and a black body with $T \approx 8000 - 15000 \text{ K}$. These estimates give an approximate temperature of the flickering light source $T_{\text{fl}} = 8000 - 15000 \text{ K}$ (we note that $(V - R)_0$ gives a lower resulting temperature ($T_{\text{eff}} = 5000 - 5500 \text{ K}$) but the R band is dominated by the contribution of the red giant).

In Fig. 3 we plot these magnitudes transformed to fluxes. Adopting $d = 2.5$ kpc and using a black body fit (*nfit1d* routine of IRAF), we calculate for the flickering light source: $T_{\text{fl}} = 11788 \pm 300$ K, $R_{\text{fl}} = 1.1 R_{\odot}$, $L_{\text{fl}} = 20 L_{\odot}$ (2009 Nov 14) and $T_{\text{fl}} = 9112 \pm 300$ K, $R_{\text{fl}} = 2.45 R_{\odot}$, $L_{\text{fl}} = 38 L_{\odot}$ (2010 Jan 11). Using all data normalized to V band we calculate $T_{\text{fl}} \approx 10100 \pm 300$ K.

3. 3. QUASIPERIODS

In our Jan 2010 observations a quasiperiod of 21.8 ± 1.2 min is visible. From the run on 2004 December 2, a quasiperiod of 11.8 ± 1.1 min is visible. From the run on 2010 December 29, a quasiperiod of 51 ± 2 min is detectable.

Quasi-periods observed in the light curves of MWC 560 range from 11 to 167 min (Tomov et al. 1996). These quasi periods correspond to Keplerian periods of gas in an accretion disk at distances $0.15 - 1.0 R_{\odot}$, around a $0.9 M_{\odot}$ white dwarf.

3. 4. ACTIVE PHASE

Our observations are obtained before and during the recent outburst, which reached the peak brightness in the end of December 2010 (Goranskij et al. 2011). The calculated parameters (Table 3) show that the flickering light source becomes hotter and more luminous, but does not change its size, during the recent outburst.

4. CONCLUSIONS

We report our CCD observations of the flickering variability of the jet-ejecting symbiotic star MWC 560, with 5 telescopes in the *UBVRIu'* bands. MWC 560 has a flickering source with $(U - B)_0 = -0.93$, $(B - V)_0 = +0.01$, $(V - R)_0 = +0.43$ (14 Nov 2009), and $(U - B)_0 = -0.61$, $(B - V)_0 = -0.01$, $(V - R)_0 = +0.46$ (11 Jan 2010).

For the flickering light source in MWC 560 we estimate $T_{\text{eff}} \approx 9100 - 11800$ K, which is similar to the temperature of the bright spot in CVs. Using a distance of $d = 2.5$ kpc, we find size $R_{\text{fl}} \approx 1 - 2.5 R_{\odot}$, and luminosity $L_{\text{fl}} \sim 20 - 40 L_{\odot}$. These values refer to November 2009 - January 2010.

References

- Bessell, M. S.: 1979, *PASP*, **91**, 589.
 Bruch, A.: 1992, *A&A*, **266**, 237.
 Cardelli, J. A., Clayton, G. C., and Mathis, J. S.: 1989, *ApJ*, **345**, 245.
 Dobrzycka, D., Kenyon, S. J., and Milone, A. A. E.: 1996, *AJ*, **111**, 414.
 Goranskij, V. P., Doroshenko, V. T., Barsukova, E. A., et al.: 2011, *The Astronomer's Telegram*, **3149**, 1.
 Gromadzki, M., Mikołajewski, M., Tomov, T., et al.: 2006, *AcA*, **56**, 97.
 Gromadzki, M., Mikołajewska, J., Whitelock, P. A., Marang, F.: 2007, *A&A*, **463**, 703.
 Henden, A., and Munari, U.: 2006, *A&A*, **458**, 339.
 Meier, S. R., Rudy, R. J., Lynch, D. K., et al.: 1996, *AJ*, **111**, 476.
 Merrill, P. W., and Burwell, C. G.: 1943, *ApJ*, **98**, 153.
 Michalitsianos, A. G., Perez, M., Shore, S. N., et al.: 1993, *ApJ*, **409**, L53.
 Schmid, H. M., Kaufer, A., Camenzind, M., et al.: 2001, *A&A*, **377**, 206.
 Sokoloski, J. L., Bildsten, L., and Ho, W. C. G.: 2001, *MNRAS*, **326**, 553.

- Sokoloski, J. L.: 2003, in *Symbiotic Stars Probing Stellar Evolution*, ed. Corradi, R. L. M., Mikolajewska, R., and Mahoney, T. J., *ASP Conf. Ser.*, **303**, 202.
- Steele, I. A., Smith, R. J., Rees, P. C., et al.: 2004, *Proc. SPIE*, **5489**, 679.
- Stute, M., and Sahai, R.: 2009, *A&A*, **498**, 209.
- Tomov, T., Zamanov, R., Kolev, D., et al.: 1992, *MNRAS*, **258**, 23.
- Tomov, T., Kolev, D., Ivanov, M., et al.: 1996, *A&AS*, **116**, 1.
- Tomov, T., and Kolev, D.: 1997, *A&AS*, **122**, 43.
- Zamanov, R., and Marziani, P.: 2002, *ApJ*, **571**, L77.
- Zamanov, R. K., Boeva, S., Latev, G., Stoyanov, K., Bode, M. F., Antov, A., Bachev, R.: 2011, *IBVS*, **5995**, 1.
- Zamanov, R., Gomboc, A., Latev, G.: 2011, *BlgAJ*, **16**, 18.
- Zamanov, R. K., Gomboc, A., Stoyanov, K. A., and Stateva, I. K.: 2010, *AN*, **331**, 282.
- Zombeck M., 1990, *Handbook of Space Astronomy and Astrophysics*, 2nd edition, Cambridge University Press.

WFPDB METADATA FORMAT PREPARATION

KATYA TSVETKOVA¹ and MILCHO TSVETKOV²

¹*Institute of Mathematics and Informatics, Bulgarian Academy of Sciences*

²*Institute of Astronomy, Bulgarian Academy of Sciences*

Abstract. We present an overview of the preparation of plate metadata for the Wide-Field Plate Database (WFPDB, <http://www.wfpdb.org>), of the accepted formats as standards for plate/archive description, the data reduction applied to original plate catalogues, as well as the work of making the existed logbooks accessible online

1. INTRODUCTION

The re-use of the old astronomical photographic plates needs a selection of worthy observations, which is dependent on the available plate metadata, i.e. the plate metadata have to contain all necessary information for future plate identification, selection and processing. In order to index and make as much as possible informative plate search and selection, the Wide-Field Plate Database (WFPDB, <http://www.wfpdb.org>) requires well-formatted plate metadata and data reduction pipeline. The first established standards of plate metadata were given in the standardized description of the ReadMe file (<http://cdsarc.u-strasbg.fr/viz-bin/Cat?VI/90>) of the WFPDB (Tsvetkov et al. 1997) which can be found through the Catalog VI/90 Selection Page in the Strasbourg Astronomical Data Center (CDS). Since the installation of the WFPDB in CDS the plate metadata standards have been developed. Here we present this development of the accepted formats as standards for plate/archive description, the used data reduction applied to original plate catalogues, as well as the work of making the existed logbooks accessible online.

2. WFPDB ARCHIVES AND PLATE INDEX METADATA

Informational sources for the plate archives included in the Catalogue of the Wide-Field Plate Archives (CWFPAs, Tsvetkova and Tsvetkov 2006, 2008) and for the individual plates in the Catalogue of the Wide-Field Plate Indexes

(CWFPs, Tsvetkov 2006) as parts of the WFPDB, are the observatories or other astronomical institutions with plate observations. In preparation of the list of such organizations we used The Strasbourg Astronomical Institutes Directory, The Nautical Astronomical Almanac, Annual Reports of different observatories, their Web pages, private correspondence and contacts, published plate data files and manual data entries or applying Optical Character Recognition tool.

The formats of the CWFPAs and CWFPs are given in Table 1 and Table 2.

Table 1: Byte-by-byte Description of file: archives

Bytes	Format	Units	Label	Explanations
1-3	A3	---	IDobs	¹ WFPDB observatory identifier
4-6	I3	cm	IDins	¹ Instrument aperture
7	A1	---	IDSuf1	¹ [A-Z]Suffix to the instrument identifier
9-25	A17	---	LOCs	Location of the plate archive, town (site)
27-40	A14	---	LOCc	Location of the plate archive, country
42-64	A23	---	OBSn	Observatory, name
66-83	A18	---	OBSs	Observatory, site
85-95	A11	---	OBSc	Observatory, country
97-99	I3	---	MNo	Marsden's number
101	A1	---	TZ-	Time zone, sign
102-103	I2	h	TZ	Time zone
105	A1	---	LON-	Observatory longitude, sign
106-108	I3	deg	LONd	Observatory longitude, deg
110-113	F4.1	arcmin	LONm	Observatory longitude, arcmin
115	A1	---	LAT-	Observatory latitude, sign
116-117	I2	deg	LATd	Observatory latitude, deg
119-122	F4.1	arcmin	LATm	Observatory latitude, arcmin
124-127	I4	m	ALT	Observatory altitude
129-130	I2	---	MULT	Multiplicity of telescope cameras
131	A1	---	---	[x] Sign 'x'
132-135	F4.2	m	APR	Clear aperture of the telescope
137-140	F4.2	m	MD	Diameter of telescope mirror
142-146	F5.2	m	FL	Focal length of the telescope
148-151	I4	arcsec/mm	SCL	Plate scale
153-155	A3	---	ITYPE	² Instrument type
157-161	F5.1	deg	FIELD	Field angular dimension
163-166	I4	yr	YEAR1	Year of beginning of telescope operation
168-171	I4	yr	YEAR2	Year of end of telescope operation
173	A1	---	PF	[F] Indication 'F' for 'film'
175-180	I6	---	NPd	Number of direct plates

Table 1: (continuation)

Bytes	Format	Units	Label	Explanations
181	A1	---	NPUNd	[:] Uncertainty of the number of plates
183-184	A2	---	CFORMd	³ Plate catalog form (direct plates)
186-190	I5	---	NPs	Number of objective prism plates
191	A1	---	NPUNs	[:] Uncertainty of the number of plates
193-194	A2	---	CFORMs	³ Plate catalog form (obj. prism plates)
196-197	A2	---	QUAL	⁴ [ABD] Code for archive quality
199-212	A14	---	ANAME	Astronomer in charge

Notes to Table 1:

¹ Fields from byte 1 to byte 7, taken together, constitute the WFPDB instrument identifier.

² Ast - astrograph, Cam - camera, FEC - fish eye camera, Men - meniscus, RCr - Ritchey-Chretien, Rfl -reflector, Rfr - refractor, Sch – Schmidt

³ C - computer-readable form, T - printed table form, TC - computer-readable form in preparation

⁴ A - very good, B - good, D – distributed

Table 2: Byte-by-byte description of file CWFPIs maindata

Bytes	Format	Units	Label	Explanations
1-3	A3	---	IDobs	¹ WFPDB observatory identifier
4-6	I3	cm	IDins	¹ Instrument aperture
7	A1	---	IDSuf1	¹ [A-Z] Suffix to the instrument identifier
8-13	I6	---	IDno	¹ Original plate number
14	A1	---	IDSuf2	¹ [A-Z] Suffix to the original plate number
15-16	I2	h	RAh	Right ascension (hours) (J2000.0)
17-18	I2	min	RAm	Right ascension (minutes)
19-20	I2	s	RA s	Right ascension (seconds)
21	A1	---	DE-	Declination sign (J2000.0)
22-23	I2	deg	DEd	Declination, degrees
24-25	I2	arcmin	DEm	Declination, arcminutes
26-27	I2	arcsec	DEs	Declination, arcseconds
28	A1	---	CCOD	[EMU] Code for Error, Missing data, or Uncertainty of coordinates
29-32	I4	yr	DATEy	Date of observation, year (UT)
33-34	I2	month	DATEm	Date of observation, month
35-36	I2	d	DATED	Date of observation, day
37-38	I2	h	UTh	Observation time (hour) (UT)
39-40	I2	min	UTm	Observation time (min)
41-42	I2	s	UTs	Observation time (sec)

Table 2: (continuation)

Bytes	Format	Units	Label	Explanations
43	A1	---	TCOD	[EMU] Code for Error, Missing data, or Uncertainty of observation time
44-63	A20	---	OBJNAM	Object or field designation
64-65	A2	---	OBJTYP	2Object type code
66-67	I2	---	METHOD	3Method of observation code
68-69	I2	---	MULTEX	Multiplicity of exposure
70-75	F6.1	min	EXP	4Exposure time
76-86	A11	---	EMULS	Emulsion type
87-93	A7	---	FILT	Filter type
94-95	A2	---	SPEC	Spectral band
96-97	I2	cm	DIMx	X dimension of plate
98-99	I2	cm	DIMy	Y dimension of plate
100	I1	---	PQUAL	[0,1] Pointer to file 'quality'
101	I1	---	PNOT	[0,1] Pointer to file 'notes'
102	I1	---	POBS	[0,1] Pointer to file 'observer'
103	I1	---	PAVA	[0,1] Pointer to file 'availability'
104	I1	---	PDIG	[0,1] Pointer to file 'digitization'

Notes to Table 2:

- ¹ Fields from byte 1 to byte 14, taken together, constitute the WFPDB plate identifier. Fields from byte 1 to byte 7 constitute the WFPDB instrument identifier.
- ² Object type in WFPDB is coded as is shown in Table 3.
- ³ Method of observation is coded as is shown in Table 4.
- ⁴ For multi-exposures with different duration of the separate exposures the 2nd, 3rd,... exposures are given in file Notes, if available in the original plate catalogues.

The plate metadata is structured in a multi-file system with conventional file names – Maindata (byte-by-byte description is given in Table 2), Quality (Table 5), Notes (Table 6), Observer (Table 7), Availability (Table 8), and Digitization (Table 9). All files belonging to this multi-file system follow certain file formats given in the respective byte-by-byte description of the files.

Table 3 and Table 4 present the assigned codes for object type and method of observation. It is common that in the plate logbooks the object type is not given. The used method of observations can be found usually in the notes of the respective logbooks. The coded information for the object type and method of observation allows making selection by these searchable constrains quickly. To code this information is a laboring work done manually up to the moment and this is a reason that very often it is missing in the WFPDB catalogues.

Table 3: WFPDB object type code

Code	Object
A1	Planet
A2	Moon
A3	Sun
A4	Asteroid
A5	Comet
A6	Meteor
A7	Artificial satellite
S1	Star
S2	Double star, or multiple star
S3	Variable star
S4	Stellar cluster
S5	HII region
S6	Nebula
S7	Planetary nebula
S8	Supernova + SN remnants
S9	Fundamental star
SR	Reference star around a radio source
SA	Stellar association
SD	Dark nebula
SH	Herbig-Haro object
SM	Molecular cloud
SP	Pulsar
G1	Galaxy
G2	QSO
G3	Group of galaxies
G4	Cluster of galaxies
G5	Supercluster
G6	Void
F	Field
G7	Radio galaxy
GR	Gamma-ray source
XR	X-ray source
RS	Radio source
IR	Infrared source
U	Object of unknown nature

Table 4: Code for method of observation

Code	Method of Observation
1	Direct photograph
2	Direct photograph, multi-exposure
3	Stellar tracks
4	Objective prism
5	Objective prism
6	Metcalf's method
7	Proper motions
8	No guiding
9	Out of focus
10	Test plate
11	Hartmann test
12	With mask
14	Sub-beam (Pickering) prism
13	Focusing
15	Raster scan/trail
24	Objective grating
25	Objective grating, multi-exposure

Table 5: Byte-by-byte description of file Quality

Bytes	Format	Units	Label	Explanations
1-3	A3	---	IDobs	WFPDB observatory identifier
4-6	I3	cm	IDins	Instrument aperture
7	A1	---	IDSuf1	[A-Z] Suffix to the instrument identifier
8-13	I6	---	IDno	Original plate number
14	A1	---	IDSuf2	[A-Z] Suffix to the original plate number
15	A1	---	CONT	Continuation sign (1, 2, ...) or blank
16-80	A65	---	QTEXT	Text of quality information

Table 6: Byte-by-byte description of file Notes

Bytes	Format	Units	Label	Explanations
1-3	A3	---	IDobs	WFPDB observatory identifier
4-6	I3	cm	IDins	Instrument aperture
7	A1	---	IDSuf1	[A-Z] Suffix to the instrument identifier
8-13	I6	---	IDno	Original plate number
14	A1	---	IDSuf2	[A-Z] Suffix to the original plate number
15	A1	---	CONT	Continuation sign (1, 2, ...) or blank
16-80	A65	---	NTEXT	Text of note

Table 7: Byte-by-byte Description of file Observer

Bytes	Format	Units	Label	Explanations
1- 3	A3	---	IDobs	WFPDB observatory identifier
4-6	I3	cm	IDins	Instrument aperture
7	A1	---	IDSuf1	[A-Z] Suffix to the instrument identifier
8-13	I6	---	IDno	Original plate number
14	A1	---	IDSuf2	[A-Z] Suffix to the original plate number
15	A1	---	CONT	Continuation sign (1, 2, ...) or blank
16-57	A42	---	OBSNAM	Observer's name(s)

Table 8: Byte-by-byte Description of file Availability

Bytes	Format	Units	Label	Explanations
1-3	A3	---	IDobs	WFPDB observatory identifier
4 6	I3	cm	IDins	Instrument aperture
7	A1	---	IDSuf1	[A-Z] Suffix to the instrument identifier
8-13	I6	---	IDno	Original plate number
14	A1	---	IDSuf2	[A-Z] Suffix to the original plate number
15	A1	---	CONT	Continuation sign (1, 2, ...) or blank
16-57	A42!	---	ATEXT	Text of availability

Table 9: Byte-by-byte Description of file Digitization

Bytes	Format	Units	Label	Explanations
1-3	A3	---	IDobs	WFPDB observatory identifier
4-6	I3	cm	IDins	Instrument aperture
7	A1	---	IDSuf1	[A-Z] Suffix to the instrument identifier
8-13	I6	---	IDno	Original plate number
14	A1	---	IDSuf2	[A-Z] Suffix to the original plate number
15	A1	---	CONT	Continuation sign (1, 2, ...) or blank
16-57	A42?	---	DTEXT	Text of digitization

3. WFPDB CATALOGUE PREPARATION

The original plate catalogues have been prepared in the computer-readable form from the existing logbooks by the staff of the observatories or in many cases by the WFPDB team. In some cases, there are even no diaries of observations and then the only option is taking the information directly from the photographic plates or plate envelopes. Another problems occurred during the catalogue preparation are missing coordinates (relying only on the given object name) and no given time of the exposure beginning. Such problems are mentioned in the

maindata file with code “M” for missing information. There are also typomistakes, which can not be corrected logically; such cases are mentioned with code "E" standing for errors.

The logbooks are an important part of every plate archive – they contain the original plate records and sometimes are the only source of information for the plate metadata, very often they contain also additional information, which facilitates the possible future plate use. There is a new opportunity for extended logbook search in the WFPDB and access to the scanned logbooks of different plate collections. For the preparation in computer readable form of the existed scanned logbooks (in typed table form) and creation of tables in the WFPDB format the Optical Character Recognition (OCR) tool (Package CuneiForm) for converting the typed original plate catalogues in table form to electronic form was applied last years (Kirov et al. 2012). Another new possibility is the linkage of the astronomical photographic plates scanned images from the WFPDB and the page images from the original astronomical journals using the segmentation of the images from the logbooks.

A comparison of the used OCR software (<http://www.cuneiForm.ru/>) for extracting data from the printed tables with original tables was made for the WFPDB TOK016 and TOK020 catalogues (Kirov et al. 2012). The OCR tool gave 90% correct recognition of the table columns.

4. WFPDB CATALOGUE DATA REDUCTION

According to our experience the most needed data conversion comprises the coordinates and the given time of the beginning of the observations. The plate centre coordinates transformation has to give the equatorial coordinates (R.A. and DEC) in the accepted epoch 2000.0. Since 2010 we used a data pipeline routine developed by N.Kirov and applied to the maindata file of the accepted WFPDB data format. Another data pipeline routine is used for the transformation of local sidereal time (LST) used very often for recording the observing data, to the required universal time (UT). For the conversion of the local standard time to UT the data for the given time zone in the CWFPAs are used, as well the information for the Daylight Saving Time (DST) for the different countries was taken in view.

Acknowledgements

This work is supported by the Bulgarian National Science Fund (grants BG NSF DO-02-273 and BG NSF DO-02-275).

References

- Kirov, N., Tsvetkov, M., Tsvetkova, K., Kalaglarsky, D.: 2012, *Proceedings of VII BSAC, Chepelare, Bulgaria, June 1-4, 2010*, Eds. M. K. Tsvetkov, M. S. Dimitrijević, K. Tsvetkova, O. Kounchev, Ž. Mijajlović, *Publ. Astron. Soc. "Rudjer Bošković"*, No 11, 147-152.
- Tsvetkov, M. K., Stavrev, K. Y., Tsvetkova, K. P., Mutafov, A. S., Semkov, E. H.: 1997, *Standardized description of the catalogue ReadMe* (<http://cdsarc.u-strasbg.fr/viz-bin/Cat?VI/90>)
- Tsvetkov, M.: 2006, *Wide-Field Plate Database: a Decade of Development*, In: *Virtual Observatory: Plate Content Digitization, Archive Mining and Image Sequence, Processing*, iAstro workshop, Sofia, Bulgaria, Eds. M. Tsvetkov, F. Murtagh, R. Molina.
- Tsvetkova, K., Tsvetkov, M.: 2006, In: *Virtual Observatory, Plate Content Digitization, Archive Mining, Image Sequence Processing*, Eds. M. Tsvetkov, V. Golev, F. Murtagh, R. Molina, Heron Press Science Series, Sofia, 45-53.
- Tsvetkova, K., Tsvetkov, M.: 2008, *VizieR Online Data Catalog*: VI/126, 10/2008.

THE LAST PLATE OBSERVATIONS WITH ROZHEN OBSERVATORY SCHMIDT TELESCOPE

KATYA TSVETKOVA¹, MILCHO TSVETKOV², NIKOLAY KIROV³,
DAMYAN KALAGLARSKY¹

¹*Institute of Mathematics and Informatics, Bulgarian Academy of Sciences*

²*Institute of Astronomy, Bulgarian Academy of Sciences*

³*Computer Science Department, New Bulgarian University*

Abstract. We present the last 549 plate observations with the 50/70/172 cm Schmidt telescope of Rozhen Observatory obtained in the period 1994 - 1998. These plate observations were carried out after the appearance of the first version of the Rozhen Schmidt telescope plate catalogue (see Mutafov et al. 1994). Statistics and analysis of these last plate observations are done.

1. INTRODUCTION

The plate observations with the 50/70/172 cm Schmidt telescope of Rozhen Observatory started immediately after the telescope installation and tests in June 1979. The first version of the Rozhen Observatory Schmidt telescope plate catalogue containing metadata information for 7348 plates obtained in the period June 1979-February 1994 was prepared by Mutafov et al. (1994). In Tsvetkova et al. (2010) one can find a statistics and analysis of this first plate catalogue version made with data retrieval from the Wide-Field Plate Database (WFPDB, <http://www.wfpdb.org>), where this catalogue is included with the WFPDB identifier ROZ050. A lot of mistakes done either by the observer or during the typing of the first version of the Schmidt telescope plate catalogue were corrected in the work of Tsvetkova et al. (2010). Recently the information for the last plate observations carried out in the period March 1994-February 1998 was put in computer-readable form using the telescope logbook.

2. WFPDB FORMAT PREPARATION OF THE PLATE METADATA

We reduced the available plate metadata to the accepted WFPDB format by:

- Structuring the plate metadata in multi-file system with conventional names of the files – Maindata, Quality, Notes, Observer, Availability, Digitization;
- Following the accepted WFPDB file format;
- Conversion of the equatorial coordinates of the plate centers (RA and DEC) given by the observer in the epoch of observations to equinox J2000.0;
- Conversion of the given time of observations LT (Local Time) to required Universal Time (UT), taking in view the information for the Daylight Saving Time (DST) for Bulgaria;
- Assigning object code in the main data file.

During the reduction of the plate metadata to the required WFPDB format we met different problems:

1. Plates without given coordinates - total number 155. The reasons that the observer did not write down the coordinates are different - the observer wrote down the name of the observed object; the observer missed to fill in the coordinates in the logbook but he has the coordinates in his notes.
2. Plates without given time of the exposure beginning - 8 of the plates are without exposure beginning.
3. Mistakes made by the observers, which were corrected logically.
4. Wrongly given time of the beginning of the exposure - this revealed itself in disturbance of the plate serial number, such cases are mentioned with "E".

3. STATISTICS AND ANALYSIS

The information about the last plate observations concerning the total number, the time period comprised, the type of the plates (different from the direct one-exposure plates) is summarized in Table 1.

Table 1: New added Rozhen Schmidt telescope plates

Number of Plates	549
Period Beginning	March 8, 1994
End	February 28, 1998
Multi-Exposure Plates	68
Objective Prism Plates	35

The time distribution of the plates obtained in the period 1994 – 1998 (Fig. 1) reflects the decreasing observing activity up to its stopping in February 28, 1998. Since that time the Rozhen Observatory Schmidt telescope has been equipped with CCD camera.

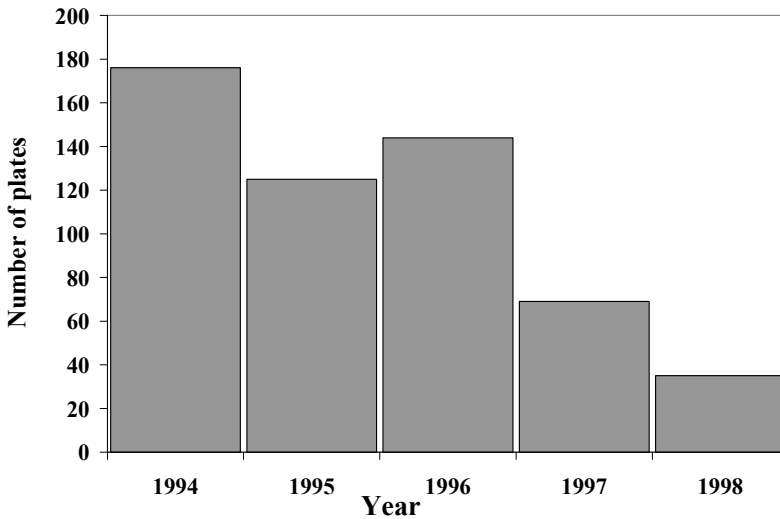


Figure 1: Time distribution versus number of the plates.

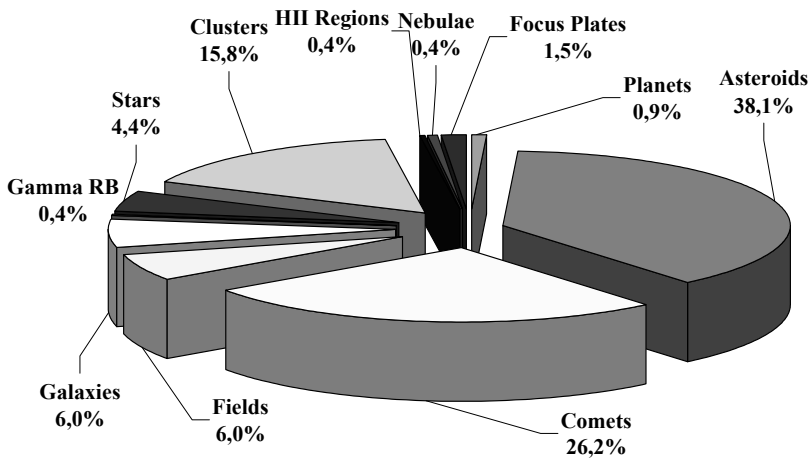


Figure 2: Observing programmes executed for the period 1994 – 1998.

Fig. 2 presents the executed observing programmes for the period 1994 – 1998. The assigned codes to the object types enable plate selection by observed object, respectively executed programme. The most observed objects were

asteroids (209 plates or 38.1% including 7 Vesta, 1094 AH2, Geographos 1620); comets (144 plates or 26.2% presented in Table 2) and stellar clusters (81 plates or 15.8%). Asteroids and comets were also the most southern objects observed with declination up to - 25 degrees. Among the observed variable stars it has to be mentioned KR Aur and AM Her.

Table 2: Observed comets

Comet	Number of Plates
Hale-Bopp (C/1995 O1)	84
6P/d'Arrest	16
Hyakutake (C/1996 B2)	11
P/1994 X1 McNaught-Russell	7
Shoemaker-Levy 9 (C/1994 F2)	6
22P/Kopff	6
9P/Tempel	4
Takamizawa-Levy (C/1994 G1)	3
31P/Schwassmann-Wachmann 2	2
65P/Gunn	1
19P/Borrelly	1
Tabur (C/1996 Q1)	1

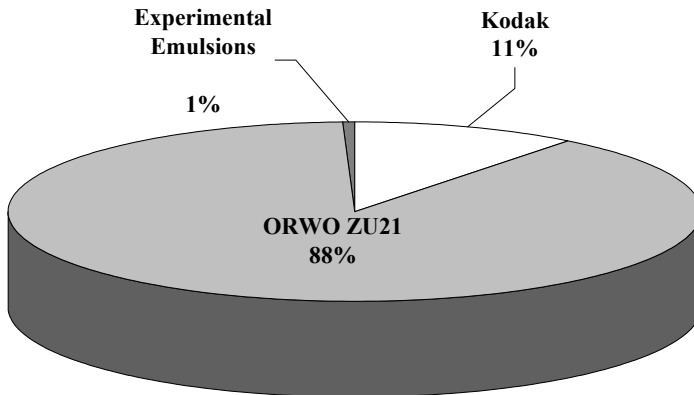


Figure 3: Emulsion type used.

In this time period with decreasing observing activity the used emulsions (Fig. 3) predominantly were ORWO ZU21 (88%) and “pg” photometric band (Fig. 4) by using Kodak IIaO or ORWO ZU21 emulsion without filter. Johnson’s UBVRI broad band photometric system was realized with the given combinations

of emulsion + filter in Table 3 valid for all plate observations with the Rozhen Observatory Schmidt telescope. For comet observations CN filters were used.

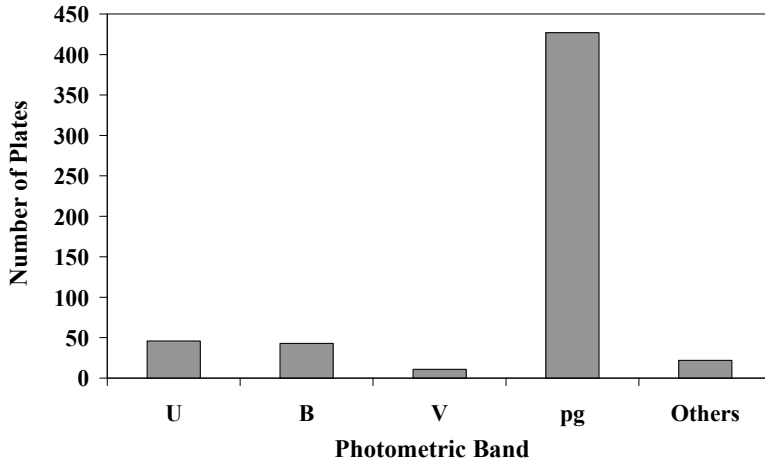


Figure 4: Broad band photometric system used for the obtained plates.

Table 3: Used combinations of emulsion and filter for Johnson's broad band photometric system (UBVRI)

Band	Emulsion	Filter
U	ORWO ZU1 ORWO ZU21 Kodak 103aO	UG1 UG1 (or UG2) UG1 (or UG2)
B	Kodak 103aO ORWO ZU21 ORWO ZU21	GG13 GG13 GG385
V	Kodak 103aD Kodak 103aD ORWO RP1 ORWO ZP3	GG11 GG495 GG11 GG11
R	ORWO ZP 3 Kodak 103aF	RG610 RG610
I	I-N (IV N)	RG715

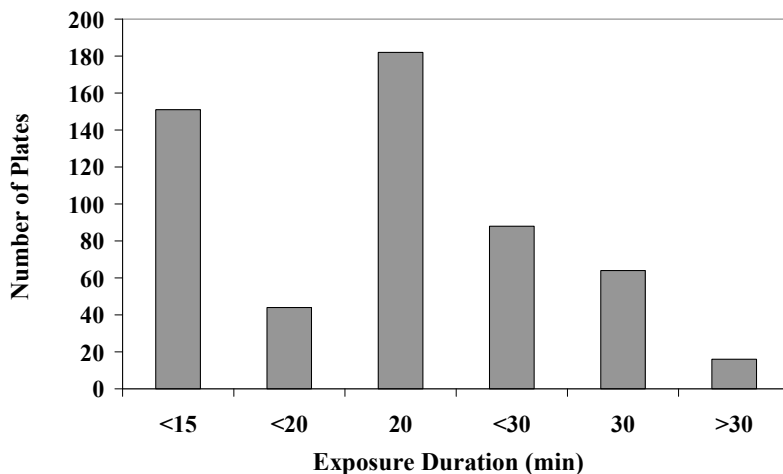


Figure 5: Distribution of the used exposure duration.

From Fig. 5 it is seen that mainly short exposure up to 15 min were used (about 34%) and exposures equal to 20min (33%) or 30 min (about 12%). Exposures with duration more than 30 min were used very rarely (3%). Mainly plates with sizes 16x16 cm were used. There are only 5 plates with sizes 9x12 cm.

From all 549 plates obtained in this period exactly 255 plates were obtained by V. Radeva in the frames of the observing programmes for asteroids and comets. Among the observers are E. Elst (Royal Observatory of Belgium), as well as G. Apostolovska and her students from the Skopje University.

4. CONCLUSIONS

With the added in 2012 new information for 549 plates concerning the last plate observations with the Rozhen Observatory Schmidt telescope done in the period 1994-1998 the upgrading catalogue includes now exactly 7897 plates. The main observing programmes during the last years of plate observations with this telescope were search of new asteroids and investigations of comets.

Acknowledgments

This work is supported by a grant of the Bulgarian National Science Foundation, Ministry of Education and Science, under number DO-02-273.

References

- Mutafov, A., Ilcheva, P., Kusheva, M., Michailov, M., Borisov, Z., Lazarov, N.: 1994, In: *Astronomy from wide-field imaging*, Proceedings of the IAU Symposium 161, Edited by H. T. MacGillivray, E. B. Thomson, B. M. Lasker, I. N. Reid, D. F. Malin, R. M. West and H. Lorenz, Kluwer Academic Publishers, Dordrecht, p.377.
- Tsvetkov, M. K.: 1991, *Wide-Field Plate Archives*, International Astronomical Union Commission 9 Working Group on Wide-Field Imaging, Newsletter No. 1, 17.
- Tsvetkova, K. P., Tsvetkov, M. K.: 2006, *Catalogue of Wide-Field Plate Archives: version 5.0* In: *Virtual Observatory: Plate Content Digitization, Archive Mining and Image Sequence Processing*, Eds. M. Tsvetkov, V. Golev, F. Murtagh, R. Molina, Heron Press, Sofia, pp. 45-53.
- Tsvetkova, K., Tsvetkov, M., Dimitrijević, M., Protić-Benišek, V., Benišek, V., Jevremović, D.: 2010, *Memorie della Societa Astronomica Italiana Supplement*, **15**.

LANGMUIR WAVES, TYPE III RADIO BURSTS AND IMPULSIVE ELECTRON EVENTS

SONJA VIDOJEVIC^{1,2}, ARNAUD ZASLAVSKY¹, MILAN MAKSIMOVIC¹,
SÄM KRUCKER³, MILAN DRAZIC², OLGA ATANACKOVIC²

¹*LESIA–Observatoire de Paris,*

CNRS, UPMC Univ. Paris 06, Univ. Paris-Diderot, France

²*Faculty of Mathematics, University of Belgrade, Serbia*

³*Space Sciences Laboratory, University of California, Berkeley, USA*

E-mail: sonja.vidojevic@obspm.fr, sonja@matf.bg.ac.rs, arnaud.zaslavsky@obspm.fr,
milan.maksimovic@obspm.fr, krucker@ssl.berkeley.edu, mdrazic@matf.bg.ac.rs,
olga@matf.bg.ac.rs

Abstract. It is known that interplanetary electron beams ejected from the sun are unstable in the solar wind and that they generate Langmuir waves (electrostatic) and electromagnetic waves (type III bursts). For the present statistical analysis we used radio observations in a range of 4 - 256 kHz from WAVES experiment onboard WIND spacecraft. A subset of 36 events, with Langmuir waves and type III radio bursts occurring at the same time, was selected. After background was removed, the remaining power spectral density is modeled by Pearson's system of probability distributions (type I, type IV and type VI). A relation in form of power-law between the power of Langmuir waves, the energy and the flux of the electrons in the impulsive electron events corresponding to the occurrence of the Langmuir waves is preliminary examined. We found a strong power-law dependence between electron fluxes and energies (power-law index γ equals 2.47 ± 0.06). The consequence of this fact is that the estimated parameters are highly unstable in numerical sense, thus the proposed model can be simplified, instead of two variables, it can be represented with only one: flux or energy.

1. INTRODUCTION

Locally generated Langmuir waves (electrostatic) and electromagnetic radio waves by the propagating of an electron beam in a surrounding plasma are some of the basic problems in plasma physics. Understanding of the conversion mechanisms by which electron beam produces Langmuir waves and radio waves is of essential importance to explain some of strong radiations in plasma astrophysics such as radio jets in active galactic nuclei, pulsars and neutron stars, or solar radio bursts. Unfortunately, for the distant objects *in situ* measurements are available only for radio emission and, sometimes, indirect measurements for the source - electron beam. Unique opportunity to study complete conversion processes, with simultaneously observed energetic

electrons and associated Langmuir and radio waves in the regions where these radio waves are generated (*in situ*), we have only for the solar radio bursts thanks to the numerous solar space missions in last few decades.

Energetic electron beams, ejected and accelerated from the sun by some violent processes - usually flares or coronal mass ejections, interact with interplanetary plasma to produce Langmuir waves and radio emissions called type III radio bursts (e.g. Lin 1985). The main characteristic of solar type III radio bursts is a fast negative frequency drift in very wide range of frequencies, from few kHz to hundreds of MHz. As the electron beam travels away from the sun along magnetic field lines, the density of surrounding plasma descends, so consequently the frequency of type III bursts decrease in time, $f_p = 9\sqrt{n_e}$ (n_e is the electron number density in m^3 , f_p in kHz). Langmuir waves and energetic electron events measured *in situ* have been directly associated with type III solar radio bursts and well-documented by many authors (e.g. Lin 1970, Frank and Gurnett 1972, Gurnett and Anderson 1977, Ergun et al. 1998).

Here, we present preliminary statistical analysis of electron beam and Langmuir waves associated with type III radio bursts. Firstly, after the background was removed, the remaining power of Langmuir waves is modeled by Pearson's system of probability distributions. It is found that the distributions belong to the three main Pearson's types: I, IV and VI. Secondly, a relation between the power of Langmuir waves, the energy and the flux of the electrons in the impulsive electron events corresponding to the occurrence of the Langmuir waves was analyzed.

The measurements obtained by the experiments onboard Wind spacecraft are used in this study. Wind spacecraft is a laboratory for long-term solar wind measurements launched on November 1, 1994 (Harten and Clark, 1995). The radio and electric field observations used, are obtained by the WAVES experiment (Bougeret et al. 1995). The locally generated Langmuir waves are recorded by the Thermal Noise Receiver (TNR, part of WAVES experiment), which provides measurements of the plasma electric field fluctuations in frequency domain from 4 kHz to 256 kHz in 5 logarithmically-spaced frequency bands including the local plasma frequency. The second used experiment is 3-D Plasma and Energetic Particle (3DP) Investigation (Lin et al. 1995) that provides the full three-dimensional distribution of suprathermal electrons. For the impulsive electron events the data detected with the electrostatic analyzers (EESAs) from ~ 0.2 keV to ~ 27 keV in 15 energy channels were used. The electron energy flux spectra are produced by summation over angular bins - omnidirectional flux. The energetic electron events are easily recognizable by its velocity dispersion, with faster electrons arriving earlier, as expected if the electrons of all energies are simultaneously accelerated at the the same point and travel the same distance along the interplanetary field to reach the spacecraft. A subset of 36 events, with Langmuir waves and type III bursts occurring at the same time, was selected.

2. DATA ANALYSIS AND RESULTS

When dealing with empirical data with significant skewness and kurtosis, the normal distribution is not the best choice for modeling. The four parameter Pearson's system of distributions is a better to use. It represents a wide class of distributions

with a wide variety of shapes and thus, provides more accurate representations of the observed data. On the other hand, it includes, as special cases, some well known distributions (normal, beta, gamma, Student's t-distribution etc.). Karl Pearson (1895) defined this distribution system by the following ordinary first order differential equation for the probability density function $p(x)$:

$$-\frac{p'(x)}{p(x)} = \frac{b_0 + b_1x}{c_0 + c_1x + c_2x^2} \quad (1)$$

where b_0, b_1, c_0, c_1 and c_2 are five real parameters. After normalizing the fraction with any of them, only four independent parameters remain. The form of the solution of this differential equation depends on the value of these parameters, resulting in several distribution types.

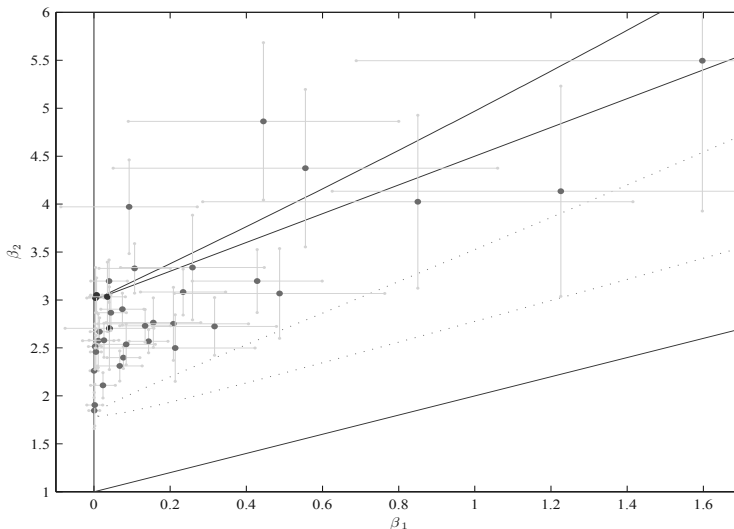


Figure 1: Beta plane. Out of the 36 events: 31 belong to Pearson's type I, 1 to type VI and 5 to type IV probability distribution. Most of the events are close to normal distribution - $(\beta_1, \beta_2) = (0, 3)$, but only for 4 (blue points) their error ellipses encompass the point of normal distribution (see electronic version).

The classification of distributions in the Pearson system is entirely determined by the first moment (mean- μ_1) and the next three central moments (variance- μ_2 , skewness- μ_3 and kurtosis- μ_4). Pearson proposed two dimensionless parameters, i.e. two moment ratios associated with the square of the skewness (β_1) and kurtosis (β_2):

$$\beta_1 = \frac{\mu_3^2}{\mu_2^3}, \quad \beta_2 = \frac{\mu_4}{\mu_2^2}. \quad (2)$$

These two parameters characterize the asymmetry and the peakedness of the distribution, respectively. They entirely determine the type of the Pearson distribution system. We have shown that the probability distributions of the power spectral density of the Langmuir waves belong to the three main types of Pearson's probability

distributions: type I, type IV and type VI (see positions of all 36 events in (β_1, β_2) plane in Fig. 1).

Next step was to extract those events where impulsive electron events can be seen at the same time as Langmuir waves. Several additional criteria had to be satisfied: (1) a clear velocity dispersion; (2) high enough signal-to-noise ratio; (3) a clear separation from surrounding events to avoid multiple events. The analysis of data detected with the electrostatic analyzers (EESAs) showed that these conditions are satisfied for 19 out of 36 previously selected events. We have analyzed a relation between power of Langmuir waves, the energy and the flux of the electrons. As a model, we proposed:

$$P_{\text{LW}} = a n_{\text{ch}}^\alpha E_{\text{ch}}^\beta. \quad (3)$$

In order to perform planned analysis, three dimensional points were created $(E_{\text{ch}}, n_{\text{ch}}, P_{\text{LW}})$. E_{ch} is energy of particular channel of EESA instrument in [keV], n_{ch} is electron flux in $[\text{cm}^2 \text{s sr eV}]^{-1}$ integrated over time interval of 12 minutes centered at electron flux maximum and P_{LW} is corresponding power of Langmuir waves in $[\text{V}^2 \text{m}^{-2}]$ integrated over the same time interval as the electron flux. Numerical integration is performed using trapezium method in both cases. The time interval of 12 minutes was chosen empirically to avoid overlapping in Langmuir waves power series and, on the other hand, to get rough approximation of electron beam flux (fair enough for a preliminary analysis) measured by particular channel. It turns out that energetic electron fluxes can be seen only in first 8 most energetic EESAs channels that spawn electron energies from about 2 to 27 keV. This fact indicates that the energies of electrons responsible for Langmuir waves emission are in range [2,27] keV. The average over all 19 events is 13.2 keV. In the Fig. 2 three-dimensional plot of the averaged variables is presented. As it can be seen, the strong linear dependence between logarithms of E_{ch} and n_{ch} in form:

$$n_{\text{ch}} = b E_{\text{ch}}^\gamma. \quad (4)$$

exists. The value of power-law index, γ , was found to be -2.47 ± 0.06 . Because of this strong dependence between n_{ch} and E_{ch} , which has the same form (power-law) as the model proposed (Eq. 3), the model given in the form $P_{\text{LW}} = P_{\text{LW}}(n_{\text{ch}}, E_{\text{ch}})$ (Eq. 3) has an infinite number of solutions. The smaller mean square errors of the fitting by Eq. (4) result in larger estimated errors for a, α and β in the model Eq. (3).

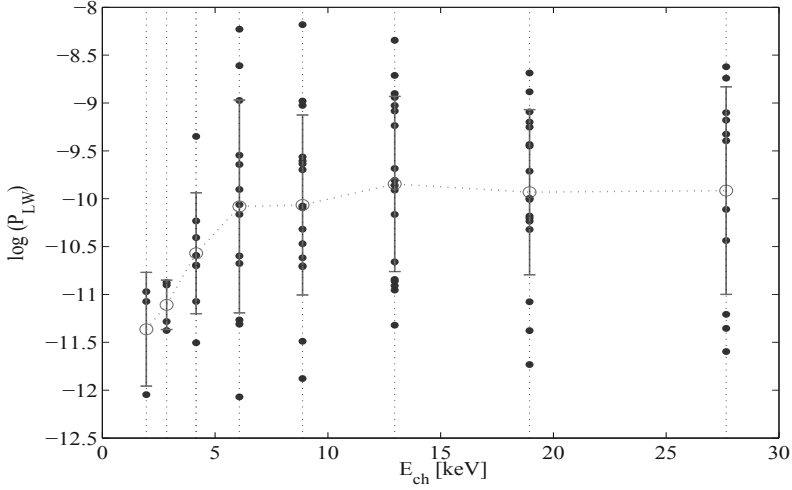


Figure 2: Relation between the logarithm of Langmuir waves power, P_{LW} , and the energies of electrons, E_{ch} . The blue points represent the integrals of Langmuir waves spectral density over the same time interval (12 min) as for the corresponding impulsive electron event fluxes, n_{ch} (see Fig. 3 for n_{ch}). Open red circles are means of Langmuir waves power at particular electron energies. The error bars are calculated as 1σ standard deviation (see electronic version).

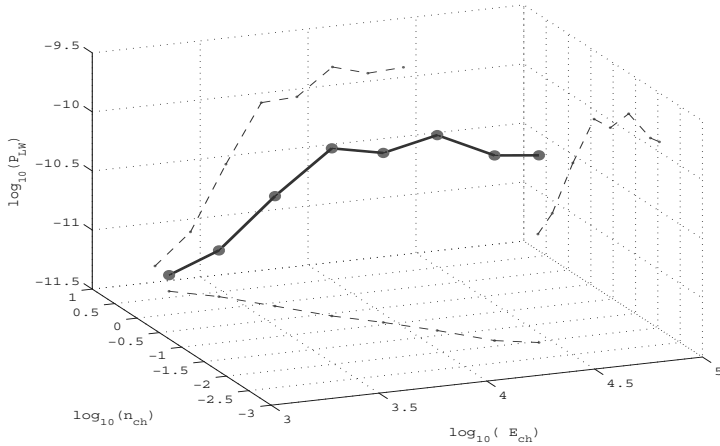


Figure 3: Spatial curve (solid line) represents the relation between logarithms of averaged Langmuir waves power, the electron energies and the averaged electron fluxes. The dashed lines are orthogonal projections of the spatial curve onto the coordinate planes. Note the projection onto horizontal plane – it can be fitted very good with logarithm of Eq. (4), i.e. with a linear model. For the projections onto vertical planes it can be seen that power-law is satisfied only partially (for lower electron energies) and then, the Langmuir waves power is flattened.

3. CONCLUSIONS

We have shown that for 36 events of intense locally formed Langmuir waves associated with type III radio bursts, the probability distributions of the power of these waves in spectral domain belong to the three main types of Pearson's probability distributions: type I, type IV and type VI. The similar result was obtained by Krasnoselskikh *et al.* (2007) for the Langmuir waves within the Earth's electron foreshock. Principal properties of the events' distributions (skewness and kurtosis) are summarized in beta plane, Fig. 1. The χ^2 goodness of fit test shows that the Pearson's probability distributions fit the data better than normal for all of the considered events. This is in contradiction with Stochastic Growth Theory proposed by Robinson (1992) which assumes log-normal distribution (or normal in logarithmic scale) for the Langmuir waves. Investigation of possible reasons of this disagreement is not within the scope of this study – further work is needed.

The power of Langmuir waves produced by the energetic electron beam can not be modeled in form of Eq. (3) by both, the flux and the energy of electrons, because of the strong power-law dependence between them. The power-law index is found to be 2.47 ± 0.06 . This result is comparable to the result recently obtained by Krucker *et al.* (2009) and earlier by Lin *et al.* (1982). The dependence between power of Langmuir waves and either the energy or either the flux, does not satisfied power-law. The partial power-law exist until the electron energy reaches approximately 10-13 keV when the saturation arises. The similar is for the dependence between power of Langmuir waves and the electron flux: the saturation starts at about $0.1 \text{ (cm}^2\text{sr s eV)}^{-1}$. A more detailed analysis is needed for an explanation of this saturation which is scope for the future study.

References

- Bougeret, J., *et al.*: 1995, Waves: The Radio and Plasma Wave Investigation on the Wind Spacecraft, *Space Science Reviews*, **71**, 231–263.
- Ergun, R. E. *et al.*: 1998, Wind Spacecraft Observations of Solar Impulsive Electron Events Associated with Solar Type III Radio Bursts, *Astrophysical Journal*, **503**, 435.
- Frank, L. A. and Gurnett, D. A.: 1972, Direct Observations of Low-Energy Solar Electrons Associated with a Type III Solar Radio Burst, *Solar Physics*, **27**, 446.
- Gurnett, D. A. and Anderson, R. R.: 1977, Plasma wave electric fields in the solar wind - Initial results from HELIOS 1, *Journal of Geophysical Research*, **82**, 632.
- Harten, R. and Clark, K.: 1995, The Design Features of the GGS Wind and Polar Spacecraft, *Space Science Reviews*, **71**, 23.
- Krasnoselskikh, V. V., Lobzin, V. V., Musatenko, K., Soucek, J., Pickett, J. S. and Cairns, I. H.: 2007, Beam-plasma interaction in randomly inhomogeneous plasmas and statistical properties of small-amplitude Langmuir waves in the solar wind and electron foreshock, *Journal of Geophysical Research (Space Physics)*, **112**, 10109.
- Krucker, S., Oakley, P. H. and Lin, R. P.: 2009, Spectra of Solar Impulsive Electron Events Observed Near Earth, *Astrophysical Journal*, **691**, 806.
- Lin, R. P.: 1970, The Emission and Propagation of 40 keV Solar Flare Electrons. I: The Relationship of 40 keV Electron to Energetic Proton and Relativistic Electron Emission by the Sun, *Solar Physics*, **12**, 266.
- Lin, R. P.: 1985, Energetic solar electrons in the interplanetary medium, *Solar Physics*, **100**, 537.
- Lin, R. P., Mewaldt, R. A. and Van Hollebeke, M. A. I.: 1982, The energy spectrum of 20 keV-20 MeV electrons accelerated in large solar flares, *Astrophysical Journal*, **253**, 946.

- Lin, R. P. et al.: 1995, A Three-Dimensional Plasma and Energetic Particle Investigation for the Wind Spacecraft, *Space Science Reviews*, **71**, 125.
- Pearson, K.: 1895, Contributions to the Mathematical Theory of Evolution. II. Skew Variation in Homogeneous Material, *Philosophical Transactions of the Royal Society of London*, **186**, 343.
- Robinson, P. A.: 1992, Clumpy Langmuir waves in type III radio sources, *Solar Physics*, **139**, 147.

GENERATION AND DEVELOPMENT OF THE DISK CORONA

KRASIMIRA D. YANKOVA

*Space Research and Technology Institute - BAS
Acad G. Bonchev Str., Bl. 1, 1113 Sofia, Bulgaria.
E-mail: f7@space.bas.bg*

Abstract. This paper considers the magneto-hydrodynamics of the advective accretion disk and its corona. The aim is to build an adequate addition to the disk evolution model, which treats the mechanisms of self-structuring in the system disk-corona. Discussed generation of the corona as a result of influences of the distribution of entropy and the development of advection in disc, over energetics (for individual components or total) of the system.

1. INTRODUCTION

In a series of papers, we develop a model, related to the interaction of the field and the plasma in the accretion disk. Accretion is qualitatively and quantitatively more effective in the presence of a magnetic field, arising more quickly and develop a more diverse range instabilities. Disks around massive objects cannot be cooled efficiently by mechanisms in the disk and its corona emerged. The corona is a macrostructure, which ensures the disk cooling, when the flow in it weakly radiates. It regulates processes in the disk and controls its stability.

2. MODEL OF THE DISK

We built a generalized model for study of magneto-hydrodynamics of the advective accretion disk under the following assumptions:

- ◆ Constructing model is non-stationary, no axis-symmetric Keplerian disk in normal magnetic field.
- ◆ The central object is a black hole. Unlike the customary consideration of relativistic flows in this case (Beloborodov, 2008), we use pseudo-

Newtonian gravitational potential in the form. $\Phi = -\frac{GM}{\mathbf{r}-r_g}$; $r_g = \frac{2GM}{c^2}$;

$\mathbf{r} = (r^2 + z^2)^{1/2}$. It is simple and convenient way to include in the consideration of purely Newtonian flow, relativistic effects which such a compact object exercises on the accretion, (Abramowicz, et al., 1988).

- ◆ The disc is geometrically thin, optically thick and without self-gravity.
- ◆ One-temperature fully ionized plasma. Temperature here is of the order of the temperature of ions, because presence of magnetic field guarantees efficient transfer of heat to the cooling components.
- ◆ In this disk there are conditions for thermal-viscous instability, but it is in controlled regime, balanced by magnetic advection; for the difference of the super-Eddington flows which inevitably become two-temperature (Spruit et al., 2001) or quickly depleted (Beloborodov, 2008). Here symbiosis of mechanisms, allowing to reach virial temperature in conditions of non-freefall.
- ◆ Own magnetic field is located vertically to the plane of the disc, respectively it is mainly determined by its vertical component, presented openly from the equatorial plane.

- ◆ Speed in the form $\mathbf{v} = (v_r, r\Omega_k = r \sqrt{\frac{GM}{r(r-r_g)^2}}, \theta)$, of its initial size and

direction depends on the degree of asymmetry of the disk (elliptical Keplerian orbits) in conditions of axis-symmetric central potential.

Model is based on the fundamental equations of the magneto-hydrodynamics fluids (1). The basic equations of MHD of accretion - disk flow: the continuity equation, equation of motion, equation of the magnetic induction, equation of heat balance and equation of state.

Equations have been obtained in the conditions of two reference systems. Coordinate system tied to the top of the flow and fixed coordinate system with centre in the acceptor. Galilean transformations are applied to the relative motion against each other. The flow will be considered as non-relativistic because $v^2/c^2 \sim 4 \cdot 10^{-2} \ll 1$.

$$\frac{\partial \rho}{\partial t} + \nabla \cdot (\rho \mathbf{v}) = 0$$

$$\nabla \cdot \mathbf{v} = 0 \quad \nabla \cdot \mathbf{B} = 0$$

$$\frac{\partial \mathbf{v}}{\partial t} + \mathbf{v} \cdot \nabla \mathbf{v} = -\frac{1}{\rho} \nabla p - \nabla \Phi + \left(\frac{\mathbf{B}}{4\pi\rho} \cdot \nabla \right) \mathbf{B} + \mathcal{G} \nabla^2 \mathbf{v}$$

$$\frac{\partial B}{\partial t} = \nabla \times (v \times B) + \eta \nabla^2 B \quad \eta = \frac{c^2}{4\pi \sigma}$$

$$\rho T \frac{\partial S}{\partial t} - \frac{\dot{M}}{2\pi r} T \frac{\partial S}{\partial r} = Q^+ - Q^- + Q_{mag}$$

$$p = p_r + p_g + p_m$$

Magnetic reconnection - feedback (Papaloizou et al., 1997) one of the fundamental mechanisms associated with the structuring of space plasmas.

- ◆ MP of the object can be its own central or external (galactic, from the donor). If its own field is located vertically to the plane of the disc, then moment in it grows inward toward the center. This effect can be compensated from powerful jets that lead the moment (Kuncic et al., 2004). But before reaching the central funnel, redistribution moment shall give an impact: Accelerated rotation releases higher amounts of energy, so by gradient of the entropy directly contributing to advection, and thus influence on the restructuring of the disk as an open system.

$$rT \frac{\partial S}{\partial t} + \frac{3}{2} H v_r \frac{v_a^2}{r} = H \vartheta (r \frac{\partial \Omega}{\partial r})^2 - \frac{c}{\chi H} (v_s^2 - \frac{v_a^2}{2} - RT) + \frac{\eta H}{4\pi \rho} (\frac{B_r}{H} + \frac{3\mu}{r^4})^2$$

- ◆ The sign of the entropy determined the basic criterion for development, equilibrium and stability of the disc. If it does not cooling efficiently in time, energy is kept in disk in form of heat and reduces the radial gradient of entropy to the center. This is a prerequisite for the disc to reach a new thermodynamic state, to remain globally stable and not to be destroyed. This transition is irreversible. Instabilities in the disk are feeding by heating, absorb the excess free energy, thus stimulate feedbacks in reshuffling the disk and instabilities become structures (vortices, spirals, corona). The effect is reinforced by the partial detention (slowdown) of the accretion, with due to such a distribution of angular momentum. Then advection helps for smooth transformation of the instabilities in the structures.

In the internal regions of the disc where the flow most difficult emits, advection carries the stored heat from the outer zones.

- ◆ More popular models suggest the flow deformation in the form of sharp increase in the radial velocity and significantly falling in orbital velocity to sub-Keplerian values – rotation of vector of the velocity. In this research advection is included in the form of advective term.

$$\frac{\partial(\rho v_i)}{\partial t} + \frac{\partial}{\partial x_j} (\rho v_i v_j) = \rho \left(\frac{\partial v_i}{\partial t} + v_j \frac{\partial v_i}{\partial x_j} \right) = \rho \frac{Dv_i}{Dt}$$

Operator $\frac{D}{Dt}$ defines the advective term.

This is not the increase in radial velocity, this is shifting of the average flow as a flux with velocity v_i in any direction. There is no rotation of the vector, although this can be considered as particular case (and works fine in the earth's atmosphere). On the total interpretation, however (and for such a powerful attraction by black holes, physically more probably) is, that the decision as a whole is transferred to smaller radii. Orbital rate of course changes, but this is due to the new orbit, and only indirectly connects it with advection. Orbital velocity is Keplerian again, because for such a packet transfer, flow does not change its nature. For a normal field to the disk, the dipole term in the equation of motion $B\Gamma\phi$ creates the conditions for the radial advection (Campbell et al., 1998) – i.e. determines the direction of displacement of the middle course. Radial pulling into a black hole can reach a speed which is about half of the rate of free fall, without weakening of the orbital rotation; on the contrary, it is accelerated due to the redistribution of the moment. Then, viscose and dynamic time-scale (which is comparable) is shorter than the thermal scale and cooling is inefficient.

Advection in similar conditions can work for relatively lower temperatures in the outer regions of the disk. Early appearances guarantee the flow to remain optically thick at temperatures of order (2-s) of higher than normally accepted, whatever show some of the new observations.

3. RESULTS

Processed results for key moments $t = 1P$ and $t \approx 0$ indicates that the disk develops spherical radiative (non-convective) corona.

- ◆ Co consideration of the radial and vertical structure of the disc:
- ◆ Monitoring of the development of the condition of stratification $|v_a| \leq |v_s|$; co set with that of the vector field of the velocity (v_r, v_z) (Iankova, 2007), gives an estimate of external radius of the corona on the disc.
- ◆ The behavior of local heating obtained (build) in the local model (Iankova, 2009a)

$$K(x) = \frac{\text{warming}}{\text{cooling}}$$

- ◆ along with $\partial_t s$, shows that the internal structure of the disk gradually changed to create a dynamic quasi-steady state - that is relatively stable, but very far from equilibrium (Yankova, 2012).
- ◆ By $K(x)$ we can also be assessed independently of the outer radius of the corona on the disc.

- ◆ Comparing the coefficients of the meeting of the global model with wave numbers in the local model (Iankova, 2009a,b, Yankova, 2012), provides independent confirmation of the idea for birth of the corona.
- ◆ In terms of our model this radius was obtained for the disk in system Cyg X-1. The expected result for the outer radius of the corona, with the coordination of observations, numerical results and simulations ranged from 15-250R_g (Novak et al., 1999) for a spherical corona to 320-640R_g for non-spherical (Pottschidt et al., 1998). In coincidence the object, evaluating value corresponds to the results of the first interval for spherical corona.

Well to note that in this case, we consider, disk and crown, without a common energetic.

To suture results in a complete model of the system we will use the output values of the perimeters from the disk surface for initial values in the functional distributions of the perimeters in the corona.

4. ADAPTATION - FORMULATION OF THE PROBLEM

Again we are based on fundamental equations of fluid MHD (1). To construct a model of the corona one should consider the general problem to adapt the system of the disk to the new conditions.

The flow in the disk is directed toward the center and is localized in the plane of the equator. Matter can be optically thick and dominated by gas or radiant pressure. Equilibrium is maintained by rotation.

Corona has reverse flow, optically thin and has a magnetic pressure.

Due to the specific nature of the almost spherical flow kinetic viscosity drops to zero $\alpha = 0$, and density decreases for orders of magnitude in the corona.

Weak rotation can not stabilize the instabilities and fell restrictions on the magnetic viscous coefficient (Iankova, Filipov, 2008):

$$\begin{aligned} \nabla \times (\eta \nabla \times B) &= \nabla [\eta \times (\nabla \times B)] = \\ &= (\nabla \cdot \eta) \times (\nabla \times B) + \eta \times (\nabla \cdot \nabla \times B) = \\ &= (\nabla \cdot \eta) \times (\nabla \times B) \pm \eta \nabla^2 B \end{aligned}$$

Then the adapted system in cylindrical coordinates is:

$$\begin{aligned} \frac{\partial \rho}{\partial t} + \frac{1}{r} \frac{\partial}{\partial r} (r \rho v_r) + \Omega \frac{\partial \rho}{\partial \varphi} + \frac{\partial}{\partial z} (\rho v_z) &= 0 \\ \frac{\partial}{\partial r} (r B_r) + \frac{\partial B_\varphi}{\partial \varphi} + r \frac{\partial B_z}{\partial z} &= 0 \end{aligned}$$

$$\frac{\partial v_r}{\partial t} + v_r \frac{\partial v_r}{\partial r} + \Omega \frac{\partial v_r}{\partial \varphi} + v_z \frac{\partial v_r}{\partial z} = -\frac{1}{\rho} \frac{\partial p}{\partial r} + \frac{1}{4\pi\rho r} (B_\varphi \frac{\partial B_r}{\partial \varphi} + rB_z \frac{\partial B_r}{\partial z})$$

$$\frac{\partial}{\partial t} (\Omega r^2) + v_r \frac{\partial}{\partial r} (\Omega r^2) + v_z \frac{\partial}{\partial z} (\Omega r^2) = \frac{1}{4\pi\rho r} [B_r \frac{\partial}{\partial r} (r^2 B_\varphi) + r^2 B_z \frac{\partial B_\varphi}{\partial z}]$$

$$\frac{\partial v_z}{\partial t} + v_r \frac{\partial v_z}{\partial r} + \Omega \frac{\partial v_z}{\partial \varphi} + v_z \frac{\partial v_z}{\partial z} = -\frac{1}{\rho} \frac{\partial p}{\partial z} - \frac{\partial \Phi}{\partial z} + \frac{B_r}{4\pi\rho} \frac{\partial B_z}{\partial r}$$

$$\frac{\partial v_r}{\partial r} + \frac{v_r}{r} + \frac{\partial v_z}{\partial z} = 0 \quad p = R\rho T + \frac{B^2}{8\pi} + \frac{aT^4}{3}$$

$$\begin{aligned} \frac{\partial B_r}{\partial t} &= \frac{1}{r} \frac{\partial}{\partial \varphi} (v_r B_\varphi) - \frac{\partial}{\partial \varphi} (\Omega B_r) + \frac{\partial}{\partial z} (v_r B_z) - \frac{\partial}{\partial z} (v_z B_r) + \frac{\eta}{r} \left[\frac{\partial}{\partial r} \frac{\partial B_r}{\partial \varphi} + \frac{\partial}{\partial r} \frac{\partial B_\varphi}{\partial \varphi} \right] + \\ &+ \frac{\eta}{r} \frac{\partial}{\partial r} (r \frac{\partial B_r}{\partial r}) + \frac{\eta}{r^2} \frac{\partial^2 B_r}{\partial \varphi^2} + \eta \frac{\partial^2 B_r}{\partial z^2} - \frac{B_\varphi}{r^2} \frac{\partial \eta}{\partial \varphi} - \frac{1}{r} \frac{\partial \eta}{\partial \varphi} \frac{\partial B_\varphi}{\partial r} + \frac{1}{r^2} \frac{\partial \eta}{\partial \varphi} \frac{\partial B_r}{\partial \varphi} + \\ &+ \frac{\partial \eta}{\partial z} \frac{\partial B_r}{\partial z} - \frac{\partial \eta}{\partial z} \frac{\partial B_z}{\partial r} \end{aligned}$$

$$\begin{aligned} \frac{\partial B_\varphi}{\partial t} &= \frac{\partial}{\partial r} (\Omega r B_r) - \frac{\partial}{\partial r} (v_r B_\varphi) + \frac{\partial}{\partial z} (\Omega r B_z) - \frac{\partial}{\partial z} (v_z B_\varphi) + \frac{\eta}{r} \left[\frac{\partial}{\partial \varphi} \frac{\partial B_r}{\partial r} + \frac{\partial}{\partial \varphi} \frac{\partial B_\varphi}{\partial r} \right] + \\ &+ \frac{\eta}{r} \frac{\partial}{\partial r} (r \frac{\partial B_\varphi}{\partial r}) + \frac{\eta}{r^2} \frac{\partial^2 B_\varphi}{\partial \varphi^2} + \eta \frac{\partial^2 B_\varphi}{\partial z^2} + \left(\frac{\eta}{r} + \frac{\partial \eta}{\partial r} \right) \left[\frac{B_\varphi}{r} + \frac{\partial B_\varphi}{\partial r} - \frac{1}{r} \frac{\partial B_r}{\partial \varphi} \right] - \\ &- \frac{\partial \eta}{\partial z} \left[\frac{1}{r} \frac{\partial B_z}{\partial \varphi} - \frac{\partial B_\varphi}{\partial z} \right] \end{aligned}$$

$$\begin{aligned} \frac{\partial}{\partial r} (rv_r B_z) - \frac{\partial}{\partial r} (rv_z B_r) - \frac{\partial}{\partial \varphi} (v_z B_\varphi) - \frac{9\eta B_z}{r} - \left(\frac{\eta}{r} + \frac{\partial \eta}{\partial r} \right) \left[\frac{\partial B_r}{\partial z} - \frac{\partial B_z}{\partial r} \right] + \\ + \frac{1}{r} \frac{\partial \eta}{\partial \varphi} \left[\frac{1}{r} \frac{\partial B_z}{\partial \varphi} - \frac{\partial B_\varphi}{\partial z} \right] = 0 \end{aligned}$$

$$\frac{\partial S}{\partial t} + \frac{3}{2} \frac{v_r v_s v_a^2}{\Omega r^2 T} = \frac{\eta v_s}{\Omega r T} \frac{1}{4\pi\rho} \left(\frac{\partial B_r}{\partial z} - \frac{\partial B_z}{\partial r} \right)^2 - \frac{c\rho}{\pi r T} \left(v_s^2 - \frac{v_a^2}{2} - RT \right)$$

Before we verify that our main modification

$$F_i = F_{i0} \mathfrak{R}_i(x = r/r_0, Z = z/r_0) \exp[k_\varphi(x, Z)\varphi + \omega(x, Z)t]$$

for the leading perimeters of the disc is applied in the new conditions, one should be noted that in this system is still incomplete adaptation and it can not be subjected to numerical treatment.

For example: The field cannot remain now in its simplest form, valid for equatorial plane and becomes:

$$B_z = \frac{\mu}{r^3} \frac{\sqrt{4r^2 + z^2}}{(r^2 + z^2)^2}$$

Also we have not given specific form of opacity $\tau = \frac{\rho v_s}{\Omega} \chi$; $\chi = ?$, and η magnetic viscosity itself.

5. COMMENTS AND EXPECTED RESULTS

Full adaptation of the model is forthcoming. It is following from its natural development in a vertical direction. The aim is to connect the physics of the corona with reordering in the disc as an open system, where the two streams do not have a total global energetic; to build an adequate addition – a model for the evolution of the corona which treats mechanisms of the self-structuring and investigates the emergence of instabilities in the disk's corona, in order to obtain a complete picture of the processes in the system disk-corona.

Literature

- Abramowicz, M. A., Czerny, B., Lasota, J. P., Szuszkiewicz, E.: 1988, *ApJ*, **332**, 646.
- Beloborodov, Andrei M.: 2008, in *Cool Discs, Hot Flows: The Varying Faces of Accreting Compact Objects*, *AIP Conf. Proc.*, **1054**, 51, arXiv:0810.2690v1.
- Campbell, C. G., Papaloizou, J. C. B., Agapitiu, V.: 1998, *MNRAS*, **300**, 315.
- Iankova, Krasimira: 2007, *V BSCASS*, Heron Press Ltd. Science series, p. 326. http://aquila.skyarchive.org/5_BSCASS/create/presentations/Iankova.pdf
- Iankova, Kr. D., Filipov, L.: 2008, *SRI-BAS*, p. 88, <http://www.space.bas.bg/SENS-2007/1-16.pdf>
- Iankova, Kr. D.: 2009a, *Publ. Astr. Soc. "Rudjer Bošković"*, **9**, 327. http://aquila.skyarchive.org/6_SBAC/pdfs/31.pdf
- Iankova, Krasimira: 2009b, *Proceedings of the International Conference MSS-09 "Mode Conversion, Coherent Structures And Turbulence"*, Space Research Institute, Moscow, p. 409.
- Kuncic, Zd., Bicknell, G.V: 2004, *ApJ*, **616**, 669, arXiv: astro-ph/0402421v1.
- Novak, M. A., Wilms, J., Vanghan, B., Dove, J., Begelman, M.: 1999, *AJ*, **515**, 726.
- Papaloizou, J. C. B., Terquem, C.: 1997, *MNRAS*, **287**, 771.
- Pottschidt, K., Konig, M., Wilms, J., Staubert, R.: 1998, *A&A*, **334**, 201.
- Spruit, H. C., Deufel, B., Dullemond, C. P.: 2001, *Hot and very hot gas around black holes*, http://www.mpa-garching.mpg.de/HIGHLIGHT/2001/highlight0110_e.html
- Yankova, Krasimira: 2012, *Publ. Astron. Soc. "Rudjer Bošković"*, **11**, 375. http://aquila.skyarchive.org/7_BSAC/html/papers.html

AUTHORS' INDEX

- Atanackovic, Olga 367
Atanasov, Emanouil 57
Atanassov, E. 105
Belcheva, Maya K. 279
Bellas-Velidis, Ioannis 279
Bode, M. F. 339
Boeva, S. 339
Bonev, Tanyu 283
Boneva, Daniela 113
Buchlin, E. 143
Chapanov, Yavor 121
Christova, Magdalena 205
Ćirić, Dušan 127
Ćirić, Luka 127
Cvetković, Zorica 135, 297
Damljanović, Goran 135, 263
Dapergolas, Anastasios 279
Dechev, M. 105, 143, 321
Dechev, Momchil 57
Dennefeld, Michel 303
Dimitrijević, Milan S. 15, 153, 173,
189, 205, 219, 333
Dimov, Dimo 219
Donkov, Sava 239
Drazic, Milan 367
Duchlev, P. 143, 321
Duchlev, Petar 283
Durchova, M. 105
Filipov, Lachezar 113
Golev, Valery K. 279
Gotchev, Deyan 113
Gurov, T. 105
Hambaryan, Valeri 7
Ignjatović, Lj. M. 333
Kacharov, N. 339
Kalaglarsky, Damyan 359
Karaivanova, A. 105
Kirilova, Daniela 249
Kirov, Nikolay 359
Koleva, K. 143, 321
Költzsch, Alexandra 7
Kontizas, Mary 279
Kovačević, Andjelka 205
Kovačević, Jelena 15
Krucker, Säm 367
Latev, G. Y. 339
Madjarska, M. S. 143
Maksimovic, Milan 367
Metodieva, Yanina 271
Metropoulos, A. 333
Mihajlov, A. A. 333
Mijajlović, Žarko 257
Milić, Ivana S. 263
Nedialkov, Petko 271
Nikolov, Grigor B. 279
Nikolov, Plamen 283
Nina, Aleksandra 289
Ninković, Slobodan 297
Ovcharov, Evgeni 271
Panayotova, Mariana 249
Pavlović, Rade 135
Pejović, Nadežda 257
Petrov, G. 105
Petrov, Georgi 57, 303
Petrov, Georgi T. 21
Petrov, N. 321
Petrov, Nikola 283
Poghosyan, Amalya 7
Popović, Luka Č. 15
Rompolt, Bogdan 283
Rudawy, Pawel 283
Sahal-Bréchet, Sylvie 205
Simić, Zoran 205
Simonović, Aleksandar 257
Slavcheva-Mihova, Lyuba 329
Srećković, V. A. 333
Stanchev, Orlin 239
Stojanović, Milan 297
Stoyanov, K. A. 339
Tsvetkov, Milcho 349, 359
Tsvetkova, Katya 349, 359
Tsvetkova, S. V. 339
Valcheva, Antoniya 271
Veltchev, Todor 239
Vial, J.-C. 143
Vidojević, Sonja 367
Vondrák, Jan 91
Yankova, Krasimira D. 375
Zamanov, R. K. 339
Zaslavsky, Arnaud 367



Figure 1. Conference photo.



Figure 2. In front of the hotel with the owner Goran Stojanović.



Figure 3. In front of St. Nicholas church in Kuršumlija.



Figure 4. In Devil's town.



Figure 5. Aleksandra Nina.



Figure 6. Daniela Boneva.



Figure 7. Daniela Kirilova, Mariyana Panayotova Manusheva.



Figure 8. Darko Jevremović.



Figure 9. Dejan Djordjević, Darinka Krstić.



Figure 10. Dejan Djordjević.



Figure 11. Dejan Urošević.



Figure 12. Dimo Dimov.



Figure 13. Djordje Petković.



Figure 14. Dragan Radović.



Figure 15. Dušan Ćirić.



Figure 16. Dušan Cvetković Lesnjak, Milan S. Dimitrijević.



Figure 17. Georgi Petrov.



Figure 18. Goran Damljanović.



Figure 19. Grigor Nikolov.



Figure 20. Jan Vondrák.



Figure 21. Jelena Kovačević.



Figure 22. Jovan Aleksić.



Figure 23. Katya Tsvetkova.



Figure 24. Krasimira Yankova.



Figure 25. Lela Popović, Luka Č. Popović.



Figure 26. Luka Č. Popović.



Figure 27. Luka Ćirić.



Figure 28. Lyuba Slavcheva-Mihova.



Figure 29. Lyuba Slavcheva-Mihova, Vasil Kolev.



Figure 30. Lyuba Slavcheva-Mihova, Vasil Popov.



Figure 31. Lyubomir Iliev.



Figure 32. Mariyana Panayotova Manusheva.



Figure 33. Marko Pavlović, Aleksandra Dobardžić.



Figure 34. Maya Belcheva, Grigor Nikolov.



Figure 35. Milan Jevtović, Miodrag Dačić.



Figure 36. Milan S. Dimitrijević.



Figure 37. Milan S. Dimitrijević, Goran Stojanović.



Figure 38. Milan S. Dimitrijević, Vasil Popov.



Figure 39. Milan S. Dimitrijević, Zdravka Sheiretova.



Figure 40. Milan Stojanović, Bojan Arbutina, Tatjana Milovanov.

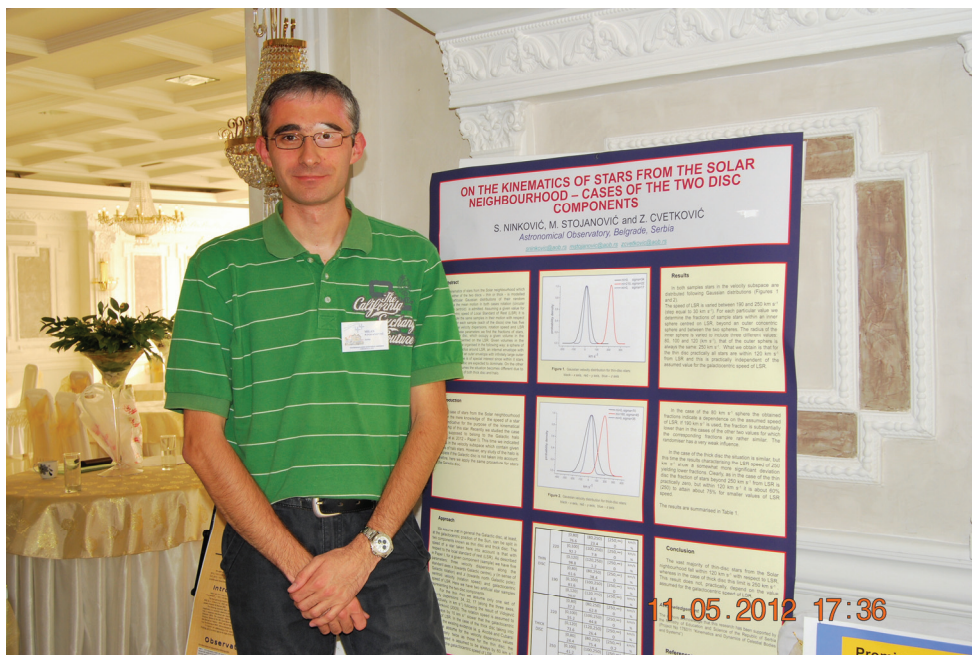


Figure 41. Milan Stojanović.



Figure 42. Milcho Tsvetkov.



Figure 43. Miodrag Dačić, Jelena Kovačević.



Figure 44. Momchil Dechev.



Figure 45. Nadežda Pejović.



Figure 46. Nemanja Rakić.



Figure 47. Nikola Petrov.



Figure 48. Nikolaj Kirov.



Figure 49. Ognyan Kounchev.



Figure 50. Orlin Stanchev, Sava Donkov, Ivana Milić.



Figure 51. Petko Nedyalkov.



Figure 52. Plamen Rusev Nikolov.



Figure 53. Rajcho Rusev Rajsyn.



Figure 54. Rositsa Miteva.



Figure 55. Svetlana Boeva.



Figure 56. Tanyu Bonev.



Figure 57. Vasil Kolev.



Figure 58. Vladimir Srečković.



Figure 59. Yavor Chapanov.



Figure 60. Žarko Mijajlović.



Figure 61. Zdravka Sheiretova.



Figure 62. Zoran Simić, Goran Damljanović.

CIP - Каталогизација у публикацији
Народна библиотека Србије, Београд

520/524(082)

SERBIAN-Bulgarian Astronomical Conference (8
; 2012 ; Leskovac)

Proceedings of the VIII Serbian-Bulgarian
Astronomical Conference, Leskovac, Serbia,
May 8-12, 2012 / eds. Milan S. Dimitrijević
and Milcho K. Tsvetkov. - Belgrade :
Astronomical Society "Rudjer Bošković", 2013
(Beograd : Sibra Star). - 413 str. : ilustr.
; 24 cm. - (Публикације Астрономског друштва
"Руђер Бошковић" = Publications of the
Astronomical Society "Rudjer Bošković" ; #sv.
#12)

Tiraž 100. - Bibliografija uz svaki rad. -
Registar.

ISBN 978-86-89035-02-5

a) Астрономија - Зборници b) Астрофизика
- Зборници
COBISS.SR-ID 199235340

